Investigation into the Molecular Mechanisms Underlying Chemoresistance in Malignant Rhabdoid Tumours

Thesis submitted to the University of Dublin, Trinity College

for the Degree of Doctor of Philosophy

By

Patricia Hannon Barroeta, B.A (Mod)

School of Biochemistry and Immunology

Trinity College Dublin

July 2023

Supervised by

Dr Daniela M. Zisterer

Declaration

I declare that this thesis has not been submitted as an exercise for a degree at this or any other University and it is entirely my own work. Figures 5.19, 5.20, 5.21 and 5. 22 were carried
out with Ms Shauna Power. I agree to deposit this thesis in the University's open access institutional repository or allow the library to do so on my behalf, subject to Irish Copyright Legislation and Trinity College Library conditions of use and acknowledgement.

.

Patricia Hannon Barroeta

Acknowledgements

First and foremost, I would like to thank my supervisor Dr Daniela Zisterer, for her guidance, advice, and infinite patience throughout this project. Thank you for staying calm even when I was not and for all the kindness you have shown me.

I would like to thank all the past members of the DZ Lab who made me feel so welcome when I started. Rachel, thank you for welcoming me even at your busiest time and for always being so kind to me. Rebecca, I will always be grateful for your friendship and all your patience. Thank you for always looking out for me! Stefania, I could not have done this project without your guidance and advice. I always miss my Monday evening tissue culture companion. Helene, thank you for all the laughs, there was never a dull day when you were in the lab! Eavan, thank you for all the after-work runs (I suppose), sushi and wine chats and your endless generosity. Tianyi, it has been a pleasure working with you these last two years. I would like to thank all the past and present members of our reading room: Marilena, Ewelina, Magda, Vinnie, Jill, Tania, Gillian, Sinead, Aidan, Louie, Callum, Mary, Claire, Chloe, Ben, Aoife, John, Jerry, Ana, Erwina and Megan. I am very grateful to have been able to work alongside such a great group of people and have made so many great memories over the past 4 years! A special mention to Ciara, who started her PhD at the same time as me and who was by my side through every step (big and small) of this process. Through all the writing and ranting about our experiments that did not work and celebrating the ones that did! You have been a source of support every hour since we started, and I will greatly miss working with you and having someone to talk to about everything.

Thank you to all the staff in Biochemistry & Immunology, everyone in the office and everyone in the teaching lab. In particular, Liam Cross for his ability to fix everything in record time and saving the day on countless occasions, and to Barry Moran for all his help with flow cytometry experiments.

I would like to thank all my friends who have offered me so much support from afar. In particular, Sorcha and Anniina, you have inspired me and cheered me on year after year. You two are the best support system I could ever ask for and I would be lost without the two of you.

A special mention to Katie, Marina, Helen, Hope and Grace, not only for their support over the last 4 years, but for 21 years of friendship. Thank you, for always being there through all the highs and lows. I am now looking forward to spending more time with each of you! Clara, thank you for your continuous empathy and kindness. Your voice messages never go unappreciated! I would like to thank all my friends here in Dublin, for their endless support and patience. In particular, to Ruth and Sara, for always checking in on me and looking out for me, from the first day I moved to Dublin. To Conor, I can't thank you enough for always listening and making me laugh. Not sure how I would have managed the last few months without your patience, generosity, and support.

To my Granny, a huge thank you for all you have invested in me. Thank you for greeting me every Sunday with a roast dinner and for always keeping scientific research articles for me to read. To Hugh, Stephen, Iseult and Ronan, thanks for helping me move so many times, and everything you have all done to support me during my studies. A special mention to my family in Spain, Carmen and Humberto. To my siblings, William and Natalia, thank you for all the motivation memes and texts!

Most importantly, I would like to thank my parents, Maurice and Delia, for everything they have done for me, every day, over the past 26 years.

Finally, I would like to dedicate this thesis to my grandfather, Bill Hannon.

Thank you to the PhD Provost Awards for funding this study.

Summary

Malignant rhabdoid tumour (MRT) is a rare and aggressive paediatric malignancy associated with poor prognosis and is, unfortunately, highly refractive to treatment. One of the major issues when treating MRT patients is the emergence of chemoresistance. The cellular mechanisms driving chemoresistance in MRT remain elusive. The aim of this study was to determine mechanisms underlying resistance to the commonly utilised chemotherapeutic agent, cisplatin, in MRT cells and whether targeting these mechanisms represents a therapeutic strategy to sensitise cells to cisplatin and improve treatment outcome. This study examined the roles of autophagy, the Nrf2/GSH antioxidant system and the Bcl-2 family of proteins in mediating cisplatin resistance in a panel of MRT cell lines.

Autophagy is a catabolic process whereby a cell degrades and recycles its own components. Autophagy has become an area of focus in the study of chemoresistance due to its reported dual role as both a pro-survival and pro-death mechanism. The role of autophagy in mediating chemoresistance in MRT remains poorly understood. Cisplatin was shown to induce autophagy and apoptosis concomitantly in a panel of MRT cell lines. Inhibition of autophagy by late-stage inhibitors, chloroquine and bafilomycin-A1, was shown to significantly enhance cisplatin-induced apoptosis but it should be noted, that off target autophagy-independent effects of these inhibitors cannot be ruled out. In contrast, inhibition of autophagy by targeting early stages of the autophagic process using the pharmacological inhibitor SAR405 or through the genetic knockdown of critical autophagic protein ATG5 by siRNA did not sensitise cells to cisplatin-induced apoptosis. Inhibition of caspase-induced apoptosis with Z-VAD-FMK also inhibited autophagy levels demonstrating a complex interplay between these two pathways. Collectively, these results suggest that autophagy does not appear to elicit a pro-survival effect in the chemotherapeutic response of MRT cells.

The balance between oxidative stress mediated by reactive oxygen species (ROS) and the antioxidant system, including the well-known antioxidant glutathione (GSH) and the transcription factor Nuclear erythroid-related factor-2 (Nrf2), has been implicated in chemoresistance. This study evaluated the role of these components in the response of MRT cells to treatment with cisplatin. This study characterised the basal levels of GSH, ROS and Nrf2 in a panel of MRT cell lines and found a correlation between the expression

profile of the antioxidant defence system and cisplatin sensitivity. Results showed that treatment with ROS scavenger N-acetylcysteine (NAC) protected cells from cisplatin-induced ROS and apoptosis. Interestingly, depleting GSH levels with the inhibitor buthionine sulphoximine (BSO) enhanced cisplatin-induced ROS and sensitised cells to cisplatin. Inhibition of Nrf2 expression with the small molecule inhibitor ML385 or by siRNA enhanced ROS and sensitised resistant MRT cells to cisplatin. These results suggest that targeting the Nrf2/GSH antioxidant system may present a novel therapeutic strategy to combat chemoresistance in rhabdoid tumours.

Finally, this study examined the role of the Bcl-2 family in mediating chemoresistance in MRT. Expression levels of a series of pro- and anti-apoptotic members of the family were characterised to assess whether they may play a role in determination of cisplatin cytotoxicity. Interestingly, cisplatin-sensitive BT12 cells were shown to be deficient in anti-apoptotic Bcl-2, whilst high levels are expressed in the more resistant BT16 and G401 cells. This study then went on to evaluate whether targeting Bcl-2 with the Bcl-2 selective BH3 mimetic ABT-199 could affect the apoptotic response to cisplatin and sensitise MRT cells to cytotoxicity. ABT-199 was found to synergistically enhance cisplatin-induced apoptosis in BT16 cells. This BH3 mimetic was shown to upregulate intracellular and mitochondrial ROS and to downregulate mitochondrial respiration and GSH levels. Moreover, ABT-199 was shown to downregulate anti-apoptotic Mcl-1 in a ROS-dependent manner and inhibition of Mcl-1 degradation and ROS production by the ROS scavenger NAC was shown to reverse the synergistic effect on apoptosis by ABT-199 and cisplatin, proposing that a ROS-dependent mechanism underlies the observed synergy. In conclusion, this study has provided novel insights into the molecular mechanisms underlying chemoresistance in MRT and proposes novel therapeutic avenues in the design of new treatment strategies for MRT.

Table of Contents

List of Figures

Chapter 1

Chapter 2

Chapter 3

Chapter 4

Chapter 5

Chapter 6

List of Tables

Abbreviations

µM	Micromolar
3-MA	3-methyladenine
ABC	ATP binding cassette
Anova	Analysis of variance
AML	Acute myeloid leukaemia
Apaf-1	Apoptotic protease activating factor-1
Ara-C	Arabinoside
ARE	Antioxidant responsive element
ATG	Autophagy-related protein
ATM	Ataxia telangiectasia mutated
ATO	Arsenic trioxide
ATP	Adenosine triphosphate
AT/RT	Atypical teratoid/rhabdoid tumour
Bad	Bcl-2 associated agonist of cell death
Baf-A1	Bafilomycin-A1
Bak	Bcl-2 antagonist/killer
Bax	Bcl-2-associated X protein
Bcl-2	B cell lymphoma-2
Bcl-xL	B-cell lymphoma-extra large
BECN1	Beclin-1
BH	Bcl-2 homology
BID	BH3 interacting domain death antagonist
BIR	Baculovirus IAP repeat domain
BSO	Buthionine sulfoximine
CARD	Caspase recruitment domains
Caspase	Cysteine-aspartic proteases
cFLIP	Cellular FLICE-like inhibitor protein
CI	Combination Index
cIAP1/2	Cellular inhibitor of apoptosis protein ½
CLL	Chronic lymphocytic leukaemia
CNS	Central nervous system
DCF	2′,7′-dichlorofluorescein
DDR	DNA damage response
DD	Death domain
DED	Death efector domain
dH_2O	Deionised water
Diablo	Direct inhibitor of apoptosis-binding protein with low pI
DISC	Death-inducing signalling complex
DMEM	Dulbecco’s Modified Eagle Medium
DMSO	Dimethyl sulfoxide
DNA	Deoxyribonucleic acid
DTT	Dithiothreitol
EBSS	Earle's Balanced Salt Solution
ECL	Electrochemiluminescence

EDTA	Ethylene-diamine-tetra-acetic acid
ERK	Extracellular signal-related kinases
ER	Endoplasmic reticulum
EZH2	Enhancer of zeste homolog 2
FADD	Fas associated protein with death domain
FasL	Fas ligand
FBS	Fetal bovine serum
FITC	Fluorescein isothiocyanate
FSC	Forward scatter
GAPDH	Glyceraldehyde 3-phosphate dehydrogenase
GPX	Glutathione peroxidase
GSH	Reduced glutathione
GSSG	Oxidazed glutathione
GST	Glutathione-S-transferase
H	Hours
H_2DCFDA	2',7'-Dichlorodihydrofluorescein-diacetate
H_2O_2	Hydrogen peroxide
HCQ	Hydroxychloroquine
HEPES	4-(2-hydroxyethyl)-1-piperazineethanesulfonic acid
HO-1	Heme oxygenase-1
IAP	Inhibitor of apoptosis protein
IC50	50% inhibitory concentration
JNK	c-Jun N-terminal kinases
kDA	KiloDalton
Keap1	Kelch-like ECH-associated protein 1
MAPK	Mitogen-activated protein kinase
Mcl-1	Myeloid cell leukaemia-1
MDR	Multidrug resistance
MFI	Median fluorescence intensity
Mg	Milligrams
MOMP	Mitochondrial outer membrane permeabilisation
MRT	Malignant rhabdoid tumour
MRTK	Malignant rhabdoid tumour of the kidney
Min	Minutes
miRNA	microRNA
mL	Millilitre
mM	Millimolar
mRNA	Messenger RNA
MRP	Multidrug resistance protein
mTOR	Multidrug associated-associated protein 1
mTORC1/2	mTOR complex ½
NAC	N-acetylcysteine
NF-κB	Nuclear factor-kB
nM	Nanomolar
Noxa	Phorbol-12-myristate-13-acetate-induced protein 1

NQO1	NAD(P)H-quinone oxidoreductase 1
Nrf2	Nuclear factor erythroid 2–related factor 2
NT siRNA	Non-targeting siRNA
OCR	Oxygen Consumption Rate
PBS	Phosphate buffered saline
PI	Propidium Iodide
PI3K	Phosphatidylinositol-3-kinase
PS	Phosphatidyl Serine
PtdIns3 complex	Phosphatidylinositol-3-kinase complex
PVDF	Polyvinylidene difluoride
Raf	Rapidly accelerated fibrosarcoma
Ras	Rat sarcoma
RIPA	Radioimmunoprecipitation
RNA	Ribonucleic acid
ROS	Reactive Oxygen Species
RTPS	Rhabdoid tumor predisposition syndrome
S.E.M	Standard error of the mean
SDS	Sodium dodecyl sulfate
SDS-PAGE	Sodium dodecyl sulphate polyacrylamide gel electrophoresis
shRNA	Short hairpin RNA
siRNA	Small interfering RNA
Smac	Second mitochondria-derived activator of caspase
SMARCA4	SWI/SNF related, matrix associated, actin dependent regulator of chromatin, subfamily A, member 4
SMARCB1	SWI/SNF –related matrix associated, actin dependent, regulator of chromatin, subfamily B, member 1
SOD	Superoxide dismutase
SQTM1	Sequestosome1
SSC	Side scatter
SWI/SNF	Switch/sucrose non-fermentable
tBid	Truncated Bid
TBS	Tris buffered saline
TBST	Tris buffered saline tween
TEMED	Tetramethylethylenediamine
TME	Tumour microenvironment
ULK	Unc-51 like autophagy activating kinase
UVRAG	UV radiation resistance-associated gene protein
XIAP	X-linked inhibitor of apoptosis protein

Thesis outputs: Publications, Presentations and Awards

Publications:

- **Patricia Hannon Barroeta**, Maureen J O'Sullivan, Daniela M Zisterer. The role of the Nrf2/GSH antioxidant system in cisplatin resistance in malignant rhabdoid tumours. *Journal of Cancer Research and Clinical Oncology.*

- **Patricia Hannon Barroeta**, Stefania Magnano, Maureen J O'Sullivan, Daniela M Zisterer. (2022). Evaluation of targeting autophagy for the treatment of malignant rhabdoid tumours. Cancer Treatment and Research Communications. 32:100584. DOI: 10.1016/j.ctarc.2022.100584.

- Stefania Magnano, **Patricia Hannon Barroeta**, Ronan Duffy, Jeff O'Sullivan, Daniela M Zisterer. (2021). Cisplatin induces autophagy-associated apoptosis in human oral squamous cell carcinoma (OSCC) mediated in part through reactive oxygen species (2021). Toxicology and Applied Pharmacology. 15;427:115646. DOI:10.1016/j.taap.2021.115646.

- A. Prasanth Saraswati, Nicola Relitti, Margherita Brindisi, Jeremy D. Osko, Giulia Chemi, Stefano Federico, Alessandro Grillo, Simone Brogi, Niamh H. McCabe, Richard C. Turkington, Ola Ibrahim, Jeffrey O'Sullivan, Stefania Lamponi, Magda Ghanim, Vincent P. Kelly, Daniela Zisterer, Rebecca Amet, **Patricia Hannon Barroeta**, Francesca Vanni, Cristina Ulivieri, Daniel Herp, Federica Sarno, Antonella Di Costanzo, Fulvio Saccoccia, Giovina Ruberti, Manfred Jung, Lucia Altucci, Sandra Gemma, Stefania Butini, David W. Christianson, and Giuseppe Campiani. (2020). Spiroindoline-Capped Selective HDAC6 Inhibitors: Design, Synthesis, Structural Analysis, and Biological Evaluation. ACS Medicinal Chemistry Letters 2020 11 (11), 2268-2276. DOI: 10.1021/acsmedchemlett.0c00395.

Presentations and Conferences:

- Ireland Association of Cancer Research (IACR) annual meeting. Cork, Ireland. 2022.
- "Harnessing Fundamental, Translational and Clinical Research for the Benefit of Cancer Patients". The 12th International Cancer Conference, 2022. Dublin, Ireland.
- "Cellular Bases for Patient Response to Conventional Cancer Therapies". 2022. European Association for Cancer Research (EACR). Berlin, Germany.

Awards:

- PhD Provost Award.
- Irish Cancer Society Translational Cancer Research Networking Award.

1. Introduction

1.1 Malignant Rhabdoid Tumours

1.1.1 Discovery of MRTs

Malignant rhabdoid tumour (MRT) is a very rare and highly aggressive form of neoplasm that occurs primarily in infants and young children. This type of tumour is most commonly found in the kidneys where it is referred to as malignant rhabdoid tumour of the kidneys (MRTK). However, it can also occur in the central nervous system (CNS), where it is termed atypical teratoid malignant tumour (AT/RT), as well as the liver and any soft tissue sites. Although diagnosed in older children and adults, MRT typically occurs in infants under the age of three[1]. The patients' age poses significant restrictions when planning intensive therapy due to low tolerance to radiotherapy and chemotherapy[2]. This factor combined with the aggressive and metastatic nature of these tumours means that the prognosis for MRT is very poor with an estimated survival rate of approximately 25%[3, 4]. A further complication in the study of MRT treatments is the rarity of this disease which greatly limits the possibilities of performing controlled clinical trials.

Rhabdoid tumours were identified in 1978 during the first National Wilms' Tumour study (NWTS)[5]. In this study, Beckwith and Palmer collected and analysed data from 427 children with malignant kidney tumours and noted a variant of Wilms' tumour. Wilms' tumour is the most common form of paediatric kidney tumour and occurs predominantly in children between the ages of 2 and 5, after which the incidence decreases notably[6]. Beckwith and Palmer noted that this variant occurred in younger infants (under the age of two) and was associated with a much poorer prognosis in comparison to Wilms' tumour. In fact, the 5-year survival rate of Wilms' tumour is 90% [6] which is significantly higher than that for MRT (approximately 25%). Further work was carried out on the characterisation of MRT in 1981, when Haas *et al*. published an ultrastructural examination of 11 of the variants that were described in the NWTS[7]. This paper confirmed the structural differences between these and Wilms' tumours and termed them malignant rhabdoid tumours due to their morphological resemblance to rhabdomyosarcomas. Furthermore, Haas *et al*. demonstrated the metastatic nature of the tumours and documented the short survival rate associated with it. After a study conducted by Weeks *et al*. on 111 MRTK cases (79 of which were tumours from NWTS), in which no histogenetic links were found between the MRTKs and Wilms' tumours[8], MRTs were recognised as a distinct entity.

Rhabdoid tumours have been reported to occur in many other sites. In 1996, AT/RTs (MRTs in the CNS), were identified as distinct to other known tumour types in the CNS[9] and in 2000, they were included by World Health Organisation (WHO) as a separate disease in their classification of CNS tumours[10]. Distinguishing AT/RTs from embryonal brain tumours was complicated due to their neuroepithelial histological similarities. In 1984, Bonnin and colleagues reviewed 7 case studies of infants under the age of two that presented with MRT in association with rhabdoid tumours in the CNS[11]. Since then, further AT/RT case studies have been published leading to its classification. Unfortunately, due the fact that AT/RT was only recently identified and is rare, it has been subject to misdiagnosis.

Aside from the CNS and kidneys, MRTs have been detected in many soft tissue sites such as pelvis, bladder, uterus, neck, thymus and more frequently, in the lungs, liver or skin[12]. As was suggested in the study by Bonnin *et al.*, it is not uncommon for children to present rhabdoid tumours in more than one location. These tumours are identified as MRTs due to certain histological characteristics such as large nucleoli, filamentous cytoplasmic inclusions, and a significant amount of eosinophilic cytoplasm. Furthermore, clinical similarities can be observed across different cases of MRTs. Most significantly, 80-95% of these tumours have a mutation in the *SMARCB1* gene in common[13].

1.1.2 Epidemiology

Rhabdoid tumours are rare. In the past, they have been frequently misdiagnosed due to a lack of diagnostic tools that detect *SMARCB1* gene mutations as well as a lack of classification and awareness around these tumours. As MRTs have only been identified relatively recently, most epidemiological data available is derived from a very limited time period and the incidence may now rise due to an increase in recognition. Much of the available information is based on individual case studies, however, there is a small number of population-based reports in literature.

In the US, the number of cases per year for children under the age of 15 is 0.19 per million for MRTKs and 0.89 per million for AT/RT[14]. A study conducted by the Austrian Brain Tumour Registry between 1996 and 2006, which evaluated 311 recently diagnosed AT/RT cases, concluded an age-standardised incidence of 1.38 per million. The peak in incidence occurred between birth and 2 years of age with a 5-year survival of 39.5%[1]. Ostrom *et al*.

confirmed some of these findings in a study which used data from the Central Brain Tumour Registry in the US to analyse the trends in incidence and survival rates in cases of AT/RT. This study looked at cases from 50 cancer registries from 2001 to 2010 and established the peak incidence of occurrence in infants as under the age of 1 after which incidence decreased with age. The 5-year survival rate was concluded to be 28.3%[15].

The European Paediatric Soft Tissue Sarcoma Study Group (EpSSG) conducted a multinational study which looked at the effect of a multimodal intensive therapy approach on 100 newly registered extra-cranial MRT patients from 2005 to 2014. The analysis of the study revealed that the risk of death was highest in patients under the age of 1. The overall survival rate was established to be 38.4% with a particularly poor prognosis in cases where metastasis had occurred. There was also a poorer prognosis in cases where patients had extra-renal tumour sites, in line with previous findings in literature[16].

In Ireland, there were only 25 paediatric patients (the criteria being patients who were under the age of 17 when diagnosed) between January 1986 and December 2013. Of this cohort of patients, the youngest age of diagnosis was 5 days and the oldest was almost 15. A review of these cases by Uwineza *et al.*, found an equal female to male ratio overall but noted AT/RTs were more common in males whereas MRTKs seemed to predominate in females. Other studies have also suggested a higher incidence in AT/RT cases in males[17]. The patients were generally treated with a multimodal approach and received some combination of surgery, chemotherapy, and radiotherapy. Relapse occurred in 43.5% of the cases. Out of the 25 patients, 19 died of their tumours, with the deaths ranging from 0.15 to 28.75 months after the initial diagnosis[18].

The EU-RHAB registry was initiated in 2005 to collect data of rhabdoid tumour patients in order to generate a common European database and establish a standardised treatment regimen of rhabdoid tumours[19, 20]. A study based on 31 ATRT patients from four countries found a correlation between prolonged overall survival and patients who were over the age of 3, received radiotherapy and underwent complete remission[20]. Nemes *et al*, conducted a study which evaluated 100 patients presenting with either extracranial extrarenal rhabdoid tumours or renal rhabdoid tumours. The 5-year overall survival was 45.8± 5.4% and the event-free survival was found to be 35.2 ± 5.1%. This study also found that being 12 months or under was associated with favourable prognosis[21].

As mentioned above, the incidence of MRT in these reports is likely to be underestimated due to misdiagnosis. However, all the studies outline a very poor prognosis for patients with rhabdoid tumours highlighting an urgent need for increased awareness and novel treatment strategies.

1.1.3 Genetics

1.1.3.1 SMARCB1-deficient rhabdoid tumours

The most prominent genetic feature in rhabdoid tumours, regardless of the origin, is a homozygous inactivation of the *SMARCB1* gene. This gene is believed to be mutated in approximately 80-90% of MRT cases[12]. The first characteristic genetic feature identified in MRTs was monosomy 22. Biegel *et al*., identified the 22q11.2 cytoband as the specific region in chromosome 22 in which deletions and translocations occurred in MRT cases[22]. Although this study was conducted in a small cohort, they proposed this mutation could serve as a biomarker of AT/RT. In 1998, Versteege *et al*., demonstrated a biallelic inactivation of *SMARCB1* in 13 MRT cell lines through PCR and southern blotting. They identified it as a key oncogenic event in the development of rhabdoid tumours as well as proposing its role as a tumour suppressor gene[23].

Chromatin complexes can be categorised into four families in accordance with similarities in their ATPase domains. These complexes are imitation switch (ISWI), INO80, chromodomain helicase DNA-binding (CHD) and switch/sucrose non-fermentable (SWI/SNF)[24]. The *SMARCB1* gene encodes for the 47 kDa SMARCB1 protein (SWI/SNF-related matrix-associated actin-dependent regulator of chromatin subfamily B member 1), which forms part of the SWI/SNF complex. This complex regulates chromatin packaging by facilitating DNA rearrangement during the remodelling of the nucleosome[25]. The SWI/SNF complex is thought to be composed of approximately 9-12 subunits[26]; which are believed to act as tumour suppressors by regulating the cell cycle[27]. Mutations in the SWI/SNF complex have been associated with various developmental diseases. In particular, it has been implicated in approximately 20-25% of all cancers[24, 28]. The role of the SMARCB1 subunit within the complex is yet unclear. However, a few studies have been conducted to examine potential functions of SMARCB1.

Wang *et al*., noted that loss of *SMARCB1* caused disassembly of SWI/SNF complexes at promoters and enhancers, but not super-enhancers. Super-enhancers are regions of the

mammalian genome comprised of clusters of the enhancer genome. This contrasts with the cells containing *SMARCB1*; which exhibited recruitment of the SWI/SNF complexes to the promoters, enhancers and super-enhancers. These results suggest that since enhancers regulate gene expression relating to cell differentiation and super-enhancers maintain cell identity, it is likely that *SMARCB*1-deficient cells lack the ability to differentiate but maintain their characteristics essential to tumour survival (proliferation, cell survival and self-renewal)[29, 30]. Nakayama *et al.*, demonstrated that *SMARCB1*-deficiency resulted in a loss of stability in SWI/SNF complexes on chromatin and that the restoration of *SMARCB1* in cells resulted in the activation of enhancers as well as that of the promoters, by blocking polycomb-mediated repression. This resulted in activation of genes involved in tumour suppression activities. However, in contrast to the findings by Wang *et al.*, this research found that reintroduction of SMARCB1 resulted in significant activation of both enhancers and super-enhancers with no notable difference between the two[31].

Studies using mouse models have shown that homozygous *SMARCB1* deficiency is lethal at the embryonic stage. In contrast, heterozygous mutation of *SMARCB1* predisposed the mice to tumours resembling human rhabdoid tumours. Of note, the mice never developed tumours on the kidney[32].

SMARB1 deficiency has been shown to impact a number of signalling pathways: the WNT signalling pathway, sonic hedgehog signalling pathway, polycomb and the p16-Rb signalling pathway. In literature, the WNT signalling pathway is categorised as either canonical or non-canonical. These are β-catenin-dependent and independent, respectively. The canonical pathway is involved in mediating cell proliferation and survival whilst the non-canonical pathway is involved in the regulation of cell migration, differentiation, and polarity[33]. SMARCB1 deficiency was observed to cause aberrant activation of canonical Wnt signalling pathway suggesting it has an essential role in the regulation of this pathway[34].

SMARCB1 expression has also been shown to impact the sonic hedgehog signalling pathway, which is involved in the signal transduction that mediates developmental cellular processes. It is involved in tissue polarity, cell differentiation and proliferation and has been implicated in tumorigenesis. This signalling cascade is induced by the binding of the Hh protein to the Patched protein 1 (Ptch 1) which binds to the smoothened (SMO) protein that activates the GLI (glioma-associated oncogene homolog) family of zinc finger

transcription factors (GLI1, GLI2 and GLI3). Knockdown of SMARCB1 correlates with overexpression of GLI1 and activation of Shh signalling. This is also observed in SMARCB1-deficient rhabdoid tumours[35].

The polycomb pathway has also become an area of focus in the study of SMARCB1 function. The polycomb group (PcG) proteins are transcriptional repressors involved in the mediation of differentiation and development. They form two complexes termed PRC1 and PRC2. The enzymatic catalytic subunit of PRC2, EZH2, has become a therapeutic target as it is overexpressed in many cancers. EZH2 alters gene expression through the trimethylation of Lys-27 in histone 3 (H3K27me3) at promoter regions[36]. SMARCB1-deficient tumours are amongst a number of cancers shown to overexpress EZH2. Inhibition of EZH2 activity can result in tumour regression and reduce expressed levels of GLI1, Ptch1, MYC[37]. Overexpression of PcG proteins results in an inability for cells to fully differentiate.

The p16-Rb pathway, which can mediate cell cycle arrest at G1 phase, has also been linked to SMARCB1 function. SMARCB1 has been demonstrated to exhibit tumour suppressor activity via this pathway resulting in the regulation of chromosomal stability and the prevention of cell cycle progression in tumour cells[33].

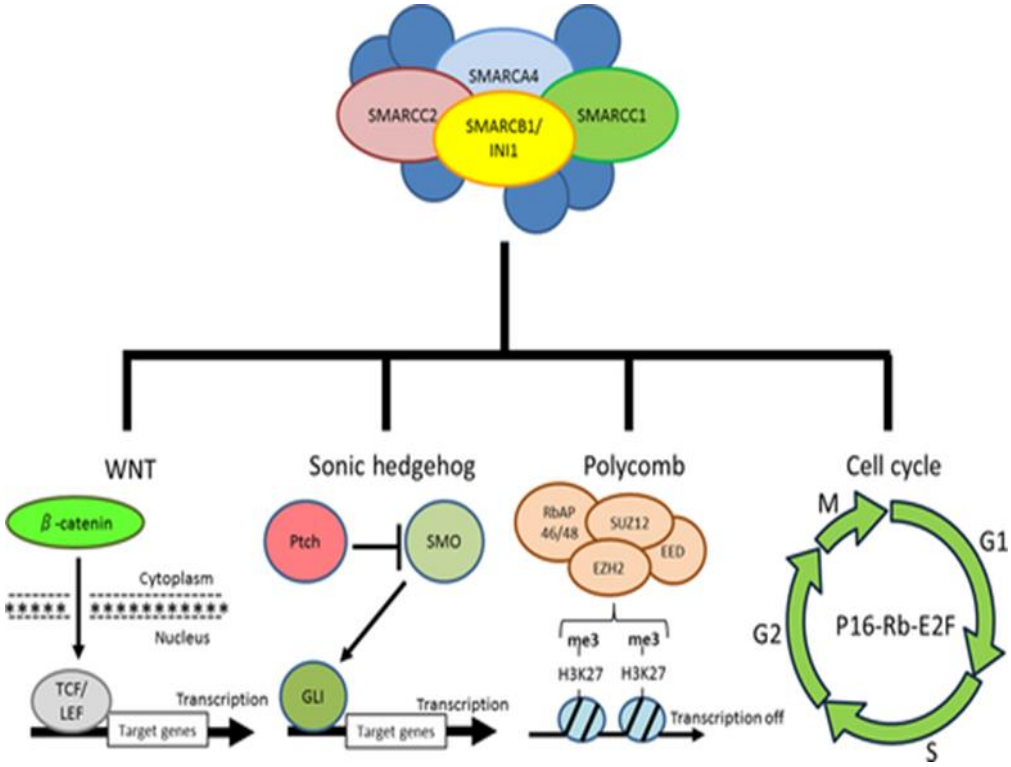

Figure 1.1 Pathways implicated in SMARCB1 tumour suppressor activity.

SMARB1 function has been implicated in various signalling pathways: the WNT signalling pathway, sonic hedgehog signalling pathway, polycomb and the p16-Rb signalling pathway. SMARCB1 deficiency causes aberrant activation of the canonical WNT signalling pathway involved in mediating cell survival and proliferation. SMARCB1 has also been shown to be involved in the sonic hedgehog signalling pathway which is implicated in tumorigenesis due to its role in cell proliferation and differentiation regulation. A link has been demonstrated between SMARCB1 and PcG proteins which are considered to maintain epigenetic cellular memory through the transcriptional repression of homeotic genes. Dysregulation of the polycomb family proteins is observed in cancer leading to an alteration in cell proliferation, metabolism, and the immune response amongst other vital cellular processes. SMARCB1 is believed to prevent progression of the cell cycle through the p16-Rb pathway. Image taken from Kohashi *et al.*[33]

Lastly c-Myc and Aurora kinase have also been demonstrated to be targets of SMARCB1. C-Myc is a regulator gene that codes for transcription factors relating to cell cycle progression, apoptosis and cell transformation. It can interact with SMARCB1 to recruit

the SWI/SNF complex for the transcription of genes involved in apoptosis. It is upregulated in the absence of SMARCB1 thereby promoting pro-tumour activity[33].

Aurora A kinase is part of the mitotic serine threonine kinase family and is important in healthy cell proliferation due to its role in mitosis and meiosis. It is downregulated in the presence of SMARCB1 and is overexpressed in SMARCB1-deficient tumours. In recent years, aurora kinases have become targets of interest in cancer research[33]. They have been found to be overexpressed in various cancers and have been demonstrated to contribute to chemo- and radio resistance[38]. Interestingly, aurora A kinase forms a positive feedback loop with c-Myc as it can promote c-Myc transcription whilst c-Myc can upregulate aurora A expression by binding to its promoter[38].

Understanding the role of SMARCB1 in the SWI/SNF complex has posed challenges, with various contradicting reports regarding the effect of SMARCB1 loss in terms of stability and composition of the complexes. SMARCB1 does not contain domains that are clearly indicative of a particular function. SMARCB1 is not reported to be essential for the formation of SWI/SNF complex[39]. However, it is clear that SMARCB1 mutations are the cause of the vast majority of MRT cases, therefore further work needs to be carried out to elucidate its role in the cancer.

1.1.3.2 SMARCA4-deficient rhabdoid tumours

Although *SMARCB1* mutations are present in almost all rhabdoid tumours, a small number do not have this mutation[2]. Instead, they present mutations in the *SMARCA4* gene. This gene is located at 19p13.2 and codes for the SMARCA4 protein, which is also a subunit in the SWI/SNF complex and functions as a tumour suppressor. SMARCA4 has been implicated in developmental processes, DNA damage repair, cell cycle regulation and regulation of transcription. SMARCA4 was identified as a tumour suppressor gene but more recently has been reported to have an oncogenic role[40]. As is the case with *SMARCB1*, these mutations consist of biallelic inactivation of the gene. More data is needed to establish the proportion of MRTs caused by *SMARCA4* deficiencies, as well as the clinical relevance of these mutations. Hasselblatt *et al*. reported a worse prognosis in *SMARCA4*-deficient tumours than in *SMARCB1*-deficient tumours[24].

Pan-cancer analyses in the field of paediatric oncology found that *SMARCA4* and *SMARCB1* were the only subunits of the SWI/SNF complex to be significantly mutated in childhood cancers[24, 41, 42]. However, in adult cancers there are four other genes from this complex that have been associated with tumorigenesis: *ARID1A, ARID1B, ARID2* and *PBRM1*[24, 39].

1.1.3.3 Rhabdoid tumour predisposition syndrome (RTPS)

Familial cases occur when there is *de novo* germline mutations giving rise to Rhabdoid Tumour Predisposition Syndrome (RTPS). This is inherited in an autosomal dominant manner where one mutated allele is inherited. An estimated 35% of SMARCB1 alterations occur as a result of *de novo* germline mutations[43]. Most cases of RTPS are associated with a *de novo* germline *SMARCB1* mutation. When this is the case, the syndrome is referred to as RTPS1. SMARCA4-related RTPS is referred to as RTPS2. In RTPS cases, patients develop tumours at a younger age than patients with bi-allelic somatic mutations and the tumours usually occur at more than one primary site. The median age of diagnosis for RTPS was found to be 6 months in a patient cohort, in contrast to a median age of 1.5 years in patients with a bi-allelic somatic mutation[12]. RTPS cases only account for a small proportion of MRT cases (25-35% for RTPS1 while the incidence of RTPS2 is unknown due to its low incidence). However, the frequency of reports of RTPS appear to be

increasing. It is still unclear if this is due to an increase in diagnoses or if there is an increase in the incidence[44].

1.1.3.4 Genome stability

Apart from the alterations in the *SMARCB1* gene, the genome of rhabdoid tumours remains notably stable[45]. This is in contrast to the majority of tumours where it is common to observe genome instability[46]. The number of mutations varies depending on the cancer, but it is usual to observe hundreds to thousands of DNA point mutations and to identify many mutated genes[47].

Lee *et al*. sequenced the exomes of 35 rhabdoid tumours and found that *SMARCB1* mutations were the only recurring event, suggesting that epigenetic dysregulation on its own is a driving force in some cancers[47]. This was first observed in 2008 by McKenna *et al*., who demonstrated that *SMARCB1*-deficient cells did not exhibit any changes in their DNA damage checkpoints or their sensitivity to DNA damaging agents. Furthermore, when looking at single-nucleotide polymorphism arrays of *SMARCB1*-deficient cancers they are identical to normal samples, aside from the *SMARCB1* mutation. They also showed that epigenetic changes driven by *SMARCB1*-deficiency directly affected the tumour phenotype, thereby indicating that epigenetic alterations due to a mutation in chromatin remodelling can drive tumorigenesis without genomic instability[48]. Moreover, human medulloblastomas were found to have a very unstable genome with many deletions and amplifications detected in multiple loci[48]. This was confirmed in 2012 by Kieran *et al*. who evaluated 25 rhabdoid tumours with SMARCB1 mutations in 115 oncogenes and found that, other than a single inactivating mutation in NRAS, there was a surprisingly complete absence of oncogenic mutations in rhabdoid tumours[49]. In 2013, this was further confirmed by Hasselblatt *et al*, who conducted a high-resolution genomic analysis which identified SMARCB1 as the only recurring mutation in rhabdoid tumours[50]. This suggests a potential for refocusing novel treatment strategies towards epigenetic pathways due to the fact that the SWI/SNF complex has a role in chromatin remodelling which regulates the packaging and unpackaging within the nucleosome thereby enabling DNA transcription, recombination, replication, and repair[51]. As previously mentioned, SMARCB1 has been shown to play an important role in Wnt/B catenin pathway, E2F-related target genes, c-MYC expression and aurora A. SMARCB1 has also been shown to

inhibit *cyclin D* transcription as well as cyclin-dependent kinase (CDK4/6) activity by recruiting HDAC during the G1 phase of the cell cycle[52]. Using SNP array analysis, McKenna *et al*. observed that the cyclin D1 locus had no mutations. However, the protein was upregulated in all rhabdoid tumours whilst only overexpressed in some of the medulloblastomas. Moreover, none of the cyclins were upregulated in the tumours. The authors postulated that cyclin D1 upregulation correlated with tumour phenotype as it has a role in promoting the progression through the G1 phase of the cell cycle. The authors also found cMyc to be upregulated at the transcript level[48]. Johann *et al*. examined the genetic and epigenetic profiles of 192 AT/RT and identified three molecular subgroups based on differences in tumour location, age of diagnosis, type of alteration, methylation, and gene expression profiles. These three profiles were named AT/RT-TYR, AT/RT-SHH and AT/RT-MYC based on what proteins were overexpressed in each molecular subgroup. This report also noted the AT/RTs to have a characteristically stable genome further confirming reports listed above. This was also seen in a mouse study whereby molecular profiling of rhabdoid tumours defined three subgroups regardless of their anatomical origin. These were found to be similar to the groups defined by Johann *et al*[53]. Another genetic and epigenetic study of 191 AT/RTs by Torchia *et al*. also found three epigenetic subgroups differing in genomic profiles, SMARCB1 genotypes, methylation patterns and therapeutic responses to epigenetic and signalling inhibitors[54].

In conclusion, the sole recurrent genetic driver of MRT are mutations in SMARCB1 or SMARCA4 components of the chromatin remodelling complex, which are typically characterised as somatically acquired biallelic inactivating truncating mutations. Although MRT tumours are considered to be the prototypical SMARCB1-deficient cancer, other SMARCB1-deficient tumours have been identified, such as renal medullary carcinoma, schwannomatosis and paediatric poorly differentiated chordoma[12]. The role of SMARCB1/SMARCA4 in driving MRT highlight the relationship between genetic and epigenetic alterations in cancer, however the exact mechanisms that underlie this remain poorly understood. SMARCB1 alterations have been shown to affect the regulation of a number of canonical cancer pathways given that the SWI/SNF chromatin remodelling complex binds to the promoters and active enhancers of a number of pathways though affecting lineage specific coordinated pathways. Recent studies have suggested that rhabdoid tumours arise from a small number of neural crest cells that become SMARCB1-deficient in the process of development, preventing further differentiation. Moreover,

polycomb repressor genes have been shown to be overactive in MRTs, impacting the cells' ability to fully differentiate[39].

1.1.4 Diagnosis

Unfortunately, it is not uncommon for MRT to be misdiagnosed. This is due to the resemblance of MRTs with other tumours on magnetic resonance imaging (MRI) and computed tomography (CT) scans. These techniques are used to detect the presence of a tumour in a patient, but to confirm that it is a rhabdoid tumour, further analysis is required[55, 56]. It is also difficult to diagnose rhabdoid tumours in early stages due to their rapid progression and metastatic nature. Additionally, rhabdoid tumours can occur in neonates[57]. Due to the young age of the patients, it can be difficult to identify the symptoms that arise with MRTs, thereby delaying the detection of the tumour. Nevertheless, there are multiple available diagnostic techniques for identifying MRTs and certain symptoms worth noting.

1.1.4.1 Clinical features

Symptoms vary amongst MRT patients depending on the location of the tumour. In most cases the first sign that is detected in MRT is a lump or a mass where the tumour is located. As it frequently occurs in young infants under the age of 3, pain and discomfort can be hard to detect and assess. However, pain can present itself as fussiness. Often symptoms are linked to the pressure exerted by the tumour mass which, depending on its location, may result in respiratory problems and airway obstruction[58], nerve palsy or abdominal distension and hepatomegaly[59]. Other symptoms include fatigue, vomiting and the child's head tilting to one side[60]. If the tumour is in the brain often a noticeable increase in head size can be reported in young infants and symptoms such as headaches, altering levels of consciousness and issues with motor coordination may arise[61]. Rhabdoid tumours in the kidney may cause haematuria, proteinuria, fevers, and hypercalcemia[62, 63]. Due to the highly progressive nature of this tumour, symptoms are only present for a short amount time before the diagnosis it made.

1.1.4.2 Histological analysis

As mentioned above, MRTs can be distinguished by characteristic histological features such as eccentric nuclei, large nucleoli, filamentous eosinophilic cytoplasmic inclusions, and an abundance of eosinophilic cytoplasm[64]. Rhabdoid tumour cells can vary in shape

and size and whorls of intermediate filaments are notable under the electron microscope. Necrosis is often detected within the tumour mass[65]. The variations that occur in the histological features of MRTs can make it difficult to classify certain tumours.

1.1.4.3 Immunohistochemical analysis

Immunohistochemistry is used in combination with other diagnostic techniques to identify rhabdoid tumours. The eosinophilic inclusions mentioned earlier stain positive for keratin. Rhabdoid tumours frequently, but not always, stain positive for epithelial membrane antigen (EMA) as well as vimentin[40, 41]. Since there is not a positive staining pattern specific to MRTs, immunohistochemical analysis is used to support and validate results provided by histology, clinical data and cytogenetics.

Immunohistochemical staining for SMARCB1 expression was developed in 2004 and has since proven to be a useful diagnostic tool in identifying MRTs[42, 43]. This detects the mutation and loss of expression of SMARCB1 protein, which occurs in approximately 80-90% of rhabdoid tumours[12] (Figure 1.2).

1.1.4.4 Cytogenetic testing

Cytogenetic testing has found abnormalities in chromosome 22 in rhabdoid tumours[44]. More specifically a loss of expression of the SMARCB1 protein, as mentioned above, is seen in an estimated 80-90% of cases. In the few cases where SMARCB1 expression is not lost, SMARCA4 expression is lost instead[26]. It should be noted however, that loss a mutation of the SMARCB1 gene is not specific to MRTs and also occurs in schwannomatosis[45]. Furthermore, SMARCB1 mutations have been detected in a subset of hepatoblastomas, epithelioid sarcoma and renal medullary carcinomas[46]. Therefore, a combination of tests with clinical assessment should be used to correctly diagnose MRTs.

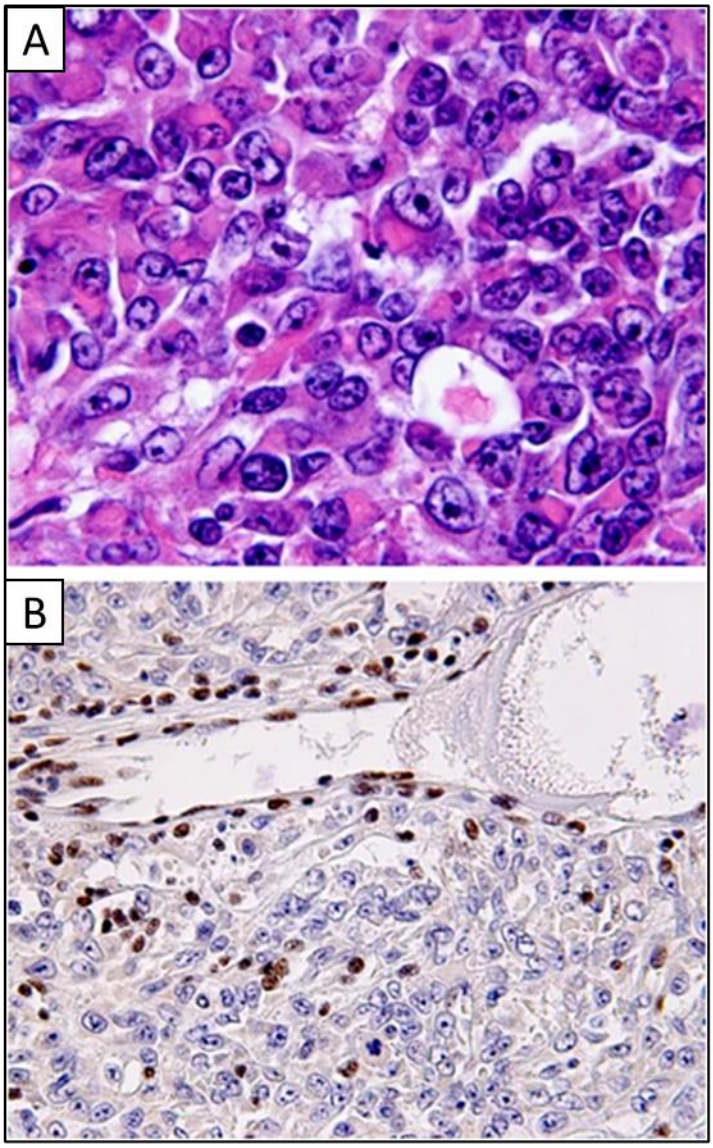

Figure 1.2 SMARCB1 expression is absent in neoplastic MRT cells.

A. SMARCB1 staining is not detected by immunohistochemistry in AT/RT. **B**. Expression of SMARCB1 in non-tumour cells. Image modified from Sigauke *et al*[66].

1.1.5 Current and emerging treatments of MRT

Unfortunately, there is no established treatment protocol for MRTs. The rarity of MRTs poses many challenges in treatment development and clinical trials. At present, rhabdoid tumours are usually treated with a combination of therapies which include surgery, chemotherapy, and radiation therapy.

1.1.5.1 Surgery

The first step in combatting MRT is often the removal of the tumour through surgery, which results in a 74% improvement in survival[67]. During the surgery, as much of the tumour as possible is resected. This is dependent on the site of the tumour and the progression of the disease. Removal of the tumour is usually performed at the same time as a biopsy. Total or near-total resection is often not possible, and this has a significant impact on the prognosis. Richards *et al*. examined overall survival for AT/RT regarding the extent of surgical resection. This study examined the data from 24 patients who underwent 38 operations. A complete total resection was performed on 25% of these cases, a near total resection was performed on 29%, 33.3% underwent a subtotal resection and 12.3% only had a biopsy. The overall survival of the group that underwent a complete total resection was found to be significantly higher than those who underwent a near total resection or a subtotal resection[68].

1.1.5.2 Chemotherapy

Chemotherapy is the most commonly used therapeutic approach to treat rhabdoid tumours and often occurs post-surgery. Patients with MRT receive chemotherapy intramuscularly or intravenously. Usually, chemotherapeutic agents are utilised in combination, however, no standard approach has been established and there is no clear evidence of the effect of different combinations on the survival outcome. The most frequently used chemotherapeutic agents for MRTs are cisplatin, carboplatin, vincristine, actinomycin D, doxorubicin, and etoposide (Figure 1.3)[48]. Cisplatin causes DNA damage to cells by binding to the N7 reactive centre on purine residues[49]. Carboplatin also targets DNA by inhibiting replication and transcription[50]. Similarly, actinomycin D binds to the transcription initiation complex, preventing DNA transcription[51]. Vincristine inhibits microtubule formation in the mitotic spindle, leading to cell cycle arrest[52]. Lastly, doxorubicin and etoposide act by targeting the enzyme topoisomerase 2, preventing cell growth and division.

In the past, AT/RT treatment was based on established treatment protocols for other infant brain tumours involving surgery, radiation, and conventional chemotherapy as well as high-dose chemotherapy with stem cell rescue. More recently, efforts have been made to adapt protocols specifically to AT/RTs by treating in accordance with rhabdomyosarcoma tumours, which has resulted in an improved prognosis. The Children's Oncology Group (COG) treatment strategy involves two cycles of induction chemotherapy including

cisplatin, cyclophosphamide, etoposide, vincristine, and methotrexate. This is followed by three cycles of consolidation chemotherapy (thiotepa and carboplatin) with stem cell rescue and then radiation therapy. This approach has shown a marked improvement in survival outcome [54]. Reddy *et al*. published the results of a clinical trial [www.clinicaltrials.gov identifier NCT00653068]) for this treatment plan and found an overall survival rate of 43% and an event-free survival of 37%, at 4 years in a group of 65 patients. This was a significant improvement from the survival outcomes of a historical cohort. However, this study also reported significant issues with toxicity as well as 4 treatment-related deaths[69].

The Dana-Farber Consortium AT/RT completed a clinical trial (Clinicaltrials.gov identifier: NCT00084838) which treated 20 patients with surgery, chemotherapy and radiation therapy, following a modified IRS-III regiment, which was based on a rhabdomyosarcoma study[70]. This consisted of 5 steps: pre-irradiation therapy, chemoradiation induction therapy, post-radiation induction therapy, maintenance therapy and continuation therapy. Multiple chemotherapeutic agents were used in the trial including cisplatin, doxorubicin, and etoposide. The overall 2-year survival was successful, with 12 out of 20 patients completing the trial. However, it should be noted that issues with toxicity posed significant challenges in this trial[12]. The "EU-RHAB" registry recommends a multimodal approach consisting of gross total resection, chemotherapy, intrathecal methotrexate and radiation therapy and allows for the use of high-dose chemotherapy with carboplatin and thiotepa[71, 72].

Unfortunately, developing a standard protocol for MRTK treatment has been less successful, with no improvement in the prognosis, which remains at 20-25%. Traditionally, MRTKs have been treated alongside Wilms' tumours. The NWTS in the US conducted trials with regimens used for Wilms' tumours that included the use of vincristine, doxorubicin and dactinomycin. This resulted in poor outcomes[4, 8] and subsequently a new approach was tested, consisting of carboplatin and etoposide or cyclophosphamide (Clinicaltrials.gov identifier: NCT00002611). The study was unsuccessful and closed after it was shown this regimen did not result in any improvement[12]. The AREN0321 regimen UH-1 alternated vincristine-doxorubicin-cyclophosphamide with cyclophosphamide-carboplatin-etoposide (ClinicalTrials.gov

Identifier: NCT00335556). Unfortunately, there was no clear improvement in the patients' response.

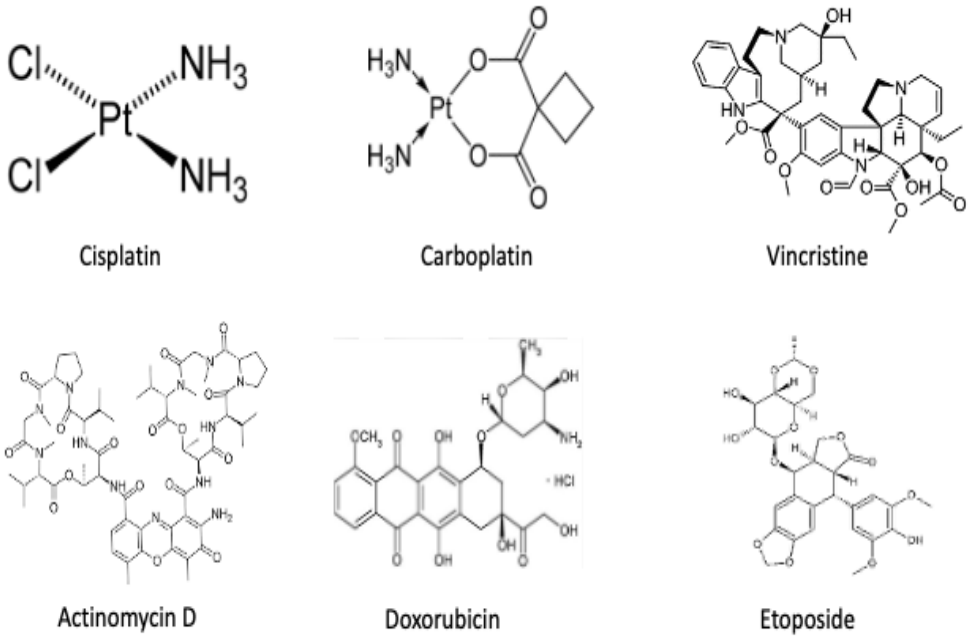

Figure 1.3 The chemical structures of chemotherapeutic drugs used in the treatment of MRT.

1.1.5.3 Radiation therapy

The use of radiation therapy as a treatment option for MRT is severely limited by the young age of the patients. For this reason, it is also difficult to evaluate the effect of radiotherapy on survival outcome, as it is more frequently utilised for older patients who are also able to tolerate higher doses of radiation. As mentioned above, radiation therapy is frequently used where possible, to treat MRT and is a recommended treatment option when used in combination with surgery and chemotherapy.

Multiple individual case studies report long term survival after treatment with radiotherapy. Additional work by NWTS, analysed 142 patients with MRTKs, 100 of which had been treated with radiotherapy. The survival at 4 years was 28.5% in patients who had received radiotherapy and 12.0% in patients who had not. However, the group who had received radiotherapy as part of their treatment were older. When the age of the patients and stage of the tumours were taken into account, the effect of radiotherapy was

significantly diminished[4]. Nevertheless, there are still reports suggesting radiation may still prove to be favourable in certain cases when the dose is adjusted[73].

1.1.5.4 Targeted therapies

As highlighted above, the survival outcome for MRT remains very poor despite efforts to optimise a treatment strategy. Therefore, there is an unmet urgent medical need for novel therapeutic strategies and current research suggests the potential of targeted therapies. There is an interest in focusing on the role of SMARCB1 in rhabdoid tumour biology. As described above, the role of SMARCB1 as part of the SWI/SNF complex defines a potential role in epigenetic regulation through chromatin remodelling, cell cycle progression and cell signalling cross-talk[52]. Further to this, Aurora A kinases and cyclins have also shown promise as potential targets for targeted therapies in MRT.

Targeting epigenetics has become a promising anti-cancer strategy in recent years. Epigenetic regulation of gene expression relies on modification through DNA methylation and histone modification[74]. As mentioned earlier, MRTs have a stable genome except for the recurring *SMARCB1* mutation. Despite this, variation is observed at a molecular level. Johann *et al*. and Chun *et al*. have shown this in AT/RTs and extra-cranial MRTs, respectively, through a combination of whole-genome DNA, RNA, microRNA, chromatin immunoprecipitation sequencing and DNA methylation assays. Johann *et al*. analysed a cohort of 192 genetically similar AT/RTs and characterised 3 sub-types of tumours by their epigenetic differences[75]. Molecular heterogeneity was also reported by Torchia *et al*., who identified 3 different subgroups within a cohort of AT/RTs that, in addition, differed in their survival outcomes[76]. Similarly, Chun *et al*. analysed the heterogeneity in extra-cranial MRTs and identified two methylation sub-groups which correlated with the age of the patient[77].

Epigenetic regulation is mediated by structural adaptations of the relevant chromatin[78]. The two complexes, trithorax (TrxG) family and the polycomb (PcG) complex, are directly involved in the epigenetic regulatory system by playing a role in the maintenance active or repressed states of gene expression[79]. Collectively, they regulate a wide range of cellular processes, in particular cell division. Both proteins are involved in the alteration of histone tails and indeed these complexes have been implicated in MRT tumours. Kuwahara *et al*. have shown that SMARCB1 expression regulates the expression of target genes through the recruitment of RNA polymerase II and K3K4 and H3K36 modifications[80]. In addition

to this, the trithorax family member MLL1, which is a histone methyltransferase specific for H3K4, interacts with SMARCB1 and potentially has a role chemoresistance in MRT[12]. The polycomb complex represses transcription through the mediation of H3K27. CBX6 and EZH2 are two members of the polycomb complex that are upregulated in rhabdoid tumours and inhibitors of these components have become potential therapeutic targets. Indeed, Johann *et al*, demonstrated that all 192 of rhabdoid tumour patients in their study expressed high levels of polycomb complex components[75]. Moreover, EZH2 is capable of interacting with the oncogene ZNF217, which is also upregulated in rhabdoid tumours. This interaction results in the methylation of H3K27 and the demethylation of K3K4me3 results in gene transcription suppression[81]. Therefore, EZH2 inhibitors have become a subject of interest in rhabdoid tumour therapeutic research. The first EZH2 inhibitor employed in *in vitro* studies is called DZNep (3-deazaneplanocin A), which showed promise as a potential anti-cancer agent in MRT. However, due to its short half-life, lack of specificity and associated toxicities, its clinical potential was limited. Instead, another EZH2 inhibitor, Tazemetostat was also demonstrated to show therapeutic promise *in vitro* and *in vivo* and is currently in clinical trials phase I and II (NCT02601950, NCT02601937)[82].

Histone deacetylase (HDAC) inhibitors have also been considered as potential targeted therapeutics for MRTs and have shown promising results in pre-clinical studies[12]. HDACs are responsible for the removal of acetyl groups from histone proteins on DNA allowing for the compaction of chromatin. In cancer biology, HDAC overexpression has been linked to the silencing of tumour suppressor genes. Overexpression of HDACs has been observed in various MRT cell lines and tumour samples. HDAC inhibitors have shown promising anti-tumour effects both alone and in combination with other treatments in rhabdoid tumours in pre-clinical studies. For example, Vorinostat, a HDAC inhibitor, was used in clinical trials alone and in combination with bortezomib or temozolomide which included MRT patients and was found to be well tolerated (NCT01076530, NCT00217412)[82].

DNA methyltransferase (DNMT) inhibitors have also been considered for the treatment of rhabdoid tumours. The oncogenic activity associated with DNMT is thought to be due to their involvement in repressing expression of genes involved in cell cycle mediation and apoptosis, amongst other cellular processes. Two DNMT inhibitors, 5-azacytidine and decitabine, were shown to deter tumour growth by promoting apoptosis, cellular

differentiation and inhibiting cell cycle progression. Phase I clinical trials showed that decitabine exhibited promising results in combination with doxorubicin and cyclophosphamide in other paediatric solid tumours[83, 84].

SMARCB1-deficiency has been associated with dysregulation of the cell cycle making it a potential therapeutic target. The cell cycle consists of two major phases: interphase and M phase. Interphase prepares cells for mitosis and is categorised into 3 stages: G1; a gap phase where the cell assesses whether it is in optimal conditions for cell division, S phase; where DNA synthesis occurs and lastly, the G2/M phase; another gap phase where the cell determines if enough DNA synthesis has occurred to move into the mitotic stage. Mitosis is divided into 4 stages known as prophase, metaphase, anaphase and telophase. Lastly, the cell undergoes cytokinesis which is the physical division where the cytoplasm separates into two daughter cells (Figure 1.4). The cell can also enter a quiescent state known as G0, which can be temporary or permanent. Uncontrolled cell division is a hallmark of cancer, therefore this process is tightly regulated by cyclins in normal cells[85]. Cyclins activate cyclin-dependent kinases (CDK) which regulate the cell cycle through phosphorylation. Numerous reports have shown that cyclin D1 is upregulated in malignant rhabdoid tumours. Cyclin D1, which forms a complex with CDK4/6, regulates the transition from G1 to S phase alongside the cyclin E-CDK2 complex. These phosphorylate the Rb protein which leads to the activation of the E2F transcription factor causing the progression from G1 to the S phase. Interestingly, loss of SMARCB1 correlates with an augmented transition from G1 to S phase. A study in mice by Tsikitis *et al,* showed that cyclin D1 repression significantly reduced rhabdoid tumour formation.[86] Kuwahara *et al.* showed that re-expression of SMARCB1 in MRT cells causes cell cycle arrest through the involvement of p16, p21 and cyclin D1[87]. In addition to these studies, a number of other studies have suggested a potential for cyclin D1 inhibitors for MRT treatment[86, 88, 89]. A phase I clinical trial recently demonstrated that ribociclib, a CDK4/6 inhibitor, was shown to be safe in paediatric rhabdoid tumour patients and in 2 out of 15 patients resulted in stable disease (NCT017747876). Other clinical trials, testing inhibitors that target the CDK4/6/cyclin D1/Rb pathway, are currently underway[82].

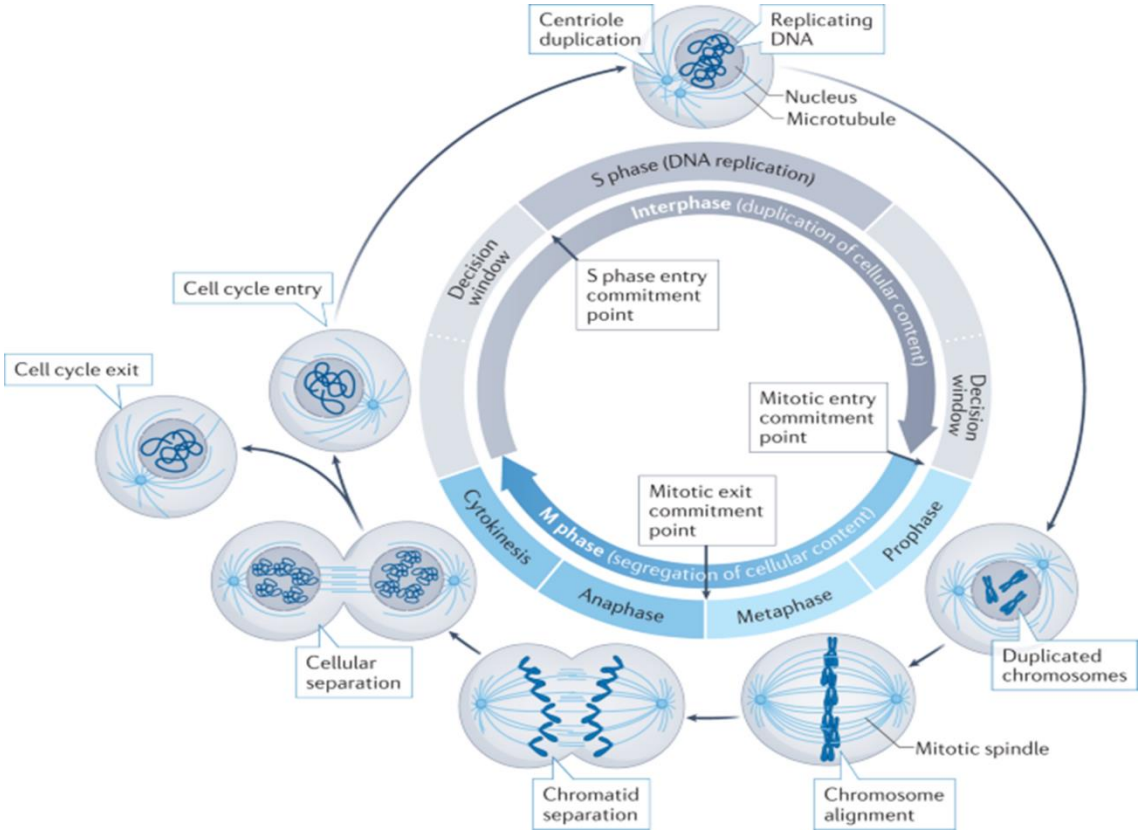

Figure 1.4 Cell division cycle.

The cell cycle is a tightly regulated series of steps that occur when the cell grows and divides. The cell spends most of its time in the interphase stage. During this phase, the cell grows and replicates its chromosomes in preparation of cell division. This stage is composed of the G1 phase (cell grows), the S phase (DNA synthesis) and G2 (cell growth). After interphase, the cell goes through mitosis which consists of prophase (chromosome duplication), metaphase (chromosome alignment), anaphase (chromatid separation) and cytokinesis (cell undergoes separation into daughter cells). Image taken from Matthews *et al*[85].

In addition to cyclin D1, Aurora A kinase is another potential target protein that has shown promising results for MRT treatment. As previously mentioned, aurora A kinase is a member of a family of mitotic serine/threonine kinases that is involved in multiple steps in mitotic progression. It has been shown to be upregulated in a number of tumours including MRT and has been associated with poor prognosis[38]. The Aurora A kinase inhibitor, MLK 8237 has shown promising activity *in vitro, in vivo* and in clinical settings[90-92].

Inhibitors of the sonic hedgehog/GLI pathway have also been considered as an area of focus due to the role of this pathway in cell proliferation and differentiation as well as tumour origin and progression. Arsenic trioxide (ATO) binds to GL2, reducing its stability and downregulating the expression of various target genes of that pathway, which in turn induces apoptosis and reduces tumour growth. This has been shown to occur in rhabdoid cells *in vitro* and *in vivo.* Moreover, ATO is being tested in clinical trials, phases I-III, in children with tumours, including rhabdoid tumours (NCT00024258, NCT00003630, NCT00095771, NCT00866918)[82].

Although the WNT/β-catenin signalling pathway has been linked to rhabdoid tumours, targeting it has proved difficult due to its critical physiological roles. However, a Wnt ligand called OMP-54F28 has shown potential in clinical trials alone and in combination with other therapies against solid tumours[82].

Other areas of potential interest in rhabdoid tumour treatment include immunotherapy, Mcl-1 inhibitors, PLK1 inhibitors and targeting inhibitors of apoptosis proteins (IAPs)[93, 94].

1.2 Chemoresistance

Chemoresistance is defined as the lack of response of cancer cells to the action of chemotherapeutics. Currently, drug resistance is one of the major challenges in the field of oncology. Despite many advancements in the study of targeted cancer therapies, chemotherapy is, to date, the most commonly used strategy to treat cancer. However, 90% of mortality in cancer patients is attributed to drug resistance[95]. The phenomenon of drug resistance mirrors that of resistance in infectious diseases and antibiotic resistance[96]. In cancer, treatment can lead to the death of drug-sensitive cells. However, resistant cells will survive and multiply thereby giving the tumour an overall resistant phenotype. This can lead to disease relapse through failure of tumour inhibition and anti-apoptotic characteristics. Resistance can occur in relation to one specific drug or multiple drugs that differ in their mechanism of action, known as multidrug resistance (MDR)[97].

Chemoresistance can be classified as primary resistance or acquired resistance (Figure 1.5)[98]. Primary resistance refers to resistance that exists intrinsically prior to treatment exposure. This could exist due to genetic factors. Moreover, tumours are often characterised by their heterogeneity meaning that they can consist of drug-sensitive and

drug-resistant cells and may also contain population of cells that do not undergo apoptosis such as sub-clonal mutant cells and cancer stem cells (CSCs)[99]. This means the patient is often observed to appear to initially response to treatment when all the sensitive cells undergo apoptosis but then will stop responding when the treatment cannot by-pass these naturally resistant tumour cells[99].

In contrast, acquired resistance refers to resistance that was developed through the exposure of the cancer cell to the treatment. Clinically, this can be observed as the gradual development of resistance over time with exposure to drug treatment. This change in sensitivity can occur due to various factors, which will be further discussed below. Examples of such factors include genetic mutations in response to treatment and a change in tumour microenvironment (TME) which occurs due to the release of miRNA and exosomes from cancer cells in response to drug exposure[100]. It is difficult to quantify occurrence of intrinsic and acquired resistance however, Verheul and Pinedo estimate that 50% of all cancer patients already present intrinsic resistance whereas the majority of the remaining patients will eventually develop acquired resistance[98]. Nonetheless, it is difficult to confirm these figures as there is no standardised diagnostic test to determine types of resistance in cancer patients.

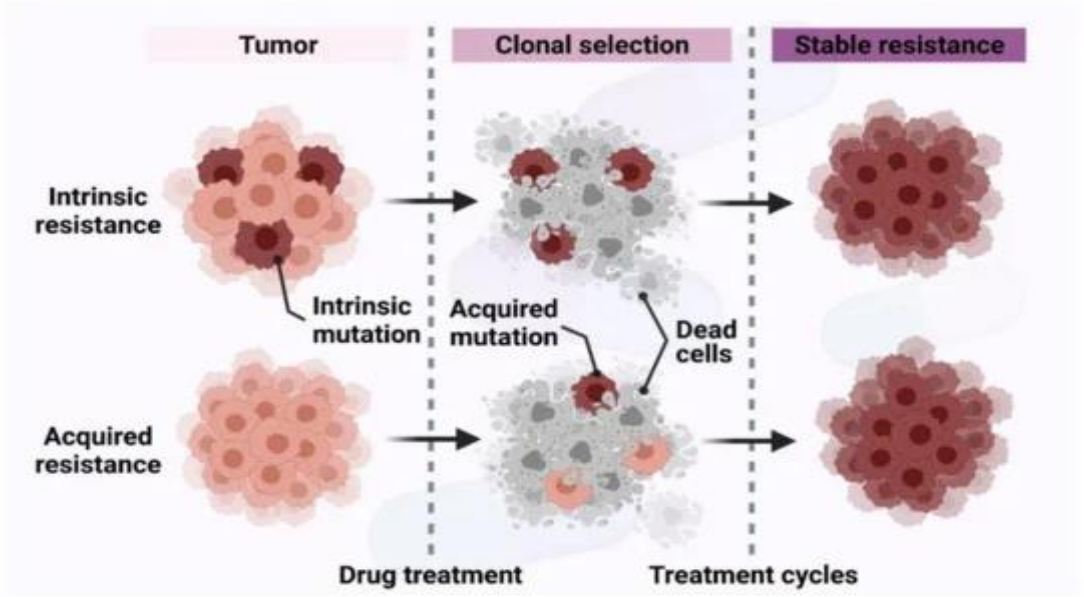

Figure 1.5 Intrinsic and acquired resistance to drug treatment in cancer cells.

Intrinsic resistance is present in cancer cells prior to drug treatment. This could be due to inherited genetic mutations, heterogenous cell population, pharmacological factors or aberrant activation of cell signalling pathways. In contrast, acquired resistance occurs after treatment. Various mechanisms behind this phenomenon have been described including mutations of drug targets, epigenetic alterations, and alterations to the tumour microenvironment. Image taken from Ramos *et al*[101].

Chemotherapeutics can be classified into different categories depending on their mechanism of action and origin. Chemotherapeutic drugs are either synthetically developed or extracted from plants and are grouped into alkylating agents, antimetabolites, and topoisomerase inhibitors, amongst other groups.

Alkylating agents have been used to treat cancer for over six decades. These agents target the cell cycle at all phases; crosslinking N-7 guanine residues, inducing DNA strand breakage leading to mispairing of bases, inhibiting cell division, and causing cell death. These agents include hydrazines such as temozolomide, oxazaphosphorines, such as cyclophosphamide and platinum-based agents such as cisplatin and carboplatin[102]. Cisplatin is one of the most effective anti-cancer treatments available and it is utilised in a number of cancers including testicular, head and neck, breast, oesophogeal, cervical, lung, bladder cancer and brain tumours. Cisplatin is a small molecule consisting of one platinum atom bonded to two chlorides and two amides. In the cytosol, cisplatin undergoes a process termed “aquation” where the chloride molecules are displaced by water molecules. This process takes place in low chloride concentrations, as is found in the intracellular environment. The process of aquation converts cisplatin into a highly reactive molecule that can interact with several biomolecules such as DNA bases, in particular the N7 site of purine bases, thereby forming DNA adducts and inducing DNA damage[103].

Antimetabolites are drugs that interfere with enzymes/metabolites required in DNA or RNA synthesis and result in interference with critical biosynthetic pathways. These are categorised into groups including purine analogues, purine antagonists, antifolates, ribonucleotide reductase inhibitors and pyrimidine antagonists such as 5-fluorouracil (5-FU), which is one of the oldest drugs that is still prescribed today[95].

Topoisomerase inhibitors block the ligation stage in the cell cycle, causing DNA strand breakage and inducing cell death. They are broadly categorised into two sub-types: type I

topoisomerases (irinotecan and topotecan) and type II topoisomerases (doxorubicin and etoposide)[95]. Another group of chemotherapeutic drugs are mitotic spindle inhibitors such as taxanes (e.g docetaxel and paclitaxel) and vinca alkaloids (e.g vincristine and vinblastine), which alter spindle microtubule formation. The other chemotherapeutic agents include enzymes, antibiotics such as actinomycin D, tyrosine kinase inhibitors and proteasome inhibitors such as bortezomib. These all differ in their mechanisms of action[95].

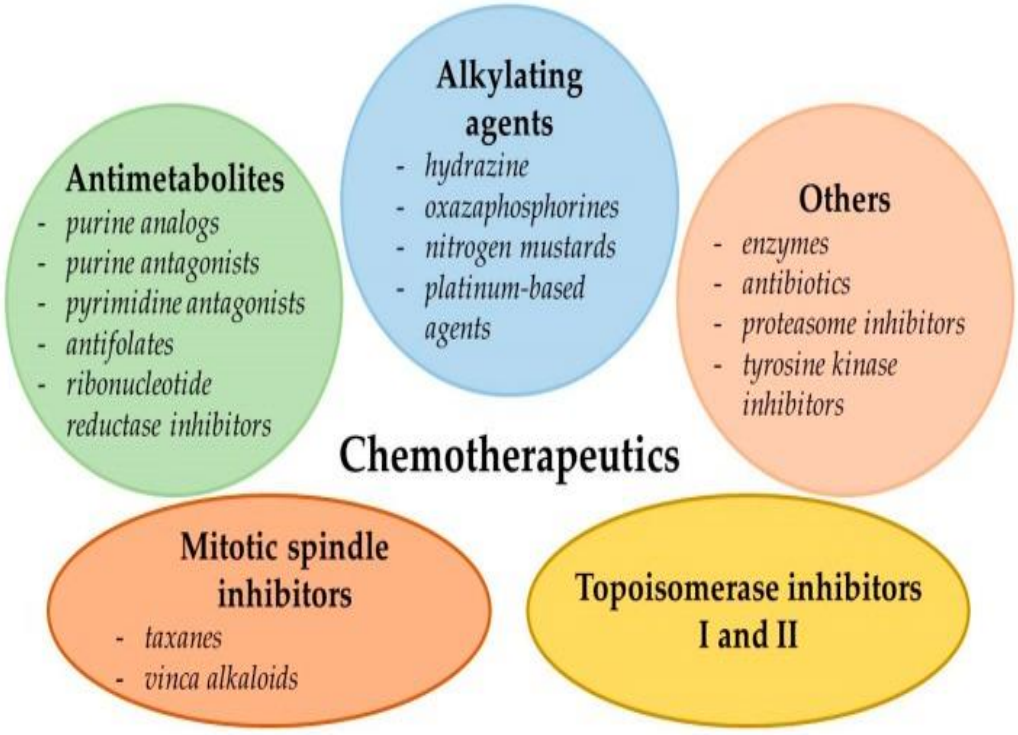

Figure 1.6 Chemotherapeutic drugs are classified in accordance with their mechanism of action.

The most commonly used chemotherapeutic drugs are dependent on their origin and mechanism of action. Topoisomerase inhibitors (I and II), such as etoposide, act by preventing the activity of topoisomerases involved in DNA replication and cause breakage of DNA strands. Mitotic spindle inhibitors, such as docetaxel inhibit nuclear division and interfere with the formation of the spindle microtubules. Antimetabolites such as 5-fluorouracil are divided into different groups based on what biosynthetic pathways they target. Alkylating agents include oxazsaphosphorines, hydrazines and platinum-based agents such as cisplatin and carboplatin. Lastly, other chemotherapeutic agents include antibiotics and proteosome inhibitors and do not share a homogenous mechanism of action. Image taken from Bukowski *et al*[95].

Resistance has been reported in almost all drugs used in the treatment of all cancers associated with poor prognosis (Figure 1.7). For example, in breast cancer, poor survival outcome and relapse has been linked with resistance to doxorubicin, paclitaxel, 5-fluorourocil, cyclophosphamide and carboplatin. In gastric cancer patients, disease recurrence has been associated with 5-fluorouracil, cisplatin, docetaxel and oxaliplatin[101]. Therefore, there is an urgent need to identify strategies that combat chemoresistance. The mechanisms underlying chemoresistance have been widely investigated and will be further discussed.

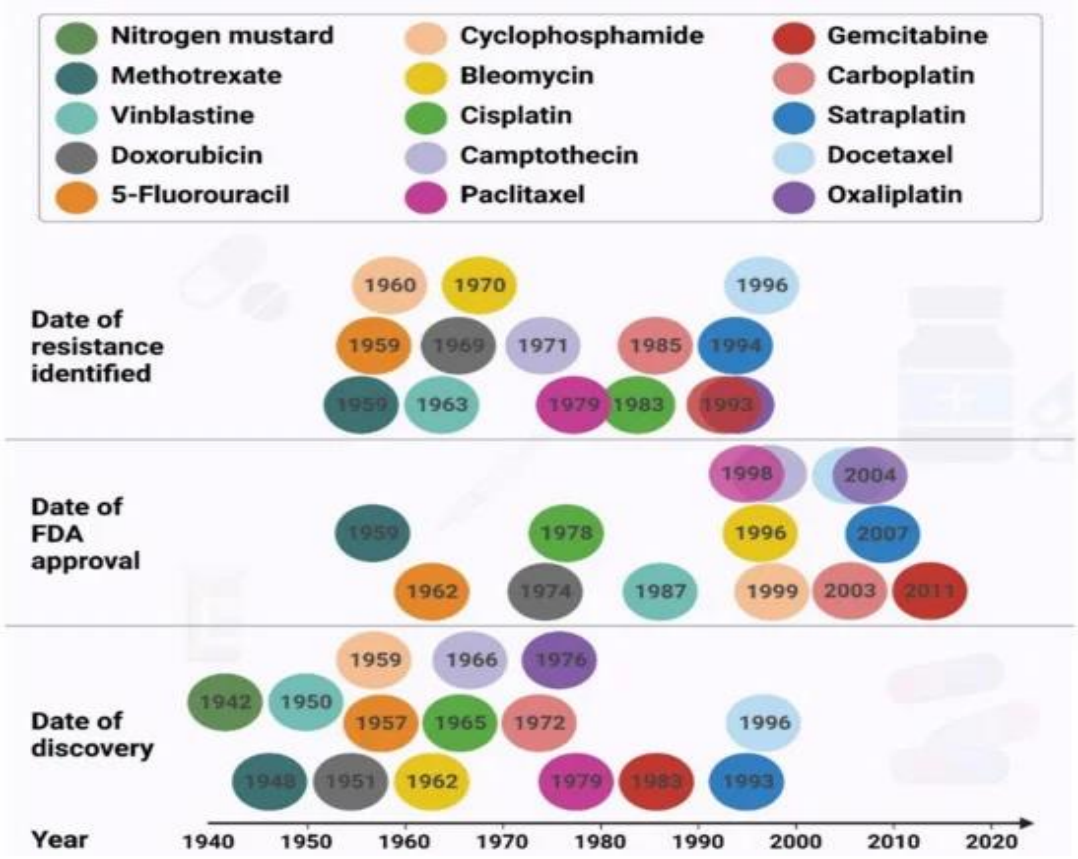

Figure 1.7 Comparison of the timelines of the discovery, FDA approval and identification of resistance in commonly used chemotherapeutic agents.

Drug resistance has been detected in all commonly used chemotherapeutic agents used to treat aggressive cancers. Image taken from Ramos *et al*[101].

1.2.1 Mechanisms of drug resistance

As mentioned above, drug resistance is one of the most significant causes for treatment failure, relapse and mortality in patients. This phenomenon is attributed to many different factors and multiple mechanism of drug resistance have been identified. Given that resistance to treatment continues to be a major challenge in oncology, there is extensive study ongoing into deciphering the mechanisms underlying drug resistance in cancer and developing strategies to overcome this issue. Some of these mechanisms that have been identified include drug efflux, DNA damage repair, EMT, changes to TME, miRNAs, alterations to signalling pathways and drug inactivation.

1.2.1.1.DNA damage repair

Chemotherapeutic agents induce cytotoxicity by causing DNA damage such as, single-strand breaks (SSBs), double-strand breaks (DSBs), alterations of bases and interstrand or intrastrand cross-links. This leads to genomic instability and mutation, which is one of the hallmarks of cancer according to Hanahan and Weinberg[104]. Upon entering the cell, cisplatin undergoes aquation (replacement of Cl^- with H_2O) to yield the single aquated species and di-aquated species. Cisplatin can then bind covalently to the N7 position of purines resulting in - intra-strand crosslinks, as well as a lower percentage of inter-strand crosslinks (ICL)[103]. In particular, cisplatin binds to the nucleophilic N7-sites on purine bases, in particular, guanine. This formation of cisplatin-DNA adducts interferes with DNA replication and transcription[103].

In order to cope with this, the cells have evolved a DNA damage repair (DDR) system. These repair pathways include nuclear and mitochondrial DNA repair pathways. Double-strand breaks are repaired by homologous recombination (HR) and non-homologous end-joining (NHEJ). The nucleotide excision repair (NER) pathway is the primary repair pathway involved in restoring damage caused by cisplatin to the DNA such as 1,2-intrastrand and 1,3-instrastrand adducts. This pathway is comprised of two sub-pathways known as the global genome repair (GGR), which identifies and repairs damage along the genome and the transcription-coupled repair (TCR), which acts on damage located on the actively transcribing strands of genes. These genes are scanned by RNA polymerases, which can detect DNA damage. The NER pathway removes recognised lesions through the cleavage of the damaged strand. A DNA polymerase then replaces the gap by using the remaining strand as a template. Another DNA damage repair pathway is the mismatch

repair pathway (MMR) which repairs single-strand DNA errors that occur during the replication process. This pathway also acts by recognition of the lesion, excision, synthesis of a new strand and ligation. The MMR pathway can repair DNA damage caused by cisplatin but ultimately fails to repair the error. In fact, it replaces the base opposite to the lesion, failing to target the adduct itself, it then restarts the process again until eventually the stress results in double-strand breakage and the activation of DNA damage signalling such as p53, resulting in apoptosis. It is also believed to inhibit the NER pathway proteins from repairing cisplatin-formed adducts suggesting that deficiencies in MMR could contribute to cisplatin resistance, in contrast to the NER pathway[103].

Oliver *et al*, observed that cisplatin resistance was acquired over time in a lung cancer mouse model. The resistant tumour cells expressed a higher level of DNA damage repair genes. Inhibition of the nucleotide excision repair (NER) pathway re-sensitised cells to cancer[104]. Inhibition of DNA damage repair by the CDK4/6 inhibitor Palbociclib in combination with radiation promoted tumour cell apoptosis in ATRT and glioblastoma[105].

In addition to generating DNA adducts through intrastrand cross-linking, cisplatin has also been shown to generate interstrand crosslinking (ICL) lesions, which are highly cytotoxic due to the binding of two DNA strands together which prevents their separation and induces double strand breakage and stalled replication forks. NER proteins such as XPD, XPF, XPG and ERCC1 have been shown to play a role in ICL repair. DNA double strand breaks are repaired through HR and NHEJ as well as ICL repair. ICL repair is highly intricate and includes numerous DNA damage repair pathways such as the Fanconi anemia (FA) proteins. The recruitment of these proteins (FANCM/FAAP24/MHF) to the ICL sites, initiate damage sensing and repair. These proteins have been implicated in cisplatin resistance (Figure 1.6)[103,104].

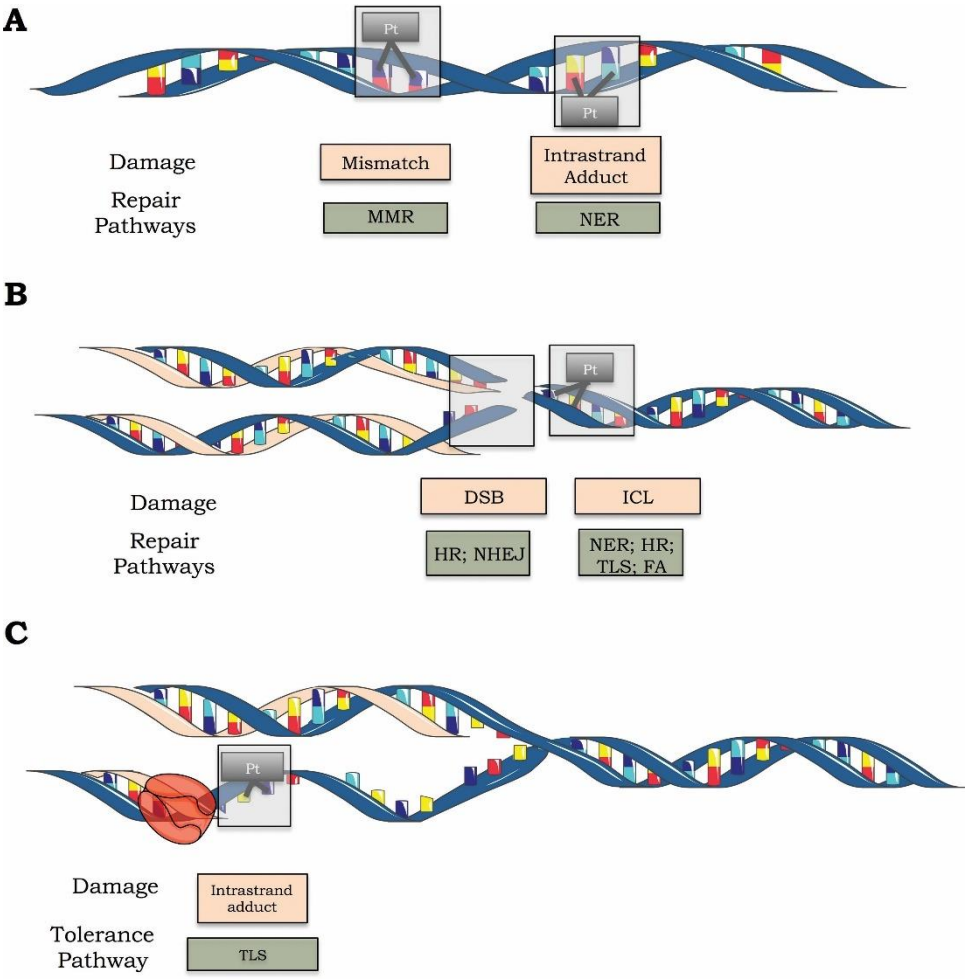

Figure 1.8 DNA Damage Repair pathways

Image taken from Reily *et al*[559].

1.2.1.2 Oncogenes and alteration to tumour suppressor pathways

Dysregulation of tumour suppressor signalling pathways is common in cancer cells. Growth factor receptors such as epidermal growth factor receptor (EGFR) overexpression are linked to chemoresistance and poor survival outcome. EGFR can trigger the activation of the Jak/Stat pathway, the PI3K/Akt/mTOR and SOS/Grb2/Ras pathways which are involved in cell proliferation, survival and differentiation. The alterations in these tumour suppressor pathways can occur due to mutations in oncogenes or key tumour suppressor genes that are directly involved in drug resistance. These mutations can be either intrinsic or acquired. In lung cancer cells, EGFR overexpression triggers NF-κB and PI3K/Akt signalling leading to chemoresistance[106]. *TP53* mutations also alter oncogenic signalling pathways. *TP53* is the most widely studied tumour suppressor gene and is referred to as

the “guardian of the genome” due to its critical function in protecting from malignancies. In non-small cell lung cancer, loss of p53 upregulates the transcription factor Nrf2, which is involved regulating response to oxidative damage in the cells. Nrf2 expression is further enhanced by the activation of the NF-κB signalling pathway. This has been shown to cause resistance to cisplatin. The mutant p53 also affects the ERK signalling pathway and therefore the transcription of Egr-1 (early growth response-1) which promotes EGFR ligand release and subsequently resistance to EGFR-inhibitor based treatment such as Cetuximab[107]. Lee *et al*., observed a feedback loop resulting in STAT3 activation in oncogene-addicted cells which correlated with limited drug response and cell survival. Inhibition of kinases such as MEK (MAP kinase kinase) triggered the activation of this feedback loop[108]. STAT3 activation has been observed in a number of cancers such as multiple myeloma, breast cancer, head and neck cancer and prostate cancer. Dysregulated STAT3 signalling is associated with angiogenesis, evasion of apoptosis and cell progression[108]. In breast cancer, MAPK signalling through the ERK pathway results in activated Ras which activates the transcription of genes involved in cell proliferation, apoptosis and survival. Targeting the MAPK signalling pathway has been shown to result in reduction of breast cancer cell proliferation and metastasis[109].

In particular, cell death signalling pathways are also altered in cancer cells through an imbalance of anti- and pro-apoptotic proteins[110]. This will be discussed in further detail below.

1.2.1.3 Drug inactivation

The efficiency of anti-cancer drugs can be highly context dependent. The interaction of drugs with certain proteins can result in molecular alterations of the drug affecting its mechanism of action. In fact, many drug treatments require metabolic activation. An example of this is cytarabine (AraC), a standard treatment used for acute myeloid leukaemia (AML). On its own, this drug is inactive however, upon phosphorylation it becomes cytotoxic. Resistance to this drug has been linked to downregulation of the expression of deoxycytidine kinase, which is the enzyme involved in phosphorylating AraC[97].

The antioxidant glutathione (GSH) is an important antioxidant that is known to also play a major role in drug inactivation. It is known to conjugate to platinum drugs such as cisplatin

and oxaliplatin facilitating substrate transport of these drugs by ABC transporters resulting in enhanced drug efflux[111]. Moreover, the GST (glutathione S-transferase) family of enzymes are also implicated in drug resistance due to their role in the detoxification of anti-cancer drugs reducing their effect on cell death[97]. Other mechanisms of cisplatin inactivation include it binding to metallothionein (MT) which can oxidise and inactivate it[111, 112]. Another example is the inactivation of the topoisomerase inhibitor I, irinotecan, used to treat colon cancer, by the enzyme CYP450 which results in resistance[111].

1.2.1.4 Drug target alteration

Chemoresistance is also acquired through molecular alterations to the drug target such as modifying expression levels or downregulating its activity. For example, there are reports in literature of cancer cell lines developing resistance to topoisomerase type II inhibitors through modifications to the topoisomerase II gene. Type II topoisomerases are important enzymes that generate double-strand DNA breaks to prevent entanglements from supercoiling or undercoiling. Drugs that target topoisomerases affect the complex they form with DNA leading to DNA damage. Resistance to these drugs can be caused by mutations to the topoisomerase gene[113]. Inhibitors of kinases are also frequently used as an anticancer drug for cancers with constitutively active kinases, however, these targets are also prone to undergo genetic alterations that confer resistance to these inhibitors after long term use. In ovarian cancer, resistance to paclitaxel and other taxanes is acquired through mutations to beta tubulin.

Alteration to enzyme expression levels at drug target sites can also confer resistance to anticancer drugs. An example of this is the enzyme thymidylate synthase (TS). TS catalyses the conversion of deoxyuridine monophosphate (dUMP) to deoxythymidine monosphosphate (dTMP). Inhibition of TS leads to excess levels of dUMP and can cause DNA damage. The anti-cancer drug 5-FU (fluorouracil) is a TS inhibitor that is activated when it is converted to FdUMP. Resistance to 5-FU is associated with dysregulation of thymidylate synthase (TS)[113, 114].

1.2.1.5 Alterations of membrane transport

Cell surface receptors and transporters can undergo alterations to affect drug efflux, which diminishes drug accumulation. This is one of the most widely studied forms of chemoresistance. One of the major contributors to this phenomenon is the family of ABC transporter proteins, which act by pumping substrates such as lipids, amino acids and ions,

across the membrane using ATP (adenosine triphosphate) hydrolysis to power these translocations. Enhanced ABC transporter expression has been associated with reduced drug accumulation and efficacy, suggesting they have an important role in mediating chemoresistance[113]. Some of the more widely studied transporters include the multidrug resistance protein 1 (MDR1) and breast cancer resistance protein (BCRP).

MDR1 is also commonly referred to as P-glycoprotein (Pgp) or ATP-binding cassette sub-family B member 1 (ABCB1). This protein is expressed in several tissues such as intestine, colon, placenta and the liver and its primary function is to pump out xenobiotic and lipid molecules[115]. MDR1 is overexpressed in a number of cancers to increase efflux of anticancer drugs such as doxorubicin and paclitaxel. Increased expression of MDR1 has been found in cancers before and after chemotherapeutic treatment indicating resistance caused by MDR1 can be either intrinsic or acquired[116, 117].

Another well characterised ABC transporter is BCRP. This protein exists in healthy tissue to regulate levels of lipids and xenobiotics in the gut, placenta and blood-brain barrier amongst other tissues. It also helps maintain heme and folate homeostasis in normal cells. In cancer cells, it helps cope with hypoxia, evades anti-cancer effects of drug treatment and is a known stem cell marker promoting self-renewal and invasiveness. Overexpression of this protein is found in a number of cancers and has mostly been studied in acute myeloid leukaemia (AML)[118, 119].

1.2.1.6 miRNAs

MicroRNAs or miRNAs are small non-protein encoding RNA molecules consisting of approximately 19-25 nucleotides. miRNAs are involved in the post-transcriptional regulation of critical genes involved in oncogenic processes such as apoptosis, cell cycle regulation and cellular proliferation. A single miRNA can regulate multiple genes in a tissue-specific manner[120]. It is estimated that miRNAs regulate 30% of all human genes. Dysregulation of miRNA has been linked to cancer drug resistance. For example, in breast cancer, resistance to tamoxifen has been linked to a dysregulation in expression of miR-221/222, which functions as an oncogene by targeting the cell cycle inhibitor, p27kip1[121].

In hepatocellular carcinoma (HCC), resistance to cisplatin can be correlated to alteration in expression of miRNA-96, miRNA-182, miRNA-340, miRNA-130a and miRNA-199a-5p. Similarly, in lung cancer, resistance to cisplatin has been linked to overexpression of a number of miRNAs[120].

1.2.1.7 Tumour microenvironment (TME)

The tumour microenvironment or TME refers to the complex environment surrounding the tumour consisting of blood cells, immune cells, fibroblasts, signalling molecules and extracellular matrix (ECM). The tumour is constantly interacting with its environment to facilitate cancer progression and resistance to therapeutics. It is not only the heterogeneity of cancer cells that contribute to drug resistance but also the diversity of the TME which can vary in levels of stromal cells, acidity, oxygen levels and ECM protein.

The tumour microenvironment is comprised of different types of stromal cells including fibroblasts, endothelial cells, adipocytes, and stellate cells. Cancer-associated fibroblasts (CAMs) are believed to contribute to chemoresistance through the production of various cytokines and chemokines. For example, secretion of IL-6 and IL-8 facilitate the progression of cancer stem cells (CSCs)[122].

Compared to normal interstitial tissue, the TME is particularly acidic and hypoxic. This is due to an accumulation of metabolic acidic waste that stems from high metabolic activity and diminished perfusion that occurs in tumours[123]. The low extracellular pH can result in the entrapment of ions which forms a physical barrier against drug uptake[124, 125].

Lastly, ECM proteins form a barrier against which a drug must pass before targeting the tumour thereby protecting it and simultaneously allowing for metastasis[126].

1.2.1.8 Epithelial-mesenchymal transition (EMT)

Epithelial-mesenchymal transition (EMT) is the mechanism by which tumours become metastatic through the loss of polarity and adhesion in epithelial cells resulting in their conversion to mesenchymal stem cells that are highly invasive and migratory. EMT has been implicated in tumour progression, cancer cell invasion and drug resistance although this is dependent on the metastatic grade of the tumour[113]. Exactly how EMT impacts drug resistance has yet to be determined, however, it is thought this is in part achieved through its role in activating survival pathways such as Akt and ERK1/2[127]. Modulation of EMT occurs through several transcription factors which inhibit epithelial gene expression[128]. For

example, a study in pancreatic adenocarcinoma mouse models has shown that suppression of EMT transcription factors enhances sensitivity to the drug gemcitabine[129].

Studies also suggest that the emergence of cancer stem cells (CSCs) may occur in part via EMT. CSCs which exhibit EMT remain after cancer treatment leading to recurrence of the cancer. Micro RNAs have been shown to be key players in the regulation of EMT and CSC[130, 131].

1.2.1.9 Cancer stem cells (CSCs)

Cancer stem cells (CSCs) have been identified in solid and hematopoietic tumours and have been associated with relapse and drug resistance due to their ability to self-renew and differentiate into heterogenous lineages even after drug treatment has killed the vast majority of a tumour. CSCs are also able to induce cell cycle arrest which facilitates their ability to become drug resistant[132]. CSCs can be identified through the detection of cell surface markers of normal stem cells which include CD44, CD24, CD133 and THY1[132].

Temozolomide (TMZ) exposure expands the glioma stem cell pool *in vitro* and *in vivo*, replenishing the original tumour population and resulting in a more resistant and invasive phenotype[133]. Similarly, preleukaemic haematopoietic stem cells (HSCs) which undergo clonal expansion at the first stage of leukaemogenesis were found to survive chemotherapeutic treatment and regenerate in the bone marrow[132, 134].

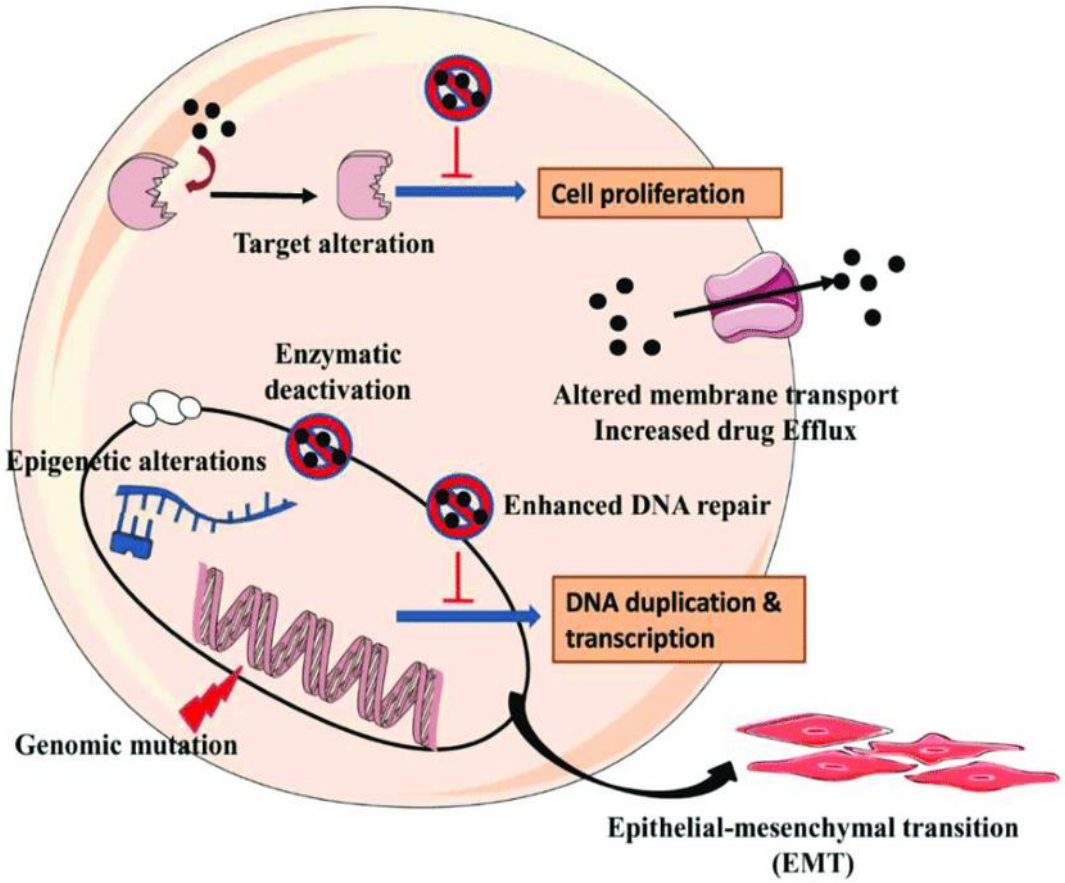

Figure 1.9 Mechanisms of chemoresistance in a cancer cell.

Chemoresistance is the leading reason for chemotherapeutic failure and is a complex phenomenon driven by various mechanisms. These include drug efflux, drug target alteration, DNA damage repair, drug inactivation, EMT and epigenetic alterations. Image taken from Palliyage *et al*[135].

1.2.2 Strategies to combat drug resistance

Advancing our understanding of the molecular mechanisms that cause chemoresistance will help in improving strategies to combat this challenge. One way to improve our response is through early detection of resistance phenotypes in cancers. Identifying biomarkers through positron emission topography (PET), tumour cell assays, metabolomics, proteomics, transcriptomics and cancer genomics are all being used to examine cell responses to drug treatment[101]. CRISPR screens and pharmacogenomic studies are currently being utilised to identify genetic mutations that can be associated with resistance[136]. Optimising drug delivery through nanomedicine could reduce cytotoxicity to

normal cells and prevent the development of acquired resistance. So far, this has proved to be effective in haematological cancers but not solid tumours. Furthermore, theoretical and animal models suggest that improving drug efficacy can be achieved by discontinuous dosing and modifying drug concentrations[101].

In addition, natural products have been demonstrated to exhibit promising results in overcoming chemoresistance through the reduction of drug efflux and the induction of non-apoptotic modes of cell death such as necroptosis, autophagy and oncosis. Vitamin C, curcumin and its derivatives have been shown to overcome cisplatin resistance in bladder cancer[137]. CSCs have also been examined as targets against chemoresistance. CSCs, a small sub-population within tumours with capabilities of self-renewal, tumour formation, metastasis, EMT and chemoresistance, is currently a promising target to overcome resistance. Targeting CSCs can be achieved through targeting the Wnt/β-catenin pathway, the sonic hedgehog signalling pathway and their surface biomarkers. Metformin, a first-line medication in the treatment of people with type 2 diabetes, has been shown to selectively target CSCs and overcome drug resistance in breast cancer[101, 138, 139].

The most common approach to overcome resistance is to use a combination of drugs. However, this could lead to MDR and therefore further study is needed to improve drug resistance in all cancers, including MRT[101]. Drug combinations which target different pathways is considered to be the preferred method to by-pass MDR. Therefore, recent studies have focused on identifying novel protein targets involved in cell death and proliferation. For example, overexpression of the anti-apoptotic protein Bcl-2 has been correlated with resistance to anti-cancer drug treatment. Bcl-2 is critical in apoptosis evasion, therefore Bcl-2 inhibitors have recently become promising therapeutic agents, particularly in CLL (chronic lymphocytic leukaemia) and AML (acute myeloid leukaemia)[140].

Another example is caspase-8 which exhibits pro-apoptotic activity by cleaving and activating the apoptotic executioner caspase-3. Although caspase-8 is often downregulated in cancers, in glioblastoma, its overexpression correlates with poor prognosis due to its role in inducing NF-kB-dependent expression of angiogenesis and pro-inflammatory cytokines which facilitate tumour progression[140].

Autophagy, the process by which a cell digests and recycles its own components, is also believed to be upregulated in tumours to help cancers cope with their rapid proliferation

and high metabolic activity. Much research has gone into determining the therapeutic potential of autophagy inhibitors. However, as will be discussed in further detail below, the role of autophagy in cancer is thought to be context-dependent as it can be either pro-survival as well as pro-death, meaning further work needs to be carried out to understand the complicated nature of autophagy activation in cancer[141].

Another potential context-dependent therapeutic target in cancer is the antioxidant system. Modulation of the intracellular antioxidant concentration has shown great promise in overcoming chemoresistance. Most conventional chemotherapeutic drugs induce ROS (reactive oxygen species), contributing to cell death in cells. The antioxidant glutathione (GSH) has been linked to chemoresistance due to its ability to help cells cope with stress caused by drug-induced ROS. Glutathione transferases (GSTs) are a family of phase II detoxification enzymes which are overexpressed in many cancers and are therefore promising targets to combat chemoresistance[140, 142].

1.2.3 Chemoresistance in MRT

Drug resistance is one of the main challenges in the treatment of MRT patients. Unfortunately, there are few studies in literature that aim to understand the molecular mechanisms underlying resistance in rhabdoid tumours.

As previously mentioned, MLL1 is a histone methyltransferase specific for H3K4, and it is transcriptionally activated via its interaction with SMARCB1, a protein that is mutated in almost all rhabdoid tumours. A study by Huo *et al*. has demonstrated that MLL1 is required for methylation of the MDR1 promoter. MDR1 codes for Pgp, a member of the ABC transporter family that can efflux anticancer agents causing resistance. MLL1 methylation of MDR1 results in the regulation of MDR[143].

EZH2, which has been shown to be overexpressed in rhabdoid tumours, has been linked to chemoresistance in ovarian cancers. Hu *et al*., demonstrated that EZH2 is overexpressed in cisplatin-resistant ovarian cell lines but not in cisplatin-sensitive cells. The report hypothesised that this was mediated through H3K27 methylation and regulation of cell proliferation[144]. EZH2 has also emerged as a potential therapeutic target in MRT. Alimova *et al.,* showed that targeting EZH2 through genetic and pharmacological means blocked AT/RT growth, tumour cell renewal and induced apoptosis. Moreover, EZH2 inhibition

sensitised AT/RT cells to radiation[145]. Knutson *et al.*, tested the effect of a novel small-molecule EZH2 inhibitor, EPZ-6438 (also known as tazemetostat), in MRT cells and xenograft mice. The results demonstrated dose-responsive tumour regression which corresponded with diminished trimethylation levels of lysine 27 on histone H3, indicating that EZH2 shows therapeutic promise for rhabdoid tumours[37]. Lastly, the EZH2 inhibitor tazemetostat has shown promise in a phase II clinical trial where it exhibited clinical activity, although the study concluded that further work is required to understand the results of the trial[146]. Furthermore, Ishi *et al*. targeted two H3K27 modifiers EZH2 and BRD4 in AT/RT cells and mice bearing human AT/RT xenografts. The study showed that treatment with EZH2 and BRD4 inhibitors blocked tumour cell proliferation and invasiveness in correlation with decreasing H3K27 trimethylation and H3K27 acetylation. Overall, treatment with a combination of the two inhibitors showed anti-cancer activity and therapeutic promise both *in vitro* and *in vivo*[147].

MicroRNAs which are downregulated in rhabdoid tumours have been linked to drug sensitivity in multiple cancers suggesting these may be of interest in MRTs[12]. The STAT3/Snail pathway has also been shown to have a role in oncogenic resistance. Snail is a transcription factor that can induce EMT and cancer progression. STAT3 knockdown downregulated Snail thereby repressing motility and invasion of cisplatin-resistant AT/RT cells and synergistically enhanced chemotherapeutic anti-cancer effects[148]. Moreover, an *in vitro* study examined resistance of a panel of MRT cell lines in response to six chemotherapeutic drugs: 5-FU, vincristine, carboplatin, doxorubicin, etoposide and paclitaxel. This study noted that doxorubicin was the only drug inducing cytotoxicity at clinically relevant concentrations (vincristine was shown to be cytostatic). The study reported that the p53 pathway was functional in all cell lines and was not considered to play a role in chemoresistance[149].

In a study conducted by Ouchi *et al*., anti-apoptotic Mcl-1 protein expression was found to be implicated in resistance in rhabdoid tumours. This study showed that the pro-apoptotic protein Noxa, that binds and inhibits Mcl-1, is not transcribed in rhabdoid tumours due to the absence of SMARCB1 and that the absence of Noxa-dependent Mcl-1 degradation led to evasion of apoptosis and chemoresistance in MRT. Pharmacological and genetic inhibition of Mcl-1 was shown to sensitise cells to doxorubicin in MRT cell lines. Moreover, ectopic expression of Noxa also increased drug sensitivity indicating that the balance between levels of expression of Noxa and Mcl-1 are potential therapeutic targets

to by-pass chemoresistance in MRT[94]. The role of other apoptotic signalling molecules in mediating chemoresistance in MRT will be discussed in section 1.3.4 below.

A recent study by Melcher *et al.* demonstrated that macrophage-tumour cell interactions contribute to tumour recurrence and therapy resistance. This study used single-cell RNA sequencing and immunofluorescent staining to determine the composition of the tumour microenvironment across AT/RT subgroups. This study determined that tumour associated macrophages (TAMs) are the most commonly found leukocytes in this tumour and that CD68+ cells had a negative prognostic significance for patient survival. Macrophage infiltration was correlated with poor survival outcome. In particular, AT/RT-MYC tumour cells were found to interact with macrophages compared to other subgroups. Moreover, these cells were implicated in chemoresistance in the murine xenograft models[150].

There have been a limited number of studies which aim to elucidate the involvement of CSCs in MRT. In order to distinguish cancer stem cells from normal stem cells, a variety of markers are used such as cell-surface protein or transcription factors. One of the most widely utilised cell surface marker protein is CD133+. This marker was observed in AT/RT from patient tissue by Chiou *et al* in the first report of CSC properties in rhabdoid tumours. Moreover CD133+ cells showed greater migratory properties, invasiveness and malignancy than CD133- cells. Moreover, levels of CD133+ cells correlated positively with resistance to radiotherapy. Increased expression of the anti-apoptotic Bcl-2 protein as well as p-ATM was also observed in CD133+ compared to CD133- cells. The study concluded that the p-ATM pathway and Bcl-2 expression in CD133+ AT/RT cells should be considered as potential therapeutic target[151]. In MRTK, Yanagisawa *et al*. suggested that CD133+ may determine metastatic fate of the cells and CD133- promotes tumour progression[152]. Furthermore, Nodomi *et al*. found that the marker CD146 (known as melanoma cell adhesion molecule and expressed in neural crest cells and other derivatives) was also a potential therapeutic target in MRT. CD146+ cells that were isolated from four MRT cell lines exhibited self-renewal activity and invasiveness *in vitro*[153]. In a xenograft model, these cells demonstrated the ability to form tumours and inhibition of CD146 suppressed tumour growth both *in vitro* and *in vivo*. Moreover, staining of CD146 in patient samples correlated with poor patient outcome[153]. Okuno *et al*. investigated six MRT cell lines for the CSC and neural stem cell (NSC) markers, CD133, Musashi-1(Msi-1) and nestin. CD133 was detected in three cell lines, nestin was observed in three of the cell lines and Msi-1 was observed in all six[154].

Lastly, a study by Carugo *et al*, proposes targeting UPR and autophagy in combination with other drug agents after observing elevated UPR and ER stress in SMARCB1-deficient malignancies[155]. The role of autophagy in chemoresistance will be further discussed below.

1.3 Apoptosis

Apoptosis is a form of highly regulated cell death that maintains cell homeostasis. It has a crucial role in multiple biological mechanisms such as development, ageing and in the regulation of the immune response. Therefore, dysregulation of apoptosis is implicated in a wide range of human diseases such as neurodegenerative disorders, autoimmune diseases, ischemic damage and numerous cancers[66]. Indeed, inherent or developed resistance to apoptosis is considered one of the eight hallmarks of cancer according to Hanahan and Weinberg[156].

During apoptosis, cells undergo characteristic morphological changes including cytoplasmic condensation, DNA fragmentation, cell shrinkage and membrane blebbing. The apoptotic cell fragments into membrane-bound apoptotic bodies in a process known as 'budding" and are subsequently, phagocytosed by neighbouring cells[66].

1.3.1 Caspases

Apoptosis is regulated by caspases (cysteine-aspartic proteases), an evolutionary conserved family of proteolytic enzymes involved in cell death and inflammation. There have been fifteen caspases identified, seven of which are implicated in apoptosis. Caspases can be broadly categorised as apoptotic or inflammatory. The inflammatory caspases consist of caspases 1, 4, 5, 11 and 12 whilst the apoptotic caspases consist of 2, 3, 6, 7, 8, 9 and 10. Caspases cleave substrates at the C-terminus of specific aspartate residues and have a structure that consists of three domains: an N-terminal pro-domain, a large subunit (20 kDa) and a C-terminal small subunit (10 kDa). They exist as inactive zymogens and can be activated through cleavage of their pro-domain[67].

Caspases are further divided into two groups, known as initiator and effector caspases. Initiator caspases have a longer pro-domain (> 90 amino acids) containing either a death effector domain (DED), caspase recruitment domain (CARD) or death domain (DD). These domains are crucial for the interaction between the caspase and upstream multiprotein complexes. Initiator caspases undergo proximity-induced autoactivation in

response to apoptotic stimuli. This process usually requires multi-component complexes, such as the apoptosome in the case of caspase 9. In contrast, effector caspases have notably shorter pro-domains (approximately 20 amino acids) and are activated by initiator caspases through the cleavage of aspartate-X sites. Once activated, effector caspases cleave cellular substrates that cause cell death[68].

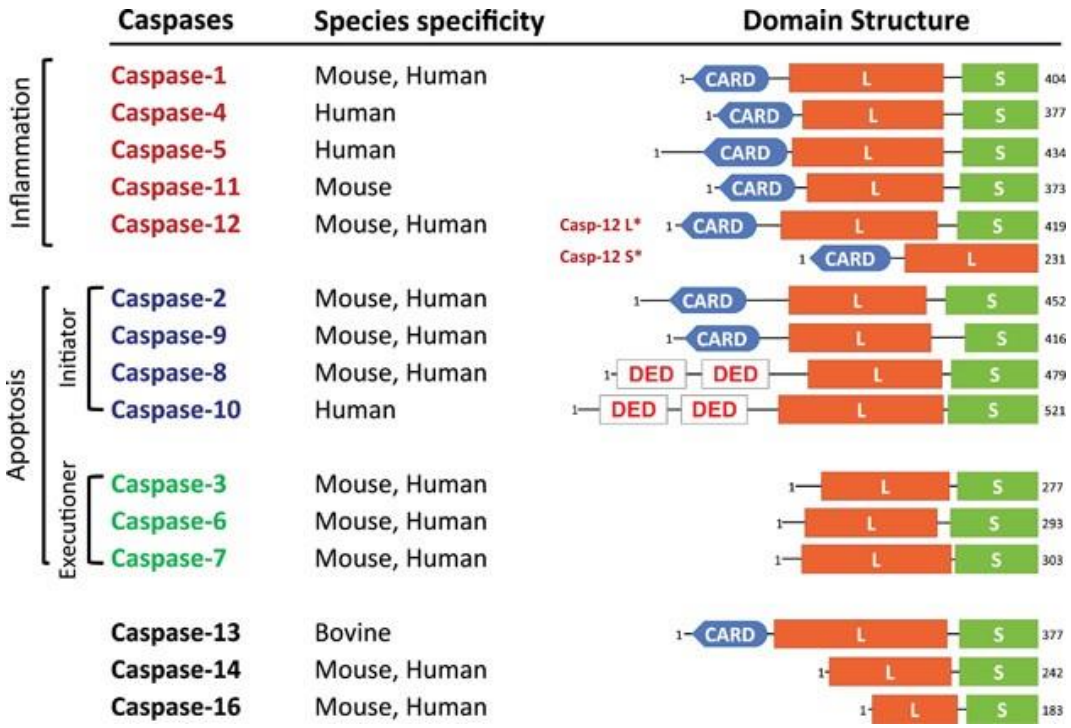

Figure 1.10 Domain structure and function of mammalian caspases.

Caspases contain 3 domains: an N-terminal pro-domain, a large domain and a shorter C-terminal domain. Caspases 1, 4, 5, 11 and 12 are inflammatory caspases. Caspases 2, 3, 6, 7, 8, 9 and 10 are apoptotic caspases and can be classified as initiator (2, 8, 9 and 10) or executioner/ effector caspases (3, 6, 7). Initiator caspases contain a CARD or DED domain. CARD, caspase recruitment domain; DED, death effector domain. L, large subunit; S, small subunit; S*, short form; L*, long form. Image taken from Shalini *et al*[157].

1.3.2 Apoptotic signalling pathways

There are two principal signalling pathways involved in apoptosis, known as the intrinsic signalling pathway and the extrinsic signalling pathway. The activation of these pathways results in the cleavage and subsequent activation of the effector caspases involved in apoptotic cell death. Crosstalk exists between the two pathways.

1.3.2.1 The intrinsic pathway

The intrinsic pathway or mitochondrial pathway is activated by intracellular stress such as oxidative stress, ischemia or genotoxic stress, which can be induced by chemotherapeutic agents, such as cisplatin[158]. The stimuli activate the BH3-only proteins in the Bcl-2 family, which in turn activate pro-apoptotic Bax and Bak proteins and inhibit anti-apoptotic Bcl-2 family members in the mitochondria and endoplasmic reticulum (ER)[159]. Bax and Bak relocate to the outer mitochondrial membrane and induce mitochondrial outer membrane permeabilization (MOMP). In response to MOMP, other pro-apoptotic proteins such as cytochrome c and Smac/DIABLO, are released into the cytosol. Smac/DIABLO inhibits XIAP, an inhibitor of apoptosis protein, thereby promoting apoptosis. Cytochrome c interacts with the adaptor protein apoptotic protease activating factor-1 (APAF-1) in the cytosol, thereby forming a heptameric wheel-like structure known as an apoptosome, exposing its CARD domains which will interact with the CARD domain of pro-caspase 9. This in turn activates caspase 9, which cleaves and induces the activation of effector caspases such as caspases 3, 6 and 7, involved in the execution of apoptosis[160].

1.3.2.2 The extrinsic pathway

The extrinsic pathway or death receptor pathway is activated by the interaction of cell death ligands with their receptors. Death receptors form part of the Tumour Necrosis Factor (TNF) receptor superfamily. Three principal ligand and receptor pairs described in literature are: Fas ligand (FasL) and Fas, TNF-alpha and TNF receptor, TRAIL and TRAIL Receptor 1/2 or Death Receptor (DR)4 and DR5[161]. These receptors are characterised by an extracellular cysteine-rich domain, which can bind to ligands, and a cytoplasmic death domain, which is involved in the recruitment of adaptor proteins to the complex, thereby propagating the signal from the cell surface to within the cell. Once the receptor has interacted with its ligand, oligomerisation occurs, and an adaptor protein is subsequently recruited. In the case of Fas/Fas ligand, the adaptor protein is FADD (Fas-associated protein with death-domain), whilst TNF-alpha and TNF receptor interaction recruits TRADD (Tumour necrosis factor receptor 1-associated DEATH domain protein). The adaptor proteins associate with the cytoplasmic portion of the receptor through their death domains and subsequently recruit the inactive initiator caspases, pro-caspase 8 or

pro-caspase 10, through their death effector domains (DED) to form a death-inducing signalling complex (DISC). This results in the autoactivation of the inactive zymogens into caspase 8 or caspase 10 which in turn cleave and activate the effector caspases; caspase 3 and caspase 7. These caspases catalyse the cleavage of key proteins involved in the execution of apoptosis. In addition to this, caspase 8 cleaves Bid into truncated or tBid which interacts with Bax and Bak and in doing so, activates the intrinsic pathway[162].

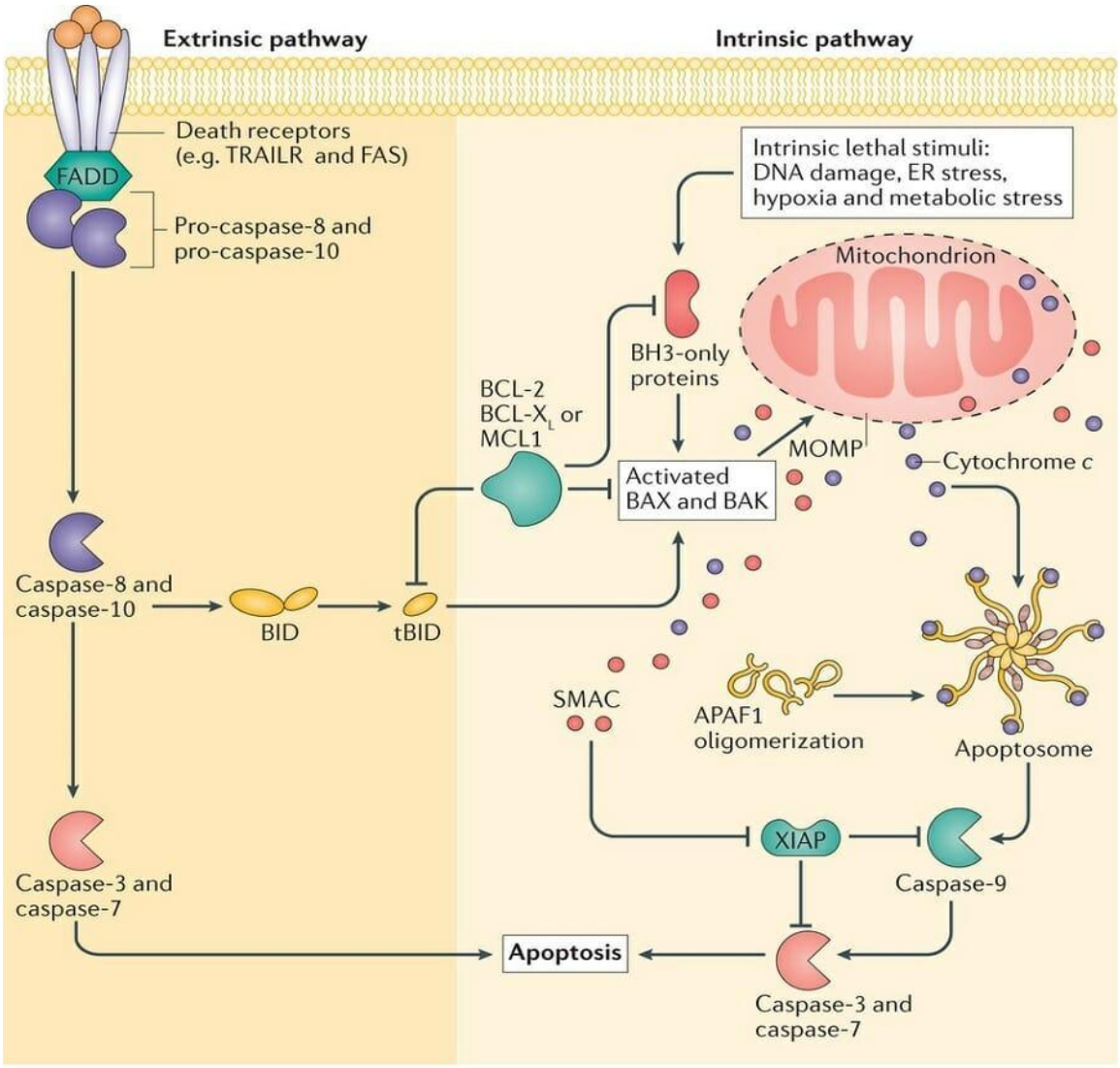

Figure 1.11 The extrinsic and intrinsic pathways in apoptosis.

The extrinsic pathway is activated by the binding of death receptors with their respective ligands, resulting in the cleavage and activation of pro-caspase 8 and pro-caspase 10. These either go on to activate the effector caspases, caspase 3 and caspase 7 or Bid, which activates the intrinsic pathway. The intrinsic pathway is activated by a number of potential intrinsic stimuli such as hypoxia or DNA damage. This results in the activation of BH3-only proteins. These proteins activate Bak and Bax which induce mitochondrial outer

membrane permeabilisation (MOMP). Cytochrome C is released into the cytosol and forms an apoptosome with APAF1. This activates caspase 9, which activates caspase 3 and caspase 7. Image taken from Ichim & Tait[163].

1.3.3 Regulation of apoptosis

1.3 IAPs

Inhibitor of apoptosis proteins (IAPs) are a family of proteins most commonly known for their role in regulation of cell survival and cell death (along with Bcl-2 family proteins). In addition to this, IAPs also have a role as innate immune sensors and are involved in various pathways including autophagy and cell division[164]. They are defined by their functional unit; the baculovirus IAP repeat (BIR) domain, which mediates their protein-protein interactions. In addition to this, IAPs also contain a RING finger domain on the C-terminal end, which facilitates protein degradation through E3 ubiquitin ligase activity[165]. When apoptosis is necessary, IAP activity can be antagonised by Smac/DIABLO to allow for the activation of caspases[166]. There are 8 members of the IAP family: NAIP, cIAP1, cIAP2, XIAP, survivin, apollon, livin/ ML-IAP and ILP-2. IAPs have been implicated in a number of processes such as inflammation, cell death and innate immunity. More specifically, cIAP1/2, XIAP, survivin and livin have been implicated in cancer progression due to their roles in regulation of programmed cell death[165]. XIAP is the most widely studied IAP family member and can directly regulate caspase activity. In particular, it has been shown to ubiquitinate capases 3 and 7 (alongside cIAP1/2 activity) leading to their proteasomal degradation and the subsequent inhibition of apoptosis[167]. cIAP1 and cIAP2 are homologous proteins. Unlike XIAP, they cannot inhibit apoptosis by direct binding to caspases, but do so indirectly through regulation of extrinsic apoptosis and NF-κB signalling[168].

Livin has two splice variants (alpha and beta), and it is believed to sequester Smac/DIABLO thereby preventing it from antagonising XIAP-mediated caspase inhibition[169]. In addition, livin has been shown to be cleaved upon effector caspase activation and this cleaved form appears to be pro-apoptotic suggesting livin has an overall regulatory effect. Lastly, survivin is the smallest member of the IAPs and has been shown

to be highly expressed in many cancers. As well as having a role in apoptosis inhibition, survivin is believed to act in the regulation of mitosis[170].

1.3.3.2 cFLIP

The anti-apoptotic protein cFLIP is a DED-containing protein that regulates the activation of caspases 8 and 10 in the extrinsic pathway. cFLIP is expressed as 3 isoforms in humans that differ functionally: $cFLIP_L$, $cFLIP_S$ and $cFLIP_R$. These 3 variants can interact with the adaptor protein FADD. This interaction results in the DISC complex recruitment. $cFLIP_S$ and $cFLIP_R$ are smaller variants with molecular weights of 26 and 24 kDa, respectively. In contrast, $cFLIP_L$ has a higher molecular weight of 55kDa and contains a caspase cleavage site that can be cleaved by caspase 8 to form p43cFLIP[171].

cFLIP is also involved in ripoptosome formation and in determining the mode of cell death that is triggered by this complex (e.g necroptotic or apoptotic). The ripoptosome is a 2-mDa protein complex, often referred to as a cell death platform, which consists of caspase 8, FADD, cFLIP isoforms and RIP1. Moreover, cFLIP also has a role in activating pro-survival pathways such as NF-κB and Akt signalling pathways[172].

cFLIP can be transcriptionally activated by a number of stimuli such as growth factors, interleukins, TNF ligands and chemotherapeutic agents. In cancer, cFLIP has been shown to be overexpressed and is a therapeutic target of interest. Developing inhibitors to target cFLIP has proved difficult due to its structural resemblance to caspase 8 and 10[172]. Nonetheless, *in vitro* downregulation has been shown to restore apoptosis via TRAIL and CD95L in melanoma cell lines[173].

1.3.3.3 Bcl-2 family of proteins

There have been approximately 25 members of the Bcl-2 family of proteins described in literature to date. The Bcl-2 family of proteins are broadly distinguished as pro-apoptotic or anti-apoptotic based on their ability to promote or inhibit apoptosis. These proteins play a vital role in the regulation of apoptosis and are characterised by their Bcl-2 homology (BH) domains. Bcl-2 family members can be categorised into three subfamilies according to their structure and function: the multi-domain anti-apoptotic subfamily, the multi-

domain pro-apoptotic subfamily and the BH3-only-pro-apoptotic subfamily. All pro-apoptotic proteins contain a BH3 domain to facilitate the interaction with other proteins and are either BH3-only proteins (e.g. Bid and Bim) or multi-domain proteins (e.g. Bax and Bak) which mediates apoptosis through permeabilization of the outer mitochondrial membrane (OMM). In contrast, anti-apoptotic proteins contain BH1, BH2 and sometimes BH3 or BH4 domains[174]. Some of the anti-apoptotic proteins include Bcl-2, Bcl-xL and myeloid cell leukaemia (Mcl-1), which inhibit Bax and Bak as well as intercepting upstream signals from BH3-only-pro-apoptotic proteins such as Bid, Bim and Puma[175, 176].

1.3.3.3.1 Structure of Bcl-2 family of proteins

Structural studies of the multi-motif Bcl-2 family of proteins indicate that they contain homologous α-helical folds which provide binding sites. The BH3 domain can bind as an amphipathic helix in a hydrophobic groove formed by BH1, BH2 and BH4 of the anti-apoptotic protein. Each anti-apoptotic protein has a similar topology; however, they differ in specificity for BH3 targets. Bid is the only BH3-only member of the family whose structure has been defined. It has a hydrophobic core structure similar to Bcl-2 and can be converted into truncated Bid or tBid through proteolytic cleavage of the α1-α2 loop by caspase-8 or granzyme B amongst other proteases[177].

1.3.3.3.2 Bcl-2

Bcl-2 was discovered in the breakpoint region of the t(14;18) translocation in patients with B-cell lymphoma. Unlike other oncogenes that had been characterised at the time, Bcl-2 was found to promote cell survival instead of proliferation. It was the first Bcl-2 family member to be identified and is considered to be the gatekeeper of the apoptotic response[178]. Bcl-2 inhibits apoptosis by inhibiting Bax/Bak oligomerisation as well as binding other pro-apoptotic proteins and suppressing their activity[179]. Inhibition of Bax/Bak oligomerisation blocks apoptosis by suppressing cytochrome c release. Bcl-2 is not only localised to the OMM, but also the ER membrane and the nuclear envelope[180]. Bcl-2 also prevents apoptosis by binding to inositol,1, 4, 5-triphosphate receptor (IP3R) via its BH4 domain to inhibit calcium release from the ER. Of note, Bcl-2 is also involved in the regulation of autophagy as it can bind to Beclin-1, a key protein in autophagosome formation. This interaction occurs through the BH3 domain of Beclin-1 and the BH3 binding groove of Bcl-2. This interaction is disrupted in response to nutrient starvation, thereby activating Beclin-1 activity.

1.3.3.3.3 Bcl-xL

Bcl-xL, another anti-apoptotic member of the family is also expressed in the OMM and acts in a similar manner to Bcl-2 by preventing the oligomerisation of Bax and Bak and the formation of pores in the OMM. In addition to this, Bcl-xL interacts with the voltage-dependent anion channel 1 (VDAC1) to protect cells from mitochondria-mediated apoptosis[181, 182].

1.3.3.3.4 Mcl-1

Mcl-1 was the second Bcl-2 family member to be discovered. It was identified in the myeloid lymphocyte line ML-1. It has a similar carboxy-terminal core to other anti-apoptotic proteins and contains four BH3 domains. In contrast, it has a longer and unstructured N-terminus containing two proline/glutamic acid/serine/threonine (PEST) domains, characteristic of rapidly degrading proteins[183]. Mcl-1 has a short half-life, is tightly regulated and its activity can be mediated by ubiquitination, phosphorylation and cleavage. Mcl-1 can be activated by a number of upstream signalling pathways such as PI3K/Akt, Jak/Stat, p38 and ERK. It acts in a similar manner to Bcl-2 and Bcl-xL by preventing the oligomerisation of Bax and Bak and has also been shown to sequester these proteins. Mcl-1 is essential in cancer cell survival[183].

1.3.3.3.5 Bax and Bak

The pro-apoptotic Bcl2 family member Bax was identified as a conserved homolog that binds to Bcl-2 with pro-death activity. Both Bax and Bak have nine alpha helices with a hydrophobic alpha helix at the core surrounded by amphipathic helices. The C-terminal alpha helix 9 has a transmembrane (TM) domain that serves to anchor the protein to the mitochondrial outer membrane. The hydrophobic BH3 domain is only exposed upon activation of these proteins and subsequently allows for homo- and hetero-oligomerisation of the proteins[184].

Bax and Bak are regulated by anti-apoptotic Bcl-2 family members. During apoptosis, Bax and Bak are activated and oligomerise, then translocate to the mitochondria and puncture the membrane by forming pores. The mechanism by which Bax/Bak are activated is a controversial matter of much debate in literature with various models proposed. One theory is that certain BH3-only proteins such as Bim, tBid and Puma are ‘activators’ and

can induce a conformational change in Bax/Bak by binding to them. This model also classifies other BH3-only proteins as 'sensitisers' that bind to Bcl-2 like proteins in order to free the 'activators'. An alternative model is the 'indirect model' where BH3-only proteins act indirectly by sequestering anti-apoptotic proteins away from Bax/Bak[185]

1.3.3.3.6 Bim

The pro-apoptotic BH3-only protein Bim links the intrinsic and extrinsic apoptotic pathways and is activated in response to stimuli such as ER stress[186]. Bim is known to bind directly to Bcl-2. In the indirect model, this is thought to be the way by which apoptosis is induced. However, the indirect model proposes that Bim can bind directly to Bax and Bak.

In cancer, reduced Bim expression correlates with tumour promotion and autoimmunity. In contrast, overexpression of Bim is associated with tumour growth inhibition and reduced drug resistance. This can be exploited therapeutically to overcome chemoresistance by treating cancer cells with a combination of chemotherapy and Bim-enhancing drugs. For example, BH3 mimetics such as ABT-263 (navitoclax) and ABT-199 (venetoclax), which enhance Bim activity by binding to Bcl-2 have entered clinical trials[187].

1.3.3.3.7 Bid

Bid is another member of the pro-apoptotic Bcl-2 family, which was discovered through its binding to anti-apoptotic protein Bcl-2 and pro-apoptotic protein Bax. During apoptosis, Bid can be cleaved by caspase 8 amongst other caspases, granzyme B, calpains and cathepsins to form truncated Bid (tBid). This form of Bid then translocates to the mitochondria where it induces Bax/Bak-dependent MOMP. Analysis of its membrane binding suggests it binds to the membrane in a similar way to Bax. Moreover, comparison of NMR structures of Bid and Bax also reveals structural similarities. Bid has eight alpha helices with two core hydrophobic helices that form a hairpin structure surrounded by six amphipathic helices. The BH3 region of Bid is necessary for its interaction with Bcl-2, Bcl-xL and Bax[188]. The expression of this pro-apoptotic protein has also been studied in cancer. In stage II and III colon cancer patients, Bid and Bad expression were concluded to serve as prognostic variables. Moreover, high levels of Bid were associated with favourable clinical outcome in prostate cancer[189, 190].

1.3.3.3.8 Noxa

Noxa is a pro-apoptotic BH3-only protein which induces apoptosis via p53-dependent and p53-independent mechanisms. On its own, Noxa does not exhibit major pro-apoptotic activity. However, it has significant impact on modulating levels of other key proteins involved in the regulation of apoptosis. Most significantly, Noxa regulates Mcl-1 by targeting it for proteasomal degradation, which results in induction of the intrinsic apoptotic pathway[191]. In cancer, Noxa itself is upregulated in response to DNA damage caused by anticancer drugs such as etoposide and irradiation[192]. Moreover, studies have shown that Noxa upregulation can sensitise cells to drug-induced apoptosis[193].

1.3.3.3.9 Puma

Puma is a pro-apoptotic BH3-only protein that mediates p53-dependent and p53-independent apoptosis induction. It can be activated in response to a number of stimuli including genotoxic stress, deregulated oncogene expression and disruption to homeostasis levels. The expression of Puma is regulated by various transcription factors and it acts by sending death signals to the mitochondria and inhibiting anti-apoptotic proteins. In cancer, low expression levels of Puma has been associated with therapeutic resistance and tumour progression[194].

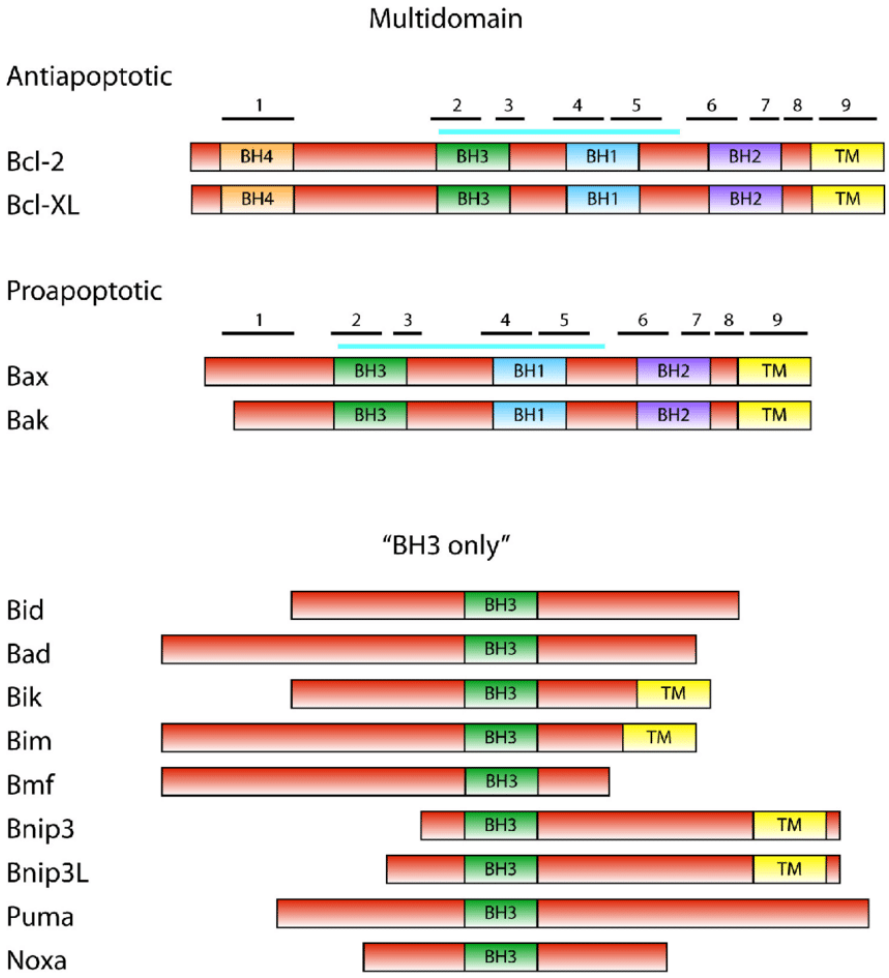

Figure 1.12 Structure of Bcl-2 proteins.

Bcl-2 family members can be categorised into three subfamilies according to their structure and function: the multi-domain anti-apoptotic subfamily, the multi-domain pro-apoptotic subfamily and the BH3-only-pro-apoptotic subfamily. Multi-domain pro-apoptotic proteins are considered to exert intrinsic activity whereas BH3-only proteins interact with anti-apoptotic proteins via their BH3-domain. They also bind to other multi-domain pro-apoptotic proteins to enhance their activity. The BH4 domain is deemed critical for the anti-apoptotic activity of Bcl-2 and Bcl-xL. Many Bcl-2 family domains have transmembrane ™ domains in their carboxy-terminal ends. Image taken from Polcic *et al*[195].

1.3.4. Apoptosis in cancer and chemoresistance

In cancer, reduced apoptosis occurs allowing for the survival of malignant cells. This concept was first outlined in the early 1970s by Kerr *et al.* who linked the process of

apoptosis to the proliferation of malignant cells, hyperplasia and tumorigenesis[196]. Malignant cells can evade apoptosis via a variety of mechanisms including increased expression of IAPs, an imbalance between pro-apoptotic and anti-apoptotic proteins, diminished caspase activity, impaired death receptor signalling, and defects in the tumour suppressor p53[197].

1.3.4.1. IAPS in cancer

IAPs have been found to be overexpressed in many malignancies with expression levels correlating with increased disease severity. In pancreatic cancer cells, many IAP family members were found to be overexpressed and were demonstrated to contribute to drug resistance[198]. In particular, c-IAP2 overexpression was found to be the most significant in mediating resistance. Furthermore, livin has been found to be consistently overexpressed in melanoma with high expression correlated to poor prognosis and cancer progression[199]. Survivin has also been reported to be overexpressed in a number of cancers. Small *et al* observed that overexpression of survivin in hematopoietic cells of transgenic mice predisposed them to the development of haematological malignancies and were less likely to undergo apoptosis[197, 200].

Interestingly, the naturally occurring IAP antagonist, Smac/DIABLO, has been shown to be downregulated in various cancers potentially contributing to drug resistance and cell survival. For example, Smac/DIABLO was shown to be downregulated in patients with renal cell carcinoma (RCC) compared to normally kidney samples and a lack of Smac/DIABLO expression corresponded to poorer prognosis. RCC cell lines also demonstrated downregulation of Smac/DIABLO. Interestingly, transfection with Smac/DIABLO sensitised these cell lines to TRAIL and cisplatin-induced apoptosis[200].

As single agents, small molecule inhibitors of XIAP termed Smac mimetics, which also induce degradation of cIAP1/2, have shown promise as pre-clinical agents in various cancerous cell lines with a number having entered clinical trials[201]. Smac mimetics have previously been shown to sensitise non-small cell lung cancer, urothelial cancer and ovarian cancer lines to cisplatin treatment[202-204]. As a monotherapy, Smac mimetics do not appear to show significant therapeutic impact, therefore they are being studied as a combination therapy with other common treatments in pre-clinical and early clinical studies. Interestingly, in MRT cells, IAPs have been shown to be a potential therapeutic

target. A report by Coyle *et al*. demonstrated that targeting XIAP with the small molecule inhibitor embelin sensitised MRT cells to TRAIL treatment. Knockdown of XIAP using siRNA also enhanced TRAIL-mediated cell death, suggesting that targeting XIAP may be a novel avenue in MRT treatment[93]. Moreover, another recent study conducted by Coyle *et al*. demonstrated that the Smac mimetic BV6 synergistically enhanced cisplatin-mediated apoptosis in MRT cell lines. Moreover, the XIAP inhibitor embelin also significantly enhanced cisplatin-induced cell death indicating pre-clinical promise for IAP as novel therapeutic targets in combination with cisplatin in rhabdoid tumours[205].

1.3.4.2. Reduced expression of caspases in cancer

As mentioned earlier, caspases are essential in the initiation and execution of apoptosis. Low levels of caspase expression and impaired caspase function is associated with abrogation of apoptosis and therefore with cancer progression.

Low caspase 3 activity is a classic characteristic of cancer cells. This low activity was found to predict local recurrence in colorectal cancer patients[197, 206]. In line with this, another study in colorectal cancer patients found that high caspase 3 expression corresponded with promising prognosis[197]. In muscle-invasive bladder cancer, low caspase 3 expression corresponded to poor prognosis[207]. Devarajan *et al* found that mRNA levels of caspase 3 were almost undetectable in breast, ovarian and cervical cancer. Further to this, induced expression of caspase 3 in caspase 3-deficient breast cancer lines restored their ability to undergo apoptosis and enhanced their sensitivity to drug treatment[208]. In oral tongue squamous carcinoma, caspase 3 and cleaved caspase 3 showed potential as clinical biomarkers[209].

Downregulation of initiator caspase, caspase 9 was identified as a recurring event in patients with stage II colorectal cancer and was linked to poor clinical outcome[210]. In choriocarcinoma, caspases 8 and 10 were found to be downregulated upon cDNA expression array analysis[211].

In aggressive childhood neuroblastomas, Teitz *et al*. found that caspase 8 was not expressed in a high proportion of cell lines. Interestingly, the cell lines that did not express caspase 8 exhibited amplification of the *MYCN* oncogene and were characterised as very resistant to chemotherapy and irradiation treatment. *CASP8*, the gene coding for caspase 8,

was silenced by methylation in the neuroblastoma cell lines and methylation of the promoter region in the patient tissue samples. Interestingly, reintroduction of caspase 8 resulted in the sensitisation of neuroblastoma cells to treatment[212].

Harada *et al*. further investigated the methylation of caspase 8 in 181 paediatric tumours. The study found frequent methylation in rhabdomyosarcomas, medulloblastomas, retinoblastomas and neuroblastomas. Methylation frequency was found to be low in Wilm's tumours. No methylation was observed in hepatoblastomas, acute leukaemias, ganglioneuromas, osteosarcomas, Ewing's sarcomas and in normal tissues. Methylation of *CASP8* was found to be elevated in all tumour types in correlation with methylation of tumour suppressor gene *RASSF1A*. The study also showed a correlation between methylation and gene inactivation[213].

1.3.4.3 Impaired receptor signalling pathway in cancer

Death receptors and their ligands are critical players in the extrinsic pathway of apoptosis[197]. Death ligands are members of the tumour necrosis factor super family (TNFSF). These include TNF-alpha, CD95L and TRAIL. In turn, their receptors are known as the TNF receptor super family. These include TNFR1/DR 1, Fas, DR3/APO-3, TRAIL1/DR4 and TRAIL2/DR5. These receptors contain a death domain (DD) that upon receiving a death signal, are able to recruit adaptor proteins in order to transduce a signalling cascade[197].

Impairment of this pathway has been observed in cancer which results in the evasion of extrinsic apoptosis. For instance, reduced expression of surface receptors such as CD95 is seen in many cancers[214, 215]. Furthermore, mutations in CD95 genes have been observed in a number of haematological malignancies[216]. In colon cancer cells, TRAIL resistance was mediated through impaired transport of TRAIL receptors to the cell surface[217]. The abnormal expression of decoy receptors is another way in which this pathway can become dysregulated. For example, decoy receptor 3 has been found to be overexpressed in a number of malignancies including glioblastoma, lung carcinoma and colon carcinoma[93, 197, 218]. As previously mentioned, Coyle *et al* enhanced the activation of the extrinsic apoptotic signalling pathway through targeting XIAP with the pharmacological inhibitor, embelin and sensitised MRT cells to TRAIL treatment[93].

1.3.4.4. p53 mutations in cancer

The p53 tumour suppressor gene transcriptionally regulates many critical apoptosis-related genes and is thus, one of the most widely studied genes. It is responsible for regulating cell proliferation by inducing cell cycle arrest and apoptosis in response to stressors such as DNA damage, ROS and hypoxia. In fact, p53 alterations have been linked to 50% of human cancers[219]. Over 75% of these mutations result in the expression of a p53 protein that has lost its wild-type functions. Moreover, mutant p53 acquire oncogenic functions independent to its loss of wild-type activity. These oncogenic functions have been described in many cancer models and include invasiveness, metastasis, angiogenesis, stem cell expansion, proliferation, tissue remodelling, genetic instability and chemoresistance[220]. Due to the high expression of mutant p53 in cancers, it has become a widely targeted protein in cancer treatment research. Popular strategies to target p53 include inactivating or destabilising it. Furthermore, re-introduction of wild type p53 has shown great therapeutic promise in mouse models of liver carcinomas. However, this strategy remains difficult to implement clinically. Mutant p53 destabilisation is achieved by targeting heat-shock proteins using histone deacetylases to restore MDM2-degradation of mutant p53. Another strategy to target mutant p53 function is to intervene in its interactions with other transcription factors. Alternatively, targeting downstream pathways and molecules of mutant p53 is also a therapeutic option. However, as p53 acts on a number of signalling pathways it is yet unclear how effective this could be[220].

TP53 mutation types vary across different populations and cancers. Somatic mutations of the p53 gene occur in almost every cancer with varying rates. For instance, these somatic mutations can be found at rates of 38-50% in ovarian, oesophageal, colorectal, colorectal, head and neck, larynx and lung cancers. In other cancers such as malignant melanoma and cervical cancer, these mutations are found at lower rates of approximately 5%. Mutations occur at a higher frequency in cancers with very aggressive nature such as triple negative or HER2-amplified breast cancers. Germline mutations of *TP53* result in Li-Fraumeni syndrome a hereditary familial pre-disposition to a wide range of tumours which include sarcomas, breast cancers, brain tumours and adrenal cortical carcinoma[221].

The role of p53 in MRT remains unclear. Kinoshita *et al.* examined p53 gene mutations through immunohistochemical staining and DNA direct sequencing in three cases of MRTK tumours and three cases of MRT of soft tissue. All of the soft tissue MRT cases

and two of the three MRTK cases showed immunopositivity for p53. Of these cases, one of rhabdoid tumours of the soft tissue and two of the MRTK cases showed missense mutations of the p53 gene[222]. Hsueh *et al*. examined p53 in one case of MRTK and did not find any mutation or amplification of the gene in agreement with other small studies conducted by Hirose *et al*. and Rosson *et al* [223-225]. However, these studies are too small to conclude that p53 mutations are not contributing factors to the progression of rhabdoid tumours. In contrast, Howard *et al.* found that MDM2 and MDM4, the canonical negative regulators of p53, exhibit therapeutic potential. Using two inhibitors of these regulators they determined that MRT cell lines were more sensitive to treatment than alternative cell lines with wild type p53. Treatment with these compounds resulted in upregulation of p53 and sensitivity was reversed by silencing TP53. Tumour regression was also observed in xenografts. The authors postulated that sensitivity to MDM2 and MDM4 inhibition was achieved through p53-mediated apoptosis[226]. Interestingly, Chun *et al.* conducted genome-wide profiles of 40 cases of extra-cranial MRT and did not detect any mutations in TP53[77]. Moreover, Johann *et al.* also examined the genetic profile of rhabdoid tumours and did not observe any TP53 alterations[75].

Carugo *et al*, developed mouse models of SMARCB-1 deficient rhabdoid tumours and discovered that p53 is a master regulator of proteostasis in these tumours resulting in enhanced levels of ER stress and UPR, displaying a high sensitivity to drugs that target autophagy and the UPR[155]. The study suggested a dual role of p53 in SMARCB1-deficient tumours; p53 signalling results in suppression of proliferation and tumour progression during initial stages of tumorigenesis, however, it can also modulate UPR and autophagic pathways to help cancer cells cope with metabolic stress. The role of MYC-p19^{ARF}-MDM2-p53 tumour suppressive axis in regulating proteostasis through autophagy was postulated to be a possible explanation for the apparent absence of TP53 mutations that was mentioned above[155].

1.3.4.5. Bcl-2 family members in cancer

Various Bcl-2 family members have been directly implicated in numerous cancers and have become the focus of pharmaceutical efforts to target members of this family in novel therapeutic approaches. As mentioned earlier, apoptosis is a tightly regulated process that highly depends on the balance of a number of proteins that exhibit either pro-death or pro-

survival activity. In cancer, this pathway becomes dysregulated due to disruptions to this delicately balanced process. Indeed in cancer, expression of proteins involved in apoptosis are often found to be downregulated. For example, the mitochondrial protein Smac/DIABLO, which potentiates apoptosis, was observed to be downregulated in certain cancers including renal carcinoma, colorectal cancer, colorectal cancer, bladder cancer, lung cancer, hepatocellular carcinoma, testicular germ cell tumours and pancreatic cancer in comparison with healthy tissue[227]. Another example is alterations to the expression of Bax; homozygous deletions and inactivating mutations have been observed in a number of cancers including colon cancer and hematopoietic cancers[228].

In contrast, overexpression of Bcl-2 has been reported to drive carcinogenesis[185]. Through direct binding, Bcl-2 and other anti-apoptotic family members such as Mcl-1 and Bcl-xl hold in check two key pro-apoptotic proteins, Bax and Bak, which when activated oligomerise on the OMM inducing MOMP, releasing cytochrome C and activating caspases that execute the destruction of the cell. Therefore, malignant cells can become dependent on Bcl-2 expression making them particularly susceptible to Bcl-2 inhibitors[229]. Thus, targeting Bcl-2 has become an area of focus in anti-cancer treatment.

Overexpression of Bcl-2 has been observed in many cancer types including glioma, neuroblastoma, melanoma, squamous carcinoma, breast, lung and colorectal cancer cells, increasing invasive and migratory properties. Moreover, overexpression of Mcl-1, Bcl-xL and Bcl-w in glioma, lung, colorectal and gastric cancer cells has also been observed[230]. Overexpression of Bcl-2 is also associated with apoptosis evasion, cell survival and drug resistance leading to cancer cells developing a dependence on Bcl-2 to survive aggressive environments induced by chemotherapeutic treatment or the immune system. These cells can become “addicted” to Bcl-2 and therefore this presents a therapeutic vulnerability that can be targeted by inhibiting Bcl-2. Some reports in literature suggest that this dependence on Bcl-2 for survival is characteristic of blood cancers while solid tumours have a tendency to display a higher reliance on the overexpression of other anti-apoptotic proteins such as Bcl-xL or Mcl-1[231].

Bcl-2 and other pro-survival proteins are naturally antagonised by the pro-apoptotic BH3-only protein subfamily which includes Bim, Bid, Noxa and Puma. There has been some interest in the generation of stabilised BH3 peptides but BH3 mimetic drugs have become

a preferred method of Bcl-2 inhibition due to their small size and selective nature[185] and many have shown promising activity *in vitro* and *in vivo.* Indeed, there are numerous preclinical and clinical trials underway using several BH3-mimetic drugs. Among these, navitoclax/ABT-263 has been shown to have significant anti-cancer activity in chronic lymphocytic leukaemia clinical (CLL) trials. However, navitoclax targets multiple Bcl-2 proteins, including Bcl-xL, which results in dose-limiting thrombocytopenia, due to the high dependency of platelets on Bcl-xL. Despite the structural and functional similarities between Bcl-2 proteins, it is possible to develop selective BH3-mimetics such as venetoclax/ABT-199 which targets only Bcl-2. *In vitro*, ABT-199 binds to Bcl-xL over three orders of magnitude less whilst still binding to Bcl-2 at sub-nanomolar concentrations[232]. ABT-199 has also shown promising results in relapsed CLL clinical trials and appears to circumvent the thrombocytopenia caused by ABT-263[185]. ABT-199 is FDA-approved and has been licensed, in combination with rituximab, to treat relapsed CLL patients that have undergone at least one prior treatment[233]. Many clinical trials are currently underway to assess the efficacy of ABT-199 alone and in combination with other anti-cancer drugs in CLL, AML and SLL (small lymphocytic lymphoma). There has also been an increased focus on assessing the pre-clinical potential of ABT199 in other cancers[232]. Xu *et al* showed that ABT-199 in combination with irinotecan (a standard treatment for small cell lung cancer and colon cancer) showed synergistic apoptotic and cell growth inhibition effects in *Kras*-mutant lung cancer cells[234]. In estrogen receptor-positive breast cancer cells, combining ABT-199 with tamoxifen showed significant tumour reduction and longer survival outcomes in breast tumour xenografts compared to treatment with either drug alone[235]. Of note, Bcl-2 inhibition alone did not induce breast tumour regression as is seen in CLL. Wang *et al*, studied the combination of ABT-199 with the Mcl-1 inhibitor, S63845 in nasopharyngeal carcinoma and demonstrated a strong synergistic anti-tumour effect in xenografted mice[236]. Of note, some studies have observed ABT-199 resistance mediated through upregulation of Mcl-1[237].

To date, ABT-199 has not been tested in MRT. Interestingly the Mcl-1 inhibitor, TW-37, has been shown to sensitise a number of MRT cell lines to doxorubicin-induced cell death in a synergistic manner. TW-37 inhibited proliferation in a dose-dependent manner[94]. The study showed that ectopic expression of the Mcl-1 regulator, Noxa became bound to Mcl-1 and promoted apoptosis in response to doxorubicin. Moreover, genetic knockdown of Mcl-1 induced a greater sensitivity to doxorubicin that ectopic Noxa expression[94].

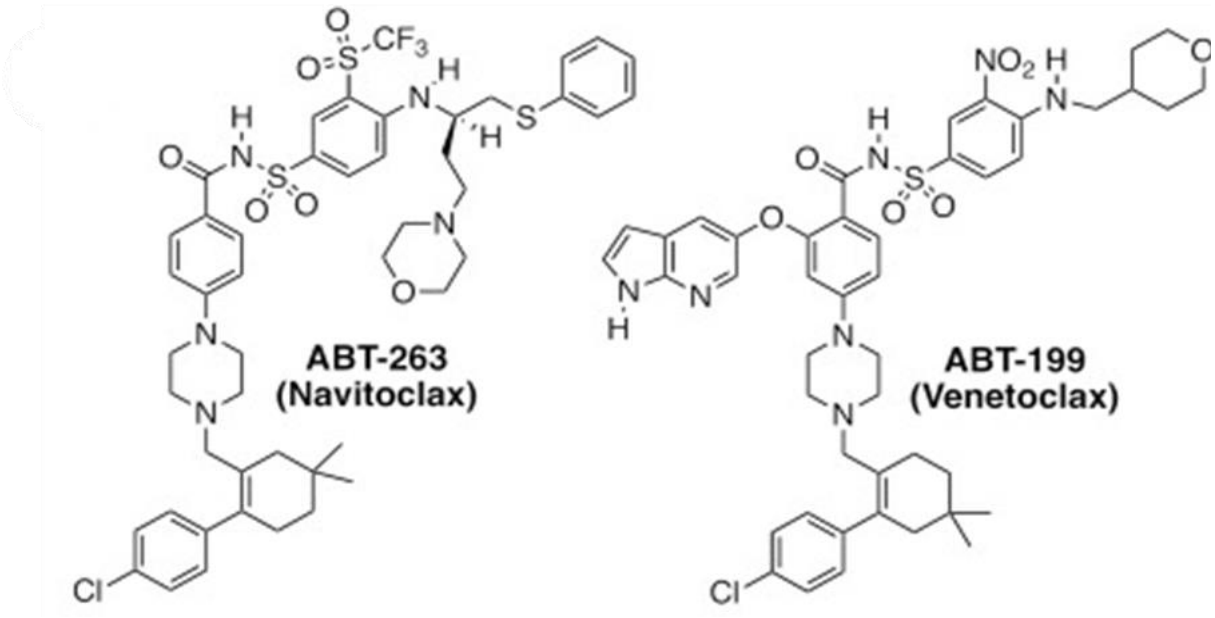

Figure 1.13 Structures of ABT-263 and ABT-199.

Adapted from Lever *et al*[238].

Thus, the balance between expression levels of pro- and anti-apoptotic Bcl-2 family proteins play a critical role in the regulation of apoptosis in cancer alongside other components of apoptotic signalling such as caspase activity, IAP expression, p53 alterations and the receptor signalling pathway Fig. 13.

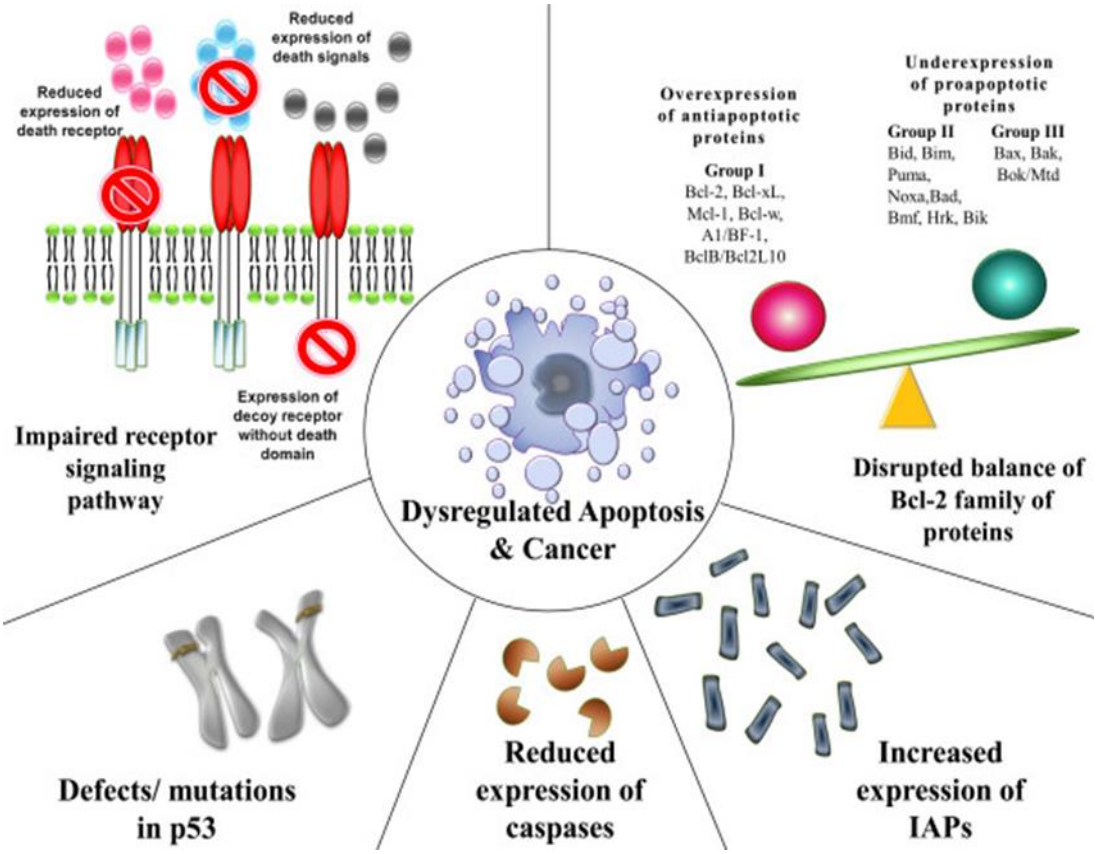

Figure 1.14 Dysregulation of apoptosis in cancer.

Apoptosis is a tightly regulated process in healthy cells. However, dysregulation of apoptosis in malignant cells results in abrogated cell death. Inhibition of apoptosis can occur at various stages of the highly orchestrated apoptotic signalling pathways. Mechanisms that contribute to evasion of apoptosis include alterations in the signalling receptor pathway in extrinsic apoptosis, an imbalance in expression levels of pro-and anti-apoptotic proteins, overexpression of IAPs, reduced expression or activity of caspases and alterations in p53. Image taken from Wong[197].

1.4 Autophagy

Autophagy is a catabolic process in which the cell recycles and degrades its own components. The term autophagy was coined by Christian De Duve in 1963 and is derived from Greek, meaning “self-devouring”. This process occurs in all eukaryotic cells to eliminate cellular waste, maintain homeostasis and provide new building blocks and energy through a recycling process[239]. Dysregulation of autophagy has been implicated in a number of diseases including neurodegenerative diseases, inflammatory diseases, metabolic diseases, obesity and cancer[240].

There are three different types of autophagy that are frequently described in literature: macroautophagy, microautophagy and chaperone-mediated autophagy (CMA). The term macroautophagy is often used interchangeably with autophagy in literature. The process of macroautophagy consists of the formation of a double-membrane sequestering compartment called the phagophore. This isolates the cytoplasmic components to form an autophagosome which then fuses with the lysosome to form an autolysosome, where the cargo is degraded. In contrast, microautophagy recycles smaller components by engulfing them through the invagination of the lysosomal membrane[241]. In chaperone-mediated autophagy, proteins that contain a KFERQ-like pentapeptide are recognised by the chaperone protein Hsc70 (heat shock cognate 70) which recruits the protein to the surface of the lysosome to be internalised and degraded[241, 242]. Autophagy can be induced by a number of factors including nutrient starvation, ER stress, rapamycin, reactive oxygen species (ROS) or viral infection. In recent, years, there have been efforts to develop autophagy inducers in clinical medicine to treat certain conditions[243].

1.4.1 Cellular mechanisms of autophagy

As summarised above, the process of autophagy is initiated with the nucleation of a phagophore, which uses lipids to expand. It is believed that phagophores form *de novo* by nucleation on a pre-existing membrane. The origin of this membrane remains unknown, despite the fact that many studies have been conducted to establish where the lipids are derived from. Some of the studies point to either the endoplasmic reticulum (ER), the Golgi apparatus or the mitochondria as potential membrane sources to the phagophore[244]. When autophagy is induced by starvation, the phagophore has been shown to nucleate at the omegasome, a lipid bilayer forming the subdomain of the ER membrane[245].
The phagophore then expands, surrounding its cargo and eventually seals it to form an autophagosome. The outer lipid bilayer membrane in the autophagosome fuses with the lipid bilayer membrane of the lysosome. The transport of the autophagosome to the lysosome is heavily reliant on the cytoskeleton. GTPase Rab7 is essential in connecting the autophagosome to the microtubule by binding to FYCO1 (FYVE and coiled-coil domain-containing 1), which acts as a linker between a kinesin motor and the autophagosome to direct transport towards the cell periphery. In addition, GTPase Rab7 mediates transport towards the perinuclear region through the formation of a complex between RILP (Rab-interacting lysosomal protein), ORP1L (oxygen-binding protein-related protein 1) and

dynein. The fusion between the autophagosome and the lysosome is mediated by tethering factors and SNARE proteins[246, 247]. The cargo is degraded within the autolysosome by lysosomal hydrolases, generating basic metabolites that are subsequently taken to the cytoplasm by lysosomal permeases to be used for biosynthesis or for energy production[248].

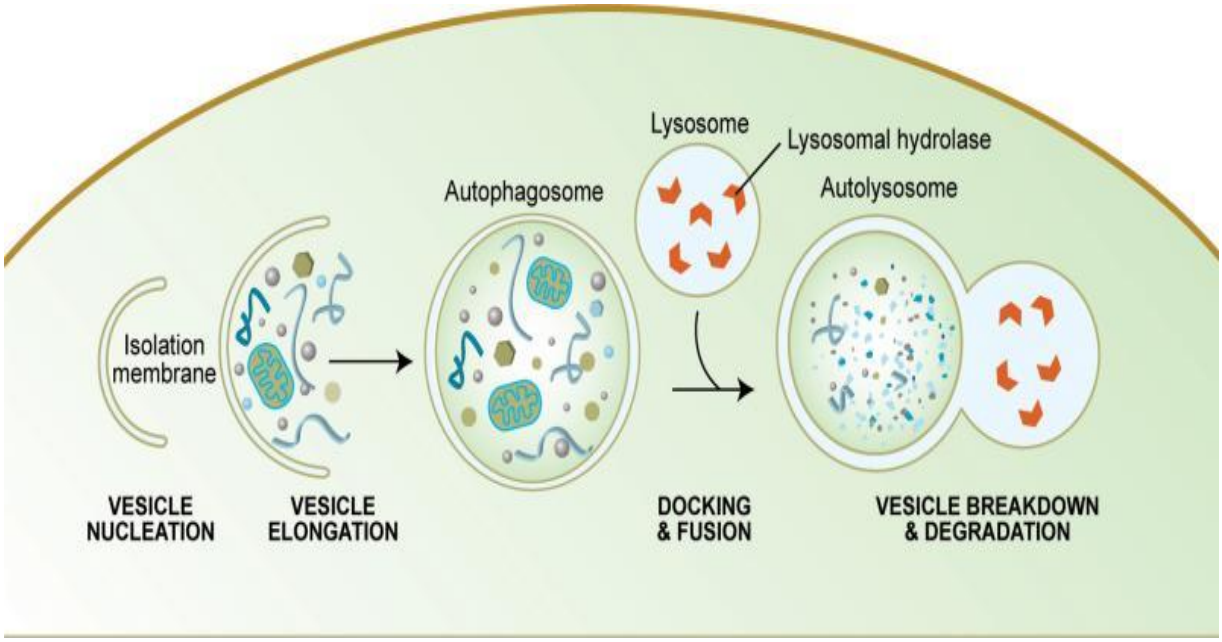

Figure 1.15 The process of autophagy.

The formation of the autophagosome is the initial stage of autophagy. The autophagosome contains cargo destined for degradation. This fuses with the lysosome, which contains lysosomal hydrolases to form an autolysosome where the contents can be degraded and recycled in biogenesis. Image taken from Melendez & Levine[249].

1.4.2 Molecular mechanisms of autophagy

The process of autophagy is regulated by a number of proteins including autophagy-related (ATG) proteins. These are considered to be the core molecular machinery and were originally defined in *S. cerevisaiae* by Tsukada and Ohsumi[250]. Yoshinori Ohsumi won the Nobel Prize in Physiology or Medicine in 2016 for his work on autophagy. Currently, there have been over 41 *ATG* genes identified in yeast, many of which are conserved in mammals and plants. This indicates that autophagy is an evolutionarily conserved mechanism[251]. The mammalian ATGs can be categorised into six functional subgroups: the ULK1 (unc-51-like kinase 1) complex, the PtdIns 3-kinase (PtdIns3K) complexes, the

PtdIns3-phosphate (PtdIns3P), the ATG9 system, the ubiquitin-like ATG12 system and the ubiquitin-like LC3 system[252].

The ULK1 complex plays a role in the initial steps of autophagy. The complex consists of the ULK1, ATG13, FIP200 (focal adhesion kinase family interacting protein of 200 kDa), and ATG101[253]. A key regulator of autophagy through the ULK1 complex, is mTORC1 (mechanistic target of rapamycin complex 1). mTORC1 is one of two forms of mTOR, a serine/threonine kinase. The other form is mTORC2, a complex involved in cell proliferation, migration and the remodelling of the cytoskeleton. In its active state, mTORC1 inhibits autophagy by phosphorylating ULK1 and ATG13. When autophagy is activated by nutrient starvation or alterations in energy and stress levels, mTORC1 is inhibited. When autophagy is induced, mTORC1 is inhibited and ULK1 and ATG13 are rapidly dephosphorylated. mTORC1 can also be inactivated by AMPK (AMP-activated protein kinase) through the phosphorylation of RAPTOR, a protein within the mTORC1[253]. AMPK is also activated by nutrient starvation, a decrease in energy levels and ER stress.

Upon activation, ULK1 phosphorylates and activates key autophagy proteins such as Beclin-1, VPS34 (vacuolar protein sorting 34) and ATG101[254]. There are two PTdIns3K complexes; complex I is involved in autophagy and complex II plays a role in vacuolar protein sorting, cytokinesis, autophagosome maturation and LC3-associated phagocytosis. Complex I consists of VPS34, VPS15, Beclin-1 and ATG4L[255]. This complex is crucial in mediating autophagosome formation and maturation. When Beclin-1 is phosphorylated by ULK1, it interacts with two forms of a PI3K-III complex, which differ depending on whether they contain ATG14L or UV resistance-associated gene (UVRAG). Both complexes are essential in mediating autophagy-related events[256]. Beclin-1 binds to AMBRA1 and UVRAG to mediate autophagosome formation. AMBRA1 binds to the dynein motor complex and tethers the Beclin-1/VPS34 complex to the cytoskeleton. When AMBRA1 is activated, the complex is released and relocates to the ER to initiate autophagosome nucleation[257]. UVRAG interacts with VPS16 to stimulate the activity of GTPase Rab7 and therefore, enhances the rate of membrane fusion. UVRAG is activated by BIF-1 (endophilin B1/Bax-interacting factor) and inhibited by Rubicon. Beclin-1 is also mediated through its interaction with Bcl-2, which mediates the balance between apoptosis and autophagy. Bcl-2 binds to Beclin-1 through its BH3 domain and blocks its ability to interact with the PTdIns3K complex[258].

The exact role and dynamics of PtdIns3P in autophagy remains elusive. It is synthesised by PIK3C3 lipid kinase and becomes phosphorylated at its inositol ring by the PtdIns3K complex during autophagosome formation at the phagophore assembly site (PAS). The levels of PtdIns3P are regulated by lipid kinases and phosphatases. When the levels of PtdIns3P are decreased, ATG proteins are not able to interact with the lipids and, as a consequence, autophagosome formation is inhibited. PtdIns3Ps are also believed to have a potential role in the later stages of autophagy[259]. It interacts with the protein WIPI2, which has a role in positioning the ATG12 conjugation system. Furthermore, PTdIns3P is believed to have a role in the regulation of fusion of the autophagosome with the lysosome[260, 261].

The nucleation phase of the autophagosome is also reliant on the recruitment of the ATG9 protein to the pre-autophagosome structure[262]. ATG9 is the only transmembrane ATG protein and is located in a number of organelle structures including the Golgi apparatus, the plasma membrane and a number of endosome-like structures[263]. Furthermore, it has been shown to be localised near the mitochondria in certain organisms. Zhou *et al*. showed that ULK1 regulates ATG9 through phosphorylation at two sites: Tyr8 and Ser14[264]. The exact function of ATG9 has not yet been determined, but it is likely involved in mediating the expansion of the phagophore[263].

Lastly, the autophagosome formation process also requires two ubiquitin-like conjugation systems mentioned above: the ATG12 system and the LC3 system. The ATG12 system is formed via a series of sequential reactions. ATG7, acts as an E1 enzyme and activates ATG12, allowing its transfer to the E2 enzyme, ATG10. Finally, it is conjugated to ATG5. The ATG12-ATG5 conjugate interacts non-covalently with ATG16 to form a complex that is required for the localisation to PAS[265, 266]. In the case of the LC3 system, LC3 is cleaved by ATG4 to form LC3-I. ATG7 activates LC3-I through its E1-like enzyme activity. This allows its transfer to the E2 enzyme, ATG3. The ATG5-ATG12-ATG16 then acts as an E3 enzyme for the conjugation of LC3 with phosphatidylethanolamine (PE). When conjugated to PE, LC3 is referred to as LC3-II. The LC3-PE conjugate acts to recruit essential autophagic molecular machinery to the phagophore. The conversion of LC3-I to LC3-II is a common marker of autophagy. This can be examined via western blot analysis whereby LC3-I and LC3-II can be observed as two distinct bands. LC3-II, despite being bound to PE has a higher molecular weight, however, due to its enhanced hydrophobicity, LC3-II

migrates faster in SDS-PAGE and therefore, appears to have a lower molecular weight[267, 268]. Notably, LC3-II interacts with the protein p62/SQTM1 to facilitate the degradation of selective cargo by autophagy[269]. p62 is a ubiquitin-binding protein that is used as a reporter of autophagy. It is also known as sequestosome 1 (SQSTM 1) due to its ability to form aggregates. p62 interacts with proteins non-covalently via their ubiquitin-binding domain and anchors them to the LIR (LC3-interacting region) domain with the LC3 protein. p62 itself is degraded by autophagy and therefore serves as a marker for autophagic flux[270].

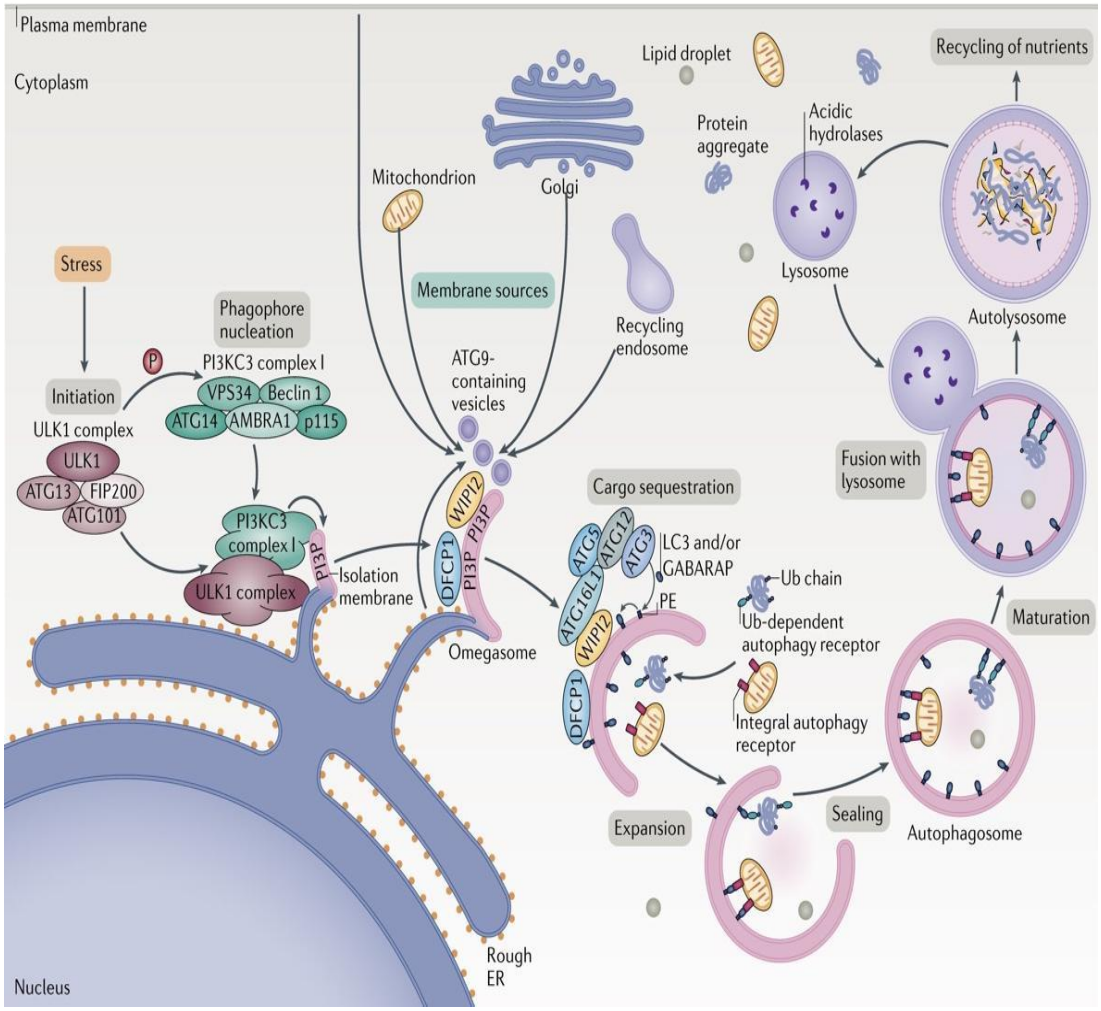

Figure 1.16 The molecular mechanisms underlying mammalian autophagy.

Phagophore nucleation is initiated by the phosphorylation of the PI2KC3 complex 1 by the ULK1 complex. The two ubiquitin-like systems mediate the expansion of the phagophore. ATG7 activates ATG12, which is transferred to ATG10 and conjugated to ATG16. LC3 is located in the autophagosome membrane. LC3-I is converted to LC3-II and is required for the recruitment of autophagic machinery as well as the closure of the autophagosome. Image taken from Dikic & Elazar [271].

1.4.3 Autophagy in cancer

Dysregulation of autophagy is implicated in a number of diseases, one of which is cancer. However, determining its exact role in cancer development and its potential as a therapeutic target is complicated and remains a matter of controversy. This is due to the fact that it has a dual role in tumorigenesis and has been shown to exhibit both anti-tumour and pro-tumour activity depending on the context. Therefore, both the inhibition and enhancement of autophagy have been considered as therapeutic strategies for cancer.

It is believed that at early stages of tumorigenesis, autophagy has a preventative role in cancer. Basal autophagy levels are considered important in cancer suppression due to the removal of cellular components. This also removes sources of reactive oxygen species (ROS)[272]. The protective effect of autophagy against cancer has been linked to autophagic cell death (ACD). ACD is a suggested form of cell death associated with high levels of autophagy that occurs in response to severe stress[273]. This is characterised by the absence of chromatin condensation and a large-scale sequestration of cytoplasmic components. This process remains elusive due to a lack of a specific underlying mechanism and with evidence consisting primarily of morphological observations[274].

However, in advanced cancers, autophagy has been shown to promote tumour cell survival and growth. For this reason, the majority of the studies targeting autophagy in cancer aim to inhibit it. During tumour formation, cancer cells experience hypoxia and nutrient starvation due to their rapidly proliferating nature. Autophagy is believed to be upregulated in response to these conditions to help cancer cells survive. Due to its dual role, autophagy is known as a "double-edged sword" in cancer[275]. Basal levels of autophagy have been shown to be particularly elevated in *KRAS* and *BRAF*-driven tumours to meet the metabolic demands of these tumours[276]. The role of autophagy in MRTs has not been clearly established and studies in this area are limited. Carugo *et al.* showed *SMARCB1*-deficient tumours expressed enhanced autophagic activity through the p53 signalling pathway[155] but further studies are required to delineate the exact role in MRT.

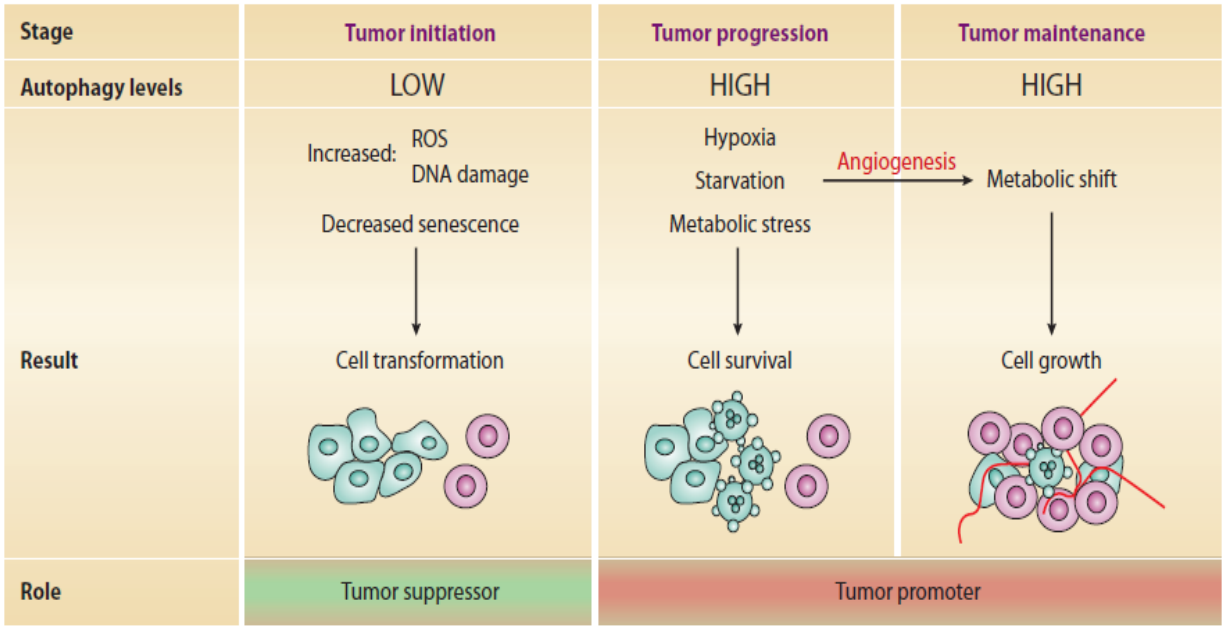

Figure 1.17 The dual role of autophagy in cancer.

Autophagy is referred as a "doubled-edged sword" in cancer. In early stages of tumorigenesis, basal autophagy levels have a preventative role against cancer and protect cells from ROS, DNA damage and undergoing senescence. However, at later stages, autophagy is induced to protect cancer cells from their stressful environment involving hypoxia, starvation and metabolic stress, promoting cell survival and growth. Image taken from Boya & Codogno[277].

1.4.4 Autophagy and chemoresistance

Chemoresistance has become an emerging challenge in oncology. A growing body of evidence points to autophagy as an important factor in chemoresistance. Interestingly, autophagy also appears to exhibit a dual role in response to chemotherapy. Multiple reports indicate elevated levels of autophagy in response to drug treatment[278, 279]. The combination of chemotherapeutic drugs with autophagic inhibitors has been shown to sensitise cancer cells to the chemotherapy in a number of cancers and may represent a potential therapeutic strategy to combat chemoresistance. Lin *et al*. have shown that inhibiting autophagy with the late-stage inhibitors chloroquine, bafilomycin-A1 or the knockdown of ATG7 and ATG12, sensitises human bladder cancer cells to cisplatin-induced apoptosis[280] indicating that autophagy is pro-survival in these circumstances. In colorectal cancer, chloroquine has been shown to enhance the effects of 5-fluorouracil (5-FU) both *in vitro* and *in vivo* [281, 282]. Similarly, in oesophageal cancer chloroquine has improved the efficacy of both cisplatin and 5-FU while in hepatocellular carcinoma

(HCC), inhibition of autophagy enhances the effects of oxaliplatin[283]. In clinical trials, hydroxychloroquine is being tested as a combination treatment with other therapies in a number of cancers, including osteosarcoma, breast cancer and pancreatic cancer. In contrast, there are other reports demonstrating that activation of autophagy may induce cell death in response to chemotherapeutics. Sulfasalazine (SSZ), an inflammatory drug, was shown to induce autophagic cell death via the Akt and ERK pathways in oral cancer cells[284]. In apoptosis-defective human colon cancer cells, autophagic cell death was used as an alternative cell death pathway[285, 286]. Depending on the context, autophagy has therefore been shown to exhibit both pro-survival and pro-death activity. The outcome appears to be dependent on the type of cancer and the type of anti-cancer drug.

Limited studies on the role of autophagy in MRT have been undertaken to date. Notably, Watanabe *et al*. performed *in vitro* and *in vivo* studies in MRT cells with the histone deacetylase (HDAC) inhibitor FK228. This drug was shown to induce both autophagy and apoptosis in MRT cells and inhibition of autophagy through treatment with the autophagy inhibitor chloroquine (CQ) enhanced FK228-induced apoptosis, suggesting autophagy may be a potential anti-cancer target in MRT[287].

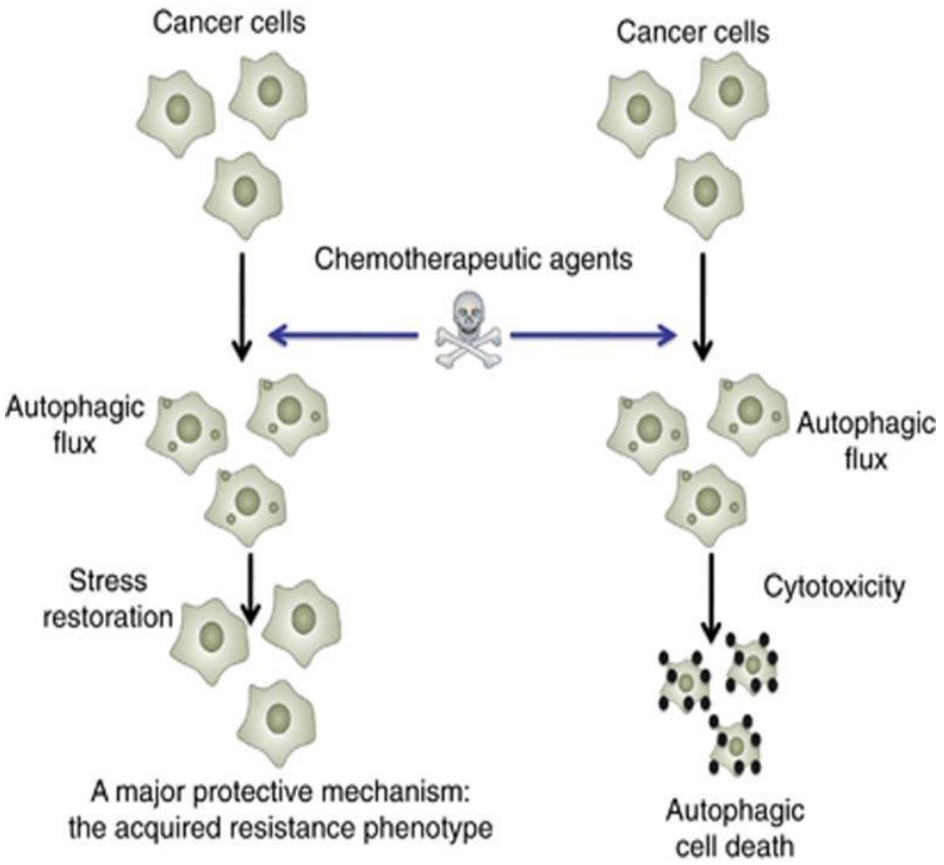

Figure 1.18 Dual role of autophagy in response to chemotherapy

Similar to the dual role of autophagy in cancer, this process also has a paradoxical role in response to cancer therapy. Autophagy is activated in response to chemotherapy to protect cancer cells from stress and help them acquire resistance, making it a potential target to combat chemoresistance. In contrast, autophagic cell death can be triggered in response to chemotherapeutic agents. The role of autophagy is dependent on the cancer type and the treatment. Image taken from Sui *et al* [283].

1.4.5 Autophagy inhibitors

The role of autophagy in cancer outlined above has led to the hypothesis that targeting autophagy may be a promising anti-cancer strategy. The research focuses primarily on autophagy inhibition. For this reason, a number of potential autophagic inhibitors have been developed. However, defining inhibitors with selective activity has been a challenge in the field. Moreover, autophagy is a dynamic process and has proven difficult to quantify. There are two approaches: static analysis of autophagic components at a certain point or alternatively, a measurement of autophagic flux through degradation analysis. Autophagic flux is the preferred method as it is a more accurate approach; however this

still remains complicated[288]. For this reason, it has become a challenge to assess the effect of inhibitors on autophagy. Autophagic inhibitors are classed into two groups; early stage autophagy inhibitors and late stage autophagy inhibitors[289].

Early-stage inhibitors target proteins involved in the initial steps of the autophagic process. These target Pan-PI3Ks, VPS34 inhibitors and ULK inhibitors. Pan-PI3Ks inhibitors include 3-methyladenine (3-MA), wortmannin and LY294002[290]. One of the most commonly used inhibitors, 3-MA, targets VPS34 as well as class I Pan-PI3Ks, which activate the mTOR signalling pathway. Therefore, it appears to inhibit starvation-induced autophagy but enhances autophagic flux after prolonged treatment, in nutrient-rich conditions. Furthermore, it has a low potency and is used at high concentrations (approximately 10 mM), which induces off-target affects. Another challenge presented by this inhibitor is poor solubility[289]. In contrast, wortmannin is a much more potent inhibitor and works at nanomolar concentrations. Wortmannin inhibits the class I PI3Ks and has been reported to exert additional effects on VPS34. Lastly, LY294002 is a synthetic class I PI3K inhibitor but has also presented challenges related to limited potency and off-target effects[289]. In contrast, VPS34 and ULK inhibitors have higher selectivity. VPS34 inhibitors include Spautin-1, which inhibit the ubiquitin-specific peptidases, USP10 and USP13. These peptidases deubiquitinate Beclin-1 thus treatment with Spautin-1 results in the ubiquitination of Beclin-1 and the degradation of the VPS34 complexes. Another commonly used VPS34 inhibitor due to its potency and selective nature, is SAR405, which was identified through chemical optimisation of a screen performed to identify autophagy inhibitors in a relevant physiological environment. SAR405 targets the catalytic activity of the two VPS34 complexes: the ATGL-and UVRAG containing complexes[291]. Lastly, due to its role in autophagosome biogenesis, ULK has become a target of interest in autophagy inhibition. Some of the ULK inhibitors outlined in literature include MRT68921, SBI-0206965 and ULK-101[292].

The late-stage autophagy inhibitors target the final stages of the autophagic process, the degradation of the cargo in the autolysosome. These include acid proteases, vacuolar-type H^+-ATPase inhibitors (V-ATPases) and lysomotropic agents. Cathepsin is involved in the degradation of autophagic material and is the target of the drugs, Pepstatin A and E64d, which inhibit the autophagic flux[289]. V-ATPases are located in the membranes of organelles, including lysosomes and are involved in proton transport across the lysosome

through ATP hydrolysis. This step is essential in maintaining a low pH in the vacuole. Thus, targeting V-ATPases, results in the inhibition of lysosomal hydrolases. The most frequently utilised V-ATPase inhibitor is bafilomycin-A1, which inhibits autophagic flux. Lastly, lysomotropic agents target the acidification of the lysosome, blocking its fusion with the autophagosome. The two principal lysomotropic agents are chloroquine (CQ) and hydroxychloroquine (HCQ). These are the only clinically available autophagy inhibitors as they are used to treat malaria, amongst other diseases. HCQ is an analogue of CQ, which was developed to combat the toxicity challenges observed with the use of CQ[289]. Current research aims to establish whether combination of CQ or HCQ with a standard cancer treatment could represent a novel therapeutic strategy. Preclinical work suggests treatment with these inhibitors can enhance drug-induced apoptosis suggesting they are a promising therapeutic strategy in a number of cancers[293].

1.4.6 Crosstalk between apoptosis and autophagy

Apoptosis and autophagy have been shown to be interconnected at various points of crosstalk[294]. The relationship between these two pathways is a complex one that is not yet fully understood. Characterising the interplay between these cellular processes is critical to develop a full understanding of the molecular background before therapeutically targeting key players of apoptosis and autophagy[295]. The suppression of autophagy has been linked to apoptosis and the inhibition of apoptosis has been shown to both suppress and induce autophagy indicating a very complicated and context-dependent link between the two molecular pathways. Moreover, there are several key proteins that are involved in both autophagy and apoptosis. The anti-apoptotic protein Bcl-2 has been shown to be essential in both apoptosis and autophagy regulation by binding the pro-autophagic protein Beclin 1 to pro-apoptotic proteins such as Bax. Long-term cellular stress can lead to loss in mitochondrial membrane potential resulting in the release of components such as AIF and cytochrome c[295]. Stress induced by starvation due to nutrient depletion results in the release of Beclin 1 which activates autophagy through PI3K signalling. It can also release Bax from Beclin 1 and thus activate apoptosis. The regulation of apoptosis and autophagy through Bcl-2 and Beclin 1 binding is mediated via the localisation of Bcl-2 to the ER or the mitochondria. Thus, damage to the mitochondria is also a key player in determining the

outcome of apoptosis and autophagy activation. The cleavage of autophagic proteins such as Beclin 1 and ATG4 can result in their translocation to the mitochondria where they obtain roles in apoptosis induction. Moreover, cleavage of ATG5 also results in its localisation to the mitochondria where it is able to bind to anti-apoptotic protein Bcl-xL and promote loss of mitochondrial membrane potential and therefore apoptosis[295].

Studies that have focused on the on the interplay between apoptosis and autophagy have determined three types of relationships: antagonism, partnership, and enablement. Antagonism refers to the ability of autophagy to antagonise apoptosis thereby promoting cell integrity and survival. In this case, blocking autophagy would result in increased levels of apoptosis. Partnership refers to the situation where autophagy can facilitate apoptosis without directly triggering cell-death so that apoptosis is autophagy-dependent. The last relationship, enablement, refers to a situation where both apoptosis and autophagy collaboratively induce cell death and autophagy can serve as a back-up cell death mechanism if apoptosis fails[296, 297].

1.5 ROS

Reactive oxygen species (ROS) are natural by-products generated during normal mitochondrial oxidative metabolism. These include the superoxide anion (O_2^-), hydrogen peroxide (H_2O_2) and the hydroxy radical ($HO\cdot$). In addition to this, ROS levels are enhanced by certain stimuli such as UV, heat exposure or cytokines. Collectively, this is known as oxidative stress and results in significant cellular damage.

ROS are primarily generated in the mitochondria in different production sites in redox signalling associated with substrate oxidation and oxidative phosphorylation electron leak. Indeed, 11 sites have been identified to date operating either at the redox potential of $NADH/NAD^+$ or of ubiquinol/ubiquinone whereby electrons are lost to oxygen to produce superoxide or hydrogen peroxide. As electrons flow from one group to another, protons are pumped across the mitochondrial inner membrane driving ATP synthesis. Electrons enter the $NADH/NAD^+$ pool through NAD-linked dehydrogenase. Electrons flow from NADH into the flavin containing site of complex I through the quinone-binding site onwards. Dehydrogenases linked to ubiquinone are implicated in electron flow, particularly complex

II, mitochondrial glycerol-3-phosphate dehydrogenase, the electron-transferring flavoprotein – oxidoreductase system and dihydroorotate dehydrogenase. Complex III and mitochondrial glycerol 3-phosphate dehydrogenase generate superoxide in the mitochondrial matrix as well as outside of the mitochondrial inner membrane. In contrast, the other sites generate superoxide and/or hydrogen peroxide exclusively in the matrix. Cytochrome P450 enzymes and NADH oxidases are also implicated in ROS generation. Aside from the mitochondria, other cellular sources of ROS are peroxisomes which can generate and scavenge ROS thereby regulating redox in cells[560].

Oxidative stress has been implicated in a number of diseases such as neurodegeneration, atherosclerosis, diabetes and cancer. In addition to this, ROS is implicated in a number of cell signalling pathways and transcription factors involved in cell survival mechanisms such as autophagy and apoptosis[298]. These include PI3K/MAPK, Nrf2/Keap1, NF-κB and p53. The activation of p53 by ROS results in the activation of pro-apoptotic Bcl-2 family members, thereby inducing apoptosis. Additionally, ROS also induces apoptosis by causing mitochondrial membrane depolarisation as well as the oxidation of cardiolipin, which results in the release of cytochrome c into the cytosol[299]. There is cross-talk between ER stress and ROS, in a positive feed-forward loop, which has been implicated in a number of human diseases[300]. Moreover, both H_2O_2 and O_2^- induce autophagy. Further crosstalk occurs between autophagy and oxidative stress through p62. A growing body of evidence suggests that ROS is a signal transducer that results in the upregulation of autophagy. This is mediated through the p62/Nrf2/Keap1. As autophagy acts to clear oxidised cellular components, it is an important contributor to the activity of the antioxidant system and DNA damage repair[301].

ROS is believed to be strongly implicated in carcinogenesis. In fact, it is believed to have a dual role as both tumour-suppressing and tumour-promoting activity. Cancer cells have been shown to have elevated ROS levels compared to healthy cells as a consequence of increased metabolic rate, gene mutation and relative hypoxia. During cancer development, ROS is believed to promote cancer survival through tumorigeneses, angiogenesis, invasion and metastasis during a “mild pre-oxidative stress”. However, past a certain threshold, the cell is under oxidative stress. At this stage, if the cell experiences further ROS stimuli due to chemotherapeutic drugs, for instance, it would undergo cell cycle arrest and/or have to

engage its repair systems (such as glutathione). If this fails, the cell will then undergo cell death[302].

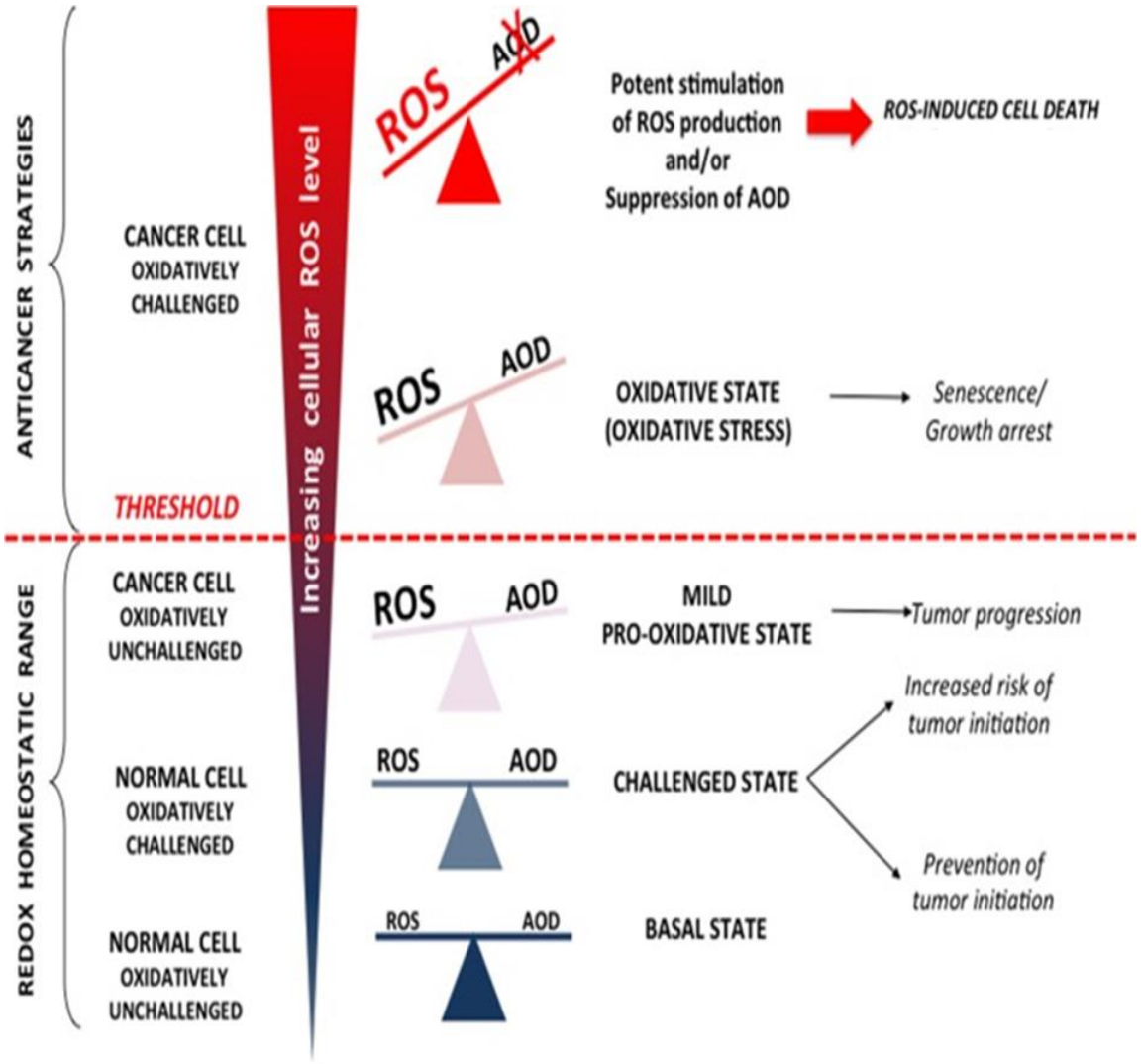

Figure 1.19 The balance of ROS in cancer

The role of reactive oxygen species or ROS in cancer can be described as a "double-edged sword". Normal cells have basal levels of ROS which are kept in balance with the antioxidant defence system. An enhancement of basal ROS levels may present a risk factor for cancer development. Cancer cells are found to have higher ROS levels than healthy cells due to their altered metabolic state. However, high ROS levels can lead to cell damage and cell death. This can be induced by a number of external stimuli such as chemotherapeutic agents. Image taken from Vucetic *et al*[303].

1.5.1 Nrf2

The nuclear factor erythroid 2-related factor 2 (Nrf2) is a basic leucine zipper (bZIP) transcription factor that regulates the expression of a number of antioxidant proteins, protecting the cell from oxidative stress. These include heme oxygenase-1 (HO-1), NADH quinone oxidoreductase 1 (NQO1), the glutamate cysteine ligase catalytic subunit (GCLC) and thioredoxin reductase 1 (TXRD1)[304]. Under basal conditions, Nrf2 is localised to the cytosol where it interacts with its negative regulator, Keap1, which suppresses its activity by promoting its degradation via the ubiquitin proteasome pathway. When the thiol groups on Keap1 becomes exposed to oxidative stress, critical cysteine residues present on the Keap1 protein become oxidised leading to a confirmational change in the Nrf2/Keap1 complex leading to the inactivation of Keap1 and stabilisation of Nrf2. As a consequence, Nrf2 dissociates from Keap1 and translocates to the nucleus where it heterodimerises with small Maf proteins (sMaf) and binds to the antioxidant response elements (AREs) located in the promoter of Nrf2 target genes. This leads to the transcription of a number of genes involved in the expression of antioxidant proteins (as described above), the synthesis of glutathione and other stress response proteins.

Aside from the Keap1-dependent pathway, Nrf2 is also regulated by phosphorylation; a process that is catalysed by glycogen synthase-3 kinase (GSK-3). This leads to degradation of Nrf2 by β-transducin repeat containing protein (β-TrCP)[305].

Cancer cells eliminate Keap1-dependent regulation of Nrf2 to enhance protective antioxidant activity. Mutations in the *Keap1* gene have been observed in a number of cancers, including colon, ovarian, breast and prostate cancer. Indeed, the upregulation of Nrf2 in cancer cells has been implicated in cell proliferation, chemoresistance and protection from oxidative stress. Nrf2 has also been shown to increase metabolism thereby facilitating cellular proliferation[306]. Nrf2 protects cancer cells from apoptosis through the increased transcription of antioxidant genes that can suppress the effects of apoptotic signalling pathways. Of note, Keap1 has been reported to bind to the BH2 domain of the anti-apoptotic protein, Bcl-2. This facilitates the degradation of Bcl-2 and enhances apoptosis. In contrast, antioxidants as well as mutations in Keap1 binding sites can disrupt this interaction. Nrf2 has been associated to the upregulation of multidrug-resistant efflux

pumps (ABCG2) and multidrug resistance proteins[306] again implicating Nrf2 in chemoresistance.

HO-1 is considered to be one of the key effectors of Nrf2 activity and plays a key role in cellular homeostasis. However, HO-1 along with Nrf2 has been implicated in tumorigenesis and has been found to be frequently elevated in a number of tumours. Although its exact role in cancer remains elusive, HO-1 expression correlates with tumour metastasis, aggressiveness and poor prognosis. Moreover, the activation of both Nrf2 and HO-1 has been linked to resistance to chemotherapy, for example, to cisplatin in ovarian cells and to doxorubicin in breast cancer cells. Therefore, the Nrf2/HO-1 axis has been considered a promising therapeutic target to combat chemoresistance[307]. A number of inhibition strategies have been considered to target Nrf2 and HO-1. These include zinc (II) protoporphyrin IX (ZnPPIX), a HO-1 inhibitor that has been shown to reduce a number of cancers in mice, including lung cancer and gastric cancer[308, 309]. The flavonoid luteolin is also a Nrf2 inhibitor that has been shown to sensitise human lung carcinoma cells to drug treatment. Additionally, ML385 is a specific small-molecule Nrf2 inhibitor that has been shown to promote the anti-cancer effect of carboplatin in lung cancer cells[310]. Another Nrf2 inhibitor, brusatol, has shown promising anti-cancer effects in pancreatic cancer cells by enhancing the chemotherapeutic effect of gemcitabine. Moreover, it has been shown to enhance the cytotoxic effects of cisplatin in A549 lung cancer cells. Thus, it is possible that pharmacological inhibition of the Nrf2/HO-1 axis may represent a promising strategy in combatting drug resistance.

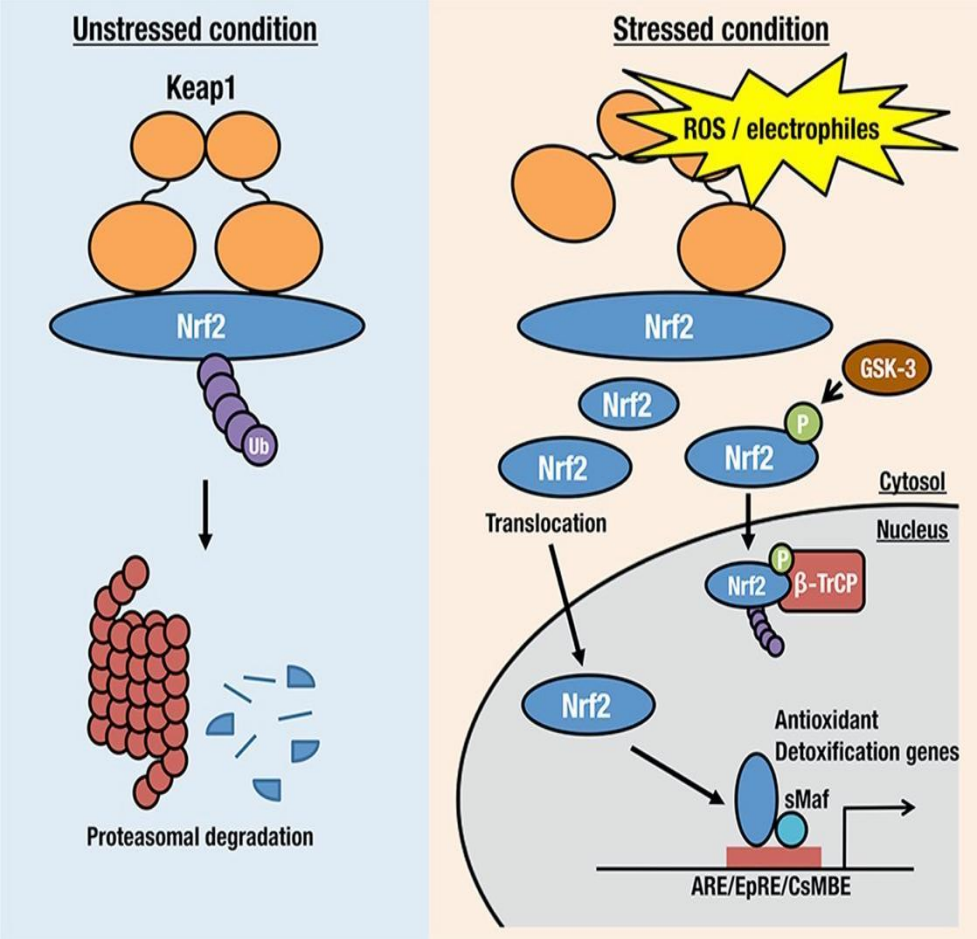

Figure 1.20 Regulation of Nrf2.

Nrf2 is regulated by forming a complex with Keap1. This results in polyubiquitination of Nrf2 and its subsequent degradation by the proteasome. In response to ROS, Nrf2 dissociates from Keap1 and translocates to the nucleus, where it binds to ARE through Maf. This leads to the transcription of antioxidant and detoxification genes. In addition, Nrf2 is also regulated through phosphorylation by GSK-3 leading to the recruitment β-TrCP. This causes the ubiquitination and degradation of Nrf2 within the nucleus. Image taken from Suzuki *et al*[305].

1.5.2 Glutathione (GSH)

One of the main regulators of ROS homeostasis is the antioxidant glutathione (GSH). GSH is a thiol-containing tripeptide consisting of glutamic acid, cysteine and glycine. It is the most abundant antioxidant in eukaryotic cells and exists in two forms: the reduced form, which constitute the vast majority of GSH in the cell and the oxidised form (GSSG), which accounts for less than 1% of overall glutathione levels. Most GSH (approximately 90%) is

distributed within the cytosol; the remaining GSH is located within the mitochondria (approximately 10%) and a small amount is found within the ER (approximately 1%)[311]. GSH is synthesised in two steps: the first (rate-limiting) step involves the ligation of cysteine to glutamate to form γ-glutamylcysteine and is catalysed by the enzyme glutamate cysteine ligase (GCL). This is then combined with glycine to form GSH and this second step is catalysed by the enzyme GSH synthase[312]. Interestingly, the levels of GCL are regulated by Nrf2. . GSSG is recycled back to GSH by glutathione reductase (GR) which requires the cofactor nicotinamide adenine dinucleotide phosphate (NADPH) to form a redox cycle. Cells dependent on NADPH to be generated by the pentose phosphate pathway[313].

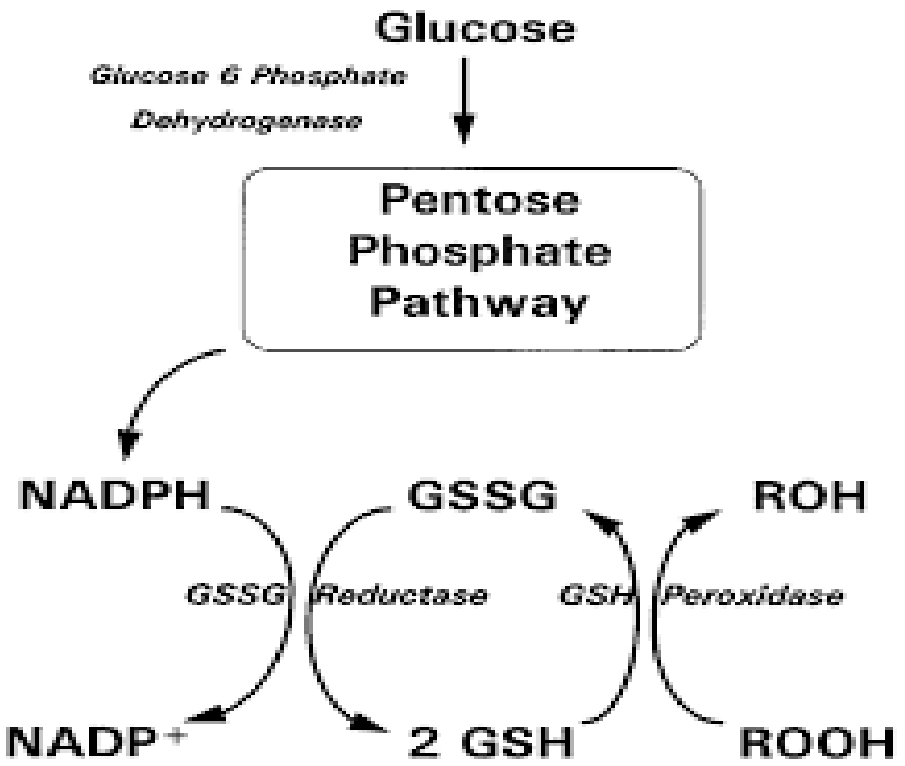

Figure 1.21 Glutathione redox cycle

Oxidized glutathione to be reduced by glutathione reductase using NADPH generated in the pentose phosphate pathway.

Like Nrf2 and HO-1, GSH has been observed to be particularly elevated in different tumour types and has been associated with the promotion of cell proliferation. Moreover, tumours displaying high levels of GSH have been shown to exhibit greater drug resistance. Depleted GSH levels leads to increased ROS levels, which induces apoptotic cell death.

Therefore, inhibiting GSH production is a potential strategy to promote apoptosis in malignant cells[314]. A commonly used GSH inhibitor is buthionine sulfoximine (BSO), which acts by targeting the enzyme GCL, thus depleting GSH levels. Lee *et al.* have shown that treatment of human stomach and ovarian cancer cells with BSO enhanced the cytotoxic effects of cisplatin, carboplatin and radiation[315]. Qiwei *et al.* also showed that BSO treatment enhanced cisplatin-induced apoptosis in biliary tract cancer cells. Interestingly, in MRT, the cisplatin-resistant BT16 cell line has been shown to have significantly elevated levels of GSH in comparison to the cisplatin-sensitive BT12 cell line. Treatment with acetaminophen (AAP), which depletes GSH, potentiated cisplatin-induced apoptosis in BT16 cells, but not in BT12 cells[316]. This indicates that glutathione levels may be linked to chemoresistance in MRT, but further studies are required to substantiate this.

In conclusion, enhanced antioxidant systems, such as glutathione and Nrf2, have been frequently found in chemoresistant cell lines, suggesting that cancer cells can overcome the cytotoxic effect of drugs by counteracting drug-induced ROS. Therefore, targeting these antioxidant systems has been proposed as a valuable strategy to reduce chemoresistance. Indeed, several studies are currently underway investigating the beneficial effects of targeting glutathione and Nrf2 to increase the sensitivity of cancer cells to chemotherapy[317-319].

1.6 Project aims.

MRT is a rare and aggressive paediatric malignancy with very poor prognosis that typically occurs in infants under the age of three. The young age of patients combined with the aggressive and metastatic nature of these tumours greatly restricts treatment options. Moreover, chemoresistance has arisen as a major challenge in the treatment of these tumours. Therefore, understanding the mechanisms that underlie chemoresistance in MRTs is essential to further develop more successful treatment plans for patients. The overall aim of this project is to evaluate some of the cellular processes underlying chemoresistance in MRT and to identify novel therapeutic strategies to combat chemoresistance.

In particular, the objectives of this project are;

1) To investigate cell death mechanisms induced in MRT in response to a representative MRT chemotherapeutic, cisplatin. Specifically, the role of autophagy in MRT as a pro-death or pro-survival mechanism will be studied to evaluate the potential of targeting autophagy therapeutically in MRT.
2) To determine the role of the Nrf2/GSH antioxidant system in mediating cisplatin resistance in MRT and whether it can provide a novel therapeutic avenue for MRT treatment.
3) To examine the role of anti-apoptotic Bcl-2 proteins in mediating chemoresistance in MRT and to evaluate any synergistic effect of combining the selective Bcl-2 inhibitor ABT-199 with cisplatin.

Overall, this study aims to uncover the molecular mechanisms underlying chemoresistance in MRT and whether they may be considered in the design of novel therapeutics for this malignancy.

2. Materials and Methods

2.1 Materials and suppliers

Materials	Suppliers
ABT-199 (Venetoclax)	Selleck Chemicals
Acrylamide	Ultra Pure
Alamar Blue	Life Technologies
Ammonium Persulfate	Sigma-Aldrich
Annexin V-FITC	iQ Products
Antimycin A	Sigma-Aldrich
Anti-Atg5	Cell Signalling
Anti-Atg7	Cell Signalling
Anti-Bak	Millipore
Anti-Bax	Cell Signalling
Anti-Bcl-2	Calbiochem
Anti-BcL-xL	BD Pharminogen
Anti-Beclin	Cell Signalling
Anti-Bid	Cell Signalling
Anti-Bim	Cell Signalling
Anti-Caspase 3	Cell Signalling
Anti-cFLIP	Millipore
Anti-cIAP1/2	Cell Signalling
Anti-Cleaved Caspase 3	Cell Signalling
Anti-GAPDH	Calbiochem
Anti-JNK (total)	Cell Signalling
Anti-JNK (phospho)	Cell Signalling
Anti-LC3-I/LC3-II	Cell Signalling
Anti-Mcl-1	Cell Signalling
Anti-Mouse	Promega

Anti-Noxa	Cell Signalling
Anti-Nrf2	Cell Signalling
Anti-p38 (total)	Cell Signalling
Anti-phospho-p38	Cell Signalling
Anti-p62	Abcam
Anti-Rabbit	Promega
Anti-Tubulin	Novus Biologicals
Anti-XIAP	Cell Signalling
Bafilomycin-A1	Sigma Aldrich
BCA protein reagents A and B	Pierce
Bortezomib	Selleck Chemicals
BSA protein standards	Pierce
Calcium chloride	Sigma-Aldrich
Cell Culture plastics	Cruinn
Chloroquine	Enzo Life Sciences
Cis-diammine platinum (II) dichloride	Sigma-Aldrich
Complete Ultra Protease Inhibitor Tablets	Roche
Cryogenic Tubes	Nalene
Cyto-ID® Autophagy Detection Kit	Enzo Life Sciences
Dichloro-dihydro-fluorescein diacetate (DCFH-DA)	Sigma-Aldrich
DMEM	Gibco
DMSO	Sigma-Aldrich
Dithiothreitol (DTT)	Sigma-Aldrich
Earle's Balanced Salt Solution	Sigma-Aldrich
ECL detection kit	Pierce
FCCP	Agilent
Foetal Bovine Serum	Sigma-Aldrich

Filter paper	Whatman
Glycerol	Sigma-Aldrich
Glycine	Sigma-Aldrich
GSH/GSSG-Glo Kit	Promega
Hepes	Sigma-Aldrich
Hydrogen peroxide (H_2O_2)	Sigma-Aldrich
Isopropanol	Sigma-Aldrich
Lipofectamine 2000	Invitrogen
Methanol	Lennox
MitoSOX	Thermofischer
ML385	Sigma-Aldrich
N-acetylcysteine	Sigma-Aldrich
N-ethylmaleimide	Promega
Non-fat dried milk	Marvel
Oligomycin	Agilent
ON-target plus non-targeting pool siRNA	Dharmacon
ON-target plus ATG5 siRNA	Dharmacon
ON-target plus Nrf2 siRNA	Dharmacon
Opti-MEM	Biosciene
PageRuler™ Plus Prestained Protein Ladder	Thermo Scientific
PBS	Gibco
PBS Tablets	Sigma-Aldrich
Penicillin-streptomycin	Sigma-Aldrich
Phosphatase Inhibitor Cocktails 2 and 3	Sigma-Aldrich
Propidium Iodide	Sigma-Aldrich
Protogel	Sigma-Aldrich
PVDF	Millipore

Rapamycin	Enzo Life Sciences
Ripa Lysis Buffer	Sigma-Aldrich
RPMI-1640	Biosciences
Rotenone	Agilent
SAR405	APExBIO
SB203580	Selleck Chemicals
SDS	Sigma-Aldrich
Seahorse plates	Agilent
Sodium chloride	Sigma-Aldrich
TEMED	Sigma Aldrich
Trizma base	Sigma-Aldrich
TrypLE Reagent	Gibco
Tween-20	Sigma Aldrich
Z-VAD-fmk	Calbiochem

All sterile tissue culture flasks, pipettes, plates, pipette tips and universal tubes were from Greiner Bio-one Ltd. The Sorvall T436 centrifuge was used to centrifuge falcon tubes and the Eppendorf® Refrigerated Microcentrifuge model 5417R was used to centrifuge 1.5 mL Eppendorf tubes. BT12, BT16 and G401 MRT cell lines were a kind gift from Prof Maureen O'Sullivan in the National Children's Research Centre, Crumlin, Dublin.

2.2 Contact details of distributors

Brennan Co: Stillorgan Industrial Park, Dublin Ireland
enquiries@brennanco.ie

Calbiochem: La Jolla, California 92-39-2087, U.S.A
CUSTOMER.SERVICE@MERCKBIOSCIENCES.CO.UK

Cell Signalling Technology: 3 Trask Lane, Denvers, Massachusetts 09123, U.S.A.
enquiries@brennanco.ie

Cruinn Diagnostics Ltd: 5b/6b Hume Centre, Park West Industrial Estate, Dublin 12, Ireland
info@cruinn.ie

GraphPad Software Inc: 2236 Avendia de la Playa, La Jolla, California 90237, U.S.A.
sales@graphpad.com

Greiner Bio-One-Ltd: Brunel Way, Stroudwater Business Park, Stonehouse, Gloustershire L10 3SX, U.K.
orders@cruinn.ie

Millipore: Tullagreen, Carrigtwohill, Co.Cork, Ireland
eiorders@europe.sial.com

MyBio: Kilkenny Research and Innovation Centre, Kilkenny, Ireland
info@mybio.ie

Biosciences: 3 Charlemont Terrace, Crofton Road, Dun Laoghaire, Co Dublin, A96 K7H7, Ireland
info@biosciences.ie

Pierce Biotechnology Ltd: P.O Box 117, Rockford, Illinois 61105, U.S.A.
info@medical-supply.ie

R&D Systems: 19 Barton Lane, Abingdon Science Park, OX14 3NB, U.K.
info@RnDSystems.co.uk

Roche Diagnostics Ltd.: Burgess Hill, West Sussex, RH159RY, U.K.
burgesshill.ras.@roche.com

Sigma-Aldrich Ireland Ltd: Vale Road, Arklow, Wicklow, Ireland

EIRCustsupport@sial.com

Tocris: Tocris House, IO Centre, Moorend Farm Avenue, Bristol BS11 0QL, U.K.
info@tocris.ie

VWR: Northwest Business Park, Dublin 15, Ireland
sales@ie.vwr.com

Abcam: 330 Cambridge Science Park, Cambridge, CB4 0FL, UK
orders@abcam.com

2.3 Cell culture

The BT12 cell line was obtained from a solid tumour in the posterior cranial fossa of a 2-month-old female AT/RT patient. The cells have a branched appearance and grow in an adherent manner. The BT16 cell line was also derived from the brain of the AT/RT patient, a 2-year-old male. The cells have a clumped and rounded morphology and are adherent. The cell lines were generously donated by Dr Peter Houghton from The Nationwide Children's Hospital, Columbus, OH, U.S. The G401 cell line was derived from a 3-month-old male patient who was originally misdiagnosed with Wilms Tumour, but it was later identified to be a kidney rhabdoid tumour cell line by Garvin *et al*[320]. G401 cells are slightly elongated and form an adherent monolayer but have a tendency to grow in a mixed cell culture, with a small percentage of the cells growing in suspension. BT12 cells are considered to be sensitive to cisplatin in literature in comparison to the BT16 and G401 cell lines, which exhibit greater cisplatin resistance[316, 321].

2.3.1 Cell maintenance

BT12 and BT16 cells were grown in Roswell Park Memorial Institute (RPMI) medium + GlutaMAX™ supplemented with 10% (v/v) Foetal Bovine Serum (FBS) and 1% (v/v) PenStrep (100units/ml penicillin, 100mg/ml streptomycin). G401 cells were grown in Dulbecco's modified Eagles (DMEM) GlutaMAX™ also supplemented with 10% (v/v) Foetal Bovine Serum (FBS) and 1% (v/v) PenStrep (100units/ml penicillin, 100mg/ml streptomycin).

The three cell lines were grown in a 75 cm^2 flask and sub-cultured approximately twice a week at 70% confluency. To passage the cells, media was removed from the flask and washed with 3 mL of Phosphate Buffered Saline (PBS). PBS was removed and TrypLE Express was added to the cells. The cells were then incubated at 37°C in TrypLE Express for the time necessary for them to detach. Once the cells were detached, complete media was added to the flask to neutralise TrypLE Express, and the contents of the flask were transferred to a falcon tube and centrifuged at 300 x g for 5 minutes. The pellet was resuspended in fresh media and the cells were then transferred into a new flask and with fresh media.

2.3.2 Cryopreservation

Multiple stocks of cells were frozen and stored in liquid nitrogen at -196°C. To prepare cells for freezing, they were grown in 75cm^2 flasks until they were approximately 70-80% confluent. At this point, they were detached and centrifuged at 300g for 5 minutes. The pellet was resuspended in freezing solution, consisting of 90% (v/v) FBS and 10% (v/v) dimethyl sulfoxide (DMSO). The cells were then transferred into 1mL aliquots and stored in cryotubes. The tubes were then placed in Mr. Frosty freezing containers filled with isopropanol and stored at -80°C for a day before being transferred to liquid nitrogen tanks.

To recover cells, a cryotube was removed from the liquid nitrogen tank and placed in a water bath at 37°C for 1 minute to thaw the cells. The cells were pipetted up and down and transferred into a falcon tube containing 9mL of fresh growth media. This was centrifuged at 300g for 5 minutes. The supernatant was discarded, thereby removing any traces of freezing solution, and the pellet was resuspended in fresh media. The cells were transferred to a 25cm^2 flask and diluted in media. The following day the media was removed and replaced with fresh media. After 2-3 passages, the cells were ready for experimentation.

2.3.3 Cell counting

Cells were detached and centrifuged as described above. The supernatant was discarded, and the pellet was resuspended in fresh media. The cells were diluted 1:10 by adding 10 ⌈l of cells to 90⌈l of fresh media in an Eppendorf tube. A bright light haemocytometer was cleaned with ethanol prior to use. A cover slip was moistened and placed over the haemocytometer to create a 0.1 mm high chamber. Therefore, the volume in each of the 9 squares in the haemocytometer was 1 x 10^{-4} mL (1 x 1 x 0.1 mm).

A 10µl aliquot was pipetted in between a cover slip and a bright light haemocytometer. The average cell number per square was determined, multiplied by the dilution factor and by 10^4 to calculate the number of cells per mL. The number of cells required for each experiment was divided by the amount of cells that were counted to determine by how much to dilute the cells.

2.4 Preparation of stock solutions of drugs and inhibitors

2.4.1 Cisplatin

8 mg of cisplatin (cis-diammine platinium (II) dichloride) was dissolved in 13.33 mL of 0.9% (w/v) NaCl to give a 2 mM stock. This was then aliquoted and stored at -20°C. The cisplatin aliquots were protected from light. Working solutions were prepared by using 0.9% (w/v) NaCl to make up the following concentrations: 50, 80, 100, 200, 500 and 1000 μM.

2.4.2 Chloroquine

Lyophilised chloroquine was provided by the CYTO-ID® Autophagy Detection kit. 7.5 μmoles of chloroquine was reconstituted in 125 μL of deionised H_2O to give a 60 mM stock solution. This was aliquoted and stored at -20°C. The working solutions of chloroquine were prepared on the day by using deionised H_2O to make up a concentration of 1 mM.

2.4.3 Rapamycin

Lyophilised rapamycin was also provided by the CYTO-ID® Autophagy Detection kit. The kit supplied 25 nmoles, which were resuspended in 50 μL of DMSO to give a stock solution of 500 μM. This was aliquoted and stored at -20°C. The working solutions were prepared on the day using sterile PBS and the cells were treated with a final concentration of 0.5 μM of rapamycin and a final concentration of 0.1% (v/v) DMSO.

2.4.4 Bafilomycin-A1

10 μg of bafilomycin-A1 was dissolved in 160 μL of DMSO to give a 100 μM stock solution. The bafilomycin-A1 stock solution was aliquoted and stored at -20°C. The working solution was prepared on the day using sterile PBS and the cells were treated with 2.5 nM bafilomycin-A1 and a final concentration of 0.1% (v/v) DMSO.

2.4.5 SAR405

5 mg of SAR405 was dissolved in 922 μL of DMSO to make 20 mM stock solution. The stock solution was stored at 4°C. Working solutions were prepared on the day. The cells were treated with varying concentrations of SAR405 and with a final concentration of 0.1% (v/v) DMSO.

2.4.6 Z-VAD-fmk

1 mg of Z-VAD-fmk (caspase inhibitor I) was dissolved in 42.7 µL DMSO to give a 50 mM stock (stored at -20ºC). Dilutions were prepared fresh on the day in sterile PBS with a final concentration of 0.1% (v/v) DMSO applied to the cells.

2.4.7 N-acetylcysteine

A stock solution of 100 mM NAC was prepared in water. The pH of the stock solution was adjusted to approximately 7 using NaOH and was then filtered using sterile syringe filters with 0.2 µm pore size to prevent bacterial contamination. The NAC solution was stored at 4ºC for a maximum of 3 months. Working concentrations of NAC were prepared using dH_2O.

2.4.8 H_2O_2

H_2O_2 was made up to a 50 mM solution in sterile H_2O. The stock solution of H_2O_2 was stored at 4ºC. A working solution was prepared on the day and cells were treated with 100 µM of H_2O_2 for an hour.

2.4.9 Menadione

Menadione was made up to a 25 mM solution in DMSO. The stock of menadione was stored at 4ºC. A working solution was prepared on the day and with a final concentration of 0.1% (v/v) DMSO in the cells.

2.4.10 Antimycin A

Antimycin A was made up to a 10 mM stock solution in DMSO. The stock solution was stored at -20ºC. Working concentrations were made up on the day with a final concentration of 0.1% (v/v) DMSO in the cells.

2.4.11 FCCP

FCCP was made up to a 100 µM stock solution in DMSO. The stock solution was stored at -20ºC. Working concentrations were made up on the day with a final concentration of 0.1% (v/v) DMSO in the cells.

2.4.12 Rotenone

Rotenone was made up to a 50 µM stock solution in DMSO. The stock solution was stored at -20ºC. Working concentrations were made up on the day with a final concentration of 0.1% (v/v) DMSO in the cells.

2.4.13 Oligomycin

Oligomycin was made up to a 100 µM stock solution in DMSO. The stock solution was stored at -20ºC. Working concentrations were made up on the day with a final concentration of 0.1% (v/v) DMSO in the cells.

2.4.14 Buthionine Sulfoximine

Buthionine sulfoximine (BSO) was prepared in a 20 mM stock solution in H_2O. The working concentrations were made from the stock solution. The principal stock solution was stored at -20ºC.

2.4.15 ML385

A stock solution of 50mM ML385 was prepared by dissolving 5 mg in 200 µL DMSO (stored at -20ºC). Dilutions were prepared fresh on the day using PBS to dilute the stock concentration to make working concentrations. DMSO was applied to the cells at a final concentration of 0.1% (v/v).

2.4.16 Venetoclax (ABT-199)

Venetoclax/ABT-199 was prepared in a 50 mM stock solution in DMSO. The stocks were aliquoted and stored at -80ºC to avoid freeze/thawing. Working concentrations were prepared from the stock. DMSO was applied to the cells at a final concentration of 0.5% (v/v).

2.4.17 Navitoclax (ABT-263)

Navitoclax/ABT-263 was prepared in a 50 mM stock solution in DMSO. The stocks were aliquoted and stored at -80ºC to avoid freeze/thawing. Working concentrations were prepared from the stock. DMSO was applied to the cells at a final concentration of 0.5% (v/v).

2.4.18 Bortezomib

Bortezomib was made up to a 10 mM stock solution in DMSO. The stock was aliquoted and stored at -80ºC to avoid freeze/ thawing cycles. Working concentrations were prepared from the stock fresh on the day. DMSO was applied to the cells at a final concentration of 0.1% (v/v) DMSO.

2.5 Cell viability assay

The Alamar Blue cell viability assay was used to determine the effects of cisplatin on BT12, BT16 and G401 cell lines. The Alamar Blue reagent is a non-toxic, REDOX indicator that is soluble. The assay is based on the reduction of active ingredient; a blue and non-fluorescent dye resazurin (7-hydroxy-3H-phenoxazin-3-one 1-oxide) to resorufin, a pink and highly fluorescent dye[322]. This reduction reaction occurs in the presence of viable cells due to the natural reductive environment. Cells that are dying and unhealthy therefore exhibit a weaker reducing environment and this colour change is not observed. The assay allows for a quantifiable method to determine cell viability through colorimetric and fluorometric detection.

In order to determine the effect of cisplatin in BT12, BT16 and G401 cell lines, the cells were seeded at a density of 10,000 cells/well for BT12 and BT16 cells and 5000 cells/ well for G401 cells into a 96-well plate. The final volume in each well was 200 μL. These were left to adhere overnight at 37°C after which they were treated in triplicate with a range of concentrations of the relevant drug by adding 2 μL of stock solution into each well. The cells were then left for the indicated incubation times. 20 μL of Alamar Blue was added to the wells 5 hours prior to measuring the fluorescence, resulting in a final concentration of 10% (v/v) of the dye. These were left to incubate in the dark after which the fluorescence was read using a Softmax Gemini EM Microplate Reader with SOFTmax Pro version 4.9 at an excitation wavelength of 544 nm and an emission wavelength of 590 nm. Media was used as a blank to normalise the values and the vehicle treated cells were set to represent 100% viability so that the cisplatin-treated cells could be expressed as a percentage of the vehicle control. Dose response curves were plotted using Prism GraphPad version 5.0.

2.6 Flow cytometric analysis

2.6.1 Apoptosis analysis

Annexin V-Fluorescein Isothiocyanate (FITC) and propidium iodide (PI) staining was used to analyse apoptosis levels in BT12, BT16 and G401 cells in response to drug treatment. This apoptosis assay relies on the ability of Annexin V, a Ca^{2+} -dependent phospholipid binding protein, to bind with a high affinity to phosphatidyl serine (PS), a membrane phospholipid. PS is located in the inner membrane but, in the early stages of apoptosis, it translocates to the outer membrane where Annexin V can access it and bind to it[323]. Annexin V is bound to the fluorochrome FITC. PI is a red fluorescent dye which binds DNA and is unable to permeate membranes. Therefore, it is only capable of binding to cells in late stages of apoptosis that have lost their membrane integrity. Cells in early stages of apoptosis will only stain positive for annexin V and not for PI as their membranes are still intact whereas cells in later stages of apoptosis or necrosis will stain positive for both Annexin V and PI[324].

2mL of MRT cells were seeded in 6-well plates and left to adhere overnight. BT12 and BT16 cells were seeded at 1 x 10^5 cells/mL and G401 cells were seeded at 5 x 10^4 cells/mL. The following day they were treated and left to incubate for the required time. Following the incubation period, the media in the wells, containing floating cells, was transferred to labelled falcon tubes. The remaining cells were detached using TrypLE Express and the detached cells were added to the falcon tubes and the contents were then centrifuged at 300g for 5 min. The supernatants were discarded, and the pellets were washed with 500 μL of 20X Annexin V binding buffer (0.1 M HEPES, 1.4 M NaCl, 25 mM $CaCl_2$ pH 7.4), diluted with PBS to give a 1X solution. The samples were centrifuged at 600g for 5 minutes at 4°C and the pellets were resuspended in 50 μL of Annexin V-FITC (diluted 1:33.3 in binding buffer). These were left on ice to incubate in the dark for 25 minutes. After the incubation period, 500 μL of binding buffer was added to the samples which were subsequently centrifuged (600g, 5 min, 4°C). The pellets were resuspended in 300 μL of PI (1mg/mL diluted 1:2000 in binding buffer). The samples

were then analysed immediately by flow cytometry. The BD Accuri C6 flow cytometer using BD Accuri C6 software was used for the analysis. Annexin V (455 nm) was detected on the 530/30 bandpass filter (FL1 channel) and PI (535 nm) was detected using the 585/40 bandpass filter (FL2 channel). Single stained vehicles were used as compensation controls (Figure 2.1).

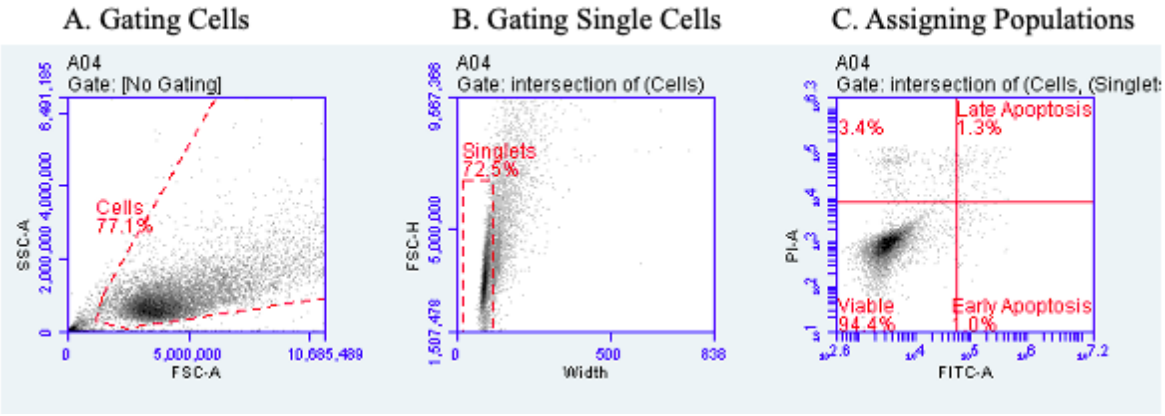

Figure 2.1 Gating strategy for Annexin V/PI flow cytometric analysis

BT12 cells were treated with the vehicle and then stained with Annexin V-FITC and PI. They were analysed using the BD Accuri flow cytometer. Unstained and singled stained vehicles were run and used as compensation controls (not shown). Forward scatter area (FSC-A) was plotted against side scatter area (FSC-A) on a dot plot and gated to exclude any debris from the cell population **(A)**. This was further analysed on another dot plot where width was plotted against forward scatter height (FSC-H) and this was gated to include singlets and exclude doublets as well as clumped cells **(B)**. This population of singlets was analysed to a greater extent using a dot plot in which PI-area (PI-A) was plotted against FITC-area (FITC-A). Cell populations were assigned as viable for Annexin V-/PI-, early apoptotic for Annexin V+/PI- or late apoptotic Annexin V+/PI+ **(C)**.

2.6.2 Autophagic analysis

The Cyto-ID Autophagy Detection Kit was used to quantitatively evaluate autophagic activity in BT12, BT16 and G401 cells. The kit supplied a CYTO-ID Green Detection Reagent, a green dye that becomes highly fluorescent in autophagic vesicles and can be detected by flow cytometry at an excitation wavelength of 488 nm[325]. Therefore, the higher the number of autophagic vesicles, the stronger the signal that is detected. This assay

represents a specific and quantitative approach for monitoring autophagy induction in live cells.

2mL of MRT cells were seeded in 6-well plates at their optimum seeding densities. BT12 and BT16 cells were seeded at 1 x 10^5 cells/mL and G401 cells were seeded at 5 x 10^4 cells/mL. They were left overnight to adhere to the plate and were treated the following day. Rapamycin and chloroquine in combination was used as a positive control for autophagy induction. Rapamycin is a commonly used inducer of autophagy and chloroquine is a lysosomal inhibitor. When used in combination, they cause cells to undergo an accumulation of autophagic vesicles, generating a strong signal[180]. The cells were treated with the positive control for 48 hours. To prepare for analysis the cells were detached from the plates using 500 µL of TrypLE Express and collected in 50 mL falcon tubes. The cells were centrifuged, the supernatant discarded, and the pellets were washed in 200 µL of 1X assay buffer, supplied by the kit. These were transferred to 1.5 mL Eppendorf tubes and centrifuged again. The pellet was resuspended in 200 µL of the CYTO-ID® Green dye solution, diluted 1:1000 with 1X assay buffer. The samples were covered with tinfoil to protect the dye from the light and left to incubate at 37°C for 30 minutes. After this incubation period, the samples were centrifuged, and the pellets were washed with assay buffer. Samples were centrifuged again, the supernatant removed, and the pellets resuspended in 200 µL of 1X assay buffer. The samples were analysed immediately with the BD Accuri C6 flow cytometer. CYTO-ID® Green dye (463/534nm) was detected using the 530/30 bandpass filter and Median Fluorescent Intensity (MFI) values were obtained (Figure 2.2).

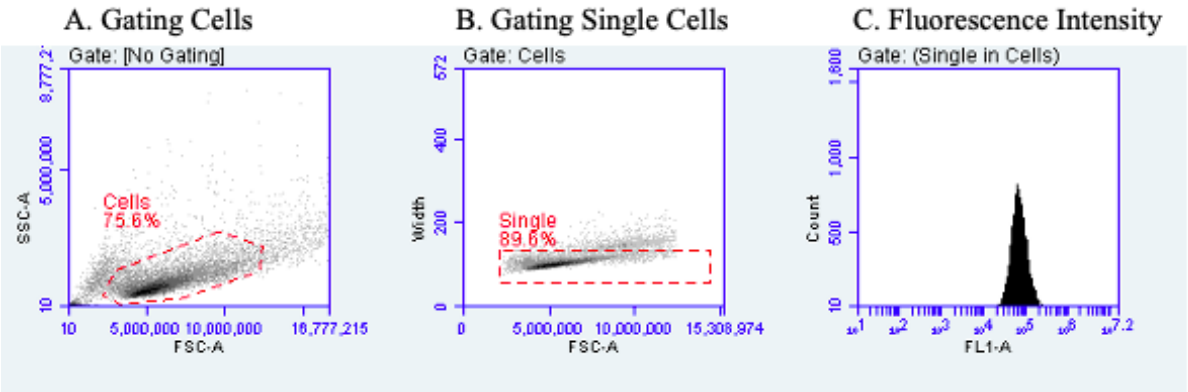

Figure 2.2 Gating strategy for Cyto ID autophagy analysis

BT12 cells were treated with the vehicle, then stained with Cyto-ID® green dye. They were analysed using the BD Accuri flow cytometer. Forward scatter area (FSC-A) was plotted against side scatter area (SSC-A) on a dot plot and gated to exclude any debris from the cell population **(A)**. This was further analysed on another dot plot where width was plotted against forward scatter height (FSC-A) and this was gated to include singlets and exclude doublets as well as clumped cells **(B)**. This was then analysed on an FL1-A histogram to obtain MFI values **(C)**.

2.6.3 Measurement of intracellular Reactive Oxygen Species (ROS)

ROS levels were monitored in MRT cells using the cell-permeant dye 2,'7'-dichlorofluorescin diacetate (H_2DCFDA). This can be oxidised to the highly fluorescent 2',7'-dichlorofluorescein (DCF) in the presence of ROS (see Figure 2.3), following the cleavage of its acetate groups by intracellular esterases and, thus, can be detected through flow cytometry[326].

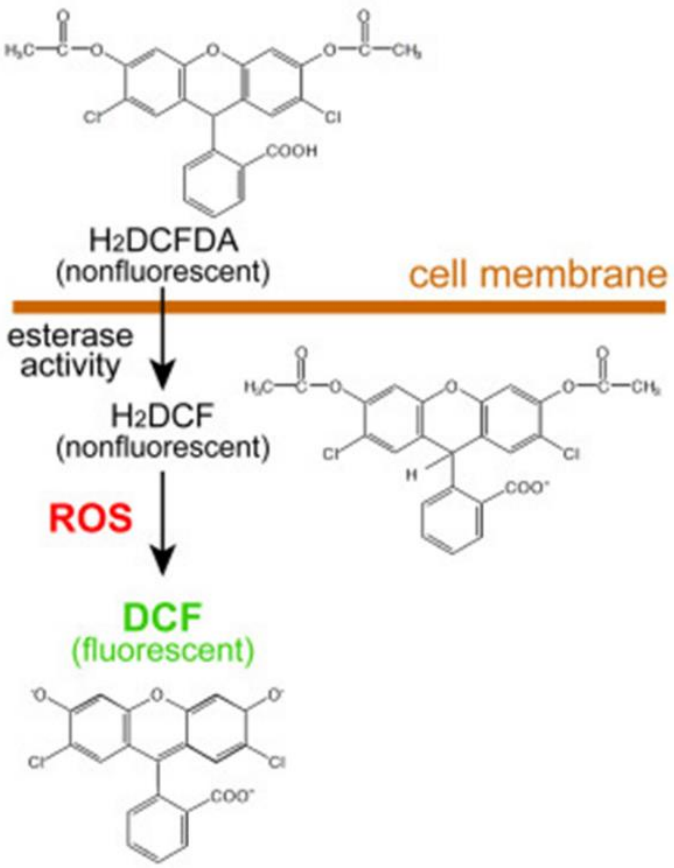

Figure 2.3 H_2DCFDA cellular staining for intracellular ROS detection

Image taken from Yoon *et al*[327].

2mL of BT12 and BT16 were seeded in 6-well plates at a seeding density of 1 x10^5 cells/mL and were left to adhere overnight. After 48 hours, cells were either pre-treated with vehicle (0.009% NaCl) or 5mM NAC for 1 hour or the required concentration of cisplatin. The cells were left to incubate for 48 hours. H_2O_2 was used as a positive control for ROS induction as H_2O_2 is a key member of the class of ROS. NAC, the ROS scavenger, was used in combination with H_2O_2 as a further control. Prior to being harvested, the cells were treated with 10 μM of H_2DCFDA and left to incubate at 37°C for 30 minutes. After this incubation period, the cells were detached and transferred to falcon tubes. They were centrifuged (300 x g, 5min) and the supernatant was discarded. The cells were washed in 200 μL of PBS and centrifuged again under the same conditions. The pellets were resuspended in 200 μL of PBS and analysed immediately by flow cytometry. The MFI values of DCF (498/522) were obtained using the bandpass filter of 530/30nm on the BD Accuri C6 flow cytometer (Figure 2.4).

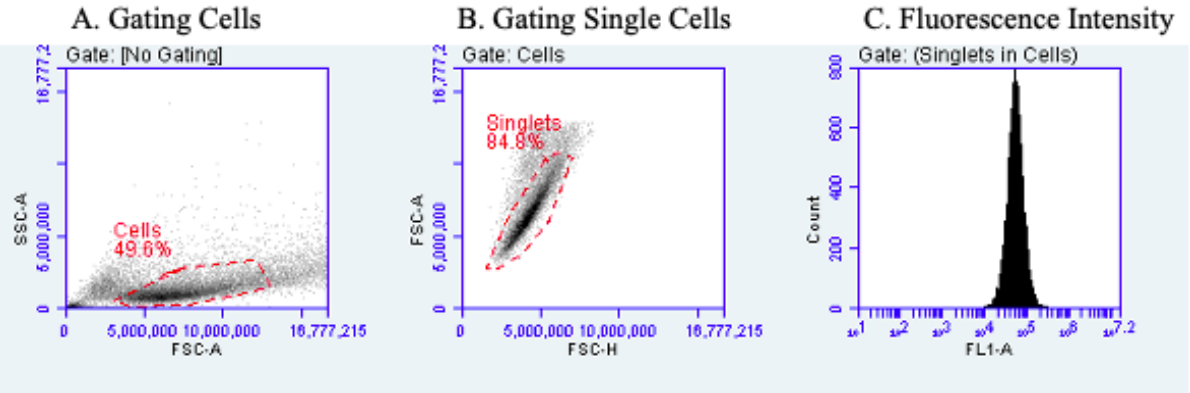

Figure 2.4 Gating strategy for DCF analysis

BT12 cells were treated with the vehicle, then stained with H_2DCFDA. They were analysed using the BD Accuri flow cytometer. Forward scatter area (FSC-A) was plotted against side scatter area (SSC-A) on a dot plot and gated to exclude any debris from the cell population **(A)**. This was further analysed on another dot plot where forward side scatter area (FSC-A) was plotted against forward scatter height (FSC-H), and this was gated to include singlets and exclude doublets as well as clumped cells **(B)**. This was then analysed on an FL1-A histogram to obtain MFI values **(C)**.

2.6.4 Measurement of mitochondrial Reactive Oxygen Species

MitoSOX™ Red reagent was used to stain MRT cells to monitor the levels of mitochondrial reactive oxygen species. MitoSOX™ Red reagent is a fluorogenic dye which specifically targets the mitochondria in live cells and can undergo oxidation by superoxide, producing red fluorescence (Figure 2.5). Dihydroethidium, also referred to as hydroethidine (HE), can be oxidised to ethidium that binds to DNA to emit fluorescence. MitoSOX is a synthetic derivative of dihydroethidium containing a cationic triphenylphosphonium moiety. It can accumulate in the mitochondria and can thus detect mitochondrial ROS which can be detected by flow cytometry, fluorometry or microscopy[328].

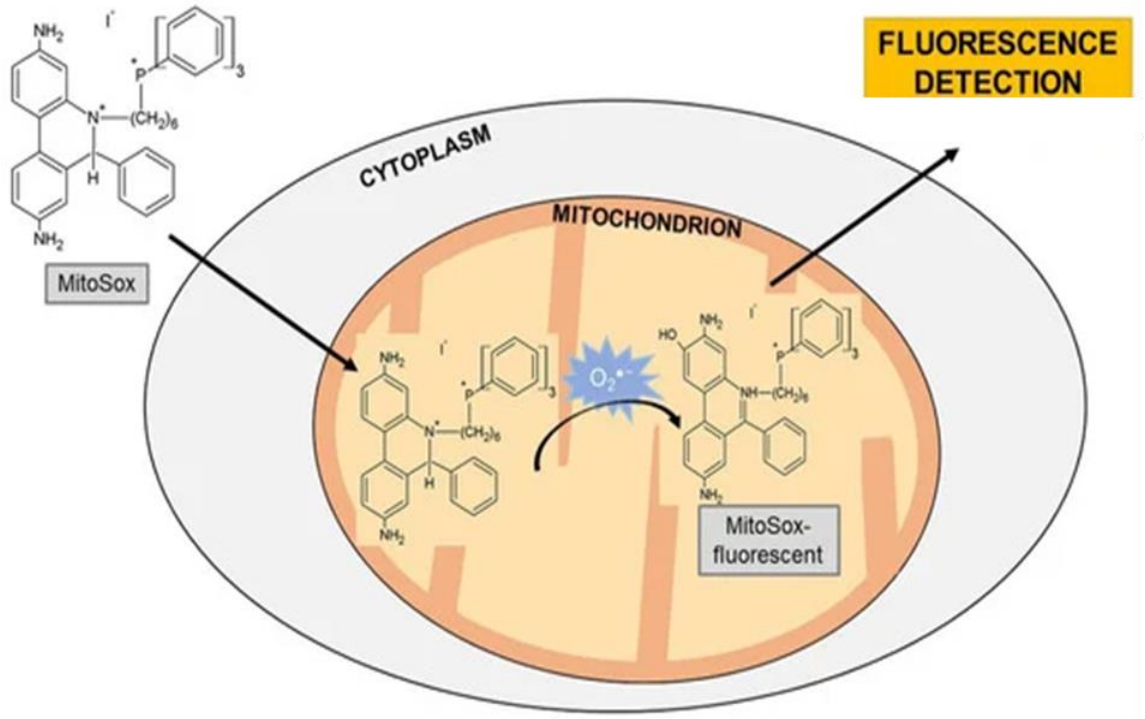

Figure 2.5 Detection of superoxides/ROS using the Mitosox fluorescent probe

Image modified from Capek *et al*.

BT16 cells were seeded in 6 well plates at a density of 1×10^5 cells/mL in complete media and the following day were treated with the relevant drugs for the required time. After incubation, cells were harvested, washed with PBS then stained with MitoSOX™ Red (2.5 μM) for 20 min at 37°C in the dark, and then washed with warm PBS and analysed by flow cytometry. The MFI values of Mitosox (510/580 nm) were obtained with the FL-2 channel using the bandpass filter of 585/340nm on a BD Accuri C6 flow cytometer[329].

2.7 Western blot analysis

Western blotting was performed to separate and identify specific proteins expressed in samples extracted from MRT cells. This technique is commonly used in cell biology research and consists of using sodium dodecyl polyacrylamide gel electrophoresis (SDS-PAGE) to separate a mixture of proteins based on their molecular weight. These proteins are then transferred onto a membrane and incubated with an antibody specific to the

protein of interest. For the purpose of visualisation, the membrane is probed with a secondary antibody and is detected through the use of electrochemiluminescence (ECL).

2.7.1 Buffer preparation

Prior to running SDS-PAGE, the necessary buffers and the milk were prepared (Table 2.1).

10X Running Buffer	10X Transfer Buffer	TBS (10X)	TBST	5% non-fat dried milk
25 mM Tris **192 mM glycine** **0.1% (v/v) SDS in dH_2O**	25 mM Tris 192 mM glycine in dH_2O	200 mM Tris 1.5 M NaCl pH 7.6 in dH_2O	100mL of 10X TBS + 890 mL dH_2O + 10 mL Tween®20 (10%)	5g of Marvel milk in 100 mL of TBST

Table 2.1 Preparation of buffers for western blot analysis

2.7.2 Sample preparation

BT12 and BT16 cells were seeded at 1x 10^5 cells/ml and G401 cells were seeded at 5x10^4 cells/ml in 25 cm^2 flasks. The cells were left to adhere overnight and the following day they were treated with drug as indicated and incubated at 37°C. After the necessary incubation period had passed, the cells were harvested using a cell scraper and centrifuged at 300 x g for 5 minutes. The supernatant was discarded, the pellets were washed with 500 µl of radioimmunoprecipitation (RIPA) buffer (50mM Tris-HCl, pH 8.0, with 150 mM sodium chloride, 1.0% (v/v) Igepal CA-630 (NP-40), 0.5% (w/v) sodium deoxycholate and 0.1% (w/v) sodium dodecyl sulfate) made up with 10% (v/v) protease inhibitor and 1% (v/v) phosphatase inhibitor 2 and 3. The samples were left on ice to lyse for 30 minutes after which they were centrifuged at 10 000 x g for 5 minutes at 4°C. The pellets were discarded, and the supernatants were transferred to fresh Eppendorf tubes for protein quantification.

2.7.3 Protein quantification

A bichinchoninic acid (BCA) assay was used to quantify the protein concentration in the samples. This involved two steps: the first step is the conversion of Cu^{2+} to Cu^{+} by peptide bonds in alkaline conditions. The amount of Cu^{2+} that is reduced is proportional to the amount of protein present. The second step is the chelation of each Cu^{+} by two molecules of bichinchoninic acid, which forms a purple-coloured complex that can absorb light at the wavelength of 562 nm[330]. To determine the protein concentration of a sample, a standard curve was plotted by reading the absorbance of a range of known concentrations of bovine serum albumin (BSA) protein. As absorbance is directly proportional to protein concentration, the value of the unknown sample can be estimated by extrapolating the standard curve.

The Pierce BCA Protein Assay kit supplies BSA stock solutions as well as two reagents which are mixed together to form the working reagent. Reagent A contains bicinchoninic acid and is mixed with Reagent B which contains cupric sulphate. As stated in the user guide, 50 parts of Reagent A were mixed with 1 part of Reagent B, thereby acquiring a green solution. Using a multichannel, 200 µl of this working reagent was then added to each well of a 96-well plate.

Serial dilutions of BSA (2mg/ml) were prepared in Eppendorf tubes using H_2O to prepare the protein standards (2, 1, 0.5, 0.25, 0.125, 0.063, 0.0315 and 0 mg/ml) as indicated in Table 2.2. A small amount of the lysates was removed and diluted 1:10 to use in the BCA assay. 20 µL of the standards and diluted lysates were pipetted in duplicate into the 96-well plate, which was wrapped in tin foil and left to incubate for 30 minutes at 37°C. After the incubation period, the plate was read using a SpectraMax 340 PC Microplate Reader (Molecular Devices, LLC, CA, USA) and the absorbance was measured at a wavelength of 562 nm. The absorbance values of the BSA standards were used to produce a standard curve which could be used to interpolate the values for the unknown samples (Figure 2.6).

The samples were prepared using 5X Laemlli buffer (5% (w/v) SDS, 50% (v/v) glycerol, 0.1% (v/v) bromophenol blue and 1M Tris-HCl, pH 6.8) and H_2O to make a 100 µg/100 µl protein solution. The cell lysates were heated for 10 minutes at 90°C and were then vortexed. 5 µl of 1M DTT (dithiothreitol) was added to each sample.

Tube	[BSA], mg/ml	Volume of BSA, µl	Volume of water, µl
A	2	600	0
B	1	300 of Tube A	300
C	0.5	300 of Tube B	300
D	0.25	300 of Tube C	300
E	0.125	300 of Tube D	300
F	0.063	300 of Tube E	300
G	0.0315	300 of Tube F	300
H	0	0	600

Table 2.2 Preparation of BSA standards

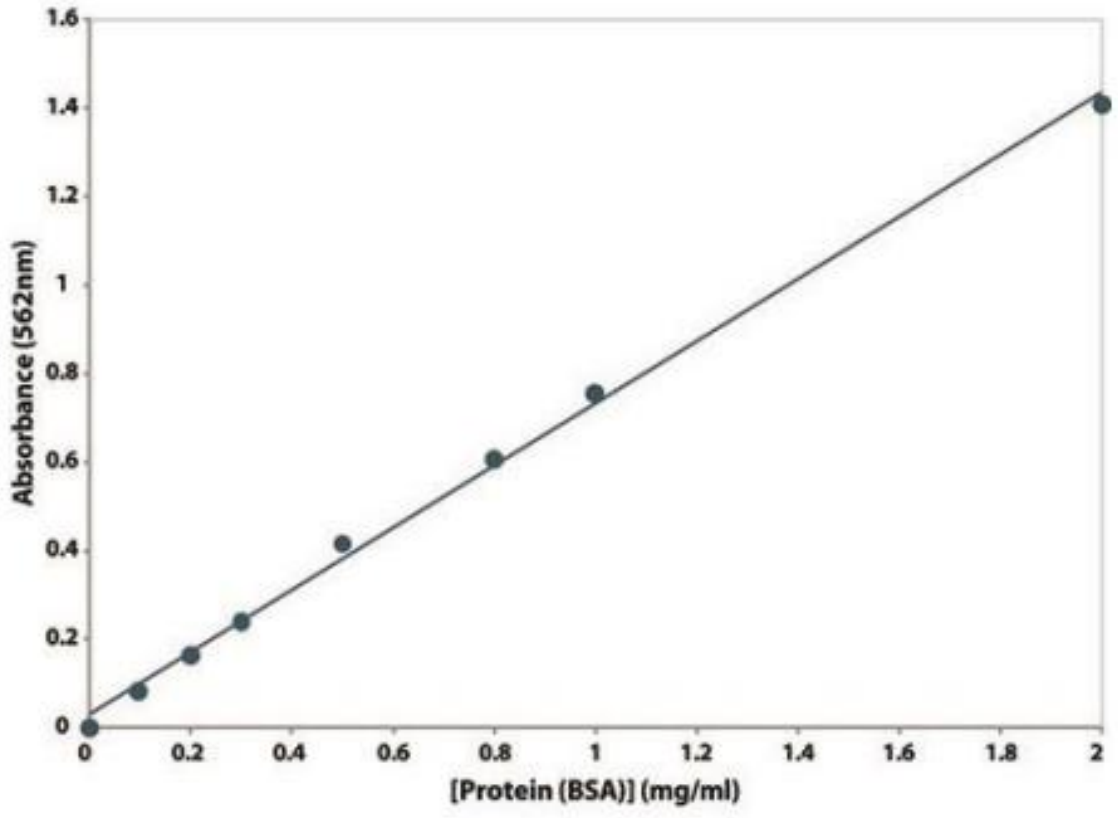

Figure 2.6 Standard curve for BCA assay

2.7.4 Sodium Dodecylsulphate-Polyacrylamide Gel Electrophoresis (SDS-PAGE)

The method of sodium dodecyl sulphate polyacrylamide gel electrophoresis (SDS-PAGE) is commonly used to separate proteins based on their molecular size. Glass plates were cleaned with hot water and wiped with methanol. Once dried, they were assembled. In a fume hood, the resolving gel was prepared (Table 2.3) and poured between the two glass plates, leaving enough space for the stacking gel. 200 µl of isopropanol was pipetted at each edge of the plate and left to run along the top of the gel, preventing the formation of any air bubbles and evening out the top of the resolving gel. The resolving gel was left to polymerise for approximately 25 minutes. Once the gel had set, the isopropanol was poured off and any traces were removed by washing with deionised water and drying with filter paper. The stacking gel was then prepared (Table 2.3) and poured into the plates. The comb was immediately inserted into the plates and the stacking gel was left to polymerise for approximately 15 minutes. Once the gel was ready, it was either used immediately or wrapped in wet tissue and stored at 4°C until it was required. The plates containing the gel were placed in the electrophoresis tank, which was filled up with 1X running buffer, diluted in dH_2O from the 10X running buffer (25 mM Tris, 192 mM glycine and 0.1% (v/v) SDS in dH_2O). The comb was then gently removed from the gel to create the wells. 5 µL of molecular weight markers was loaded into the first well of the gel. 10-20 µg of lysate samples were loaded into each subsequent gel and the gel was run at 80 V until the samples ran through the stacking gel (approximately 25 minutes). At this point, the current was increased to 120V until the samples reached the base of the resolving gel.

Components	8% Resolving gel	10% Resolving gel	12% Resolving gel	15% Resolving gel	5% Stacking gel
H_2O	4.6	4	3.3	2.3	3.4
30% acrylamide mix	2.7	3.3	4	5	0.83
Tris-Cl (1.5M, pH 8.8)	2.5	2.5	2.5	2.5	-
Tris-Cl (1M, pH 6.8)	-	-	-	-	0.63
10% SDS	0.1	0.1	0.1	0.1	0.05
10% Ammonium persulfate (APS)	0.1	0.1	0.1	0.1	0.05
TEMED	0.006	0.004	0.004	0.004	0.005

Table 2.3 Preparation of resolving gel (10mL) and stacking gel (5mL) for SDS-PAGE

2.7.5 Transfer

The protein on the SDS gels was transferred onto polyvinylidene difluoride (PVDF) membranes. PVDF membranes were activated in 100% methanol for 2 minutes, after which they were soaked in 1X transfer buffer, diluted 1:10 from 10X transfer buffer (25 mM Tris and 192 mM glycine in dH_2O) and supplemented with 10% (v/v) methanol. Sponges, transfer cassettes and filter papers were also soaked in 1X transfer buffer. After the gel had finished running, the current was stopped, and the gel was removed from the chamber. The stacking gel was cut off and disposed of. The gel was removed from the two plates and was placed on top of blotting paper that was placed on a sponge on one end of the cassette. PVDF membrane was placed on top of the gel and covered with 2 layers of filter paper. A tube was used to roll over the layers of filter paper to remove any air bubbles. A sponge was placed on top and the cassette was closed firmly to avoid the formation of any air bubbles. The cassette was placed into a transfer tank and filled with 1X transfer buffer. An ice pack was also placed in the cassette to avoid the system overheating during the transfer procedure. The gel was transferred to the PVDF membrane

for 40-90 minutes (depending on protein size) at 150 mA. To determine the success of the transfer, the quality of the transfer of the pre-stained molecular weight markers onto the PVDF membrane was assessed visually.

2.7.6 Probing Membranes

Once transfer was complete, the membrane was incubated in 5% non-fat dried milk (Marvel) at room temperature for 1 hour (blocking reagent). The membrane was then incubated in the primary antibody (diluted in 5% milk) overnight. The following day, the membrane was washed 3 times for 10 minutes with TBST made up of 1x TBS solution diluted in dH_2O and supplemented with 0.1% (v/v) Tween®20. This was then incubated for 1 hour in the secondary antibody (either anti-rabbit or anti-mouse secondary antibodies from Promega. These polyclonal secondary antibodies were derived in goat, immunoaffinity-purified using immobilized antigens and conjugated to horseradish peroxidase (HRP) enzyme) conjugated to horseradish peroxide (HRP) for 1 hour. The secondary antibody was also diluted in 5% milk. After this incubation period in the secondary antibody, the membrane was washed in TBST a further 3 times for 10 minutes.

After the proteins of interest were detected, the membranes were re-probed in GAPDH. GAPDH was included as a loading control to ensure equal loading across the gel.

Antibody	Host	Dilution
Anti-Atg5	Rabbit	1:1000
Anti-Atg7	Rabbit	1:1000
Anti-Bak (active form)	Rabbit	1:1000
Anti-Bax	Rabbit	1:1000
Anti-Bcl-2	Rabbit	1:1000
Anti-BcL-xL	Rabbit	1:1000
Anti-Beclin	Rabbit	1:1000
Anti-Bid	Rabbit	1:1000
Anti-Caspase 3	Rabbit	1:1000
Anti-cFLIP	Rabbit	1:1000
Anti-cIAP1	Rabbit	1:1000
Anti-Cleaved Caspase 3	Rabbit	1:1000
Anti-GAPDH	Mouse	1:5000
Anti-JNK (total)	Rabbit	1:1000
Anti -JNK (phosphor)	Rabbit	1:1000
Anti-LC3I/II	Rabbit	1:1000
Anti-Mcl-1	Rabbit	1:1000
Anti-Mouse	Goat	1:5000
Anti-Noxa	Rabbit	1:1000
Anti-Nrf2	Rabbit	1:500
Anti-p38 (total)	Rabbit	1:1000
Anti -p38 (phosphor)	Rabbit	1:1000
Anti-p62	Mouse	1:1000
Anti-Rabbit	Goat	1:2500
Anti-γ-Tubulin	Mouse	1:2500
Anti-XIAP	Rabbit	1:1000

Table 2.4 Antibodies used for analysis of MRT cells

2.7.7 Protein detection

Electrochemiluminescence (ECL) was used to detect the protein bands. When HRP is combined with peroxide it oxidises luminol to 3-aminophthalate, which is its excited state product[331]. This excited form releases light which can be detected by the Biorad Geldoc™ XR+System.

The membranes were covered with equal amounts of HRP substrate luminol reagent and HRP substrate peroxide reagent (Pierce ECL Western Blotting Substrate) for one minute and images were acquired using both chemiluminescent and colorimetric settings. These were merged together using the Image Lab software to obtain an image containing both the protein of interest as well as the protein marker in order to estimate the protein size.

2.7.8 Densitometric analysis of western blots

Image Lab software was used to perform densitometric analysis on the protein bands. The programme quantifies the number of pixels in each protein band and automatically removes any background noise. The relative density of each band was normalised by the relative density of the loading control and the data was plotted on GraphPad Prism version 5.0.

2.8 Knockdown using siRNA

2.8.1 siRNA reconstitution

On-target plus human ATG5 siRNA SMARTpool and Nrf2 siRNA SMARTpool was purchased from Dharmacon as a 5 nmol aliquot. As a negative control, an On-target plus non-targeting pool was also purchased from Dharmacon as a 5 nmol aliquot. The siRNA aliquots were each dissolved in 50 μL of sterile DNAse and RNAase free cell culture grade water to make a 100 μM stock. To ensure reconstitution, the solutions were placed on an orbital mixer for 30 minutes at room temperature. The tubes were then briefly centrifuged at 600 x g to collect the solutions at the base of the tube. The reconstituted siRNA was then aliquoted and stored at -80°C for future use.

2.8.2 ATG5 siRNA

2 mL of BT12 cells were seeded at 1 x 10^5 cells/mL in a 6-well plate, in antibiotic-free

media. The cells were left to adhere overnight. The following day, the cells were washed 3 times with sterile PBS and the media was replaced with antibiotic-free and serum-free media.

The cells were left to incubate for 2 hours prior to transfecting with lipofectamine, NT siRNA or ATG5 siRNA. Lipofectamine was diluted 1 in 50 in Opti-MEM media. The ATG5 siRNA was diluted in Opti-MEM to a concentration of 500 nM. This was then incubated for 5 minutes at room temperature. After this time, the siRNA was diluted 1 in 2 in lipofectamine, mixed gently and left to incubate for 20 minutes at room temperature. Finally, the siRNA was added to the cells at a further dilution of 1 in 5 to give a final concentration of 50 nM. After 4 hours, the siRNA was removed, and the cells were washed three times with sterile PBS and media with FBS was added to the wells. The cells were left for 48 hours prior to harvesting and analysed by western blotting and flow cytometry. Cisplatin was added to cells 24 hours prior to harvesting.

2.8.3 Nrf2 siRNA

2 mL of BT16 cells were seeded at 1 x 10^5 cells/mL in a 6-well plate, in antibiotic-free media. The cells were left to adhere overnight. The following day, the cells were washed 3 times with sterile PBS and the media was replaced with antibiotic-free and serum-free media.

The cells were left to incubate for 2 hours prior to transfecting with lipofectamine, NT siRNA or Nrf2 siRNA. Lipofectamine was diluted 1 in 50 in Opti-MEM media. The Nrf2 siRNA was diluted in Opti-MEM to give a concentration of 250 nM. This was then incubated for 5 minutes at room temperature. After this time, the siRNA was diluted 1 in 2 in lipofectamine, mixed gently and left to incubate for 20 minutes at room temperature. Finally, the siRNA was added to the cells at a further dilution of 1 in 5 to give a final concentration of 25 nM. After 4 hours, fresh media with FBS was added to the cells. The cells were left for 24 hours prior to harvesting and analysed by western blotting

2.9 Drug combination studies

BT16 cells were seeded at 1 x 10^5 cells/mL and treated the next day with different combinations of cisplatin and ABT-199 concentrations as indicated. After the relevant incubation time the cells were harvested and stained with Annexin/PI and analysed by flow cytometry. The computer software CompuSyn was used to study interactions between the different concentrations of drugs. The programme relies on the Chou-Talay methodology which is based on the median effect principle, to determine the Combination Index (CI) values for each combination. CI values <1, =1 and > 1 indicate synergistic, additive, and antagonistic effects respectively (see Table 2.5). Furthermore, lower CI values indicate stronger synergism whereas high CI values are indicative of higher antagonism. To determine the CI values, the effects of each drug alone (effect on viability) is entered into the programme and dose effect plots are calculated. Then, the effect of the drug combination is entered into the programme as well and the CI values can then be determined.

Combination Index (CI) Range	Symbol	Description
<0.1	+ + + + +	Very strong synergism
0.1-0.3	+ + + +	Strong synergism
0.3-0.7	+ + +	Synergism
0.7-0.85	+ +	Moderate synergism
0.85-0.9	+	Slight synergism
0.9-1.1	±	Nearly additive
1.1-1.2	-	Slight antagonism
1.2-1.45	--	Moderate antagonism
1.45-3.3	---	Antagonism
3.3-10	----	Strong antagonism
> 10	-----	Very strong antagonism

Table 2.5 Range of CI values describing synergism and antagonism in drug combination studies

2.10 Determination of glutathione levels in MRT cells

In cells, glutathione can exist in reduced state (GSH) or in oxidised state (GSSG). Total glutathione (GSH + GSSG) and the ratio of GSH to GSSG was assessed using the

GSH/GSSG-Glo™ assay. This assay is a luminescence-based assay that can detect and quantify the levels of GSH, GSSG and total glutathione. The assay relies on monitoring the GSH-dependent conversion of Luciferin-NT to luciferin. This reaction is then coupled to a firefly luciferase reaction which emits a detectable luminescent signal. The light emitted is dependent on the amount of Luciferin present which in turn is dependent on the levels of GSH present. The reduction of GSSG to GSH allows for the quantification of total glutathione which is comprised of the sum of GSSG and reduced GSH (GSSG+GSH). Blocking endogenous GSH with N-Ethylmaleimide (NEM) allows for the quantification of GSSG alone (Figure 2.7).

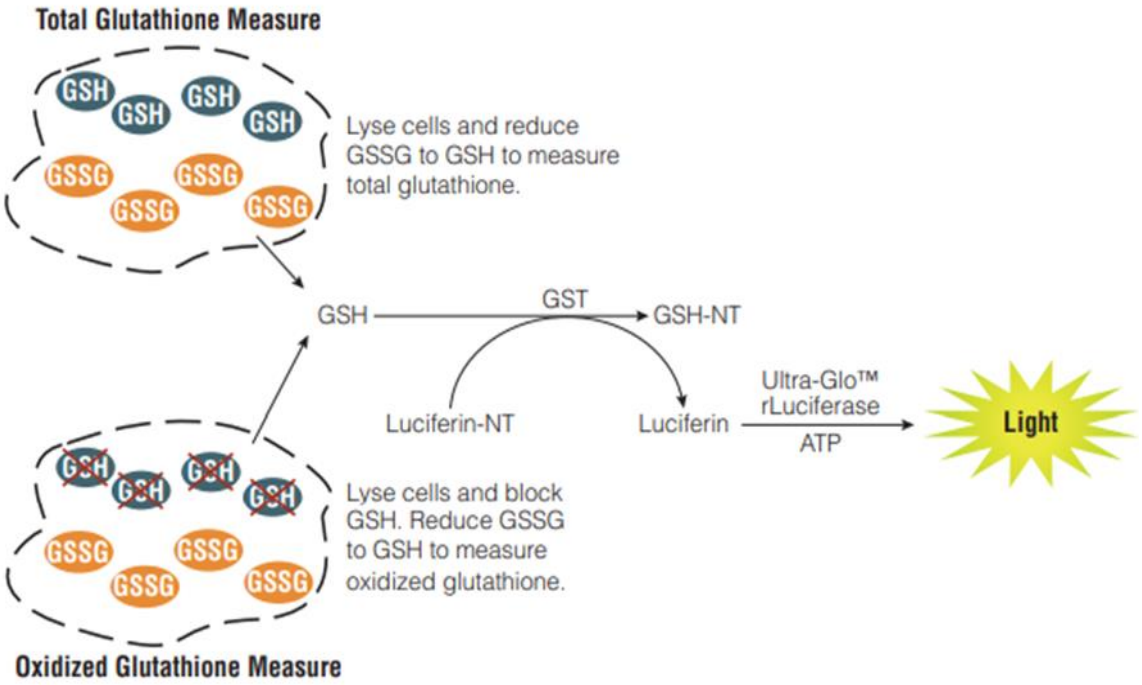

Figure 2.7 Reaction behind the principle of the GSH/GSSG-Glo Assay

The cells were seeded in a 96-well plate and allowed to adhere overnight. Two sets of cells were seeded: one set for the measurement of the total glutathione levels and one set for oxidised glutathione levels. Both sets of cells were seeded for in duplicate. The following day cells were treated with the relevant drugs for the required treatment time. After the relevant incubation time, the GSH/GSSG-Glo assay was performed according to the manufacturer's protocol. The reagents were prepared using components provided in the assay kit. Total Glutathione Lysis Reagent was made up using 2% Luciferin-NT and 20% Passive Lysis Buffer 5X and H_2O. The Oxidised Glutathione Lysis Reagent was prepared using 2% Luciferin-NT, 1% NEM (25mM), 20% Passive Lysis Buffer 5X and H_2O. Finally,

the Luciferin Generation Reagent was prepared with 2.5% DTT (100mM), 3% Glutathione-S-Transferase and Glutathione Reaction Buffer. Total Glutathione Lysis Reagent (50 µl) was added to wells of the plate that was seeded to determine the total glutathione levels. In contrast, Oxidised Glutathione Lysis Reagent (50 µl) was added to the set of cells to measure oxidised glutathione levels. The cells were incubated in the lysis reagents for 5 minutes at room temperature. Following this incubation time, 50 µl of Luciferin Generation Reagent was added to generate luciferin from the GSH-probe, Luciferin-NT, and the plate was left to incubate for 30 minutes at room temperature. Prior to measuring luminescence, the contents of the wells were transferred to a 96-well opaque plate and 100 µl of Luciferin Detection Reagent was added to the wells. Luciferin Detection Reagent contains Ultra-Glo™ Luciferase which halts the luciferin generation reaction and initiates a luminescent signal proportional to the amount of GSH derived from total glutathione or GSSG alone. The plate was incubated for 15 minutes at room temperature. After this time, luminescence was measured using SpectraMax Gemini EM Microplate Reader using SOFTmax Pro version 4.9.

The luminescence measurements provided the values in relative light units (RLU), and these were normalised by the blank values. The mean of the duplicate values was calculated. The values of reduced GSH were calculated by subtracting GSSG from total glutathione. The ratio of GSH:GSSG was calculated as per guideline recommendations. In this assay two moles of GSH were generated from one mole of GSSG, so a twofold adjustment was applied to the GSSG values to obtain the measurement of the GSSG levels. Accordingly, the GSH/GSSG ratio was calculated using the formula:

$$GSH/GSSG = Total\ glutathione - GSSG\ /\ GSSG \div 2$$

The values obtained from this assay were plotted and graphed using GraphPad Prism version 5.0.

2.11 Seahorse bioenergetic assay

The Agilent Seahorse XF Cell Mito Stress Test was conducted to measure key parameters of mitochondrial function in response to drug treatment. This assay measures the oxygen consumption rate (OCR) and extracellular acidification rate (ECAR) of live cells in response

to serial injections of various inhibitors of the electron transport chain (Figure 2.8) that allow for the monitoring of basal respiration, ATP production, proton leak, maximal respiration, spare respiratory capacity, and non-mitochondrial respiration (Figure 2.9).

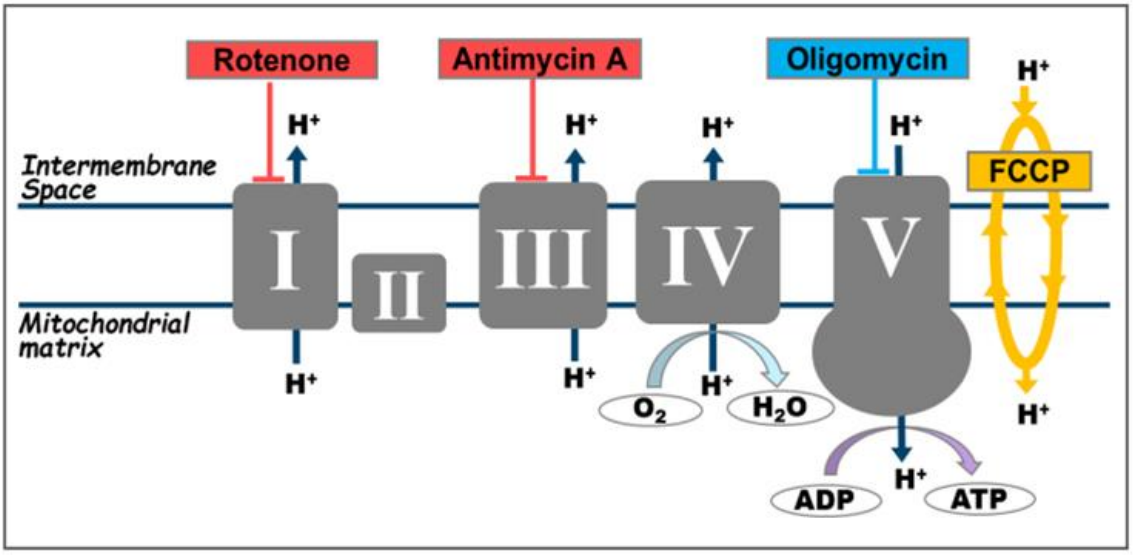

Figure 2.8 Inhibitors of the electron transport chain

Image taken from Seahorse XF Cell Mito Stress Test Kit User Guide.

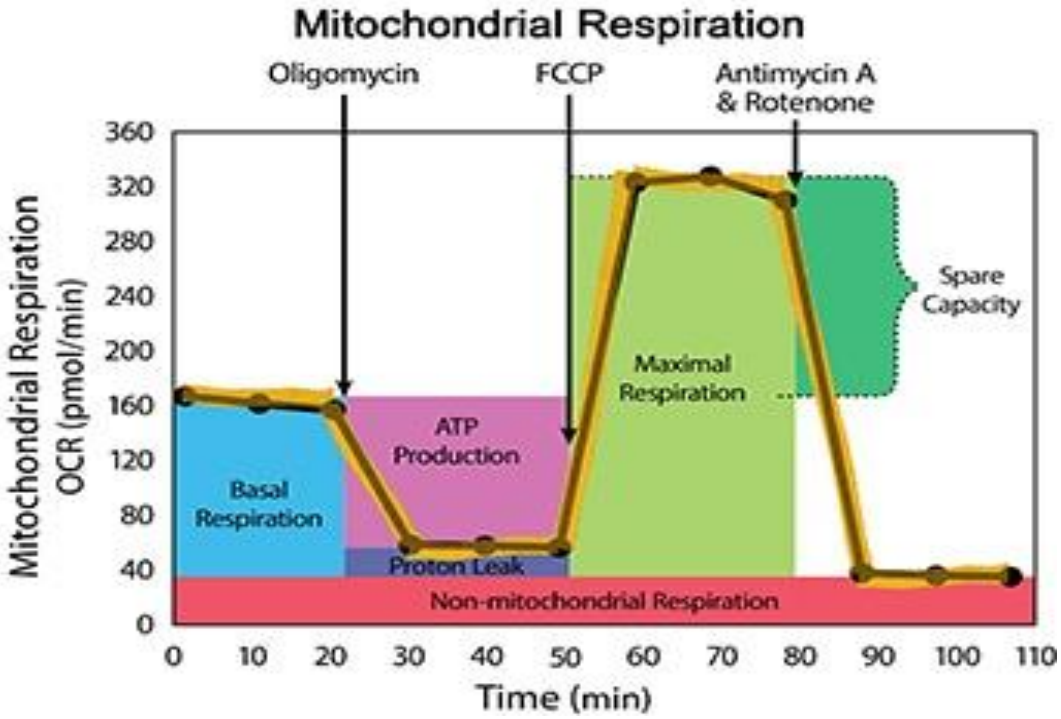

Figure 2.9 Seahorse FX Cell Mito Stress Test Profile

Image taken from Seahorse XF Cell Mito Stress Test Kit User Guide

The Seahorse XFe24/XFp Analyser monitors the OCR and ECAR in an 8-well plate format. Following optimisation of the seeding density, the cells were seeded in a Seahorse XFp Cell Culture Microplate at a seeding density of 20,000 cells/well in 80 µl growth medium (RPMI medium supplemented with 10% foetal bovine serum, 1 % penicillin and streptomycin). Two wells were left as blanks i.e. these contained only 80 µl of growth medium with no cells to serve as background temperature correction wells. The cells were left to adhere overnight. The following day the cells were treated with the relevant drug for the required time.

The day prior to running the assay, the sensory cartridges were hydrated. In order to do this, the utility plate and the sensory cartridge were separated. The sensory cartridge was placed upside down on the bench. The wells of the utility plate were filled with 200 µl of XF calibrant. Subsequently, the sensory cartridge was lowered onto the utility plate slowly to avoid the formation of air bubbles. This was then incubated in a non-CO_2 37ºC incubator for 24 hours prior to initiating the assay.

The day of the assay the Seahorse medium was prepared fresh by supplementing the XF base medium pyruvate solution, glutamine solution and D-glucose. The assay was pre-warmed to 37ºC prior to use. The cell growth medium was removed from the XFp Cell Culture Microplate and 180 µl of assay medium was added into the wells. To de-gas, the XFp Cell Culture Microplate was incubated in a 37ºC non-CO_2 incubator for 1 hour. In the meantime, the XF Cell Stress Test compounds were prepared. Stocks of oligomycin, FCCP and rotenone/antimycin A were prepared. For the Cell Mito Stress Test, the injection ports A, B and C (see Figure 2.10) of the XFp sensor cartridge were loaded with the relevant volumes of the compounds (20 µl in port A, 22 µl in port B and 25 µl in port C). A 100 µM stock solution of oligomycin was diluted to 15 µM working concentration using assay medium. The final concentration of oligomycin in the well was thus 1.5 µM. The final working concentration of FCCP was determined by conducting a FCCP titration. A 100 µM stock solution of FCCP was made up in ethanol. This was diluted to a concentration of 20 µM to give a final concentration of 2 µM in the wells.

Finally, a mixture of Antimycin A and Rotenone was prepared with a concentration of 5 µM each, the final working concentration in the well was 0.5 µM each. The XF Cell Mito Stress Test was selected, and calibration was performed on the sensory cartridge. When the

calibration was complete, the utility plate was removed and replaced with the XFp Cell Culture Microplate.

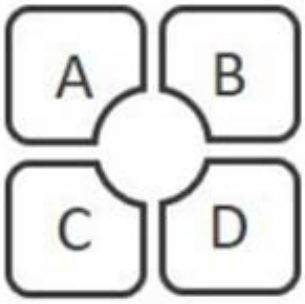

Figure 2.10 The 4 injection ports of XFp Cartridge

2.11.1 Seahorse analyser data analysis

The XF Cell Mito Stress Test parameters were calculated from Wave data that was exported to Excel using the Seahorse XF Stress Test Report Generator.

2.12 Statistical analysis

All statistical analysis was performed on GraphPad Prism 5.0. Results were expressed as mean ± standard error of the mean (S.E.M). A paired two-tailed t-test was used for statistical analysis for comparison of two groups. When appropriate, a one-way ANOVA followed by Tukey's or Dunnett's multiple comparison tests was conducted. Values of *p< 0.05, **p<0.01 and p**<0.001 were considered to be significant.

3. Evaluation of targeting autophagy for the treatment of Malignant Rhabdoid Tumour

3.1 Introduction

Malignant rhabdoid tumour (MRT) is an aggressive and lethal tumour that occurs in infants, often under the age of 3[12]. The prognosis for these tumours is poor and the survival rate is currently estimated to be 20-30% with most deaths occurring within the first year of tumour presentation[4, 14]. These tumours can be found in the brain, kidney or other soft tissues sites and are characterised by a mutation in *SMARCB1*. MRTs were discovered relatively recently and in the past, have often been subject to misdiagnosis, hindering the treatment of patients. Furthermore, these tumours are extremely rare. Due to these factors, there is not sufficient epidemiological data to fully determine the incidence of MRTs. Current data suggests that in the US, the incidence is 0.19 per million for renal MRTs, 0.89 per million for rhabdoid tumours of the CNS and 0.32 per million for tumours located in other sites[14].

At present, treatment for rhabdoid tumours relies on a combination of surgery, chemotherapy and radiation therapy[12]. Where possible, depending on the location of the tumour, it is resected. Total or near-total removal of the tumour has a significant impact on the survival rate of the patient[67]. Radiation therapy is also recommended in combination with surgery and chemotherapy. However, due to the young age of MRT patients, the use of radiation therapy is severely limited and is more often recommended in the treatment of older patients[73]. Chemotherapy is the most relied upon treatment strategy for rhabdoid tumours and is administered intravenously or intramuscularly. Thus far, there is no standardised chemotherapeutic regimen for treating MRT, but current regimens include cisplatin, cyclophosphamide, carboplatin, etoposide, vincristine and methotrexate[332].

Cisplatin is a commonly utilised chemotherapeutic drug in the treatment of a variety of cancers such as ovarian, lung and breast cancer[333]. It is also one of the most frequently used chemotherapeutic agents for MRT[12]. Cisplatin is a square planar metallic coordination compound that induces DNA damage through inter-strand cross-linking between purine residues though the N7 reactive centres[333]. Although current treatment options improve the prognosis for some patients (particularly older patients with lower stages of the cancer), there are various complications that limit the success of such therapies[12]. The young age of MRT patients poses significant restrictions on the dosage of radiation therapy and chemotherapy that can be administered to treat these aggressive tumours[334]. Patients who receive cisplatin treatment often experience undesirable side effects such as anaemia, petechiae, fatigue, gastro-intestinal disorders, kidney damage or hearing loss[335]. In order to

avoid this, various analogues of cisplatin have been developed such as carboplatin, ormaplatin, enloplatin and oxaliplatin[333]. Carboplatin is used to treat cancers in the ovaries, lungs, head, and neck. A major advantage of carboplatin is reduced nephrotoxicity in comparison to cisplatin. However, it is considerably less potent than cisplatin. The clinical dosage of carboplatin is four times higher than cisplatin to achieve the same effect and due to its stable and inert nature, 90% of carboplatin that is administered will pass straight through the body and be expelled in urine[333].

Currently, cisplatin is included in the treatment of 50% of all cancer patients and continues to have significant impact on patient prognosis[333]. However, resistance to cisplatin, amongst other chemotherapeutic agents, has emerged as a major challenge in the treatment of many cancers, including MRT. This is referred to as chemoresistance; whereby cancer cells possess the ability to overcome the effects of chemotherapeutics to enable their survival and evade chemo-induced apoptosis[336]. This key issue in oncology is the focus of many studies which aim to determine the molecular mechanisms by which cancer cells exhibit resistant properties. These properties can be either innate or acquired; they can be present prior to the administering of the treatment or afterwards[337]. Chemoresistance has been linked to various cellular processes and mechanisms such as increased drug export, decreased drug import, increased DNA damage repair and inactivation of cell death signalling[338]. Treating patients with a combination of different anti-cancer therapies is one of the proposed strategies to overcome resistance[140]. For rhabdoid tumours, the European registry study (Eu-rhab) recommends surgery, radiotherapy and chemotherapy, intrathecal methotrexate and high-dose chemotherapy with stem-cell rescue. However, as mentioned above the prognosis is very poor and toxicity-related mortality with these regimens is 5%[12]. For this reason, further insights into the cellular processes that underly chemo-resistant tumours is required to develop novel therapeutic strategies for MRT.

Autophagy is a catabolic and self-degradative process by which the cell recycles and removes unnecessary or dysfunctional components[339]. In doing so, autophagy plays a housekeeping role for the cell through the removal of misfolded proteins, damaged organelles or intracellular pathogens[239]. Of note, different specific processes of autophagy have been described which are involved in the removal of damaged organelles. For example, damaged mitochondria, which can lead to pathogenesis are removed through mitophagy, which occurs when excess and dysfunctional mitochondria are engulfed by the autophagosome and degraded by the lysosome. Autophagy occurs at basal levels in the cell

but is also known to be strongly induced in response to starvation to promote survival until nutrients become accessible. In addition to this, autophagy has been shown to be activated in various pathological contexts. It is implicated in neurodegenerative disorders, ageing and cancer[340]. In cancer biology, autophagy is referred to a double-edged sword as it has been shown to have both tumour-suppressing and tumour-promoting activity[341]. In early stages of tumorigenesis, low levels of autophagy prevent chromosome instability and cell proliferation[342]. At more advanced stages of tumorigenesis, high levels of autophagy facilitate cancer cell survival and proliferation by protecting the cells from metabolic stress and starvation[279]. Of note, although autophagy is a cell survival mechanism, high autophagic levels are also believed to lead to a form of cell death, known in literature as autophagic cell death (ACD)[274]. However, the physiological and molecular mechanisms that underly this are poorly understood. Most evidence in support of this is based on morphological observations of dying cells with high levels of autophagosomes and autolysosomes but it remains unclear if autophagy is coinciding with apoptosis, triggering apoptosis or whether it is occurring as a form of cell death that is completely independent of apoptosis[343].

Autophagy has also been implicated in chemoresistance. Further to its paradoxical role in tumour progression, autophagy is also believed to have a dual role in response to anti-cancer therapeutics. On one hand, autophagy has been shown to be upregulated in response to chemotherapy as a protective mechanism against therapeutic stress[283]. On the other hand, there are reports that autophagy is induced in response to anti-cancer drugs to enhance their cytotoxicity and cause autophagic cell death. Whether autophagy is upregulated as a pro-survival or pro-death mechanism seems to depend on the cancer type and the drug[283, 344]. However, there is mounting evidence to suggest that in many cancers, inhibiting autophagy is a promising strategy to circumvent chemoresistance[345].

The result of autophagy manipulation is dependent on the combined influence of several factors including cell type, autophagy initiator, the combined stimuli to the autophagy initiator and selected combination. Given the varied and complex outcome of autophagy manipulation it is not yet fully understood how to effectively modulate autophagy to enhance the therapeutic efficacy of individual anticancer therapies. Hydroxychloroquine and chloroquine are to date the only clinically approved autophagy inhibitors but there are multiple autophagy inhibitors in the pre-clinical stage at various stages of development[346]. Additional studies on the mechanism of these autophagy inhibitors are still required to answer questions surrounding how these agents will eventually be used in the clinic[347].

Given the infancy of autophagy manipulation as a novel anti-cancer strategy there is an urgent need to accumulate pre-clinical data on a broad spectrum of chemotherapeutics in various cancer types including in MRT. Autophagy modulation may represent a new approach for MRT treatment. With novel and more specific autophagy modulators in production our understanding of this process in cancer will continue to evolve. To date, the role of autophagy in the pathogenesis of MRT remains unclear. In one study in MRT, the histone deacetylase inhibitor FK228 was shown to induce both apoptosis and autophagy[287]. Inhibition of autophagy by the pharmacological autophagy inhibitors chloroquine and 3-methlyadenine enhanced FK228-induced cell death suggesting that under these circumstances, autophagy is activated as a pro-survival protective mechanism. A more recent study examined the radio-sensitising effects of disulfiram (DSF), an irreversible inhibitor of aldehyde dehydrogenase, in MRT. DSF significantly increased the expression of DNA double strand breaks markers (H2AX and p-ATM), an apoptosis marker (cleaved caspase-3), an autophagy marker (LC3B), and a cell cycle arrest protein (p21) in MRT cells[348]. Whether autophagy observed in the treated MRT cells represented a mechanism that allowed the tumour cells to survive therapy or a mechanism for initiating a non-apoptotic form of cell death was not investigated. Further study into the role of autophagy in response to chemotherapeutics in MRT is justified. Therefore, the aim of this chapter was to firstly investigate the cell death pathway(s) initiated by a representative MRT chemotherapeutic agent, cisplatin, in a panel of MRT cell lines and to determine if autophagy is indeed activated. Secondly, this chapter examined whether targeting autophagy, using early and late-stage pharmacological autophagy inhibitors and through genetic knockdown of key autophagic proteins, enhanced sensitivity of the tumour cells to cisplatin. A combination of cisplatin with autophagy inhibition may represent a useful treatment strategy to enhance chemotherapy and improve clinical outcomes for MRT patients.

3.2 Results

3.2.1. The effect of cisplatin on the viability of a panel of MRT cell lines

The alamar blue assay was used to determine the effect of cisplatin on the viability of a panel of MRT cell lines. BT12 and BT16 cells were chosen as representative AT/RT cells with reported differential susceptibility to cisplatin whilst G401 cells were utilised as a representative MRT of the kidney[349, 350]. Cisplatin was selected for this study as a representative chemotherapeutic agent as it is widely used for the treatment of MRT. In the clinic, cisplatin is administered as a single dose of 50 to 70 mg/m2 IV per cycle once every 3 to 4 weeks. The BT16 and G401 cell lines were treated with a range of increasing concentrations of cisplatin (0.5 to 20 µM) whereas the BT12 cell line was treated with the same concentrations of the drug except for the highest concentration (0.5 to 10µM). Following treatment with cisplatin, cell viability was evaluated at three different timepoints: 24, 48 and 72 hours.

Cisplatin (CDDP) decreased the viability of the three cell lines in a dose- and time-dependent manner. A higher sensitivity to cisplatin was observed in BT12 cells when compared to BT16 and G401 cells. A decrease in cell viability was observed as early as 24 hours in BT12 cells. At this time point, 10 µM cisplatin reduced the viability of BT12 cells to 36%, whereas in BT16 and G401 cells the viability was reduced to only 86% and 84%, respectively, indicating a higher level of resistance. In order to further determine the variation in cell sensitivity to the drug, IC50 values, the concentration of cisplatin required to inhibit 50% cell viability in each case, were calculated. At the 24-hour timepoint, IC50 values for BT16 and G401 cells could not be determined as even the highest concentration of 20 µM cisplatin did not reduce the viability below 50%. In BT12 cells however, an IC50 value of 7.72±1.12 µM was determined.

Following 10 µM cisplatin treatment for 48 hours, BT16 cell viability was reduced to 34% whilst G401 and BT12 cell viability was reduced to 21% and less than 5% respectively (Figure 3.1). BT12 cells exhibited the lowest IC50 value of 2.67±1.10 µM. A similar IC50 value of 2.59±1.27µM was determined in G401 cells. BT16 cells had a higher IC50 value of 6.76±1.18µM, suggesting that this cell line exhibits the highest levels of resistance to cisplatin.

Following 72 hours of cisplatin treatment, IC50 values for BT12 and G401 cells were determined as 1.18 ± 1.09 µM and 1.45 ± 1.15 µM respectively. Finally, in the BT16 cell line, the IC50 value was determined to be 5.13±1.09 µM (Table 3.1). Taken together, these results confirm reports in literature that BT16 exert a higher resistance to cisplatin induced cytotoxicity in comparison to BT12 cells[316]. G401 cells were shown to be slightly more resistant than BT12 cells, but still notably more sensitive than BT16 cells.

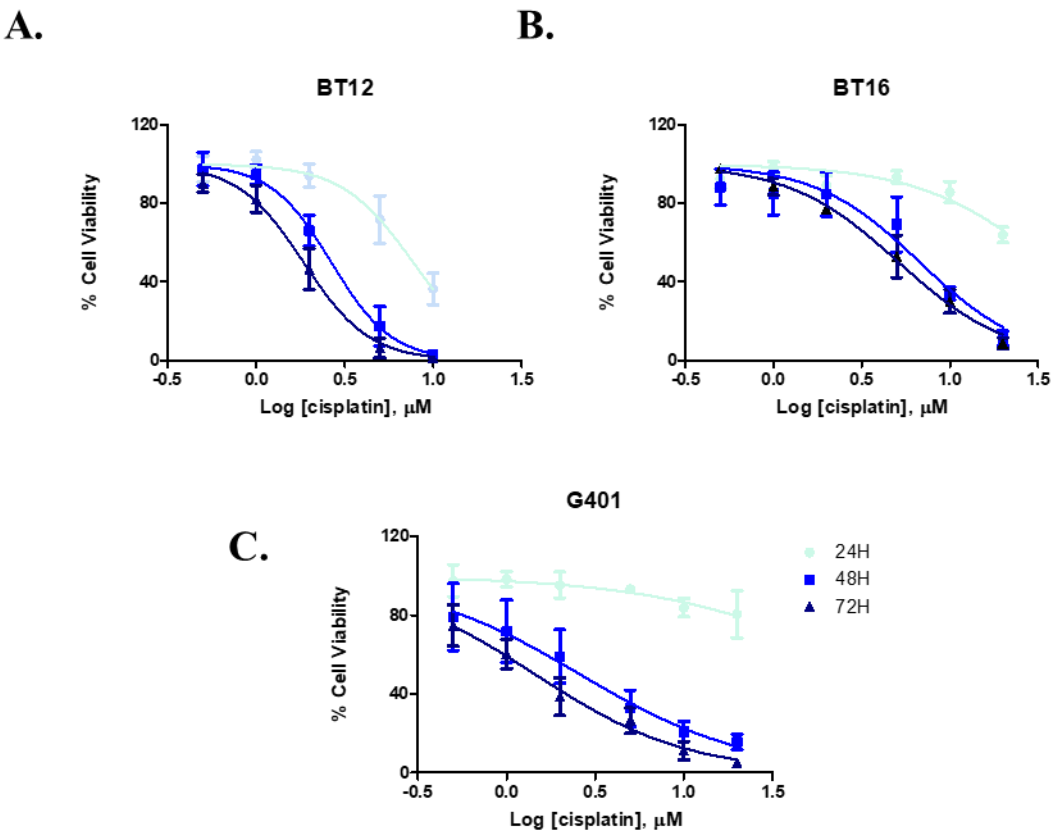

Figure 3.1 Cisplatin reduces the viability of MRT cell lines in a dose- and time-dependent manner

BT12 and BT16 cells were seeded at 1 x 10^5 cells/well whilst G401 cells were seeded at 5 x 10^3 cells/well. Cells were left to adhere overnight and were subsequently treated with vehicle (0.009% (v/v) NaCl) or a range of concentrations of cisplatin (CDDP): 0.5-10 µM for BT12 cells (**A**) and 0.5-20 µM for both the BT16 (**B**) and G401 cell lines (**C**). These were left to incubate for 24, 48 and 72 hours. Alamar blue (10% (v/v)) was added to the wells 5 hours prior to analysis and the cells were incubated in the dark at 37°C. The fluorescence was measured using a Softmax Gemini EM Microplate Reader at an excitation wavelength of 544 nm and an emission wavelength of 590 nm. Media was used to obtain blank values. The values obtained from the cisplatin-treated cells were corrected by the blank values and normalised against vehicle treated cells and results were plotted using Graphpad Prism 5. Values represent the mean ± S.E.M of at least three independent experiments performed in triplicate.

	BT12	BT16	G401
24h	7.72±1.12 µM	ND	ND
48h	2.67±1.10 µM	6.76±1.18µM	2.59±1.27µM
72h	1.18 ± 1.09 µM	5.13±1.09 µM	1.45 ± 1.15 µM

Table 3.1 IC50 values for 24-, 48- and 72-hour treatments with cisplatin in a panel of MRT cell lines

ND = not determined.

3.2.2 Cisplatin induces apoptotic cell death in a dose- and time-dependent manner in MRT cell lines

Results from the alamar blue assay showed that cisplatin reduces viability in MRT cells. This was further analysed by flow cytometric analysis of Annexin V/PI-stained cells to determine whether apoptosis is induced in response to cisplatin. In addition to this, caspase 3 activation (a hallmark of apoptosis) in cisplatin treated cells was examined through western blot analysis.

3.2.2.1 Flow cytometric analysis of cisplatin-induced apoptosis in MRT cell lines

BT12, BT16 and G401 cells were seeded and left to adhere overnight. The following day the cells were treated with either the vehicle (0.009% (v/v) NaCl or varying concentrations of cisplatin (0.8 to 10 µM). The cells were incubated for 48 hours and were then double stained with Annexin V-FITC and PI. The percentage of cells staining positive for one or both stains was determined using the BD Accuri flow cytometer. A dot plot showed the different cell populations: healthy cells (Annexin V-/ PI-) in the lower left quadrant, early apoptosis (Annexin V+/ PI-) in the lower right quadrant, and late apoptosis (Annexin V+/ PI+) in the upper right quadrant.

Cisplatin induced apoptosis in a dose-dependent manner in all three MRT cell lines. In BT12 cells, cisplatin significantly induced apoptotic death from a concentration of 1µM. Of note, apoptosis did not increase between 5 and 10 µM as the apoptotic rate was already at 80%. (Figure 3.2). In contrast, cisplatin only caused a statistically significant increase in BT16 cell death at 10 µM, where it induced approximately 30% apoptosis. This again suggests that BT16 cells exhibit a higher resistance to the effects of cisplatin in comparison to BT12 cells (Figure 3.3) and correlates with the alamar blue viability results. Similarly, in G401 cells statistically significant apoptosis was detected at the higher concentrations of 5 and 10 µM (Figure 3.4).

In addition to this, the effects of cisplatin over time on apoptosis was also examined in MRT cells. A single concentration was selected for each cell line and the apoptotic response to that concentration was measured over the following timepoints: 8, 16, 24, 48 and 72 hours. The BT12 cell line was treated with 1 µM whereas the BT16 and G401 cell lines were treated with 10 µM. Cisplatin induced apoptosis in a time-responsive manner in the three cell lines. In the BT12 cell line, a statistically significant increase in apoptosis was seen at 48 hours

when treated with 1 µM cisplatin (Figure 3.5). In the BT16 and G401 cell lines, apoptosis was seen from 24 hours when treated with 10 µM cisplatin (Figure 3.6 and Figure 3.7).

Collectively, these results confirm the reports of enhanced resistance of BT16 cells to cisplatin in comparison to BT12 and G401 cells[316].

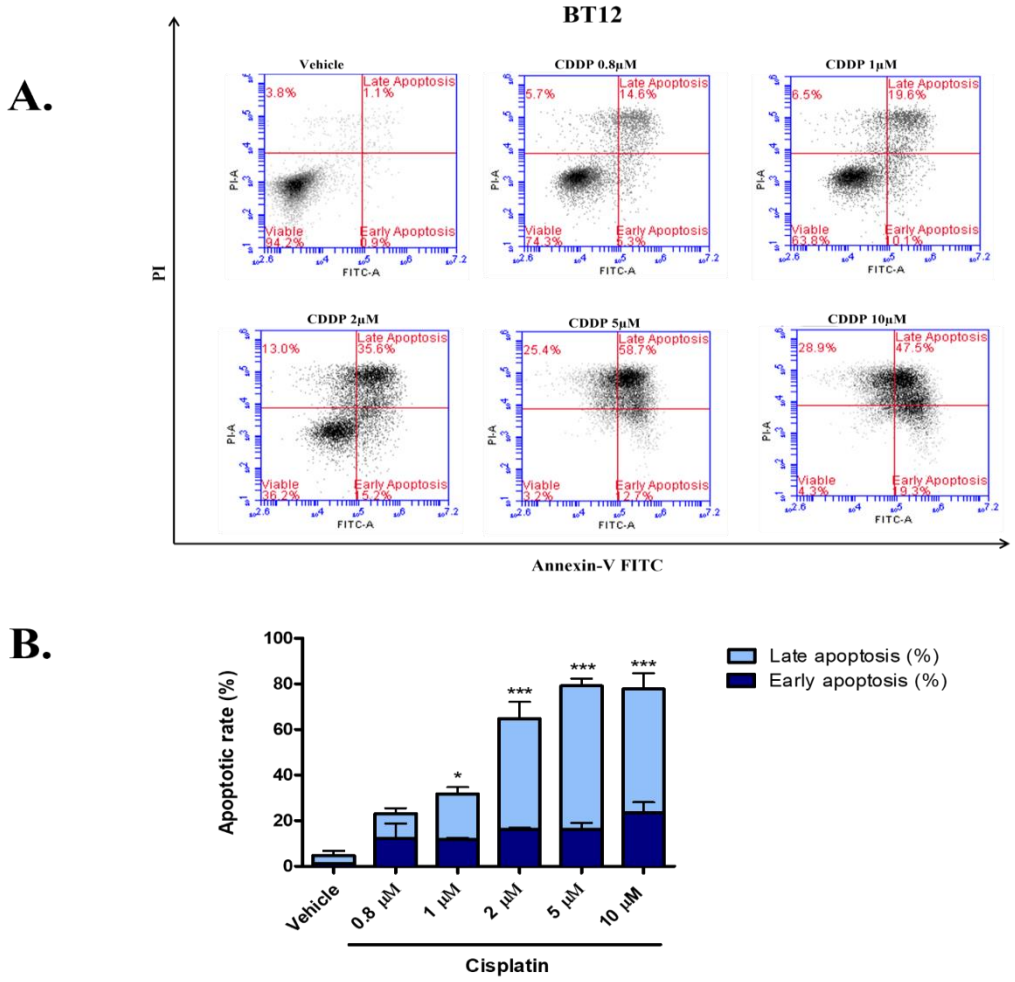

Figure 3.2 Cisplatin induces apoptosis in the BT12 cell line in a dose-dependent manner

2mL of BT12 cells were seeded in a 6-well plate at a seeding density of 1 x 10^5 cells/mL Cells were left to adhere overnight and were then treated with the vehicle (0.009% (v/v) NaCl) or varying concentrations of cisplatin (CDDP) (0.8, 1, 2, 5, 10µM). After 48 hours, the cells were detached and stained with Annexin V-FITC and propidium iodide (PI). The cells were immediately analysed by flow cytometry using the BD FACS Accuri software. 10,000 cells were gated on vehicle treated cells and the percentage of cells undergoing early and late apoptosis was determined to be those stained with Annexin V only or stained with both Annexin V and PI, respectively. Cells stained by only PI suggest another non-apoptotic form of cell death, such as necrosis. **A.** Representative dot plot of treated cells. **B.** Values represent mean ± S.E.M of three independent experiments. Statistical analysis was performed using a one-way ANOVA with Tukey's post hoc test. * $p < 0.05$, *** $p < 0.001$.

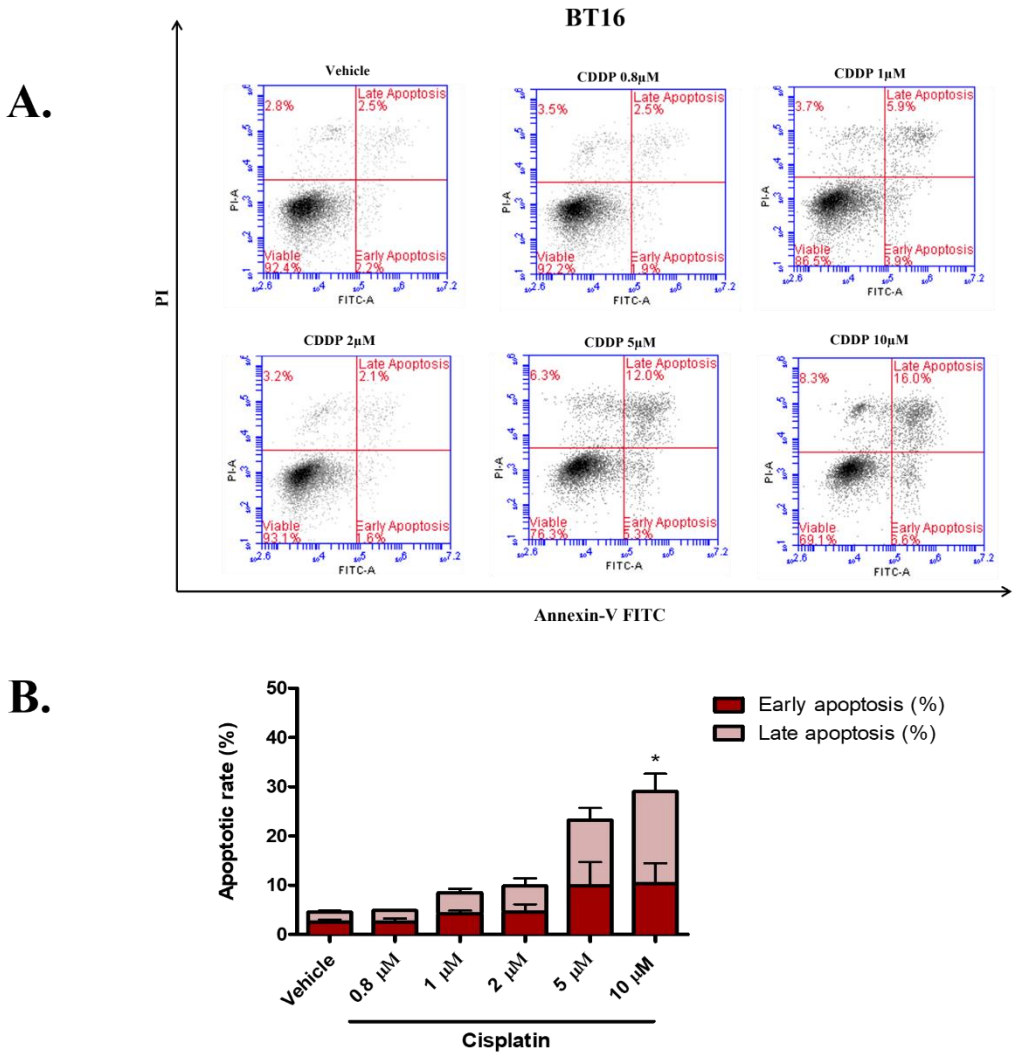

Figure 3.3 Cisplatin induces apoptosis in the BT16 cell line in a dose-dependent manner

2mL of BT16 cells were seeded in a 6-well plate at a seeding density of 1 x 10^5 cells/mL and were left to adhere overnight. The following day cells were treated with the vehicle (0.009% (v/v) NaCl) or varying concentrations of cisplatin (CDDP) (0.8, 1, 2, 5, 10µM) and were left to incubate for 48 hours. The cells were subsequently detached, stained with Annexin V-FITC and PI and were analysed by flow cytometry using the BD FACS Accuri software. Vehicle treated cells were used to gate for 10,000 cells. The percentage of cells undergoing early apoptosis was determined to be those stained with Annexin V only whereas the cells that were stained with both Annexin V and PI were undergoing late apoptosis. **A.** Representative dot plot of treated cells. **B.** Values represent mean ±S.E.M of three independent experiments. Statistical analysis was performed using a one-way ANOVA with Tukey's post hoc test. * $p < 0.05$.

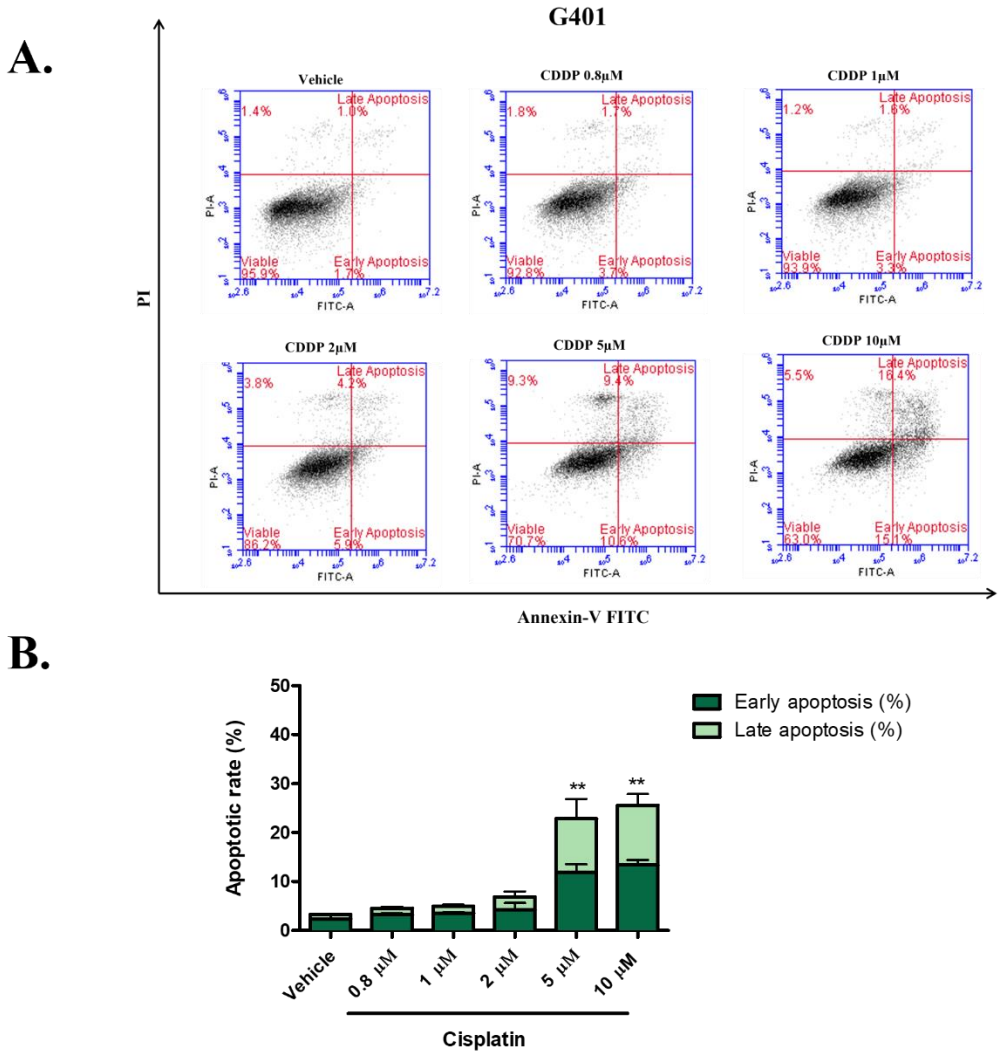

Figure 3.4 Cisplatin induces apoptosis in the G401 cell line in a dose-dependent manner

2mL of G401 cells were seeded in a 6-well plate at a seeding density of 5 x 10^4 cells/mL and were left to adhere overnight. The cells were subsequently treated with the vehicle (0.009% (v/v) NaCl) or varying concentrations of cisplatin (CDDP) (0.8, 1, 2, 5, 10µM). After 48 hours, the cells were detached, stained with Annexin V and PI, then analysed by flow cytometry using the BD FACS Accuri software. The gating was adjusted to count for 10,000 vehicle treated cells. Flow cytometric analysis determines the percentage of cells that are viable, in early apoptosis or in late apoptosis. **A.** Representative dot plot of treated cells. **B.** Values represent mean ± S.E.M of three independent experiments. Statistical analysis was performed using a one-way ANOVA with Tukey's post hoc test. ** $p < 0.01$.

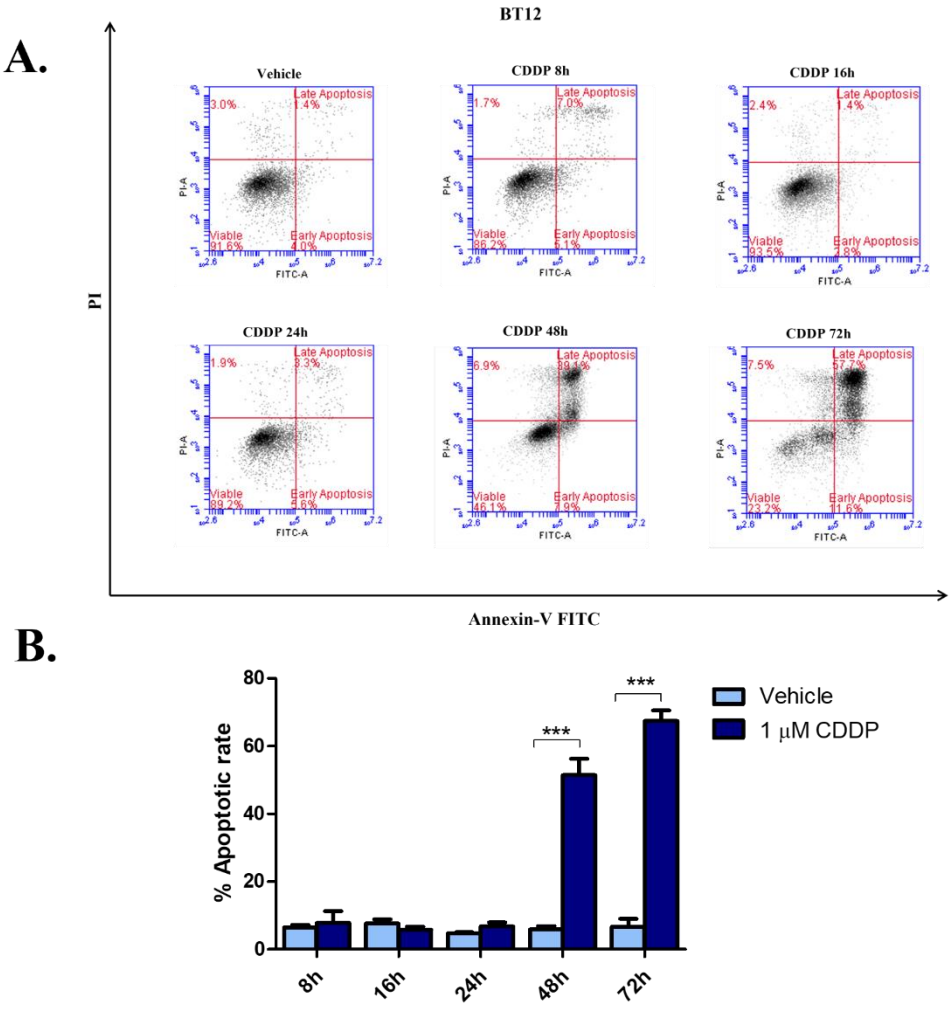

Figure 3.5 Cisplatin induces apoptosis in the BT12 cell line in a time-dependent manner

2mL of BT12 cells were seeded in a 6-well plate at a seeding density of 1 x 10^5 cells/mL. Cells were left to adhere overnight and were then treated with either the vehicle (0.009% NaCl) or CDDP (1 µM) for 8, 16, 24, 48 and 72 hours. At each time point, the cells were detached and stained with Annexin V and propidium iodide (PI). The cells were immediately analysed by flow cytometry using the BD FACS Accuri software. 10,000 cells were gated on vehicle treated cells and the percentage of cells undergoing early and late apoptosis was determined to be those stained with Annexin V only or stained with both Annexin V and PI, respectively. **A.** Representative dot plot of treated cells. **B.** Values represent mean ± S.E.M of three independent experiments. Statistical analysis was performed using a one-way ANOVA with Tukey's post hoc test. *** $p < 0.001$.

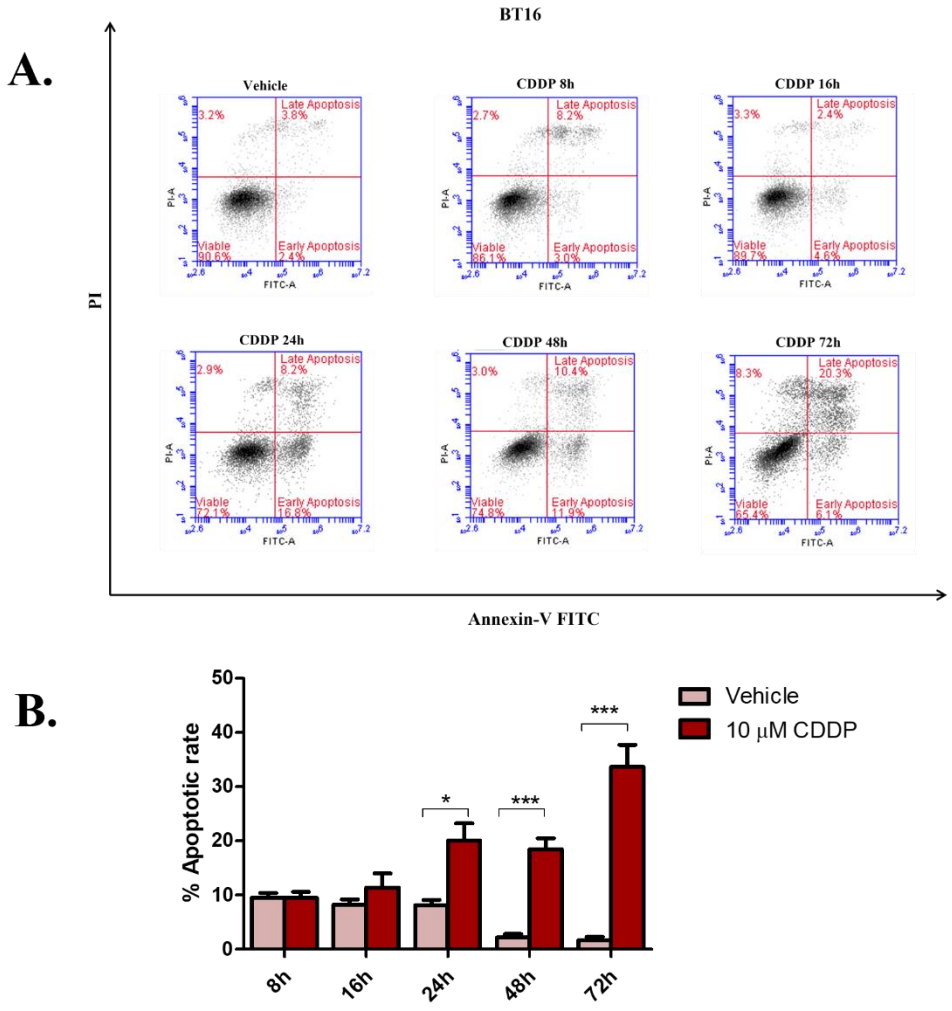

Figure 3.6 Cisplatin induces apoptosis in the BT16 cell line in a time-dependent manner

2mL of BT16 cells were seeded in a 6-well plate at a seeding density of 1 x 10^5 cells/mL. Cells were left to adhere overnight and were then treated with the vehicle (0.009% NaCl) or CDDP (10 μM) for 8, 16, 24, 48 and 72 hours. After each time point, the cells were detached and stained with Annexin V and PI. The cells were analysed by flow cytometry using the BD FACS Accuri software. 10,000 cells were gated on vehicle treated cells and the percentage of cells undergoing early and late apoptosis was determined to be those stained with Annexin V only or stained with both Annexin V and PI, respectively. **A.** Representative dot plot of treated cells. **B.** Values represent mean ± S.E.M of three independent experiments using a one-way ANOVA with Tukey's post hoc test. * $p < 0.05$, *** $p < 0.001$.

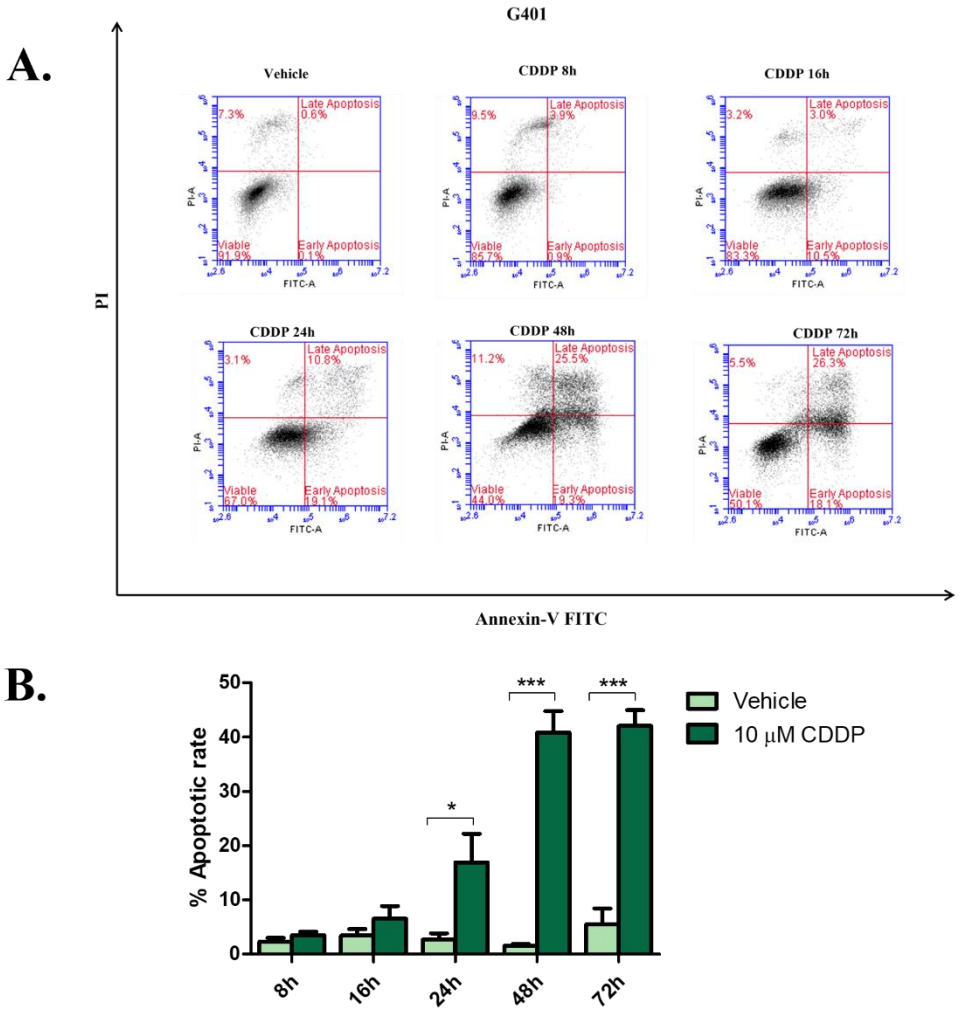

Figure 3.7 Cisplatin induces apoptosis in the G401 cell line in a time-dependent manner

2mL of G401 cells were seeded in a 6-well plate at a seeding density of 5 x 10^4 cells/mL. Cells were left to adhere overnight and were then treated with the vehicle (0.009% NaCl) or CDDP (10 µM) for 8, 16, 24, 48 and 72 hours. Following each time point, the cells were detached, stained with Annexin V and PI and examined through flow cytometric analysis using the BD FACS Accuri software. 10,000 cells were gated on vehicle treated cells and the percentage of cells undergoing early and late apoptosis was determined to be those stained with Annexin V only or stained with both Annexin V and PI, respectively. **A.** Representative dot plot of treated cells. **B.** Values represent mean ± S.E.M of three independent experiments using a one-way ANOVA with Tukey's post hoc test * $p < 0.05$, *** $p < 0.001$.

3.2.2.1 Western blot analysis of caspase 3 activation in BT12 cells

Caspase 3 is an effector caspase that is frequently activated by both the intrinsic and extrinsic apoptotic signalling pathways and is generally considered a reliable marker of apoptosis[351]. This occurs by the cleavage of pro-caspase 3 (32kDa) resulting in the formation of various cleaved caspase 3 fragments (12-23kDa). To further investigate apoptotic cell death, the disappearance of the pro-enzyme form of caspase 3 along with the appearance of cleaved fragments was evaluated by western blot in the BT12 cell line as a representative MRT cell line.

BT12 cells were left to adhere overnight and then treated with a range of concentrations of cisplatin (0.8, 1, 2, 5 and 10 µM). After 48 hours they were harvested, lysates were prepared and run on SDS-PAGE gels. Subsequently, they were transferred to PVDF membranes and probed with caspase 3 and cleaved caspase 3 antibodies. To establish the time-dependent effect of cisplatin, BT12 cells were also treated for 4, 8, 16, 24, 48 and 72 hours with 1 µM cisplatin and caspase 3 activation was monitored at each of these timepoints.

The disappearance of pro-caspase 3 and the appearance of cleaved caspase 3 fragments was displayed following treatment with cisplatin. Pro-caspase 3 was observed to be significantly decreased when compared to the vehicle (Figure 3.8) following treatment with 2 µM cisplatin and increased up to 10µM. In terms, of a time-dependent response, activation of caspase 3 was observed from 48 hours (Figure 3.9). These results correlate with the flow cytometric analysis findings, suggesting that cisplatin induces apoptosis in MRT cells in a dose-and time-dependent manner.

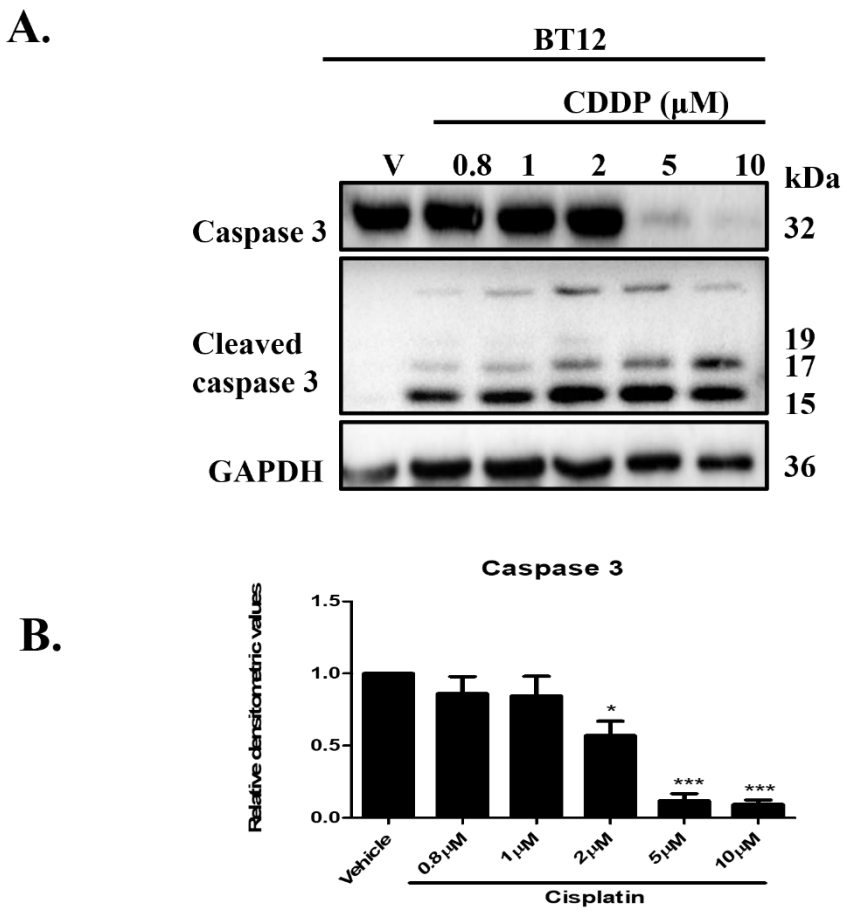

Figure 3.8 Cisplatin induces activation of caspase 3 in BT12 cells in a dose-dependent manner

10 mL of BT12 cells were seeded in a T25 flask at a seeding density of 1 x 10^5 cells/mL. Cells were left to adhere overnight and were then treated with the vehicle (0.009% NaCl) or varying concentrations of cisplatin (CDDP) (0.8, 1, 2, 5, 10μM). After 48 hours, the cells were detached, and lysates were prepared. 20μg of protein was loaded on a 15% gel and transferred onto PVDF membrane which was incubated overnight in caspase 3 and cleaved caspase 3 antibodies. GAPDH served as a loading control. **A.** Results are representative of three experiments. **B.** Densitometric analysis was performed using ImageLab software and the loading control was used to normalise the values obtained. Values represent mean ± S.E.M. of three experiments. Statistical analysis was performed using a one-way ANOVA with Tukey's post hoc test. * $p < 0.05$, *** $p < 0.001$.

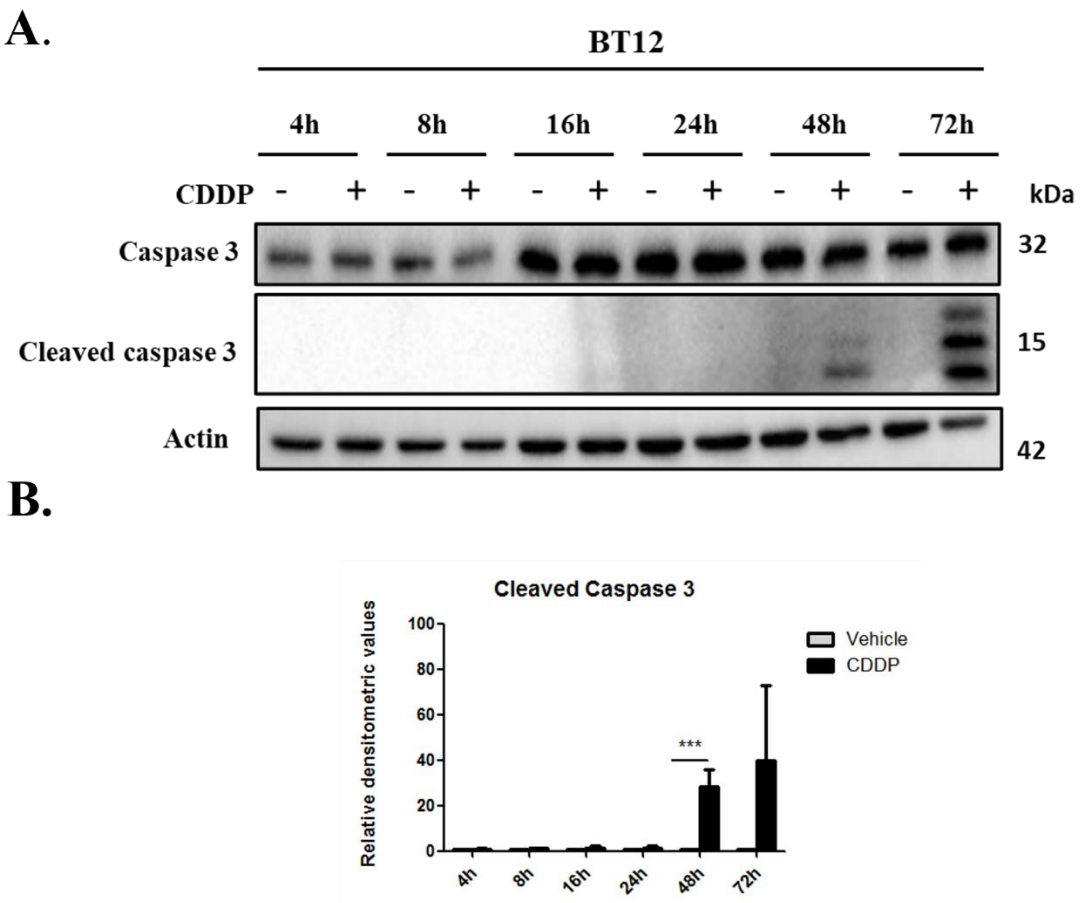

Figure 3.9 Cisplatin induces activation of caspase 3 in BT12 cells in a time-dependent manner

10 mL of BT12 cells were seeded in a T25 flask at a seeding density of 1 x 10^5 cells/mL. Cells were left to adhere overnight and were then treated with the vehicle (0.009% (v/v) NaCl) or CDDP (1 µM) for 8, 16, 24, 48 and 72 hours. At each time point, the cells were detached, and lysates were prepared. 20 µg of protein was loaded on a 15% gel and transferred onto PVDF membrane which was incubated overnight in caspase 3 and cleaved caspase 3 antibodies. GAPDH served as a loading control. **A.** Results are representative of three experiments. **B.** Densitometric analysis of caspase 3 and cleaved caspase 3 was performed using ImageLab software and the loading control was used to normalise the values obtained. Values represent mean ± S.E.M of three independent experiments using a one-way ANOVA with Tukey's post hoc test *** $p < 0.001$.

3.2.3 Basal expression levels of autophagic proteins in a panel of MRT cell lines

Having established that cisplatin induces apoptosis in MRT cells, this study next aimed to establish whether cisplatin also induces an autophagic response in these cells. There are various reports in literature that indicate crosstalk between apoptotic and autophagic pathways[352]. As a starting point, the expression levels of various autophagic proteins were analysed in the panel of MRT cell lines (BT12, BT16 and G401). Some key proteins implicated in autophagy include ATG5, ATG7, Beclin 1, p62 and LC3. The proteins ATG5 and ATG7 are part of the ATG protein family, ATG meaning "autophagy-related". ATG genes are a group of evolutionarily conserved genes characterised namely in yeast[353]. ATG5 and ATG7 are generally considered to be essential components in autophagy and are involved in the elongation and closure of the autophagosome[354]. For this reason, ATG7 and ATG5, are commonly targeted by RNA-based interference knockdown in the field of autophagy research[355, 356]. Beclin 1, encoded by the BECN1 gene, is a mammalian orthologue of ATG6 in yeast. Beclin 1 is a core component of the PI3KC3 complex and is essential in regulating the initiation of autophagosome formation[357]. The protein LC3-I is converted to LC3-II during autophagy and is often used a marker of autophagy activation. Both LC3-I and LC3-II can be detected via western blot analysis due to their varying molecular weights. Along with LC3-II conversion, autophagy activation is also commonly monitored through the degradation of p62 which can be visualised using western blotting[358]. The basal expression levels of these proteins were examined via western blot analysis in BT12, BT16 and G401 cells.

All the autophagic proteins examined were expressed in the three cell lines (Figure 3.10). Significantly higher expression levels of ATG5 were observed in G401 cells when compared to BT12 and BT16 cells (Figure 3.11). A slight increase in expression levels of ATG7, beclin and p62 was also observed in G401 cells when compared to BT12 and BT16 cells but this increase was not deemed significant. Finally, when comparing BT12 and BT16 cells, there was no difference in the expression levels of any of the autophagic proteins under examination.

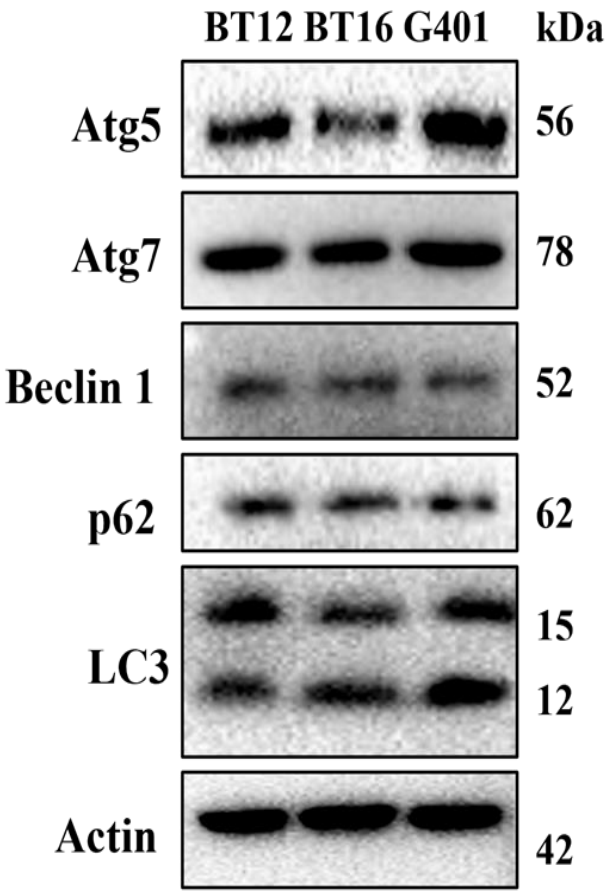

Figure 3.10 Expression of basal levels of autophagic proteins in a panel of MRT cell lines

MRT cell lines (BT12, BT16 and G401) were seeded at various densities in T175 flasks and grown to sub-confluency. The cells were then harvested, and lysates prepared for western blot analysis. 20 ug of protein was loaded, separated on an SDS page gel, transferred to PVDF and probed with the relevant antibodies. Results are representative of three independent experiments. Actin was used as a representative loading control.

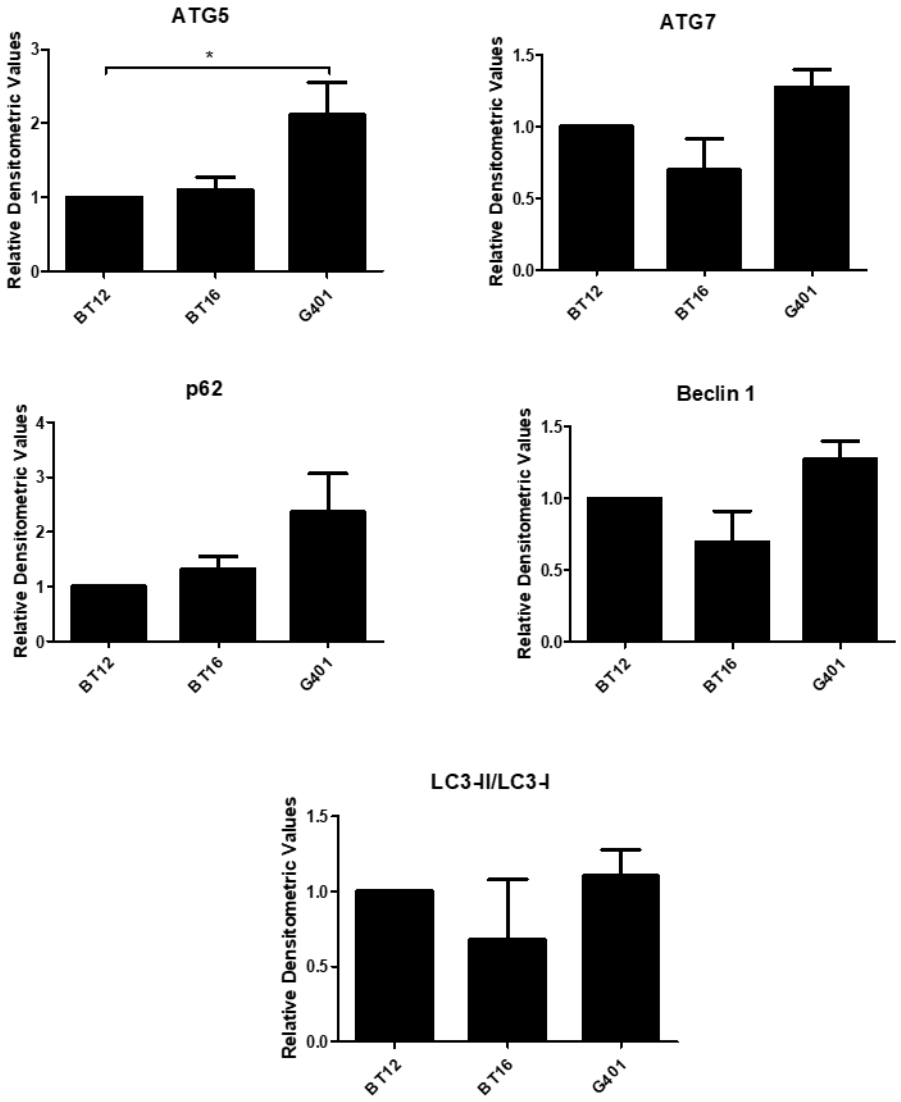

Figure 3.11 Densitometric analysis of expression of basal levels of autophagic proteins in a panel of MRT cell lines

MRT cell lines (BT12, BT16 and G401) were seeded at various densities in T175 flasks and grown to sub-confluency. The cells were then harvested, and lysates prepared for western blot analysis. 20 ug of protein was loaded, separated on an SDS page gel, transferred to PVDF and probed with the relevant antibodies. Results are representative of three independent experiments. Actin was used as a representative loading control. All the values were normalised against BT12 to obtain the relative densitometric value. Results represent the mean and S.E.M of at least three experiments. Statistical analysis was performed using one way ANOVA with Tukey's post hoc test. *$p<0.05$.

3.2.4 Evaluation of basal levels of autophagic flux in a panel of MRT cell lines

Next, the basal levels of autophagy in the panel of MRT cell lines were evaluated. According to the literature, this is typically achieved by inducing autophagy through starvation and blocking the flux with a late-stage autophagy inhibitor[288]. The degradation of p62 and the conversion of LC3-I to LC3-II is indicative of autophagy activation. The degradation of p62 is visualised by the decrease of p62 expression levels on a western blot. The p62 protein is internalised and degraded by the autophagosome itself during autophagy. The protein LC3 is cleaved by ATG4 to form LC3-I. During the autophagic process, LC3-I is conjugated to phosphatidylethanolamine (PE) to form LC3-II. The two forms of LC3-I and LC3-II can be distinguished on a western blot due to their different molecular weights. In fact, the conversion of LC3-I to LC3-II is a commonly utilised method of monitoring autophagy[267].

Autophagic flux is defined as the measurement of autophagic degradation activity. Blocking the degradation step in autophagy results in an accumulation of autophagosomes corresponding to the levels of autophagic activity[359]. The lysosomal inhibitor, bafilomycin-A1, is commonly used to block autophagy when measuring autophagic flux[360].

A panel of MRT cell lines were untreated or treated with EBSS (Earle's Balanced Salt Solution) for 4 hours, in order to starve the cells. In some cases, bafilomycin-A1(100nM) was added for the last hour of incubation. The cells were harvested and analysed by western blotting. An accumulation of p62 and LC3 in samples treated with bafilomycin-A1 was observed, demonstrating that autophagy is active at a basal level in the MRT cells. Moreover, starvation with EBSS caused a decrease in p62 levels and a conversion of LC3-I to LC3-II indicating that autophagy can be induced in MRT cells by external stimuli, such as starvation (Figure 3.12). Following on from this, EBSS was selected as a positive control in further experiments monitoring autophagy.

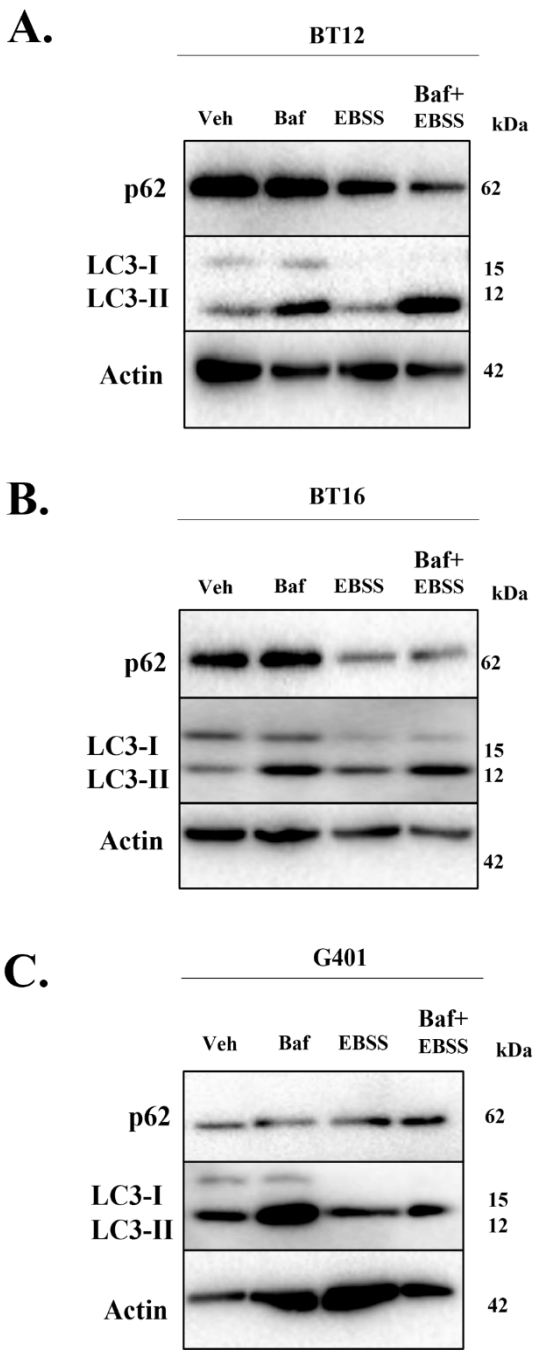

Figure 3.12 Evaluation of basal levels of autophagy in a panel of MRT cell lines

The MRT cell lines BT12 (**A**), BT16 (**B**) and G401 (**C**) were seeded at various seeding densities. The cells were left untreated, treated with EBSS for 4 hours, treated with bafilomycin-A1 (100nM) for one hour or a combination of EBSS and bafilomycin. After the incubation period, the cells were harvested and lysed. 20 µg of protein lysate was loaded onto a 15% SDS-PAGE gel. The protein was then transferred onto a PVDF membrane, incubated in blocking milk for one hour and probed for LC3 and p62. Actin

was used as a loading control. This figure is representative of three independent experiments.

3.2.5 Cisplatin induces autophagy in a dose- and time-dependent manner in MRT cell lines

Several reports have indicated that cisplatin can simultaneously induce autophagy and apoptosis in cancerous cells such as oesophageal and ovarian cancer[319, 361-363]. Following the observation that cisplatin induces apoptosis in MRT cell lines, the effect of cisplatin on autophagy was investigated through western blotting and flow cytometric analysis of Cyto-ID-stained cells.

3.2.5.1 Western blot analysis of autophagic markers in response to cisplatin in MRT cells

Western blot analysis of LC3-I/LC3-II and p62 was conducted in BT12 cells following treatment with cisplatin. Cells were seeded and treated the following day for 48 hours with either vehicle (0.009% (v/v) NaCl) or increasing concentrations of cisplatin (0.8, 1, 2, 5 and 10 µM) to evaluate the dose-responsive effect of cisplatin on autophagy. As a positive control, cells were starved with Earle's balanced salts solution (EBSS) for 4 hours to induce autophagy. Moreover, the effect of cisplatin on autophagy over time was also examined. Cells were treated with 1 µM cisplatin for 4, 8, 16, 24, 48 and 72 hours and LC3-I to LC3II conversion and p62 degradation was monitored. Densitometric analysis was performed using ImageLab software and the ratio of LC3-I to LC3-II conversion was calculated.

Conversion of LC3-I to LC3-II and degradation of p62 was observed in BT12 cells treated with EBSS for 4 hours, indicating activation of the autophagic flux under starvation conditions (Figure 3.13).

Cisplatin was also shown to induce autophagy in BT12 cells in a dose-dependent manner. A statistically significant conversion of LC3-I to II was observed upon cisplatin treatment. p62 was also observed to significantly decrease in response to increasing concentrations of cisplatin (Figure 3.14) with a significant reduction of p62 demonstrated from 48 hours. Thus, cisplatin induces autophagy in MRT cells in a dose- and time-dependent manner. Interestingly, these results indicate that cisplatin induces apoptosis and autophagy simultaneously in BT12 cells.

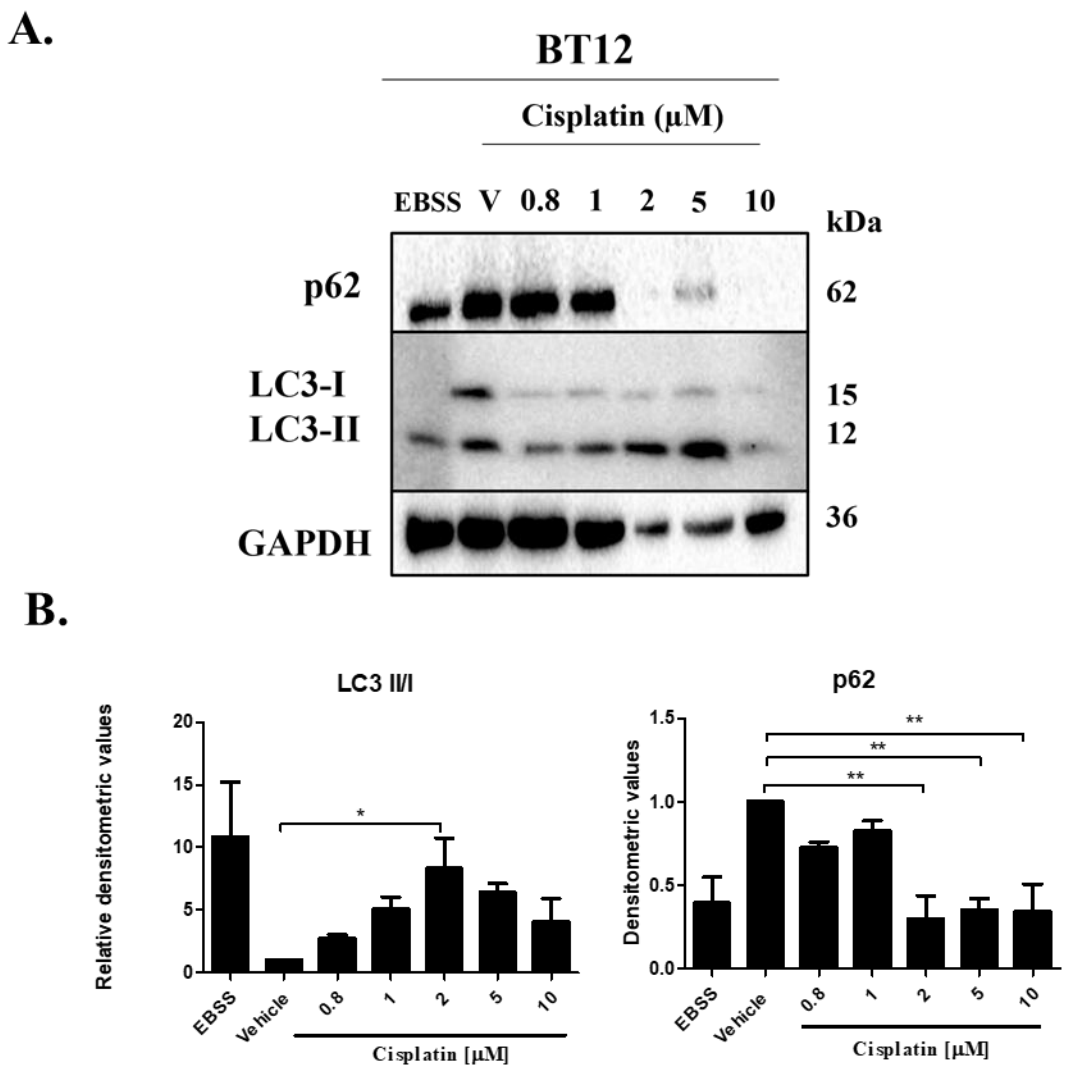

Figure 3.13 Cisplatin induces autophagy in BT12 cell line in a dose-dependent manner

10 mL of BT12 cells were seeded in a T25 flask at a seeding density of 1 x 10^5 cells/mL. Cells were left to adhere overnight and were then treated with the vehicle (0.009% (v/v) NaCl) or varying concentrations of cisplatin (0.8, 1, 2, 5, 10µM). EBSS treatment for 4 hours was used as a positive control. After 48 hours, the cells were detached, and lysates were prepared. 20µg of protein was loaded on a 15% gel and transferred onto PVDF membrane which was incubated overnight in p62 and LC3 antibodies. GAPDH served as a loading control. **A.** Results are representative of three experiments. **B.** Densitometric analysis of LC3 and p62 was performed using ImageLab software and the loading control was used to normalise the values obtained. Statistical analysis was performed using a one-way ANOVA with Tukey's post hoc test. * $p < 0.05$, **$p < 0.01$.

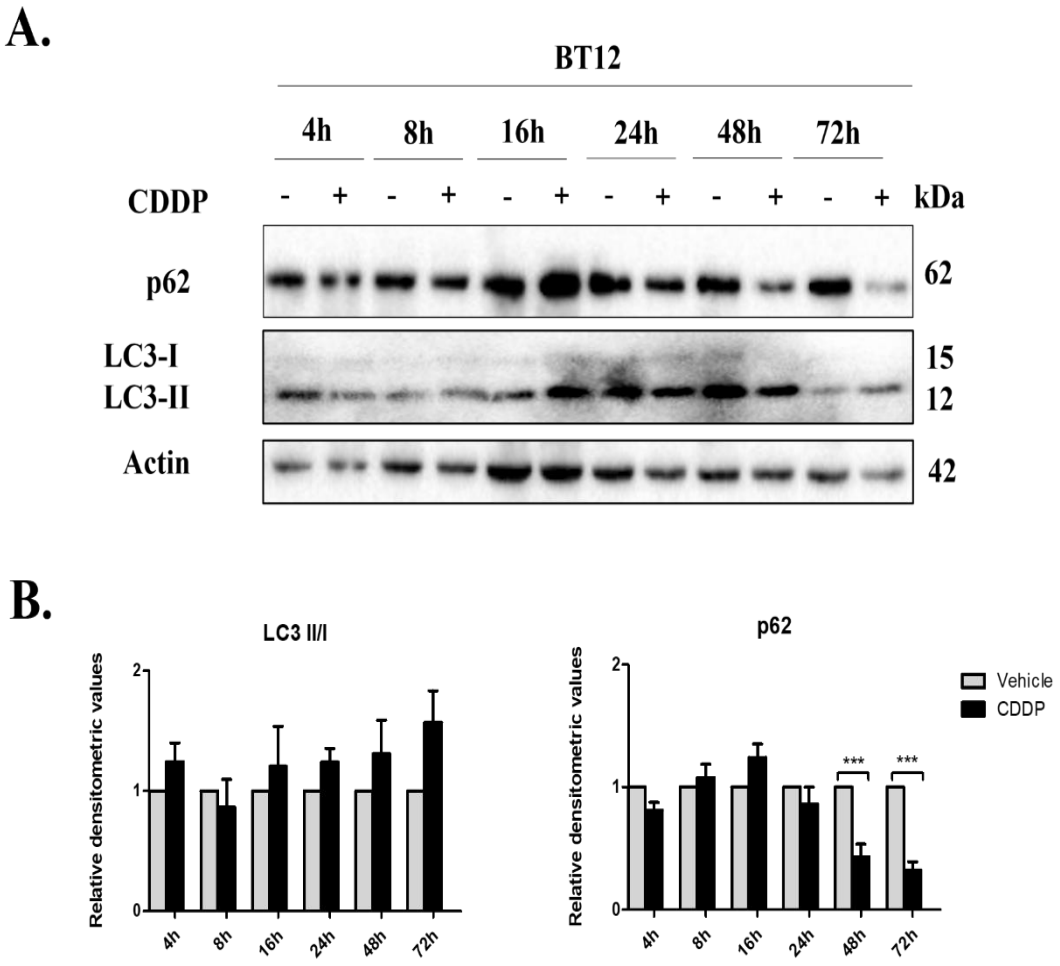

Figure 3.14 Cisplatin induces autophagy in the BT12 cell line in a time-dependent manner.

10 mL of BT12 cells were seeded in a T25 flask at a seeding density of 1 x 10^5 cells/mL. Cells were left to adhere overnight and were then treated with the vehicle (0.009% (v/v) NaCl) or CDDP (1 µM) for 8, 16, 24, 48 and 72 hours. At each time point, the cells were detached, and lysates were prepared. 20µg of protein was loaded on a 15% gel and transferred onto PVDF membrane which was incubated overnight in a p62 antibody. Actin served as a loading control. **A.** Results are representative of three experiments. **B.** Densitometric analysis of p62 and LC3-II/LC3-I was performed using ImageLab software and the loading control was used to normalise the values obtained. Values represent the mean and the S.E.M of three independent experiments. Statistical analysis was performed using one-way ANOVA with Tukey's post hoc test. ***$p<0.001$.

3.2.5.2 Flow cytometric analysis of autophagosome formation in response to cisplatin in MRT cells

The effect of cisplatin on autophagosome formation in MRT cells was next established through flow cytometric analysis of Cyto-ID-stained cells. The Cyto-ID green autophagy dye (Enzo Life Sciences) becomes highly fluorescent when it is integrated in autophagic vesicles and represents a quantitative approach of monitoring autophagy at a cellular level[364].

The effect of cisplatin on autophagosome formation was monitored at a range of concentrations in BT12, BT16 and G401 cell lines to confirm autophagy induction. The cells were treated with 0.8, 1, 2, 5 and 10 µM cisplatin for 48 hours. As a positive control (as recommended by Enzo Life Sciences), cells were treated with rapamycin and chloroquine in combination. Rapamycin induces autophagy through the inhibition of mTOR and chloroquine is a late-stage inhibitor, which causes an accumulation of autophagosomes by blocking autophagic flux, resulting in a strong fluorescent signal[365, 366]. After a 48-hour treatment, the cells were harvested and stained with Cyto-ID green dye and the fluorescence was detected using a BD Accuri flow cytometer. The Median Fluorescence Intensity (MFI) values were obtained.

Rapamycin/chloroquine treatment resulted in an enhancement of autophagosome formation in all three cell lines demonstrating the validity of the assay. Moreover, autophagy was induced in MRT cells in response to cisplatin in a dose-responsive manner. In BT12 cells, a significant enhancement of autophagosome formation was first observed following treatment with the lowest concentration of cisplatin (0.8 µM) and this increased up to 2 µM. Notably, at the higher concentrations of 5 and 10 µM cisplatin, autophagy was dramatically reduced below basal levels, which correlated with the LC3-I/LC3-II western blot result (Figure 3.13). This is likely due to the fact that the BT12 cells are no longer viable when treated at these high cisplatin concentrations (Figure 3.15). In BT16 cells, autophagosome formation increased in response to cisplatin a dose-dependent manner, with a significant enhancement at the highest concentration of cisplatin (10µM). In G401 cells, a significant enhancement of autophagosome formation was observed from 5 µM. Collectively this demonstrates the decreased sensitivity of BT16 and G401 cells to cisplatin-induced autophagy when compared to the BT12 cells.

To assess the time-dependent effect of cisplatin on autophagosome formation, BT12 cells were treated with 1 µM of cisplatin for 8, 16, 24 and 48 hours. In line with the western blot results (Figure 3.14), a statistically significant increase in autophagy was seen at 48 hours (Figure 3.16).

Overall, these results support those obtained via western blot analysis and confirm that autophagy is induced in response to cisplatin in a dose- and time-dependent manner in MRT cell lines.

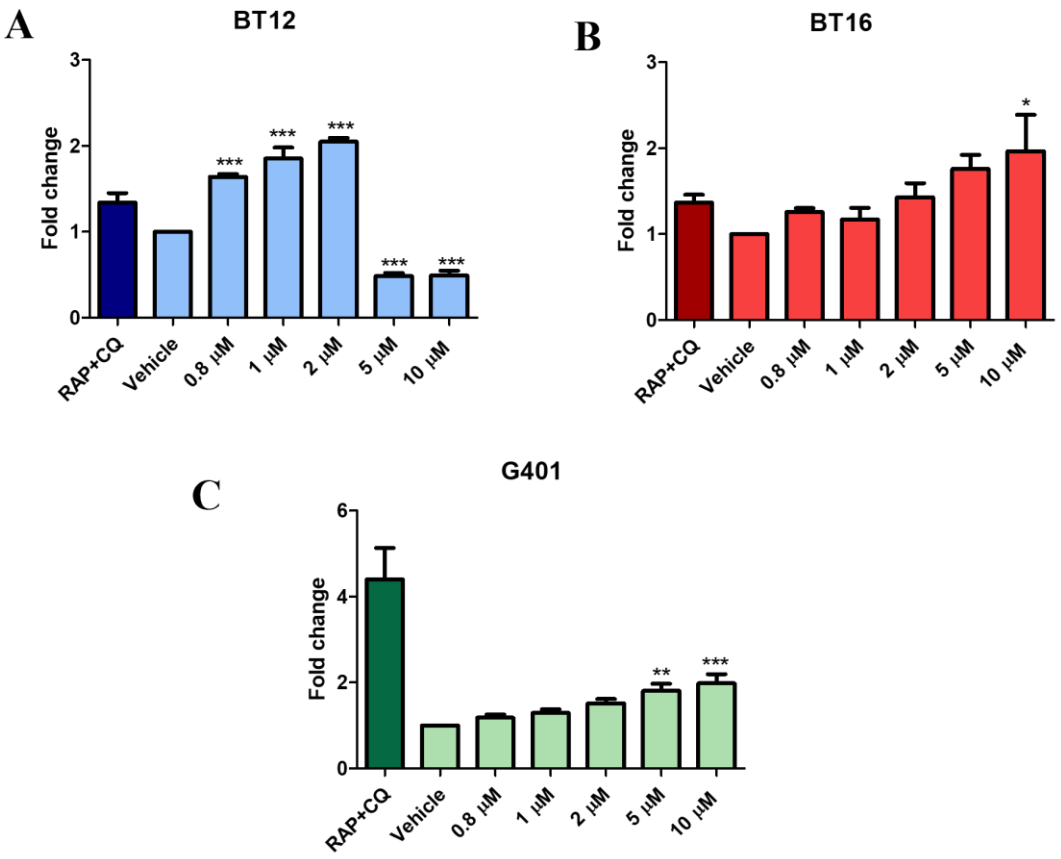

Figure 3.15 Cisplatin enhances autophagosome formation in BT12, BT16 and G401 cell lines

2mL of BT12, BT16 and G401 cells were seeded at various densities and left to adhere overnight. After 24 hours, the cells were treated with the vehicle (0.009% NaCl) or varying concentrations of cisplatin (CDDP) (0.8, 1, 2, 5, 10µM). Rapamycin (0.5 µM) and chloroquine (10 µM) was used as a positive control. After 48 hours, the cells were detached from the wells and stained with CytoID green autophagy dye. The cells were immediately analysed by flow cytometry using the BD FACS Acurri software. 10,000 cells were gated on vehicle treated cells and the media fluorescence values were acquired for BT12 (**A**), BT16 (**B**) and G401 (**C**) cells. Values represent mean with S.E.M of three independent and were normalised by the vehicle. Statistical analysis was performed using a one-way ANOVA with Dunnett's Multiple Comparison Test to compare mean values between vehicle and treated cells. *p<0.05, ** p < 0.01., *** p < 0.001.

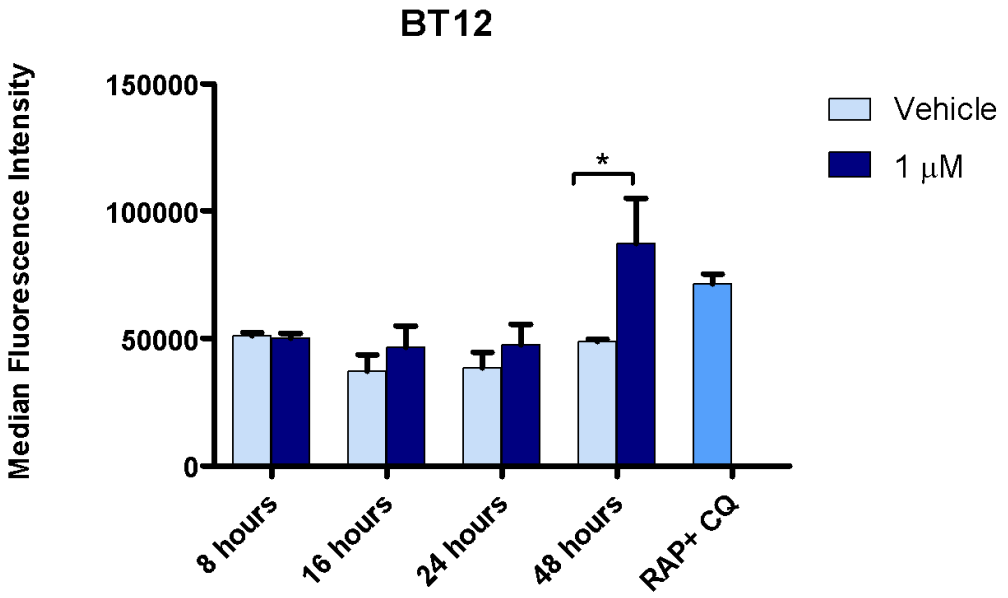

Figure 3.16 Cisplatin enhances autophagosome formation in BT12 cell lines in a time-responsive manner

2mL of BT12 cells were seeded at 1 x 10^5 cells/mL and left to adhere overnight. After 24 hours, the cells were treated with the vehicle (0.009% NaCl) or with cisplatin (CDDP) (1 μM). Rapamycin (RAP) (0.5 μM) and chloroquine (CQ) (10 μM) was used as a positive control in a 48-hour treatment. After the indicated time points, the cells were detached from the wells and stained with CytoID green autophagy dye and cells were immediately analysed by flow cytometry using the BD FACS Accuri software. 10,000 cells were gated on vehicle treated cells and the media fluorescence values were acquired for the cells. Values represent mean with S.E.M of three independent experiments and were normalised by the vehicle. Statistical analysis was performed using one-way ANOVA with Tukey's post hoc test p *< 0.05.

3.2.6 Cisplatin induces the activation of autophagic flux in MRT cells

The results presented herein suggested that autophagy is activated in response to cisplatin treatment in MRT cells. This was shown through an increase in LC3-I/LC3-II conversion and p62 degradation by western blot analysis and an increase in autophagosome formation by flow cytometric analysis of Cyto-ID-stained cells. However, these results were insufficient to definitively determine that the dynamic process of autophagic flux is occurring in the MRT cells. The number of autophagosomes is a function of the balance between the rate of their generation and the rate of their conversion into autolysosomes. Therefore, an increase in autophagosomes can be indicative of either autophagy activation or the inhibition of autophagosome maturation resulting in an accumulation of vesicles. Similarly, a low level of autophagosomes can signify autophagy inhibition or an enhanced turnover rate of autophagic vesicles[367]. Therefore, to confirm that cisplatin induces autophagy in MRT cell lines a late-stage lysosomal autophagy inhibitor, chloroquine, was utilised to block the autophagic flux. This inhibits autophagosome turnover. Thus, a combination treatment of cisplatin and chloroquine should result in a higher level of autophagosomes than a treatment of either cisplatin or chloroquine alone [288, 367, 368].

BT12 and BT16 cells were treated with vehicle, cisplatin alone (1 or 10 µM of cisplatin, respectively), chloroquine alone (20 µM) or cisplatin and chloroquine in combination. In addition, cells were treated with rapamycin and chloroquine in combination as a positive control. After 48 hours, cells were harvested, stained with Cyto-ID green autophagy dye and analysed using the BD Accuri flow cytometer. As expected, the combination of rapamycin and chloroquine treatment resulted in a notable enhancement of MFI values when compared to vehicle treatment. An increase in MFI values was also observed in MRT cells when treated with cisplatin or chloroquine alone. Furthermore, a significant enhancement in fluorescence was observed in the cells treated with a combination of cisplatin and chloroquine when compared to cisplatin and chloroquine treatments on their own (Figure 3.17). This suggested that the autophagosome levels observed following cisplatin treatment were due to the induction of autophagy as when the flux was blocked, an increase in fluorescence was still observed.

Taken together, this result suggests that cisplatin promotes an increase of autophagic vesicles in MRT cells due to the activation of the autophagic flux and excludes secondary accumulations due to autophagic degradation blockade.

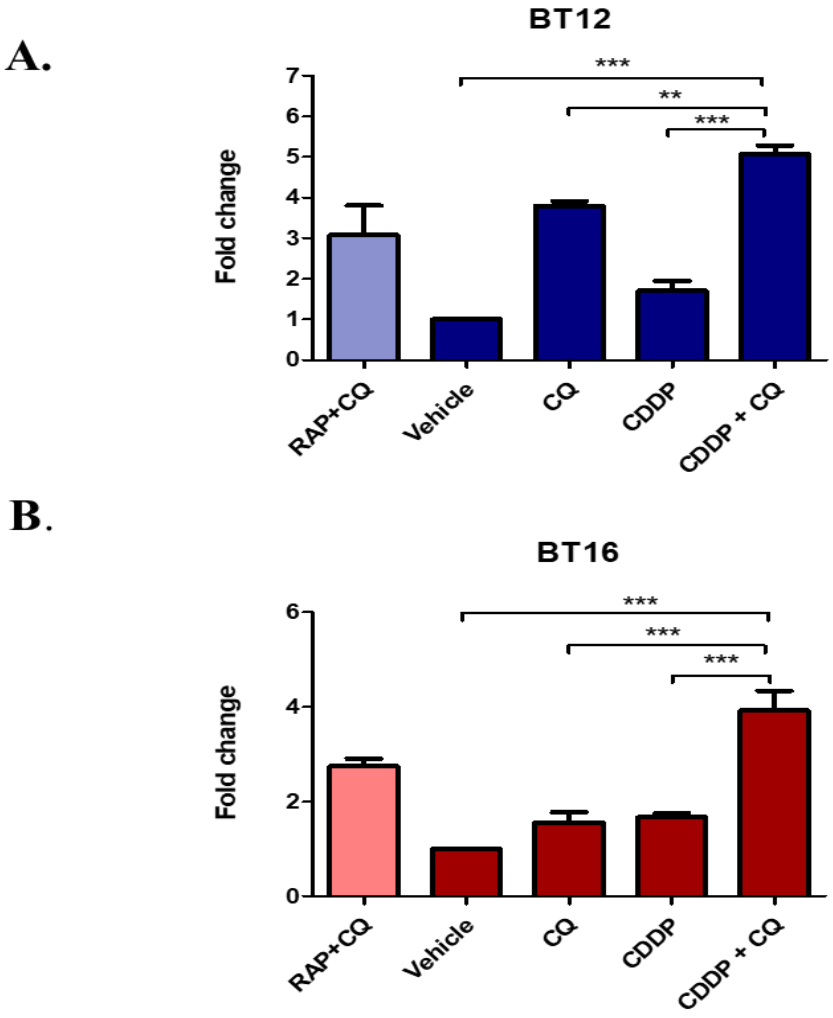

Figure 3.17 Cisplatin induces autophagic flux in BT12 and BT16 cell lines

2mL of BT12 and BT16 cells were seeded at 1 x 10^5 cells/mL and left to adhere overnight. After 24 hours, the cells were treated with the vehicle (0.009% (v) NaCl), chloroquine (CQ) (20 μM), cisplatin (CDDP) (1 μM and 10 μM in BT12 and BT16 cells respectively) or cisplatin and chloroquine in combination. Rapamycin (RAP) (0.5 μM) and chloroquine (10 μM) in combination was used as a positive control. After 48 hours, the cells were detached from the wells and stained with Cyto ID green autophagy dye. The cells were immediately analysed by flow cytometry using the BD FACS Accuri software. 10,000 cells were gated on vehicle treated cells and the median fluorescence values were acquired for BT12 (**A**) and BT16 (**B**) cells. Values represent mean ± S.E.M of three independent and were normalised by the vehicle. Statistical analysis was performed using a using a one-way ANOVA with Tukey's post hoc test. ** $p < 0.01$, ***$p<0.001$.

3.2.7 Evaluation of targeting autophagy for the treatment of MRT

Results presented herein demonstrated that autophagy is activated in MRT cells in response to cisplatin. To determine the role of autophagy in mediating chemoresistance, autophagy was first targeted using pharmacological inhibitors. In the field of autophagy, pharmacological inhibitors are classified as early-stage inhibitors or late-stage inhibitors depending on at which step of the process the inhibitors act on[345]. Early-stage inhibitors target the initial steps of the autophagic process to block the activation of autophagy machinery whereas late-stage inhibitors target the lysosome[369].

3.2.7.1 Targeting autophagy with an early-stage autophagy inhibitor has no effect on cisplatin-induced apoptosis in MRT cells

SAR405 is a potent and selective early-stage autophagy inhibitor, which acts by blocking two Vps34 complexes: Vps18 and Vps35 which in turn blocks the formation of autophagosomes[291].

The effect of SAR405 on autophagy was first assessed via western blot analysis. Treatment of cells with increasing concentrations of SAR405 resulted in a notable accumulation of p62 in all three MRT cell lines as well as a decrease in the conversion of LC3-I to LC3-II (significant in BT12 and BT16 cell lines), indicating that, as expected, SAR405 appears to block autophagy.

Next, the effect of SAR405 on cisplatin-induced apoptosis was determined through flow cytometric analysis of Annexin V/PI-stained cells. Cells were treated with increasing concentrations of either SAR405 alone, or in combination with cisplatin. Results demonstrated that SAR405 had no effect on cisplatin-induced apoptosis in any of the MRT cells lines, at any concentration tested (Figure 3.19-3.21).

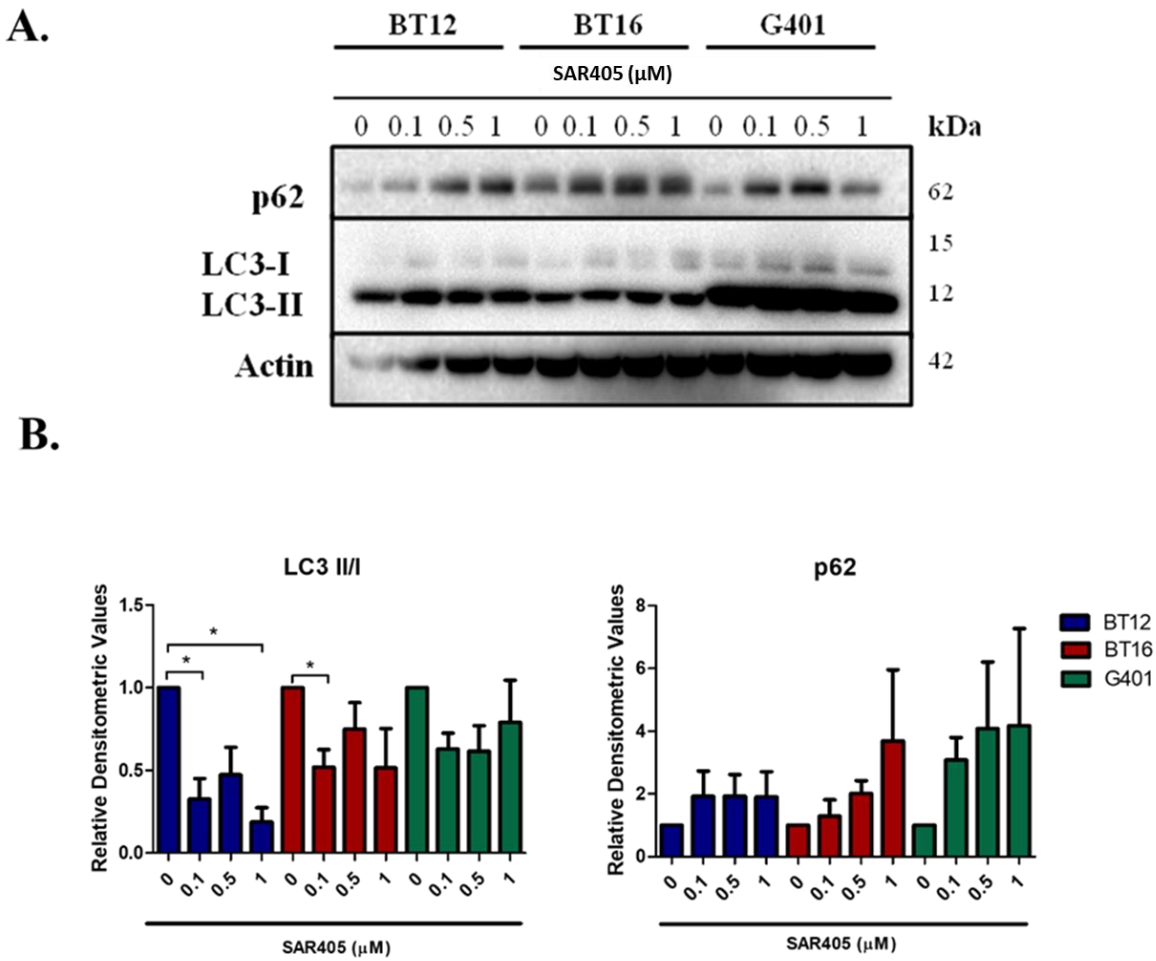

Figure 3.18 SAR405 inhibits autophagy in panel of MRT cell lines.

The BT12, BT16 and G401 cell lines were seeded at their optimum cell densities in a T25 flask. Cells were left to adhere overnight and were treated with various concentrations of SAR405 (0, 0.1, 0.5 or 1 μM) for 48h. After incubation, cells were harvested and lysed. 20 μg of protein was loaded onto a 15% SDS-gel, transferred onto a PVDF membrane and probed with anti-p62 and anti-LC3-I/LC3-II antibodies. Actin was used as a loading control **A**. Results are representative of at least 3 independent experiments. **B**. Densitometric analysis was conducted and statistical analysis was performed using paired two-tailed t-test. (GraphPad Prism 5). * $p<0.05$.

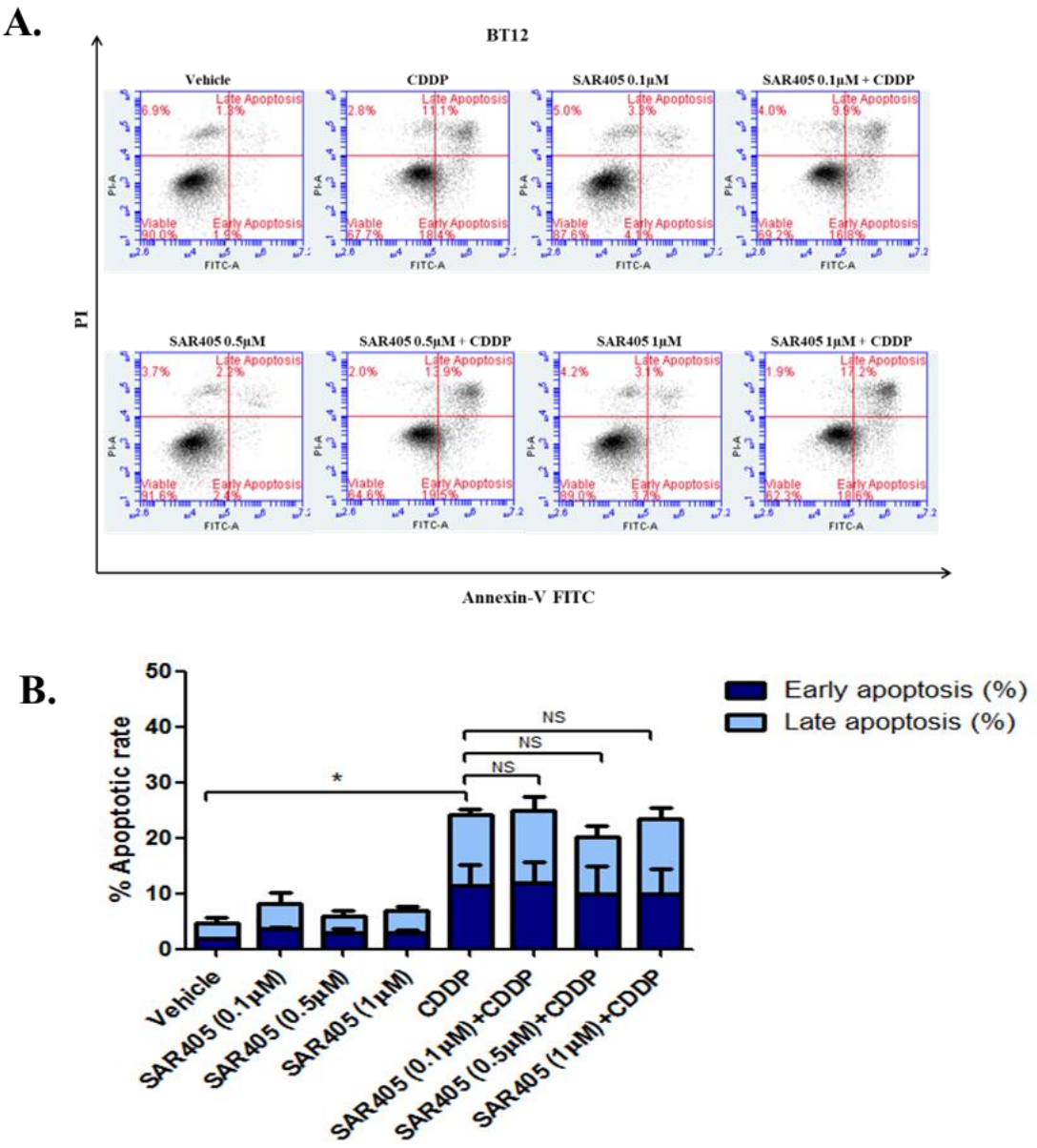

Figure 3.19 SAR405 has no effect on cisplatin-induced apoptosis in BT12 cells

BT12 cells were seeded at 1 x 10^5 cells/mL in a 6-well plate. Cells were pre-treated for 1 h with various concentrations of SAR405 (0, 0.1, 0.5 and 1µM). After an hour, cells were treated with cisplatin (1µM) on its own or in combination with SAR405 for 48h. Cells were analysed by flow cytometry using BD FACS Accuri software. 10,000 cells single cells were gated on vehicle treated cells and the percentage of cells undergoing early and late apoptosis was acquired. **A**. Representative dot plot of treated cells. **B**. Values represent the mean and S.E.M of three independent experiments. Statistical analysis was performed using one-way ANOVA with Tukey's Multiple Comparison Test (GraphPad Prism 5). *p<0.05; NS: non-significant.

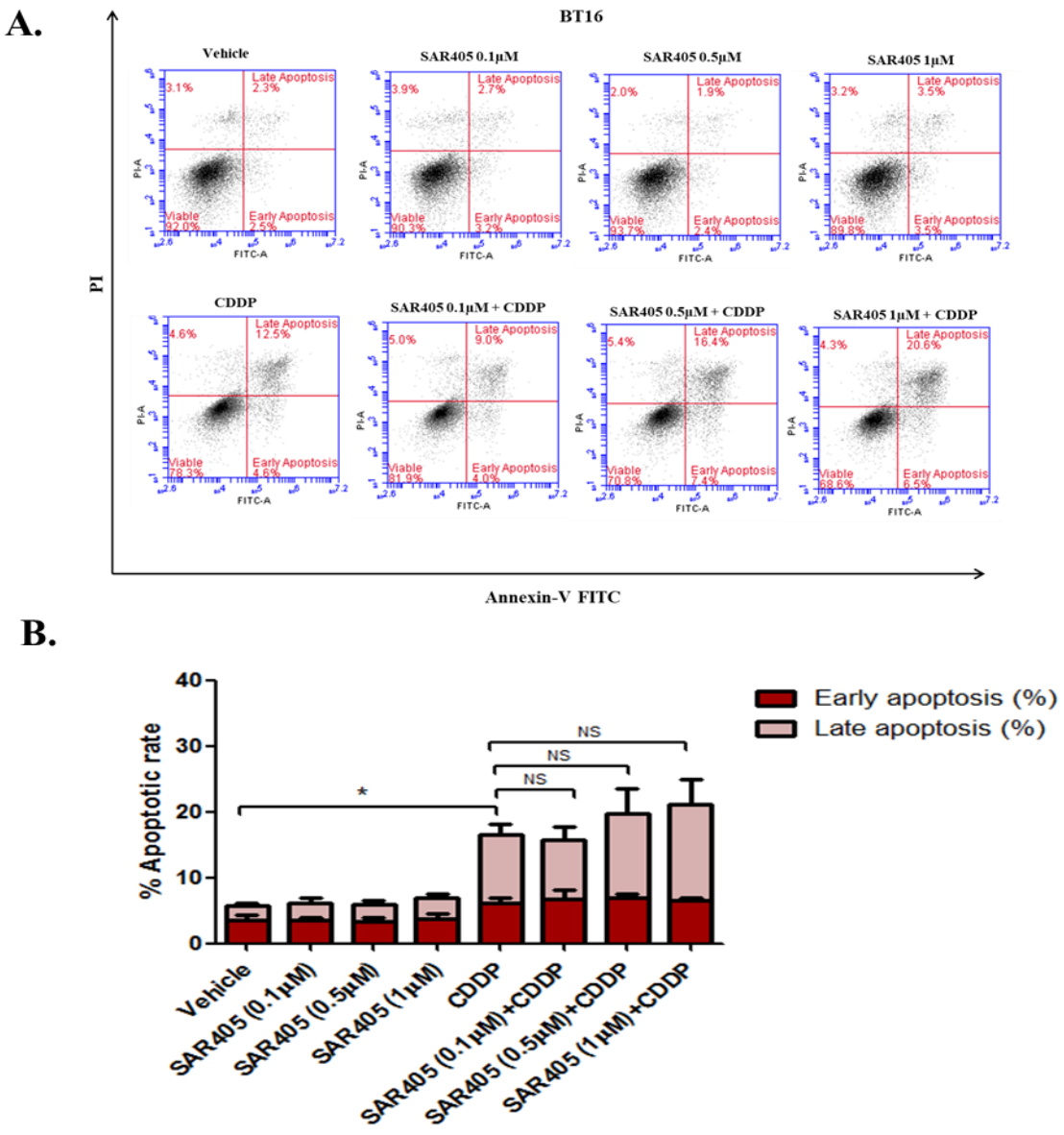

Figure 3.20 SAR405 has no effect on cisplatin-induced apoptosis in BT16 cells

BT16 cells were seeded at 1 x 10^5 cells/mL in a 6-well plate. Cells were pre-treated for 1 h with various concentrations of SAR405 (0, 0.1, 0.5 and 1µM). After an hour, cells were treated with cisplatin (1µM) on its own or in combination with SAR405 for 48h. Cells were analysed by flow cytometry using BD FACS Accuri software. 10,000 cells single cells were gated on vehicle treated cells and the percentage of cells undergoing early and late apoptosis was acquired. **A**. Representative dot plot of treated cells. **B**. Values represent the mean and S.E.M of three independent experiments. Statistical analysis was performed using one-way ANOVA with Tukey's Multiple Comparison Test (GraphPad Prism 5). *p<0.05; NS: non-significant.

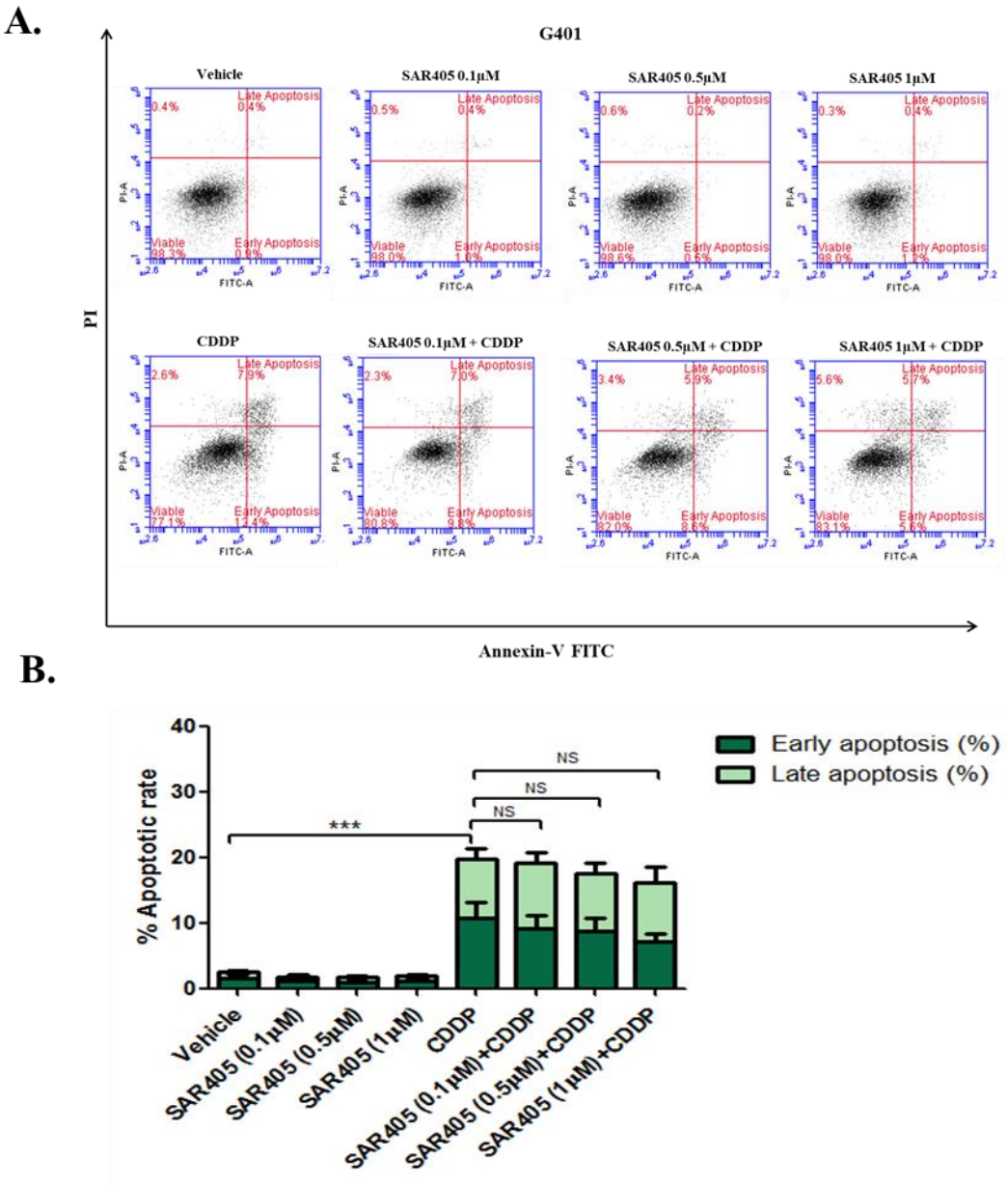

Figure 3.21 SAR405 has no effect on cisplatin-induced apoptosis in G401 cells

G401 cells were seeded at 5 x 10^4 cells/mL in a 6-well plate. Cells were pre-treated for 1 h with various concentrations of SAR405 (0, 0.1, 0.5 and 1µM). After an hour, cells were treated with cisplatin (1µM) on its own or in combination with SAR405 for 48h. Cells were analysed by flow cytometry using BD FACS Accuri software. 10,000 cells single cells were gated on vehicle treated cells and the percentage of cells undergoing early and late apoptosis was acquired. **A**. Representative dot plot of treated cells. **B**. Values represent the mean and S.E.M of three independent experiments. Statistical analysis was performed using one-way ANOVA with Tukey's Multiple Comparison Test (GraphPad Prism 5). ***p<0.001; NS: non-significant.

3.2.7.2 Targeting autophagy with late-stage autophagy inhibitors enhances cisplatin-induced apoptosis in MRT cells

The results obtained above showed that the early-stage inhibitor SAR405 had no effect on cisplatin-induced apoptosis. Next, autophagy was targeted with late-stage autophagy inhibitors, chloroquine and bafilomycin-A1, to determine whether blocking autophagy at later stages sensitises cells to cisplatin. The effect of these inhibitors on cisplatin-induced autophagy and apoptosis was evaluated through flow cytometric analysis of Annexin V/PI-stained cells and through western blot analysis of LC3-I/LC3-II conversion, p62, caspase 3 and cleaved caspase 3.

3.2.7.3 Chloroquine

Chloroquine is a late-stage inhibitor that blocks autophagic flux by inhibiting the fusion of the autophagosome and the lysosome[365]. Firstly, western blot analysis was conducted to establish whether chloroquine inhibited autophagy in MRT cells. BT12 cells were starved with EBSS for 4 hours as a positive control. The cells were also treated with the vehicle, cisplatin (1 μM) alone, chloroquine (20 μM) alone or cisplatin and chloroquine in combination for 48 hours. High expression of LC3-II was observed in the co-treated cells, indicating an accumulation of autophagosomes, confirming the results observed by Cyto-ID flow cytometric analysis (Figure 3.17). Furthermore, upon treatment with chloroquine, an increase in p62 levels was observed, suggesting that the later stage of autophagy was blocked and p62 was no longer being degraded. In contrast, when treated with cisplatin, p62 levels in BT12 cells decreased. Co-treatment of cells with chloroquine and cisplatin resulted in an increase of p62 when compared to cisplatin on its own (Figure 3.22).

The effect of chloroquine on cisplatin-induced apoptosis was next investigated by flow cytometric analysis of Annexin V/PI-stained cells in both BT12 and BT16 cell lines. Cells were treated with cisplatin (1 μM for BT12 cells and 10 μM for BT16 cells) alone, chloroquine (20 μM) alone or cisplatin and chloroquine in combination. After 48 hours, the cells were either stained with Annexin V/PI and analysed with the BD Accuri flow cytometer or lysates were prepared for western blotting. As shown in Figure 3.23, BT12 cells treated with chloroquine alone exhibited no significant increase in the apoptotic rate when compared to vehicle treated cells. On the other hand, and in line with the western blot result of caspase 3 activation, BT12 cells treated with chloroquine in combination with cisplatin displayed a substantial and significant increase in the rate of apoptosis when

compared to cells treated with cisplatin alone, again indicating that chloroquine sensitises cells to cisplatin-induced apoptosis in BT12 cells. A similar result was obtained in BT16 cells (Figure 3.24). These results were supported by western blot analysis in BT12 cells; chloroquine treatment alone did not result in caspase 3 activation whereas cisplatin treatment induced the marked appearance of cleaved caspase 3. Interestingly, chloroquine was shown to significantly enhance cisplatin-induced caspase 3 activation in BT12 cells, indicating that chloroquine is sensitising the cells to the effects of cisplatin. These results suggest that combining cisplatin treatment with chloroquine could serve as a potential novel strategy to maximise the anti-cancer effects of cisplatin in MRT.

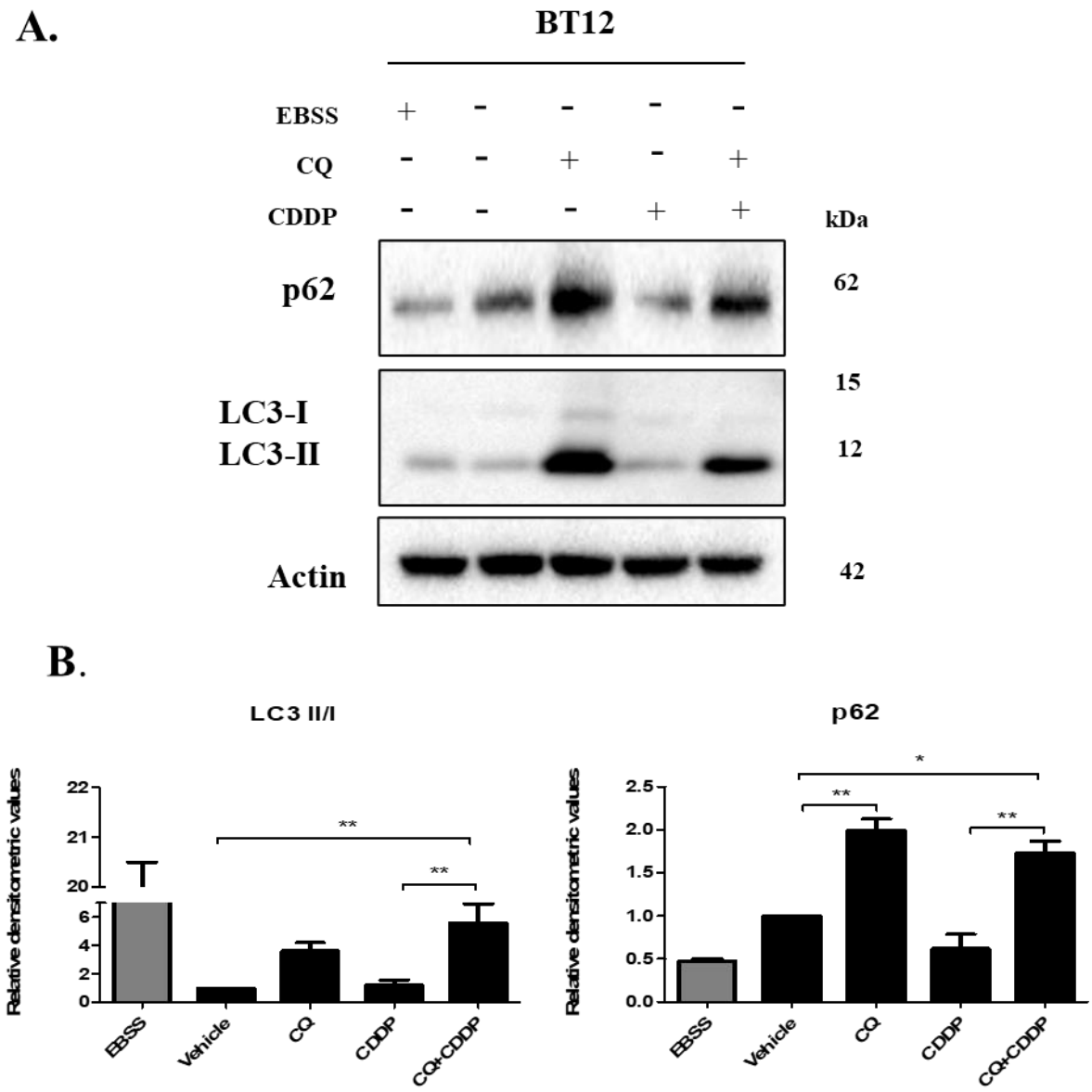

Figure 3.22 Chloroquine inhibits autophagic flux in BT12 cells

10mL of BT12 cells were seeded in T25 flasks at a seeding density of 1 x 10^5 cells/mL. Cells were left to adhere overnight and were then treated with the vehicle (0.009% (v/v) NaCl), cisplatin (CDDP) (1 µM), chloroquine (CQ) (20 µM) or cisplatin and chloroquine in combination. After 48 hours, the cells were detached, and lysates were prepared. Treatment of cells with EBSS for 4 h was used as a positive control. 20µg of protein was loaded on a 15% gel and transferred onto PVDF membrane which was incubated overnight in p62 and LC3. Actin served as a loading control. **A** Results are representative of three experiments **B.** Densitometric analysis of LC3 II/I and p62 was performed using ImageLab software and the loading control was used to normalise the values obtained. Statistical

analysis was performed using a one-way ANOVA with Tukey's post hoc test. * $p < 0.05$, ** $p < 0.01$.

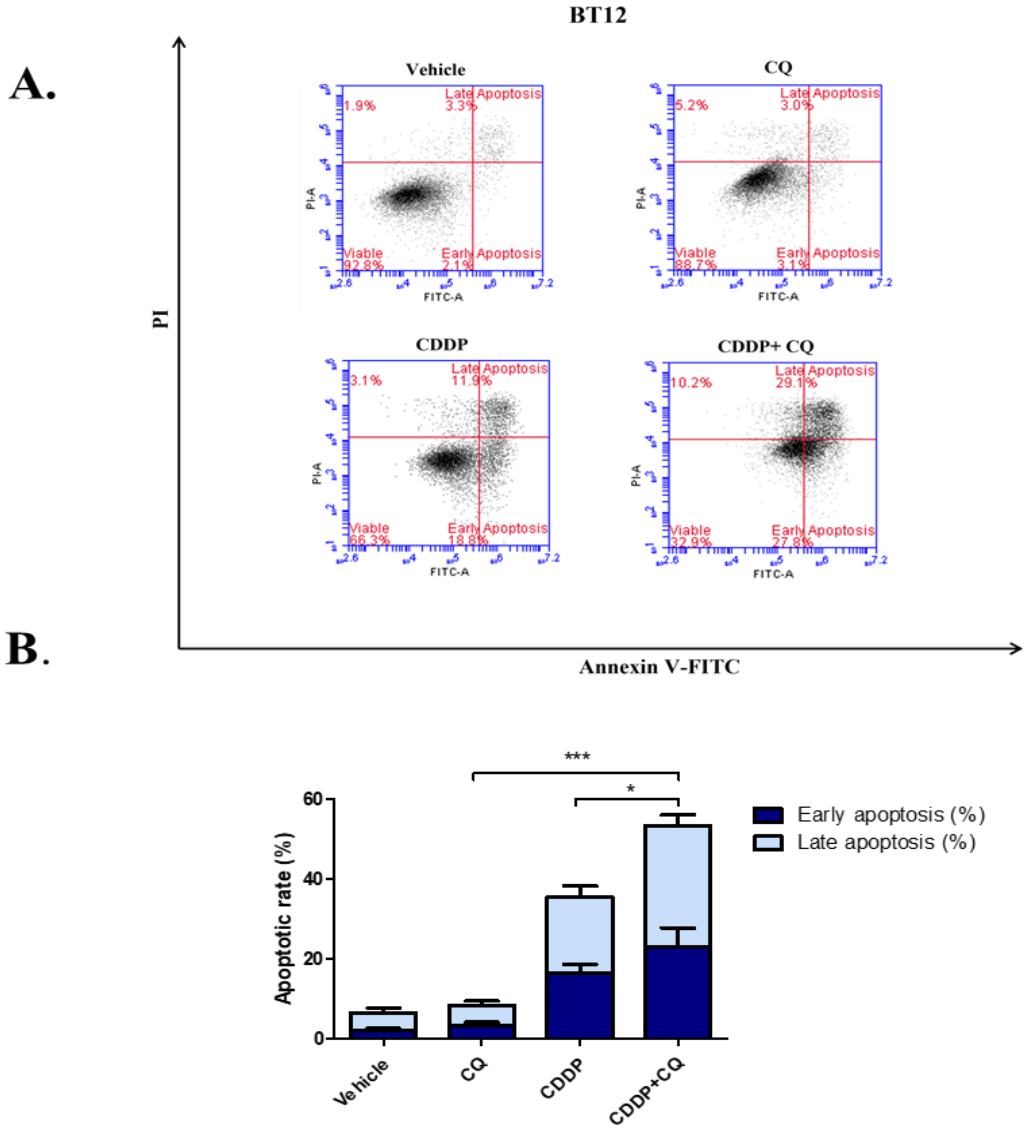

Figure 3.23 Chloroquine enhances cisplatin-induced apoptosis in BT12 cells

2mL of BT12 cells were seeded in a 6-well plate at a seeding density of 1 x 10^5 cells/mL. Cells were left to adhere overnight and were then treated with the vehicle (0.009% (v/v) NaCl), cisplatin (CDDP) (1 µM), chloroquine (CQ) (20 µM) or cisplatin and chloroquine in combination. After 48 hours, the cells were detached and stained with Annexin V and propidium iodide (PI). The cells were immediately analysed by flow cytometry using the BD FACS Accuri software. 10,000 cells were gated on vehicle treated cells and the percentage of cells undergoing early and late apoptosis was determined to be those stained with Annexin V only and stained with both Annexin V and PI, respectively. **A.** Representative dot plot of treated cells. **B.** Values represent mean ± S.E.M of three

independent experiments. Statistical analysis was performed using a one-way ANOVA with Tukey's post hoc test. * $p < 0.05$, ***$p<0.05$.

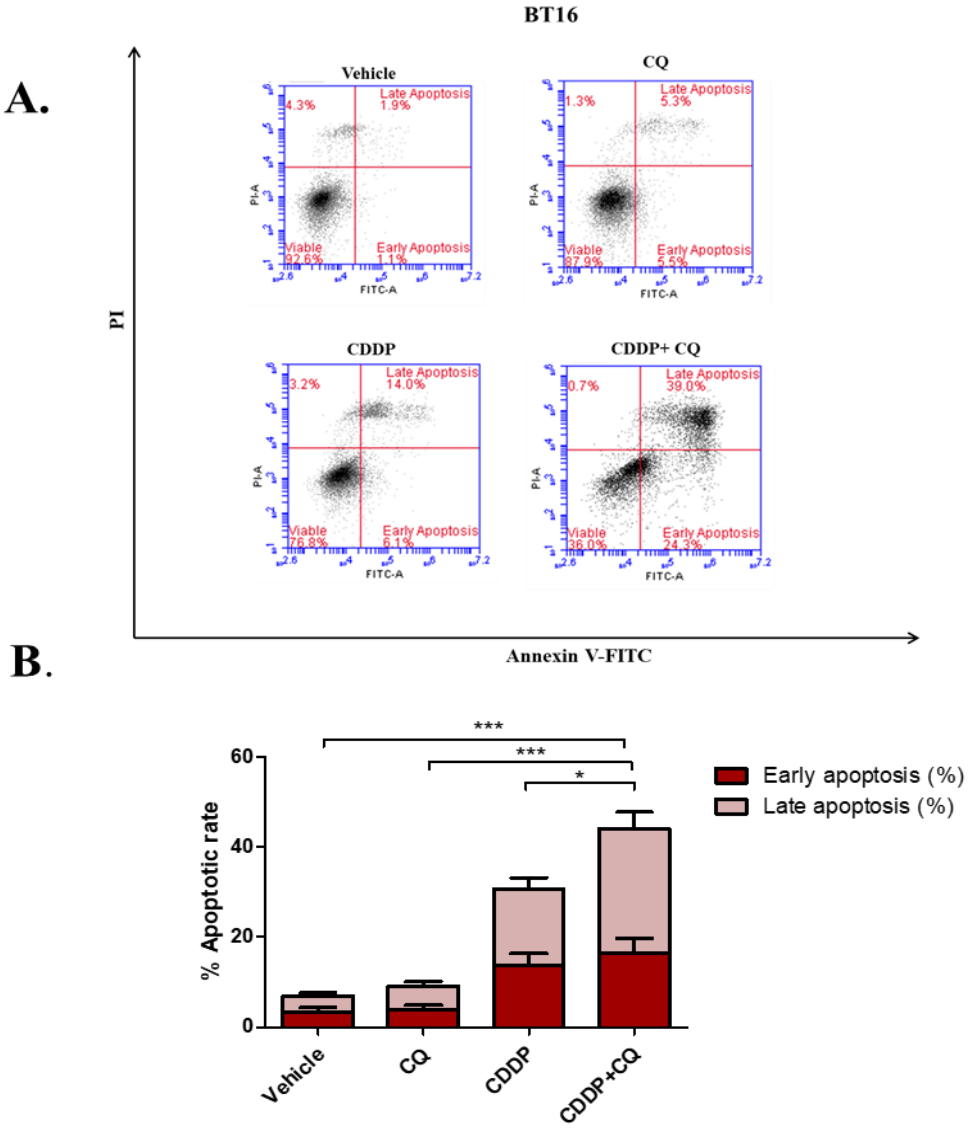

Figure 3.24 Chloroquine enhances cisplatin-induced apoptosis in BT16 cells

2mL of BT16 cells were seeded in a 6-well plate at a seeding density of 1 x 10^5 cells/mL. Cells were left to adhere overnight and were then treated with the vehicle (0.009% NaCl), cisplatin (CDDP) (10 µM), chloroquine (CQ) (20 µM) or cisplatin and chloroquine in combination. After 48 hours, the cells were detached and stained with Annexin V and propidium iodide (PI). The cells were immediately analysed by flow cytometry using the BD FACS Acuri software. 10,000 cells were gated on vehicle treated cells and the percentage of cells undergoing early and late apoptosis was determined to be those stained with Annexin V only and stained with both Annexin V and PI, respectively. **A.** Representative dot plot of treated cells. **B.** Values represent mean ± S.E.M of three

independent experiments. Statistical analysis was performed using a one-way ANOVA with Tukey's post hoc test * p < 0.05, ***p<0.05 .

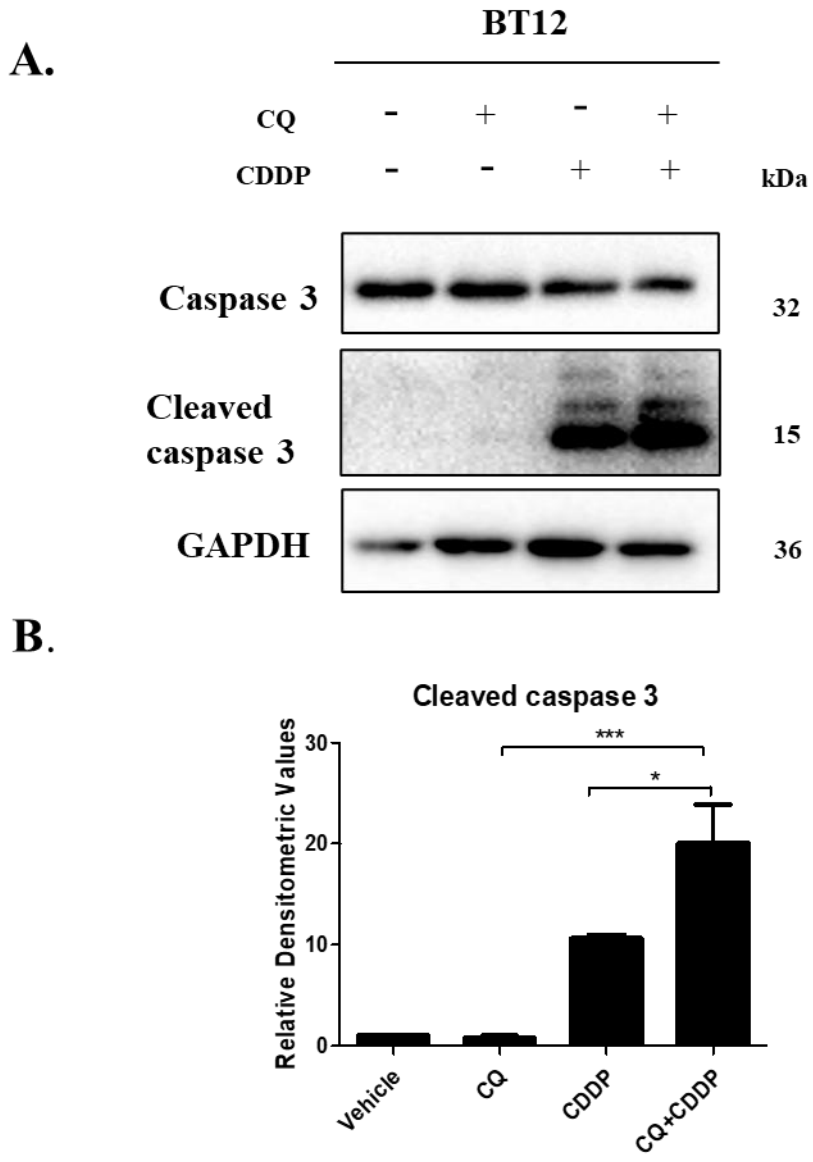

Figure 3.25 Chloroquine enhances cisplatin-induced caspase 3 activation in BT12 cells

10mL of BT12 cells were seeded in T25 flasks at a seeding density of 1 x 10^5 cells/mL. Cells were left to adhere overnight and were then treated with the vehicle (0.009% (v/v) NaCl), cisplatin (CDDP) (1 µM), chloroquine (CQ) (20 µM) or cisplatin and chloroquine in combination. After 48 hours, the cells were detached, and lysates were prepared. 20µg of protein was loaded on a 15% gel and transferred onto PVDF membrane which was incubated overnight in caspase 3 and cleaved caspase 3 antibodies. GAPDH served as a loading control. **A.** Results are representative of three experiments **B.** Densitometric

analysis of cleaved caspase 3 was performed using ImageLab software and the loading control was used to normalise the values obtained. Statistical analysis was performed using a one-way ANOVA with Tukey's post hoc test. * $p < 0.05$, ** $p < 0.01$.

3.2.7.2 Bafilomycin-A1

Bafilomycin-A1 is another commonly used late-stage autophagy inhibitor that acts by preventing the fusion of lysosomes with autophagosomes by blocking vacuolar H+ ATPase (V-ATPase)[370]. Given that chloroquine enhanced cisplatin-induced apoptosis, the effect of a second late-stage autophagy inhibitor bafilomycin-A1 was next examined in MRT cells.

Firstly, western blot analysis was conducted to confirm that bafilomycin-A1 inhibits autophagy. BT12 cells were starved with EBSS for 4 hours as a positive control. The cells were also treated with the vehicle, cisplatin (1 µM) alone, bafilomycin-A1(2.5 nM) alone or cisplatin and bafilomycin-A1 in combination. An accumulation of LC3-II was observed in the co-treated cells compared to cisplatin treated cells suggesting that bafilomycin-A1 had blocked cisplatin-induced autophagic flux. This was confirmed through the analysis of p62 degradation. Expression of p62 was observed to be substantially upregulated upon co-treatment when compared to cisplatin treatment alone (Figure 3.26).

The effect of bafilomycin-A1 on cisplatin-induced apoptosis was next assessed through flow cytometric of Annexin V/PI cells. BT12 cells were treated with vehicle (0.009% (v/v) NaCl), bafilomycin-A1 (2.5 nM), cisplatin (1µM) or bafilomycin-A1 and cisplatin. A statistically significant increase was seen in cisplatin-induced apoptosis when co-treated with bafilomycin-A1 when compared to cells that were just treated with cisplatin alone (Figure 3.27). Similar results were obtained in BT16 cells, with bafilomycin-A1 also significantly enhancing the sensitivity of cells to cisplatin (Figure 3.28). Additionally, and as was seen with chloroquine, a significant increase in cleaved caspase 3 levels was observed in BT12 cells that were co-treated with bafilomycin-A1 and cisplatin when compared to cells that were just treated with cisplatin alone (Figure 3.29), confirming the flow cytometric results.

These results, taken together with the experiments conducted with chloroquine, suggest that targeting late-stage autophagy may increase sensitivity of MRT cells to cisplatin. This is in marked contrast to the results obtained with the early-stage autophagy inhibitor

SAR405 which was shown to have no effect on cisplatin-induced apoptosis in MRT cells (Figures 3.19 to 3.21).

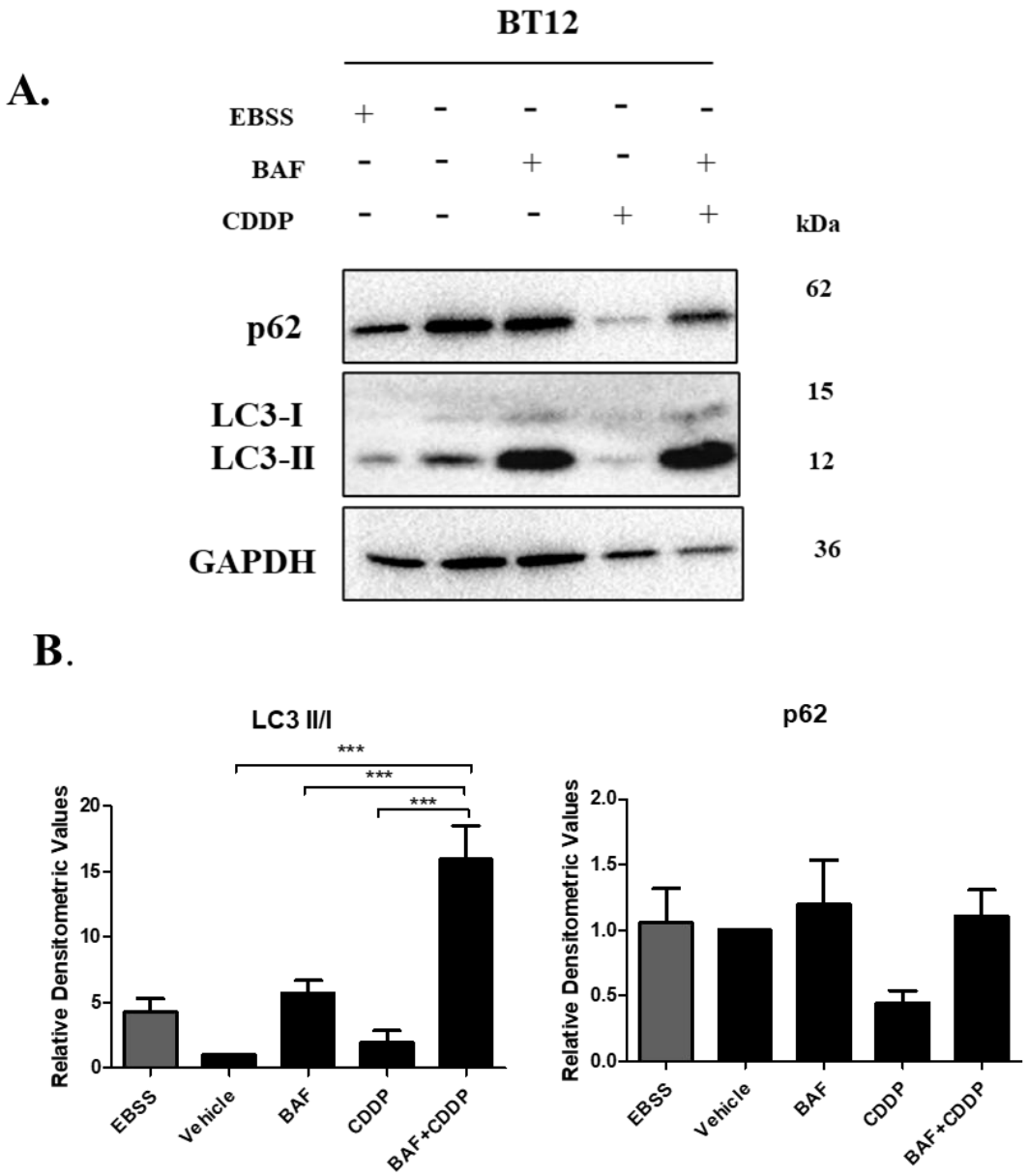

Figure 3.26 Bafilomycin A1 inhibits the autophagic flux in BT12 cells

10mL of BT12 cells were seeded in T25 flasks at a seeding density of 1 x 10^5 cells/mL. Cells were left to adhere overnight and were then treated with the vehicle (0.009% (v/v) NaCl), cisplatin (CDDP) (1 µM), bafilomycin A1 (BAF) (2.5 nM) or cisplatin and bafilomycin-A1 in combination. After 48 hours, the cells were detached, and lysates were prepared. 20µg of protein was loaded on a 15% gel and transferred onto PVDF membrane which was incubated overnight in p62 and LC3 antibodies. GAPDH served as a loading control. **A**. Results are representative of three experiments. **B**. Densitometric analysis of three experiments. Statistical analysis was performed using a one-way ANOVA with Tukey's post hoc test *** $p < 0.001$.

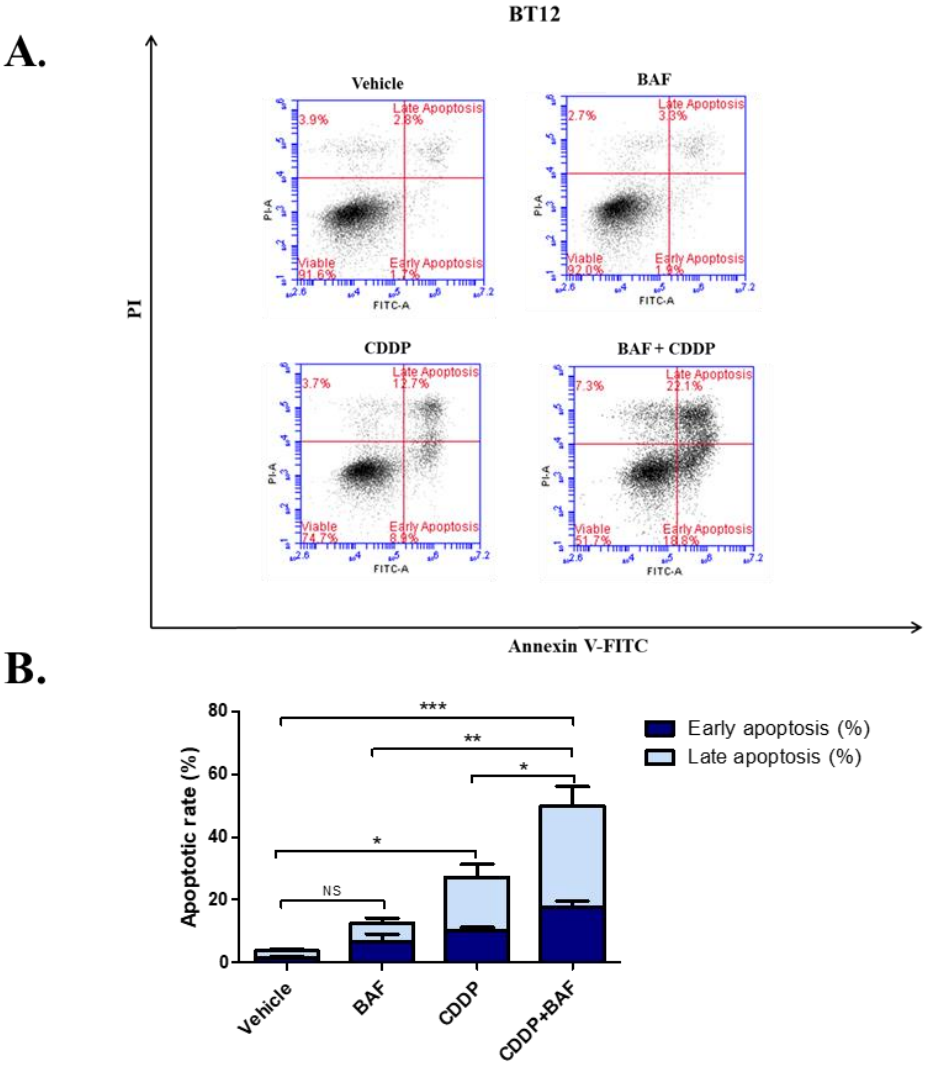

Figure 3.27 Bafilomycin A1 enhances cisplatin-induced apoptosis in BT12 cells

2mL of BT12 cells were seeded in a 6-well plate at a seeding density of 1 x 10^5 cells/mL. Cells were left to adhere overnight and were then treated with the vehicle (0.009% NaCl), cisplatin (CDDP) (1 µM), bafilomycin A1 (BAF) (2.5 nM) or cisplatin and bafilomcyin A1 in combination. After 48 hours, the cells were detached and stained with Annexin V and propidium iodide (PI). The cells were immediately analysed by flow cytometry using the BD FACS Accuri software. 10,000 cells were gated on vehicle treated cells and the percentage of cells undergoing early and late apoptosis was determined to be those stained with Annexin V only and stained with both Annexin V and PI, respectively. **A.** Representative dot plot of treated cells. **B.** Values represent mean ± S.E.M of three independent experiments. Statistical analysis was performed using a one-way ANOVA with Tukey's post hoc test. * $p < 0.05$, ** $p < 0.05$, *** $p < 0.001$.

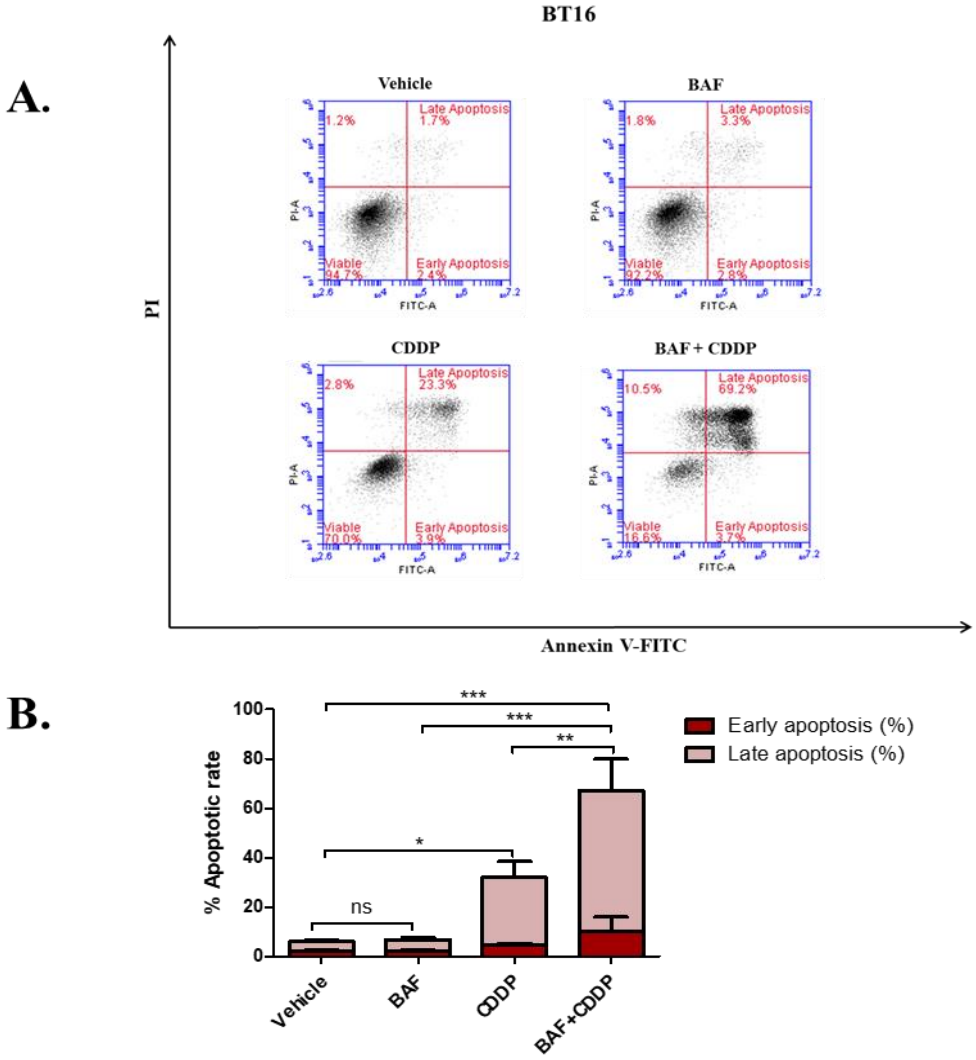

Figure 3.28 Bafilomycin A1 enhances cisplatin-induced apoptosis in BT16 cells

2mL of BT16 cells were seeded in a 6-well plate at a seeding density of 1 x 10^5 cells/mL. Cells were left to adhere overnight and were then treated with the vehicle (0.009% NaCl), cisplatin (CDDP) (10 µM), bafilomycin A1 (BAF) (2.5 nM) or cisplatin and bafilomycin A1 in combination. After 48 hours, the cells were detached and stained with Annexin V and propidium iodide (PI). The cells were immediately analysed by flow cytometry using the BD FACS Accuri software. 10,000 cells were gated on vehicle treated cells and the percentage of cells undergoing early and late apoptosis was determined to be those stained with Annexin V only and stained with both Annexin V and PI, respectively. **A.** Representative dot plot of treated cells. **B.** Values represent mean ± S.E.M of three independent experiments. Statistical analysis was performed using a one-way ANOVA with Tukey's post hoc test. * $p < 0.05$, **$p<0.01$ ***$p<0.001$.

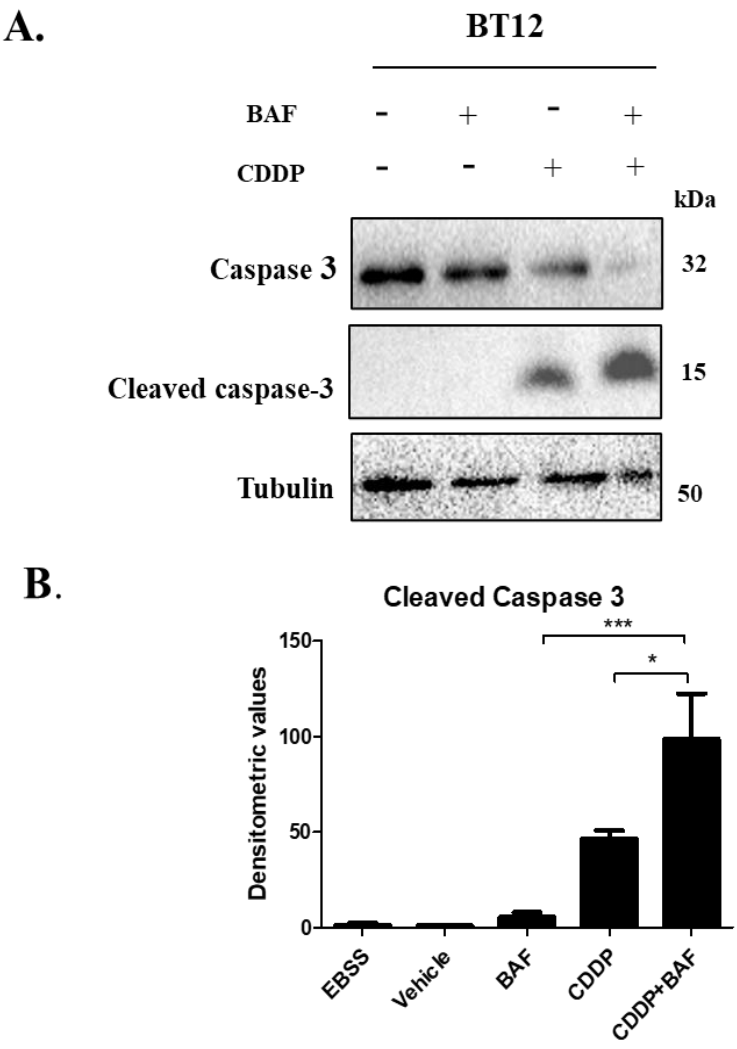

Figure 3.29 Bafilomycin A1 enhances cisplatin-induced apoptosis in BT12 cells

10mL of BT12 cells were seeded in T25 flasks at a seeding density of 1 x 10^5 cells/mL. Cells were left to adhere overnight and were then treated with the vehicle (0.009% (v/v) NaCl), cisplatin (CDDP) (1 µM), bafilomycin A1 (BAF (2.5 nM) or cisplatin and bafilomycin-A1 in combination. After 48 hours, the cells were detached, and lysates were prepared. 20µg of protein was loaded on a 15% gel and transferred onto PVDF membrane which was incubated overnight in caspase 3 and cleaved caspase 3 antibodies. Tubulin served as a loading control. **A**. Results are representative of three experiments. **B**. Statistical analysis was performed using a one-way ANOVA with Tukey's post hoc test * $p < 0.05$, ***$p < 0.001$.

3.2.8 Targeting autophagy via RNAi does not enhance cisplatin-induced apoptosis

Due to the contrasting results obtained on the role of autophagy in mediating cisplatin resistance using pharmacological late-stage and early-stage inhibitors, a genetic approach was next employed. Genetic inhibition is a more specific method of targeting autophagy as pharmacological inhibitors have been associated with a range of off-target effects[289, 345]. As mentioned previously, ATG5 is a critical autophagic protein involved in the lipidation steps of autophagosome formation. During this step, ATG5 forms a complex with ATG12. The ATG5 protein is a common genetic target in autophagy inhibition studies[371].

First, the efficiency of the siRNA was assessed through western blot analysis. BT12 cells were transfected with Non-Targeting (NT) Control siRNA or with ATG5 siRNA using lipofectamine. Cells treated with lipofectamine were considered as a negative control. After 48 hours, the cells were harvested and analysed via western blot analysis. As shown in Figure 3.30, a significant decrease in ATG5-ATG12 protein expression was observed when compared to NT siRNA transfected cells and lipofectamine treated cells. To ensure that the knockdown of ATG5 was inhibiting autophagy, LC3 expression levels were also examined. A significant decrease in LC3-I to LC3-II conversion was observed indicating that ATG5 knockdown results in failure of LC3 activation. Taken together this result confirms that ATG5 expression was inhibited, and that autophagy activation had indeed been blocked.

The effect of genetic inhibition of autophagy on cisplatin-induced apoptosis was next examined. The cells were transfected for 48 hours, and cisplatin was added 24 hours before the end of this incubation period. As seen in Figure 3.31, genetic inhibition of ATG5 had no effect on cisplatin-induced apoptosis. These results agree with the results obtained using SAR405, suggesting that blocking autophagy at early stages in the process does not sensitise MRT cell lines to the effects of cisplatin. In conclusion, these results suggest that autophagy may not mediate cisplatin resistance in MRT. However, the effects of targeting autophagy on cisplatin sensitivity in MRT may be dependent on the stage at which the process is blocked.

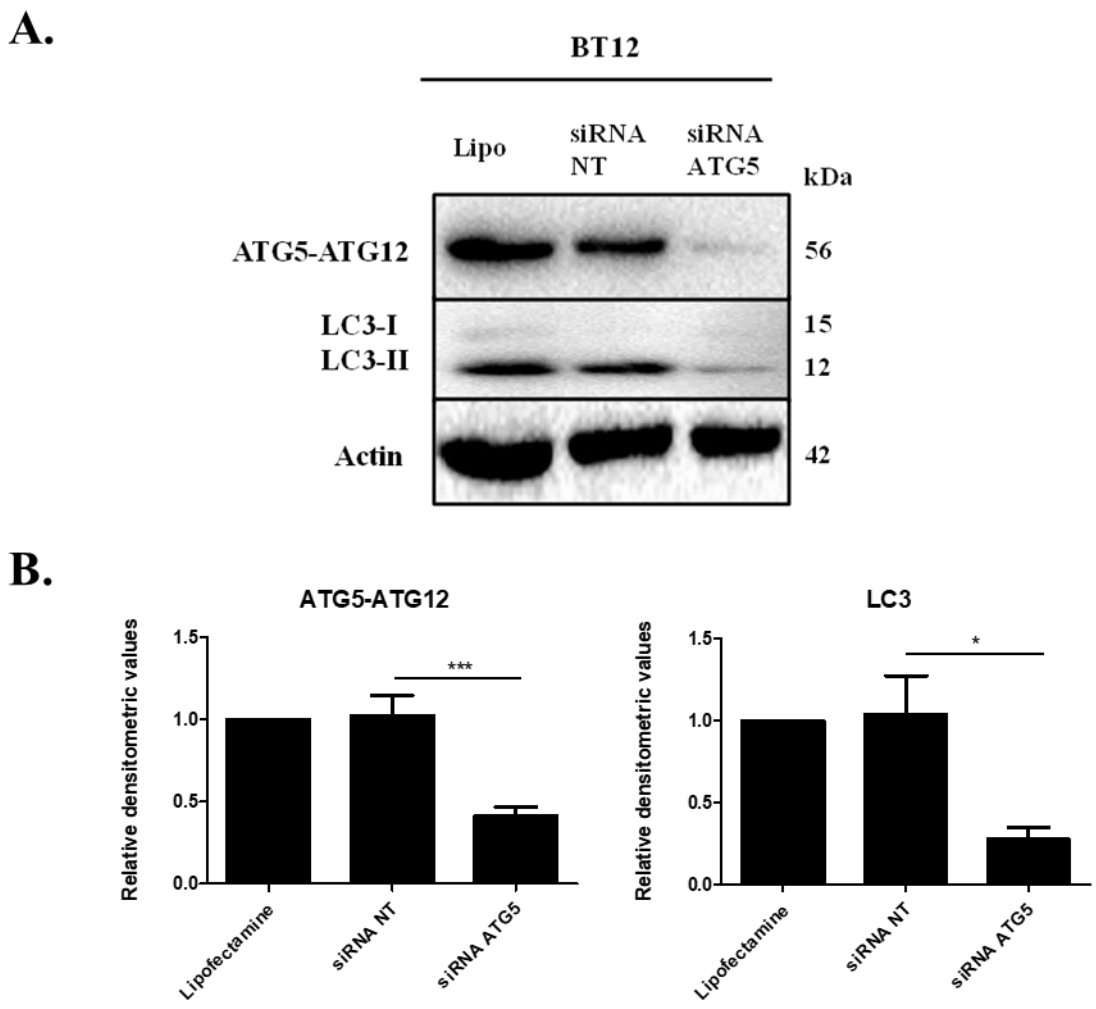

Figure 3.30 Knockdown of ATG5 protein inhibits autophagy in BT12 cells

BT12 cells were seeded at 1 x 10^5 cells/mL in a T25 flask. Cells were transfected with non-targeting control siRNA or ATG5 siRNA for 48h using lipofectamine. Cells treated with lipofectamine on its own served as a negative control. After incubation, cells were harvested and lysed. 20 µg of protein was loaded onto a 15% SDS-gel, transferred onto a PVDF membrane and probed with anti-ATG5-ATG12 and anti-LC3-I/LC3-II antibodies. Actin was used as a loading control **A**. Results are representative 3 independent experiments. **B**. Densitometric analysis of ATG5-ATG12, LC3-I and LC3-II bands was performed using ImageLab software and values were normalised to the loading control. Statistical analysis was performed using a one-way ANOVA with Tukey's post hoc test. * $p < 0.05$, ***$p<0.001$.

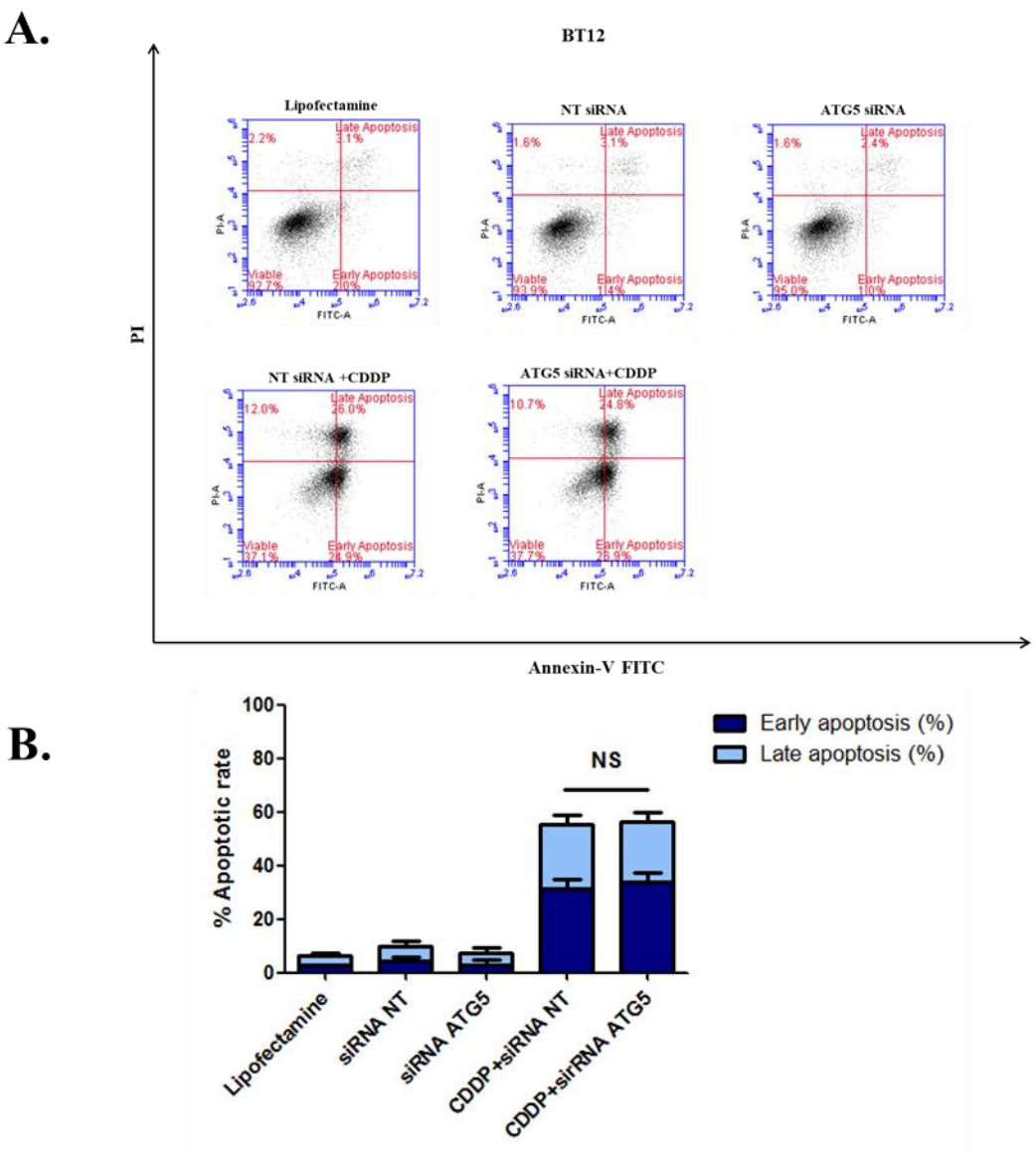

Figure 3.31 Knockdown of ATG5 protein does not sensitise BT12 cells to cisplatin

BT12 cells were seeded at 1 x 10^5 cells/mL in a 6-well plate. Cells were transfected with NT control siRNA or ATG5 siRNA for 24h before the addition of cisplatin (10µM) for a further 24h. Cells treated with lipofectamine or transfected with either NT siRNA or ATG5 siRNA on its own served as negative controls. Cells were harvested 48h after transfection and analysed by flow cytometry using BD FACS Accuri software. 10,000 cells single cells were gated on vehicle treated cells and the percentage of cells undergoing early and late apoptosis was acquired. **A**. Representative dot plot of treated cells. **B**. Values represent the mean and S.E.M of three independent experiments. Statistical analysis was performed using unpaired two-tailed t-test to compare mean values between siRNA NT

and siRNA ATG5 transfected cells treated with cisplatin. (GraphPad Prism 5). NS: non-significant.

3.9 The pan-caspase inhibitor Z-VAD-FMK abrogates cisplatin-induced apoptosis and autophagy

Apoptosis is known to be activated by caspase-dependent and independent pathways[372]. This study previously demonstrated that cisplatin induced apoptosis in MRT cells through caspase 3 activation (Figures 3.8 and 3.9). The significance of the role of caspase 3 in cisplatin-induced apoptosis was further investigated using the pan-caspase inhibitor, Z-VAD-FMK. Cells were pre-treated with Z-VAD-FMK for 1 hour and then treated with cisplatin for 48 hours. After this incubation period, cells were double stained with Annexin V and PI and analysed. Treatment with Z-VAD-FMK had a significant protective effect in both BT12 and BT16 cell lines from cisplatin-induced apoptosis (Figure 3.32 and Figure 3.33). This result confirms our previous findings suggesting that apoptosis is occurring in a caspase dependent manner.

The effect of Z-VAD-FMK on autophagy levels was also examined to determine the relationship between apoptosis and autophagy in response to cisplatin. A significant accumulation in p62 and LC3-II was observed in BT12 cells that were treated with cisplatin and z-VAD-FMK in combination when compared to cells that were treated with cisplatin alone, indicating an inhibition of autophagic flux (Figure 3.34). Collectively, these results suggest complex cross talk between the apoptotic and autophagic pathways in MRT upon cisplatin treatment where inhibition of one pathway results in an alteration in the other pathway.

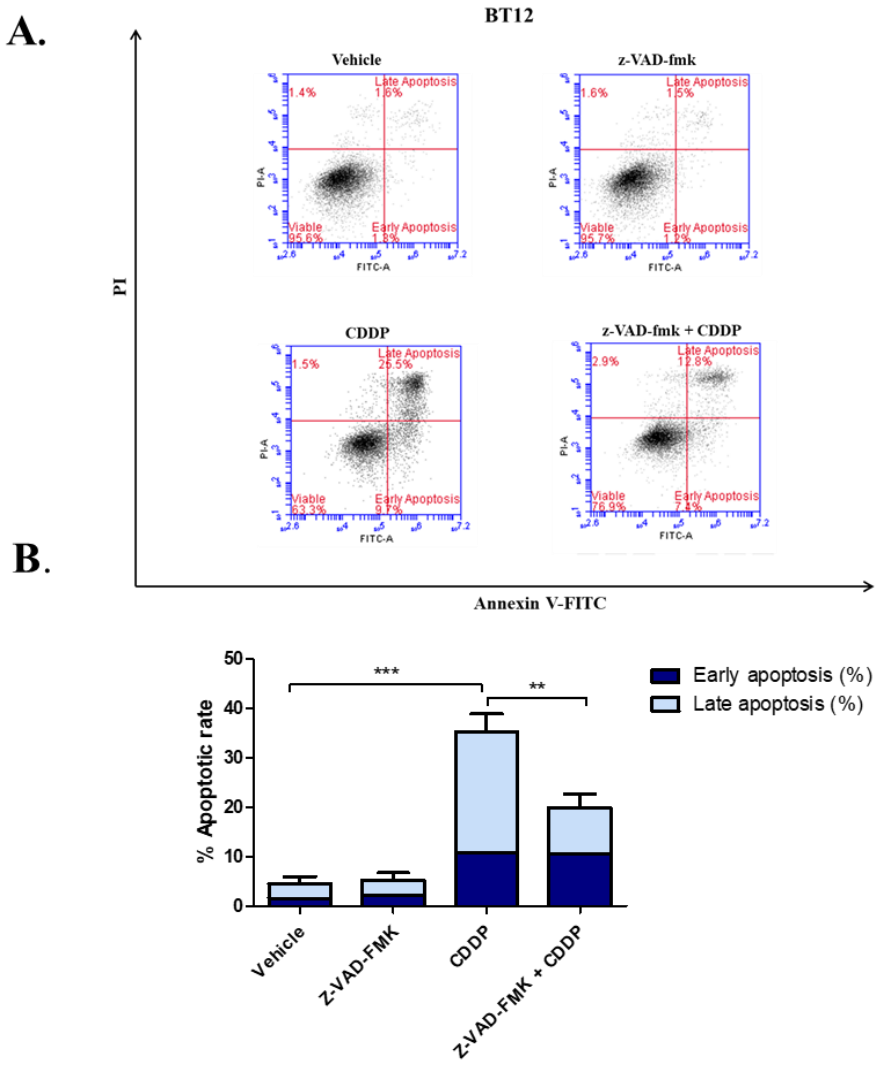

Figure 3.32 Z-VAD-FMK elicits a protective effect against cisplatin-induced apoptosis in BT12 cells

2mL of BT12 cells were seeded in a 6-well plate at a seeding density of 1 x 10^5 cells/mL. Cells were left to adhere overnight and were treated with the vehicle (0.009% NaCl), cisplatin (CDDP) (1 µM), Z-VAD-FMK (20 µM) or cisplatin and Z-VAD-FMK in combination. The Z-VAD-FMK treatment was left for an hour prior to cisplatin treatment. After 48 hours, the cells were detached and stained with Annexin V and propidium iodide (PI). The cells were immediately analysed by flow cytometry using the BD FACS Accuri software. 10,000 cells were gated on vehicle treated cells and the percentage of cells undergoing early and late apoptosis was determined to be those stained with Annexin V only and stained with both Annexin V and PI, respectively. **A.** Representative dot plot of treated cells. **B.** Values represent mean ± S.E.M of three independent experiments using a one-way ANOVA with Tukey's post hoc test ** $p < 0.01$., *** $p < 0.001$.

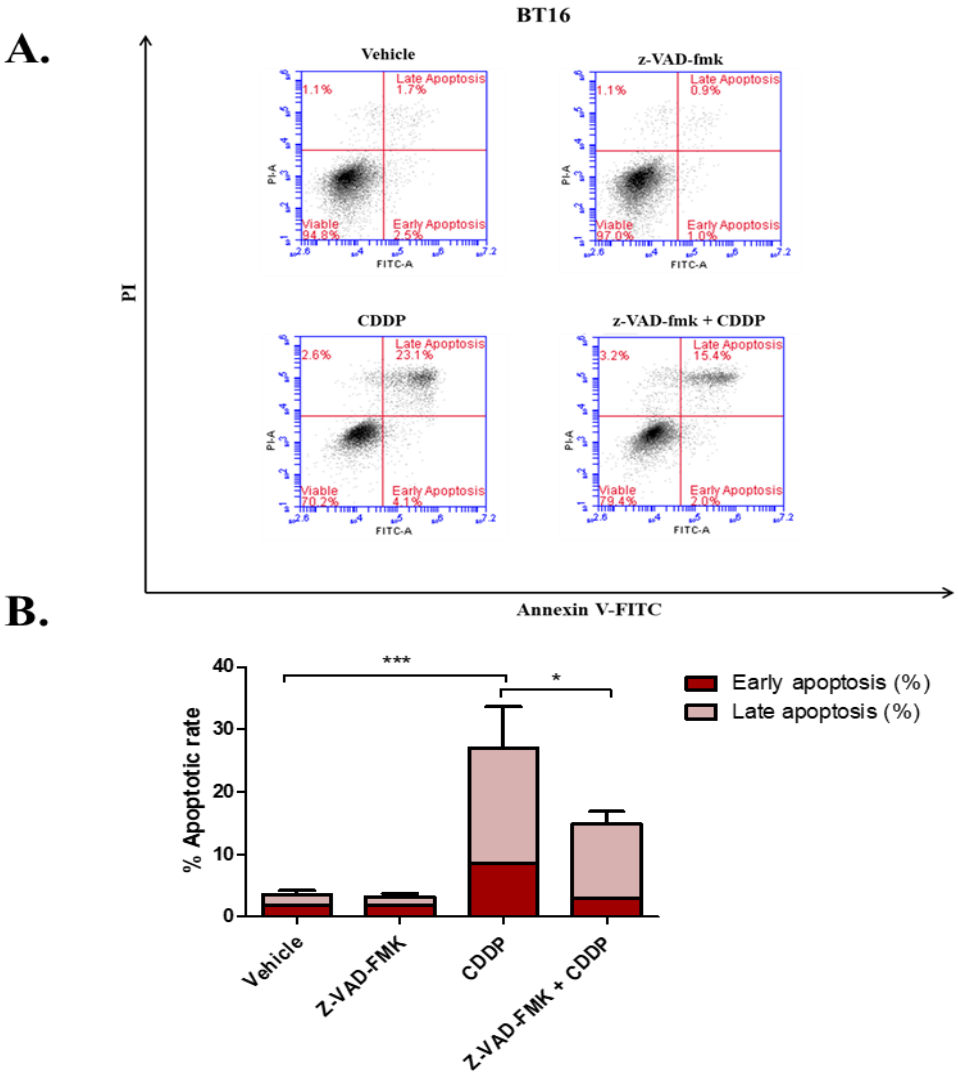

Figure 3.33 Z-VAD-FMK elicits a protective effect against cisplatin-induced apoptosis in BT16 cells

2mL of BT16 cells were seeded in a 6-well plate at a seeding density of 1 x 10^5 cells/mL. Cells were left to adhere overnight and were treated with the vehicle (0.009% NaCl), cisplatin (CDDP) (10 µM), Z-VAD-FMK (20 µM) or cisplatin and Z-VAD-FMK in combination. The Z-VAD-FMK treatment was left for an hour prior to cisplatin treatment. After 48 hours, the cells were detached and stained with Annexin V and propidium iodide (PI). The cells were immediately analysed by flow cytometry using the BD FACS Accuri software. 10,000 cells were gated on vehicle treated cells and the percentage of cells undergoing early and late apoptosis was determined to be those stained with Annexin V only and stained with both Annexin V and PI, respectively. **A.** Representative dot plot of treated cells. **B.** Values represent mean ± S.E.M of three independent experiments using a one-way ANOVA with Tukey's post hoc test * $p < 0.05$., *** $p < 0.001$.

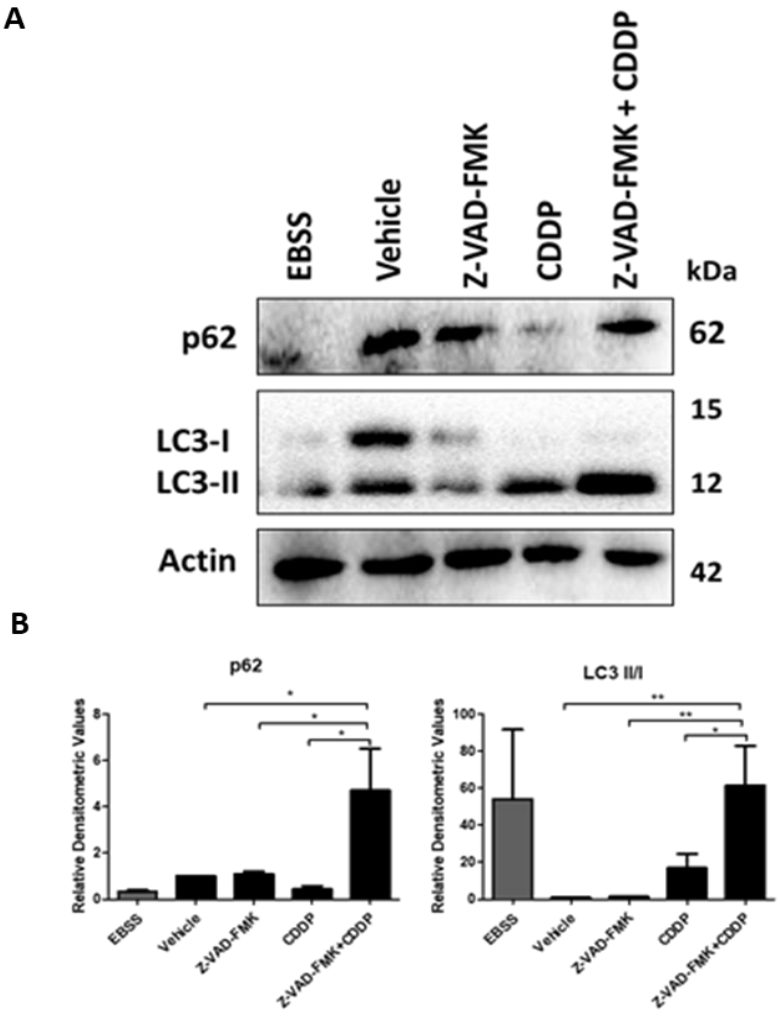

Figure 3.34 Z-VAD-FMK inhibits cisplatin-induced autophagy in BT12 cells

10mL of BT12 cells were seeded in T25 flasks at a seeding density of 1 x 10^5 cells/mL. Cells were left to adhere overnight and were treated with the vehicle (0.009% NaCl), cisplatin (CDDP) (1µM), Z-VAD-FMK (20 µM) or cisplatin and Z-VAD-FMK in combination. After incubation, cells were harvested and lysed. 20 µg of protein was loaded onto a 15% SDS-gel, transferred onto a PVDF membrane and probed with anti-p62 and anti-LC3-I/LC3-II antibodies. Actin was used as a loading control **A.** Results are representative 3 independent experiments. **B.** Values represent mean ± S.E.M of three independent experiments using a one-way ANOVA with Tukey's post hoc test. *$p<0.05$, ** $p < 0.01$.

3.3 Discussion

MRT is a rare childhood tumour located in the kidneys and the CNS as well as various soft tissue sites. These tumours typically occur in children under the age of 3 and are associated with a very poor survival rate due to its aggressive nature. Chemotherapy is the principal treatment course for MRT, often used in combination with surgery and radiation therapy. Despite this, the prognosis for rhabdoid tumour patients remains very low. This is in part due to the aggressive nature of the tumour as well as a poor understanding of the molecular and clinical characteristics of MRT. Moreover, resistance to chemotherapeutics is a major challenge in oncology and has emerged as a significant problem in the treatment of MRT, limiting the effectiveness of anticancer therapies[12].

A variety of factors has been linked to chemoresistance such as: the tumour microenvironment, genetic factors, and oncogenic signalling pathways. In recent years, autophagy has also become an area of focus in the study of chemoresistance. Studies in various cancers have proposed autophagy as a potential therapeutic target. Autophagy is thought to be upregulated in response to chemotherapeutics as a pro-death or pro-survival mechanism, depending on the cancer and on the drug. The dual role of autophagy in cancer and chemoresistance remains poorly understood in cancer cell biology and is still a matter of debate in literature[272, 373]. In MRT, the role of autophagy remains unclear. This study therefore aimed to establish the role of autophagy in MRT and whether it may serve as a potential therapeutic target to overcome chemoresistance.

Cisplatin was selected as a model chemotherapeutic agent for MRT. Cisplatin is a commonly used chemotherapeutic drug that acts through the interference of DNA repair mechanisms by cross-linking with purine bases, which results in the inhibition of DNA transcription and replication as well as the induction of cell cycle arrest and apoptosis[333]. It has been incorporated into several treatment regimens for MRT with varying success. While cisplatin is a highly potent anti-cancer drug, its efficacy is limited by drug resistance and dose-limiting toxic side effects including nephrotoxicity and neurotoxicity[374]. One strategy to improve cisplatin responses is the use of effective drug combination therapies to allow increased cytotoxic activity at reduced doses of cisplatin thus alleviating the toxic side effects. Furthermore, combining cisplatin with a drug which has a different mechanism of action may prevent the development of resistance.

In this chapter, the effect of cisplatin on the viability of a panel of representative cell lines was assessed; BT12, BT16 and G401 cells lines. BT12 and BT16 cell lines are epithelial AT/RT cells isolated from a 2-month-old female and a 2-year-old male, respectively[93]. In contrast, G401 cells were derived from a 3-month-old male who was originally misdiagnosed with Wilms Tumour, but it was later identified to be a kidney rhabdoid tumour cell line[320]. Cisplatin decreased the viability of these cell lines in a dose- and time-responsive manner. BT12 cells were shown to be more sensitive to the effects of cisplatin than BT16 cells. BT16 cells were observed to be the most resistant to the effects of cisplatin. This agrees with a report by Neuwelt, *et al* from 2014, who conducted an MTS viability assay as well as a CytoToxGlo demonstrating that BT16 cells were significantly more resistant to cisplatin than BT12 cells[316]. The MTS assay conducted in the Neuwelt study showed that 6.64 µM cisplatin (or 2µg/mL) resulted in 10% relative viability in BT12 cells and 75% relative viability in BT16 cells. This study obtained LD50 values as opposed to IC50 values and reported an LD50 value of 7 µg/mL cisplatin (or 23.25 µM) at 48 hours. A report published by Jangra *et al.* in 2020 also showed a difference in sensitivity between the two AT/RT cell lines. This study showed that a 5 µM cisplatin treatment reduced viability to approximately 60% in BT12 cells and 80% in BT16 cells indicating BT16 have a higher resistance to cisplatin[375]. The results obtained in the present study showed that the IC50 values after 48 hours were 2.67±1.10 µM for BT12 cells, 6.76±1.18µM for BT16 cells and 2.59±1.27µM for G401 cells. At 72 hours, the IC50 values were 1.18 ± 1.09 µM for BT12 cells, 5.13±1.09 µM for BT16 cells and 1.45 ± 1.15 µM for G401 cells. The molecular differences that account for the variation in sensitivity in these MRT cell lines remains unknown. Moreover, the cell lines are not well characterised due to the rare nature of the tumour. The Genomics of Drug Sensitivity website lists the G401 cell line, but not BT12 and BT16 cells. The GDSC2 dataset listed the IC50 of cisplatin for G401 cells at 72 hours using CellTitreGlo as 1.43 µM. This is in close agreement to the value of 1.45 µM obtained in this study. A report by Birks *et al* in 2019 studied the differences between AT/RTs and MRTKs at a molecular level as well as looking at molecular processes. Whilst a loss in functional SMARCB1 protein was the common characteristic in all the rhabdoid tumours, variations were noted between AT/RTs and MRTKs. The molecular differences between the two tumour types suggested that they may arise from the difference in cell types[376].

To determine whether apoptotic cell death occurs in MRT cells following treatment with cisplatin, flow cytometric analysis of Annexin V and PI-stained cells was performed. Cisplatin induced apoptotic cell death in a dose-and time-dependent manner, which correlated with results obtained from the viability assay. The same range of cisplatin concentrations produced a varying response in the different cell lines. As was seen in the viability assay, BT12 cells were observed to be particularly sensitive to the effects of cisplatin. At 48 hours, a significant increase in apoptosis was observed with 1 µM cisplatin treatment. These results correlated with results obtained from western blot analysis of caspase 3 activation in BT12 cells where the appearance of cleaved caspase 3 fragments appear upon cisplatin treatment (0.8-10 µM). In contrast, a statistically significant increase in apoptosis was only noted in BT16 cells following treatment with 10 µM cisplatin. Similarly, G401 cells responded to cisplatin in a dose-dependent manner with significant apoptosis first observed at 5 µM. The time-dependent nature of apoptotic induction in MRT cells in response to cisplatin was also examined through flow cytometry and western blot analysis. Apoptosis was first observed in G401 and BT16 cells at 24 hours and increased thereafter whilst apoptosis was first detected in BT12 cells at the later time point of 48 hours. This may be because BT12 cells were treated with a 10-fold lower concentration of cisplatin when compared to BT16 and G401 cells. The time-dependency of cisplatin-induced apoptosis was again confirmed through western analysis of caspase 3 cleavage in BT12 cells. Cleaved caspase 3 fragments were detected at 48 hours and 72 hours, in correlation with the results obtained through flow cytometric analysis. This result is in line with previous reports in the literature which demonstrate that cisplatin induces caspase 3 mediated apoptosis. For example, Wu *et al.* also showed caspase 3 cleavage occurred in response to cisplatin in a time-responsive manner in small-cell lung cancer cells[377].

Taken together, these results suggest that cisplatin induces apoptosis in a dose- and time-responsive manner in MRT cell lines with BT12 cells exhibiting greatest sensitivity. Although there are limited studies in the literature on the effect of cisplatin on MRT cell lines, the results presented here are in line with those reports. For example, Neuwelt *et al.* showed that cisplatin (3.32µM) induced approximately 13% apoptosis in Annexin V/PI stained BT16 cells at 20 hours[316]. Furthermore, in a study which evaluated the effect of the heparin-binding growth factor midkine on cisplatin-induced apoptosis in G401 cells, Qi, *et*

al. showed a decrease in viability and an induction of apoptosis at 12 and 24 hours in response to treatment with 100 µM cisplatin[321].

Given that cisplatin induced apoptosis in MRT cell lines, the activation of autophagy in response to cisplatin treatment was next examined. Cisplatin has previously been reported to induce autophagy as well as apoptosis in several cancer cell types including oesophageal, lung and ovarian cancer cells[280]. The role of autophagy in cancer is complex, as it has been shown to have a dual effect on both tumour promotion and suppression. Basal autophagy maintains cellular homeostasis and is considered to play a role in cancer prevention through the removal of damaged proteins and organelles. In contrast, autophagy can be activated at advanced stages of tumorigenesis to promote pro-survival activity by recycling substrates for the metabolic requirements of cancer cells and promoting cell proliferation. The role of autophagy is therefore often described as "context-dependent". Further to this, autophagy has been shown to be upregulated in response to chemotherapeutics in several cancers and is believed to contribute to chemoresistance. However, like its context-dependency in cancer, autophagy has a paradoxical role in chemoresistance. It is also believed by some to act as a death executioner in response to stress invoked by drug treatment. The role of autophagy in MRT remains unclear. In the present study it was hypothesised that autophagy may be activated in MRT in response to chemotherapeutics and may lead to chemoresistance.

Autophagy can occur basally to maintain cellular homeostasis or be induced by external stimuli such as starvation, oxidative stress, or drug treatment. One of the preferred methods to assess autophagy is through western blot analysis of the autophagy markers p62 and LC3-I/LC3-II[367]. p62 delivers cargo to the autophagosome for degradation, a process during which p62 itself is also degraded. Therefore, a decrease in p62 is a good indicator of autophagy activation. Another commonly used indicator is the conversion of LC3-I to LC3-II. The cysteine protease ATG4 cleaves LC3 to form LC3-I, which conjugates with phosphatidylethanolamine (PE) to form LC3-II. Western blot analysis can detect a band for both LC3-I and LC3-II. Thus, the conversion from LC3-I to LC3-II in combination with degradation of p62, is a commonly used method to detect autophagy induction alongside the assessment of autophagosome formation through electron microscopy[367]. In this study, the basal expression levels of various autophagic proteins were assessed in all three MRT cell lines through western blot analysis. Both LC3-I and LC3-II were found to be expressed at similar levels in the three cell lines, as was p62.

Additionally, the Atg5-Atg12 complex was expressed in all three MRT cell lines, with a somewhat higher expression demonstrated in the G401 cell line. Atg5 is an autophagic protein which forms a complex with Atg12 and has a critical role in the formation of the phagosome. This may be perhaps because G401 cells are from MRTKs. In contrast, BT12 and BT16 cells are AT/RT cell lines. The Atg7 protein is another critical autophagic protein which plays a role in autophagosome biogenesis by serving as a E1-ligase enzyme in the conjugation of Atg5 to Atg12. Furthermore, the beclin 1 protein is a central regulator of autophagy by interacting with the Class III PI3K complex[240]. Similar levels of Atg7 and beclin 1 expression were again demonstrated in all three MRT cell lines. Beclin 1 interacts with the anti-apoptotic protein Bcl-2 to form a complex which has been implicated in the regulation of autophagy-associated death. Bcl-2 inhibits apoptosis by blocking the effect of Bax and Bak. It binds to beclin 1 through its Bcl-2 homology 3 (BH3) domain-only protein. In doing so, Bcl-2 prevents beclin 1 from recruiting key autophagic proteins to form the pre-autophagosome structure[378].

Having assessed the levels of expression of several key autophagic proteins, the basal levels of autophagy were next examined in the MRT panel. To do this, the cells were treated with the autophagy inhibitor, bafilomycin-A1, which acts by blocking autophagosome-lysosome fusion and autolysosome acidification. The inhibition of lysosomal degradation by bafilomycin A1 is a commonly used method to assess autophagic flux[288, 368]. Autophagic flux is the term used to refer to the entire process of autophagy from the formation of the autophagosome to the degradation of substrates within the autophagolysosome. Where there are high levels of basal autophagy, treatment with bafilomycin-A1 will result in the accumulation of p62 and LC3-II due to the inhibition of the degradative process in autophagy. Contrary to this, no accumulation could be indicative of a defective vesicular trafficking pathway. Interestingly, treatment with bafilomycin-A1 resulted in the accumulation of p62 and LC3-II suggesting that autophagy is constitutively activated at a basal level in all three cell lines examined. In addition to this, starvation with EBSS for 4h resulted in the conversion of LC3-I to LC3-II and the degradation of p62 thereby showing that autophagy can be induced by external stressors such as starvation. Indeed, external stress through starvation is the gold standard for autophagy induction. Taken together these findings indicate functional autophagy pathways in all three MRT cells lines used in this study.

Next, the ability of cisplatin to induce autophagy in BT12 cells was investigated. Western blot analysis showed that cisplatin induced autophagy in a dose-dependent manner in BT12 cells, resulting in an increase in LC3-II levels and a concomitant decrease in p62 levels. Autophagy was first observed at a concentration of 0.8 µM and peaked at 2 µM. At the higher concentrations of 5 and 10 µM autophagy levels were reduced. These cisplatin concentrations induced a very high rate of apoptosis therefore it is possible that at this point, the cells were damaged beyond a point of which autophagy could be detected.

A previous study by Levy *et al* examined autophagy's role in the treatment of paediatric brain tumours[379]. They studied the effect of lomustine (CCNU), an alkylating nitrosourea compound and cisplatin on several paediatric medulloblastoma and MRT cell lines with varying results. Treatment of cells for 8 hours with lomustine appeared to cause an increase in LC3-II in all the cell lines tested. Cells treated with cisplatin showed varying effects in the different cell lines under examination. A small increase in LC3-II was reported in BT16 cells and the two medulloblastoma cell lines. In contrast a reduction in LC3-II was observed in BT12 cells in response to cisplatin. However, the Levy study only quantified the total levels of LC3-II and did not assess the conversion of LC3-I to LC3-II, which is considered a more accurate method to monitor autophagy[379]. p62 degradation in response to chemotherapy treatment was not evaluated and no other assays to monitor autophagy were utilised. Furthermore, statistical analysis was not conducted on LC3-II expression levels therefore the level of significance, if any, was not reported, hence the need for further studies in this area to clarify the role of autophagy in the response to chemotherapy in MRT.

Several reports in the literature recommend the employment of more than one experimental approach to firmly conclude induction of autophagy[288, 367]. In the present study, to further examine autophagy, cells were stained with Cyto-ID green autophagy dye, which stains autophagic vesicles and is detected by flow cytometry. Cyto-ID is reported to stain autophagic vesicles in a more specific manner than other lysosomotropic dyes such as acridine orange[364]. In agreement with the western blot results, autophagosome formation was increased in response to cisplatin in all three MRT cell lines cells in a dose-dependent manner. In BT12 cells at the two highest cisplatin concentrations tested the formation of autophagosomes was notably reduced possibly due to the low cell viability levels as described above. Interestingly, a decrease in autophagosome formation did not occur at these higher cisplatin concentrations in BT16 and G401 cells. Instead, these cisplatin

concentrations resulted in a continued enhancement of autophagy, perhaps since these cell lines were shown to exhibit a greater resistance to cisplatin.

The time-dependent nature of autophagic induction was also assessed by monitoring the degradation of p62 as well as LC3 conversion in BT12 cells. The levels of p62 were significantly reduced at 48 and 72 hours. These results are in agreement with those obtained by flow cytometric analysis of Cyto-ID-stained cells which demonstrated a statistically significant increase in autophagosome formation at 48 hours. They are also in agreement with a study examining the effect of cisplatin on non-small cell lung carcinoma cells where the expression of p62 and LC3-I/LC3-II in response to cisplatin was assessed and indicated a decrease in p62 and an increase in the conversion from LC3-I to LC3-II[380].

Taken together, these results suggest that cisplatin may induce autophagy and apoptosis in a concomitant manner in MRT cells. This agrees with several reports in the literature that demonstrate that cisplatin induces both apoptosis and autophagy concomitantly in human bladder cells[280], lung cancer cells[380] and in breast cancer cells[381].

Monitoring autophagy is a major challenge due to its complex and dynamic nature. Upon autophagy induction, LC3-I and PE conjugate to become LC3-II. The levels of LC3-II correlate with autophagosome formation as it is in the autophagosome membrane. Eventually, it is degraded in the autolysosomal lumen. However, static measurements of LC3-II and autophagosome levels are not enough to determine that the dynamic process of autophagy is efficiently induced. According to Mizushima *et al* (2010), this is only representative of the balance between the rate of generation and the rate of conversion to autolysosomes[367]. Late-stage inhibition which targets the conversion of autophagosomes to autolysosomes could result in an accumulation of autophagosomes and this may be mistaken for high levels of autophagy. Similarly, low levels of LC3-II may indicate rapid turnover. Thus, late-stage autophagy inhibitors are commonly used, which block later steps in the autophagic process such as acidification within the lysosome or the fusion between autophagosomes and lysosomes. The difference in LC3-II formed between samples treated with and without late-stage inhibitors such as chloroquine is representative of the LC3 that is recruited to the lysosomes for degradation upon the activation of autophagic flux. To

confirm that autophagy was indeed induced upon cisplatin treatment, BT12 and BT16 cells were treated with cisplatin or chloroquine alone as well as cisplatin and chloroquine in combination and stained with Cyto-ID autophagy green dye. The difference between the fluorescence values obtained from cells treated with cisplatin alone and cells that were co-treated with chloroquine and cisplatin represents the autophagic flux. In both BT12 and BT16 cell lines, co-treatment with cisplatin and chloroquine significantly enhanced autophagy in comparison to chloroquine or cisplatin alone suggesting that cisplatin activates autophagic flux in MRT cell lines and confirms functional autophagy in these cell lines.

Given that cisplatin induced both autophagy and apoptosis in MRT cell lines, an examination of the role of cisplatin-induced autophagy was next undertaken. To date, the role of autophagy in cancer remains highly controversial. It can act as a pro-tumour mechanism that allows cells to adapt to stressful conditions, or as an anti-tumour mechanism leading to autophagic cell death (ACD)[343]. Furthermore, this dual role of autophagy has been reported in response to treatment with anti-cancer drugs. In human ovarian cancer cells, cisplatin induced caspase 3-dependent apoptosis in a dose-dependent manner alongside autophagy[382]. Upon treatment with chloroquine and cisplatin in combination, the apoptotic rate in the cancer cells was enhanced significantly. This was confirmed *in vivo*, where chloroquine in combination with cisplatin, significantly suppressed xenograft tumour growth in mice. Thus, this study concluded that autophagy is induced by cisplatin as a cytoprotective mechanism[382]. In 2017, Qu *et al* also showed that chloroquine enhanced cisplatin-induced apoptosis in cholangiocarcinoma cells[383]. Indeed, autophagy induced specifically by cisplatin has also been shown to exhibit a pro-survival role in several other types of cancer, including breast cancer, oesophageal cancer, and cervical cancer[279, 384, 385]. Collectively, such studies support the suggestion that cisplatin-induced autophagy contributes to chemoresistance and acts as a survival pathway in a wide range of malignancies.

In contrast, there have also been reports in the literature that autophagy may be involved in tumour suppression and may lead to ACD. However, studies to determine the role of ACD are limited. This is due to the limitation in our ability to interpret cause of death as many cells contain morphological and biochemical features of various forms of cell death. Moreover, there are various difficulties associated with developing a model for the study of autophagic cell death. An example of this is the use of *ATG* gene knockout mice, which

has been hindered by lethality, alternative overt phenotypes, or redundant gene function[343]. In human ovarian epithelial cancer cells, knockdown of *ATG5* and *ATG7* prevented cell death triggered by autophagy linked to the overexpression of H-Ras[386]. In A549 lung carcinoma cells, resveratrol treatment induced an increase in autophagic flux and cell death without induction of apoptosis or necroptosis. Furthermore, this cell death was linked with an increase in autophagic markers and could not be blocked through inhibition of apoptosis and necroptosis[343, 387]. Temozolomide (TMZ), a DNA-alkylating agent, was shown to activate autophagy in malignant glioma cells. Inhibition of autophagy using 3-methyladenine blocked autophagosome formation and reduced TMZ-induced cytotoxicity in malignant glioma cells. Furthermore, RNAi gene silencing of the autophagic proteins ATG5 and Beclin 1 reduced cell death induced by TMZ. It has been suggested that these contrasting roles of autophagy may be dependent on the anti-cancer drug utilised and the cancer type[388, 389]. Magnano *et al.* (2021), showed that autophagy did not have a pro-survival effect in OSCC cells through the inhibition of early-stage autophagy[319].

The role of autophagy in MRT remains controversial, and whether autophagy inhibition may represent a strategy to overcome cisplatin resistance in this type of cancer has been poorly reported. In the present study, to determine whether autophagy is a potential anti-cancer therapeutic target for MRT, cells were treated with autophagy inhibitors (chloroquine and bafilomycin-A1) in combination with cisplatin. As described above, chloroquine is a frequently used autophagy inhibitor, which targets the fusion of the autophagosome with the lysosome and alters the acidic environment within the lysosome. Chloroquine inhibited p62 degradation and LC3-I/LC3-II conversion, alone and in combination with cisplatin. The effect of cisplatin on caspase 3-mediated apoptosis was also assessed. Western blot analysis demonstrated that co-treatment of cisplatin with chloroquine enhanced the expression levels of cleaved caspase 3 when compared to treatment with cisplatin. Further to this, chloroquine enhanced cisplatin-induced apoptosis in both BT12 and BT16 cells at 48 hours, indicating that targeting autophagy at the late stage may indeed sensitise MRT cells to cisplatin treatment. These results are somewhat in contrast with a study published in 2012 by Levy *et al*, who performed an MTS viability assay on BT12 and BT16 cells treated with chloroquine and either a range of concentrations of cisplatin (0 to 200μM) or lomustine (0 to 250ug/ml) for 24 hours. They reported no effect of chloroquine in sensitising BT12 cells to cisplatin whereas they observed a small effect in BT16 cells, where chloroquine treatment in combination with

the higher concentrations of cisplatin (25 to 100μM) resulted in improved survival[379]. No effects were observed in the chloroquine/lomustine combinations compared to either drug alone in either BT12 or BT16. However, this assay was conducted an earlier time time-point when compared to the present study and the concentration of chloroquine used was not reported. Moreover, the effect of chloroquine on autophagy at this time point was not confirmed via western blot analysis or through other methods and no statistical analysis was conducted. On the other hand, Carugo *et al.* published data supporting targeting autophagy, as well as the proteosome, in rhabdoid tumours. They developed embryonic mouse models of MRT and found that SMARCB1 deficient tumours were associated with high levels of autophagy and ER stress. Moreover, targeting these tumours with proteosome inhibitors and chloroquine, resulted in a dramatic regression of the tumours via apoptosis. This study also found that genetic suppression of autophagy through short hairpin RNA against ATG7 in combination with proteosome inhibition also resulted in complete tumour regression. These results were confirmed in secondary orthotopic transplants and in tumour models of different organ sites. This sensitivity to proteosome and autophagy inhibition was confirmed *in vitro* in the G401 cell line[155]. Taken together, these studies provide a rationale for furthering our understanding of autophagy in MRT to determine whether pharmacological manipulation of autophagy in combination with chemotherapeutic agents may potentially serve as a novel therapeutic strategy.

Another late-stage inhibitor of autophagy is bafilomycin-A1 which blocks autophagic flux by targeting V-ATPase. Interestingly, inhibition of autophagy with bafiloymcin-A1 has been shown to sensitise gastric cancer cells to the anti-cancer effects of 5-fluorouracil. In 2013, Dragowska *et al*, demonstrated that autophagy levels in breast cancer cells increased in response to treatment with gefitinib and that late-stage autophagy inhibition with either bafilomycin-A1 or hydroxychloroquine sensitised the cells to the effects of gefitinib[390]. In the present study in BT12 cells, bafilomycin A-1 was shown to block p62 degradation upon co-treatment with cisplatin when compared to cisplatin alone confirming its effect as a late-stage autophagy inhibitor. Additionally, as was seen with chloroquine, bafilomycin-A1 also sensitised BT12 and BT16 cells to cisplatin-induced apoptosis. This was confirmed via western blot analysis of caspase 3 activation. Co-treated samples showed higher expression of cleaved caspase 3 fragments than samples treated with cisplatin only.

Taken together, these results suggest that inhibiting autophagy at late stages may sensitise MRT to chemotherapy. However, a similar study by Magnano *et al* in OSCC cells reported

that late-stage inhibition of autophagy using pharmacological inhibitors sensitised the cells to cisplatin but early-stage pharmacological inhibition and ATG5 inhibition did not[319]. Moreover, some studies in breast and tongue carcinoma have reported that both these late-stage autophagy inhibitors may sensitise cells to chemotherapy through autophagy-independent mechanisms[391, 392]. These studies propose that chloroquine and bafilomycin-A1 may sensitise cells to chemotherapy due to off-target effects which are unrelated to autophagy suppression. For example, chloroquine and its derivative hydroxychloroquine have been reported to exhibit anti-neoplastic and immunomodulatory activity that are unrelated to autophagy. This is dependent on the cell line (cancerous as well as normal cells) and on the concentration[393]. Studies in literature report an increase in lysosomal pH upon exposure with chloroquine which can be restored, indicating alternative effects of chloroquine and hydroxychloroquine which are unrelated to autophagy. Off-target effects of chloroquine and hydroxychloroquine may in turn induce apoptosis and necroptosis unrelated to autophagy inhibition[393]. Both these-late stage inhibitors can induce lysosomal membrane permeabilization thereby activating the mitochondrial apoptosis pathway[394]. In addition, chloroquine has been shown to inhibit JAK2 signalling in cancer stem cells[395]. Another study in oncogenic KRAS-dependent tumours demonstrated that chloroquine elicited synergistic effects with tyrosine kinase inhibitors but not with ATG7 deficiency suggesting autophagy inhibition may not be the principal mechanism of action[396]. Moreover, bafilomycin-A1 has been reported to exert various potential off-target effects on the mitochondria and it remains unclear whether this activity is related to autophagy inhibition. Bafilomycin-A1 has been shown to inhibit mitochondrial ATPase in primary neurons[397]. Nevertheless, regardless of their mechanism of action, treatment of MRT with either chloroquine or bafilomycin may represent a new strategy to enhance the chemotherapy and improve the clinical outcome of MRT patients.

Chloroquine and its derivative hydroxychloroquine are currently the only clinically approved late-stage autophagy inhibitors. The use of bafilomycin-A1 in the clinic has been limited by its high level of toxicity. Due to the high concentrations of bafilomycin-A1 (>0.1 μM) required to elicit an effect and broad mechanism of action, secondary effects in normal cells have been reported eliciting doubt regarding its future potential as a clinical drug[398, 399]. Of note, this study used a low non-toxic concentration of 2.5 nM to inhibit autophagic flux and enhance cisplatin-induced apoptosis.

Interestingly, there are multiple clinical trials ongoing using combinations of chloroquine and hydroxychloroquine in combination with standard drug agents in various types of cancers. A meta-analysis of clinical trials using chloroquine showed that the outcome of combining the inhibitor with a standard drug provided a better outcome than treating patients with chemotherapy or radiotherapy on its own[400]. As there is a wide range of trials studying combinations with different chemotherapeutic drugs and radiotherapies at different stages of cancer progression and in different cancers, there is still significant variations in the studies and further analyses and large-scale studies would be required to determine any trends in the variations[401]. In a study published in 2015, patients with pancreatic adenocarcinoma were treated with hydroxychloroquine and gemcitabine in combination. Interestingly, the patients that had a 51% increase in the autophagy marker LC3-II in their peripheral blood mononuclear cells were observed to have a significant improvement in overall survival with this treatment[402]. Another clinical trial which treated glioblastoma patients with chloroquine in combination with chemotherapy and radiotherapy reported an improvement in overall survival rate[403]. Collectively, these clinical reports suggested that autophagy was induced as a protective mechanism against the cytotoxic effects of cisplatin. On the other hand, the pro-death effect of autophagy has been reported in oral squamous cell carcinoma cells following treatment with curcumin and in glioma cells treated with cannabinoids[404, 405]. Magnano *et al.*, showed that early-stage inhibition through pharmacological as well as genetic inhibition did not sensitise OSCC cells to cisplatin. Further work comparing autophagy activation in response to cisplatin did not support a link between autophagy and chemoresistance[319]. It has therefore been suggested that this paradoxical role of autophagy may be dependent on the anti-cancer drug employed and the cancer type.

Due to the reported off-target effects of these late-stage inhibitors, this study next considered evaluating the effect of early-stage autophagy inhibition on sensitising MRT cells to the effects of cisplatin. SAR405 is a frequently used early-stage autophagy inhibitor due to its potency and selective nature. SAR405 is small kinase inhibitor of PIK3C3 and interestingly has been shown to enhance the anti-proliferative effect of everolimus in renal cell carcinoma[291]. Furthermore, in urothelial carcinoma, SAR405 enhanced cisplatin-mediated cell death in both cisplatin-sensitive and cisplatin-resistant cells[406]. The effect of targeting early-stage autophagy in MRT remains to be established. In this study, SAR405 was shown to inhibit early stages of autophagy, demonstrated by the

accumulation of p62 and a trend towards the inhibition of the conversion of LC3-I to LC3-II in all three MRT cell lines. Having confirmed that SAR405 was inhibiting autophagy, the three cell lines were treated with a range of concentrations of SAR405 alone, and in combination with cisplatin and the levels of apoptosis was assessed. SAR405 was found to have no effect on cisplatin-induced apoptosis in any of the MRT cell lines. This result is in contrast with the findings obtained using the late-stage inhibitors chloroquine and bafilomycin-A1 in this study. It is also in contrast with the study in urothelial carcinoma cells mentioned above. Interestingly though, and similar to the findings presented herein, a study in 2015 has reported the effect of autophagy inhibition at different stages in glioblastoma (GBM) cells with opposing results. Inhibition of early steps of autophagy decreased the cytotoxic effect of arsenic trioxide (ATO) in GBM cell lines, whilst inhibition of autophagy flux at late stage enhanced ATO cytotoxicity[407]. According to the authors, the opposing effects observed can be linked to the complex mechanism of crosstalk between the autophagic and the apoptotic pathways. The study showed that ATO induced cytotoxic cell death in a dose and time-dependent manner and induced autophagy activation. Inhibition of autophagy with the early-stage inhibitor 3-MA reversed ATO-induced cell death. In contrast, inhibition of autophagy with the late-stage inhibitor chloroquine dramatically enhanced ATO-induced caspase-3-dependent apoptosis. The opposing results observed with 3-MA and chloroquine were also reported with the autophagy inducers LY294002 and rapamycin[407]. Furthermore, the findings presented in this study in MRT are similar to those reported by Magnano *et al.* (2021) who demonstrated that chloroquine and bafilomycin A1 sensitised oral cancer cells to cisplatin-induced apoptosis whereas early-stage autophagy inhibition using SAR405 did not.[319].

Given the contrasting effects of late and early-stage autophagy inhibitors on cisplatin-induced apoptosis observed herein, genetic inhibition of autophagy through the knockdown of ATG5 was conducted. As mentioned above, pharmacological autophagy inhibitors lack specificity and may also affect other cellular processes including mitosis and endocytosis. For this reason, Mizushima *et al.*, recommend genetic suppression of autophagy to support data obtained with pharmacological inhibitors[367]. This provides a more specific approach to targeting autophagy and is often achieved through the genetic knockdown or knockout of ATG genes. One of the most widely reported ways to genetically block autophagy is through the suppression of ATG5. As previously

mentioned, ATG5 catalyses ATG8 lipidation, a crucial step in the formation of the autophagosome[339].

BT12 cells transfected with ATG5 siRNA exhibited a substantial and significant decrease in ATG5-ATG12 protein expression and a concurrent significant reduction in the conversion of LC3-I to LC3-II compared to NT siRNA transfected cells and lipofectamine treated control cells. Interestingly, and in agreement with the results obtained using the early-stage inhibitor, SAR405, this inhibition of autophagic flux via the knockdown of ATG5, had no effect on cisplatin-induced apoptosis suggesting that cisplatin-induced autophagy does not represent a protective mechanism in MRT cell lines. This finding is also in agreement with results reported by Levy *et al* who demonstrated that genetic manipulation of autophagy through RNAi targeting of another key autophagic protein, ATG7, in BT12 and BT16 cells had no effect on short term cell survival in response to cisplatin treatment evaluated by an MTS viability assay. Additionally, the finding is in line with a recent study reported by Magnano *et al*, (2021) which demonstrated that late-stage pharmacological autophagy inhibition sensitised OSCC cells to cisplatin induced apoptosis but early-stage inhibition and ATG5 knockdown did not significantly modulate sensitivity to cisplatin. In contrast, Chen *et al* have demonstrated that siRNA targeting of ATG5 and Beclin 1 enhanced cisplatin-induced apoptosis in human lung cancer cells[408] while ATG5 knockdown was also shown to enhance bufalin-induced apoptosis in human gastric cancer cells suggesting that the role of chemotherapy-induced autophagy (pro-death or pro-survival) may be context dependent[409]. Interestingly, Holloman *et al*, found opposing effects on campothecin (CPT)-induced cytotoxicity when conducting an ATG5 knockdown in two murine osteosarcoma cell lines. In one cell line the knockdown appeared to elicit a protective effect whereas in another it enhanced CPT-induced cytotoxicity. In this case, the authors hypothesised that this was due to different basal autophagy levels between the two cell lines[410]. Moreover, the authors also suggested that the high level of basal autophagy in one of the cell lines is a contributor to its overall cancer phenotype. A dependence on basal autophagy has also been reported for other cell lines in literature such as pancreatic cancer cells[411]. The report further examined the cell line in which ATG5 knockdown had a protective effect to determine the mechanism underlying this. CPT induced DNA damage, as determined by phosphorylation of p53 at Ser15. The levels of DNA damage were similar between autophagy-competent and autophagy-inhibited cells and the authors concluded that the protection provided by

autophagy inhibition from CPT was not due to a reduction in DNA damage or cell division but was associated with reduced oxidative stress and mitochondrial damage[410].

There is a considerable amount of evidence to suggest that the signalling pathways regulating autophagy and apoptosis are interconnected. Moreover, the pathways involved in autophagy and apoptosis share some key molecules, the modulation of one mechanism influences the execution of the other and vice versa. Therefore, how apoptosis and autophagy collaborate to decide cancer cells fate are complex. For example, as mentioned earlier, beclin-1, a known tumour suppressor and autophagy initiator, interacts with Bcl-2 a central regulator of both autophagy and apoptosis. Bcl-2 functions by interacting with both beclin-1 and pro-apoptotic proteins Bax/Bak. Cellular stress can cause the displacement of Bcl-2 from beclin-1 and Bax triggering autophagy and apoptosis, respectively. The Bcl-2 inhibitor ABT-263 has been shown to induce both apoptosis and autophagy. Upregulation of p62 results in enhanced caspase 8 activation by ABT-263[412]. Moreover, the pro-apoptotic proteins Bad, Bak, Nix and $BNIP_3$ have been shown to disrupt the interaction between Bcl-2 and beclin-1 thereby regulating autophagy. Another anti-apoptotic Bcl-2 family member, Mcl-1 has also been shown to bind to beclin-1. The pro-apoptotic protein Noxa, can disrupt this interaction thereby inducing autophagy. Just as apoptotic proteins are implicated in autophagy regulation, autophagic proteins have also been shown to be involved in apoptosis. For example, ATG5 has been implicated in spontaneous apoptosis in neutrophils and in several different cell types, the N-terminal cleavage product of ATG5 was demonstrated to translocate to the mitochondria where it interacts with Bcl-xL and induces cytochrome C release. ATG12 has been shown to also regulate mitochondrial apoptosis by inactivating Bcl-2 and Bcl-xL. Likewise, autophagic proteins have also been implicated in extrinsic apoptosis. Namely, caspase-8 has been observed to cleave ATG3 resulting in the inhibition of death receptor activation by autophagy[413].

The results obtained thus far suggest that apoptosis and autophagy are simultaneously upregulated by cisplatin in MRT cells and inhibiting autophagy has different outcomes on cisplatin-induced apoptosis suggesting a complex interplay between the two pathways that warrants further investigation. To study the crosstalk between the two pathways, the pan-caspase inhibitor Z-VAD-FMK was employed. BT12 and BT16 cells were treated with Z-VAD-FMK alone and in combination with cisplatin. Z-VAD-FMK treatment elicited a significant protective effect in both cell lines from cisplatin-induced apoptosis. Furthermore, an accumulation of p62 and LC3 levels, hallmarks of impaired autophagic

flux, were observed in response to Z-VAD-FMK treatment suggesting that apoptosis inhibition via Z-VAD-FMK also resulted in the inhibition of autophagosome clearance and degradation. These results are in agreement with a study by Magnano *et al* (2021) which showed that Z-VAD-FMK completely abrogated cisplatin-induced apoptosis in OSCC cell lines whilst simultaneously inhibiting cisplatin-induced apoptosis[319]. Z-VAD-FMK was also shown to impair autophagic flux in renal tubular epithelial cells (RTEC) through western blot analysis of accumulated levels of p62 and LC3[414]. These results support observations above that apoptosis and autophagy are upregulated simultaneously in response to cisplatin and have a complex dependency on each other. The crosstalk between these pathways may be context-dependent as there are also reports in literature demonstrating contrasting results on the effect of Z-VAD-FMK on autophagy. An example of this was reported by Zhao *et al.* in a study that examined the potential effect of pristimerin on human breast cancer. Pristimerin is a naturally occurring quinonemethide triterpenoid extracted from plants that is known to exhibit potential anti-tumour effects on various cancers. This study reported that Z-VAD-FMK reduced pristimerin-induced autophagy in breast cancer *in vivo* and *in vitro*[415]. These contrasting results indicate further study is warranted to better understand the context in which Z-VAD-FMK treatment may result in autophagy inhibition or induction.

In conclusion, this chapter has shown that cisplatin induces parallel activation of both apoptosis and autophagy in MRT cells, suggesting an interplay of the two pathways in response to chemotherapeutics. Autophagy inhibition using the late-stage autophagy inhibitors chloroquine and bafilomycin-A1 sensitised MRT cells to cisplatin-induced apoptosis. However, both these pharmacological inhibitors have been reported to exert off-target effects therefore no firm conclusions can be made on whether their modulation of cisplatin sensitivity is solely due to autophagy inhibition. Nonetheless, these results demonstrate that combining chemotherapy with chloroquine or bafilomycin-A1 may represent a novel treatment strategy to improve clinical outcome in MRT patients. In contrast, autophagy inhibition using a specific early-stage autophagy inhibitor SAR405 had no effect on cisplatin sensitivity, suggesting that cisplatin-induced autophagy may not represent a protective mechanism in MRT. This conclusion was supported by data demonstrating that the genetic knockdown of ATG5 had no effect on sensitivity of MRT cells to cisplatin. Thus, the role of autophagy in MRT is complex and results presented in this chapter justify further study into understanding the intricate relationship between

apoptosis and autophagy in MRT. Further study is also required into other molecular mechanisms underlying chemoresistance in MRT.

4. The role of ROS and the Nrf2/GSH antioxidant system in chemoresistance in Malignant Rhabdoid Tumour

4.1 Introduction

ROS (reactive oxygen species) are naturally occurring by-products generated during mitochondrial oxidative metabolism[416]. These highly reactive molecules regulate a number of critical signalling pathways in the cell. Redox homeostasis is maintained through a balance between ROS generation and elimination through antioxidant scavenging systems[417]. High levels of ROS generation can result in oxidative stress resulting in damage of proteins, lipids and DNA, eventually leading to cellular damage that can result in a number of pathologies, including cancer[418]. Prolonged oxidative stress can also result in the cell undergoing programmed cell death. Examples of ROS include peroxides, superoxides and hydroxyl radicals.

To maintain cellular redox homeostasis, the cell is equipped with an antioxidant defence system. Many of the cytoprotective genes involved in this system have a sequence known as the antioxidant response element (ARE), which is mediated by the basic leucine zipper (bZIP) transcription factor, Nrf2 (nuclear factor erythroid 2-related factor 2)[419]. Nrf2 is often referred to as the master regulator of anti-oxidative responses. Nrf2 itself is negatively regulated by the cytosolic protein Keap1 (Kelch-like ECH associated protein 1), a component of the Cullin 3 (Cul3) E3 ubiquitin ligase protein which interacts with Nrf2 through DLGex and ETGE sites in the Nrf2 Neh domain and targets Nrf2 for proteosomal degradation[305]. ROS and electrophiles can alter Keap1 cysteine residues thereby inactivating ubiquitin E3 ligase activity and allowing for Nrf2 to escape Keap1-mediated degradation[420]. Thus, Nrf2 can then translocate to the nucleus to activate antioxidant gene expression including those involved in the antioxidant glutathione (GSH) pathway, heme-oxygenase-1 (HO-1) and NAD(P)H: quinone oxireductase 1 (NQO1)[421]. Glutathione (GSH) is one of the most widely studied antioxidants due to its abundance and powerful activity and it is one of the main scavengers of ROS[422]. It is a tripeptide composed of cysteine, glutamic acid and glycine. It is synthesised within the cell by γ-glutamylcysteine synthetase (γ-GCS) and glutathione synthetase[422]. Glutathione exists in its reduced form (GSH) or in an oxidised form (GSSG). Both forms are found in healthy cells, however, the majority of glutathione is found in its reduced form and the ratio of GSH:GSSG is a marker of oxidative stress.

Cancer cells have particularly high levels of ROS due to their characteristically high metabolic rate, hypoxia and microenvironment-associated instability[423]. Chemotherapeutic agents exploit this vulnerability; they typically induce the generation of intracellular ROS in cancer cells, leading to the induction of oxidative stress and ROS-mediated cell death[424].

Cisplatin is one of the most widely used chemotherapeutic agents used to treat many cancers including bladder cancer, ovarian cancer and rhabdoid tumours[333]. Indeed, in 2019 it was estimated that 50% of cancer patients received a treatment plan which included cisplatin[425]. Often, a significant anti-cancer response is observed in response to cisplatin treatment however, patients frequently relapse due to chemoresistance. Cisplatin induces oxidative stress in the cancer cell in addition to DNA damage[425]. However, some cancer cells adapt to the high basal ROS generation by upregulating their antioxidant system and are therefore equipped to better cope with drug-induced oxidative stress leading to chemoresistance[426]. Indeed, studies have shown that high expression of components of the antioxidant system such as Nrf2 are observed in chemoresistant cancer cells. Studies have also suggested that basal intracellular ROS levels may affect the sensitivity of a cancer cell to drug treatment[425]. Interestingly, elevated GSH levels have previously been linked with chemotherapeutic resistance including resistance to platinum-based anti-cancer agents. Levels of cellular thiols such as GSH play a critical role in detoxification of these platinum agents. GSH can bind and inactivate cisplatin through its reactive thiol group, preventing cisplatin from binding to DNA and inducing its damage. Indeed, increased inactivation of cisplatin by thiol-containing proteins has been reported to be an important mechanism underlying tumour resistance in many cancers including cervical cancer, osteosarcoma and glioblastoma[427-429].

Silva *et al*. have shown that the cisplatin-sensitive lung cancer cell line H23, has a much lower GSH:GSSG ratio than cisplatin-resistant lung cancer cells A549[430]. Interestingly, in MRT, Neuwelt *et al* have previously shown that basal levels of GSH are higher in the cisplatin-resistant BT16 cell line compared to the cisplatin-sensitive BT12 cell line. Furthermore, treatment with the glutathione inhibitor acetaminophen (AAP) improved apoptotic response to cisplatin in these MRT cells[316] This indicates that glutathione levels may be linked to chemoresistance in MRT, but further studies are required to substantiate this.

.

Activation of Nrf2 is involved in the regulation of not only antioxidant genes but also detoxification genes, drug metabolism genes and multidrug resistance associated genes. Thus, many studies have examined the role of Nrf2 in mediating chemoresistance. Nrf2 overexpression has been linked to drug resistance in non-small cell lung cancer (NSCLC), stomach cancer, endometrial cancer and osteosarcoma[306]. In acute myeloid leukaemia (AML) patients, Nrf2 overexpression correlated with higher mutation frequency, disease progression and increased drug resistance[431]. Targeting Nrf2 has shown pre-clinical promise in a variety of cancer studies. For example, ML385, a small molecule inhibitor of Nrf2 that can bind to Neh1, the Cap 'N' Collar Basic Leucine Zipper (CNC-bZIP) domain of Nrf2 and inhibit its downstream targets, has shown promising pre-clinical anti-cancer activity in the treatment of advanced NSCLC[432].

The role of Nrf2 in chemoresistance in rhabdoid tumours remains elusive. Parkhurts *et al.* have shown the mTORC1/2 inhibitor TAK-228 also interferes with Nrf2 transcriptional activity in ATRT cell lines and potentially plays a protective role in MRT against drug-induced oxidative stress and subsequent apoptosis[433].

Furthermore, the role of oxidative stress in response to chemotherapeutics in MRT is still unclear. Further study into the involvement of ROS and the role of the Nrf2/GSH antioxidant system in mediating cisplatin resistance in MRT is therefore warranted. Thus, the aim of this chapter was firstly to investigate whether basal ROS levels, Nrf2 or GSH play a role in determination of cisplatin cytotoxicity in a panel of MRT cells lines. Secondly, this chapter, aimed to determine whether modulating the levels of these three key cellular components involved in redox homeostasis could affect the apoptotic response to cisplatin and sensitise resistant MRT cells to cytotoxicity. Targeting the Nrf2/GSH antioxidant system may present a novel therapeutic strategy to combat chemoresistance in rhabdoid tumours.

4.2 Results

4.2.1 Basal intracellular ROS levels in a panel of MRT cell lines

Flow cytometric analysis of H_2DCFDA stained cells was employed to examine the basal levels of intracellular ROS in a panel of MRT cell lines. H_2DCFDA or 2',7'-dichlorohydrofluoroscein -diacetate is a cell permeant dye which is a chemically reduced form of fluorescein widely used as an indicator of ROS in cells. After this dye diffuses into the cell, the acetate groups undergo cleavage by intracellular esterases and oxidation thereby converting the non-fluorescent H_2DCFDA into the fluorescent 2',7'-dichlorolfuorescein (DCF). The highly fluorescent DCF can be detected by flow cytometry and therefore ROS levels in cells can be measured[434].

The validity of the assay was first assessed by using the non-radical ROS, hydrogen peroxide (H_2O_2) and the ROS scavenger, N-acetylcysteine (NAC). Exposure to H_2O_2 is a widely used method to induce oxidative stress in cellular models. BT12 cells were treated with 100 µM H_2O_2 for 1 hour. Cells were also pre-treated with NAC (5 mM) for an hour before H_2O_2 treatment. Cells were stained with H_2DCFDA and evaluated using the BD Accuri flow cytometer. Both positive and negative controls appeared effective with H_2O_2 causing a significant increase in fluorescence, which was reversed by NAC. This result validates the efficacy of the assay in measuring ROS (Figure 4.1).

Levels of basal intracellular ROS were next examined in BT12, BT16 and G401 cells. Cells were stained with H_2DCFDA dye and analysed with the BD Accuri flow cytometer. Cisplatin-sensitive BT12 cells had significantly higher levels of ROS when compared to cisplatin-resistant BT16 cells with G401 cells having intermediary levels. This suggests a potential correlation between basal ROS levels and cisplatin sensitivity. In order to further examine this, relative ROS levels were plotted against percentage cellular viability in response to treatment with 10 µM cisplatin. An inverse relationship was observed between the two variables with r value of 0.9999 and a statistically significant p value of 0.0072 (Figure 4.2), suggesting inverse correlation between basal ROS levels and cisplatin resistance.

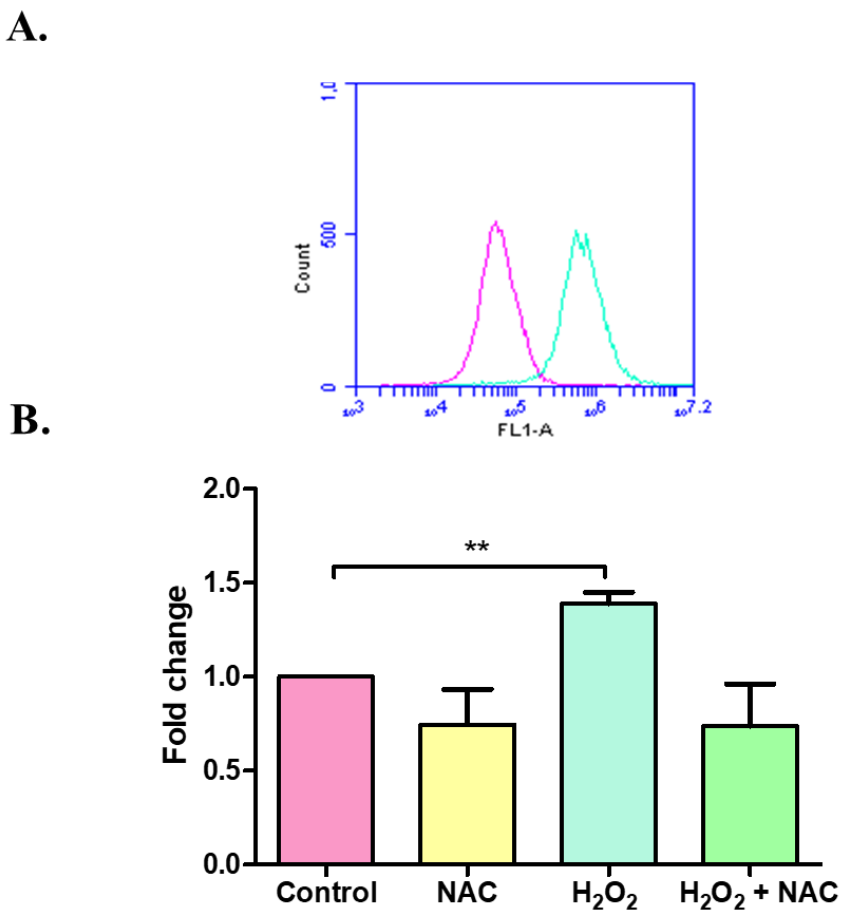

Figure 4.1 Validation of the H_2DCFDA cellular ROS assay using H_2O_2 as a positive control in BT12 cells

2mL of BT12 cells were seeded in a 6-well plate at a seeding density of 1 x 10^5 cells/mL. Cells were left to adhere overnight before being treated with vehicle (0.009% (v/v) NaCl), NAC (5mM), vehicle and NAC in combination, H_2O_2 (100 µM for 1 hour), or H_2O_2 and NAC in combination. Cells were pre-treated with NAC for one hour prior to H_2O_2 treatment. The cells were stained H_2DCFDA for 30 minutes after which they were harvested then washed and resuspended in PBS. The cells were immediately analysed by flow cytometry using the BD FACS Accuri software. 10,000 cells were gated on vehicle treated and the MFI values were obtained and normalised by the vehicle. **A**. Representative flow cytometric histogram of vehicle (pink line) and H_2O_2 treated cells (green line). **B**. Bar graph showing ROS levels in presence of NAC, H_2O_2 alone or in combination, relative to the vehicle control. Values represent mean ± S.E.M. of at least three independent experiments. Statistical analysis was performed using two-tailed paired t test. **p<0.01.

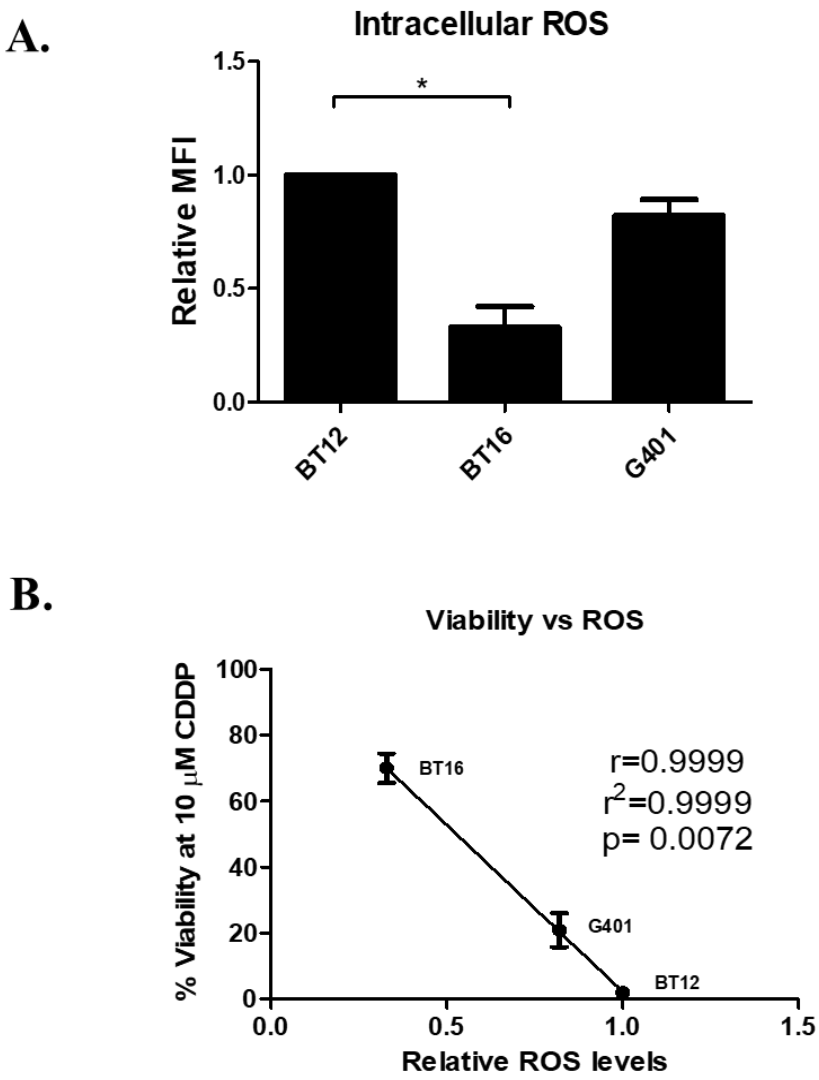

Figure 4.2 Basal levels of intracellular ROS in MRT cells

2mL of BT12, BT16 and G401 cells were seeded in a 6-well plate at various seeding densities. Cells were left to adhere and after 48 hours, the cells were stained H_2DCFDA for 30 minutes after which they were washed and resuspended in PBS. The cells were immediately analysed by flow cytometry using the BD FACS Accuri software. 10,000 cells were gated on vehicle treated and the MFI values were obtained and normalised by the vehicle. **A**. Values represent mean ± S.E.M of three independent experiments. Statistical analysis was performed using a two-tailed paired t test. *$p<0.05$. **B**. Relative densitometric values were plotted against percentage viability at 10 uM cisplatin treatment for the three cell lines to determine the correlation between the two variables. Correlation analysis was performed on GraphPad Prism to obtain r values and p values.

4.2.2. Cisplatin induces intracellular ROS generation in a panel of MRT cell lines

Having established that basal intracellular levels of ROS in MRT cell lines correlated with cisplatin sensitivity, this study next examined the effect of cisplatin on ROS in the panel of cell lines. BT12 cells were treated with 1 µM cisplatin whereas BT16 and G401 cell lines were treated with 10 µM cisplatin, for 48 hours. After this incubation period, cells were stained with H_2DCFDA dye and analysed on the BD Accuri flow cytometer.

A statistically significant increase in ROS production was observed in the three cell lines compared to vehicle treated cells. Moreover, in BT12 cells, there was a 2-fold increase in ROS production in cisplatin-treated cells compared to vehicle treated cells while in BT16 cells, a 2.5-fold increase of ROS generation was detected. Lastly, in G401 cells a 3.6-fold increase in ROS generation was observed in cisplatin treated cells compared to vehicle treated cells (Figure 4.3). Together, these results suggest that treatment with cisplatin promotes ROS accumulation on MRT cells.

To further examine the source of this ROS generation, MitoSOX™ Red staining was used to detect any alterations in mitochondrial ROS. MitoSOX™ Red is a fluorogenic dye that permeates the cell and specifically targets the mitochondria. Upon oxidation, the reagent produces red fluorescence that can be detected by flow cytometry[328]. BT16 cells were treated with vehicle (0.009% NaCl) or cisplatin (10 µM) for 48h. Antimycin A (10 µM for 1 h) was used as a positive control. After 48h, the cells were harvested and stained with MitoSOX™ Red (2.5 µM) for 15 min at 37 °C in the dark, washed with warm PBS and analysed by flow cytometry. As expected, treatment of cells with the positive control antimycin A induced an increase in fluorescence confirming the validity of the assay. Results also indicated that cisplatin induces significant production of mitochondrial ROS.

Collectively, these results indicate that cisplatin treatment induces a mitochondrial-dependent ROS accumulation in MRT cells, suggesting it may have a critical role to play in cisplatin-induced apoptosis.

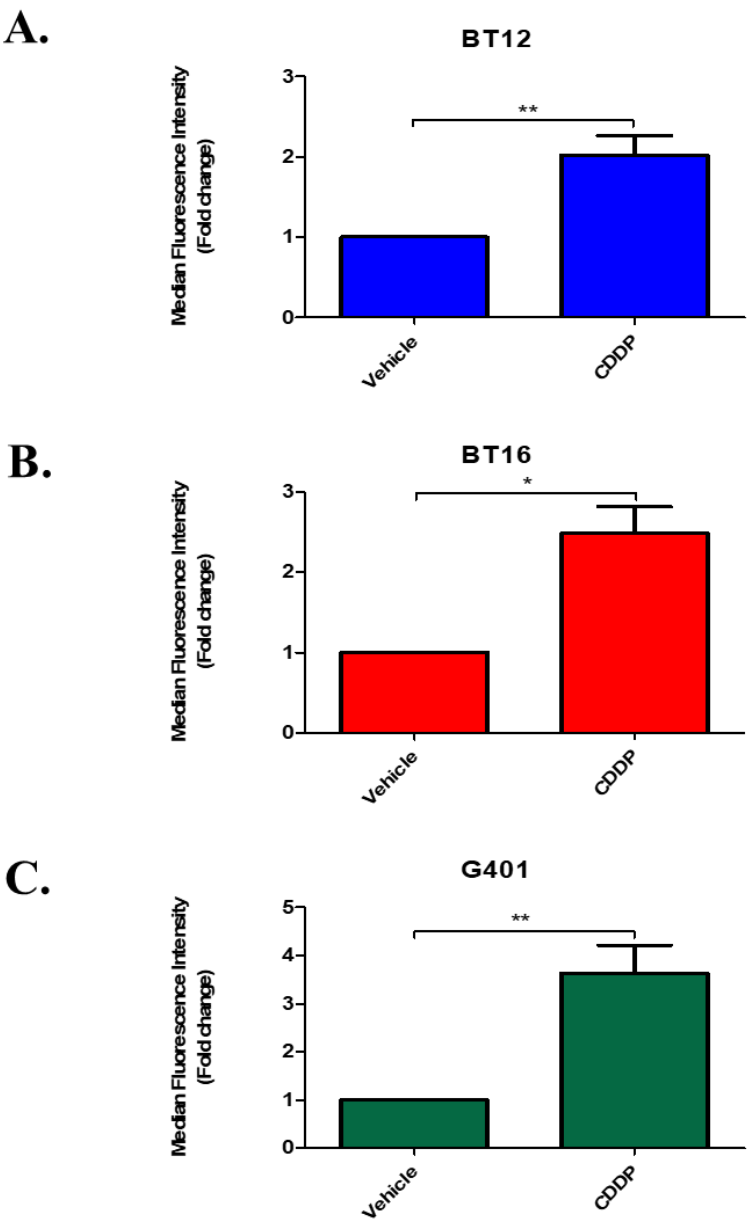

Figure 4.3. Cisplatin induces ROS generation in a panel of MRT cells

2mL of BT12, BT16 and G401 cells were seeded in a 6-well plate at various seeding densities. Cells were left to adhere overnight and were treated with the vehicle (0.009% NaCl) or cisplatin (CDDP) (1 µM in BT12 cells or 10 µM in BT16 and G401 cells). After 48 hours, the cells were stained H_2DCFDA for 30 minutes after which they were washed and resuspended in PBS. The cells were immediately analysed by flow cytometry using the BD FACS Accuri software. 10,000 cells were gated on vehicle treated and the MFI values were obtained and normalised by the vehicle. Values represent mean ± S.E.M of three independent experiments in BT12 cells (**A**), BT16 cells (**B**) and G401 cells (**C**). Statistical analysis was performed using two-tailed paired t test. *$p<0.05$, ** $p < 0.01$.

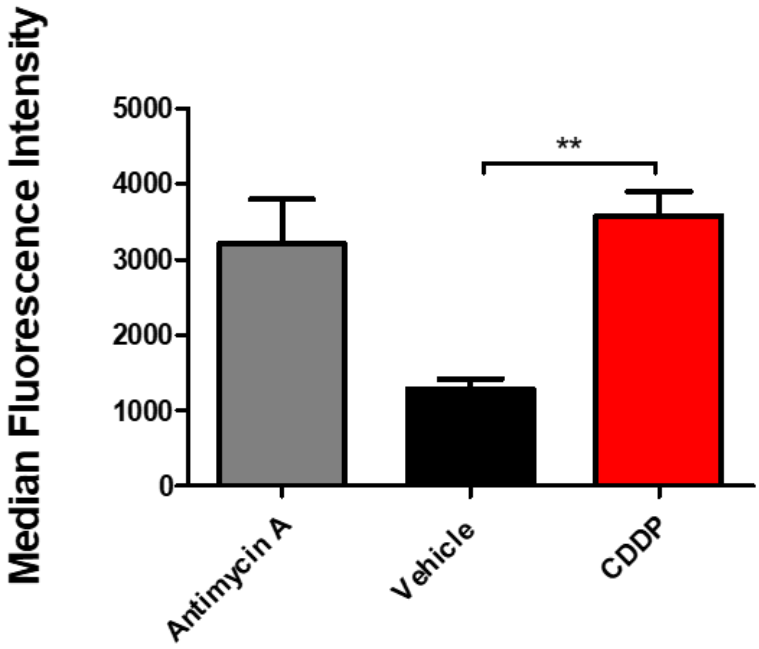

Figure 4.4. Cisplatin induces mitochondrial ROS in BT16 cells

2mL of BT16 cells were seeded in a 6-well plate at a seeding density of 1 x 10^5 cells/mL. Cells were left to adhere overnight and were treated with the vehicle (0.009% NaCl) or cisplatin (CDDP). Antimycin A was used as a positive control. After 48 hours, the cells were harvested, washed and resuspended in 2.5 µM Mitosox for 20 minutes. The cells were immediately analysed by flow cytometry using the BD FACS Accuri software. 10,000 cells were gated on vehicle treated and the MFI values were obtained and normalised by the vehicle. Bar graph showing mitochondrial ROS levels of antimycin A, vehicle, or cisplatin. Values represent mean ± S.E.M of three independent experiments in BT16 cells. Statistical analysis was performed using two-tailed paired t test. ** $p < 0.01$.

4.2.3. The antioxidant N-acetylcysteine abrogates cisplatin-induced apoptosis by reversing cisplatin-induced ROS generation

Having determined a potential correlation between basal intracellular ROS levels and sensitivity to cisplatin in a panel of MRT cell lines and that cisplatin induces significant ROS generation in all three cell lines, the effect of ROS modulation on cisplatin-induced cell death was next evaluated.

The antioxidant N-acetylcysteine (NAC) was employed to target ROS in MRT cell lines. NAC is a synthetic precursor of glutathione and intracellular cysteine that is frequently used to study the role of ROS and oxidative stress in drug-induced apoptosis. The antioxidant properties of NAC have been linked to its free radical scavenging activity via redox potential of thiols and its ability to increase intracellular levels of GSH[435].

To investigate the ROS scavenging properties of NAC in MRT, ROS levels were measured by flow cytometric analysis of H_2DCFDA-stained cells. BT12 and BT16 cells were pre-treated with 5mM of NAC for 1h before being treated for 48h with 1 or 10 µM cisplatin, respectively. As shown in Figure 4.5, cisplatin treatment significantly increased ROS levels in BT12 and BT16 cells. However, pre-treatment with NAC completely reversed this effect, returning ROS to basal levels. This result suggests the antioxidant activity of NAC is achieved through its ROS scavenging properties.

As results shown above demonstrate a potential implication of ROS generation in cisplatin-induced cell death, this study next evaluated the effect of NAC on cisplatin-induced apoptosis. BT12 and BT16 cells were left untreated or were pre-treated with 5mM NAC for 1h before being treated with 1 or 10 µM cisplatin, respectively for 48h. After this incubation time, cells were stained with Annexin V and PI and examined with the BD Accuri flow cytometer. Results obtained show a significant decrease in cisplatin-induced apoptosis in cells that had been pre-treated with NAC when compared to cells that had only been treated with cisplatin alone, in both BT12 and BT16 cell lines (Figure 4.6 and Figure 4.7). NAC treatment completely reversed cisplatin-induced apoptosis in BT12 cells. However, this reversal was only partial in BT16 cells, perhaps because BT16 cells have elevated Nrf2/GSH and that these cells are only partially affected by ROS-dependent apoptosis. This result demonstrates that NAC can inhibit cisplatin-induced apoptosis, implicating ROS as an important component in drug cytotoxicity.

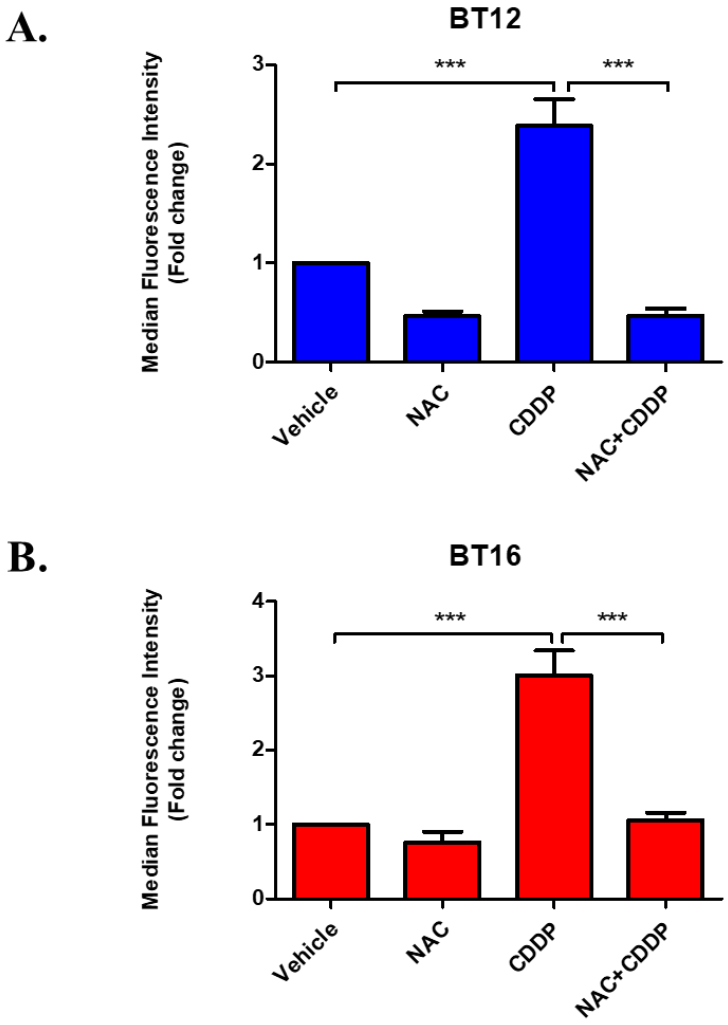

Figure 4.5 N-acetyl cysteine exhibits a protective effect against cisplatin-induced ROS in BT12 and BT16 cells

2mL of BT12 and BT16 cells were seeded in a 6-well plate at a seeding density of 1 x 10^5 cells/mL. Cells were left to adhere overnight and were treated with the vehicle (0.009% NaCl), NAC (5mM), cisplatin (CDDP) (1 µM in BT12 cells and 10 µM in BT16 cells), or cisplatin and NAC in combination. The NAC treatment was left for an hour prior to cisplatin treatment. After 48 hours, the cells were stained H_2DCFDA for 30 minutes after which they were harvested, washed and resuspended in PBS. The cells were immediately analysed by flow cytometry using the BD FACS Accuri software. 10,000 cells were gated on vehicle treated cells and the MFI values were obtained and normalised by the vehicle. Values represent mean ± S.E.M of three independent experiments in BT12 cells (**A)** and BT16 cells (**B)**. Statistical analysis was performed using Statistical analysis was performed using one-way ANOVA with Tukey's post hoc test. ***$p<0.001$

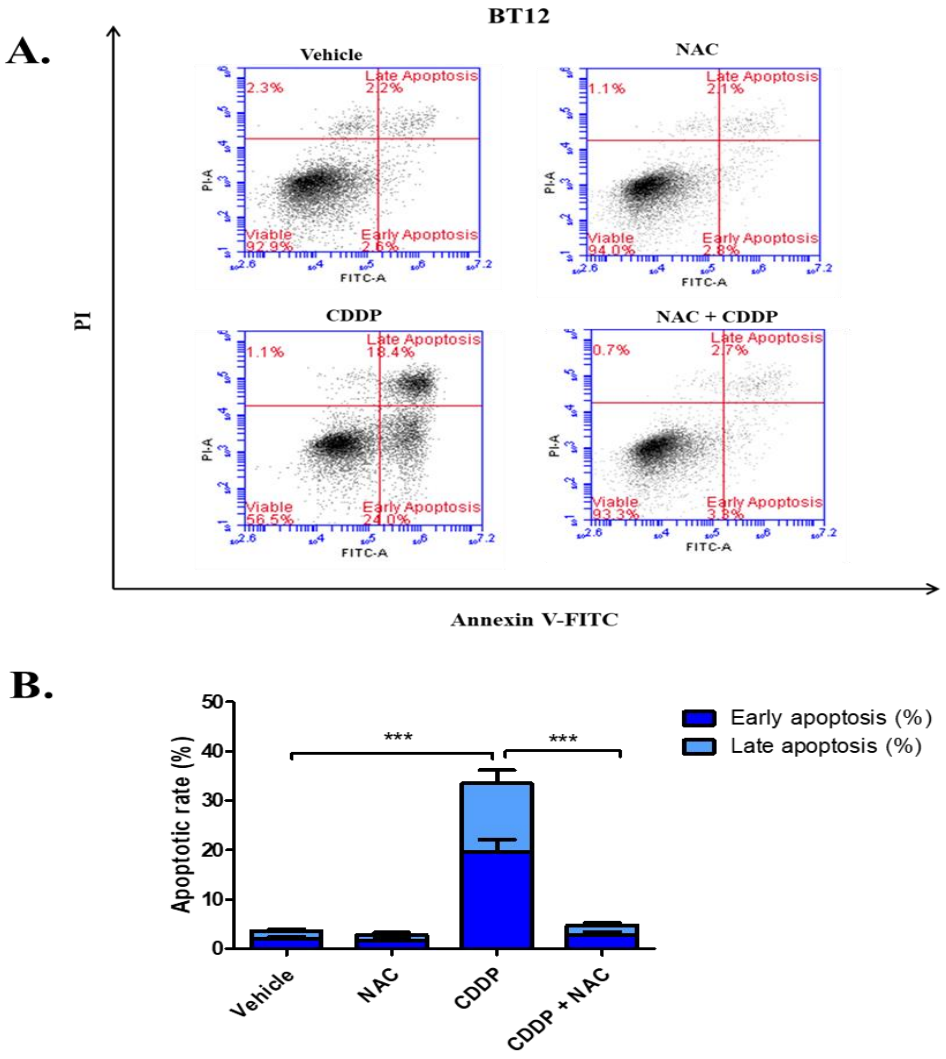

Figure 4.6 N-acetyl cysteine exhibits a protective effect against cisplatin-induced apoptosis in BT12 cells

2mL of BT12 were seeded in a 6-well plate at a seeding density of 1 x 10^5 cells/mL. Cells were left to adhere overnight and were treated with the vehicle (0.009% NaCl), NAC (5mM), 1 µM cisplatin (CDDP) or cisplatin and NAC in combination. The NAC treatment was left for an hour prior to cisplatin treatment. After 48 hours, the cells were detached and stained with Annexin V and propidium iodide (PI). The cells were immediately analysed by flow cytometry using the BD FACS Acuri software. 10,000 cells were gated on vehicle treated cells and the percentage of cells undergoing early and late apoptosis was determined to be those stained with Annexin V only and stained with both Annexin V and PI, respectively. **A** Representative dot plot of treated cells. **B** Values represent mean ± S.E.M. of three independent experiments. Statistical analysis was performed using a one-way ANOVA with Tukey's post hoc test ***$p<0.001$.

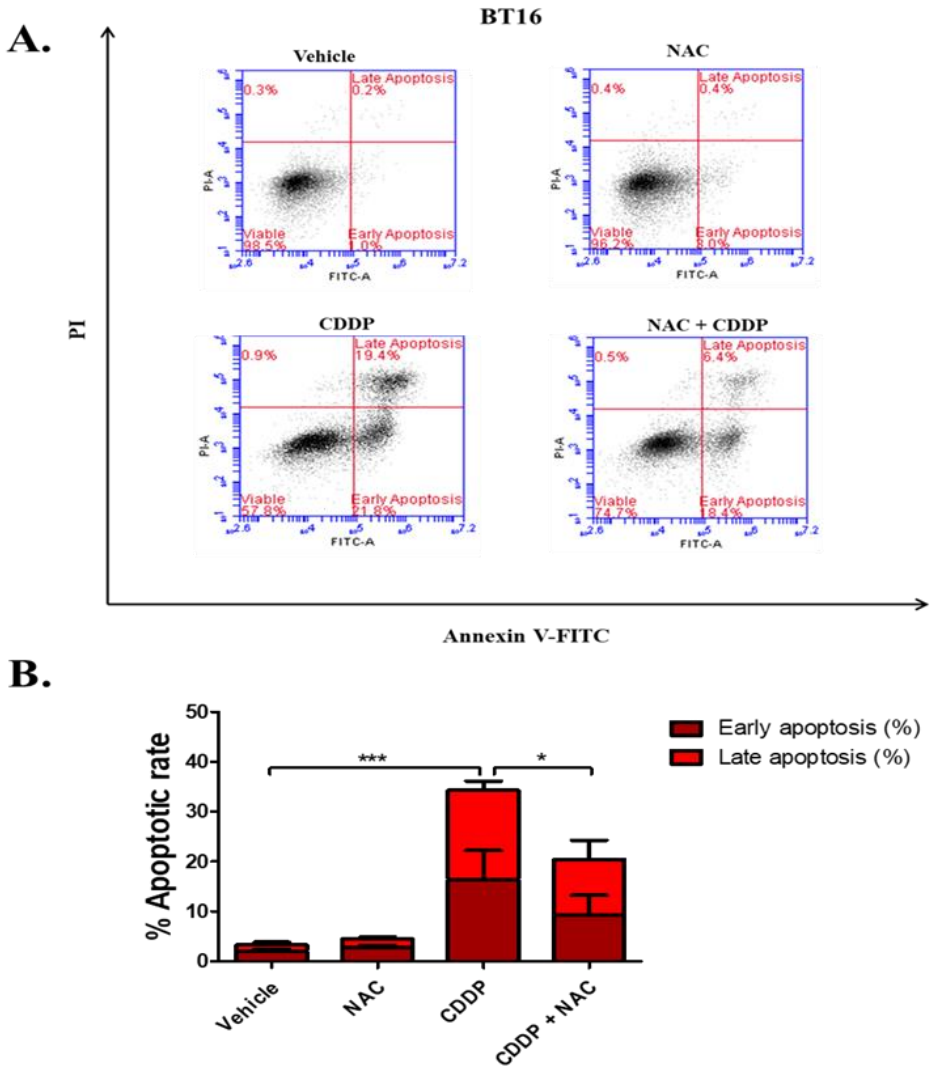

Figure 4.7 N-acetyl cysteine exhibits a protective effect against cisplatin-induced apoptosis in BT16 cells

2mL of BT16 were seeded in a 6-well plate at a seeding density of 1 x 105 cells/mL. Cells were left to adhere overnight and were treated with the vehicle (0.009% NaCl), NAC (5mM), 10 µM cisplatin (CDDP), or cisplatin and NAC in combination. The NAC treatment was left for an hour prior to cisplatin treatment. After 48 hours, the cells were detached and stained with Annexin V and propidium iodide (PI). The cells were immediately analysed by flow cytometry using the BD FACS Accuri software. 10,000 cells were gated on vehicle treated cells and the percentage of cells undergoing early and late apoptosis was determined to be those stained with Annexin V only and stained with both Annexin V and PI, respectively. **A**. Representative dot plot of treated cells. **B**. Values represent mean ± S.E.M. of three independent experiments. Statistical analysis was performed using a one-way ANOVA with Tukey's post hoc test. *p<0.05, ***p<0.001.

4.2.4. The antioxidant GSH is significantly higher in cisplatin resistant BT16 cells.

As a correlation between basal intracellular ROS and cisplatin sensitivity was observed in a panel of MRT cell lines, the basal levels of the antioxidant glutathione across this panel of cell lines were next examined. Glutathione or GSH is reported to be one of the most important and abundant antioxidants in the cell.

The GSH/GSSG-Glo™ assay was employed to measure basal GSH levels in BT12, BT16 and G401 cells. This assay consists of a luminescence-based system that measures a luciferin-based reaction to quantify and detect total GSH, reduced GSH, GSSG and thus, calculate the GSH:GSSG ratio. The reaction relies on the conversion of a GSH probe, Luciferin-NT to luciferin by a glutathione transferase enzyme, GST, in the presence of glutathione. This is coupled to a firefly luciferase reaction. The light from luciferase is dependent on the amount of luciferin detected and thus luminescence is proportional to GSH levels. The assay can measure either the reduced form, GSH or the oxidised form GSSG by adding a reagent that blocks GSH while leaving GSSG intact, allowing for its quantification. This GSSG is then reduced to GSH for quantification.

In this study, the GSH/GSSG kit was first used to measure basal reduced GSH levels in BT12, BT16 and G401 cells and luminescence was measured using the Luminoskan™ Microplate Luminometer. Significantly higher GSH levels were observed in the cisplatin-resistant BT16 cells when compared to cisplatin-sensitive BT12 cells (Figure 4.8). The levels of GSH in BT12 and G401 cells were similar, with G401 cells having only slightly more GSH. These results correlate with the profile of basal ROS levels demonstrated in Figure 4.2, suggesting a relationship between the balance of glutathione, ROS and susceptibility to cisplatin in MRT. BT16 cells which had the highest resistance to cisplatin and the lowest basal ROS levels also exhibited the highest basal levels of GSH. In contrast, BT12 cells which are the most sensitive to cisplatin, had the highest levels of intracellular ROS and the lowest basal levels of GSH. G401 cells appeared to consistently have an intermediary phenotype. In order to further examine the correlation between cisplatin resistance and basal GSH levels, a correlation analysis was performed. Relative GSH levels were plotted against percentage viability in MRT cells treated with 10 µM cisplatin and a positive correlation was observed between the two variables with an r value of 0.9843 suggesting a potential correlation between cisplatin and GSH levels. However, this was non-significant with a p-value of 0.1130.

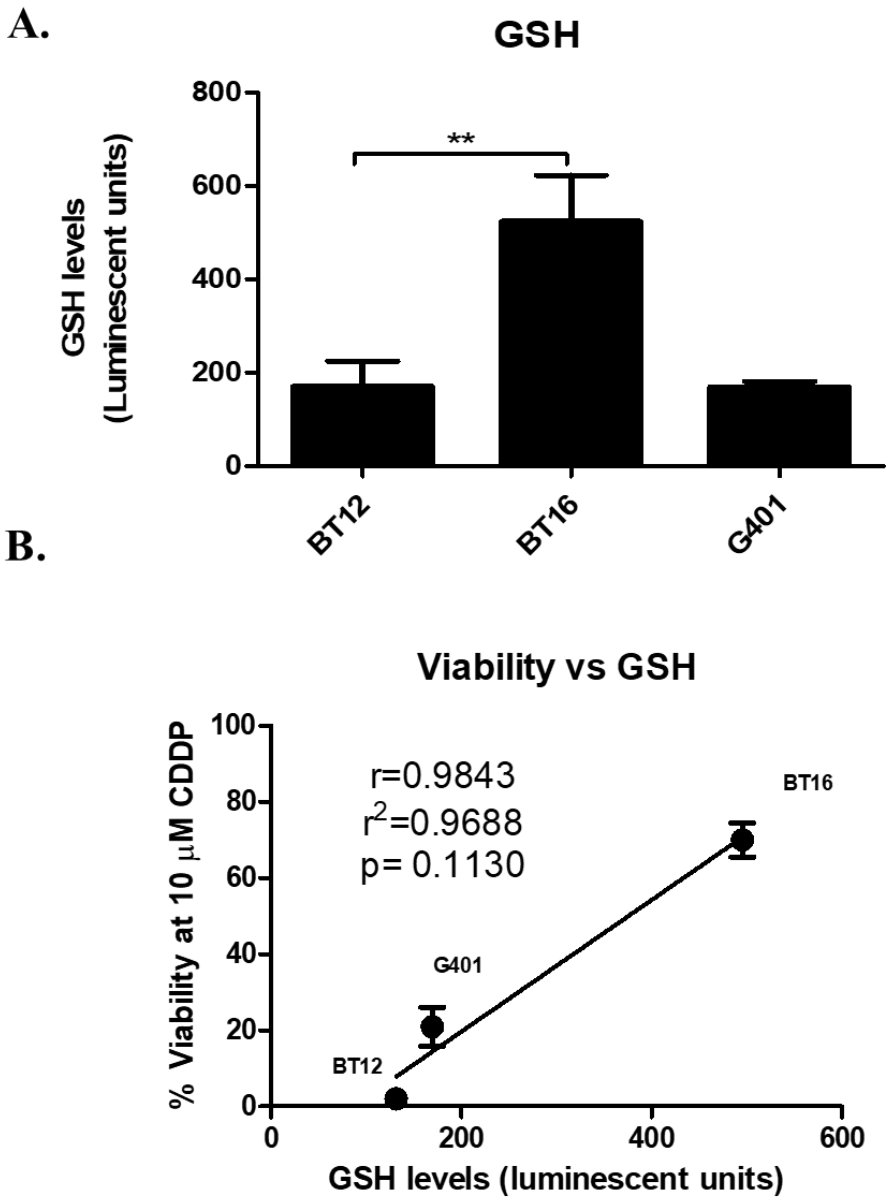

Figure 4.8 Basal glutathione levels in MRT cells correlate with cisplatin sensitivity

BT12, BT16 and G401 cells were seeded at various seeding densities in a 96-well plate. The cells were left to incubate for 72h. After this incubation time, the cells were analysed using the GSH/GSSG-Glo Kit. Luminescence was measured using the Luminoskan™ Microplate Luminometer. **A**. Bar graph depicting reduced GSH levels in BT12, BT16 and G401 cells. Values represent the mean ± S.E.M. of at least three independent experiments performed in duplicate. Statistical analysis was performed using two-tailed paired t test. **B.** Relative densitometric values were plotted against percentage viability at 10 µM cisplatin treatment for the three cell lines to determine the correlation between the two variables. Correlation analysis was performed on GraphPad Prism to obtain r values and p values.

4.2.5. Cisplatin reduces GSH and induces oxidative stress in MRT cell lines

Oxidative stress is a term used to define an imbalance between the generation of ROS and the antioxidant capacity of the cell resulting in an excess of free radicals. Oxidative stress has been linked with a number of pathologies including neurodegenerative disease, cardiovascular disease and cancer[436]. This study has shown that MRT cell lines with different levels of GSH exhibit varying responses to cisplatin. Moreover, results have also shown that cisplatin induces a significant generation of ROS. In order to determine whether this cisplatin-induced ROS production results in oxidative stress**,** the GSH/GSSG-Glo™ assay was utilised. As previously mentioned, glutathione can exist in its reduced form (GSH) or in its oxidised form (GSSG). Most of the glutathione found in healthy cells exists in its reduced form. This is because the enzyme glutathione reductase, which converts free glutathione from its oxidised form to its reduced form is constitutively active and is induced in response to oxidative stress. The ratio of GSH to GSSG is commonly used as a marker of oxidative stress[422].

BT12 cells were treated with 1 µM cisplatin whereas BT16 and G401 cells were treated with a higher concentration of 10 µM cisplatin. Following incubation for 48h, the cells were analysed with the GSH/GSSG-Glo™ assay and luminescence was measured with Luminoskan™ Microplate Luminometer. A significant reduction in GSH and GSH:GSSG ratio was observed in BT12 cells (Figure 4.9) suggesting that ROS accumulation caused by cisplatin results in oxidative stress. In contrast, in BT16 cells, which were shown to have much higher basal levels of GSH, no significant depletion of GSH or a decrease in the GSH:GSSG ratio was observed (Figure 4.10). These results suggest that BT16 may rely strongly on its antioxidant defence system to cope with stress induced by cisplatin treatment. Lastly, G401 cells were shown to elicit a significant decrease in GSH levels in response to cisplatin as well as a notable decrease in GSH:GSSG ratio, with a near significant p value of 0.0675 (Figure 4.11). Of note, cisplatin can be detoxified by GSH, as GSH can bind covalently to cisplatin and these formed GSH conjugates is then exported from the cells, preventing the drug from accessing DNA.

Collectively, these results suggest that ROS accumulation may induce cisplatin-induced oxidative stress in BT12 and G401 cells, however, the more resistant BT16 cell line is better adapted to cope with cisplatin-induced ROS generation.

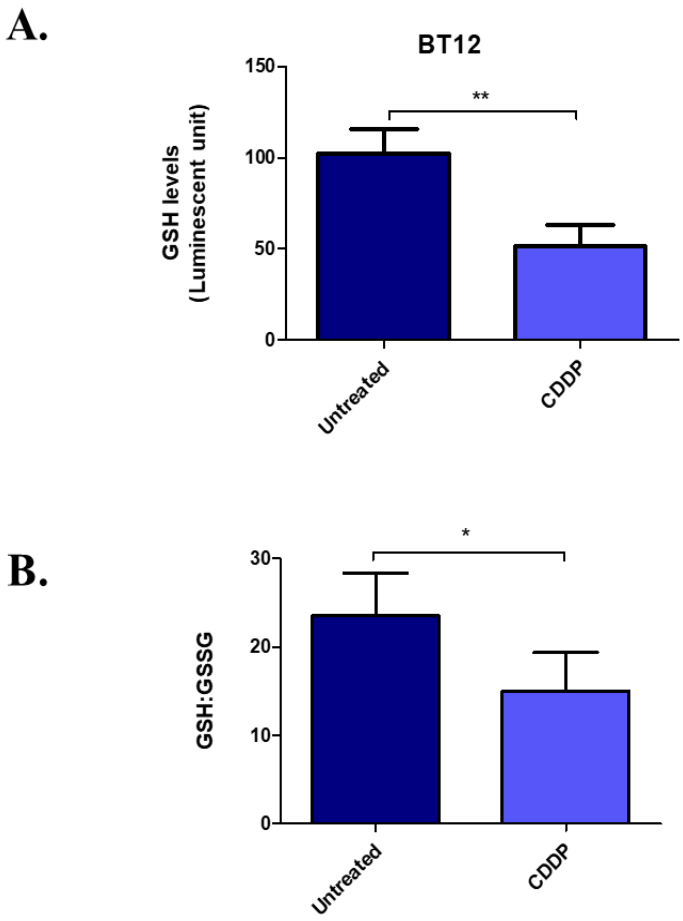

Figure 4.9 Cisplatin decreases GSH and the GSH/GSSG ratio in BT12 cells

BT12 cells were seeded at 1 x 10^4 cells/ well in a 96-well plate. The cells were left to adhere for 24h and were then treated with 1 µM cisplatin. After 48h, the cells were analysed using the GSH/GSSG-Glo Kit. And luminescence was measured using the Luminoskan™ Microplate Luminometer. **A**. GSH levels **B**. GSH/GSSG ratio. Values represent the mean ± S.E.M. of three independent experiments each performed in duplicate. Statistical analysis was performed using two-tailed paired t test. *$p<0.05$, **$p<0.01$.

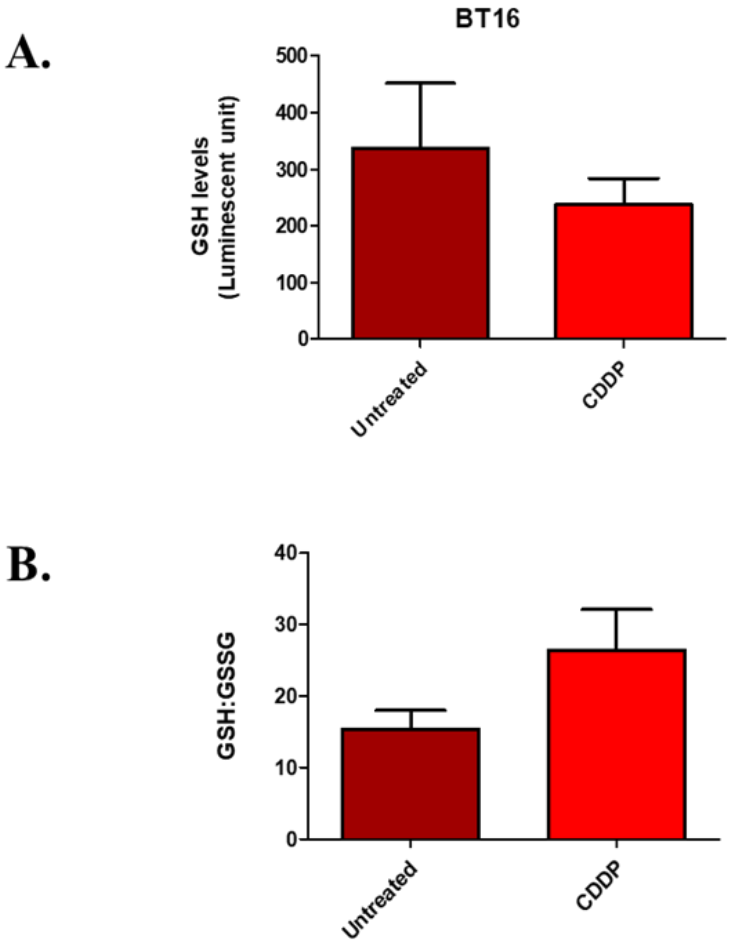

Figure 4.10 Lack of effect of cisplatin on glutathione and GSH/GSSG levels in BT16 cells

BT16 cells were seeded at 1 x 10^4 cells/ well in a 96-well plate. The cells were left to adhere for 24h and were then treated with 10 µM cisplatin for 48h. After this incubation time, the cells were analysed using the GSH/GSSG-Glo Kit and luminescence was measured using the Luminoskan™ Microplate Luminometer. **A**. GSH levels **B**. GSH/GSSG ratio. Values represent the mean ± S.E.M. of three independent experiments each performed in duplicate. Statistical analysis was performed using two-tailed paired t test.

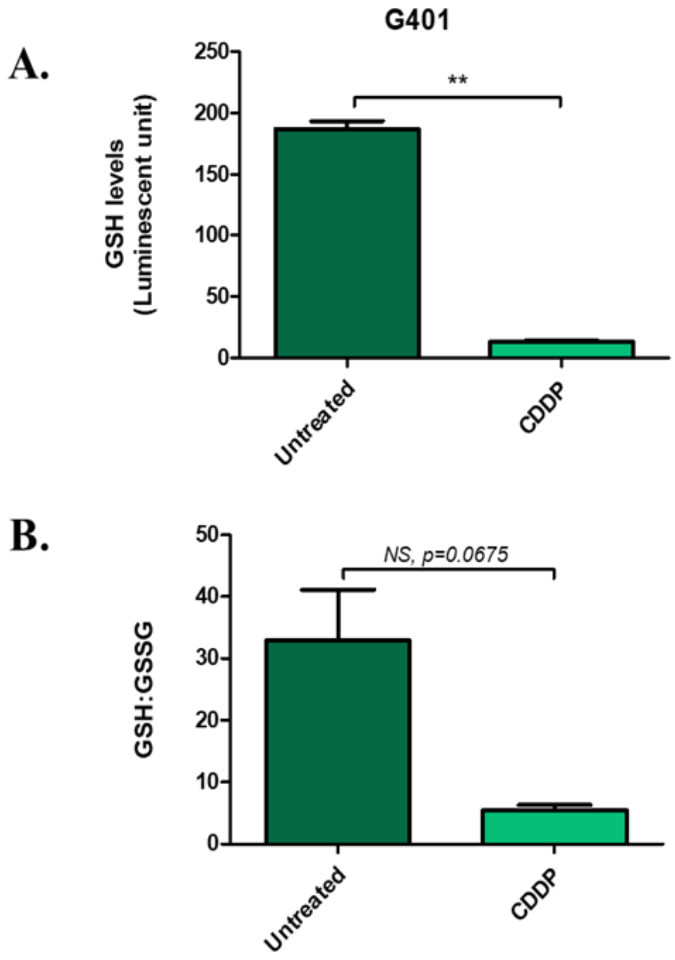

Figure 4.11 Cisplatin induces glutathione depletion and reduces the GSH/GSSG ratio in G401 cells

G401 cells were seeded at 5 x 10^3 cells/ well in a 96-well plate. The cells were left to adhere for 24h and were then treated with 10 µM cisplatin. After 48h, the cells were analysed using the GSH/GSSG-Glo Kit and luminescence was measured using the Luminoskan™ Microplate Luminometer. **A**. GSH levels **B**. GSH/GSSG ratio. Values represent the mean ± S.E.M. of three independent experiments each performed in duplicate. Statistical analysis was performed using two-tailed paired t test. NS= non-significant, **p<0.01.

4.2.6. Glutathione depletion enhances cisplatin-induced ROS and cisplatin-induced apoptosis in MRT cell lines

Earlier results presented in this chapter demonstrated a potential correlation between basal glutathione levels and cisplatin resistance. In order to further investigate the importance of glutathione in cisplatin-induced cytotoxicity and resistance in MRT the effect of glutathione depletion on cisplatin sensitivity was next examined in cisplatin-sensitive BT12 and cisplatin-resistant BT16cell lines.

The glutathione inhibitor, buthionine sulfoximine (BSO) was employed to target this component of the antioxidant system by inhibiting gamma-glutamylcysteine synthetase, the enzyme required in the first step of glutathione synthesis. To validate the inhibitor activity of BSO, GSH and GSH: GSSG levels were assessed in BT16 cells following treatment with 200 µM BSO for 48 hours. After this incubation period, cells were analysed with the GSH/GSSG-Glo™ assay and luminescence was measured with Luminoskan™ Microplate Luminometer. As shown in Figure 4.12, GSH levels were significantly depleted and the GSH:GSSG ratio was also significantly reduced in response to BSO compared to control cells confirming the inhibitory activity of BSO on glutathione.

Moreover, to determine the effect of glutathione depletion on cisplatin-induced ROS, BT16 cells were treated with BSO and cisplatin, alone and in combination for 48h. After this incubation period, cells were stained with H_2DCFDA and analysed with flow cytometry. A significant enhancement in ROS production was observed in cells treated with BSO and cisplatin when compared to cells that were treated with cisplatin alone (Figure 4.13). This result indicates that GSH plays a critical role in regulating cisplatin-induced ROS.

In order to determine the therapeutic potential of targeting glutathione, the effect of BSO on cisplatin-induced apoptosis was then examined. BT12 and BT16 cells were treated with cisplatin (1 and 10 µM, respectively) alone or in combination with BSO for 48h. After this time period, cells were stained with Annexin V and PI and percentage of early and late apoptosis was obtained using the BD Accuri flow cytometer. Results showed that BSO significantly enhanced cisplatin-induced apoptosis in both cisplatin-sensitive BT12 cells (Figure 4.14) and cisplatin-resistant BT16 cells (Figure 4.15). Of note, BSO treatment alone does not cause an increase in apoptosis compared to vehicle control cells. This

suggests that GSH depletion alone does not cause cell death however, it can enhance drug-induced apoptosis.

Taken together, these results suggest that glutathione may play an important role in chemoresistance and may present a potential therapeutic target in MRT to combat resistance.

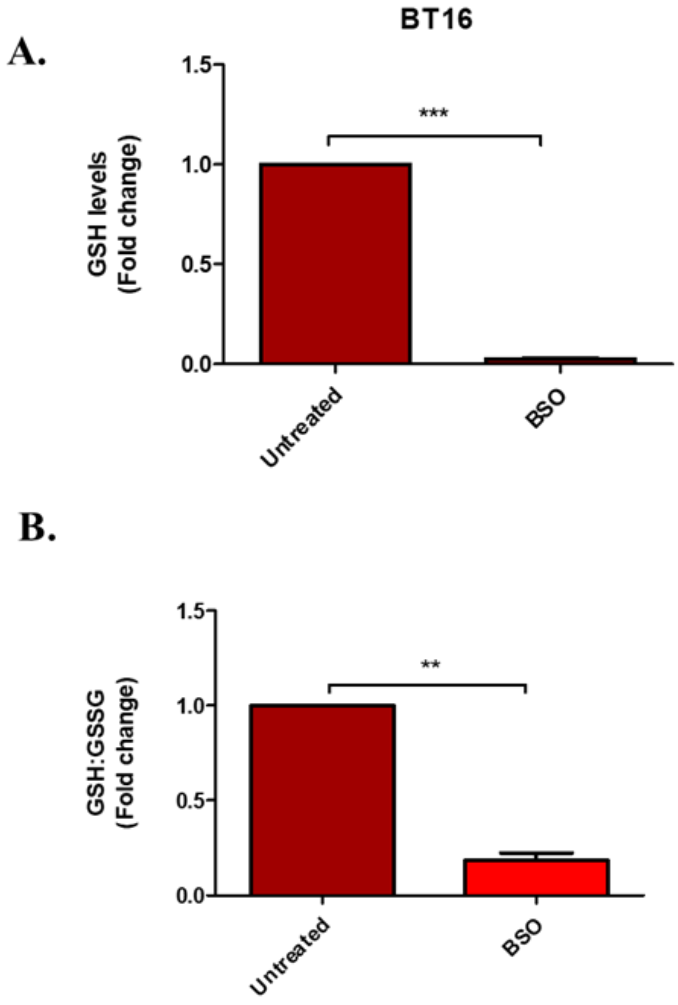

Figure 4.12 BSO induces glutathione depletion and oxidative stress in BT16 cells

BT16 cells were seeded at 1 x 10^4 cells/ well in a 96-well plate. The cells were left to adhere for 24h and were then treated with 200 µM BSO. After 48h, they were analysed using the GSH/GSSG-Glo Kit. And luminescence was measured using the Luminoskan™ Microplate Luminometer. **A**. GSH levels **B**. GSH/GSSG ratio. Fold change values were obtained by normalising data from treated cells against the data obtained for the untreated cells. Values represent the mean ± S.E.M. of three independent experiments each performed in duplicate. Statistical analysis was performed using a paired two-tailed t test. **p<0.01, ***p<0.001.

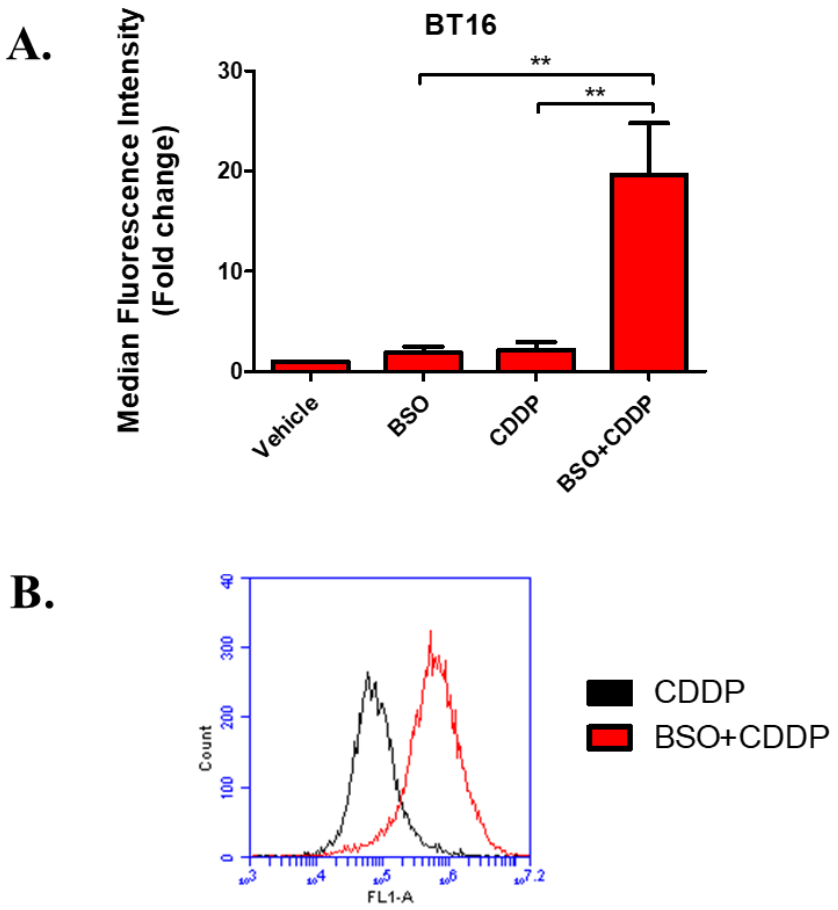

Figure 4.13 BSO enhances cisplatin-induced ROS in BT16 cells

2mL BT16 cells were seeded in a 6-well plate at a seeding density of 1 x 10^5 cells/mL. Cells were left to adhere overnight and were treated with the vehicle (0.009% NaCl), BSO (200 µM), cisplatin (10 µM or cisplatin and BSO in combination. The BSO treatment was left for an hour prior to cisplatin treatment. After 48 hours, the cells were stained H_2DCFDA after which they were harvested, washed and resuspended in PBS. The cells were immediately analysed by flow cytometry using the BD FACS Accuri software. 10,000 cells were gated on vehicle treated and the MFI values were obtained and normalised by the vehicle. **A**. Bar graph showing ROS levels of BSO, cisplatin alone or in combination, relative to the vehicle control. Fold change values were obtained by normalising data from treated cells against the data obtained for the vehicle control cells. Values represent mean ± S.E.M of three independent experiments in BT16 cells. Statistical analysis was performed using Statistical analysis was performed using one-way ANOVA with cells treated with cisplatin and cisplatin with BSO. **p<0.01. **B**. Representative flow cytometric histogram of cells treated with cisplatin alone or in combination with BSO.

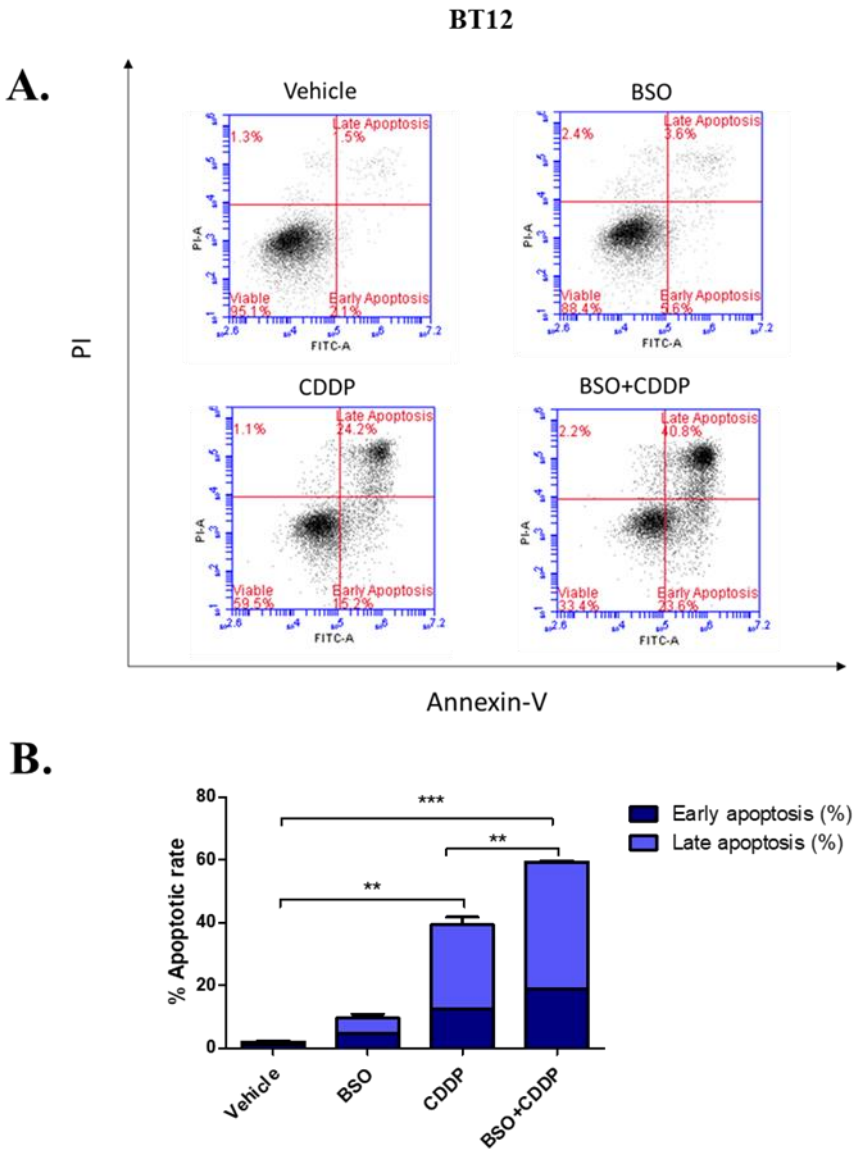

Figure 4.14 BSO enhances cisplatin-induced apoptosis in BT12 cells

2mL of BT12 were seeded in a 6-well plate at a seeding density of 1 x 10^5 cells/mL. Cells were left to adhere overnight and were treated with the vehicle (0.009% NaCl), BSO (200 µM), 1 µM cisplatin (CDDP) or cisplatin and BSO in combination. The BSO treatment was left for an hour prior to cisplatin treatment. After 48 hours, the cells were detached and stained with Annexin V and propidium iodide (PI). The cells were immediately analysed by flow cytometry using the BD FACS Accuri software. 10,000 cells were gated on vehicle treated cells and the percentage of cells undergoing early and late apoptosis was determined to be those stained with Annexin V only and stained with both Annexin V and PI, respectively. **A** Representative dot plot of treated cells. **B**. Values represent mean ± S.E.M of three independent experiments. Statistical analysis was performed using a one-way ANOVA with Tukey's post hoc test. **p<0.01, ***p<0.001.

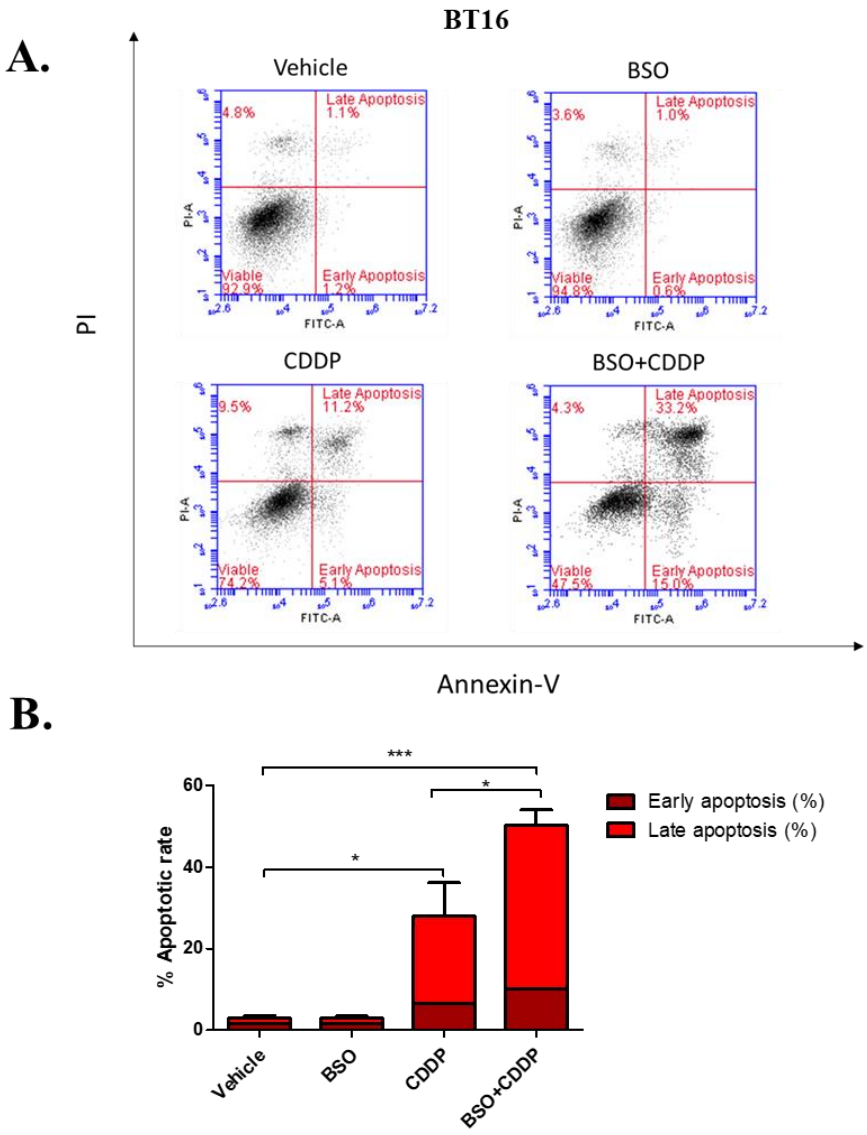

Figure 4.15 BSO enhances cisplatin-induced apoptosis in BT16 cells

2mL of BT16 were seeded in a 6-well plate at a seeding density of 1 x 10^5 cells/mL. Cells were left to adhere overnight and were treated with the vehicle (0.009% NaCl), BSO (200 µM), 10 µM cisplatin (CDDP), or cisplatin and BSO in combination. The BSO treatment was left for an hour prior to cisplatin treatment. After 48 hours, the cells were detached and stained with Annexin V and propidium iodide (PI). The cells were immediately analysed by flow cytometry using the BD FACS Accuri software. 10,000 cells were gated on vehicle treated cells and the percentage of cells undergoing early and late apoptosis was determined to be those stained with Annexin V only and stained with both Annexin V and PI, respectively. **A** Representative dot plot of treated cells. **B**. Values represent mean ± S.E.M of three independent experiments. Statistical analysis was performed using a one-way ANOVA with Tukey's post hoc test. *p<0.05 , ***p<0.001.

4.2.7. Analysis of endogenous and cisplatin-induced Nrf2 protein expression in MRT cells.

This present study has indicated a role for GSH in mediating cisplatin resistance in MRT and the potential of exploiting this role therapeutically to circumvent resistance. Nrf2, a transcription factor widely known as the master regulator of the antioxidant system and a mediator of genes involved in the GSH pathway, was next investigated to determine whether it was implicated in GSH-mediated chemoresistance.

Firstly, basal protein expression levels of Nrf2 were examined by western blot analysis in the panel of MRT cell lines (Figure 4.16). Interestingly, the lowest levels of Nrf2 expression were observed in the most cisplatin-sensitive BT12 cell line. The most resistant BT16 cells exhibited the highest levels of Nrf2 whereas G401 cells had intermediary levels of Nrf2 expression. These levels were consistent with the varying sensitivities of this panel of MRT cell lines to cisplatin. In order to determine the relationship between Nrf2 expression and cisplatin resistance, the relative densitometric values were plotted against the percentage viability of cells in response to 10 μM cisplatin treatment. Correlation analysis was performed in GraphPad Prism and an r value of 0.9268 was obtained indicating some correlation. This was however not deemed statistically significant with a p-value of 0.2451. A limitation of this correlation analysis is the low number of samples examined (3 cell lines). However, this trend of correlation is consistent with the results obtained when looking at the basal profile of ROS and glutathione in relation to sensitivity of the three MRT cell lines to cisplatin suggesting that there is a relationship between cisplatin resistance and the antioxidant system in MRT.

Subsequently, protein expression of levels of Nrf2 were examined in response to cisplatin treatment. BT12 and BT16 cells were treated with the vehicle (0.009% NaCl) or cisplatin (1 and 10 μM, respectively) for 48h. After this time, cells were harvested and lysed. Samples were prepared, ran on a SDS-PAGE gel and probed with an anti-Nrf2 antibody. Cisplatin did not induce any significant change in total Nrf2 levels in either cell line (Figure 4.17). Once again, significantly higher basal Nrf2 protein expression levels were observed in BT16 cells when compared to BT12 cells.

Collectively, the results presented herein demonstrate that MRT cells with the highest resistance to cisplatin, the BT16 cells, also have the highest levels of basal GSH and Nrf2 expression as well as the lowest levels of intracellular ROS. BT12 cells, which were the

most sensitive to cisplatin, were shown to have significantly higher levels of ROS, the lowest levels of GSH and the lowest basal expression of Nrf2. These results may suggest an important role of the antioxidant system in mediating the cytoprotective response to cisplatin treatment in MRT.

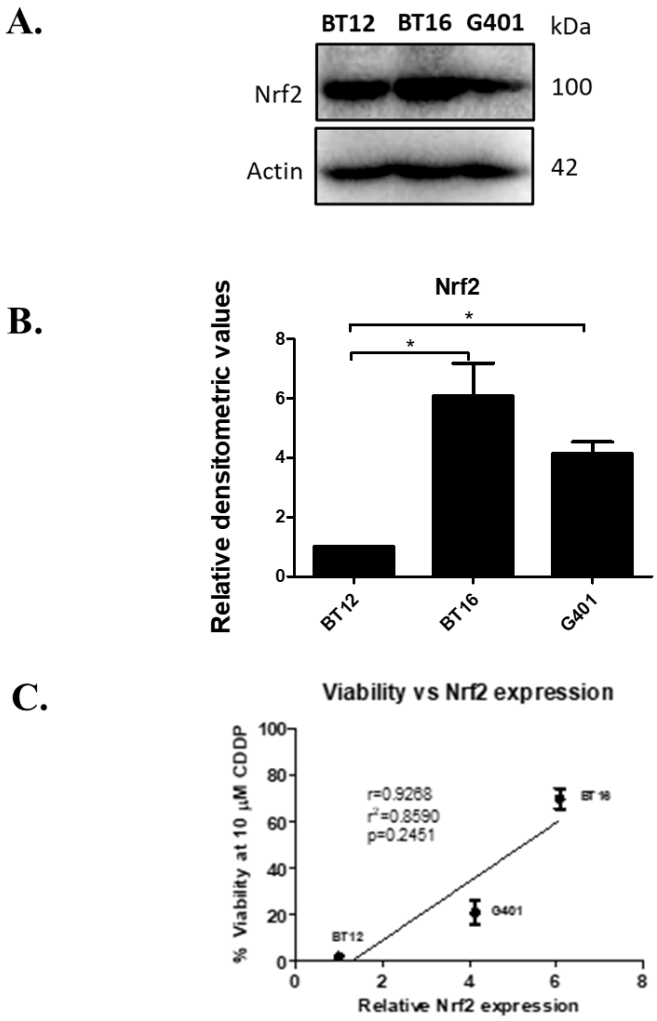

Figure 4.16 Basal expression levels of Nrf-2 in a panel of MRT cell lines

A. MRT cell lines (BT12, BT16 and G401) were seeded at various densities in T175 flasks and grown to sub-confluency. The cells were then harvested and lysates prepared for western blot analysis. 20 ug of protein was loaded, separated on an SDS page gel, transferred to PVDF and probed with the relevant antibodies. Results are representative of three independent experiments. Western blots were normalised to total actin as a loading control. **B**. Densitometric analysis of the bands was carried out using Image Lab software. Statistical analysis was performed using a two-tailed paired t-test. *$p<0.05$. Results represent the mean and S.E.M of three independent experiments. **C**. Relative densitometric values were plotted against percentage viability at 10 uM cisplatin treatment for the three lines to determine the correlation between the two variables using GraphPad Prism.

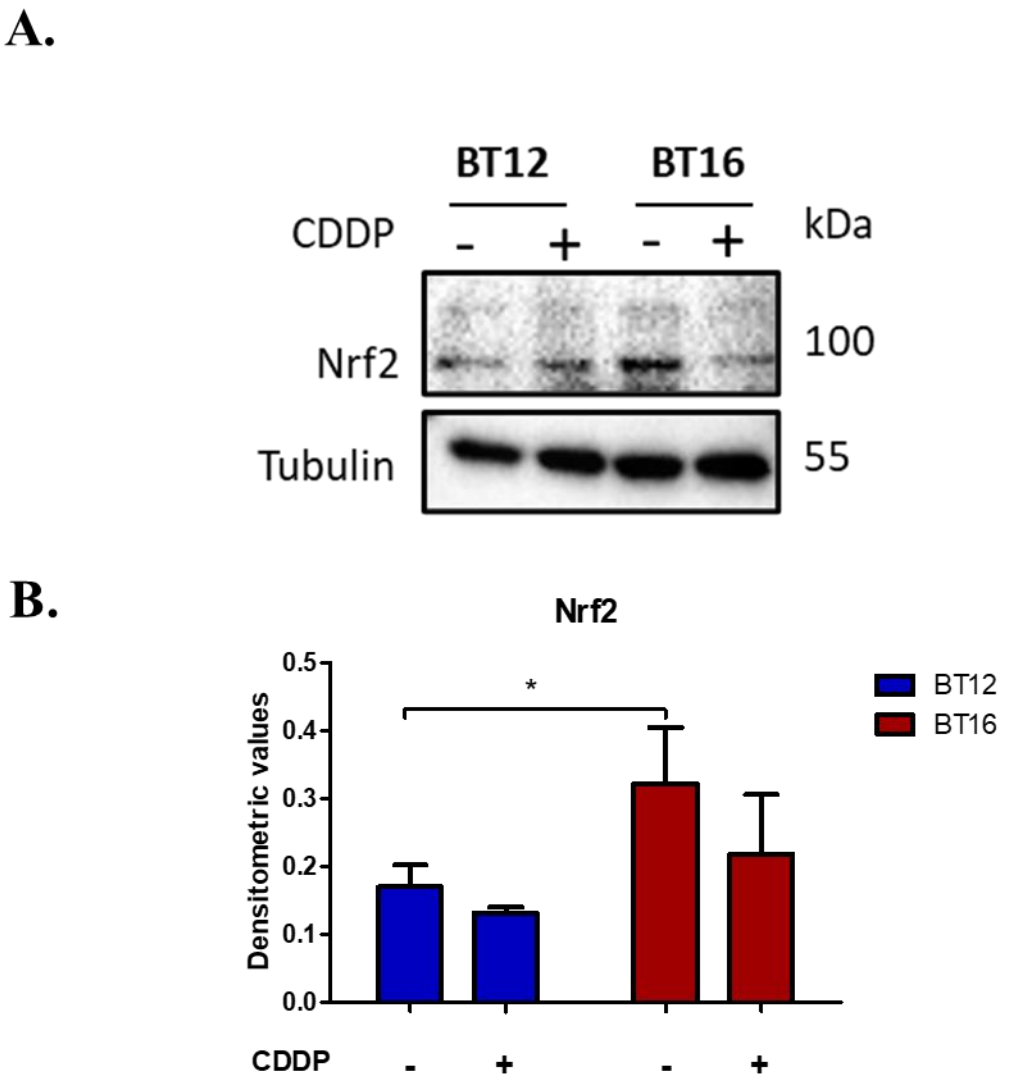

Figure 4.17 Effect of cisplatin on Nrf2 expression levels in MRT cells

A. BT12 and BT16 were seeded at various densities in T175 flasks and grown to sub-confluency. The cells were then harvested and lysates prepared for western blot analysis. 20 ug of protein was loaded, separated on an SDS page gel, transferred to PVDF and probed with the relevant antibodies. Results are representative of three independent experiments. Western blots were normalised to total tubulin as a loading control. **B**. Densitometric analysis of the bands was carried out using Image Lab software. Statistical analysis was performed using one way ANOVA with Tukey's post hoc test. *$p<0.05$. Results represent the mean and S.E.M of three independent experiments.

4.2.8. Nrf2 inhibition decreases GSH levels, enhances cisplatin-induced ROS and sensitises BT16 cells to cisplatin-mediated cell death

This study previously demonstrated a potential correlation between GSH levels and cisplatin resistance in MRT cell lines. Indeed, GSH depletion sensitised MRT cells to the cytotoxic effects of cisplatin. Given that the same pattern of correlation was observed between cisplatin resistance and Nrf2 expression in MRT cell lines, it was hypothesised that levels of Nrf2 may determine cisplatin sensitivity in MRT cell lines by regulating GSH production. In order to test this hypothesis, a small molecule inhibitor of Nrf2, ML385, was firstly employed to inhibit Nrf2 expression levels in the cisplatin-resistant BT16 cells and examine the effect on GSH levels, ROS production and sensitisation to cisplatin. This was followed up by using an siRNA approach to target Nrf2. In both cases Nrf2 inhibition was confirmed using western blot analysis and sensitisation to cisplatin was examined using flow cytometric analysis of Annexin/PI stained cells.

4.2.8.1 ML385

ML385 binds to the Neh1, the Cap 'N' Collar Basic Leucine Zipper (CNC-bZIP) domain of Nrf2 and inteferes with its target downstream gene expression by interfering with the binding of the V-Maf Avian Musculoaponeurotic Fibrosarcoma Oncogene Homolog G (MAFG)-NRF2 protein complex to regulatory DNA binding sequences[432].

To determine the inhibitory effect of ML385 on Nrf2, BT16 cells were treated with 40 µM ML385 for 48h. As demonstrated by western blotting, Nrf2 expression levels were significantly downregulated validating the inhibitory activity of ML385 (Figure 4.18). ML385 binds to Neh1, the Cap 'N' Collar Basic Leucine Zipper (CNC-bZIP) and downregulates total intracellular Nrf2 levels by inhibiting transcriptional activity of Nrf2 itself, as well as various downstream target genes.

Given that this study has shown that ML385 can efficiently downregulate Nrf2 levels and that GSH plays a potential role in mediating cisplatin resistance, this study next evaluated whether Nrf2 inhibition could affect GSH levels. Cells were treated with 40 µM ML385 for 48h and GSH levels and the GSH:GSSG ratio analysed with the GSH/GSSG-Glo kit. A significant decrease in GSH levels was observed in response to ML385 and a trend of decrease was also observed in the GSH:GSSG ratio (Figure 4.19) indicating that Nrf2 can indeed regulate GSH production in MRT.

Moreover, the effect of Nrf2 inhibition on ROS levels was next evaluated. Cells were treated with cisplatin (10 µM) or ML385 (40 µM) alone or in combination for 48h. After this time, the cells were harvested and stained with H_2DCFDA. Subsequently, ROS levels were examined by flow cytometric analysis. As expected, and in agreement with previous results presented herein (Figure 4.3) cisplatin treatment on its own caused ROS generation (Figure 4.20). Interestingly, a combination of ML385 and cisplatin treatment caused a significant enhancement of ROS levels when compared to cisplatin or ML385 on its own indicating that Nrf2 downregulation sensitised MRT cells to cisplatin-induced ROS. Following on from this, the effect of ML385 treatment on cisplatin-induced apoptosis was assessed. BT16 cells were treated with ML385 (40 µM) or cisplatin (10 µM) alone or in combination and stained with Annexin V/PI-stained apoptosis. A statistically significant increase in the apoptotic rate of BT16 cells was observed in cells treated with the combination of cisplatin and ML385 compared to cisplatin treatment alone, indicating that Nrf2 inhibition may restore cisplatin sensitivity in resistant MRT cells (Figure 4.21).

A.

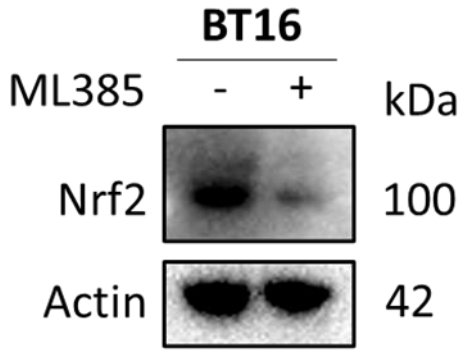

B.

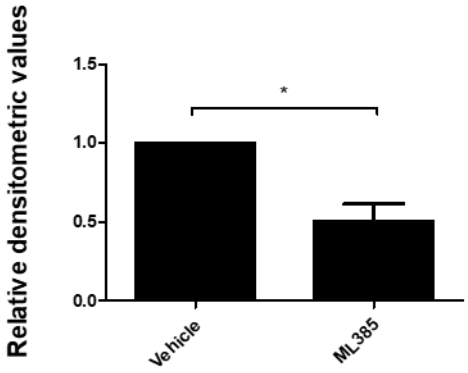

Figure 4.18. The Nrf2 small molecule inhibitor ML385 reduces levels of Nrf2 in BT16 cells

A. BT16 cells was seeded at 1 x 10^5 cells/mL. The cells were then harvested and lysates prepared for western blot analysis. 20 ug of protein was loaded, separated on an SDS page gel, transferred to PVDF and probed with the relevant antibodies. Results are representative of three independent experiments. Western blots were normalised to total actin as a loading control. **B**. Densitometric analysis of the bands was carried out using Image Lab software. Statistical analysis was performed using using a paired two-tailed t test. Results represent the mean and S.E.M of three independent experiments.

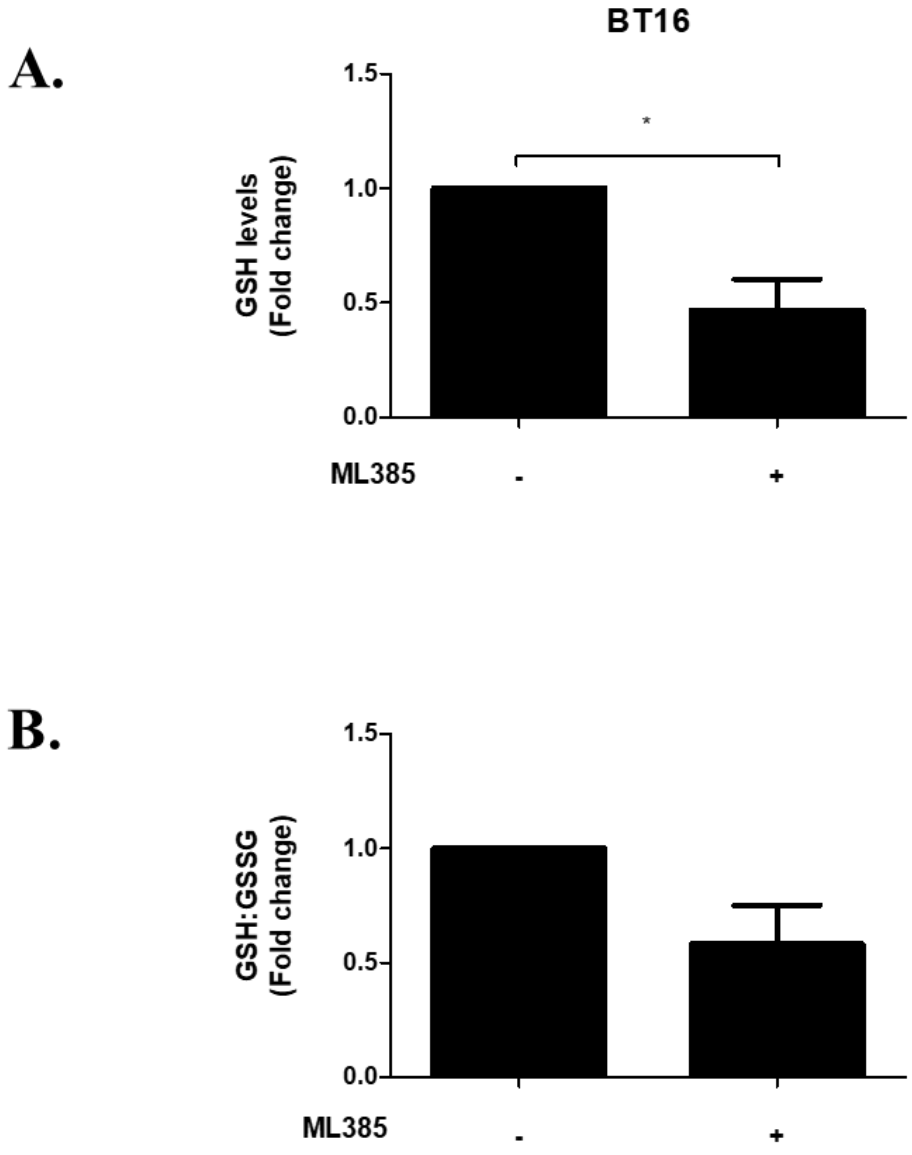

Figure 4.19 Effect of ML385 on GSH levels and the GSH:GSSG ratio

BT16 cells were seeded at 1 x 10^4 cells/ well in a 96-well plate. The cells were left to adhere for 24h and were then treated with 40 µM ML385. After 48h, they were analysed using the GSH/GSSG-Glo Kit. And luminescence was measured using the Luminoskan™ Microplate Luminometer. **A**. GSH levels **B**. GSH/GSSG ratio. Fold change values were obtained by normalising data from treated cells against the data obtained for the untreated cells. Values represent the mean ± S.E.M. of three independent experiments each performed in duplicate. Statistical analysis was performed using a paired two-tailed t test. *$p<0.05$.

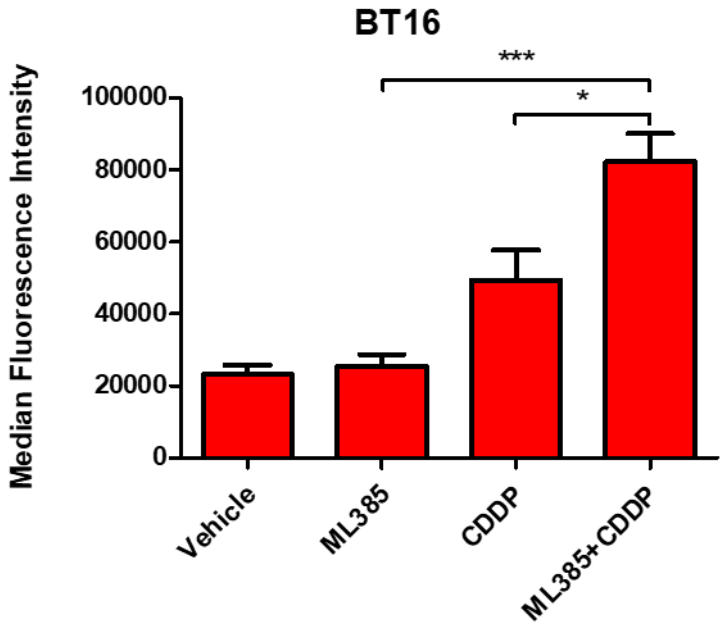

Figure 4.20 Targeting of Nrf2 with ML385 enhances cisplatin-induced ROS in BT16 cells

2mL of BT16 were seeded in a 6-well plate at a seeding density of 1 x 10^5 cells/mL. Cells were left to adhere overnight and were treated with the vehicle (0.009% NaCl), ML385 (40 µM), 10 µM cisplatin (CDDP) or cisplatin and ML385 in combination. After 48 hours, the cells were stained H_2DCFDA for 30 minutes after which they were harvested, washed and resuspended in PBS. The cells were immediately analysed by flow cytometry using the BD FACS Accuri software. 10,000 cells were gated on vehicle treated cells. Values represent mean ± S.E.M of three independent experiments. Statistical analysis was performed using a one-way ANOVA with Tukey's post hoc test. *$p<0.05$, ***$p<0.001$.

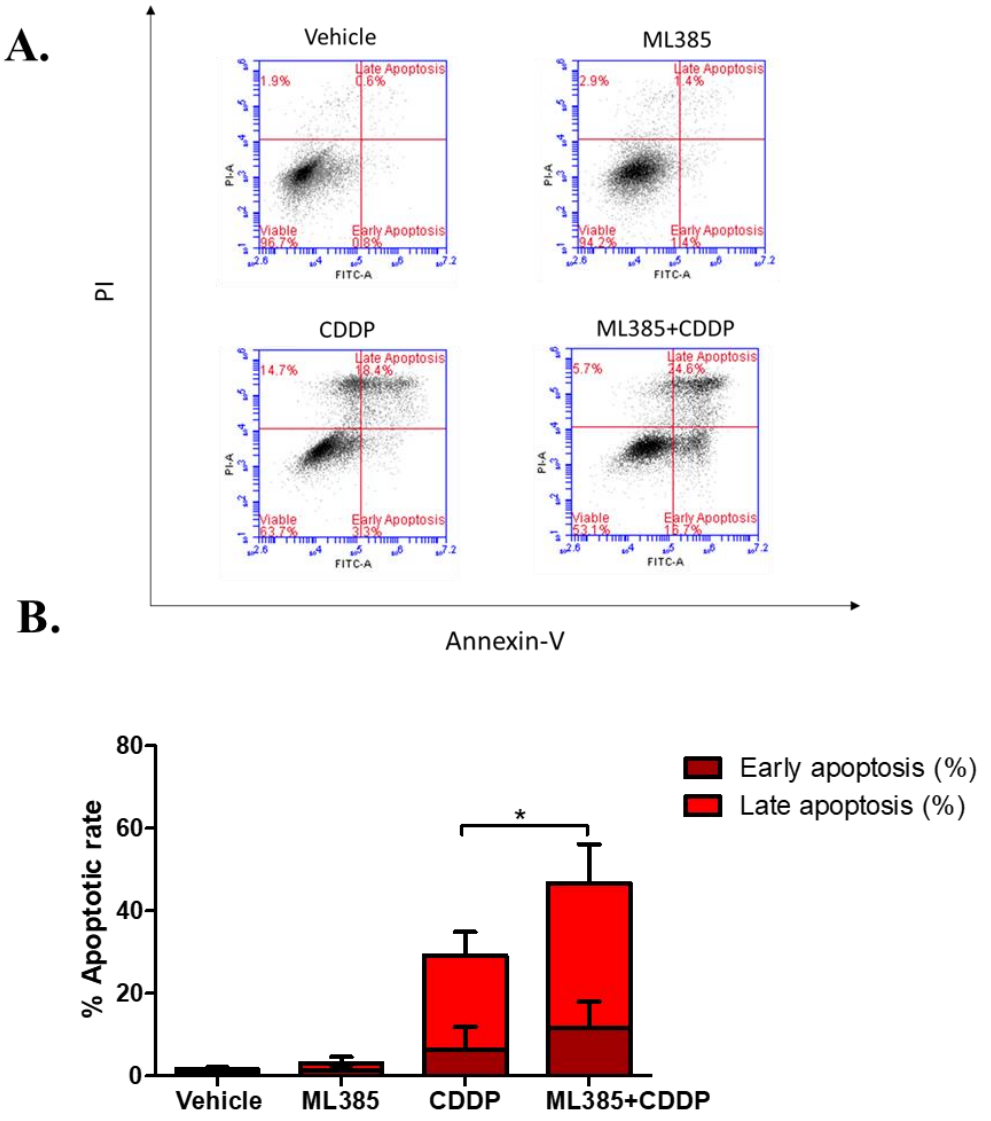

Figure 4.21 ML385 enhances cisplatin-induced apoptosis in BT16 cells

2mL of BT16 were seeded in a 6-well plate at a seeding density of 1 x 10^5 cells/mL. Cells were left to adhere overnight and were treated with the vehicle (0.009% NaCl), ML385 (40 µM), 10 µM cisplatin (CDDP) or cisplatin and ML385 in combination. After 48 hours, the cells were detached and stained with Annexin V and propidium iodide (PI). The cells were immediately analysed by flow cytometry using the BD FACS Accuri software. 10,000 cells were gated on vehicle treated cells and the percentage of cells undergoing early and late apoptosis was determined to be those stained with Annexin V only and stained with both Annexin V and PI, respectively. **A** Representative dot plot of treated cells. **B**. Values represent mean ± S.E.M of three independent experiments. Statistical analysis was performed using a one-way ANOVA with Tukey's post hoc test. *$p<0.05$.

4.3.8.2 Nrf2 siRNA

In order to validate the results obtained with the pharmacological Nrf2 inhibitor, ML385, a genetic approach was also used to target Nrf2 protein expression. Nrf2 siRNA was employed to downregulate Nrf2 protein expression. This RNA-interference approach represents a more accurate strategy to specifically target Nrf2, avoiding any possible non-specific off-target effects of ML385 treatment.

Firstly, the efficiency of Nrf2 siRNA was assessed. BT16 cells were transfected with Non-Targeting (NT) Control siRNA or with Nrf2 siRNA using lipofectamine. Cells treated with lipofectamine alone were considered as a negative control. After 24 hours, the cells were harvested and analysed via western blot analysis. As shown in Figure 4.22, a significant decrease in Nrf2 protein expression was observed in cells that had been transfected with Nrf2 siRNA when compared to NT siRNA transfected cells and lipofectamine treated cells. This result confirmed and validated the efficiency of the Nrf2 siRNA.

The results presented above demonstrated that targeting Nrf2 through the use of the small molecule Nrf2 inhibitor ML385 enhanced cisplatin-induced ROS suggesting Nrf2 may play a role in mediating ROS levels in response to drug treatment. In order to further examine this, the effect of genetic inhibition of Nrf2 on cisplatin-induced ROS levels was assessed. The cells were transfected for 24 hours, and cisplatin was added 20 hours before the end of this incubation period. As seen in Figure 4.23, genetic inhibition of Nrf2 significantly enhanced cisplatin-induced ROS generation confirming the results obtained using ML385.

The effect of genetic inhibition of Nrf2 on cisplatin-induced apoptosis was also assessed. The cells were transfected for 24 hours, and cisplatin was added 20 hours before the end of this incubation period. Cells were harvested, stained with Annexin V/PI and examined by flow cytometry. Interestingly, cells transfected with Nrf2 siRNA and cisplatin exhibited a significant enhancement in cisplatin-induced apoptosis (an apoptotic rate approximately 20% higher) than cells transfected with NT siRNA and cisplatin (Figure 4.24).

Taken together, these results suggest that targeting the Nrf2/GSH antioxidant system may provide a novel therapeutic strategy for the treatment of MRT and a means of overcoming resistance.

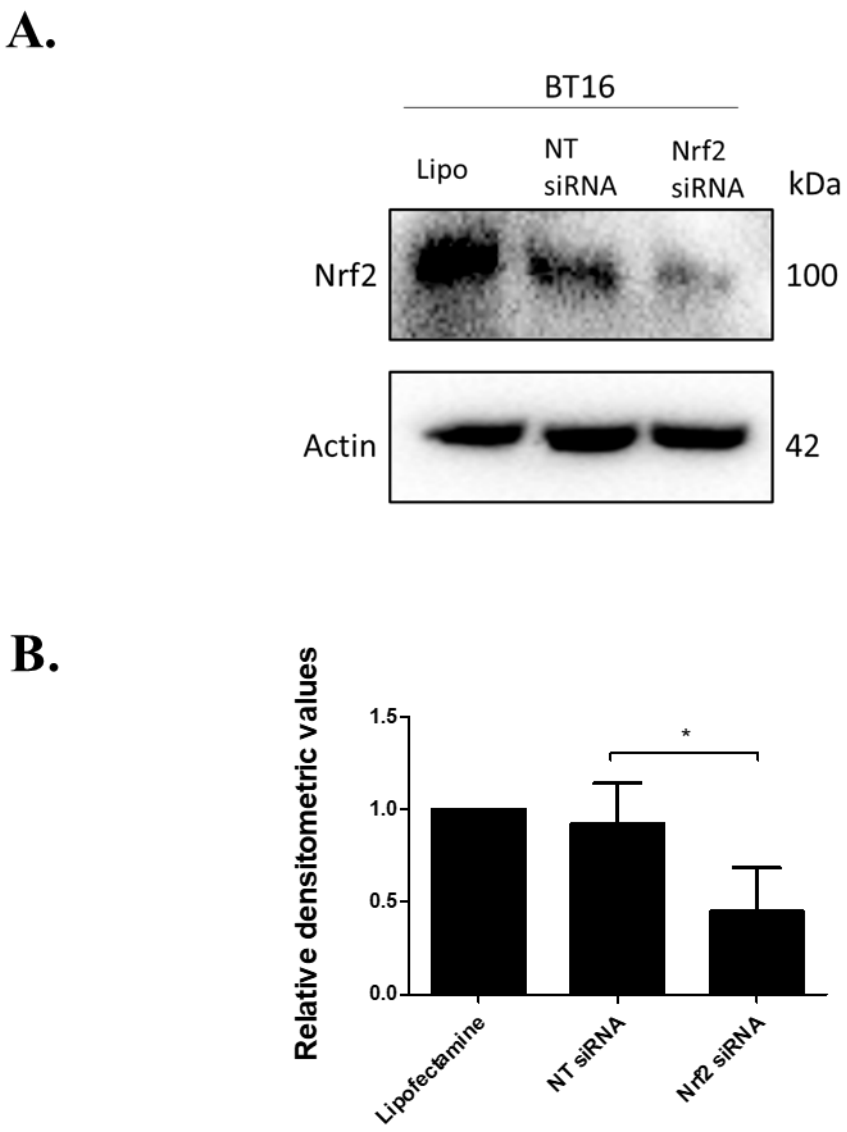

Figure 4.22. Knockdown of Nrf2 in the BT16 cell line using an siRNA approach

A. BT16 cells were seeded at 1 x 10^5 cells/mL in a T25 flask. Cells were transfected with non-targeting control siRNA or Nrf2 siRNA for 24h using lipofectamine. After 24h, the cells were then harvested and lysates prepared for western blot analysis. 20 ug of protein was loaded, separated on an SDS page gel, transferred to PVDF and probed with the relevant antibodies. Results are representative of three independent experiments. Western blots were normalised to total actin as a loading control. **B**. Densitometric analysis of the bands was carried out using Image Lab software. Statistical analysis was performed using one way ANOVA with Tukey's post hoc test. *$p<0.05$. Results represent the mean and S.E.M of three independent experiments.

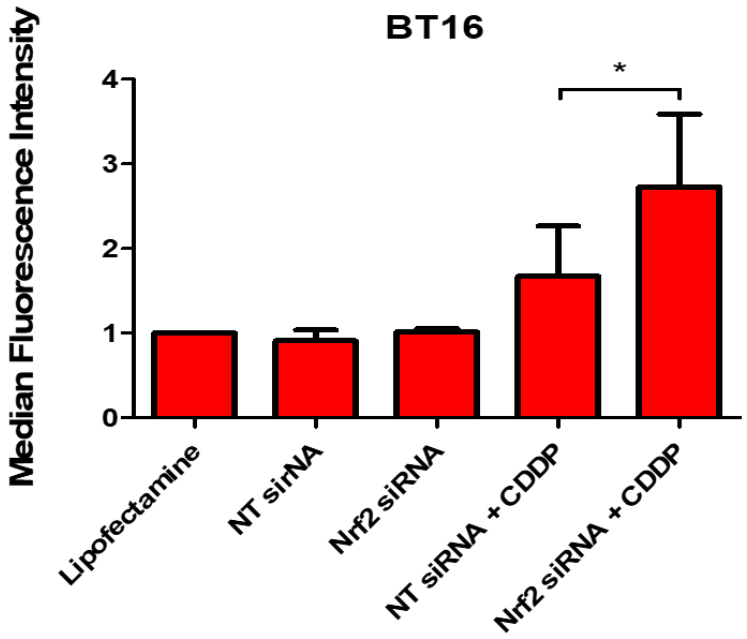

Figure 4.23. Knockdown of Nrf2 enhances cisplatin-induced ROS in BT16 cells

BT16 cells were seeded at 1 x 10^5 cells/mL in a T25 flask. Cells were transfected with non-targeting (NT) control siRNA or Nrf2 siRNA for 24h using lipofectamine. The cells were treated with cisplatin (CDDP, 10 µM) 20 h before the end of this inclubation period. After 24 h, the cells were stained H_2DCFDA for 30 minutes, washed and resuspended in PBS. The cells were immediately analysed by flow cytometry using the BD FACS Accuri software. 10,000 cells were gated on vehicle treated cells. Values represent mean ± S.E.M of three independent experiments. Statistical analysis was performed using a paired two-tailed t test. *$p<0.05$.

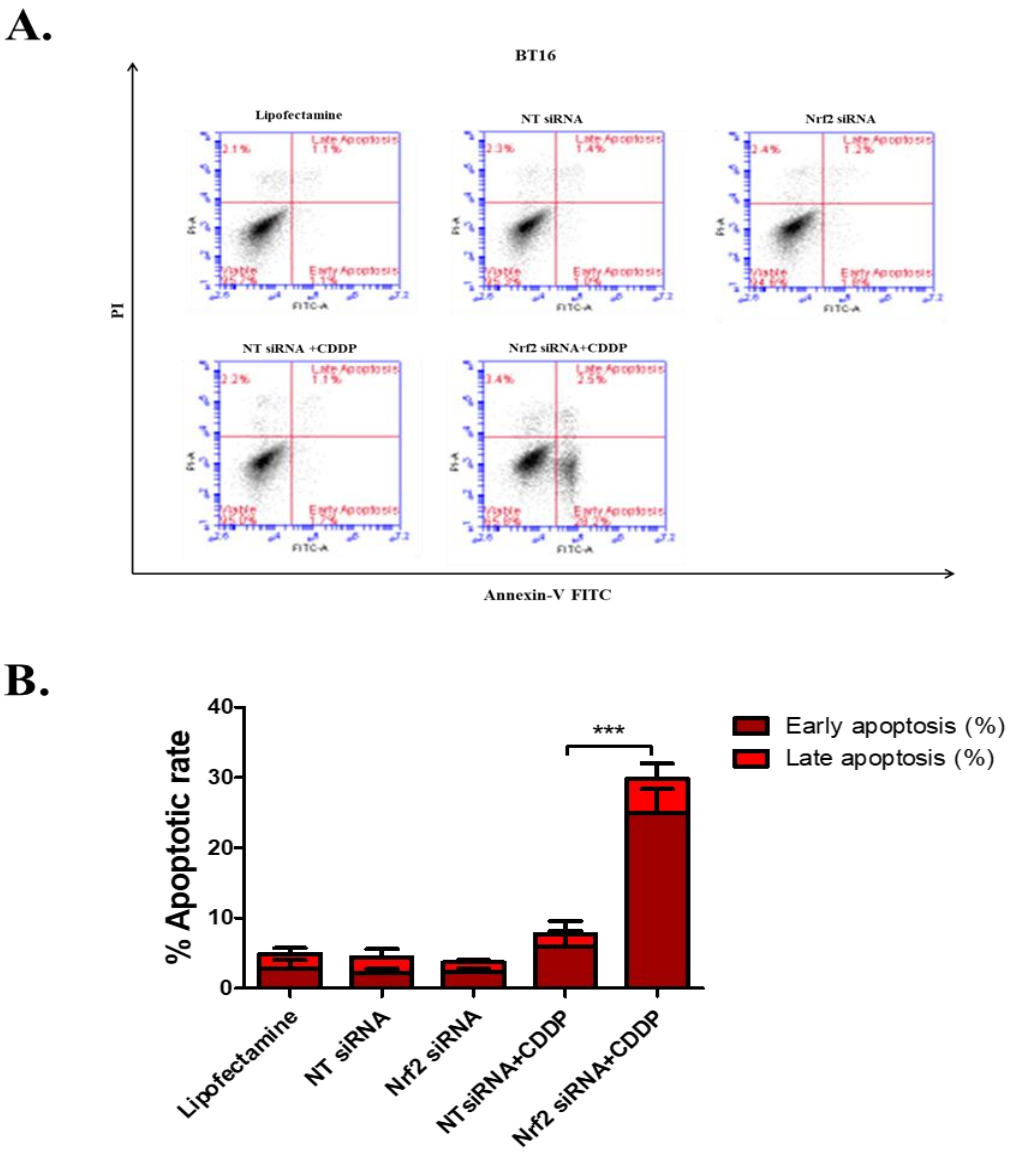

Figure 4.24. Knockdown of Nrf2 sensitises BT16 cells to cisplatin-induced apoptosis.

A. BT16 cells were seeded at 1 x 10^5 cells/mL in a T25 flask. Cells were transfected with non-targeting (NT) control siRNA or Nrf2 siRNA for 24h using lipofectamine. The cells were treated with cisplatin (CDDP, 10 µM) 20 h before the end of this inclubation period. After 24 h, the cells were stained Annexin V and PI. The cells were immediately analysed by flow cytometry using the BD FACS Accuri software. 10,000 cells were gated on vehicle treated cells. **A**. Representative dot plot of treated cells **B**. Values represent mean ± S.E.M of three independent experiments. Statistical analysis was performed using one way ANOVA with Tukey's post hoc test. ***$p<0.001$.

4.3 Discussion

Cisplatin was first approved by the Food and Drug Administration (FDA) in 1978 for the treatment of testicular cancer. It is now one of the most widely used chemotherapeutic agents to treat a wide range of cancers such as bladder, ovarian, cervical, breast cancer, and the head and neck. Cisplatin acts by binding to and cross-linking DNA, forming DNA adducts leading to DNA damage and subsequently inducing apoptosis. Cisplatin treatment has been shown to significantly improve the survival outcome in cancer patients[333]. However, there are two major limitations that have been associated with the use of cisplatin as an anti-cancer treatment. Firstly, this platinum-based chemotherapeutic agent has been associated with toxic side effects such as nausea, allergic reactions, nephrotoxicity, cardiotoxicity, gastrointestinal disorders, hepatotoxicity, neurotoxicity or hearing loss in young patients[437]. Secondly, cancer cells typically develop resistance against cisplatin limiting its therapeutic efficiency. Cancer cells can achieve this by a number of drug defence mechanisms. To by-pass these limitations, research has explored the therapeutic potential of combining cisplatin with other drugs. Research into this area aims to understand the mechanisms underlying cisplatin resistance and target these specific mechanisms with various combination strategies. These chemoresistant mechanisms include decreasing drug import, increase drug export, upregulating DNA damage repair, upregulation of cellular mechanisms such as autophagy or cisplatin inactivation by detoxification enzymes[338]. Cisplatin is also utilised in a number of treatment regimens for MRT but efficacy in the clinic is again hampered by primary and acquired resistance. For this reason, further study into the molecular and cellular responses to cisplatin in MRT is warranted in order to gain a greater understanding of the mechanisms underlying cisplatin resistance.

In addition to forming DNA adducts, cisplatin can cause intracellular generation of ROS. High levels of ROS in response to cisplatin has been observed in a number of cancers including oral squamous carcinoma cells, bladder cancer, ovarian cancer and malignant mesothelioma[319, 438-440]. Moreover, cancer cells have higher basal levels of ROS than healthy cells as a result of an imbalance between oxidants and antioxidants. This is due to the high metabolic rate and hypoxic conditions that is characteristic of cancer cells. These high levels of ROS also confer cancer cells with a higher vulnerability to drug-induced oxidative stress. However, cells can upregulate their antioxidant system as a resistance

mechanism in response to treatment with chemotherapeutic agents such as cisplatin to cope with this drug-induced oxidative stress[441]. This is primarily mediated by the transcription factor Nrf2, which is often referred to as a master regulator of the antioxidant response system and is involved in mediating the expression of a wide variety of antioxidant genes, including those involved in the GSH pathway[305]. The present chapter investigated whether the Nrf2/GSH pathway is a critical determinant in cytotoxicity mediated by cisplatin in MRT.

Previous studies have reported that higher basal levels of ROS generation in cancer cells are associated with higher sensitivity to drug-related cytotoxicity. For example, Salatino *et al*. examined the role of the antioxidant H-Ferritin in the modulation of ROS and cisplatin cytotoxicity in ovarian cancer cells and observed a correlation between cisplatin resistance and baseline intracellular ROS levels[442]. Diehn *et al*., have also examined ROS levels in cancer stem cells (CSCs) and proposed a potential correlation between low ROS levels, high ROS defences and radioresistance[443].

This present study first assessed the intracellular baseline levels of ROS in a panel of MRT cell lines with varying sensitivities to cisplatin. Interestingly, the most cisplatin-sensitive BT12 cell line, had the highest basal levels of ROS whereas the cisplatin-resistant BT16 cells had the lowest basal levels of intracellular ROS. Moreover, G401 cells exhibited intermediary levels of ROS as well as an intermediary phenotype in cisplatin resistance. In order to further explore the relationship between basal intracellular ROS levels and cisplatin, the relative ROS levels were plotted against the percentage of viability of cells treated with 10 µM cisplatin and an inverse relationship between the two variables with an r value of 0.9999 was determined. These results are in agreement with Neuwelt *et al*. who examined relative peroxide levels in BT12 and BT16 cells treated with the GSH inhibitor AAP and cisplatin. They also reported higher relative peroxide levels in BT12 cells compared to BT16 cells[316]. The results presented herein are also in agreement with a study by Kleih *et al*. who measured basal mitochondrial ROS levels in a panel of ovarian cancer cell lines consisting of three cisplatin-resistant cell lines and three cisplatin-sensitive cell lines. The sensitive cell lines (OVCAR-3, OVCAR-4 and IGROV-1) were shown to exhibit higher basal levels of mitochondrial ROS compared to the resistant cell lines (OVCAR-5, OVCAR-8, A2780)[439].

This study next evaluated the effect of cisplatin treatment on ROS generation in the BT12, BT16 and G401 cell lines. BT12 cells were treated with 1 µM cisplatin whereas the more resistant G401 and BT16 cells were treated with 10 µM cisplatin. Intracellular ROS generation was significantly enhanced in response to cisplatin treatment, in all three cell lines. These results are somewhat in contrast to those reported by Neuwelt *et al*. who found a significant increase in peroxide levels in response to cisplatin treatment in BT12, but not in BT16 cells. However, in the Neuwelt study the two cell lines were treated with the same concentration of cisplatin (1µg/mL) despite their varying sensitivities to cisplatin[316]. The results presented herein are similar to those observed by Magnano *et al*, who treated two OSCC cell lines, SCC4 and SCC9, with cisplatin and found a significant increase in ROS generation[319]. Moreover, Wang *et al* found that cisplatin increased ROS generation in two ovarian cell lines, SKOV3 and OVCAR8, in a dose-dependent manner[444].

Intracellular ROS can be generated from various sources within the cells. These include mitochondria, cytosol, peroxisomes and the endoplasmic reticulum. However, a major source of ROS production is the mitochondria through electron leakage from complexes I and III in the electron transport chain[445]. Marullo *et al*. demonstrated this by using a panel of normal and cancer cell lines and the budding yeast *Saccaromyces cerevisiae* as model systems. Their study reported that H_2DCFDA and Mitosox-stained cells depicted a time-dependent increase in ROS in a parallel manner suggesting that the source of ROS was the mitochondria. To further evaluate this, ROS levels in response cisplatin treatment were measured in DU145p^o, a respiratory incompetent prostate cancer cell line that lacks mitochondrial DNA and its parental cell line, DU145p. Interestingly, the study found that whilst cisplatin induces accumulation of ROS in the parental DU145p cell line, no difference in ROS levels was observed in the respiratory incompetent prostate cancer cell line, suggesting that the primary source of cisplatin-induced ROS production is the mitochondria[446].

In the present study, in order to determine the source of intracellular ROS accumulation observed in MRT upon cisplatin treatment, BT16 cells were stained with Mitosox dye, a fluorogenic dye that specifically detects mitochondrial ROS. A significant enhancement in mitochondrial ROS accumulation was detected in response to cisplatin treatment compared to the vehicle control cells, suggesting the source of intracellular ROS observed is indeed the mitochondria.

To further examine the role of ROS in cisplatin-mediated cytotoxicity in MRT, ROS levels were next modulated using the antioxidant N-acetyl cysteine (NAC), a ROS scavenger that targets oxidant species. In addition to this, NAC is a synthetic precursor of the critical cellular antioxidant GSH and can replenish GSH levels in the cell. GSH can bind to cisplatin through its reactive thiol group and prevent its DNA-interfering cytotoxic activity[430]. To assess the role of ROS in cisplatin-induced toxicity on MRT cells, the cells were pre-treated with NAC prior to cisplatin treatment. NAC significantly reduced cisplatin-induced ROS generation and importantly abrogated the cytotoxic effects of cisplatin on both BT12 and BT16 cells. Notably, in the BT12 cell line the apoptotic rate was completely reversed back to basal levels whereas in the BT16 cell line, NAC reduced the apoptotic rate by 20%. This data suggests that cisplatin-induced apoptosis in MRT is at least partially mediated by oxidative stress through ROS generation.

These results are in agreement with results reported by Neuwelt *et al*. who observed that NAC protected BT12 cells from peroxide accumulation induced by cisplatin and the glutathione inhibitor acetaminophen (AAP). In addition, this protective effect was also observed when examining mitochondrial damage induced by AAP and cisplatin[316]. Magnano *et al*. reported that NAC treatment protected two OSCC cell lines from cisplatin-induced ROS and cell death[319]. Interestingly, this protective effect from NAC has been considered to help treat toxicities associated with cisplatin treatment. Huang *et al*, showed that NAC treatment improved cisplatin-induced nephrotoxicity in mice by inhibiting inflammation[447]. Abdel-Wahab *et al.* examined the protective effect of NAC on cisplatin-induced neurotoxicity in rats suggesting NAC treatment can be employed to salvage cells from toxic effects[448].

Having observed that ROS generation is induced by cisplatin and that this plays an important role in apoptosis in MRT, this study further examined how the balance of oxidants and antioxidants affect sensitivity to cisplatin. Glutathione or GSH is an important component of the antioxidant system in the cell. Moreover, GSH has been implicated in chemoresistance. Studies have reported that high basal glutathione levels have been observed in drug resistant cell lines compared to drug-sensitive cells[449]. Temozolomide (TMZ)-resistant glioblastoma cell lines have been shown to exhibit lower endogenous ROS levels and higher levels of antioxidant capacity and GSH when compared to sensitive cell lines. Moreover, resistant cell lines have higher expression levels of glutathione reductase (GSR)[450]. Overexpression of glutathione-S-transferases

(GSTs), a family of detoxification enzymes that conjugate GSH to electrophiles, has also been observed in a number of drug-resistant cancer cell lines[451].

As a correlation between basal intracellular ROS and cisplatin sensitivity was observed across the three MRT cell lines analysed in this study, the basal levels of the antioxidant glutathione across this panel of cell lines were next examined. Interestingly, GSH levels correlated with the profile of basal ROS levels suggesting a relationship between the balance of glutathione, ROS and susceptibility to cisplatin in MRT. BT16 cells which had the highest resistance to cisplatin and the lowest basal ROS levels also exhibited the highest basal levels of GSH. In contrast, BT12 cells which are the most sensitive to cisplatin, had the highest levels of intracellular ROS and the lowest basal levels of GSH. G401 cells appeared to consistently have an intermediary phenotype. To further analyse the relationship between GSH and cisplatin resistance, the GSH basal levels were plotted against percentage viability in response to 10 μM cisplatin treatment. A positive correlation was observed with a r value of 0.9843, with a non-significant p value of 0.1130. These results are in agreement with Neuwelt *et al*. who examined the role of GSH in BT12 and BT16 cell lines by employing the GSH inhibitor, AAP. They also reported that the BT16 cells had higher basal GSH levels compared to BT12 cells. Furthermore, the study showed that BT16 cells were less responsive to cisplatin but exhibited a greater chemo-enhancive effects with AAP[316].

Drug-induced oxidative stress can occur as a result of ROS accumulation. Having observed that cisplatin induces high ROS levels that mediate apoptosis, this study next determined the effect of cisplatin on GSH levels and on the GSH:GSSG ratio, a marker of oxidative stress. A decrease in GSH and GSH:GSSG levels in response to cisplatin treatment was observed in both BT12 and G401 cell lines. In contrast, this increase in oxidative stress was not observed in BT16 cells, perhaps in part due the high basal GSH levels these cells exhibit. In agreement, increased inactivation of cisplatin by thiol-containing proteins has been reported to be an important mechanism underlying tumour resistance in many cancers including cervical cancer, osteosarcoma and glioblastoma[427-429].

As a number of studies have shown a link between glutathione and drug resistance, research has aimed to determine whether this may serve as a potential therapeutic target in cancer. The most commonly utilised method of GSH inhibition is through the treatment of BSO, which blocks the rate-limiting step of GSH synthesis, specifically the enzyme GCL.

Treatment with BSO has been shown to have pre-clinical promise in a number of cancers including neuroblastoma, biliary tract cancer and glioma cells[450, 452-454]. The effect of combining cisplatin and BSO treatments in MRT has not yet been reported. Results presented herein for the first time demonstrate that GSH became depleted in BT16 cells in response to BSO treatment, confirming the inhibitory effect of BSO in cells with high basal levels of GSH. Interestingly, a combination of BSO and cisplatin treatment resulted in a significant increase of ROS production and a significant enhancement in cisplatin-induced apoptosis in BT16 cells. These results are in agreement with those published by Silva *et al* who demonstrated that depletion of GSH in lung cancer cells with BSO resulted in a significant increase in sensitivity to cisplatin[430]. Similarly, Li *et al* have observed that sub-toxic concentrations of BSO synergistically enhanced the apoptotic response and the anti-proliferative activity of cisplatin and gemcitabine in biliary tract cancer cell lines[453]. Moreover, Neuwelt *et al*, also showed that combining cisplatin treatment with another glutathione inhibitor, acetaminophen, enhanced the effect of cisplatin. This confirms the importance of GSH in determining cisplatin resistance and suggests that GSH could be a potential therapeutic target to overcome chemoresistance in MRT[316]. Collectively, these results suggest that GSH plays a role in chemoresistance in MRT and that targeting glutathione may represent a novel potential therapeutic avenue for overcoming cisplatin resistance in rhabdoid tumours.

Given the potential significance of the antioxidant GSH in mediating cisplatin resistance in MRT, the role of Nrf2, the master regulator of the antioxidant defence system was then examined. As the results presented above showed a strong correlation between basal GSH and ROS levels and cisplatin resistance in the panel of MRT cell lines, the study assessed the basal expression levels of Nrf2 in the same panel of cell lines. BT16 was shown to have significantly higher Nrf2 protein expression than BT12 cells consistent with results obtained showing higher levels of its downstream target, GSH. Nrf2 expression was also found to be significantly higher in BT16 cells compared to G401 cells. A correlation analysis comparing relative densitometric values of Nrf2 protein expression to percentage viability of cells in response to 10 μM cisplatin treatment was conducted. An r value of 0.9268 was observed with a p value of 0.2451. Although this correlation is non-significant, the same trend was observed as when looking at GSH and ROS levels. A limitation to these correlation analyses is the low number of cell lines. Cisplatin treatment did not significantly alter total Nrf2 levels in BT12 and BT16 cells as shown by western analysis.

In agreement with results presented here, Nrf2 upregulation has previously been observed in resistant cancer cell lines. Moreover, expression of its downstream targets such as haem oxygenase 1 (HO-1) have also been shown to correlate with drug resistance. For example, Bao *et al*., examined Nrf2 and HO-1 in the parental ovarian cancer cell line A2780 and its derived cisplatin-resistant cell line A2780cp. Interestingly, A2780cp cells were shown to have significantly higher mRNA expression levels of Nrf2 and HO-1[455]. Moreover, Silva *et al*. found higher GSH and Nrf2 expression levels in the cisplatin-resistant lung cancer cell line A549 compared to the more sensitive cell line NCI H23[430]. These studies found that targeting Nrf2 through genetic knockdown sensitised the resistant cell lines to drug treatment. However, the role Nrf2 in mediating chemoresistance in MRT remains elusive. A study by Parkhurts *et al*. has found that dual mTORC1/2 inhibition with the compound TAK-228 leads to downregulation of Nrf2 thereby sensitising AT/RT cells to oxidative stress and apoptosis suggesting that Nrf2 expression plays a critical role against oxidative stress-induced apoptosis[433]. Song *et al*. have found that SWI/SNF chromatin remodelling alters Nrf2 signalling in non-small cell lung carcinoma (NSCLC). Mutations in the SWI/SNF complex, characteristically found in rhabdoid tumours, was studied in these NSCLC cells. Loss of the complex resulted in activation of Nrf2-mediated downstream target genes[456]. However, to the best of our knowledge, the role of Nrf2 in mediating chemoresistance in rhabdoid tumours has not yet been examined. In this chapter, in order to study the role of Nrf2 in MRT and its potential as a therapeutic target to circumvent resistance, its expression was blocked through treatment with both a small molecule pharmacological inhibitor and through genetic inhibition (siRNA approach).

Despite an increased focus of anti-cancer research on the role of Nrf2 in recent years there are currently no pharmacological inhibitors available in the clinic or under assessment in clinical trials. This study utilised the Nrf2 inhibitory activity of a novel pharmacological inhibitor, ML385, identified in a recent report by Singh *et al.* To identify novel Nrf2 inhibitors, the study screened approximately 400,000 small molecules (Molecular Libraries Small Molecule Repository Library, MLSMR) at the National Center for Advancing Translational Sciences[432]. The screen identified the compound ML385 as a probe molecule that could bind to Nrf2. More specifically, this compound was shown to bind to Neh1, the Cap 'N' Collar Basic Leucine Zipper (CNC-bZIP) domain of Nrf2, and was found to interfere with the binding of the V-Maf Avian Musculoaponeurotic Fibrosarcoma Oncogene Homolog G (MAFG)-Nrf2 protein complex to regulatory DNA binding

sequences. The study went on to examine the anti-cancer effect of ML385 on Keap-1 deficient NSCLC tumours. Tumours with Keap1 mutations that allowed for Nrf2 gain of function were selected and were found to be particularly sensitive to the effects of ML385 treatment. The inhibitor was shown to sensitise these cells to cytotoxicity induced by doxorubicin, taxol and carboplatin indicating pre-clinical promise as a potential novel treatment for NSCLC[432]. Moreover, treatment with ML385 was also shown to significantly downregulate downstream gene targets of Nrf2 such as NQO1 and GCLm. Interestingly, ML385 inhibition also downregulated intracellular GSH in a dose-dependent manner[174].

In the present study, inhibition of Nrf2 with ML385 resulted in a decrease of GSH and GSH:GSSG ratio in BT16 cells confirming that Nrf2 can regulate GSH production in MRT. Additionally, ML385 also significantly enhanced cisplatin-induced ROS and cisplatin-mediated apoptotic cell death indicating the Nrf2/GSH antioxidant pathway modulates cisplatin resistance in MRT. These results agree with the reports by Singh *et al*. which demonstrate downregulation of GSH in response to ML385 in a dose-dependent manner in NSCLC cell lines[432]. Moreover, Silva *et al*. observed that Nrf2 inhibition through genetic knockdown also significantly decreased GSH levels[430]. Similar results were also recently observed by Sun *et al*, who showed that ML385 enhanced ROS levels and cisplatin mediated cell death in ovarian cancer cells[457]. Ren *et al*. also examined the role of Nrf2 in cisplatin resistance through the use of another Nrf2 inhibitor, brusatol. Brusatol selectively inhibits Nrf2 expression by targeting it for ubiquitination and degradation. The study demonstrated that treatment with brusatol sensitised a panel of cancer cell lines and A549 xenografts to cisplatin[458]. Collectively, these studies suggest that developing pharmacological inhibitors for clinical use that target Nrf2 may present a novel strategy to circumvent chemoresistance.

To further confirm the chemoresistant role of Nrf2 in MRT, a genetic approach was used to inhibit Nrf2 protein expression. Knockdown of Nrf2 has previously been performed in a variety of cancers, however, not in rhabdoid tumours. Genetic inhibition of Nrf2 elicited a significant increase in cisplatin-induced ROS and importantly, a significant enhancement in cisplatin-induced apoptosis when comparing cells that were transfected with Nrf2 siRNA and treated with cisplatin to cells that were transfected with NT siRNA and treated with cisplatin.

This is agreement with the study conducted by Silva *et al.* that demonstrated that cells which were transduced with Nrf2 shRNA lentiviral recombinant vector were found to have higher sensitivity to cisplatin than their parental cell lines[430]. Additionally, a report by Bao *et al*. into the role of Nrf2 in cisplatin resistance in ovarian cancer also found that genetic knockdown of Nrf2 in the cisplatin-resistant A2780cp cell line, sensitised the cells to cisplatin treatment[455].

In addition to alterations in the antioxidant system, it should be noted that Nrf2 inhibition may result in modulations in signal transduction pathways such as MAPK cascades and furthermore expression of multidrug resistance proteins, which exerts cisplatin efflux in cancer cells, has been known to be regulated by Nrf2[459]. For example, disruption of the Ras/ERK signalling pathway has been implicated in chemoresistance in various cancers and has been associated with tumour progression[460]. It would be of interest in future studies to examine the contribution of these components to alterations in cisplatin sensitivity following inhibition of the Nrf2 pathway.

In conclusion, this chapter examined the role of ROS generation and oxidative stress in cisplatin-induced cytotoxicity in MRT. In addition, the role of the GSH/Nrf2 antioxidant system in protecting cells from the effects of cisplatin was also examined. MRT cells with higher resistance to cisplatin were also shown to have higher levels of GSH and Nrf2 expression as well as lower levels of intracellular ROS. A relationship between cisplatin resistance and these characteristics was observed through correlation analysis. Cisplatin was shown to reduce GSH levels and induce oxidative stress in the more sensitive cell lines (BT12 and G401) but not in BT16 cells, which exhibit the highest levels of GSH, Nrf2 and cisplatin resistance. Moreover, cisplatin was shown to induce ROS accumulation in a panel of cell lines. This accumulation of ROS was shown to mediate cisplatin-induced apoptosis, as treatment with the ROS scavenger NAC reversed cisplatin cytotoxicity. Glutathione depletion by treatment with the GSH synthesis inhibitor, BSO, sensitised both BT12 and BT16 cells to cisplatin. Moreover, Nrf2 inhibition by treatment with the pharmacological inhibitor ML385 as well as through Nrf2 siRNA transfection resulted in downregulation of GSH levels, GSH:GSSG and accumulation of cisplatin-generated ROS. Lastly, ML385 and Nrf2 siRNA sensitised resistant BT16 cells to cisplatin suggesting targeting the Nrf2/GSH antioxidant system may present a novel therapeutic avenue in the design of new treatment strategies for rhabdoid tumours and a means of overcoming chemoresistance.

5. The role of Bcl-2 proteins in mediating chemoresistance in Malignant Rhabdoid Tumours

5.1 Introduction

Drug resistance is one of the most significant causes of treatment failure, relapse, and mortality in cancer patients. MRT is highly drug refractory and there is currently an unmet need for novel treatment strategies which elicit a more effective anti-tumour response. In many tumours, deregulation of apoptotic cell death underlies drug resistance and is a major reason for failure of conventional anticancer therapy. The mitochondrial pathway of apoptosis (also known as intrinsic pathway of apoptosis) is the most common form of cell death in cancer cells[461]. This pathway is characterised by mitochondrial outer membrane permeabilisation (MOMP), which results in the release of cytochrome c to the cytoplasm and subsequently, the activation of caspases and apoptosis induction. Regulation of this pathway is mediated by the Bcl-2 family of proteins, which are divided into three groups; the anti-apoptotic multi-domain proteins (e.g. Bcl-2 and Mcl-1), the pro-apoptotic multi-domain proteins (e.g. Bax and Bak), and the pro-apoptotic BH3-only proteins (e.g. Bid and Bim)[462]. Cells express many pro- and anti-apoptotic Bcl-2 proteins, and the balance between these different groups and their interactions determine if the pro-apoptotic proteins Bax/Bak will oligomerise and form pores on the outer membrane of the mitochondria, allowing for release of cytochrome c. Anti-apoptotic proteins block this step by binding to pro-apoptotic proteins through their hydrophobic groove that interacts with the BH3 domain of pro-apoptotic proteins[462].

The founding member of the Bcl-2 family, Bcl-2 was originally identified from the *t* (14; 18) chromosomal translocation in follicular lymphoma through chromosomal mapping[463]. Overexpression of the anti-apoptotic Bcl-2 protein has since been observed in many cancer types including neuroblastoma, melanoma, squamous carcinoma, breast, lung, and colorectal cancer cells[230]. In addition, overexpression of other Bcl-2 anti-apoptotic family members such as Mcl-1, Bcl-xL and Bcl-w has also been observed in various cancer types[464-466]. Overexpression of Bcl-2 is also associated with apoptosis evasion, cell survival and drug resistance leading to cancer cells developing a dependence on Bcl-2 to survive aggressive environments induced by chemotherapeutic treatment or the immune system[228]. These cells can become “addicted” to Bcl-2 or “Bcl-2 dependent” and therefore this presents a therapeutic vulnerability that can be targeted by inhibiting Bcl-2[467]. Moreover, current research suggests a link between overexpression of Bcl-2 and cisplatin resistance in various cancers[468]. Little is known about the link between Bcl-2 overexpression and cisplatin resistance in MRT.

BH3 mimetics are a class of compounds capable of mimicking BH3-proteins by binding to anti-apoptotic Bcl-2 proteins and inducing apoptosis[462]. These small molecules have shown a high level of effectiveness at pre-clinical and clinical level both as a monotherapy and as part of combination therapies leading to increasing interest in further developing these drugs for greater efficacy[469]. A number of compounds have been developed through the use of natural library screening, peptide therapeutics and structure-based design. Variation in specificity and effectiveness has been observed across these developed compounds[469].

BH3 mimetics were initially trialled as a monotherapy in haematological malignancies such as chronic lymphocytic leukaemia (CLL) and acute myeloid leukaemia (AML) due to the observed high expression levels of Bcl-2. ABT-737 which targets Bcl-2, Bcl-xL and Bcl-W with high affinity was one of the first BH3 mimetics to be developed and showed promise in animal models and patient xenografts by eliciting tumour regression and improved survival rate[470]. Unfortunately, ABT-737 did not translate into the clinic as it is not bioavailable post oral administration[471]. Hence, Navitoclax (ABT-263) was developed. Navitoclax/ABT-263 is an orally bioavailable BH3 mimetic with a high binding affinity for Bcl-2, Bcl-xL and Bcl-W, which was originally evaluated for the treatment of patients with non-Hodgkin's lymphoma (NHL) and CLL[472]. These early studies showed an improvement in overall response rate of both NHL and CLL patients; 22% and 35% respectively[473]. However, the overall improvement in progression-free survival was only moderate. Furthermore, the use of ABT-263 in the clinic was hindered by the toxic side effect of thrombocytopenia, caused by the affinity of this BH3 mimetic for Bcl-xL, which is essential in platelets, thus limiting its dose to 300 mg per day [473]. Therefore, the selective Bcl-2 inhibitor, Venetoclax/ABT-199 was developed and has shown great success in the treatment of haematological malignancies. For example, Venetoclax/ABT-199 treatment in CLL as a monotherapy showed an 80% response rate and was well tolerated[474]. It was clinically approved in 2013 for the treatment of both CLL and AML[475]. Currently, clinical trials are evaluating the effect of ABT-199 in multiple myeloma (MM) and lymphomas although the response rate for these cancers is more heterogenous when compared to the response rate observed in CLL patients[476]. Combining ABT-199 with other therapies such as chemotherapeutic agents is an ongoing avenue of investigation to optimise response rates in these cancers.

In solid tumours, a number of *in vitro* and *in vivo* studies have been conducted to evaluate the efficacy of ABT-199 alone and in combination with chemotherapy, with some

promising results. [477, 478]. Xu *et al* showed that a combination of ABT-199 and irinotecan, a standard treatment for small cell lung cancer, resulted in synergistic apoptosis and cell growth inhibition effects in *Kras*-mutant lung cancer cells[479]. In estrogen receptor-positive breast cancer cells, a combination of ABT-199 with tamoxifen showed significant tumour reduction and longer survival outcomes in breast tumour xenografts compared to treatment with either drug alone[235]. As solid tumours are commonly more difficult to treat in the clinic, further work is required to determine whether the success obtained in treating CLL with ABT-199 will be replicated in non-haematological malignancies[462]. There are limited studies examining the efficacy of BH3 mimetics in MRT and to date, there are no reports in the literature focused on ABT-199 treatment of MRT. A recent study by Parkhurst *et al*., examined the effect of combining TAK-228, an inhibitor of mTORC1 and mTORC2 that has shown pre-clinical potential in the treatment of AT/RT, with the BH3 mimetic, Obatoclax, a pan Bcl-2 inhibitor of anti-apoptotic proteins including Mcl-1. This study proposed that this novel combination therapy of TAK-228 and Obatoclax could be added to standard frontline therapies or used for treatment of relapsed and refractory AT/RT patients. This suggests that further research should be conducted to assess the combination of standard therapies such as cisplatin with BH3 mimetics in AT/RT[433].

Another limitation to ABT-199/Venetoclax treatment is resistance to the monotherapy[480]. Studies indicate that resistance to ABT-199 can be caused by overexpression of the other anti-apoptotic proteins; Mcl-1 and Bcl-xL. This issue of resistance to BH3 mimetics provides a rationale for the combining ABT-199 with other drugs. Moreover, an array of combinations is currently being tested in clinical and pre-clinical models. As such, this includes combining chemotherapeutic agents with BH3 mimetics[480]. Indeed, several studies are currently underway investigating the beneficial effects of targeting anti-apoptotic Bcl-2 proteins to increase the sensitivity of cancer cells to chemotherapy.

Interestingly, there have been some previous pre-clinical studies evaluating BH3 mimetics in combination with cisplatin for the treatment of various solid tumours with promising results. Steele *et al*., showed that the BH3 mimetic Obatoclax enhances cisplatin-induced apoptosis in muscle-invasive bladder cancer cells[481]. In SCLC cell lines, a synergistic reduction in cell viability was observed between cisplatin-etoposide and ABT-199 combinations (ratio 1:1.5) suggesting the therapeutic potential for combining BH3 mimetics with chemotherapeutics[477]. Moreover, in head and neck cancer cells, cisplatin resistance was reversed when cells were treated with the BH3 mimetic gossypol which

binds to the BH3 domains of both Bcl-2 and Bcl-xL. This study compared cisplatin-resistant cell lines to parental cell lines and postulated that Bcl-xL and wild-type p53 were responsible for resistance. Treatment with gossypol resulted in 70-80% apoptosis in cisplatin-resistant cell lines and 25-40% apoptosis in the parental cell lines further suggesting that BH3 mimetic agents, such as gossypol may potentially help overcome cisplatin resistance[482].

Collectively, these studies indicate the potential of combining chemotherapeutic agents and BH3 mimetics in both haematological and solid tumours, warranting further work in this area. Targeting anti-apoptotic Bcl-2 proteins with BH3 mimetics has been proposed as a valuable strategy to reduce chemoresistance. The role of the Bcl-2 family of proteins in mediating chemoresistance in rhabdoid tumours is not yet clear. The aim of this chapter was firstly to characterise the expression levels of a series of anti-apoptotic and pro-apoptotic members of the Bcl-2 family of proteins in a panel of MRT cell lines and assess whether they may play a role in determination of cisplatin cytotoxicity. Moreover, this chapter evaluated whether targeting Bcl-2 with the selective BH3 mimetic, ABT-199 could affect the apoptotic response to cisplatin and sensitise MRT cells to cytotoxicity. The use of BH3 mimetics may present a novel therapeutic strategy to overcome chemoresistance in MRT.

5.2 Results

5.2.1 MRT cells display varying protein expression levels of Bcl-2 family members

In order to evaluate whether basal expression levels of Bcl-2 family members may play a role in determination of cisplatin cytotoxicity in MRT, a panel of MRT cells (BT12, BT16 and G401), with varying sensitivities to cisplatin, was analysed via western blotting. (Figure 5.1, Figure 5.2).

Firstly, expression of a series of anti-apoptotic Bcl-2 proteins (Mcl-1, Bcl-2, and Bcl-xL) was assessed in the three cell lines (Figure 5.1). The cells displayed varying expression levels of these proteins. Significantly higher expression of Mcl-1 was observed in the cisplatin-sensitive BT12 cells when compared to the more resistant G401 and BT16 cells. In contrast, BT12 cells expressed significantly less Bcl-xL compared to the cisplatin-resistant BT16 cells. More notably, BT12 cells did not express any detectable levels of Bcl-2 protein whereas BT16 and G401 cells expressed high levels of this protein. As previously mentioned, cells vary in their dependencies on different anti-apoptotic Bcl-2 proteins[483]. Results herein suggest that BT12 cells may be more Mcl-1 dependent than BT16 and G401 cells. Notably, the absence of Bcl-2 in the cisplatin-sensitive BT12 cells versus its high expression in cisplatin-resistant BT16 cells may suggest a role for Bcl-2 in determining different sensitive/resistant phenotypes of rhabdoid tumour cells.

Next, a series of pro-apoptotic Bcl-2 proteins (Bim, Bax and Bid) were examined in the three rhabdoid tumour cell lines. Interestingly, differential expression of the three proteins was observed in the panel of MRT cell lines. The BH3-only pro-apoptotic family member Bim was found to be significantly more highly expressed in BT16 cells compared to BT12 and G401 cells. Bax, which is involved in MOMP, was found to be the least expressed in BT12 cells, however this difference was not significant. Lastly, Bid, a BH3-only protein involved in inducing Bak/Bax-activated MOMP, appeared to be less expressed in BT16 than the other MRT cell lines. However, this difference was again not significant.

In conclusion, all cell lines examined expressed varying levels of several Bcl-2 family members with the exception of cisplatin-sensitive BT12 cells, which expressed no detectable Bcl-2 protein. To determine if the presence of Bcl-2 has a role in mediating chemoresistance, this study next aimed to evaluate if targeting Bcl-2 in the cisplatin-resistant cell line BT16 may present a strategy to sensitise these cells to cisplatin.

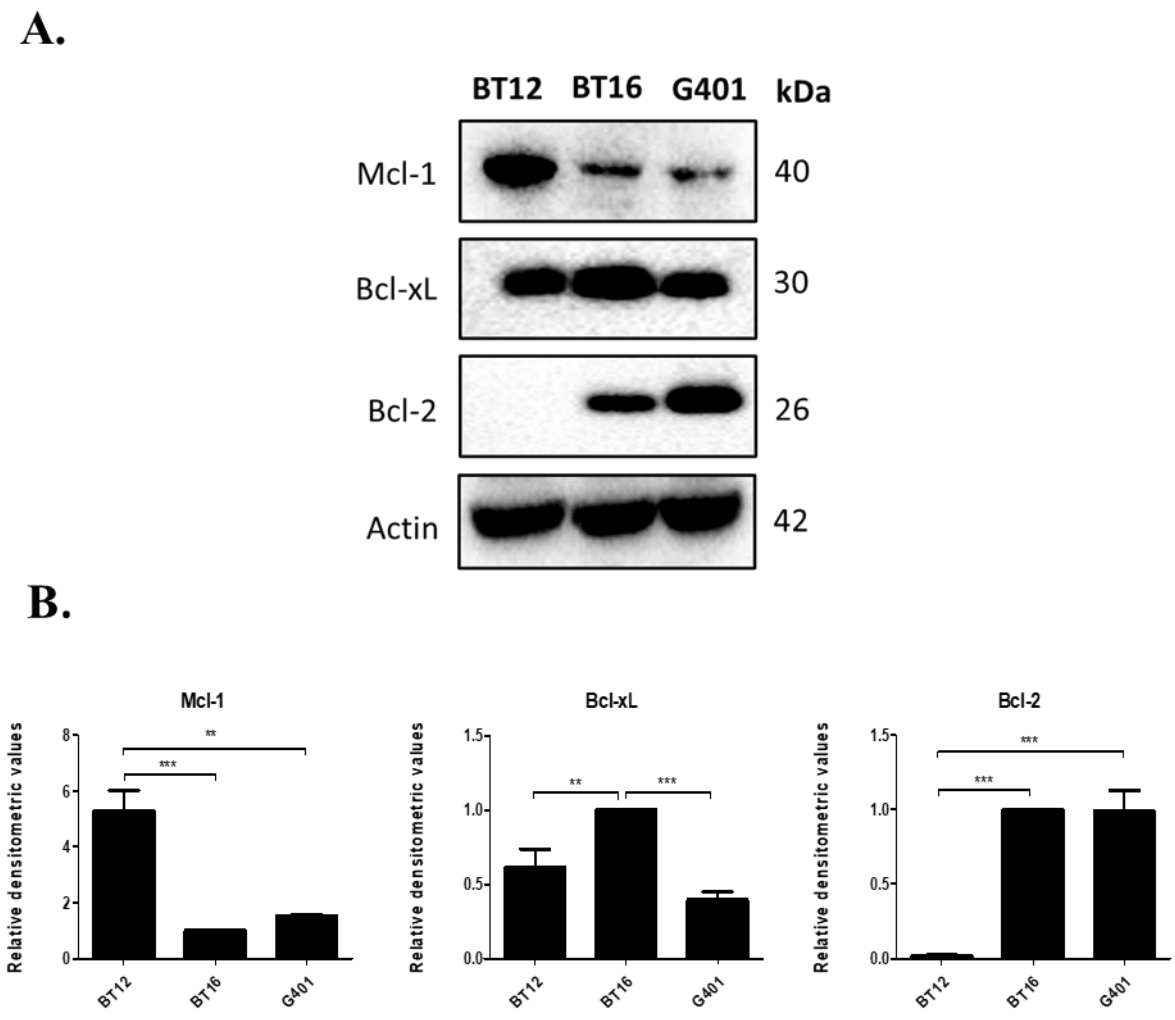

Figure 5.1 Basal expression levels of anti-apoptotic Bcl-2 proteins in a panel of MRT cell lines

MRT cell lines (BT12, BT16 and G401) were seeded at various densities in T175 flasks and grown to sub-confluency. The cells were then harvested, and lysates prepared for western blot analysis. 15 µg of protein was loaded, separated on an SDS page gel, transferred to PVDF and probed with the relevant antibodies. **A.** Results are representative of three independent experiments. Western blots were normalised to total actin as a loading control. **B**. Densitometric analysis of the bands was carried out using Image Lab software. Statistical analysis was performed using one way ANOVA with Tukey's post hoc test. ** $p<0.01$, ***$p<0.001$. Results represent the mean and S.E.M of three independent experiments.

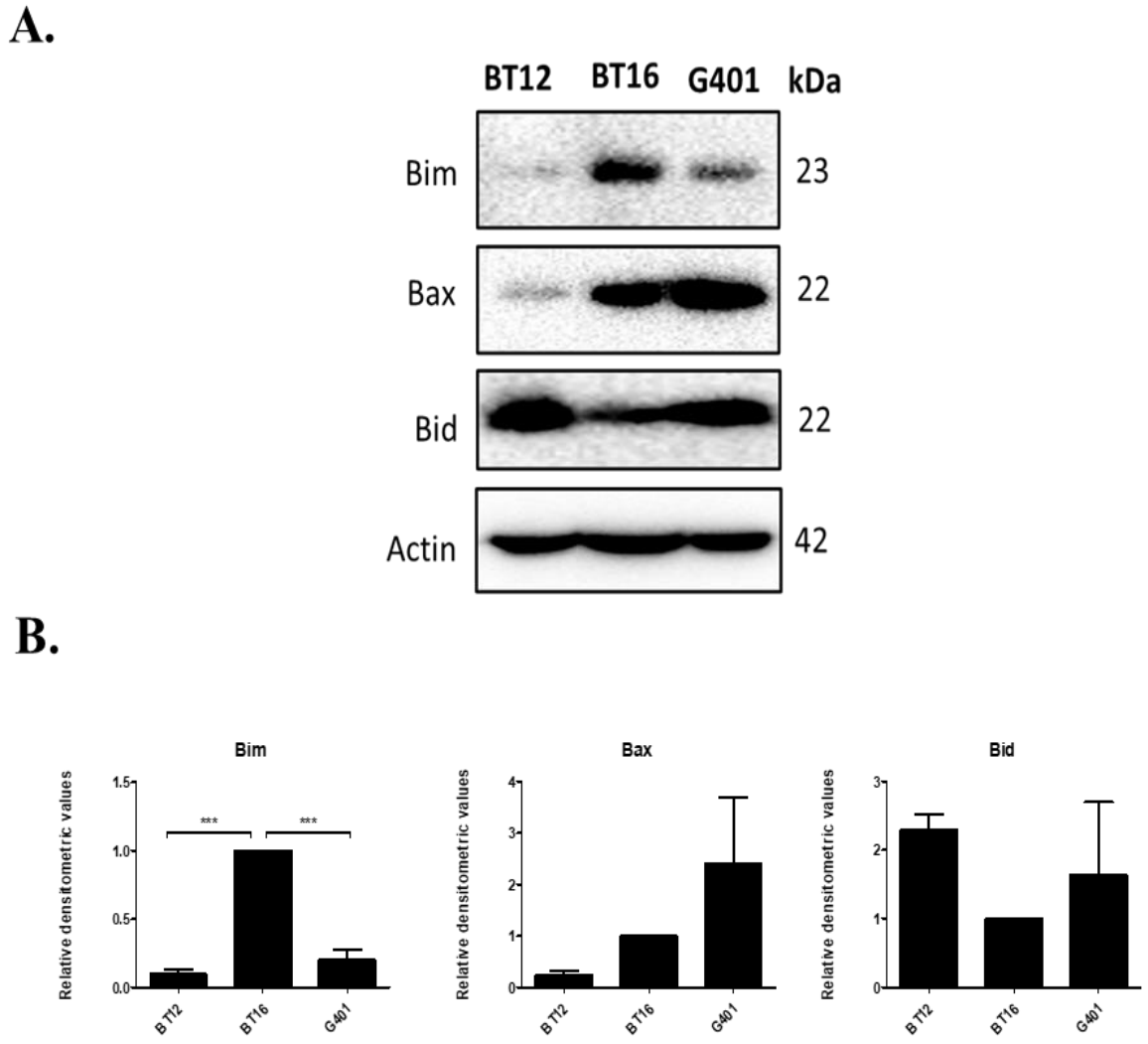

Figure 5.2 Basal expression levels of pro-apoptotic Bcl-2 proteins in a panel of MRT cell lines

MRT cell lines (BT12, BT16 and G401) were seeded at various densities in T175 flasks and grown to sub-confluency. The cells were then harvested, and lysates prepared for western blot analysis. 15 µg of protein was loaded, separated on an SDS page gel, transferred to PVDF and probed with the relevant antibodies. **A**. Results are representative of three independent experiments. Western blots were normalised to total actin as a loading control. **B**. Densitometric analysis of the bands was carried out using Image Lab software. Results represent the mean and S.E.M of three independent experiments. Statistical analysis was performed using one way ANOVA with Tukey's post hoc test. ***$p<0.001$.

5.2.2 The effect of the BH3 mimetics, ABT-263 and ABT-199 on the viability of a panel of MRT cell lines

The BH3 mimetic agents, ABT-263 and ABT-199, are small selective inhibitors used for the treatment of Bcl-2-dependent cancers. ABT-263 exhibits selectivity for both Bcl-xL and Bcl-2 whereas ABT-199 is selective for Bcl-2 only. An alamar blue assay was used to determine the effect of increasing concentrations (0-20 µM) of ABT-199 and ABT-263 on the viability of BT12, BT16 and G401 cell lines at 72 hours. The viability of all three cell lines was decreased in response to treatment with either ABT-199 or ABT-263 in a dose-dependent manner. Surprisingly, the IC50 value for ABT-199 treatment of BT12 cells was 9.82 ±1.13 µM, only slightly lower than that determined in BT16 cells, which had a IC50 8.60±1.10 µM (Table 5.1). Moreover, it was noted that G401 cells seem to exhibit a higher IC50 value of 12.50±1.15 µM (Figure 5.3). However, this was not observed in the response of G401 cells to ABT-263; where a lower IC50 value of 7.15±1.39 µM was determined (Figure 5.4). BT16 cells also had a lower IC50 value for ABT-263 (5.793 ± 1.06 µM) than BT12 cells (9.36±1.05 µM). These differences may suggest that dual inhibition of Bcl-2 and Bcl-xL may be more effective in reducing cellular viability in MRT cell lines.

The use of ABT-263 is limited due to its propensity to cause thrombocytopenia as a side effect, as platelets are highly dependent on Bcl-xL. For this reason, this study aimed to focus on the therapeutic potential of ABT-199 in rhabdoid tumour cells.

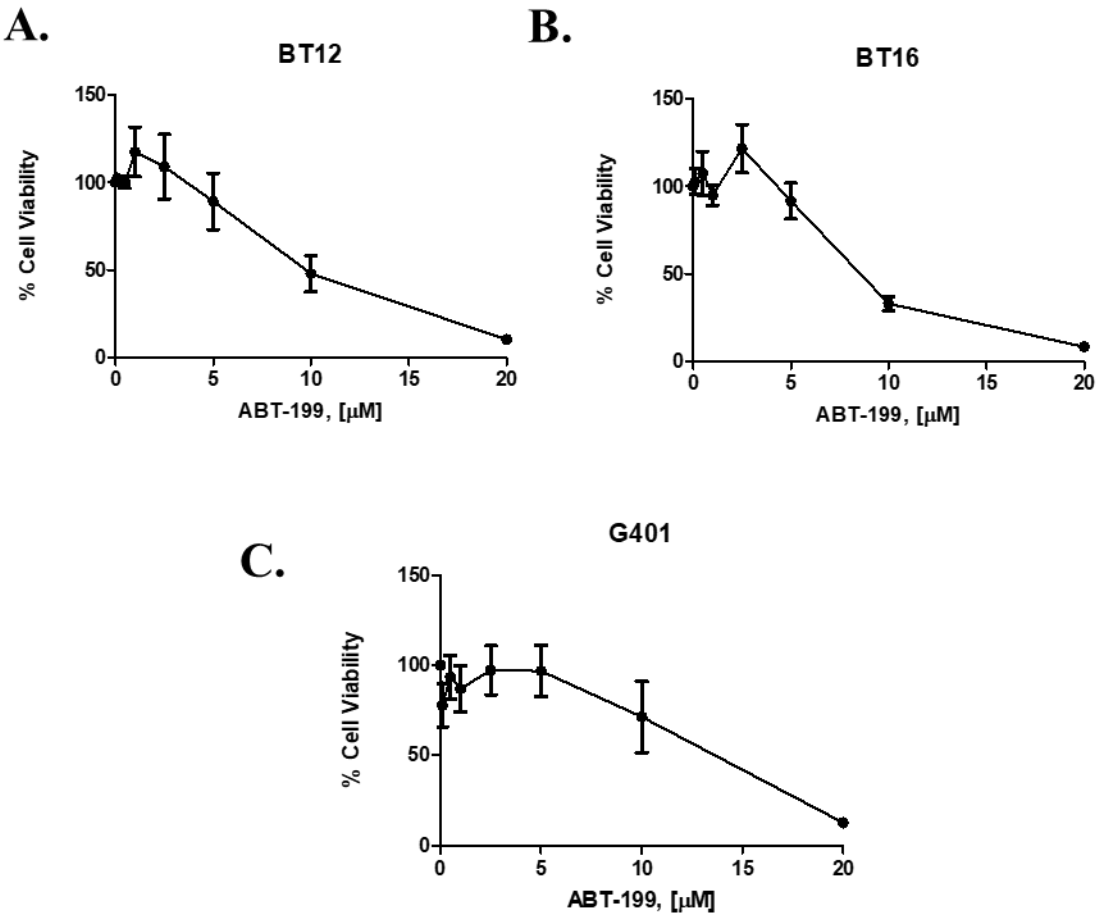

Figure 5.3 ABT-199 reduces the viability of MRT cell lines in a dose-dependent manner

BT12 and BT16 cells were seeded at 1 x 10^4 cells/well whilst G401 cells were seeded at 5 x 10^3 cells/well. Cells were left to adhere overnight and were subsequently treated with vehicle (0.5% (v/v) DMSO) or a range of concentrations of ABT-199 (0.1-20 μM) for 72 hours. Alamar blue (10% (v/v)) was added to the wells 5 hours prior to analysis and the cells were incubated in the dark at 37°C. The fluorescence was measured using a Softmax Gemini EM Microplate Reader at an excitation wavelength of 544 nm and an emission wavelength of 590 nm. Media was used to obtain blank values. The values obtained from treated cells were corrected by the blank values and normalised using the vehicle. Values represent the mean ± S.E.M of three independent experiments. Each experiment was performed in triplicate.

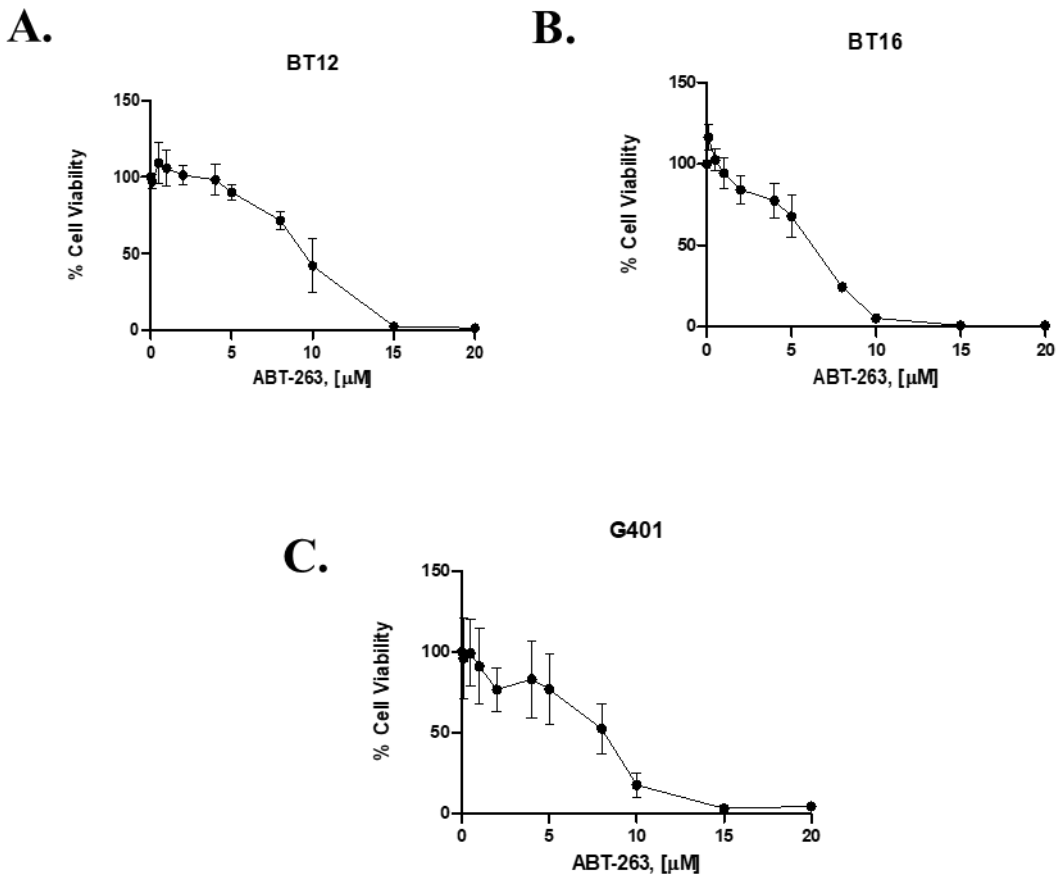

Figure 5.4 ABT-263 reduces the viability of MRT cell lines in a dose-dependent manner

BT12 and BT16 cells were seeded at 1 x 10^4 cells/well whilst G401 cells were seeded at 5 x 10^3 cells/well. Cells were left to adhere overnight and were subsequently treated with vehicle (0.5% (v/v) DMSO) or a range of concentrations of ABT-263 (0.1-20 μM for 72 hours). Alamar blue (10% (v/v)) was added to the wells 5 hours prior to analysis and the cells were incubated in the dark at 37°C. The fluorescence was measured using a Softmax Gemini EM Microplate Reader at an excitation wavelength of 544 nm and an emission wavelength of 590 nm. Media was used to obtain blank values. The values obtained from treated cells were corrected by the blank values and normalised using the vehicle. Values represent the mean ± S.E.M of three independent experiments. Each experiment was performed in triplicate.

	ABT-199 (µM)	ABT-263 (µM)
BT12	9.82±1.13	9.36±1.05
BT16	8.60±1.10	5.793±1.06
G401	12.50± 1.15	7.15±1.39

Table 5.1 IC50 values of ABT-199 and ABT-263 in a panel of MRT cell lines

5.2.3 The effect of the BH3 mimetic ABT-199 on apoptosis in a panel of MRT cell lines

Results from the Alamar blue assay elicited similar IC50 values with ABT-199 in Bcl-2-positive BT16 cells and Bcl-2-deficient BT12 cells. Moreover, G401 cells showed a higher IC50 to ABT-199 despite expressing its target protein, Bcl-2. Therefore, the ability of ABT-199 to induce apoptosis in MRT cell lines, was subsequently investigated.

BT12, BT16 and G401 cells were treated with increasing concentrations of ABT-199 (1, 2.5, 5, 10 and 15 µM) for 48 hours. Annexin V/PI-stained cells were analysed by flow cytometry and showed G401 cells to be resistant to ABT-199-induced apoptosis up to a concentration of 15 µM (Figure 5.5). Interestingly, ABT-199 significantly induced apoptosis in a dose-dependent manner in BT12 and BT16 cells. This agrees with the Alamar blue results which demonstrate a similar response to ABT-199 by the BT12 and BT16 cell lines, despite the differential expression of Bcl-2 in these cells. This would suggest that ABT-199 may elicit off-target effects to induce cell death in Bcl-2-deficient BT12 cells. Moreover, the observed resistance of G401 cells to ABT-199-induced apoptosis in response to treatments up to 15 µM may be as a result of upregulation of other anti-apoptotic proteins such as Mcl-1 and Bcl-xL.

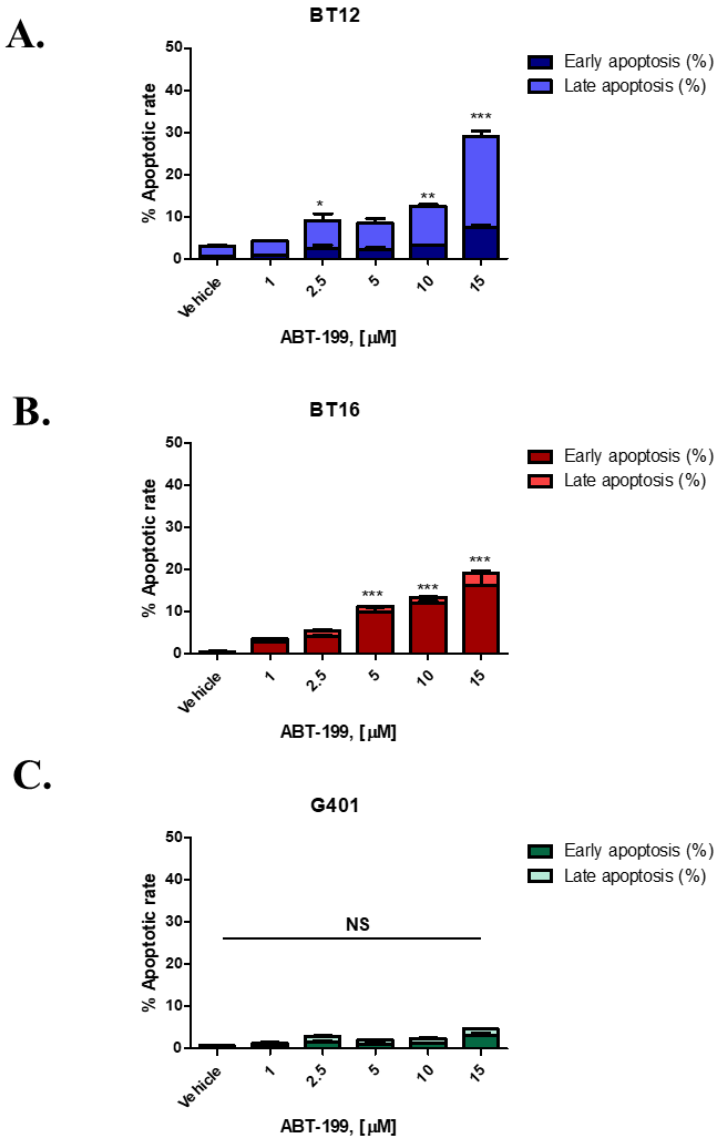

Figure 5.5 The effect of the BH3 mimetic ABT-199 on apoptosis in MRT cell lines

2mL of BT12 (**A**), BT16 (**B**) and G401 (**C**) cells were seeded in a 6-well plate at various seeding densities. Cells were left to adhere overnight and were then treated with the vehicle (0.5% (v/v) DMSO) or varying concentrations of ABT-199 (1, 2.5, 5, 10, 15µM). After 48 hours, the cells were detached and stained with Annexin V-FITC and propidium iodide (PI). The cells were immediately analysed by flow cytometry using the BD FACS Accuri software. 10,000 cells were gated on vehicle treated cells and the percentage of cells undergoing early and late apoptosis was determined to be those stained with Annexin V only or stained with both Annexin V and PI, respectively. Values represent mean ± S.E.M of three independent experiments. Statistical analysis was performed using a one-way ANOVA with Tukey's post hoc test. * $p < 0.05$, **$p<0.01$, *** $p < 0.001$.

5.2.4 ABT-199 treatment does not sensitise BT12 cells to cisplatin

This chapter previously showed that BT12 cells have no detectable protein levels of Bcl-2 (Figure 5.1). However, BT12 cells exhibited a similar IC50 value for ABT-199 when compared to the Bcl-2-positive BT16 cells. Moreover, despite not expressing Bcl-2, ABT-199 induced 30% apoptosis in BT12 cells at a concentration of 15 µM, potentially due to Bcl-2 independent off-target effects. Next the ability of ABT-199 to affect cisplatin-induced apoptosis in BT12 cells was evaluated.

Cisplatin-sensitive BT12 cells were treated with cisplatin (1 µM) alone and in combination with increasing sub-cytotoxic concentrations of ABT-199 (0.5, 1 and 2 µM). Flow cytometric analysis of Annexin V/PI-stained cells showed no enhancement in the apoptotic rate of cells treated with cisplatin alone and cells treated with a combination of ABT-199 and cisplatin (Figure 5.6). This would suggest that despite inducing apoptosis at higher concentrations, ABT-199 is not a suitable drug to sensitise Bcl-2-deficient MRT cells to cisplatin treatment. In addition, these results suggest that the apoptosis induced in BT12 by higher concentrations of ABT-199 may be due to off-target effects that do not prime cells to become more sensitive to cisplatin treatment.

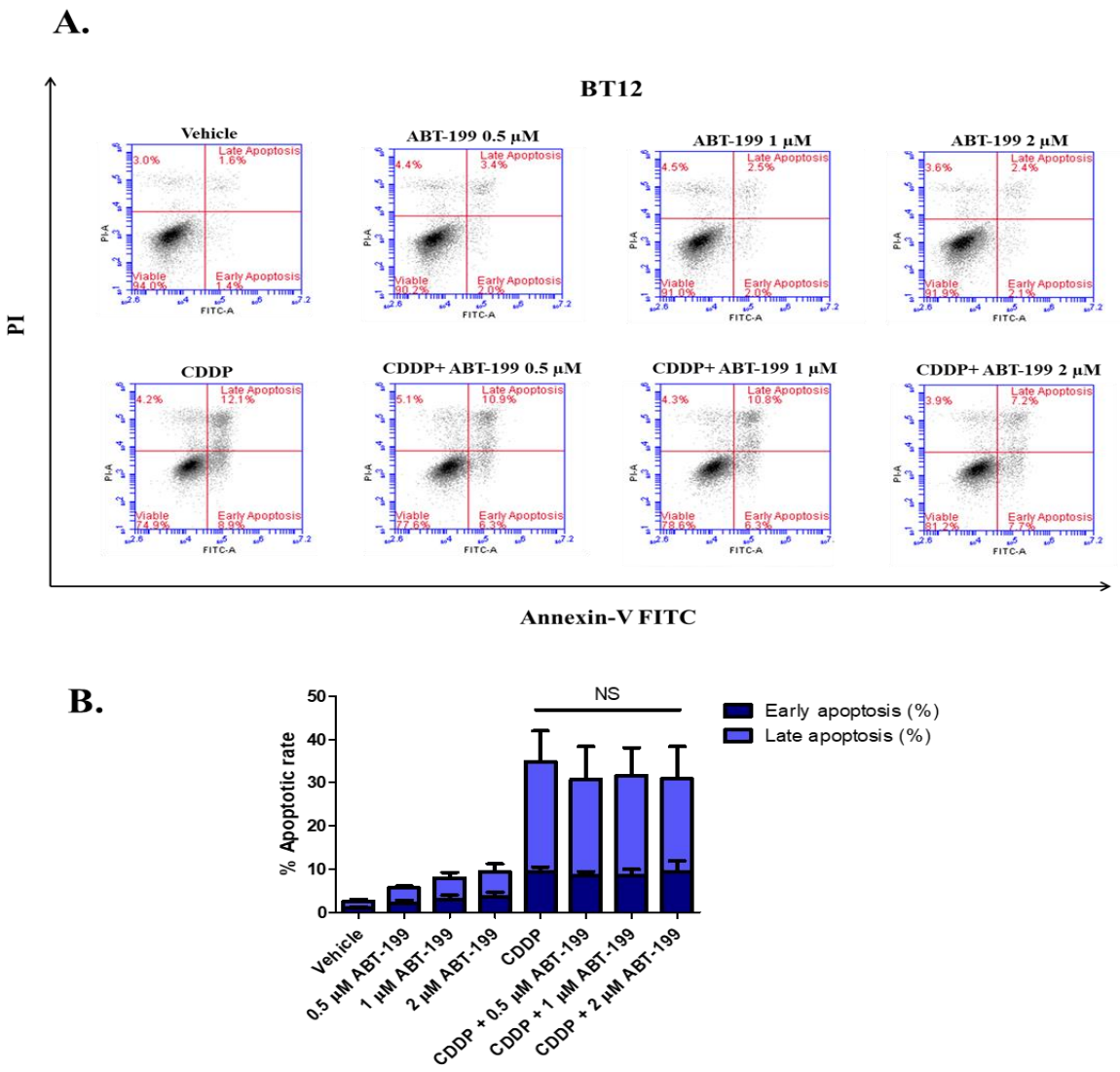

Figure 5.6 ABT-199 does not enhance cisplatin-induced apoptosis in BT12 cells

2mL of BT12 cells were seeded in a 6-well plate at a seeding density of 1 x 10^5 cells/mL. Cells were left to adhere overnight and were then treated with the vehicle (0.5% (v/v) DMSO), cisplatin (1µM) or varying concentrations of ABT-199 (0.5, 1, 2µM) alone or in combination. After 48 hours, the cells were detached and stained with Annexin V-FITC and propidium iodide (PI). The cells were immediately analysed by flow cytometry using the BD FACS Accuri software. 10,000 cells were gated on vehicle treated cells and the percentage of cells undergoing early and late apoptosis was determined to be those stained with Annexin V only or stained with both Annexin V and PI, respectively. **A** Representative dot plot of treated cells. **B** Values represent mean ± S.E.M of three

independent experiments. Statistical analysis was performed using a one-way ANOVA with Tukey's post hoc test. NS=non-significant.

5.2.5 ABT-199 synergistically enhances cisplatin-induced apoptosis in BT16 cells

Previous research has shown that cancers which overexpress Bcl-2 may exhibit resistance to chemotherapeutics. For example, in human ovarian cancer cells, Bcl-2 overexpression increased resistance to cisplatin[484]. Moreover, in human bladder cancer cell lines, upregulation of Bcl-2 was also found to be linked to cisplatin resistance via inhibition of Bax translocation to the mitochondria[468]. Furthermore, in nasopharyngeal carcinoma cells, genetic suppression of Bcl-2 sensitised cells to cisplatin[485]. As such, this chapter next evaluated whether targeting Bcl-2 with the selective BH3 mimetic ABT-199 could affect the apoptotic response to cisplatin and sensitise BT16 cells to cytotoxicity.

Cisplatin-resistant BT16 cells were treated with cisplatin (10 µM) alone and in combination with increasing sub-cytotoxic concentrations of ABT-199 (0.5, 1 and 2 µM). Flow cytometric analysis of Annexin V/PI-stained cells showed that cisplatin-induced apoptosis was significantly enhanced when cells were pre-treated with all concentrations of ABT-199 tested (Figure 5.7). Moreover, western blot analysis of caspase 3 cleavage depicted a significant increase in expression of cleaved caspase 3 (Figure 5.8) with the combination treatment compared to cisplatin alone, supporting results obtained by flow cytometry.

This study next determined whether BT16 cells could be sensitised by ABT-199 to non-cytotoxic concentrations of cisplatin. A concentration of 1 µM cisplatin was selected for this experiment. Results demonstrated that despite both ABT-199 and 1 µM cisplatin on their own causing minimal cell death compared to vehicle, a combination of both caused a significant increase in the apoptotic rate (Figure 5.9).

To further examine this effect, a drug combination study was conducted whereby the concentration of 2 µM ABT-199 was kept fixed and its effect was monitored alone and in combination with three concentrations of cisplatin (1, 5, 10 µM). The computer program Compusyn was then used to determine synergistic or additive effects. Compusyn calculates the combination index (CI) value of each combination. Values <1, =1 and >1 indicate synergistic, additive, and antagonistic effects respectively. Lower CI values are indicative of greater synergism. The combinations of ABT-199 and cisplatin was

synergistic at all concentrations tested with CI values ranging from 0.24-0.76 (Table 5.2) with the combination of 2 μM ABT-199 and 10 μM cisplatin showing the greatest level of synergism. It should be noted that higher concentrations of ABT-199 induced significant levels of apoptosis in BT16 cells whereas 2 μM ABT-199 was not cytotoxic (Figure 5.5). Thus, this sub-cytotoxic concentration of ABT-199 was selected for further experimentation.

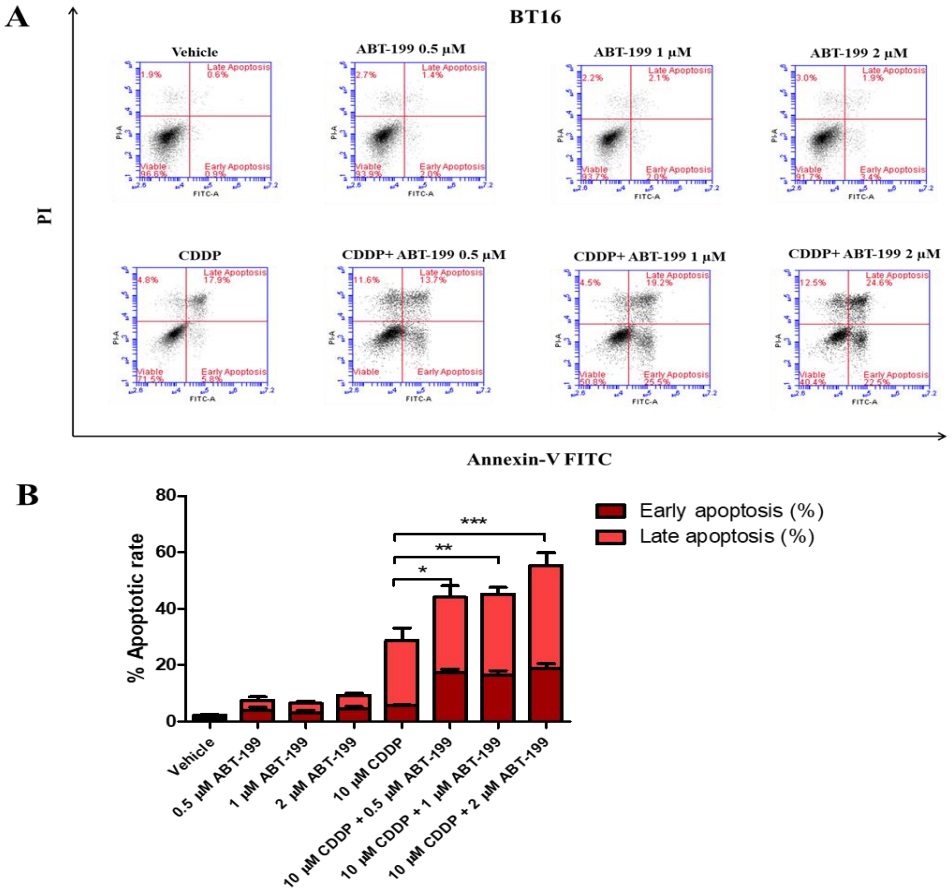

Figure 5.7 ABT-199 significantly enhances cisplatin-induced apoptosis in BT16 cells

2mL of BT16 cells were seeded in a 6-well plate at a seeding density of 1 x 10^5 cells/mL. Cells were left to adhere overnight and were then treated with the vehicle (0.5% (v/v) DMSO), cisplatin (10µM) or varying concentrations of ABT-199 (0.5, 1, 2µM) alone or in combination. After 48 hours, the cells were detached and stained with Annexin V-FITC and propidium iodide (PI). The cells were immediately analysed by flow cytometry using the BD FACS Accuri software. 10,000 cells were gated on vehicle treated cells and the percentage of cells undergoing early and late apoptosis was determined to be those stained with Annexin V only or stained with both Annexin V and PI, respectively. **A** Representative dot plot of treated cells. **B** Values represent mean ± S.E.M of at least three independent experiments. Statistical analysis was performed using a one-way ANOVA with Tukey's post hoc test. * $p < 0.05$, **$p<0.01$, *** $p < 0.001$.

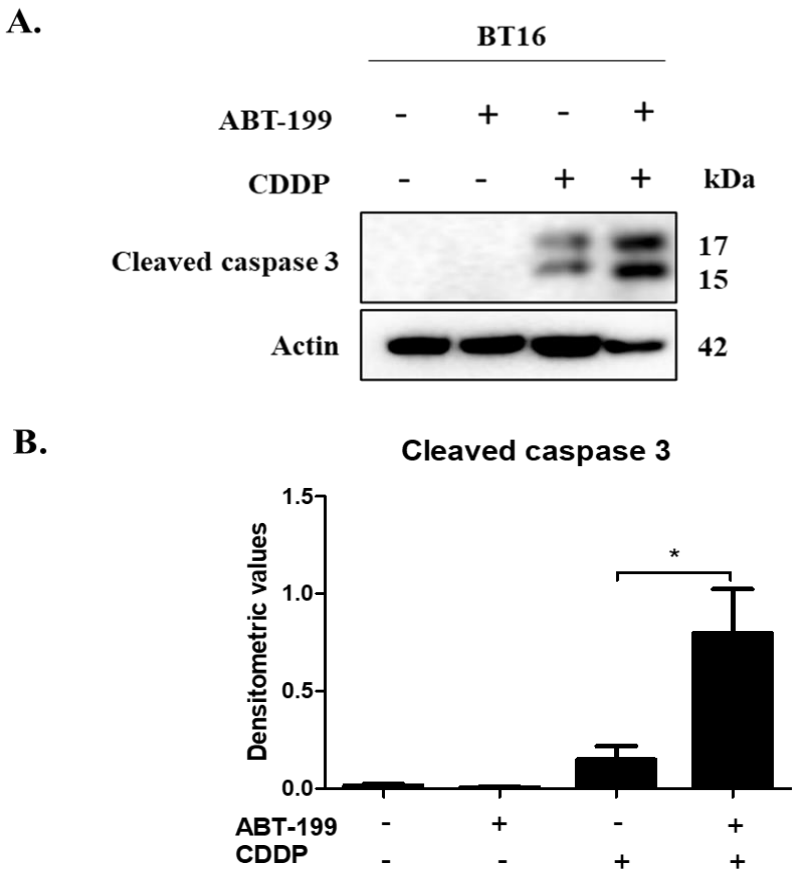

Figure 5.8 ABT-199 enhances cisplatin-induced activation of caspase 3

10 mL of BT16 cells were seeded in a T25 flask at a seeding density of 1 x 10^5 cells/mL. Cells were left to adhere overnight and were then treated with the vehicle (0.5% (v/v) DMSO), ABT-199 (2 µM) or cisplatin (CDDP) (10µM) alone and in combination. After 48 hours, the cells were detached, and lysates were prepared. 15 µg of protein was loaded on a 15% gel and transferred onto PVDF membrane which was incubated overnight in cleaved caspase 3 antibody. Actin served as a loading control. **A** Results are representative of three experiments. **B** Densitometric analysis was performed using ImageLab software and the loading control was used to normalise the values obtained. Values represent mean ± S.E.M. of three experiments. Statistical analysis was performed using a one-way ANOVA with Tukey's post hoc test. * $p < 0.05$, **$p<0.01$, *** $p < 0.001$.

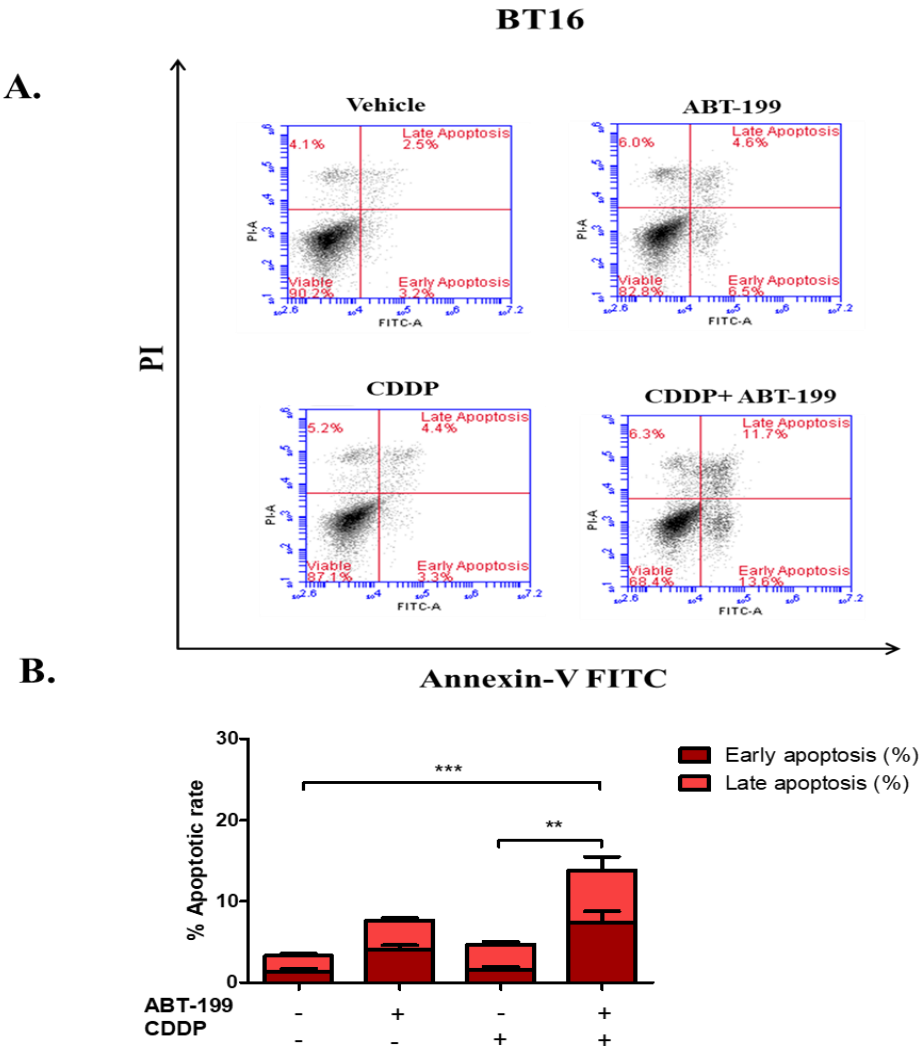

Figure 5.9 ABT-199 sensitises BT16 cells to sub-cytotoxic concentrations of cisplatin

2mL of BT16 cells were seeded in a 6-well plate at a seeding density of 1 x 10^5 cells/mL. Cells were left to adhere overnight and were then treated with the vehicle (0.5% (v/v) DMSO), cisplatin (1µM) or ABT-199 (2µM) alone or in combination. After 48 hours, the cells were detached and stained with Annexin V-FITC and propidium iodide (PI). The cells were immediately analysed by flow cytometry using the BD FACS Accuri software. 10,000 cells were gated on vehicle treated cells and the percentage of cells undergoing early and late apoptosis was determined to be those stained with Annexin V only or stained with both annexin V and PI, respectively. **A** Representative dot plot of treated cells. **B.** Values represent mean ± S.E.M of three independent experiments. Statistical analysis was performed using a one-way ANOVA with Tukey's post hoc test. ** $p < 0.01$, *** $p < 0.001$.

Cisplatin (µM)	ABT-199 (µM)	Fa	CI Value	Level of Synergism
1	2	0.173	0.55687	Synergism
5	2	0.266	0.76107	Moderate Synergism
10	2	0.51767	0.24230	Strong Synergism

Table 5.2 Synergism between cisplatin and ABT-199 in BT16 cells

2mL of BT16 cells were seeded at $1x10^5$ cell/mL in a 6 well plate and left to adhere overnight. The following day, cells were treated for 48 hours with a vehicle (0.009% NaCl for cisplatin, 0.5% DMSO for ABT199), and a range of concentrations of cisplatin alone or in combination with 2 µM ABT-199. After 48 hours, cells were harvested, and stained with Annexin V and propidium iodide. Cells were analysed by flow cytometry using BD FACS Accuri software. 10,000 single cells were gated on vehicle treated cells. The mean of at least three independent experiments was entered into Compusyn. CI Values <1, =1 and >1 indicate synergistic, additive, and antagonistic effects respectively

5.2.6 ABT-199 does not sensitise G401 cells to cisplatin treatment

Despite expressing high levels of Bcl-2, G401 was previously shown to have a higher IC50 value for ABT-199 treatment when compared to BT12 and BT16 cells (Table 5.1). Moreover, G401 was also shown to resist apoptosis in response to treatment with concentrations of ABT-199 as high as 15 µM (Figure 5.5). Thus, this study next evaluated whether combining ABT-199 with cisplatin may enhance cytotoxicity in G401 cells, despite its potential higher resistance to ABT-199 as a monotherapy. The concentration of 2 µM ABT-199 was selected as this showed a synergistic effect when combined with cisplatin in the other Bcl-2 positive MRT cell line, BT16. ABT-199 was treated in combination with three concentrations of cisplatin: two lower concentrations of 1 and 2 µM and one higher concentration of 10 µM. However, unlike in BT16 cells, ABT-199 did not affect cisplatin-induced apoptosis (Figure 5.10).

An Alamar blue assay was then conducted to examine further combinations of ABT-199 and cisplatin on overall cell viability. Three concentrations of cisplatin (1, 2 and 10 µM) were tested against three concentrations of ABT-199 (0.5, 1 and 2µM). In agreement with results presented in chapter 3, cisplatin alone induced a decrease in viability of G401 cells in a dose-dependent manner. No further decrease in viability was observed when cisplatin was combined with any of these concentrations of ABT-199. In fact, at the higher concentrations of 5 and 10 µM cisplatin, co-treatment with ABT-199 showed a slight but non-significant enhancement of viability (Figure 5.11). This validates the results obtained with flow cytometric analysis of Annexin V/PI-stained cells. In conclusion, these results taken together suggest that the Bcl-2 positive G401 cell line appears to be resistant to the effects of ABT-199, alone and in combination with cisplatin.

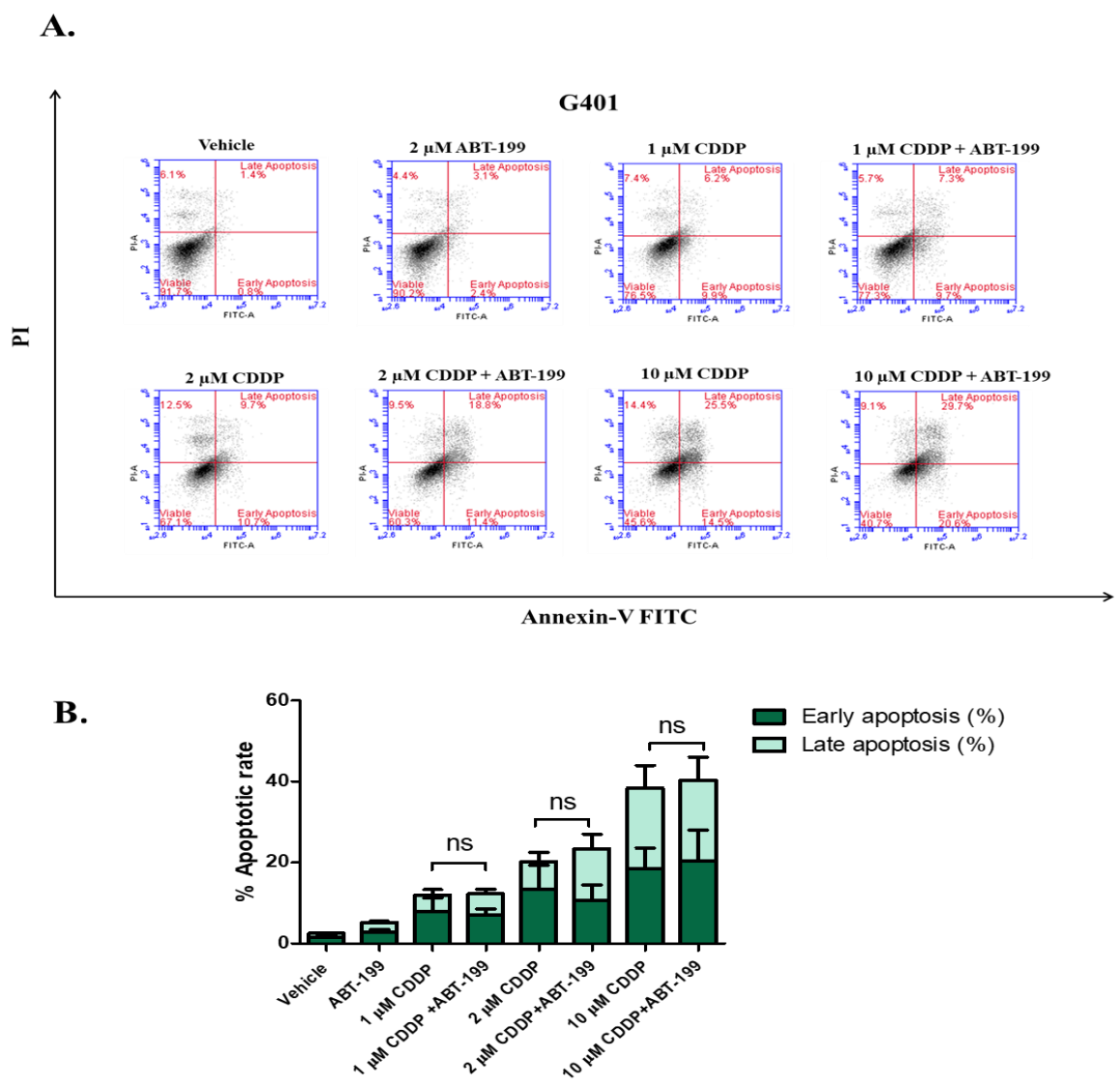

Figure 5.10 ABT-199 does not enhance cisplatin-induced apoptosis in G401 cells

2mL of G401 cells were seeded in a 6-well plate at a seeding density of 1 x 10^5 cells/mL. Cells were left to adhere overnight and were then treated with the vehicle (0.5% (v/v) DMSO), ABT-199 (2µM), or varying concentrations of cisplatin (1, 2 or 10 µM) alone or in combination. After 48 hours, the cells were detached and stained with Annexin V-FITC and propidium iodide (PI). The cells were immediately analysed by flow cytometry using the BD FACS Accuri software. 10,000 cells were gated on vehicle treated cells and the percentage of cells undergoing early and late apoptosis was determined to be those stained with Annexin V only or stained with both Annexin V and PI, respectively. **A**. Representative dot plot of treated cells. **B**. Values represent mean ± S.E.M of three

independent experiments. Statistical analysis was performed using a one-way ANOVA with Tukey's post hoc test. NS=non-significant.

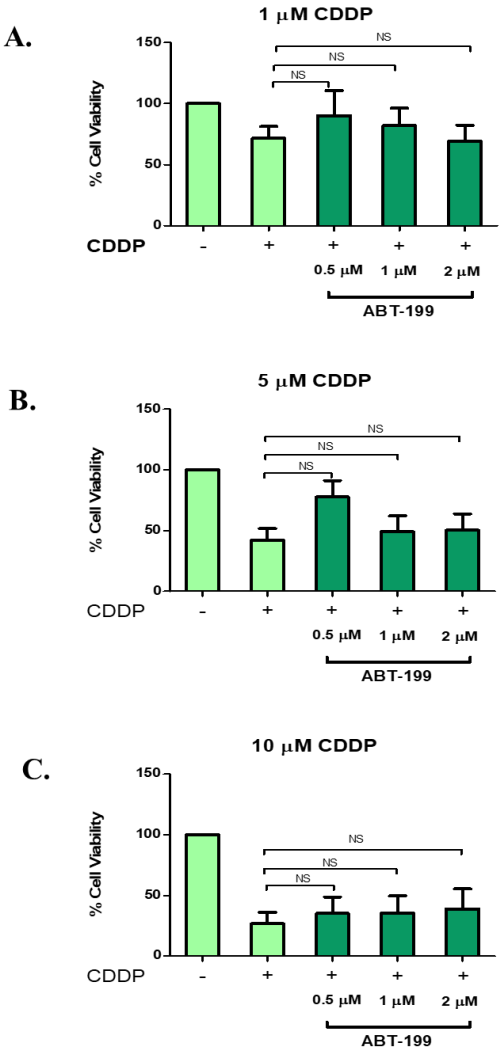

Figure 5.11 ABT-199 does not enhance cisplatin-induced reduction in viability in G401 cells

G401 cells were seeded in a 96-well plate at a seeding density of 5 x 10^3 cells/well. Cells were left to adhere overnight and were then treated with the vehicle (0.5% (v/v) DMSO), cisplatin (1, 5 or 10 μM) or ABT-199 (0.5, 1, 2μM) alone or in various combinations for 72 hours. Alamar blue (10% (v/v)) was added to the wells 5 hours prior to analysis and the cells were incubated in the dark at 37°C. The fluorescence was measured using a Softmax Gemini EM Microplate Reader at an excitation wavelength of 544 nm and an emission wavelength of 590 nm. Media was used to obtain blank values. The values obtained from the treated cells were corrected by the blank values and normalised using the vehicle. Values represent the mean ± S.E.M of three independent experiments. Each experiment was performed in triplicate.

5.2.7 Effect of ABT-199 on intracellular ROS levels in MRT cell lines

The previous chapter demonstrated that cisplatin induced apoptosis in part through an accumulation of ROS leading to oxidative stress. Interestingly, certain reports in literature suggest Bcl-2 inhibition by ABT-199 may affect ROS regulation. Lee *et al*, have previously demonstrated that ABT-199 activates T cell-mediated anti-leukaemic activity through enhanced ROS production. Moreover, Aharoni-Simon *et al*., demonstrated that targeting Bcl-2 through ABT-199 treatment induced ROS and redox-sensitive mitochondrial proton leak in mouse pancreatic β-cells[486]. This study next evaluated whether ABT-199 induces ROS accumulation in MRT cell lines and whether this could be involved in the differential sensitivities of this panel of MRT cell lines to ABT-199-induced apoptosis.

BT12, BT16 and G401 cells were seeded at various densities in 6-well plates and treated the following day with increasing concentrations of ABT-199. After 48 hours, cells were harvested, stained with H_2DCFDA, and examined by flow cytometric analysis. Results obtained demonstrated that ABT-199 induced a statistically significant and dose-dependent increase in ROS levels in BT16 cells but not in BT12 or G401 cell lines (Figure 5.12). The increase in ROS levels observed in BT16 cells, occurred at concentrations as low as 1 μM ABT-199. This result suggested that ABT-199 may sensitise BT16 cells to cisplatin through an enhancement in ROS accumulation but further studies were required to test this hypothesis.

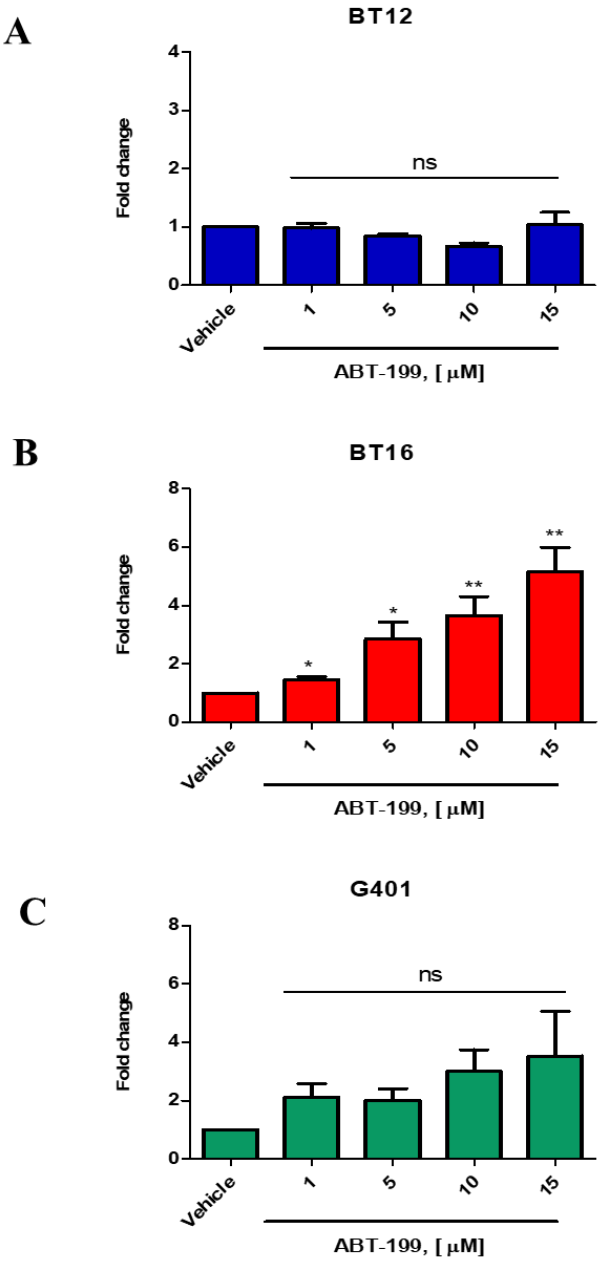

Figure 5.12 The effect of ABT-199 on intracellular ROS accumulation in MRT cell lines

2mL of BT12, BT16 and G401 cells were seeded at various densities and left to adhere overnight. After 24 hours, the cells were treated with the vehicle (0.5% DMSO) or varying concentrations of ABT-199 (1, 5, 10, 15 µM). After 48 hours, the cells were stained with H_2DCFDA and analysed by flow cytometry using the BD FACS Accuri software. 10,000 cells were gated on vehicle treated cells and the median fluorescence values were acquired for BT12 (**A**), BT16 (**B**) and G401 (**C**) cells. Values represent mean with S.E.M of at least

three independent and were normalised by the vehicle. Statistical analysis was performed using a one-way ANOVA with Tukey's post hoc test, * $p < 0.05$, **$p<0.01$.

5.2.8 ABT-199 does not enhance cisplatin-induced ROS levels in BT12 and G401 cell lines

Previous results have shown that ABT-199 induces cell death in BT12 cells only at very high concentrations, potentially due to off-target effects while G401 cells were shown to exhibit higher resistance to ABT-199-induced apoptosis than BT12 and BT16 cells even at high concentrations (Figure 5.5). Furthermore, no significant response to a range of concentrations of ABT-199 was observed when intracellular ROS was monitored in either of these cell lines. To confirm, ROS levels are not affected by ABT-199, both cell lines were treated with ABT-199 in combination with cisplatin. As shown in Figure 5.13, ABT-199 (2 μM) did not significantly enhance intracellular ROS either alone or in combination with cisplatin in either BT12 or G401 cells which may explain why no enhancement was observed in cisplatin-induced apoptosis by ABT-199 in either of these cell lines.

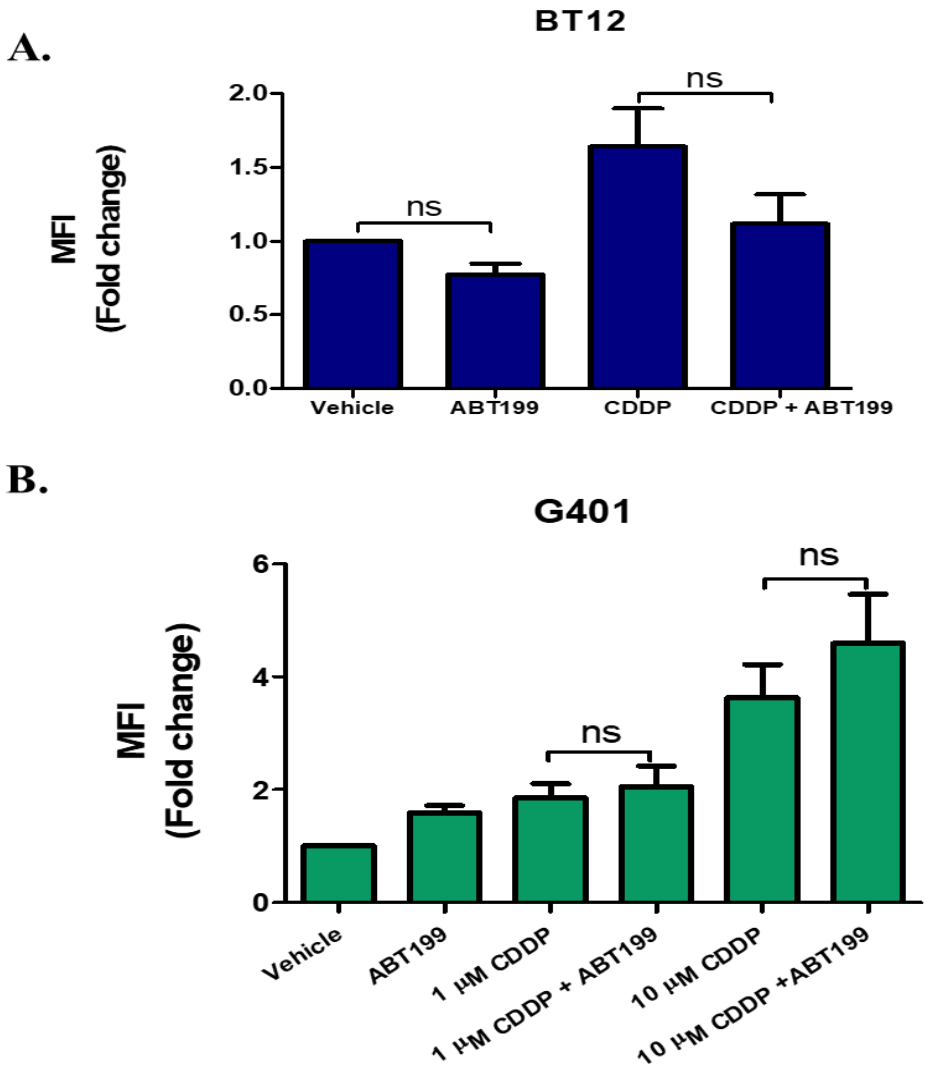

Figure 5.13 ABT-199 does not enhance cisplatin-induced ROS in BT12 and G401 cells

2mL of BT12 and G401 cells were seeded in 6-well plates at a seeding density of 1 x 10^5 cells/mL and 5x 10^4 cells/mL respectively. Cells were left to adhere overnight and were then treated with the vehicle (0.5% (v/v) DMSO), cisplatin (CDDP) (1µM or 10 µM) or ABT-199 (2 µM) alone or in combination. After 48 h, 10 µM H_2DCFDA dye was added to each well for 30 min. Cells were then harvested and analysed on the flow BD FACS Accuri cytometer. 10,000 single cells were gated on vehicle treated cells and the median fluorescence intensity (MFI) was acquired. MFI values of cisplatin/ABT-199 treated cells were normalised by MFI values of vehicle treated cells to determine the fold change in ROS levels. Values represent the mean ±S.E.M. of at least three independent experiments. Statistical analysis was performed using a one-way ANOVA with Tukey's post hoc test. NS- non-significant.

5.2.9 ABT-199 significantly enhances cisplatin-induced ROS in BT16 cells

Results thus far have demonstrated that ABT-199 did not induce ROS accumulation either alone or in combination with cisplatin in BT12 or G401 cells and did not induce an enhancement in cisplatin-induced cell death. This study next evaluated whether ABT-199 can enhance cisplatin-induced ROS in BT16 cells, which undergo a synergistic enhancement in apoptosis in response to ABT-199 and cisplatin treatment.

BT16 cells were treated with cisplatin, both a sub-cytotoxic and cytotoxic concentration (1 and 10μM respectively), and ABT-199 (2 μM) alone and in combination and intracellular ROS levels were monitored (Figure 5.14). Significant accumulation of ROS was observed in cells treated with ABT-199 alone compared to vehicle. Moreover, ABT-199 treatment in combination with cisplatin significantly enhanced ROS levels compared to cells treated with cisplatin alone. This suggests that the enhanced accumulation of ROS in cells treated with both ABT-199 and cisplatin, compared to cisplatin alone may play a role in the synergistic effect this drug combination exhibits on cell death in BT16 cells.

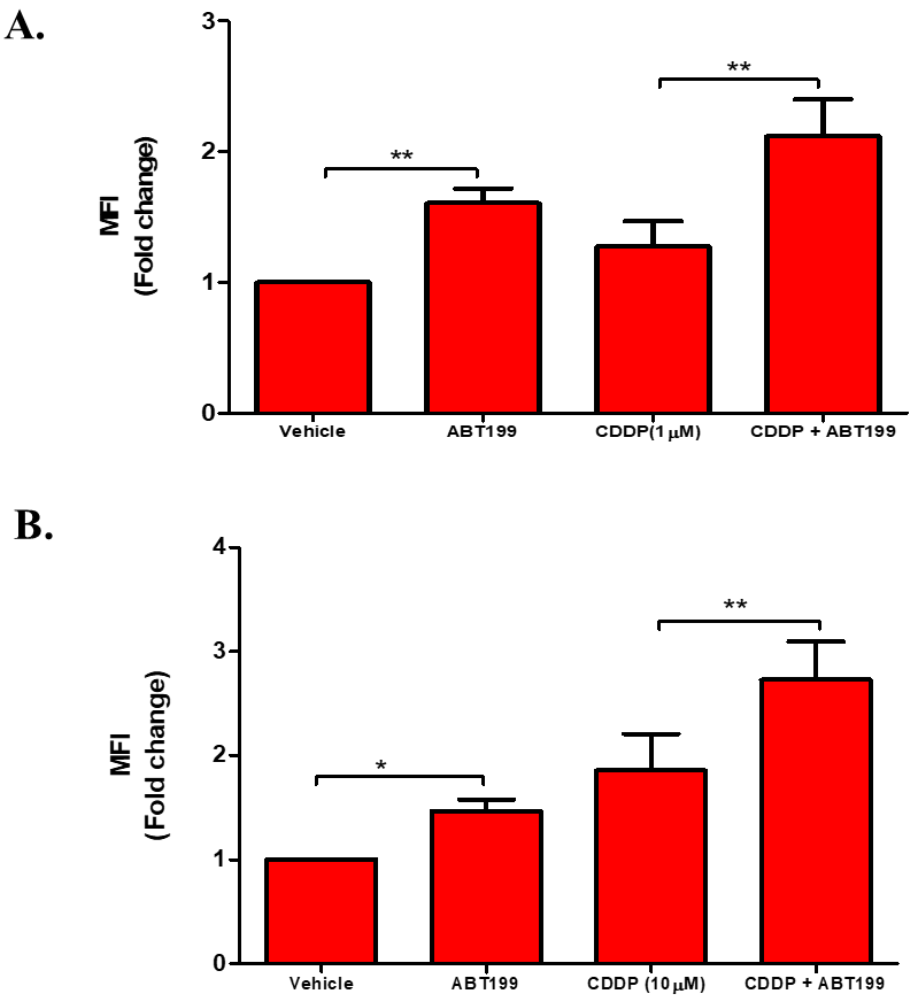

Figure 5.14 ABT-199 enhances cisplatin-induced ROS in BT16 cells

2mL of BT16 cells were seeded in a 6-well plate at a seeding density of 1 x 10^5 cells/mL. Cells were left to adhere overnight and were then treated with the vehicle (0.5% (v/v) DMSO), cisplatin (CDDP) (1 or 10 µM) or ABT-199 (2 µM) alone or in combination. After 48 h, 10 µM H_2DCFDA dye was added to each well for 30 min. Cells were then harvested and analysed on the flow BD FACS Accuri cytometer. 10,000 single cells were gated on vehicle treated cells and the median fluorescence intensity (MFI) was acquired. **A**. Cells treated with 1 µM cisplatin and ABT-199. **B**. Cells treated with 10 µM cisplatin and ABT-199. MFI values of cisplatin/ABT-199 treated cells were normalised by MFI values of vehicle treated cells to determine the fold change in ROS levels. Values represent the mean ±S.E.M. of at least three independent experiments. Statistical analysis was performed using a one-way ANOVA with Tukey's post hoc test * $p < 0.05$, ** $p < 0.01$.

5.2.10 ROS is involved in ABT-199 and cisplatin synergism in BT16 cells

ABT-199 and cisplatin showed a synergistic effect on apoptosis in BT16 cells, a cisplatin-resistant MRT cell line that highly expresses Bcl-2. Moreover, ABT-199 was shown to significantly enhance cisplatin-induced ROS accumulation in combination with either 1 or 10 µM cisplatin. Next, this study aimed to establish whether accumulation of intracellular ROS plays a role in the synergism observed between cisplatin and ABT-199.

To this end, cells were pre-treated with the ROS scavenger, NAC (5mM) for 1 hour followed by treatment with ABT-199 (2 µM) and cisplatin (10 µM). After 48 hours cells were harvested, stained with Annexin V/PI, and analysed by flow cytometry. Results demonstrated that NAC reverses the synergistic induction of apoptosis mediated by ABT-199 and cisplatin in combination (Figure 5.15) back down to the levels seen with cisplatin alone (a reduction of approximately 20%).

This result confirms the hypothesis that ROS production which is enhanced by ABT-199, is at least partially responsible for the synergism observed between ABT-199 and cisplatin.

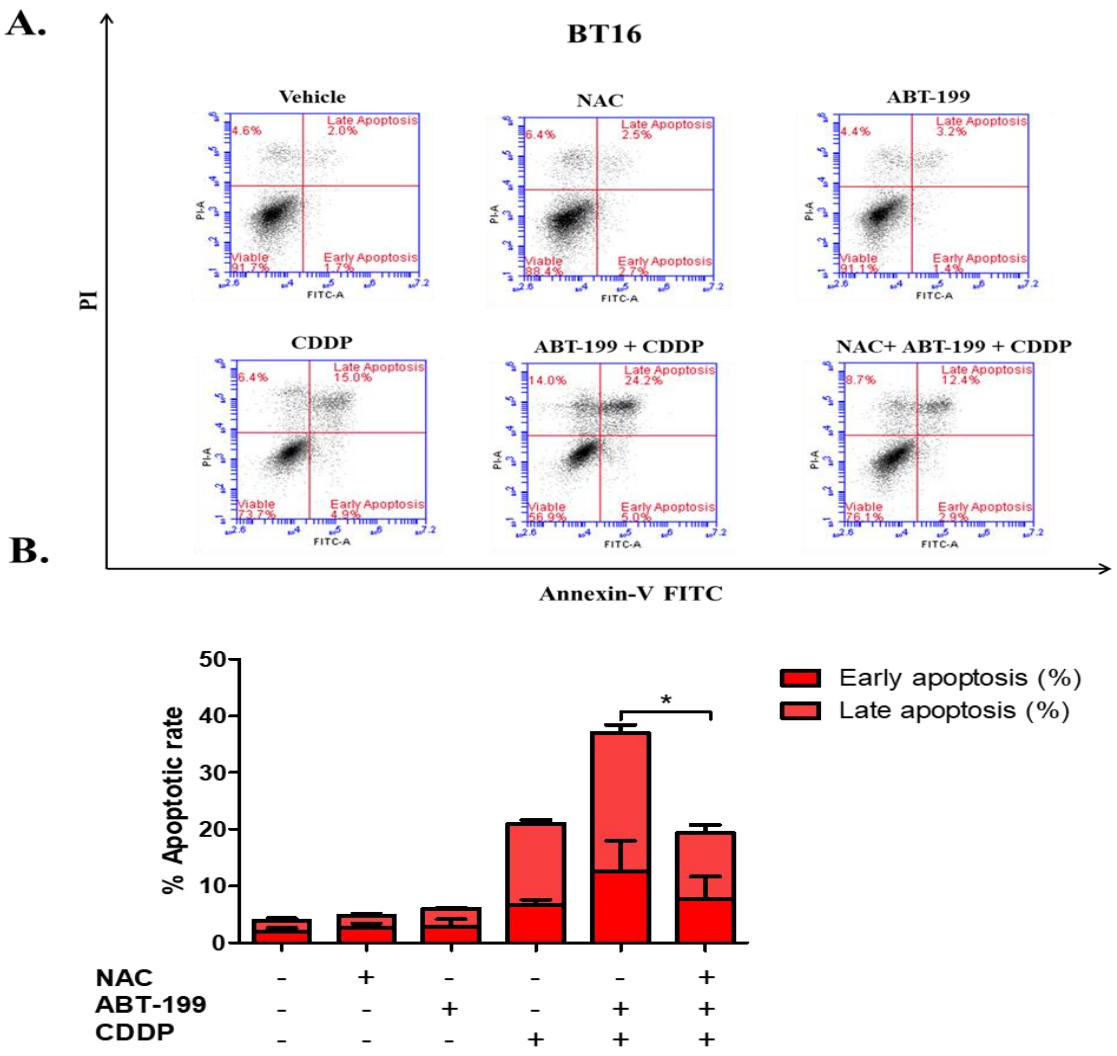

Figure 5.15 N-acetylcysteine reverses the synergistic effect on cell death mediated by ABT-199 and cisplatin

2mL of BT16 cells were seeded in a 6-well plate at a seeding density of 1 x 10^5 cells/mL. Cells were left to adhere overnight and were then treated with the vehicle (0.5% (v/v) DMSO), cisplatin (CDDP) (10µM) or varying concentrations of ABT-199 (2µM) alone or in combination. Cells were pre-treated with NAC for 1 hour prior to ABT-199 treatment. After 48 hours, the cells were detached and stained with Annexin V-FITC and propidium iodide (PI). The cells were immediately analysed by flow cytometry using the BD FACS Accuri software. 10,000 cells were gated on vehicle treated cells and the percentage of cells undergoing early and late apoptosis was determined to be those stained with Annexin V only or stained with both Annexin V and PI, respectively. **A** Representative dot plot of treated cells. **B** Values represent mean ± S.E.M of three independent experiments. Statistical analysis was performed using a paired t test.* $p < 0.05$

5.2.11 ABT-199 induces intracellular ROS in BT16 cells as early as 4 hours post-treatment

As demonstrated in the results above, ROS production plays an important role in mediating the synergism between ABT-199 and cisplatin. A significant enhancement in apoptosis was observed in cisplatin-treated BT16 cells when co-treated with ABT-199 for 48 hours. Similarly, a significant enhancement of ROS was observed at this time point. To further understand the role of ROS in cisplatin/ABT-199-mediated cell death, a time-course was conducted to establish how early ABT-199 induces intracellular ROS in BT16 cells.

Cells were treated with 2 μM ABT-199 for a series of timepoints; 4, 8, 12 and 24 hours. At the required time point, cells were harvested, stained with H_2DCFDA and analysed by flow cytometry. ROS was observed to be consistently elevated at every time point examined. In fact, a statistically significant elevation in ROS was observed as early as 4 hours (Figure 5.16). Moreover, pre-treatment of cells with the ROS scavenger NAC at 4 hours significantly reversed ABT-199 induced accumulation of ROS, back down to levels seen with NAC alone (Figure 5.17) to further support this observation.

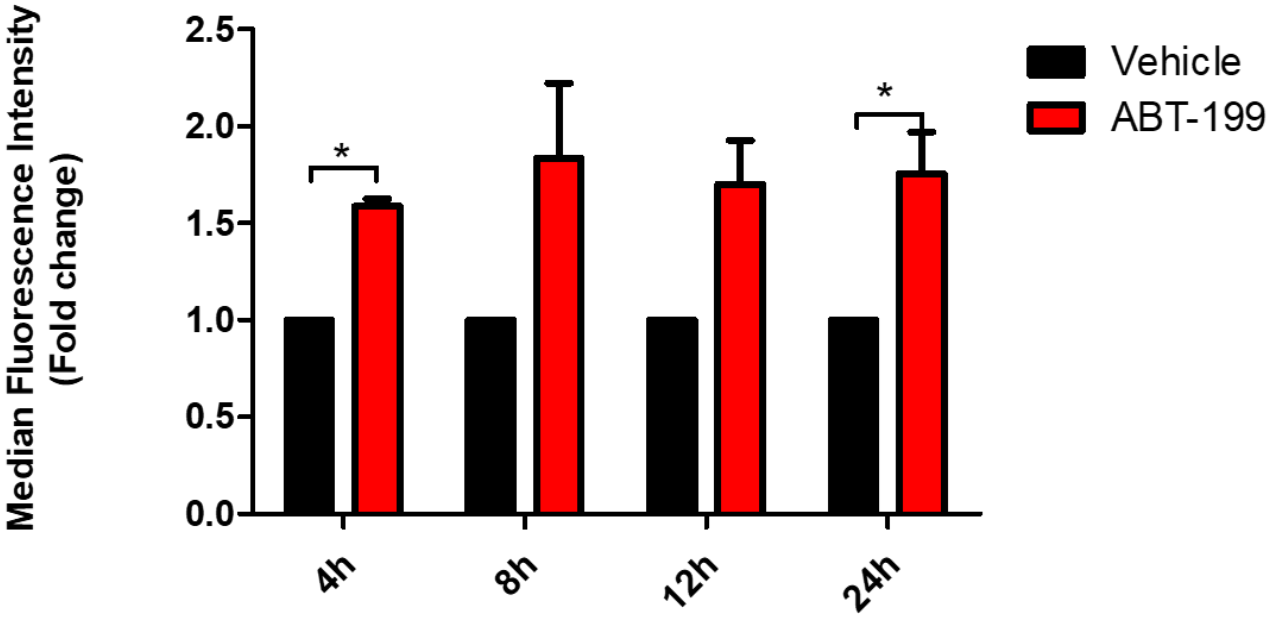

Figure 5.16 ABT-199-induced ROS production occurs as early as 4 hours in BT16 cells.

2mL of BT16 cells were seeded in a 6-well plate at a seeding density of 1 x 10^5 cells/mL. Cells were left to adhere overnight and were then treated with the vehicle (0.5% (v/v) DMSO) or ABT-199 (2 µM) for 4, 8, 12 or 24h. After the required incubation times, 10 µM H_2DCFDA dye was added to each well for 30 min. Cells were then harvested and analysed on the flow BD FACS Accuri cytometer. 10,000 single cells were gated on vehicle treated cells and the median fluorescence intensity (MFI) was acquired. MFI values of treated cells were normalised by MFI values of vehicle treated cells to determine the fold change in ROS levels. Values represent the mean ± S.E.M. of three independent experiments. Statistical analysis was performed using a paired t test. * $p < 0.05$.

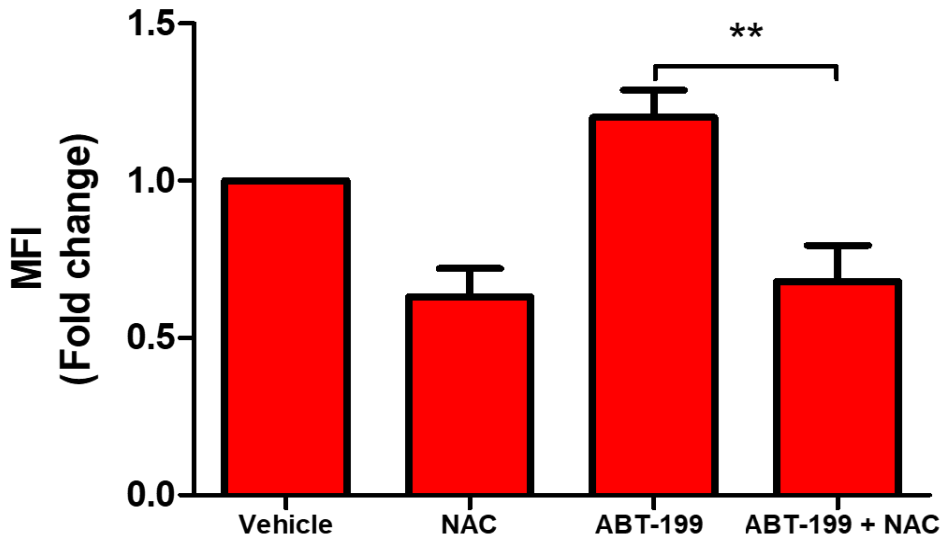

Figure 5.17 NAC reverses ABT-199-induced ROS at a 4h timepoint.

2mL of BT16 cells were seeded in a 6-well plate at a seeding density of 1 x 10^5 cells/mL. Cells were left to adhere overnight and were then treated with the vehicle (0.5% (v/v) DMSO), NAC (5mM), ABT-199 (2 μM), or a combination of both. After 4 hours, 10 μM H_2DCFDA dye was added to each well for 30 min. Cells were then harvested and analysed on the flow BD FACS Accuri cytometer. 10,000 single cells were gated on vehicle treated cells and the median fluorescence intensity (MFI) was acquired. MFI values of treated cells were normalised by MFI values of vehicle treated cells to determine the fold change in ROS levels. Values represent the mean ± S.E.M. of three independent experiments. Statistical analysis was performed using a one-way ANOVA with Tukey's post hoc test. ** $p < 0.01$.

5.2.12 ABT-199 treatment increases mitochondrial ROS at 4 and 48 hours.

Given the important role of intracellular ROS in mediating the anti-cancer activity of ABT-199 and cisplatin in BT16 cells, further work was carried out to understand the source of the ROS production. Recent reports in literature have suggested that ABT-199 may affect mitochondrial function[487]. To further examine the effect of ABT-199 on the mitochondria, one early time point of 4 hours was selected alongside the later time point of 48 hours to further explore the steps that lead to the synergistic activity of ABT-199 and cisplatin on apoptosis.

Mitochondrial derived ROS is commonly evaluated using MitoSOX™ Red[488], a fluorogenic dye which specifically targets the mitochondria in live cells and can undergo oxidation by superoxide, producing red fluorescence. It can accumulate in the mitochondria and can thus detect mitochondrial ROS which can be detected by flow cytometry[328].

The validity of the assay was first assessed by treating cells with Antimycin A (10 µM for 1 h) as positive control. Antimycin A is commonly used as a positive control to measure superoxide generation as it inhibits electron flow through complex III of the ETC by blocking passage of electrons from cytochrome b to cytochrome c[489].

BT16 cells were treated with vehicle (0.5% DMSO) or ABT-199 (2 µM) for either 4 or 48h timepoints. Cells were stained with MitoSOX Red dye (2.5 µM) and examined by flow cytometric analysis. Mitochondrial ROS was shown to be elevated by ABT-199 as early as 4 hours and remained elevated at the 48-hour time point indicating that the source of ROS induced by ABT-199 is at least in part mitochondrially derived.

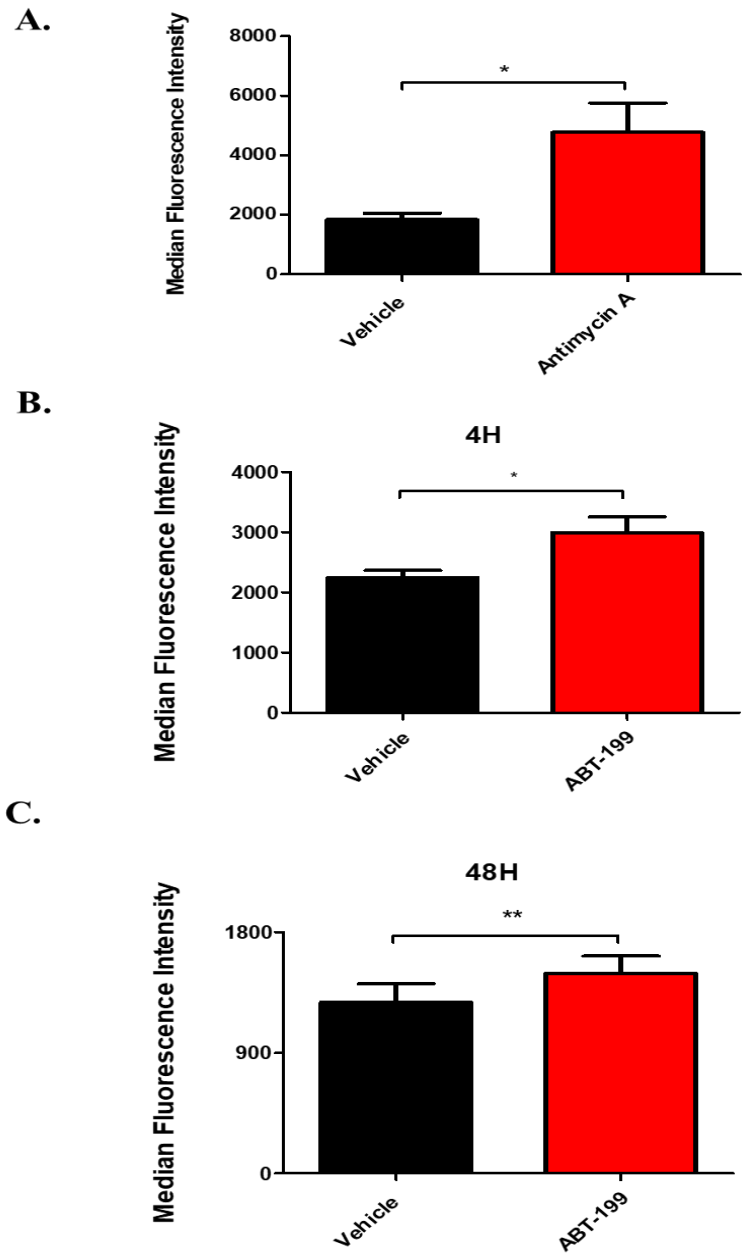

Figure 5.18. ABT-199 induces mitochondrial ROS in BT16 cells

2mL of BT16 cells were seeded in a 6-well plate at a seeding density of 1 x 10^5 cells/mL. Cells were left to adhere overnight and were treated with the vehicle (0.5% DMSO) or ABT-199 (2 µM). Antimycin A (**A**) was used as a positive control to validate the assay (10 µM treatment for 1h). After 4 (**B**) or 48 (**C**) hours, the cells were harvested, washed, and resuspended in 2.5 µM Mitosox for 20 minutes. The cells were immediately analysed by flow cytometry using the BD FACS Accuri software. 10,000 cells were gated on vehicle treated and the MFI values were obtained and normalised by the vehicle. Values represent mean ± S.E.M of three independent experiments. Statistical analysis was performed using two-tailed paired t test. *<0.5, ** $p < 0.01$.

5.2.13 ABT-199 treatment decreases oxygen consumption rate (OCR) of BT16 cells

Various studies have implicated Bcl-2 family proteins in metabolic regulation independent of cell death. Moreover, Bcl-2 overexpression has been shown to increase COX activity and promote mitochondrial respiration whereas suppression of Bcl-2 using a shRNA approach was demonstrated to inhibit mitochondrial respiration[490, 491]. Interestingly, ABT-199 has recently been shown to also inhibit basal oxygen consumption rate (OCR) in CT26 colorectal cancer cells, indicating an inhibitory effect on mitochondrial oxidative phosphorylation[487]. Given the elevation of mitochondrial ROS in response to ABT-199 treatment in BT16 cells demonstrated herein, this study next examined the effect of ABT-199 on mitochondrial respiration. To do this, the Seahorse XF Mito Stress Test was conducted on the Seahorse XFp analyser to calculate the oxygen consumption rate (OCR) as a measure of mitochondrial respiratory function. In order to optimise experimental conditions, different cell densities were plated to determine the optimal cell density for this assay (Figure 5.19). The Seahorse manufacturer Agilent recommends that the basal OCR range should be 20-160 pmol/min for optimal signal. Based on the data presented in Figure 5.19, the seeding density of 20,000 cells/well was selected for the 8-well plate. Further optimisation was carried out to determine the appropriate concentration of FCCP for use in the assay (Figure 5.20). FCCP is a potent uncoupler that disrupts ATP synthesis through proton transportation across the mitochondrial membrane. The optimal concentration of FCCP is cell-type dependent. Thus, a titration of FCCP was conducted using 6 concentrations of FCCP to determine the lowest concentration of FCCP that will elicit the highest maximal respiration rate. As shown in Figure 5.20, this dose response of FCCP showed maximal respiration at 2 µM, thus, this concentration was chosen for future experiments.

As elevated levels of mitochondrial and intracellular ROS were observed in response to 4h ABT-199 treatment, a Seahorse XF Cell Mito Stress was conducted to compare vehicle treated and ABT-199 treated cells. Results showed a significant decrease of basal OCR in response to ABT-199 and a trend of a decrease in mitochondrial OCR indicating the drug may affect mitochondrial function (Figure 5.21). To determine if this effect is enhanced over time, a longer treatment of 24 hours was performed. ABT-199 significantly decreased both basal cellular OCR and mitochondrial OCR of BT16 cells at 24 hours (Figure 5.22).

These results indicate that ABT-199 treatment can affect cellular metabolism at sub-cytotoxic concentrations.

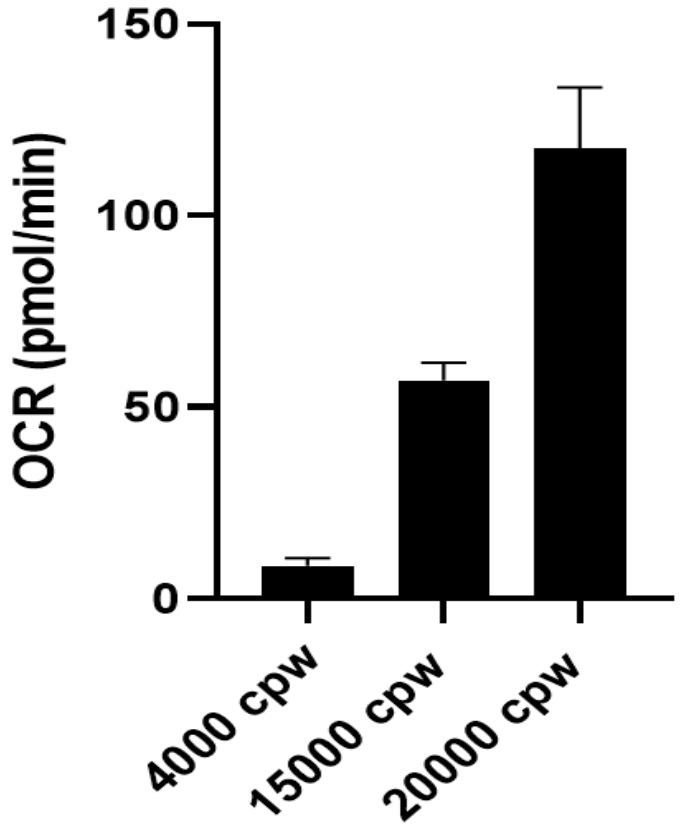

Figure 5.19 Optimisation of seeding density in BT16 cells using the Seahorse XFp analyser

BT16 cells were seeded at densities of 4,000, 15,000 and 20,000 cells per well (cpw) in XPF 8-well miniplates with a volume of 180 µL media in each well and were left to adhere overnight and reach 90% confluency. A Cell Mito Stress Test was performed the next day using the Seahorse XFp Analyser. Each seeding density was performed once in triplicate. Results were plotted using GraphPad Prism 5. Error bars represent mean ± S.E.M of triplicate determinations.

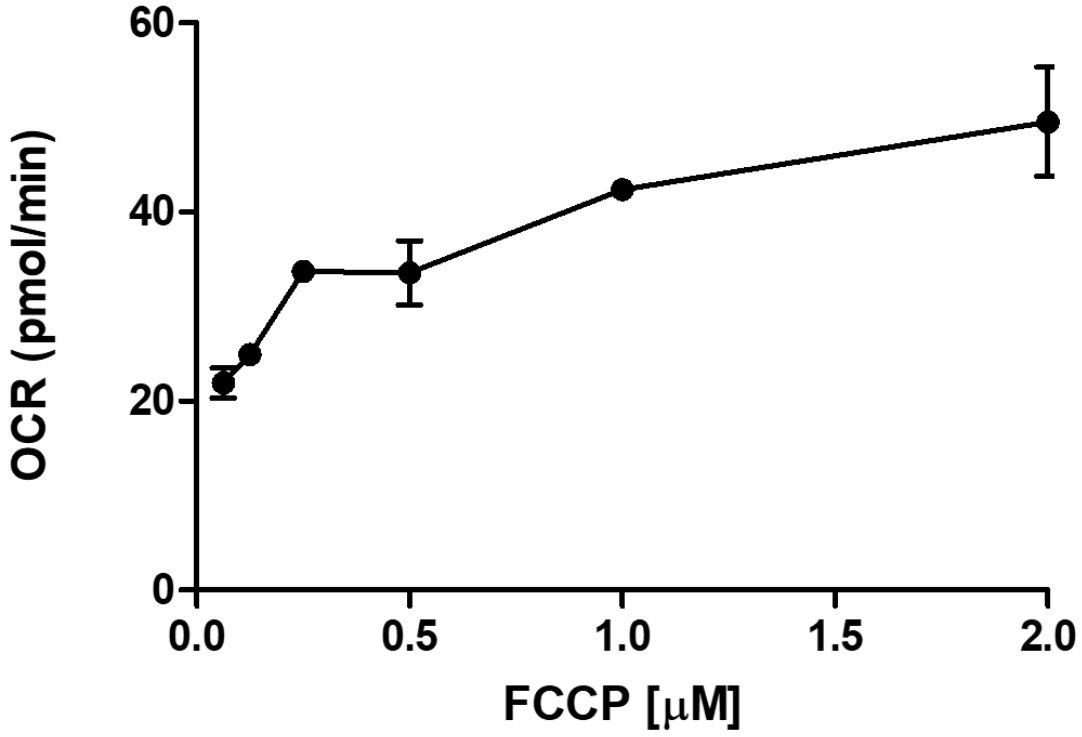

Figure 5.20 Optimisation of FCCP concentration for use in the Seahorse Analyser XFp in BT16 cells

BT16 cells were seeded at a seeding density of 20,000 cells/well. A Seahorse Cell Characterization FCCP titration test was conducted to optimise FCCP concentrations. Oxygen consumption rates (pmol/min) were measured in response to a range of FCCP concentrations (0.0625, 0.125, 0.25, 0.5, 1 and 2μM). Values represent the mean ± range of one experiment. Results were plotted using GraphPad Prism 5.

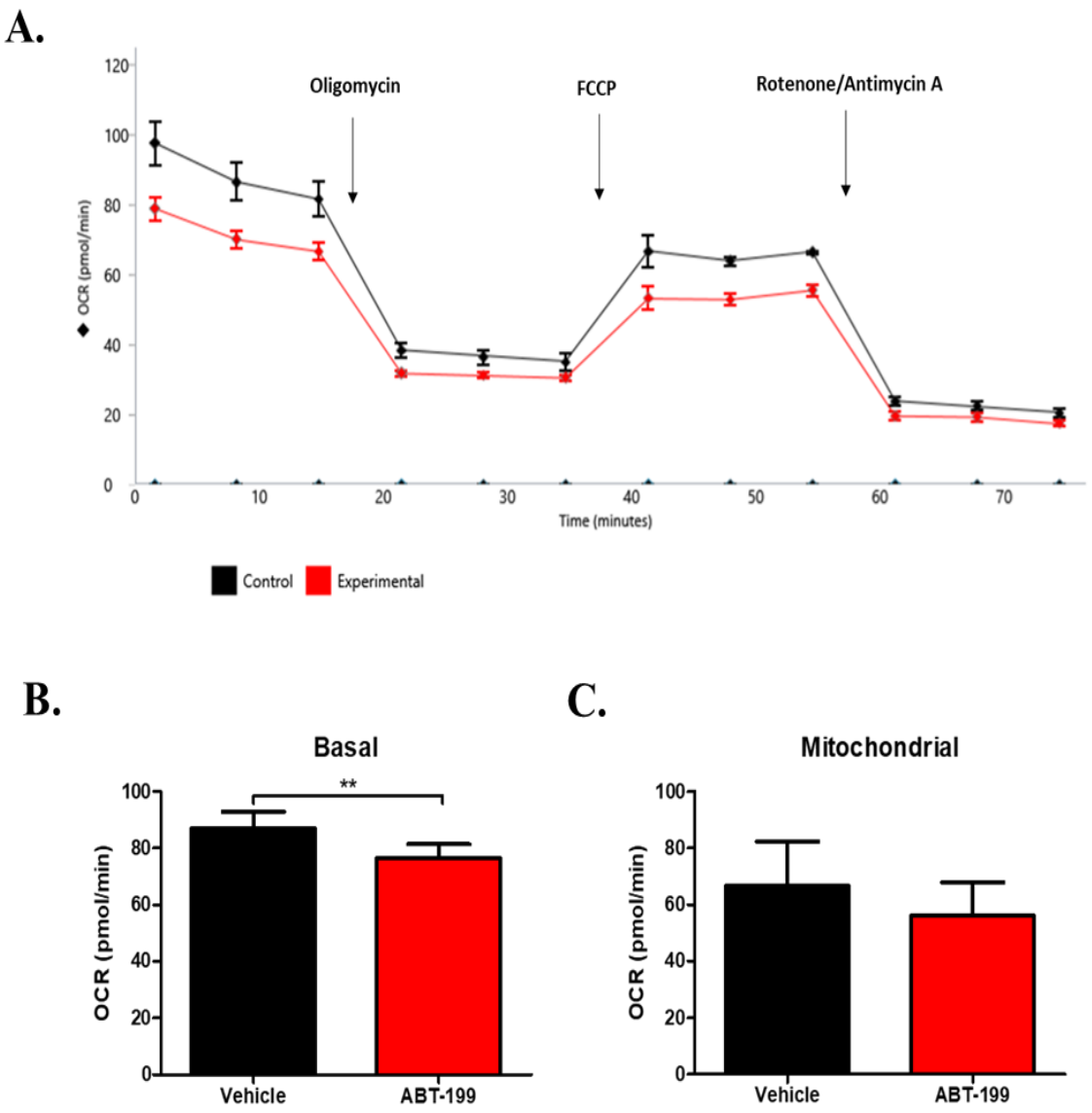

Figure 5.21 Effect of 4-hour ABT-199 treatment on cellular and mitochondrial basal oxygen consumption rates

BT16 cells were seeded at 20,000 cells/well in a Seahorse 8-well cell miniplate. Cells were treated with ABT-199 (2 µM) for 4 hours and a Cell Mito Stress Test was performed. OCR was measured in response to Oligomycin (1 µM), FCCP (2 µM) and a combination of Rotenone and Antimycin A (0.5 µM of both). **A**. A representative OCR curve of a Seahorse assay conducted three times showing the influence of the mitochondrial inhibitors. **B**. Total basal respiration. **C**. Mitochondrial respiration was calculated by subtracting the non-mitochondrial oxygen consumption rates from the total basal respiration. Values represent the mean ± S.E.M of at least 3 independent experiments

performed in triplicate. Statistical analysis was performed using two-tailed paired t test. ** $p < 0.01$.

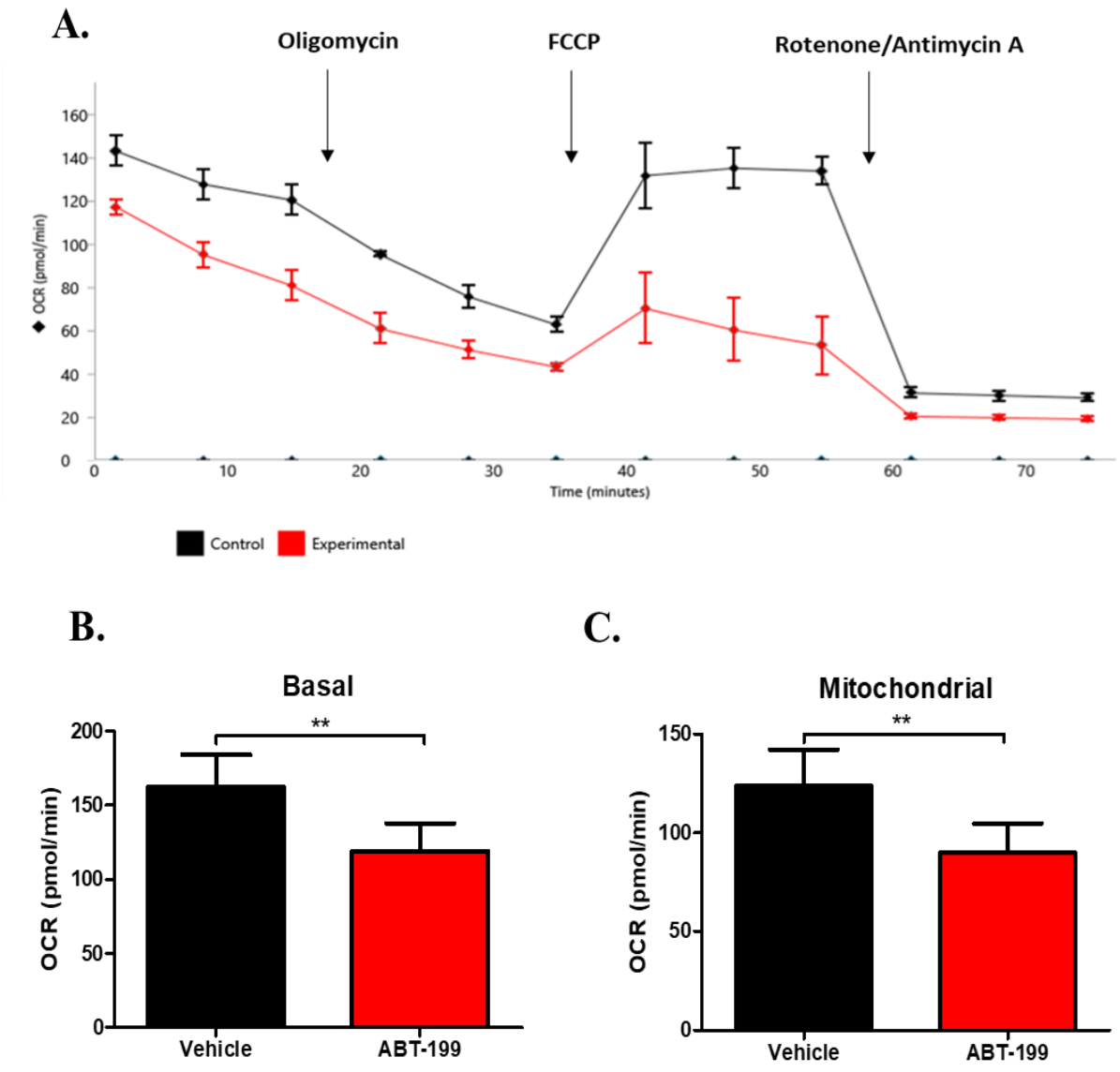

Figure 5.22 Effect of 24-hour ABT-199 treatment on cellular and mitochondrial oxygen consumption rates

BT16 cells were seeded at 20,000 cells/well in a Seahorse 8-well cell miniplate. Cells were treated with ABT-199 (2 µM) for 24 hours and a Cell Mito Stress Test was performed. OCR was measured in response to Oligomycin (1 µM), FCCP (2 µM) and a combination of Rotenone and Antimycin A (0.5 µM of both). **A**. A representative OCR curve of a Seahorse assay conducted three times showing the influence of the mitochondrial inhibitors. **B**. Total basal respiration. **C**. Mitochondrial respiration was calculated by subtracting the non-mitochondrial oxygen consumption rates from the total basal

respiration. Values represent the mean ± S.E.M of at least 3 independent experiments performed in triplicate. Statistical analysis was performed using two-tailed paired t test. ** $p < 0.01$.

5.2.14 Evaluating the effect of ABT-199 on the antioxidant response

As discussed in Chapter 4, the antioxidant response plays a critical role in mediating the cellular response to cisplatin-induced apoptosis. BT16 cells exhibit high basal levels of GSH to help them cope with the effect of oxidative stress induced by chemotherapeutics. As these cells are sensitised to cisplatin by ABT-199, this study next examined how ABT-199 impacts the antioxidant system.

Pollyea *et al*. have previously shown that ABT-199 in combination with azacytidine, diminishes glutathione thereby affecting complex II activity of the electron transport chain and thus inhibiting oxidative phosphorylation[492]. As ABT-199 has been shown to upregulate intracellular and mitochondrial ROS and downregulate basal and mitochondrial OCR in BT16 cells, GSH levels in response to ABT-199 were next monitored. Total levels of glutathione and reduced GSH were examined, and total levels were found to be significantly downregulated in response to ABT-199 (Figure 5.23).

Previous studies have linked Bcl-2 expression to GSH and ROS levels in the context of cisplatin resistance[493-495]. Given that Bcl-2 inhibition through ABT-199 treatment leads to an increase in ROS levels and a small albeit non-significant decrease in GSH in cisplatin-resistant BT16 cells, this study next examined the effect of GSH inhibition on Bcl-2 expression. Thus, cells were treated with the GSH inhibitor, BSO, cisplatin alone or a combination of cisplatin and BSO. In chapter 4, BSO has previously been shown to significantly deplete GSH levels in BT16 cells. No difference in Bcl-2 expression was observed between vehicle-treated cells and BSO-treated cells. However, Bcl-2 levels were significantly downregulated when comparing cells treated with cisplatin to cells treated with a combination of ABT-199 and cisplatin. This is perhaps due to an increase in apoptosis leading to the downregulation of the anti-apoptotic Bcl-2 protein (Figure 5.24).

Thus, this result suggests GSH depletion alone may not affect Bcl-2 expression. However, Bcl-2 inhibition through ABT-199 treatment appears to downregulate glutathione levels in BT16 cells. This may be linked to the effect of ABT-199 in upregulating ROS and its effect on impacting mitochondrial function.

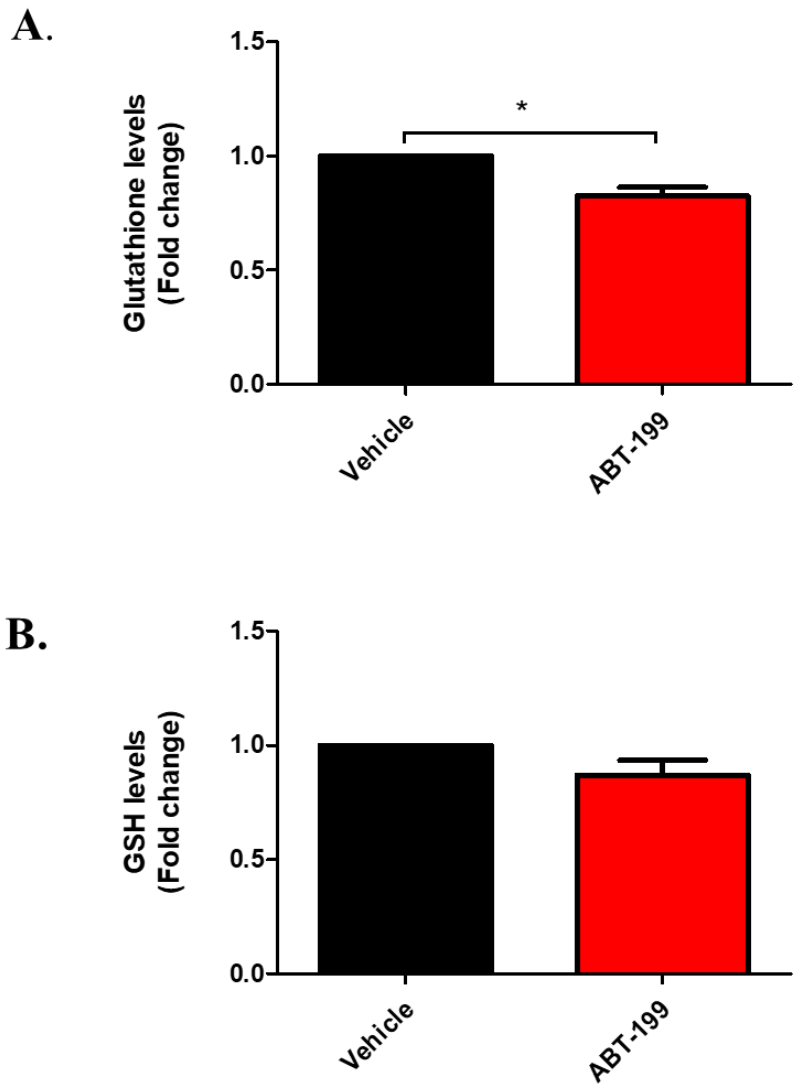

Figure 5.23 The effect of ABT-199 on total glutathione and reduced GSH levels

BT16 cells were seeded at 1 x 10^4 cells/ well in a 96-well plate. The cells were left to adhere for 24h and were then treated with 2 µM ABT-199. After 48h, they were analysed using the GSH/GSSG-Glo Kit and luminescence was measured using the Luminoskan™ Microplate Luminometer. **A**. Total glutathione levels **B**. Reduced GSH levels. Fold change values were obtained by normalising data from treated cells against the data obtained for the vehicle treated cells. Values represent the mean ± S.E.M. of three independent experiments each performed in duplicate. Statistical analysis was performed using a paired two-tailed t test. *$p<0.05$.

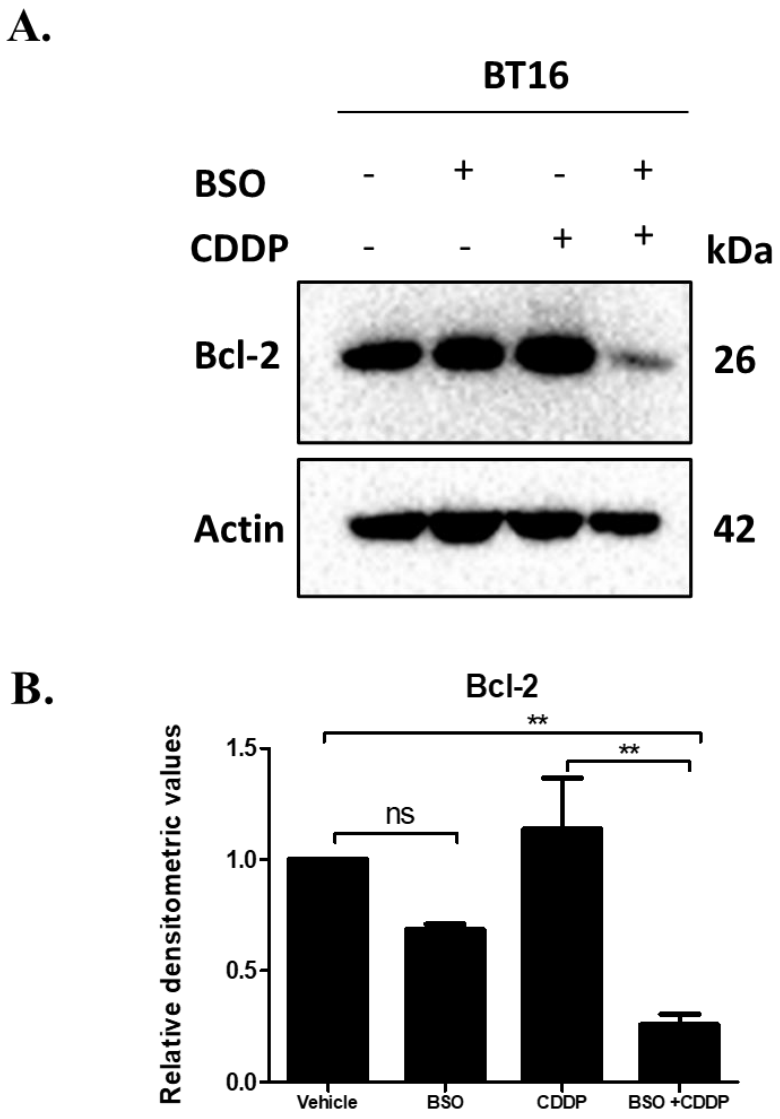

Figure 5.24 Effect of the GSH inhibitor BSO on the expression level of anti-apoptotic Bcl-2

10mL of BT12 cells were seeded in T25 flasks at a seeding density of 1 x 10^5 cells/mL. Cells were left to adhere overnight and were treated with the vehicle (0.009% NaCl), 1 µM cisplatin (CDDP), BSO (200 µM) or cisplatin and BSO in combination. After incubation, cells were harvested and lysed. 15 µg of protein was loaded onto a 15% SDS-gel, transferred onto a PVDF membrane and probed with anti-caspase 3 and anti-cleaved caspase 3 antibodies. Actin was used as a loading control **A**. Results are representative 3 independent experiments. **B** Values represent mean ± S.E.M of three independent experiments using a one-way ANOVA with Tukey's post hoc test. NS=non-significant, ** $p < 0.01$.

5.2.15 Evaluating the effect of ABT-199 on anti-apoptotic Bcl-2 family members in BT12 cells

Results presented herein have demonstrated the anti-cancer effect of ABT-199 on a panel of MRT cell lines; BT12, BT16 and G401 cells. These three cell lines have shown varying responses to ABT-199 treatment, alone and in combination with cisplatin. Results have shown that despite not expressing detectable levels of Bcl-2, the IC50 of ABT-199 in BT12 cells was similar to that of Bcl-2-positive BT16 cells (Table 5.1). Moreover, at high concentrations of ABT-199, apoptosis was induced in BT12 cells, indicating Bcl-2 independent effect of ABT-199. Furthermore, ABT-199 had no effect on cisplatin-induced apoptosis in BT12 cells. Interestingly, although ABT-199 and ABT-263 inhibit the growth of various cancer cells, there are reports that upregulation of Mcl-1 and Bcl-xL expression induced by these drugs adversely affects their anti-cancer activity[496, 497]. To further evaluate the different responses to this drug across the panel of MRT cell lines, the effect of ABT-199 alone on the expression levels of a panel of anti-apoptotic Bcl-2 family members was next examined.

BT12 cells were shown above to have no detectable levels of Bcl-2 via western blot analysis. Moreover, these cells were shown to exhibit significantly lower Bcl-xL expression levels when compared to BT16 cells. However, higher expression levels of Mcl-1 were observed in BT12 cells compared to BT16 and G401 cells (Figure 5.1). Thus, the expression levels of these proteins were next examined in response to ABT-199 treatment (2 μM). Consistent with findings with Figure 5.1, vehicle treated cells were shown to not express any detectable levels of Bcl-2, moreover no upregulation of Bcl-2 was observed in ABT-199 treated cells. Whilst BT12 cells were shown to basally express Bcl-xL and Mcl-1 in Figure 5.1, this experiment found that the expression levels were not altered upon treatment with ABT-199 (Figure 5.25).

In conclusion, ABT-199 showed no significant effect on the expression levels of selected anti-apoptotic Bcl-2 proteins in BT12 cells in response to ABT-199 treatment.

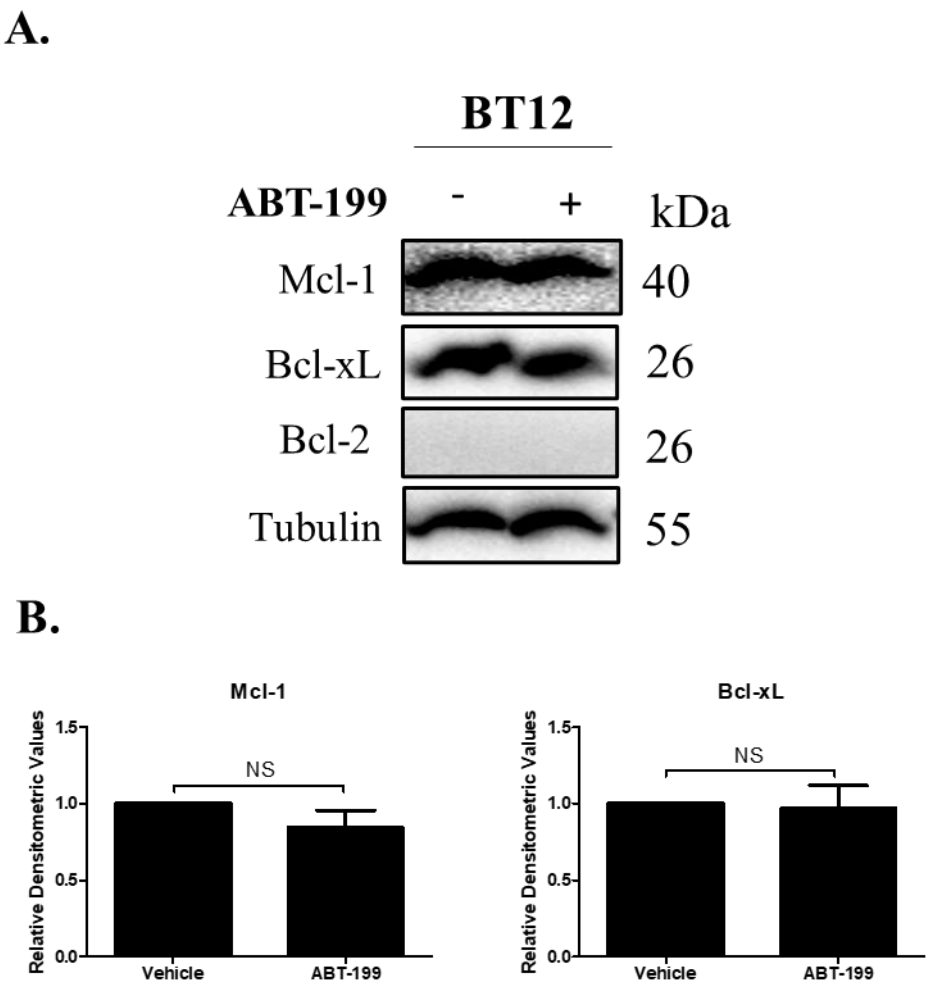

Figure 5.25 The effect of ABT-199 on Mcl-1, Bcl-xL and Bcl-2 protein expression in BT12 cells

10 mL of BT16 cells were seeded in a T25 flask at a seeding density of 1 x 10^5 cells/mL. Cells were left to adhere overnight and were then treated with the vehicle (0.5% DMSO) or ABT-199 (2 μM). After 48 hours, the cells were detached, and lysates were prepared. 15 μg of protein was loaded on a 15% gel and transferred onto PVDF membrane which was incubated overnight in Mcl-1, Bcl-xL and Bcl-2 antibodies. Tubulin served as a loading control as indicated. **A**. Results are representative 3 independent experiments. **B.** Densitometric analysis was performed using ImageLab software and the loading control was used to normalise the values obtained. Values represent mean ± S.E.M of three independent experiments using a paired t-test, NS= non-significant.

5.2.16 Evaluating the effect of ABT-199 on anti-apoptotic Bcl-2 family members in G401 cells

Alamar blue assay of ABT-199 on G401 cell viability indicated G401 cells had a higher IC50 to ABT-199 when compared to BT12 and BT16 cells (Table 5.1). Moreover, a dose-response of increasing concentrations of ABT-199 in Annexin V/PI-stained cells supported the observation that G401 cells are somewhat more resistant to ABT-199 than BT12 and BT16 cells (Figure 5.5). Furthermore, a combination of ABT-199 with both a low and high concentration of cisplatin (1 and 10 µM) showed no effect on cisplatin-induced apoptosis (Figure 5.10). It is possible G401 cells upregulate a protective compensatory pathway in response to ABT-199 treatment through the upregulation of other anti-apoptotic proteins. Indeed, ABT-199 resistance is commonly associated with Mcl-1 and Bcl-xL overexpression. For example, Choudhary *et al*., examined the mechanisms of resistance to ABT-199 in non-Hodgkin lymphoma (NHL) cell lines and described an association between acquired resistance and upregulation of Mcl-1 and Bcl-xL[497]. Thus, this study next examined the effect of ABT-199 on expression levels of Bcl-xL and Mcl-1 in G401 cells.

As seen in Figure 5.26, ABT-199 caused a significant increase in Mcl-1 and Bcl-xL. Bcl-2 was shown to be increased as well, although due to variability between replicates, this effect was not statistically significant. This result suggests a potential role for Mcl-1 and Bcl-xL upregulation in the observed resistance of G401 cells to ABT-199.

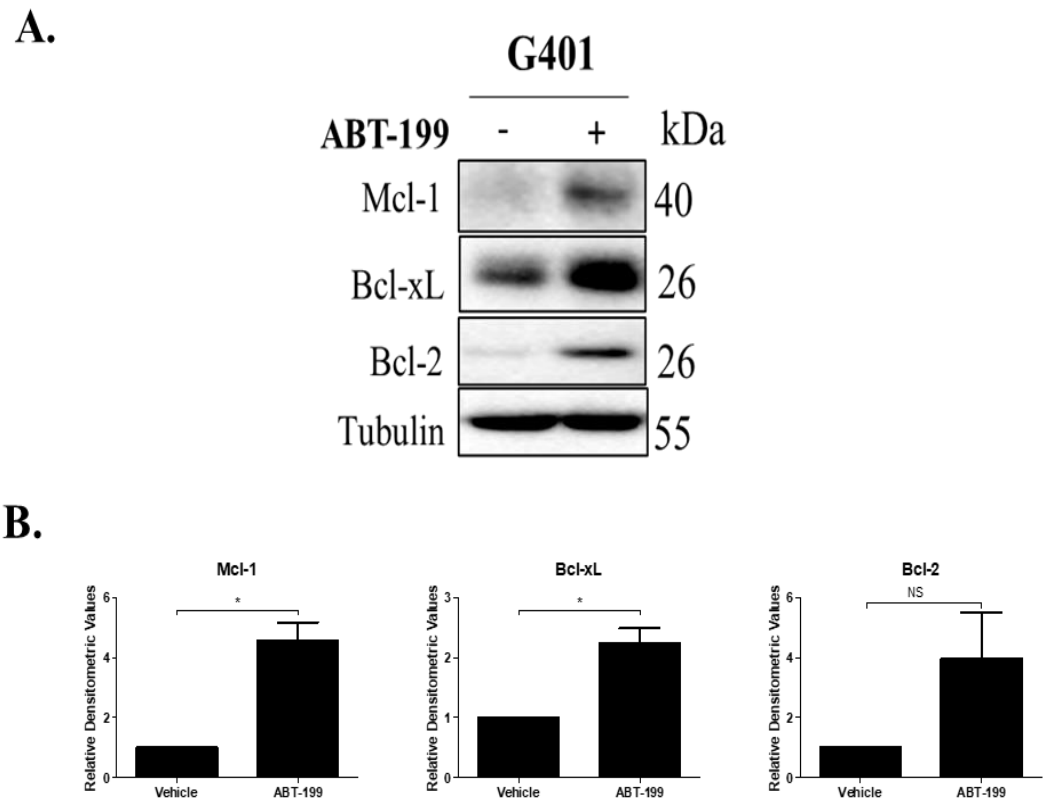

Figure 5.26 The effect of ABT-199 on Mcl-1, Bcl-2 and Bcl-xL protein expression in G401 cells

10 mL of G401 cells were seeded in a T25 flask at a seeding density of 1 x 10^5 cells/mL. Cells were left to adhere overnight and were then treated with vehicle (0.5% DMSO) or ABT-199 (2 µM). After 48 hours, the cells were detached, and lysates were prepared. 15 µg of protein was loaded on a 15% gel and transferred onto PVDF membrane which was incubated overnight in Mcl-1, Bcl-2 or Bcl-xL antibodies. Tubulin served as a loading control. **A**. Results are representative of three independent experiments. **B**. Densitometric analysis was performed using ImageLab software and the loading control was used to normalise the values obtained. Values represent mean ± S.E.M of three independent experiments using a paired two-tailed t-test. *$p<0.05$.

5.2.17 Evaluating the effect of ABT-199 anti- apoptotic Bcl-2 family members in BT16 cells

In a panel of MRT cell lines, BT12, BT16 and G401, the only cell line whereby ABT-199 showed synergistic effects with cisplatin was the cisplatin-resistant BT16 cell line. This cell line also demonstrated high basal expression levels of Bcl-2. To further understand the mechanism of action behind the synergism of ABT-199 with cisplatin in BT16 cells, the effect of treatment with these drugs on the expression levels of a series of anti-apoptotic Bcl-2 family member proteins was assessed.

ABT-199 is believed to selectively bind directly to the BH3-binding groove of Bcl-2, displacing Bim and other BH3-only proteins which can then activate Bax/Bak[498]. However, recent studies have shown that ABT-199 may have other effects on the apoptotic machinery in cancer cells. For example, ABT-199 has been shown to induce Mcl-1 upregulation in AML cells[499]. In contrast, Weller *et al*, observed downregulation of Mcl-1 in sarcoma cell lines[500]. Thus, this study aimed to examine the mechanism of action of ABT-199 in BT16 cells by assessing whether it may affect the expression level of other Bcl-2 family proteins involved in apoptosis.

BT16 cells were treated with 2 µM ABT-199, which was previously shown to elicit a synergistic effect on cell death with cisplatin. However, no significant effect was observed on Bcl-2 expression levels (Figure 5.27). This is often observed in studies on ABT-199. As the BH3 mimetic binds directly to Bcl-2, it does not necessarily decrease its expression levels[501, 502]. Furthermore, no difference was observed in Bcl-xL expression levels in response to ABT-199 treatment, either alone or in combination with cisplatin. Interestingly, Mcl-1 degradation was observed in response to ABT-199 treatment, both alone and in combination with cisplatin, suggesting that ABT-199 may indeed target anti-apoptotic Bcl-2 proteins other than Bcl-2 alone.

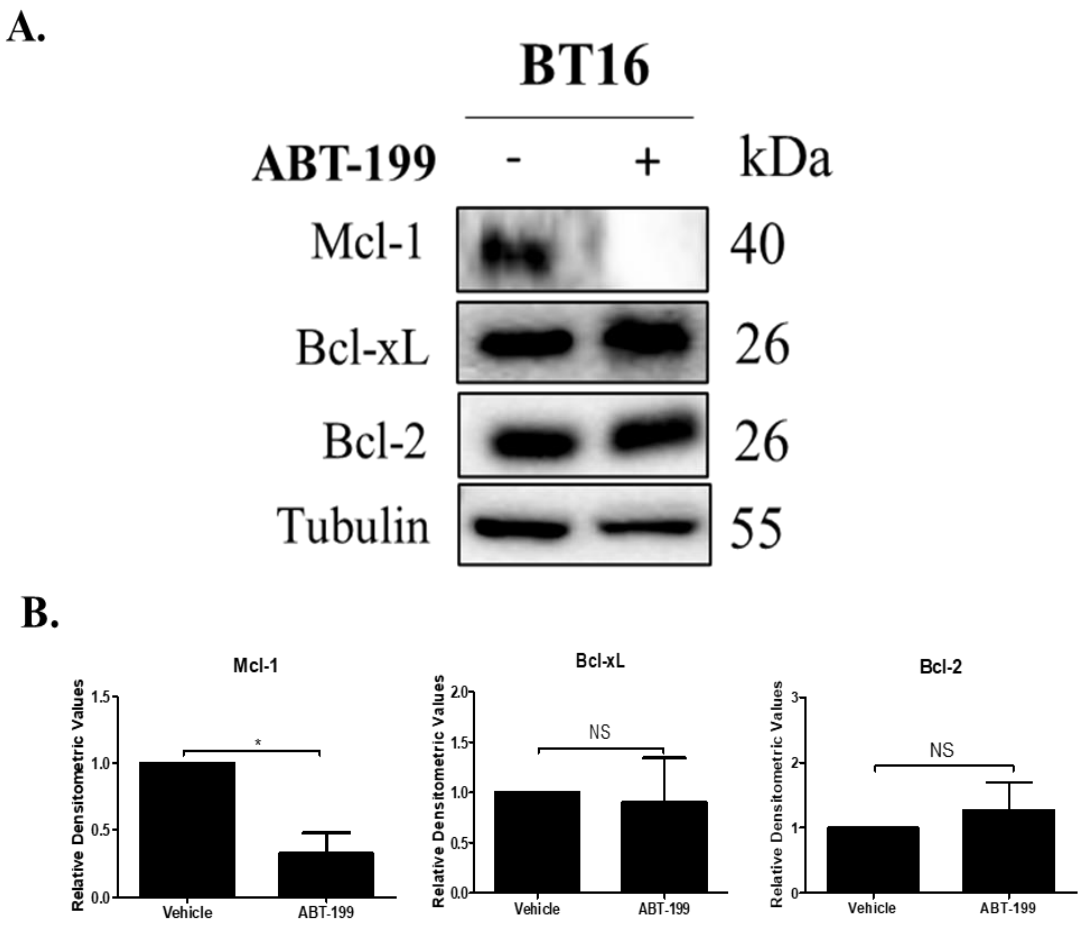

Figure 5.27 The effect of ABT-199, alone and in combination, on Mcl-1, Bcl-xL and Bcl-2 protein expression in BT16 cells

10 mL of BT16 cells were seeded in a T25 flask at a seeding density of 1 x 10^5 cells/mL. Cells were left to adhere overnight and were then treated with the vehicle (0.05% DMSO) or ABT-199 (2 µM). After 48 hours, the cells were detached, and lysates were prepared. 15 µg of protein was loaded on a 15% gel and transferred onto PVDF membrane which was incubated overnight in Mcl-1, Bcl-2 and Bcl-xL antibodies. Tubulin served as a loading control. **A** Results are representative of three experiments for Bcl-2, Mcl-1 and Bcl-xL. **B** Densitometric analysis was performed using ImageLab software and the loading control was used to normalise the values obtained. Values represent mean ± S.E.M. of three experiments. Statistical analysis was performed using a paired two-tailed test.* $p < 0.05$.

5.2.18 Mcl-1 degradation contributes to the synergistic effect of ABT-199 and cisplatin on cell death in BT16 cells

Despite the reported selective nature of ABT-199 for Bcl-2, significant degradation of Mcl-1 expression was observed in response to treatment with ABT-199 (Figure 5.27). This result was unexpected, as 2 μM ABT-199 is non-cytotoxic in BT16 cells, therefore Mcl-1 downregulation is not a result of high levels of cell death in these cells. Mcl-1 has a short half-life and is reported to be rapidly degraded by the ubiquitin proteasome system[503, 504]. This study next examined whether this Mcl-1 downregulation is related to the synergistic effect of ABT-199 and cisplatin on cell death.

To do this, BT16 cells were pre-treated with the proteosome inhibitor, bortezomib (10nM), to prevent Mcl-1 degradation, prior to treatment for a further 48 hours with ABT-199 and cisplatin in combination. Rapino *et al*, have previously demonstrated that Bortezomib attenuated apoptosis induced by taxol by inhibiting Mcl-1 degradation[505]. As observed in Figure 5.28, Mcl-1 degradation was prevented by bortezomib treatment and moreover, this reversed the synergistic effect of ABT-199 and cisplatin on apoptosis in BT16 cells. This result suggests that ABT-199 induced Mcl-1 degradation is involved in the mechanism underlying ABT-199 and cisplatin synergy.

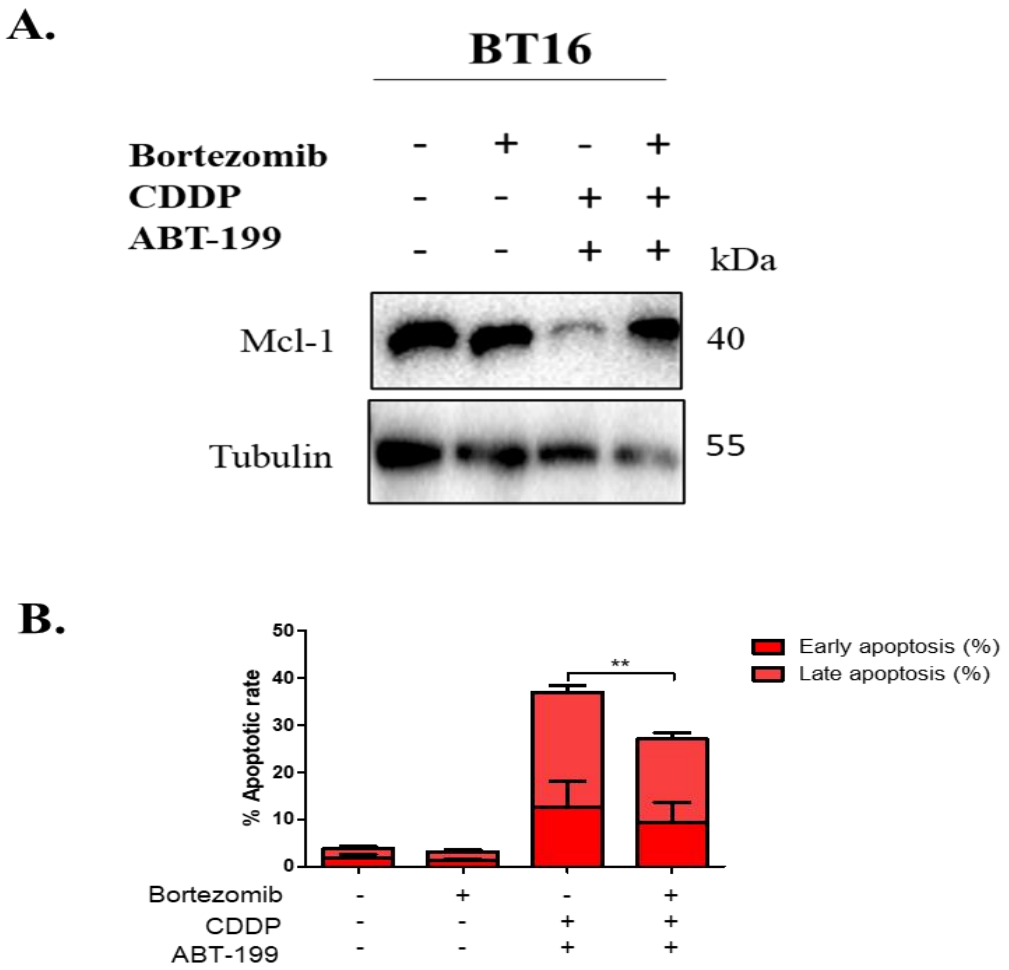

Figure 5.28 Bortezomib reverses the synergistic effect on cell death mediated by ABT-199 and cisplatin

2mL of BT16 cells were seeded in a 6-well plate at a seeding density of 1 x 10^5 cells/mL. Cells were left to adhere overnight and were then treated with the vehicle (0.5% (v/v) DMSO) or a combination of cisplatin (10µM) and ABT-199 (2µM) alone, or with a pre-treatment of Bortezomib (10 nM for 1 hour). After 48 hours, the cells were harvested and **(A)** lysed and loaded on 15% gel SDS-page gel, transferred to PVDF, and probed with Mcl-1 antibody. Tubulin served as a loading control. Results are representative of three independent experiments. **B**. Cells were collected and stained with Annexin V-FITC and propidium iodide (PI). The cells were immediately analysed by flow cytometry using the BD FACS Accuri software. 10,000 cells were gated on vehicle treated cells and the percentage of cells undergoing early and late apoptosis was determined to be those stained with Annexin V only or stained with both Annexin V and PI, respectively. Values represent mean ± S.E.M of three independent experiments. Statistical analysis was performed using a paired t test.**$p < 0.01$.

5.2.19 Co-treatment of BT16 cells with ABT-199 and cisplatin upregulates expression of active Bak

The pro-apoptotic protein Bak is often considered to be functionally equivalent with Bax, despite their distinct localisation. Bax is mostly cytosolic, whereas Bak is mostly situated in the outer membrane of the mitochondria and endoplasmic reticulum[506]. Bak and Bax are known to dimerise and lead to MOMP. Bax is believed to be negatively regulated through binding to Bcl-2. In contrast, Bak is sequestered by Mcl-1. Thus, regulation of these proteins can be categorised by the Bcl-2/Bax axis and the Mcl-1/Bak axis [500, 506]. Willis *et al*, characterised the interaction between Mcl-1 and Bak and proposed that Bak is inhibited through sequestration by Mcl-1. Bak can be displaced and activated by Noxa, which has been shown to displace Mcl-1 and promote its degradation[506]. Therefore, this study hypothesised that Mcl-1 degradation may lead to upregulation of the active form of Bak. Upon activation, Bak undergoes a conformational change for the purpose of homo-dimerisation and permeabilisation of the outer mitochondrial membrane[184].

ABT-199 was shown to synergistically enhance apoptosis levels induced by 10 µM cisplatin by 20% (Figure 5.7). In addition to this, ABT-199 sensitised BT16 cells to a non-cytotoxic concentration of 1 µM cisplatin (Figure 5.0). Thus, BT16 cells were treated with ABT-199 alone or combination with both concentrations of cisplatin (1 and 10 µM) and the levels of active Bak were assessed by western blotting. As shown in Figure 5.29, co-treatment of ABT-199 with either 1 or 10 µM cisplatin significantly enhanced expression of active Bak when compared to either treatment alone, indicating that this may be linked to the observed synergistic enhancement in apoptosis and decrease in Mcl-1 levels.

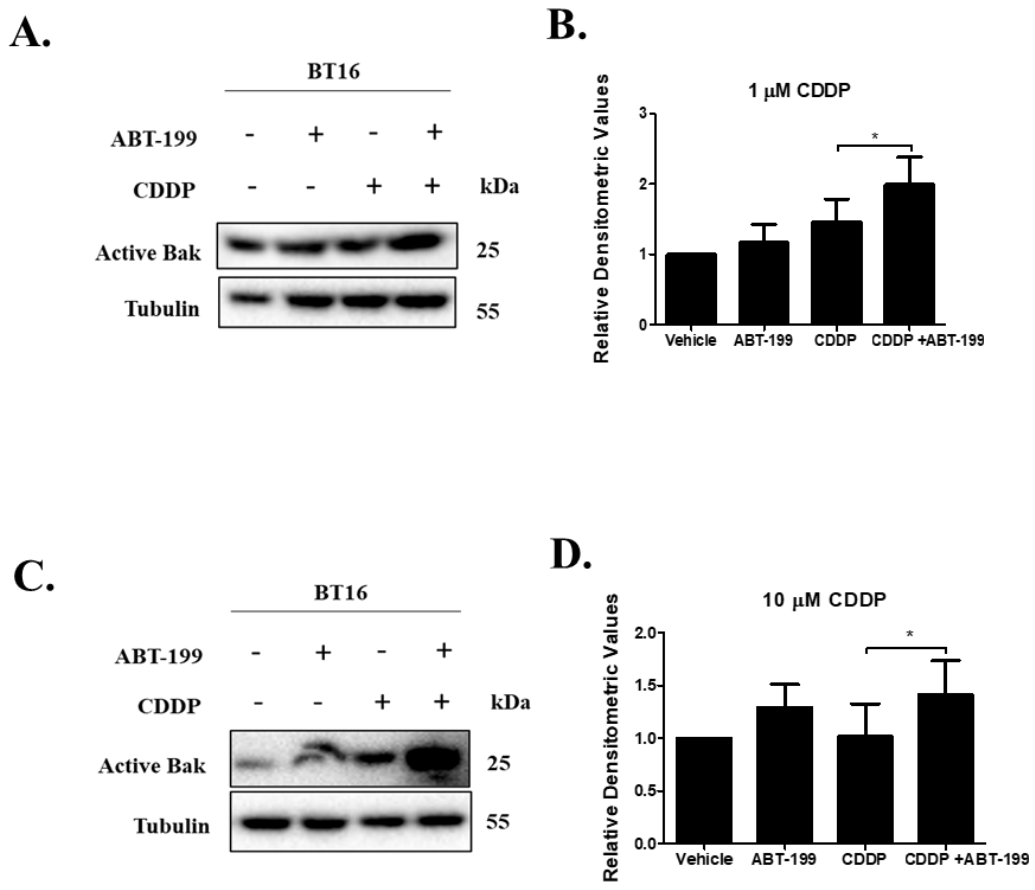

Figure 5.29 The effect of ABT-199 and cisplatin on active Bak protein expression in BT16 cells

10 mL of BT16 cells were seeded in a T25 flask at a seeding density of 1 x 10^5 cells/mL. Cells were left to adhere overnight and were then treated with the vehicle, ABT-199 (2 µM) or CDDP (1 or 10µM) alone and in combination. After 48 hours, the cells were detached, and lysates were prepared. 15 µg of protein was loaded on a 15% gel and transferred onto PVDF membrane which was incubated overnight in active Bak antibody. Tubulin served as a loading control. **A** Results are representative of three experiments of cells treated with 1 µM cisplatin and ABT-199 alone or in combination. **B** Densitometric analysis was performed using ImageLab software and the loading control was used to normalise the values obtained. **C**. Results are representative of three experiments of cells treated with 10 µM cisplatin and ABT-199 alone or in combination. **D**. Densitometric analysis was performed using ImageLab software and the loading control was used to normalise the values obtained. Values represent mean ± S.E.M. of three experiments. Statistical analysis was performed using a one-way ANOVA with Tukey's post hoc test.* $p < 0.05$.

5.2.20 ABT-199 has no effect on expression levels of the anti-apoptotic proteins XIAP, cIAP1 and cFLIP

Results presented so far have demonstrated that ABT-199 sensitises BT16 cells to cisplatin and both ROS accumulation and Mcl-1 degradation are involved in this process. Further work was carried out to understand the link between ABT-199-induced ROS upregulation and Mcl-1 downregulation by examining the effect on expression levels of various other anti-apoptotic proteins including c-FLIP, an endogenous negative regulator of DISC formation and XIAP, a member of the inhibitor of apoptosis (IAP) protein family

A study by Lee *et al*., previously demonstrated that ROS-induced Mcl-1 degradation was observed alongside proteasome-mediated degradation of cFLIP, thereby sensitising cells to TRAIL-induced apoptosis by the anti-tumour isoquinoline alkaloid berberine[507]**.** BT16 cells were treated with ABT-199 and cisplatin, alone and in combination and western blot analysis of the expression levels of cFLIP was examined, alongside the expression levels of IAPs, cIAP1 and XIAP (Figure 5.30). Results demonstrated that ABT-199 did not induce degradation of any of these three proteins. This result suggests that the ROS/cFLIP degradation pathway observed by Lee *et al*., is not activated by ABT-199 in BT16 cells. Moreover, the two IAP proteins, XIAP and cIAP1 are also not affected by ABT-199 treatment.

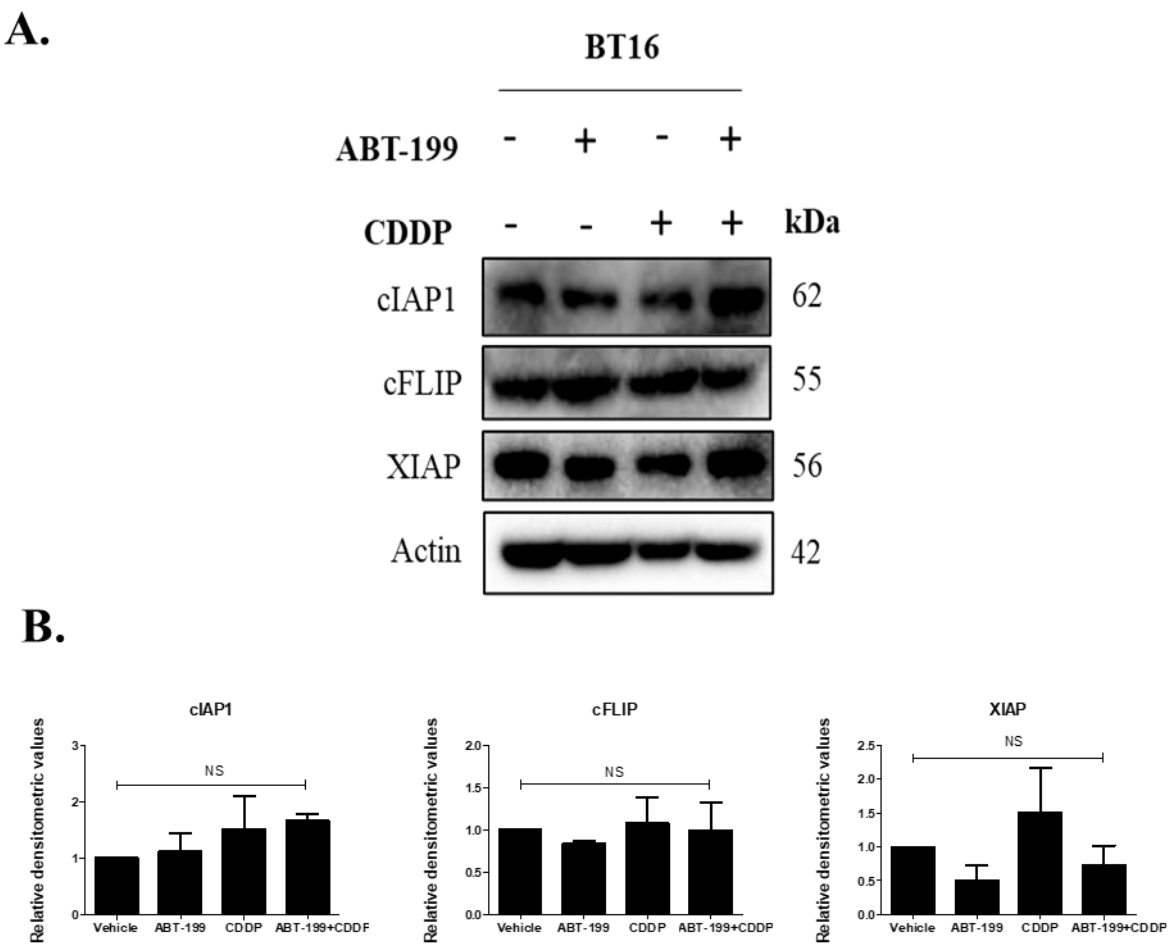

Figure 5.30 ABT-199, both alone and in combination with cisplatin, has no effect on cIAP1, cFLIP and XIAP protein expression levels in BT16 cells

10 mL of BT16 cells were seeded in a T25 flask at a seeding density of 1 x 10^5 cells/mL. Cells were left to adhere overnight and were then treated with the vehicle, ABT-199 (2 µM) or CDDP (10µM) alone and in combination. After 48 hours, the cells were detached, and lysates were prepared. 15 µg of protein was loaded on a 15% gel and transferred onto PVDF membrane which was incubated overnight in cIAP1, cFLIP and XIAP antibodies. Actin served as a loading control. Results are representative of three experiments. Statistical analysis was performed using a one-way ANOVA with Tukey's post hoc test. NS= non-significant.

5.2.21 ABT-199 treatment upregulates the expression of the negative Mcl-1 regulator, Noxa

This study next turned its focus on another potential mechanism by which Mcl-1 may be degraded, namely Noxa. The pro-apoptotic BH3-only protein Noxa is one of the key binding partners and inhibitors of Mcl-1, preventing it in turn from binding to and neutralising Bax and Bak[508]. Moreover, proteasome-dependent degradation of Mcl-1 involves this interaction with Noxa[509, 510]. In addition, previous reports have shown that Noxa can be upregulated by ROS accumulation. Tonino *et al*, have shown that Noxa is upregulated in response to ROS generated by cisplatin and fludarabine (F-ara-A), an antimetabolite, which together were shown to synergistically enhance cell death in CLL through ROS/Noxa upregulation[511]. Moreover, in mantle-cell lymphoma (MCL), treatment with ROS scavenger inhibited Noxa upregulation[512]. Thus, this study hypothesised that Mcl-1 degradation observed in response to ABT-199 treatment may be induced by upregulation of Noxa.

To test this hypothesis, BT16 cells were treated with 2 μM ABT-199 for 48 hours; the sub-cytotoxic concentration that sensitises BT16 cells to cisplatin, induces ROS, inhibits mitochondrial respiration and induces Mcl-1 degradation. Western blot analysis was conducted on Noxa expression levels and results demonstrated that Noxa was indeed significantly upregulated in response to ABT-199 treatment.

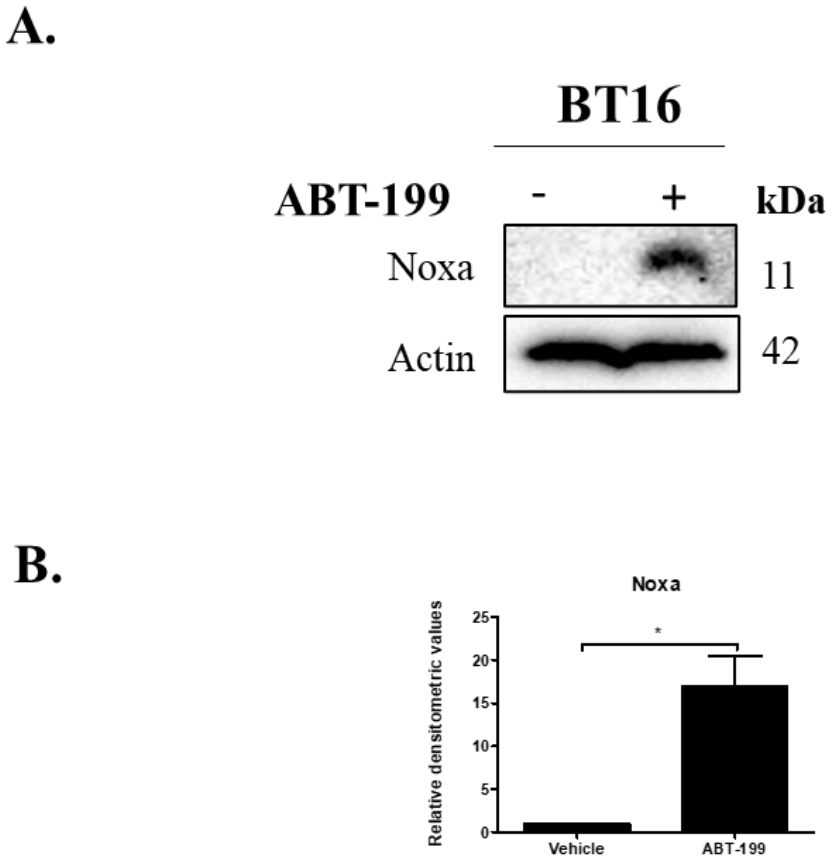

Figure 5.31 ABT-199 significantly upregulates Noxa expression levels in BT16 cells

10 mL of BT16 cells were seeded in a T25 flask at a seeding density of 1 x 10^5 cells/mL. Cells were left to adhere overnight and were then treated with the vehicle (0.05% DMSO) or ABT-199 (2 μM). After 48 hours, the cells were detached, and lysates were prepared. 15 μg of protein was loaded on a 15% gel and transferred onto PVDF membrane which was incubated overnight in anti-Noxa antibody. Actin served as a loading control. **A**. Results are representative of three experiments. **B**. Densitometric analysis was performed using ImageLab software and the loading control was used to normalise the values obtained. Values represent mean ± S.E.M. of three experiments. Statistical analysis was performed using a paired two-tailed test.* $p < 0.05$.

5.22 ABT-199 treatment induces activation of the p38 MAPK pathway but not JNK

Having proposed that ABT-199 induced Noxa upregulation and Mcl-1 degradation, which may potentially be linked to ROS accumulation, the effect of ABT-199 on the JNK and p38 MAPK signalling pathways was next examined.

Chiou *et al*, have shown that ABT-199 in combination with the Bcl-xL inhibitor WEHI-597 can synergistically enhance Mcl-1 degradation and apoptosis in human leukaemia cells mediated through ROS/p38 MAPK/Noxa upregulation[57]. However, there are a limited number of studies that have linked ROS mediated Noxa upregulation with JNK activation. Thus, this study next evaluated whether either of these pathways is potentially activated in response to ROS accumulation induced by ABT-199.

BT16 cells were treated with ABT-199 alone and in combination with cisplatin. Results demonstrated induction of phosphorylated and thus activated p38 in response to ABT-199 treatment. Moreover, and similar to results observed by Chiou *et al*, in leukaemia cells, ABT-199 had no effect on JNK signalling.

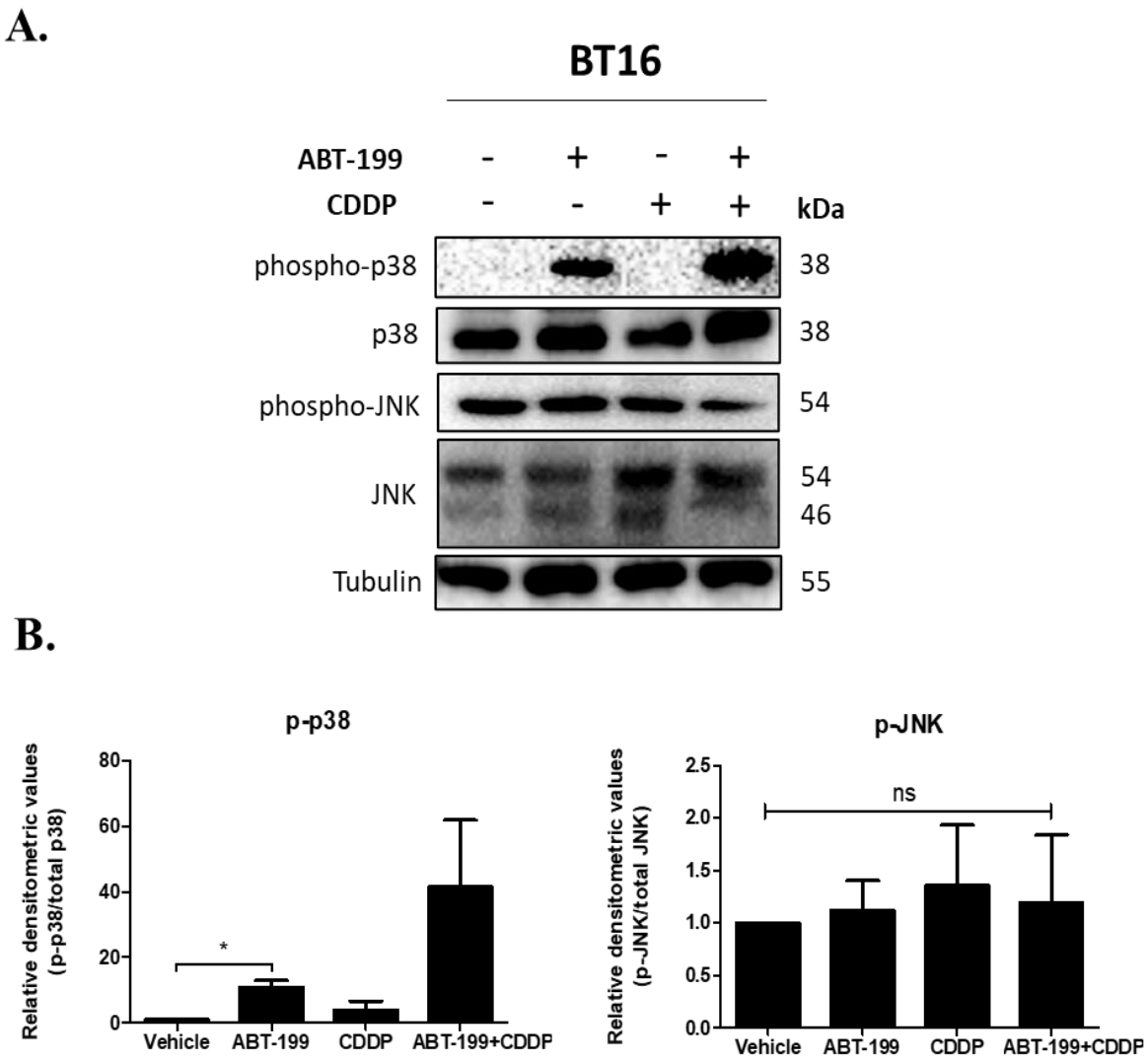

Figure 5.32 ABT-199, alone and in combination with cisplatin, induces activation of p38 MAPK but has no effect on JNK

10 mL of BT16 cells were seeded in a T25 flask at a seeding density of 1 x 10^5 cells/mL. Cells were left to adhere overnight and were then treated with the vehicle, ABT-199 (2 μM) or CDDP (10μM) alone and in combination. After 48 hours, the cells were detached, and lysates were prepared. 15 μg of protein was loaded on a 15% gel and transferred onto PVDF membrane which was incubated overnight in phospho-p38, total p38, phospho-JNK and total JNK antibodies. Tubulin served as a loading control. **A.** Results are representative of three experiments. **B**. Densitometric analysis was performed using ImageLab software and the loading control was used to normalise the values obtained. Statistical analysis was performed using a paired two-tailed test.* $p < 0.05$ Values represent mean ± S.E.M. of three experiments.

5.2.23 NAC treatment reverses ABT-199 induced Mcl-1 degradation in BT16 cells

Results so far have shown that 2 µM ABT-199, although non-cytotoxic alone, enhances cisplatin-induced apoptosis by approximately 20%. Moreover, at this concentration ROS levels have been shown to be significantly enhanced alone and in combination with cisplatin. Pre-treatment with the ROS scavenger NAC has been shown to prevent this enhancement of cisplatin-induced apoptosis observed in response to treatment with ABT-199. Mitochondrial ROS levels are significantly elevated and basal /mitochondrial OCR is significantly inhibited. Interestingly, Mcl-1 appears to be degraded upon treatment with this concentration of ABT-199 and this degradation has been shown to contribute to its synergy with cisplatin. In order to establish whether Mcl-1 degradation may be linked to the elevated ROS levels observed, cells were pre-treated with NAC for 1 hour prior to ABT-199 and cisplatin treatment and Mcl-1 expression was examined by western blot analysis (Figure 5.33). Results showed that Mcl-1 degradation was significantly reduced by NAC pre-treatment when compared to cells that were treated with ABT-199 and cisplatin.

This result suggests that Mcl-1 degradation is linked to the elevated levels of ROS in response to ABT-199 treatment and this is a crucial part of the mechanism underlying ABT-199 and cisplatin synergy. Moreover, no synergy was observed in BT12 and G401 cells which also displayed no degradation of Mcl-1 or elevation of ROS in response to ABT-199 treatment.

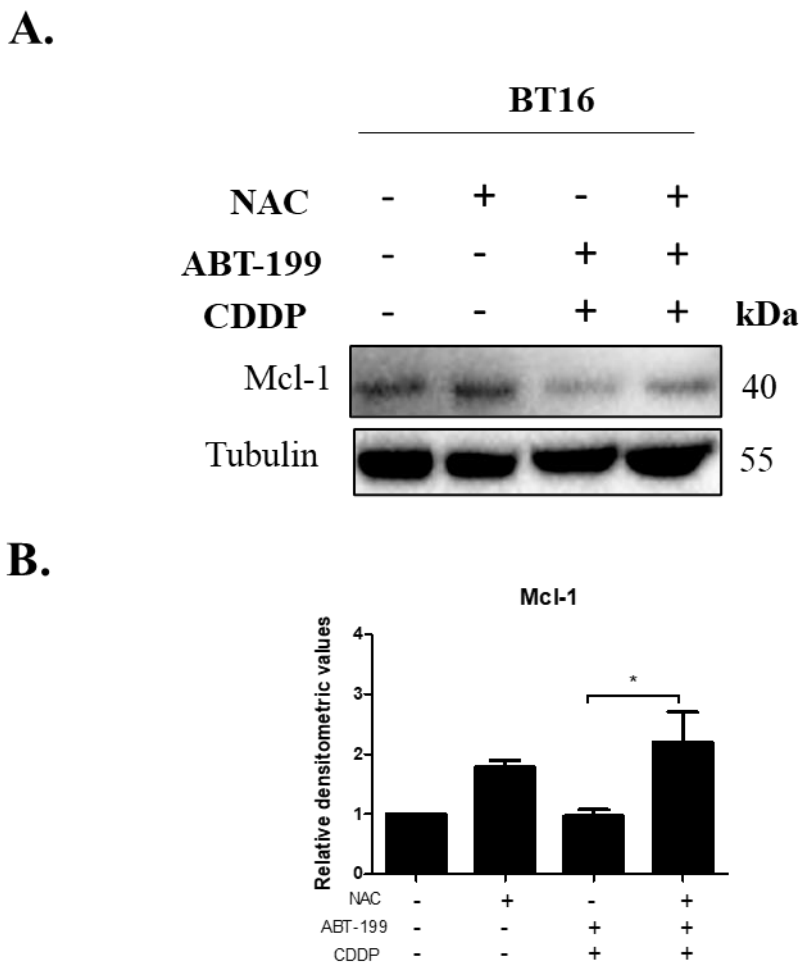

Figure 5.33 NAC treatment reduces Mcl-1 degradation induced by ABT-199 and cisplatin

10 mL of BT16 cells were seeded in a T25 flask at a seeding density of 1 x 10^5 cells/mL. Cells were left to adhere overnight and were then treated with the vehicle, NAC (5 mM), a combination of ABT-199 (2 µM) and CDDP (10µM) alone or with 1 hour pre-treatment of NAC. After 48 hours, the cells were detached, and lysates were prepared. 15 µg of protein was loaded on a 15% gel and transferred onto PVDF membrane which was incubated overnight in Mcl-1 antibody. Tubulin served as a loading control. **A.** Results are representative of three experiments. **B**. Densitometric analysis was performed using ImageLab software and the loading control was used to normalise the values obtained. Values represent mean ± S.E.M. of three experiments. Statistical analysis was performed using a one-way ANOVA with Tukey's post hoc test.* $p < 0.05$.

5.3 Discussion

Currently, the standard treatment for MRT, is a combination of surgical resection with chemotherapy and radiation therapy, as is the case for most cancers. Unfortunately, rhabdoid tumours present a high level of resistance to treatment and are associated with very poor prognosis due to their aggressive and metastatic nature. These characteristics also lead to the need for aggressive therapeutic regimens to improve survival, often in very young patients. However, this can lead to severe side effects. Therefore, novel treatment strategies are necessary to improve patient survival and health.

Evasion of apoptosis is one of the hallmarks of cancer. Overall, the relative expression and interaction of pro-apoptotic, anti-apoptotic, and BH3-only proteins regulate apoptosis in cells. Ample evidence indicates that promotion of chemoresistance and survival of cancer cells may be attributed to altered anti-apoptotic protein expression and inhibition of pro-apoptotic proteins. Indeed, many cancer cells have been found to overexpress one or more anti-apoptotic Bcl-2 proteins such as Bcl-2, Bcl-xL and Mcl-1. These proteins contain a hydrophobic groove that binds to the face of the amphipathic, alpha helical BH3 domain in every Bcl-2 protein. BH3 mimetics are a class of compounds that can compete for this hydrophobic groove in order to inhibit anti-apoptotic protein activity. The development of these BH3 mimetics has shown great pre-clinical promise and many have now passed regulatory approval and entered the clinic[462]. The Bcl-2 inhibitor, ABT-737, which targets Bcl-2, Bcl-xL and Bcl-w was one of the first BH-3 mimetics to be developed and was shown to be effective *in vitro* against myeloma, acute leukaemia and lymphoma. Moreover, this effectiveness was replicated *in vivo* in mouse xenograft models. Unfortunately, ABT-737 did not enter the clinic as it was not orally bioavailable and had low solubility. ABT-263 (Navitoclax), another inhibitor of Bcl-2, Bcl-xL and Bcl-w, was developed and having shown great pre-clinical promise, entered clinical trials in lymphoid malignancies and CLL[513]. However, due to its ability to target Bcl-xL, a protein which platelets are dependent on, thrombocytopenia emerged as a toxic side effect that limited the utility of this drug. Therefore, a selective Bcl-2 inhibitor, ABT-199, was developed and is now clinically approved for the treatment of AML and CLL[514].

ABT-199 has been shown to be very effective alone and in combination with other therapies such as tyrosine kinase inhibitors (TKI) including imatinib, in haematological malignancies[514]. However, resistance to ABT-199 has been observed in certain cancers

primarily due to overexpression of other anti-apoptotic Bcl-2 proteins such as Mcl-1 and Bcl-xL. This was observed through BH3 profiling in a phase II study of ABT-199 monotherapy in relapsed/refractory AML patients where those patients with higher dependencies on Bcl-xL and Mcl-1 showed poorer responses to ABT-199 treatment. Therefore, one avenue of research is focusing on Mcl-1 inhibitors as potential combination therapies with ABT-199[237].

Furthermore, recent studies are now examining the potential of BH-3 mimetics in the treatment of solid tumours, more specifically in combination with other known effective cancer therapies[469]. Oakes *et al*. have shown that breast tumours that overexpress Bcl-2 are sensitised to chemotherapeutics by ABT-737[515]. Potter *et al.*, used dynamic BH3 profiling to construct drug regimens for NSCLC and found that the combination of ABT-263 and etoposide significantly reduced tumour burden in a xenograft mouse model[33]. Interestingly, Alcon *et al*, have shown that chemotherapeutic agents vincristine and doxorubicin combined with BH3 mimetics such as S63845 and A-1331852 exhibited anti-cancer efficacy in patient-derived xenografts of rhabdomyosarcoma[516].

The role of the Bcl-2 family of proteins in mediating chemoresistance in rhabdoid tumours remains unclear. This present study characterised the expression levels of a series of anti-apoptotic and pro-apoptotic members of the Bcl-2 family of proteins in a panel of MRT cell lines and assessed whether they may play a role in determination of cisplatin cytotoxicity.

Firstly, expression of a series of anti-apoptotic Bcl-2 proteins (Mcl-1, Bcl-2 and Bcl-xL) was assessed in the three MRT cell lines with cells displaying varying levels of these proteins. Most notably, cisplatin-sensitive BT12 cells did not express any detectable levels of Bcl-2 protein when compared to the more cisplatin resistant BT16 and G401 cells which expressed significantly higher levels of this protein. This result indicates a possible role for Bcl-2 in mediating cisplatin resistance in MRT. Interestingly, Michaud *et al*, have shown that Bcl-2 overexpression is also correlated with cisplatin resistance in advanced oropharyngeal squamous cell carcinoma[517]. Moreover, Bahar *et al*, established two cisplatin-resistant ovarian cancer sublines from parental SKOV3 and OV-90 cell lines, each through pulse dosing and stepwise dose escalation methods. Both these cisplatin-resistant cell lines expressed significantly elevated Bcl-2 levels when compared to their parental cell line[518]. In this study, the cisplatin-resistant BT16 cell line was also found to

have the highest expression of Bcl-xL while expression levels of Mcl-1 were significantly higher in cisplatin sensitive BT12 cells. It is widely accepted that cancer cells have dependencies on different anti-apoptotic proteins, suggesting that despite expressing low levels of Bcl-xL and no Bcl-2, BT12 cells may have a higher dependency on Mcl-1 and therefore this may present a therapeutic vulnerability. Interestingly, Ouchi *et al*, previously investigated the role of Mcl-1 in chemoresistance in MRT and reported downregulation of the BH3-only protein Noxa, which binds to and inhibits Mcl-1. Ectopic expression of Noxa was found to bind Mcl-1 and promote doxorubicin-induced apoptosis. Moreover, genetic knockdown of Mcl-1 and pharmacological inhibition with the inhibitor TW-37, had a synergistic effect on cell death with doxorubicin[94].

Having determined a significant difference in Bcl-2 expression in cisplatin-sensitive cells and cisplatin-resistant cells, this study evaluated whether targeting Bcl-2 with BH3 mimetics could sensitise MRT cells to cisplatin cytotoxicity. Numerous studies have reported that high levels of Bim indicate potential sensitivity to ABT-199/Venetoclax and can be used as a predictive marker[501, 519]. In this study, the levels of Bim, Bax and Bid were assessed, and Bim was found to be significantly elevated in cisplatin resistant BT16 cells compared to both BT12 and G401 cell lines whereas no significant difference was observed regarding the basal expression levels of Bid and Bax. In diffuse large B cell lymphomas (DLBCL), Pham *et al* showed that, Bim, Bak and Bcl-2 correlated positively with ABT-199 sensitivity whereas Mcl-1, Bid and Bax did not [520]. Moreover, in follicular lymphoma, cell lines with high levels of Bim were found to be more susceptible to ABT-199[519]. Due to the high levels of Bcl-2 and Bim observed in cisplatin-resistant BT16 cells, this study hypothesised that this cell line may potentially exhibit sensitivity to Bcl-2 inhibition

A viability assay was conducted in the panel of MRT cell lines in response to ABT-263 and ABT-199 treatment. Despite the lack of Bcl-2 expression in BT12 cells, the IC50 value at 72 hours was similar to that determined in the Bcl-2-positive BT16 cells. A study by Wong *et al*, screened a panel of myeloma cell lines against ABT-199 and found 25% of them had IC50 values lower than 100 nM and 75% of the cell lines had IC50s from 140.87 nM to above 10 µM at 48h[521]. In T-cell acute lymphoplastic leukemia, a panel of 11 cell lines were treated with increasing concentrations of ABT-199 for 48 hours and IC50 values ranging from 0.2-10 µM were determined[502]. Tanos *et al*, studied the potential of ABT-199 in a range of neuroblastoma cell lines. This study categorised three cell lines as

either Mcl-1-dependent or Bcl-2-dependent and found a high difference in sensitivity to ABT-199. Whilst the IC50 of Mcl-1-dependent cells could not be determined due to lack of response, Bcl-2-dependent cells were found to be highly sensitive with IC50 values of 1.5 nM and 5 nM. It should be noted that Tanos *et al* only assessed the effect of ABT-199 up to 500 nM. These results differ to the micromolar IC50 values obtained in this study in rhabdoid tumour cell lines and furthermore, no discernible difference was observed in sensitivity to ABT-199 between Mcl-1 dependent and Bcl-2 dependent cell lines. A reason for this may be due to the higher concentration of ABT-199 required to induce cytotoxicity which may have off-target effects in BT12 cells and may be also targeting Bcl-xL.

ABT-263 was also examined in the panel of MRT cell lines. In BT16 cells, a somewhat lower IC50 was observed for ABT-263 compared to ABT-199. In small cell lung cancers, a range of IC50 values of 0.05-3 µM was determined following 72-hour ABT-263 treatment[522]. Cerella *et al*, examined the IC50s of ABT-199 and ABT-263 in a panel of AML cell lines with differential expression of anti-apoptotic proteins. HL-60 cells were shown to have high levels of Bcl-2 and exhibited a high sensitivity to ABT-199 and ABT-263 with IC50 values of 0.1 and 0.4 µM at 24 hours, respectively[523]. Hel cells were shown to have high levels of Bcl-xL and no detectable levels of Bcl-2. The IC50 of these cells at 24 hours for ABT-199 was 6.7 µM, and 0.5 µM for ABT-263. This is similar to the results obtained in this study, which showed an IC50 value of 9.82 µM at 72 hours despite a deficiency in Bcl-2 levels[523]. Altogether, this suggests that while expression levels of Bcl-2 and Bcl-xL may help predict the susceptibility to ABT-199 and ABT-263, there are other factors at play which influence cellular response. Due to the preferred clinical potential of ABT-199 compared to ABT-263, this study selected ABT-199 as a model BH3 mimetic to study its potential as a combination treatment with cisplatin.

In line with the results obtained from the alamar blue assay, BT12 and BT16 cells elicited a similar dose-dependent apoptotic response in both cell lines. In BT16 cells significant apoptosis was seen from 5 µM onwards with 20% cell death observed at 15 µM. Meanwhile, in BT12 cells, despite not expressing Bcl-2, apoptosis was significant from 2.5 µM onwards with approximately 28% apoptosis observed at 15 µM, potentially due to Bcl-2 independent off-target effects. In contrast, G401 cells were found to exhibit higher resistance to ABT-199 treatment with no apoptosis observed at the highest concentration tested of 15 µM. The results obtained in BT12 and BT16 cells agree with those observed by Wang *et al*., who examined the anti-cancer effect of ABT-199 in nasopharyngeal

carcinoma (NPC). These cell lines exhibited IC50 values in the range of 2-3 µM at 48 hours. Two of these NPC cell lines were stained with Annexin V/PI following treatment with 3 µM ABT-199 and exhibited approximately 30% apoptosis [236].

Next the ability of ABT-199 to affect cisplatin-induced apoptosis in MRT cells was evaluated. Despite having similar IC50 values and apoptotic response to ABT-199, BT12 and BT16 cells responded differently to the effect of ABT-199 in combination with cisplatin. BT12 cells were not sensitised to cisplatin when treated in combination with cisplatin, possibly due to the absence of Bcl-2 in these cells. However, in BT16 cells, increasing concentrations of ABT-199 sensitised cells to cisplatin in a dose-dependent manner. Moreover, this effect was found to be synergistic in BT16 cells, with the strongest synergism observed at a combination of 2 µM ABT-199 and 10 µM cisplatin. This was further confirmed by the levels of cleaved caspase 3, which was significantly higher in cells co-treated with ABT-199 and cisplatin compared to cells treated with cisplatin alone. In addition, at a non-cytotoxic concentration of 1 µM cisplatin, ABT-199 was able to sensitise the cells to cisplatin. Interestingly, and similar to results found in BT12 cells, G401 cells were also resistant to any sensitisation by ABT-199 to cisplatin-induced apoptosis.

Numerous studies have previously demonstrated a link between cisplatin and Bcl-2. Overexpression of Bcl-2 has been often reported as a characteristic of cancers with chemotherapeutic resistance. Leisching *et al*., showed that Bcl-2 conferred cisplatin resistance to cervical cancer cell lines. Genetic knockdown of Bcl-2 sensitised cervical cancer cells to cisplatin treatment[524]. In NPC, genetic knockdown of Bcl-2 by small-hairpin RNA (shRNA) or with the Bcl-2 inhibitor YC137 sensitised cells to cisplatin[485]. In triple negative breast cancer, ABT-199 and cisplatin also elicited synergistic anti-tumour effects. [525].

Having determined that the three MRT cell lines respond differently to ABT-199, both alone and in combination with cisplatin, this study aimed to examine the mechanism underlying the synergistic effect observed in BT16 cells that is not apparent in BT12 and G401 cells. The previous chapter demonstrated that cisplatin induced apoptosis in part through an accumulation of ROS leading to oxidative stress. Interestingly, there are reports in literature suggesting Bcl-2 inhibition by ABT-199 may affect ROS regulation. Lee *et al*, have previously demonstrated that ABT-199 activates T cell-mediated anti-leukaemic

activity through enhanced ROS production. Moreover, Aharoni-Simon *et al*., demonstrated that targeting Bcl-2 through ABT-199 treatment induced ROS in mouse pancreatic β-cells[486]. This study next evaluated whether ABT-199 induces ROS accumulation in MRT cell lines and whether this could be involved in the different sensitivities of this panel of MRT cell lines to ABT-199-induced apoptosis.

Interestingly, BT16 cells were the only cell line that showed significant, dose-dependent accumulation of intracellular ROS in response to ABT-199 indicating that ROS may indeed be involved in the observed synergy between ABT-199 and cisplatin in BT16 cells. To further examine this hypothesis, the three cell lines were treated with 2 μM ABT-199 (the concentration where synergy was observed with cisplatin in BT16 cells) alone and in combination with cisplatin, and intracellular ROS levels were assessed. Notably, BT16 was the only cell line that showed significant enhancement of cisplatin-induced ROS accumulation, with both a non-cytotoxic and cytotoxic concentration of cisplatin. In literature, there have been a few reports linking Bcl-2 and ROS production. In pancreatic β-cells, treatment with either the Bcl-2/Bcl-xL inhibitor, Compound 6 or the selective Bcl-2 inhibitor, ABT-199 induced elevated peroxide levels and stimulated superoxide dismutase activity. Moreover, conditional knockdown of Bcl-2 amplified peroxide formation. Thus, the study concluded that Bcl-2 modulated ROS signalling and that this non-canonical role of Bcl-2 that may be important for β-cell survival[486]. A further study by Amstad *et al*., overexpressed Bcl-2 in mouse epidermal cells and found these cells were resistant to cell death induced by hydrogen peroxide, superoxide or other oxygen radical-generating agents with glutathione levels increasing in response to oxidative stress. This study hypothesised that Bcl-2 interferes in ROS-induced cell death, in part, through glutathione upregulation[526].

Results herein show that the ROS scavenger NAC reverses the synergistic effect of cisplatin and ABT-199, further suggesting that ROS accumulation plays an important role in the ability of ABT-199 to sensitise BT16 cells to cisplatin. To further examine ROS upregulation in response to ABT-199, a time course was conducted which demonstrated that ROS was significantly induced by ABT-199 as early as 4 hours and remained elevated up to 48 hours. Importantly, NAC pre-treatment of BT-16 cells significantly reduced ROS accumulation.

Yu *et al.*, recently observed that ABT-199 induced mitochondrial dysfunction, associated with increased ROS levels and decreased GSH levels in porcine oocytes[527]. Furthermore, Zhang *et al*. observed enhanced ROS production and reduced mitochondrial respiration as a result of Bcl-2 inhibition through ABT-199 in preclinical AML models[528]. These studies suggest that inhibition of Bcl-2 using the antagonist ABT-199 may affect mitochondrial activity. In the present study mitochondrial ROS was shown to be elevated by ABT-199 in BT16 cells as early as 4 hours and remained elevated at 48 hours indicating that the source of ROS induced by ABT-199 is at least in part mitochondrially derived.

This result agrees with reports presented in recent literature. Nguyen *et al*. examined novel strategies to enhance the effect of hypomethylating agents (HMAs) in AML cells. This study found that combining HMAs with ABT-199 resulted in an increase in mitochondrial ROS induction and apoptosis compared to HMAs alone[529]. Furthermore, Hoang *et al* found that co-treatment of arsenic trioxide with ABT-199 augmented mitochondrial ROS[530].

Having observed a significant increase in mitochondrial ROS in response to ABT-199 in BT16 cells, this study next aimed to assess its effect on mitochondrial function. To do this, the Seahorse XFp Analyser was used to determine the effect of ABT-199 on the basal oxygen consumption rate (OCR) at 4 and 24 hours. ABT-199 was shown to cause a decrease in OCR, 4- and 24-hour timepoints. This agrees with reports in literature of ABT-199 affecting mitochondrial function in other cancer cell types. Zhang *et al*., found that ABT-199 partially reduced OCR in primary AML cell lines. Moreover, when combined with a Complex I inhibitor, IACS-010759, which also partially reduced OCR (<15%), ABT-199 fully inhibited basal consumption rate as early as 2 hours[528]. A study by Roca-Portoles *et al*, assessed the effect of 1 µM ABT-199 treatment at 24 hours in CT26 cells, a murine colorectal cancer cell line. Results demonstrated a significant decrease in OCR suggesting an inhibitory effect on mitochondrial oxidative phosphorylation (OXPHOS). The study also assessed the effect of ABT-199 on CT26 cells over a 4-hour time period to assess if the effects were immediate. Although no immediate effect was observed upon treatment, after 4 hours a decrease in OCR became apparent in ABT-199 treated cells. Roca-Portoles *et al* repeated these experiments in a human colorectal cancer cell line (HCT116), a breast cancer cell line (MCF7) and human AML cells (OCI-AML-3) and again observed a decrease in OCR following a 24-hour ABT-199 treatment.

As discussed in Chapter 4, the antioxidant response plays a critical role in mediating the cellular response to cisplatin-induced apoptosis. BT16 cells exhibit high basal levels of GSH that helps them cope with the effect of oxidative stress induced by chemotherapeutics such as cisplatin. As ABT-199 had been shown to upregulate intracellular and mitochondrial ROS and downregulate basal OCR in BT16 cells, glutathione levels in response to ABT-199 were next monitored. Total levels of glutathione and reduced GSH were examined, and total levels were found to be significantly downregulated in response to ABT-199. This result is in agreement with Yu *et al*, that showed that ABT-199 decreased intracellular GSH levels caused by mitochondrial dysfunction in porcine oocytes[527]. Pollyea *et al*. demonstrated that ABT-199 combined with azacytidine decreases OCR and glutathione in leukaemia stem cells from AML patients. Interestingly, the study postulated ABT-199 and azacytidine-induced glutathione reduction resulted in succinate dehydrogenase A glutathionylation which in turn impacted ETC complex II activity, inhibiting OXPHOS[492].

Chapter 4 showed a potential correlation between GSH and cisplatin-resistance in MRT cells, in agreement with several reports in literature. BT16 cells were shown to have the highest resistance to cisplatin and the highest levels of GSH. Moreover, this chapter has shown high expression of Bcl-2 in BT16 cells and higher sensitivity to ABT-199 and cisplatin combinations compared to BT12 and G401 cells. In literature, numerous reports have demonstrated a correlation between Bcl-2 levels and GSH levels and depletion of GSH is an early indicator of cell death progression in response to apoptotic stimuli[531]. In human cholangiocyte H69 cells, depletion of antioxidants such as GSH through pharmacological inhibitors resulted in Bcl-2 degradation and apoptosis[532]. In contrast Brozovic *et al*, did not observe a change in Bcl-2 expression in response to either GSH addition or GSH depletion[531]. There are few reports in literature linking GSH, cisplatin and Bcl-2. Rudin *et al*. transfected MCF-7 cells with Bcl-2 and observed an increase in GSH and reduced cisplatin sensitivity. Furthermore, GSH depletion mediated by GSH inhibitor BSO, normalised GSH levels and reversed cisplatin resistance[495]. Having demonstrated that the Bcl-2 inhibitor, ABT-199 sensitises BT16 cells to cisplatin and reduces GSH levels, further work was carried out to evaluate any link between Bcl-2, GSH and cisplatin resistance. BT16 cells were treated with cisplatin and BSO either alone or in combination and effects on Bcl-2 expression was examined through western blotting. Results demonstrated no significant difference between control cells and BSO-treated cells. These

results agree with Brozovic *et al*, who observed no difference in Bcl-2 expression in response to GSH depletion[531]. The combination of cisplatin and BSO showed significant Bcl-2 degradation, most likely as a result of the enhanced apoptosis, compared to cells treated with cisplatin alone.

Interestingly, although ABT-199 and ABT-263 inhibit the growth of various cancer cells, there are reports that upregulation of Mcl-1 and Bcl-xL expression induced by these drugs adversely affects their anti-cancer activity[464]. To further evaluate the different responses to ABT-199 across the panel of MRT cell lines, the effect of this drug on the expression levels of a panel of anti-apoptotic Bcl-2 family members was next examined.

No effect on the expression levels of Bcl-2, Bcl-xL or Mcl-1 was observed in response to ABT-199 treatment in BT12 cells. However, in G401 cells, Bcl-2, Mcl-1 and Bcl-xL proteins were found to be upregulated in response to treatment of ABT-199 at a non-cytotoxic concentration of ABT-199. This is not surprising, as upregulation of these proteins in response to ABT-199 is commonly observed in resistant cell lines. Current theories suggest that due to complex interplay between Bcl-2 and other anti-apoptotic proteins from the Bcl-2 family, ABT-199 as a monotherapy will lead to failure from acquired resistance. Resistance to ABT-199 is reported to be associated with sequestration of Bim, which is usually induced through ABT-199 binding to Bcl-2, by other anti-apoptotic proteins such as Mcl-1[533]. In AML cell lines which acquired resistance to ABT-199 by continuous exposure, higher expression levels of Mcl-1 and Bcl-xL were also acquired over time indicating a shift in Bcl-2 dependency to dependency on Mcl-1 and Bcl-xL. Furthermore, genetic and pharmacological inhibition of Bcl-xL was shown to restore sensitivity to ABT-199 in these cells[534]. In neuroblastoma cell lines, Mcl-1 was shown to be upregulated in response to ABT-199 in a dose-dependent manner. Moreover, its negative regulator, Noxa was shown to be decreased in a dose-dependent manner suggesting that neuroblastoma patients may benefit from combining ABT-199 treatment with Mcl-1 inhibitors[501]. Thus, using ABT-199 in combination with other therapies will most likely be a more successful therapeutic strategy.

Next, the expression levels of Bcl-2, Bcl-xL and Mcl-1 were examined in BT16 in response to ABT-199. Interestingly, Mcl-1 was shown to be significantly reduced in response to ABT-199 whereas Bcl-2 and Bcl-xL levels did not change. Mcl-1 has a short half-life and is reported to be rapidly degraded by the ubiquitin proteasome system[503, 504].

To determine if Mcl-1 downregulation was involved in the mechanism underlying ABT-199 and cisplatin synergy, Mcl-1 degradation was prevented through treatment with non-cytotoxic concentrations of the proteosome inhibitor bortezomib. Inhibition of Mcl-1 degradation reversed this synergistic effect indicating that downregulation of Mcl-1 mediates, at least in part, the synergistic effect on cell death mediated by cisplatin and ABT-199. Interestingly, when Chiou *et al.* combined the Bcl-xl inhibitor WEHI-539 with ABT-199 they observed a synergistic effect on cell death in human leukaemia cells. Moreover, WEHI-539 sensitised ABT-199-resistant cells to ABT-199 induced cell death through Noxa-mediated Mcl-1 degradation[535]. Furthermore, the tyrosine kinase inhibitor Gilteritinib and ABT-199 were shown to elicit a synergistic effect on apoptosis in AML cells mediated by Mcl-1 degradation[536]. Collectively, these studies would suggest that, in addition to the classic mechanism of action assigned to ABT-199 whereby binding to Bcl-2 releases Bim and induces intrinsic apoptosis, ABT-199 can also prime cells to apoptosis through Mcl-1 degradation in certain cell types.

Broadly speaking, there are two axes associated with Bcl-2-like in pro-apoptotic family proteins; the Bcl-2-Bax and Mcl-1-Bak axes[500]. Mcl-1 regulates Bak-dependent MOMP and apoptosis by sequestering it whereas Bcl-2 regulates Bax-dependent apoptosis. Having established a role for Mcl-1 degradation in cisplatin and ABT-199 synergy, this study examined Bak activation (induced by Bak undergoing conformational changes) in response to ABT-199 treatment, alone and in combination with cisplatin. Results herein demonstrate that Bak activation is significantly higher in cells treated with cisplatin and ABT-199 than cells treated with cisplatin only. Moreover, this is also the case in cells treated with a sub-apoptotic concentration of cisplatin (1 μM) in correlation with the previous observation that ABT-199 sensitises cells to sub-apoptotic concentrations of cisplatin indicating that this may be due to Bak activation.

Results presented so far demonstrated that ABT-199 sensitises BT16 cells to cisplatin and both ROS accumulation and Mcl-1 degradation are involved in this process. Further work was carried out to understand the link between ABT-199-induced ROS upregulation and Mcl-1 downregulation by examining the effect on expression levels of various other anti-apoptotic proteins including c-FLIP, an endogenous negative regulator of DISC formation and cIAP1 and XIAP, members of the inhibitor of apoptosis (IAP) protein family.

Lee *et al.*, recently reported that treatment of human renal cancer cells with Berberine (BBR), an anti-cancer isoquinoline alkaloid, induced Mcl-1 and cFLIP degradation through activation of the proteosome dependent pathway. Treatment with the proteosome inhibitor, MG132, prevented Mcl-1 and cFLIP degradation. Moreover, ROS inhibition through NAC treatment prevented cFLIP and Mcl-1 degradation. Thus, this study concluded that BBR sensitised cells to TRAIL-induced apoptosis via Mcl-1 and cFLIP degradation through the, ROS-mediated, proteasomal signalling pathway. Results presented herein demonstrated that ABT-199 did not induce degradation of either cFLIP or the IAP proteins, suggesting the ROS/cFLIP degradation pathway described by Lee *et al* is not activated by ABT-199 in BT16 cells. Interestingly, in lung cancer cells, treatment with human hormone Ouabain resulted in ROS-mediated Mcl-1 degradation, which sensitised cells to TRAIL-induced apoptosis. However, similar to our results with ABT-199, this hormone had no significant effect on cFLIP levels[537].

In literature, degradation of Mcl-1 in cancer cells has often been associated with Noxa upregulation. Moreover, Noxa has been shown to be upregulated by ROS in CLL cells. Interestingly, this upregulation of Noxa by ROS was demonstrated to be necessary to overcome cisplatin resistance in CLL[511]. Having observed an accumulation of ROS in BT16 cells in response to ABT-199, this study examined Noxa expression levels in response to ABT-199. Indeed, Noxa levels were found to be significantly upregulated in response to ABT-199 treatment. Weller *et al*., have shown significant upregulation of Noxa by ABT-199 in soft tissue derived sarcoma cells and postulated that ABT-199 has a double impact on apoptosis, both through Bcl-2 binding and Mcl-1 degradation[500].

Ouchi *et al*, have previously shown an important role for the Noxa/Mcl-1 axis in mediating chemoresistance in MRT. This group demonstrated that SMARCB1, a characteristic mutation in MRT, contributes to Noxa transcriptional activity and therefore, Noxa is commonly found to be downregulated in MRT cell lines. Ectopically expressed Noxa was shown to inhibit Mcl-1 activity and sensitise MRT cells to doxorubicin. In addition, Mcl-1 inhibition through knockdown and pharmacological inhibition also sensitised MRT cells to doxorubicin treatment[94]. Therefore, the ability of ABT-199 to upregulate Noxa, potentially through ROS, may contribute to its ability to sensitise cells to cisplatin.

Having determined that ABT-199 induced Noxa upregulation and Mcl-1 degradation may be linked to ROS accumulation, the effect of ABT-199 on the ROS-mediated JNK and p38

MAPK signalling pathways was next examined. Chiou *et al*, have shown that ABT-199 in combination with the Bcl-xL inhibitor WEHI-597 can synergistically enhance Mcl-1 degradation and apoptosis in human leukaemia cells mediated through a ROS/p38 /Noxa pathway. However, this study found that levels of phosphorylated JNK remined unchanged after ABT-199 and WEHI-597 treatment[535]. Lynch *et al*., conducted a study to examine the role of glucocorticoid receptor phosphorylation on Mcl-1 and Noxa gene expression and found that phosphorylation of JNK resulted in altered expression of Noxa and Mcl-1[538]. In addition, Sun *et al*. observed ROS-induced Mcl-1 degradation in liver cancer cells in response to dichloroacetate and sorafenib treatment and found that Mcl-1 degradation induced by ROS was mediated by JNK phosphorylation[539]. To determine whether ROS may upregulate Noxa through p38 or JNK, the activation of both signalling pathways in response to ABT-199 treatment, alone and in combination with cisplatin was assessed. Results demonstrated a significant activation of the p38 signalling pathway in response to ABT-199 treatment, while no effect on the JNK signalling pathway was observed. It would be of interest in future studies to determine the importance of p38 activation in Noxa upregulation and Mcl-1 degradation through the use of the p38 inhibitor SB202190.

Previous results in this chapter observed that accumulation of ROS partially mediates cisplatin and ABT-199 synergy. Interestingly, NAC treatment also reversed the ABT-199/cisplatin-mediated Mcl-1 degradation, confirming that Mcl-1 degradation is ROS-dependent. This is similar to results observed by Lee *et al* and Chanvorachote *et al* who both observed ROS-mediated Mcl-1 degradation in their respective cancer cell lines[507, 537].

In conclusion, this study characterised the basal expression levels of a series of pro- and anti-apoptotic proteins in three MRT cell lines to assess whether they may play a role in determination of cisplatin cytotoxicity. Interestingly, cisplatin-sensitive BT12 cells were shown to be deficient in anti-apoptotic Bcl-2, whilst high levels were expressed in the more resistant BT16 and G401 cells. This study then examined the effect of the Bcl-2 specific BH3 mimetic ABT-199 on MRT cell lines and demonstrated that BT16 cells showed the greatest sensitivity to ABT-199 treatment. Moreover, a combination treatment of cisplatin and ABT-199 elicited a synergistic effect on apoptosis in BT16 cells alone. Despite expressing high levels of Bcl-2, G401 cells were not sensitised to ABT-199 treatment possibly due to the observed upregulation of Bcl-xL and Mcl-1 in response to ABT-199 treatment. Interestingly, ABT-199 was shown to significantly enhance intracellular and mitochondrial ROS, decrease glutathione levels, and decrease

mitochondrial basal respiration in BT16 cells. Furthermore, ABT-199 treatment resulted in the upregulation of the Mcl-1 negative regulator, Noxa, concomitant with degradation of Mcl-1. Interestingly, activation of p38 MAPK, which has been shown in literature to upregulate Noxa and to be mediated by ROS accumulation, was also observed. Moreover, ABT-199 was shown to enhance levels of the active form of pro-apoptotic protein Bak, which is normally sequestered by Mcl-1. Mcl-1 degradation was prevented by the ROS scavenger NAC, suggesting ABT-199-induced Mcl-1 degradation is linked to ROS upregulation. Importantly, NAC was also shown to reverse the synergistic effect on apoptosis by ABT-199 and cisplatin, proposing that a ROS-dependent mechanism underlies the observed synergy. Collectively, these results suggest that combining cisplatin with ABT-199 may present a potential treatment strategy in certain rhabdoid tumours Further study into the ability of BH-3 mimetics to overcome chemoresistance in solid tumours including MRT is warranted.

6. Concluding Remarks

Malignant rhabdoid tumour (MRT) is one of the most aggressive paediatric malignancies typically occurring in patients under the age of three. Characterisation of this tumour is relatively recent; AT/RTs were classified by the WHO as a distinct tumour from other CNS tumours in the year 2000[10]. The young age of the patients, metastatic nature of the tumour, the rarity of the disease and the recent characterisation of this tumour all contribute to late diagnosis and the poor prognosis associated with MRT. Indeed, the estimated survival rate of MRT is only approximately 25%[4, 10]. Diagnosis of these tumours is highly dependent on identifying mutations in *SMARCB1*, a component of the SWI/SNF chromatin remodelling complex, which occurs in 80-95% of MRT cases, with the rest of the cases being characterised by a mutation in *SMARCA4*[12].

To date, these is no standardised treatment protocol for patients diagnosed with MRT. Large data sets of uniformly treated patients are rare and most information on therapeutic success stems from retrospective studies. The current treatment approach is a combination of surgical resection, where possible, followed by chemotherapy and radiation therapy. However, like many cancers, rhabdoid tumours often develop resistance to these therapies. Recent efforts have been made to establish a database of MRT treatments to address the deficiency in assessing therapies in controlled clinical settings. The European rhabdoid registry was established in 2005 and reported a 46% improvement in the 6-year survival rate of patients treated with high dose chemotherapy and radiation therapy[72]. The Dana Faber consortium reported a 70% improvement in the 2-year survival of patients treated with a combination of surgery, chemotherapy and radiation therapy between February 2004 and September 2006. Nonetheless, these regimens are associated with undesirable side effects[540]. To address these side effects and the poor prognosis, research has focused on SMARCB1 and epigenetic modulation with targets such as the methyl transferase EZH2, cyclin D1, a downstream effector of SNF5 and Aurora kinase, a direct downstream target of SMARCB1[37, 88, 146]. However, further work is required to elucidate the molecular mechanisms in MRT that may present therapeutic vulnerabilities. Given the relative success rate of standard chemotherapeutic agents in MRT, studies have also aimed to overcome chemoresistance and reduce associated toxicities[205]. Combination therapies have so far been successful in enhancing the efficacy of chemotherapeutics. The current project sought to examine the molecular mechanisms underlying chemoresistance to one of the most the commonly used chemotherapeutic agents in MRT, cisplatin, and to establish novel therapeutic strategies to sensitise cells to cisplatin.

In this study, a panel of three MRT cells were examined; BT12, BT16 and G401 cells. BT12 and BT16 cells are derived from AT/RTs and G401 cells are derived from MRTK. This study examined the sensitivity of the three cell lines to cisplatin and found BT16 cells were particularly resistant to cisplatin whereas BT12 cells were shown to be the most sensitive, with G401 cells falling in an intermediary phenotype. The molecular mechanisms underlying this differential response to cisplatin were examined in this project.

Autophagy is a homeostatic cellular process whereby the cell degrades and recycles proteins, lipids, and organelles. This process has been associated with ageing, differentiation, and development. Moreover, dysregulation of this process has been associated with a number of diseases, including cancer[541]. The role of autophagy in cancer has recently garnered huge interest, with a wide range of reports indicating that it may be of therapeutic importance. However, the field is complex as autophagy is widely believed to have a dual role in cancer. Autophagy has been shown to play both a pro-survival and pro-death role in cancer, and this role appears to be context dependent. This dual role is thought to extend to the response of cancer cells to stressors such as chemotherapeutics[542]. On one hand, there are reports of it being induced in order to result in autophagic cell death. In contrast, autophagy has also been shown to be upregulated as a protective mechanism against the stress imposed by chemotherapeutic agents. This paradoxical role of autophagy is believed to be context-dependent; it may be dependent on the drug and cell type. However, it may also depend on the threshold of stress induced by chemotherapy[542]. For example, in response to moderate stress signals from drug treatment, autophagy may be upregulated to aid the cell in coping with this. In contrast, in cases where the damage is too severe, it has been proposed that autophagy may be upregulated in order to induce autophagic cell death[319]. The role of autophagy in MRT remains unclear. The present study examined the role of autophagy in response to cisplatin treatment in the panel of MRT cell lines. Cisplatin was shown to upregulate autophagy and apoptosis in a concurrent manner in MRT cells suggesting autophagy may be involved in cisplatin-induced cell death. Upregulation of autophagy in response to cisplatin has been observed in a number of studies; however, as previously mentioned, whether its role is pro-death or pro-survival is context dependent[543]. The present study investigated the role of autophagy in cisplatin-induced cell death through the use of pharmacological inhibitors. Pharmacological inhibitors of autophagy are classified as early or late-stage inhibitors depending on what

stage of the process of autophagy is blocked. Early-stage inhibition refers to blocking early steps of autophagy initiation (i.e. inhibiting the formation of the autophagosome) whereas late-stage autophagy inhibition refers to blocking the flux (i.e. the formation of the autophagolysosome)[368]. This study demonstrated that inhibiting early and late-stage autophagy resulted in different outcomes when monitoring cisplatin sensitisation. Whilst treatment with late-stage autophagy inhibitors, like chloroquine and bafilomycin-A1, significantly enhanced cisplatin-induced apoptosis, early-stage inhibition with SAR405 had no effect on cisplatin-induced cell death. Due to these contrasting results, genetic knockdown of key autophagic protein ATG5 was conducted. However, this had no effect on cisplatin-induced apoptosis. Nonetheless, inhibition of apoptosis with the pan-caspase inhibitor Z-VAD-FMK resulted in downregulation of cisplatin-induced autophagy, suggesting crosstalk between apoptotic and autophagic signalling pathways. This study showed clinical potential in combining cisplatin with late-stage autophagy inhibitors such as chloroquine and bafilomycin-A1. Thus, it is possible that therapeutic benefits of targeting autophagy are relevant in late-stage autophagy but are not the case in early-stage autophagy. Alternatively, it is possible that the ability of these inhibitors to sensitise MRT cells to cisplatin is independent of autophagy. This could be because the accumulation of autophagosomes due to inhibition of flux, result in cytotoxicity[544]. Chloroquine and bafilomycin-A1 have been widely used in many cancer types and have shown promising *in vitro* and *in vivo* effects in combination with cisplatin. Due to its poor toxicity profile, bafilomycin A1 has not been approved for use in the clinic. In contrast, chloroquine is a clinically approved drug which is widely used for the treatment of malaria[400]. There are multiple clinical trials underway examining the potential of combining chloroquine with cisplatin[400]. Future studies examining the effect of chloroquine and bafilomycin A1 in combination with cisplatin in an *in vivo* in a model of MRT, such as subcutaneous rhabdoid tumour xenografts would be of interest. The mice could then randomly be divided into 4 groups and treated with vehicle control, late-stage autophagy inhibitor, cisplatin, and late-stage autophagy inhibitor /cisplatin. Subsequently, tumour growth and survival would be monitored[545].

Moreover, further study could be carried out to elucidate whether the enhancement of cisplatin-induced apoptosis by bafilomycin-A1 and chloroquine, is independent of autophagy. Experiments could be carried out by combining other late-stage inhibitors of autophagy such as toosendanin (a novel potent vacuolar-type H^+-translocating ATPase

inhibitor) and LAI-1 (a novel inhibitor that causes lysosomal dysfunction and blockage of autophagolysosome formation), with cisplatin[546, 547]. The ability of chloroquine to sensitise MRT cell lines to cisplatin could also be assessed in ATG5/ATG7/ATG12-deficient cells to confirm whether autophagy upregulation is involved in the enhanced apoptotic rate. Moreover, given the complexity of autophagic signalling, a more comprehensive genetic targeting study of autophagy in the context of cisplatin-induced apoptosis is warranted. Additionally, it is possible that the inhibition of autophagic flux by late-stage inhibitors results in the accumulation of autophagic vesicles that in turn result in the activation of ROS signalling thereby inducing apoptotic signalling. Numerous reports have demonstrated that autophagosome accumulation can trigger cytotoxicity, rather than autophagy activation[544, 548]. Thus, the involvement of ROS-induced signalling pathways in response to chloroquine and bafilomycin-A1 treatment could be examined in the future.

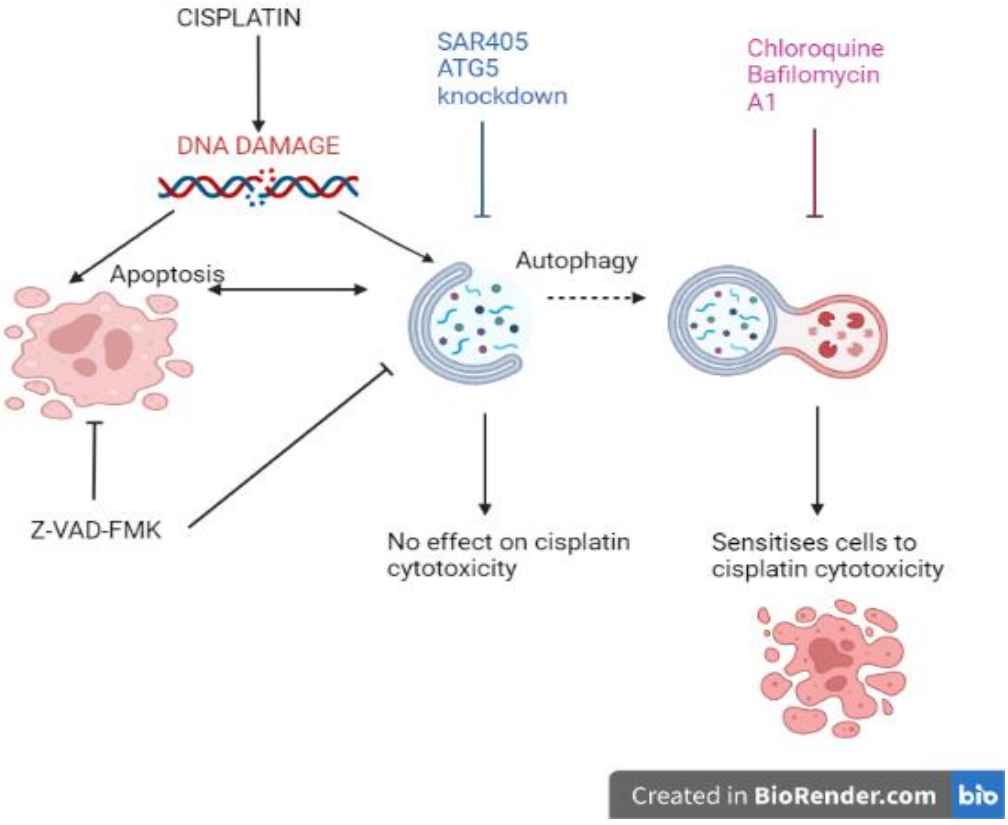

Figure 6.1 The effect of cisplatin on apoptosis and autophagy in MRT cell lines.

This study proposes cisplatin upregulates apoptosis and autophagy concurrently. Apoptosis inhibition by the pan-caspase inhibitor Z-VAD-FMK results in abrogation of cisplatin-induced autophagy. Late-stage autophagy inhibitors sensitise MRT cells to cisplatin. However, early-stage inhibitors do not sensitise MRT cells to cisplatin.

The balance between oxidative stress mediated by reactive oxygen species (ROS) and the antioxidant system has become a subject of interest in cancer therapy research. Previous studies have implicated certain key players of the antioxidant system in chemotherapeutic resistance in various malignancies including the well-known antioxidant glutathione (GSH) and the transcription factor Nuclear erythroid-related factor-2 (Nrf2), the master regulator of antioxidant response. The second part of the study examined the role of ROS and the Nrf2/GSH antioxidant system in mediating cisplatin resistance MRT. This antioxidant system maintains cellular redox homeostasis by counteracting free radicals and neutralising oxidants. Platinum-based anti-cancer drugs have been shown to elicit high levels of oxidative stress in response to DNA damage. It is believed that cancer cells upregulate their antioxidant system to cope with intrinsic and drug-induced oxidative stress[302, 311]. This is important as cancer cells typically have high basal ROS levels making them particularly sensitive to further ROS accumulation. Reports in literature suggest that lower levels of ROS and higher levels of key components of the antioxidant system are often observed in chemoresistant cancer cells[430]. For example, mutations in Nrf2 and its negative regulator Keap1 have been associated with poor survival in cancer patients[311]. Moreover, high Nrf2 expression has also been correlated with chemoresistant phenotype in several malignancies such as lung cancer and gall bladder cancer, as it can help cells overcome oxidative stress induced by anti-cancer drug treatment[317]. Elevated GSH levels have also been linked with chemotherapeutic resistance including resistance to platinum-based anti-cancer agents [312]. Levels of cellular thiols such as GSH play a critical role in detoxification of these platinum agents. GSH can bind and inactivate cisplatin through its reactive thiol group, preventing cisplatin from binding to DNA and inducing its damage[430].

The role of the Nrf2/GSH antioxidant pathway and oxidative stress in mediating chemoresistance in MRT remains poorly understood. This study next investigated whether the Nrf2/GSH antioxidant system plays a role in determination of cisplatin cytotoxicity in a panel of MRT cells lines. This study characterised the basal levels of GSH, ROS and Nrf2 in the panel of MRT cell lines and found a correlation between the expression profile of the antioxidant defence system and sensitivity to cisplatin. Elevated levels of GSH and Nrf2 expression along with reduced basal levels of ROS were observed in cisplatin-resistant MRT cells when compared to sensitive cells. Moreover, targeting ROS levels by treatment with the ROS scavenger NAC significantly protected MRT cells from cisplatin-

mediated apoptotic cell death. Depleting GSH levels with a GSH inhibitor BSO enhanced cisplatin-induced ROS leading to an enhancement of cisplatin-mediated cell death. Lastly, targeting Nrf2, a key mediator of the antioxidant defence system, both through a pharmacological approach utilising ML385 and through genetic knockdown sensitised resistant MRT cells to cisplatin-induced cell death. These novel findings provide insights into the therapeutic potential of targeting components of the antioxidant system in MRT to circumvent chemoresistance and a further insight into the involvement of the Nrf2/GSH antioxidant system in response to cisplatin in MRT. A proposed mechanism of antioxidant response in MRT cells to cisplatin-induced oxidative stress is depicted in Figure 6.2. Interestingly, approximately 40% of currently used anti-cancer drugs, including the anthracycline doxorubicin, have been reported to induce oxidative stress[549], indicating that targeting Nrf2 may be a useful strategy to overcome chemoresistance mediated by anti-cancer agents other than solely platinum based compounds.

One limitation of the current study is that the analysis of components of the antioxidant system was conducted on only three cell lines and future work warrants repeating this as a larger scale study with a wider range of MRT cell lines. Moreover, the generation of a cisplatin-resistant cell line from a parental MRT cell line could be developed as a model to further the Nrf2/GSH antioxidant system by comparing its components in cisplatin-sensitive and cisplatin-resistant cell populations derived from the same cell line. This could be conducted through pulsed stepwise exposure to cisplatin over a long period of time (approx. 12 months). The generation of a cisplatin resistant BT12 cell line was previously attempted, however, due to the sensitivity of BT12 cells, increasing cisplatin dosage led to cytotoxicity issues.

Further work is also warranted to elucidate the effect of cisplatin on Nrf2 activation by conducting a Nrf2 ARE luciferase activity assay. Nrf2 activity is regulated by Keap1, which determines its inhibition and degradation through the proteosomal degradation pathway. Upon ROS accumulation, Nrf2 is released and translocates to the nucleus and binds to the antioxidant response element (ARE) of antioxidant genes. As cisplatin has been shown to upregulate Nrf2 expression levels, it is likely that treatment results in the release of Nrf2 and higher presence of nuclear Nrf2 in order to upregulate the antioxidant response as a cytoprotective mechanism. Moreover, experiments could be conducted to assess the role of Nrf2 inhibition on ROS-mediated signalling pathways such as the NF-κB pathway as well as the downstream targets of Nrf2, such as *HMOX-1* and *NQO1*[550, 551]. It

should be noted that Nrf2 inhibition may also result in modulations in additional signal transduction pathways such as MAPK cascades[552]. Furthermore, expression of multidrug resistance proteins, which exerts cisplatin efflux in cancer cells, has been shown to be regulated by Nrf2[553]. It would be of interest in future studies to examine the contribution of these components to alterations in cisplatin sensitivity following inhibition of the Nrf2 pathway in MRT.

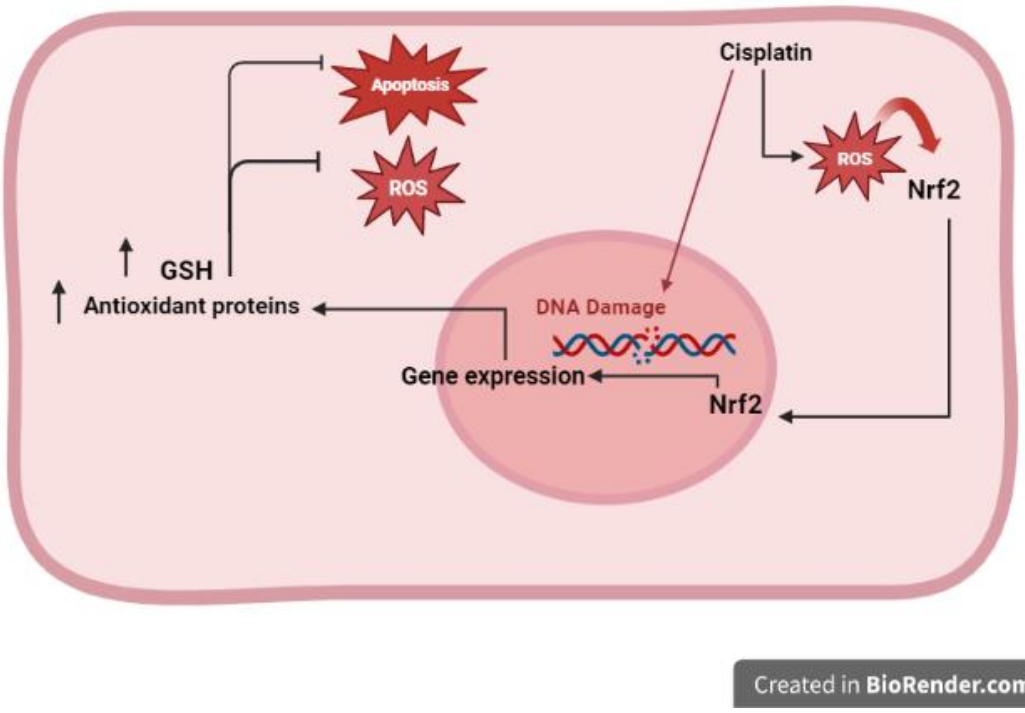

Figure 6.2 Proposed mechanism of antioxidant response in MRT cells to cisplatin-induced oxidative stress

This study proposes that cisplatin-induced apoptosis in MRT is partially mediated by ROS accumulation, leading to oxidative stress. Oxidative stress results in the translocation of the key antioxidant transcription factor Nrf2, to the nucleus, where it transcribes a series of antioxidant genes and replenishes GSH stores to counteract ROS accumulation. This effect protects the cell from cisplatin-induced cytotoxicity suggesting that targeting Nrf2 and GSH (with pharmacological inhibitors such as ML385 and BSO, respectively) may present a potential therapeutic strategy to overcome chemoresistance. Created with Biorender.com.

Whilst genetic knockdown of Nrf2 was shown in the present study to reduce GSH and cisplatin resistance, it would be of interest to determine the effect of Nrf2 overexpression in BT12 cells through plasmid transfection to assess whether this confers the cells with cisplatin resistance. Lastly, the results of Nrf2 inhibition have proven to be promising in *in vitro* studies of BT16 cells, therefore further work could examine the effect of Nrf2 inhibition *in vivo* by monitoring tumour progression and survival in Nrf2 knockout mice.

In the last part of the study, the role of the Bcl-2 family of proteins in mediating chemoresistance in MRT was assessed. Firstly, the expression levels of a series of anti-apoptotic and pro-apoptotic members of the Bcl-2 family of proteins in a panel of MRT cell lines was characterised to examine whether they may play a role in determination of cisplatin cytotoxicity. MRT cells displayed varying protein expression levels of Bcl-2 family members. Most notably, cisplatin sensitive BT12 cells did not express any detectable levels of Bcl-2 protein whereas the more resistant BT16 and G401 cells expressed high levels of this protein suggesting a possible role for Bcl-2 in determining different sensitive/resistant phenotypes of rhabdoid tumour cells. This study then went on to evaluate whether targeting Bcl-2 with the Bcl-2 selective BH3 mimetic ABT-199 could affect the apoptotic response to cisplatin and sensitise MRT cells to cytotoxicity. Surprisingly, similar IC50 values were obtained for ABT-199 in Bcl-2-positive BT16 cells and Bcl-2-deficient BT12 cells indicating that ABT-199 may exhibit off target Bcl-2 independent effects. Moreover, G401 cells showed higher IC50 to ABT-199 despite expressing its target protein, Bcl-2. These results were confirmed by flow cytometric analysis of AnnexinV/PI-stained cells. Next the ability of ABT-199 to affect cisplatin-induced apoptosis in each of the three cell lines was evaluated. ABT-199 elicited no effect on cisplatin-induced apoptosis in either BT12 or G401 cells whereas it synergistically enhanced cisplatin-induced apoptosis in BT16 cells and moreover sensitised these cells to sub-cytotoxic concentrations of cisplatin. These results provide a rationale for evaluating the therapeutic potential of combining BH3 mimetics with chemotherapeutic agents in Bcl-2-dependent rhabdoid tumours to circumvent chemoresistance and reduce toxicities by lowering dosage.

This study also demonstrated high levels of basal Mcl-1 expression in BT12 cells. This observation suggests that although ABT-199 did not sensitise BT12 cells to cisplatin, combinations of cisplatin with other mimetics such as Mcl-1 inhibitors may present a potential strategy in rhabdoid cells with this profile. Additionally, future work could expand combination studies in these cells to determine if a synergistic effect on cell death can be observed at higher concentrations of ABT-199 with cisplatin. Moreover, G401 cells were shown to have a higher sensitivity to the Bcl-2/Bcl-xl specific BH-3 mimetic ABT-263 than ABT-199, suggesting Bcl-xL may contribute to potential ABT-199 resistance. It is possible that G401 cells upregulate a protective compensatory pathway in response to ABT-199 treatment through the upregulation of other anti-apoptotic proteins. Indeed,

ABT-199 resistance is commonly associated with Mcl-1 and Bcl-xL overexpression[497]. For example, Choudhary *et al*, investigated the mechanisms of ABT-199 resistance in lymphoid malignancies and linked upregulation of Bcl-xL and Mcl-1 to acquired resistance of ABT-199[497]. Interestingly, western blot analysis which demonstrated upregulation of Bcl-2, Bcl-xL and Mcl-1 in response to ABT-199 treatment in G401 cells in this study further suggests this could be the case. Thus, further work could test whether combinations of cisplatin with ABT-263 or Mcl-1 inhibitors may sensitise G401 cells to ABT-199 and cisplatin combination treatments.

The BH3 profiling assay was developed to help predict the quantity and type of pro-apoptotic signalling required for a cell to undergo apoptosis[554]. Therefore, BH3 profiling can be used to predict what cell types will exhibit heightened vulnerabilities to certain BH3 mimetics[462]. The BH3 profiling assay is based on measuring the amount of MOMP that occurs in response to pro-apoptotic peptides, which mimic the activity of BH3-only proteins from the pro-apoptotic family[554]. A larger-scale study employing BH3 profiling to identify the dependencies of different rhabdoid tumour types could be conducted to predict which BH3 mimetics would have the most success and may provide data to compare against other cancer types to determine if there is a significant difference in therapeutic vulnerability between cancer types.

This study then went on to examine the mechanism underlying the ABT-199/cisplatin synergy. The classic mechanism of action of ABT-199 is based on the drug binding to the BH3 groove of Bcl-2, releasing Bim, thereby inducing Bax/Bak mediated intrinsic apoptosis[480]. In future studies, the interaction between Bcl-2 and Bim could be validated through immunoprecipitation experiments. Interestingly, an increase in conformationally active Bak was observed in response to co-treatment of BT16 cells with ABT-199 and cisplatin. This study also showed ABT-199 treatment results in the upregulation of cellular ROS and mitochondrial ROS. Moreover, ABT-199 reduced mitochondrial oxygen consumption suggesting that ABT-199 treatment impacts mitochondrial function. These observations are in agreement with recent reports in literature demonstrating that ABT-199 treatment affects mitochondrial activity[527]. Roca-Portoles *et al.* have shown that ABT-199 impaired mitochondrial respiration and the TCA cycle, however, these effects were independent of Bcl-2 inhibition and cell death induction[487]. Further work would be required to determine if the observed effects of ABT-199 on ROS and mitochondrial respiration in the present study is as a consequence of Bcl-2 inhibition or if it is through a

Bcl-2 independent mechanism. This could be achieved by repeating these experiments in BT16 cells where Bcl-2 has been silenced using siRNA to assess whether similar results are obtained. Moreover, these experiments could be repeated on a wider panel of rhabdoid tumour cell lines for a clearer depiction of how dependent this effect of ABT-199 is on cell type.

Next, the expression levels of Bcl-2, Bcl-xL and Mcl-1 were examined in BT16 in response to ABT-199 alone and in combination with cisplatin at concentrations where synergy was observed. Interestingly, Mcl-1 was shown to be significantly reduced in response to ABT-199 whereas Bcl-2 and Bcl-xL levels did not change. Whilst Mcl-1 upregulation has been commonly associated with ABT-199 resistance, degradation of Mcl-1 has previously been observed in cases when ABT-199 synergises with another drug to induce cell death[536, 555]. To determine if Mcl-1 downregulation was involved in the mechanism underlying ABT-199 and cisplatin synergy, Mcl-1 degradation was prevented through treatment with the proteasome inhibitor bortezomib. Inhibition of Mcl-1 degradation reversed this synergistic effect indicating that downregulation of Mcl-1 mediates, at least in part, the synergistic effect on cell death mediated by cisplatin and ABT-199. Future experiments could include knockdown of Mcl-1 to determine if ABT-199 can enhance-cisplatin induced apoptosis. Moreover, ectopic expression of Mcl-1 could be conducted to determine if this synergy could be reversed. Degradation of Mcl-1 in cancer cells has often been associated with upregulation of its negative regulator Noxa[511]. Indeed, Noxa levels were found to be upregulated in response to ABT-199 treatment indicating that ABT-199 may have a double impact on apoptosis, both through Bcl-2 binding and Mcl-1 degradation. Importantly, pre-treatment of BT16 cells with the ROS scavenger NAC, prior to treatment with ABT-199/cisplatin, reduced the elevated ROS levels, prevented Mcl-1 degradation, and reversed the synergistic effect on apoptosis. Preliminary results presented herein also demonstrate phosphorylation and thus activation of the p38 MAPK, in line with previous reports of a ROS/p38 MAPK/Noxa axis mediating suppression of Mcl-1[535]. Thus, this study proposes that a dual action on apoptosis is exerted by ABT-199 treatment: on one hand, ABT-199 binds to Bcl-2 resulting in the release of Bim causing the activation of intrinsic apoptosis, and on the other hand, ABT-199 treatment impacts mitochondrial function and results in accumulation of mitochondrial ROS which in turn results in p38 phosphorylation and Noxa upregulation. Noxa upregulation promotes Mcl-1 inhibition and thus the release of Bak which induces intrinsic

apoptosis. A summary diagram of the proposed pathway is depicted in Figure 6.3. However, further work is required to substantiate this proposal. Future experiments could examine the effect of a p38 inhibitor, such as SB203580, on Noxa expression and Mcl-1 degradation to establish whether blocking the phosphorylation of p38 would inhibit Noxa upregulation and Mcl-1 degradation. Moreover, the effect of ROS inhibition by NAC on p38 phosphorylation and Noxa could also be examined to confirm p38 phosphorylation by ROS. Lastly, knockdown of Noxa by siRNA could be conducted to assess its role in Mcl-1 degradation and Bak activation and to determine the effect on apoptosis induced by cisplatin and ABT-199.

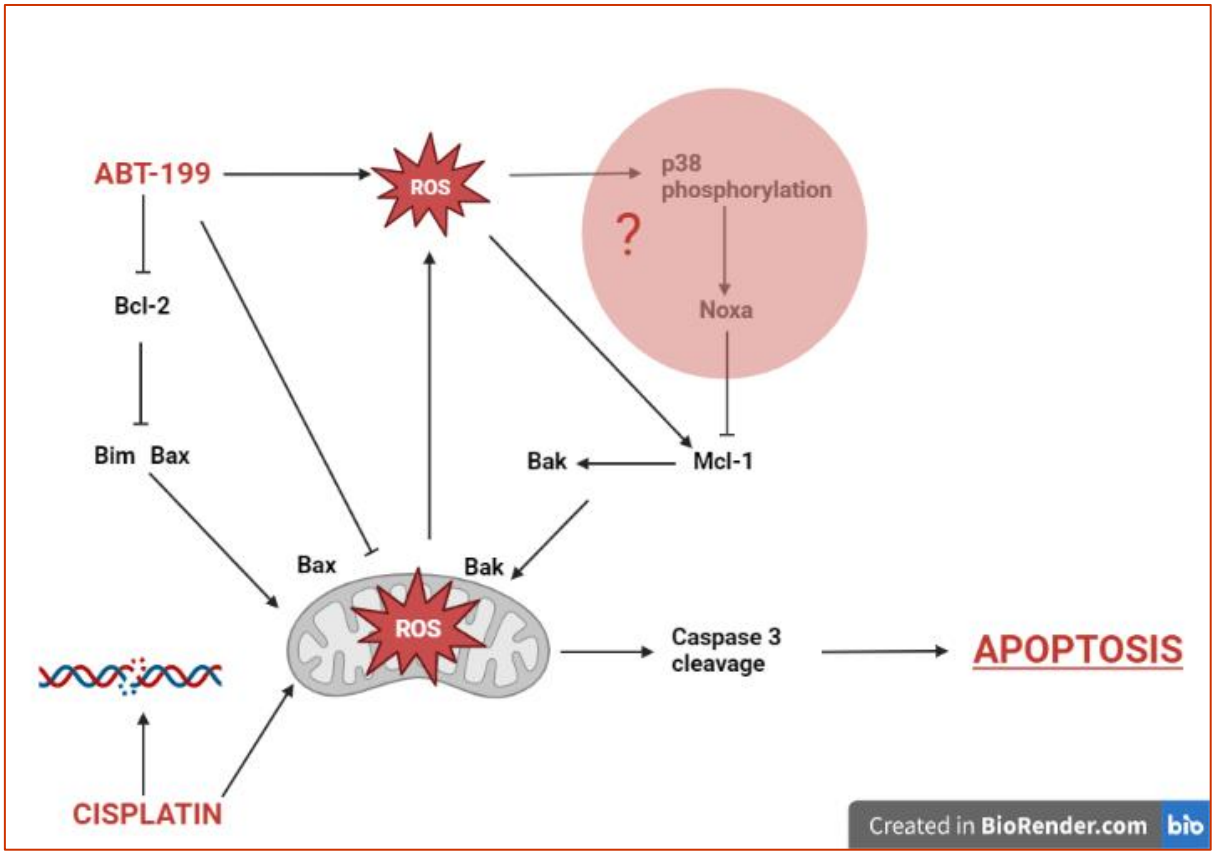

Figure 6.3 Proposed mechanism of enhanced cell death upon co-treatment with ABT-199 and cisplatin

This project proposes the synergistic effect of cisplatin and ABT-199 on cell death could be mediated through a dual action on apoptosis. On one hand, ABT-199 binds to Bcl-2 to release BIM and induce MOMP. On the other hand, ABT-199 induces ROS and impacts mitochondrial function with elevated ROS levels potentially leading to the phosphorylation of p38 which upregulates Noxa, a negative regulator of Mcl-1. Noxa

binding of Mcl-1 targets it for proteasomal degradation resulting in Bak release and activation and the subsequent induction of MOMP. Created with Biorender.com.

Results in this chapter have demonstrated that ABT-199 upregulation of ROS is of critical importance in mediating the synergistic effect on cell death with cisplatin. Reports in literature suggest that drug-induced ROS can be mediated by the ROS producing enzyme, NOX4 (NADPH oxidase 4). For example, Seo *et al* found that combined treatment of curcumin and thioridazine results in Mcl-1 degradation mediated by NOX4-mediated ROS[556]. Therefore, it is possible the upregulation of ROS by ABT-199 may be mediated by NOX4. In chapter 3, upregulation of autophagy was observed in response to cisplatin treatment. Chiou *et al* observed upregulation of NOX4/ROS/p38 axis resulting in autophagy-induced downregulation of β-TrCP mediating the increase of Noxa and Mcl-1 degradation[535]. β-TrCP is a ubiquitin E3 ligase involved in regulating various cellular processes. Future work could examine whether NOX4 is upregulated in BT16 cells treated with ABT-199 and whether inhibition with NOX4 inhibitor, GLX351322, prevents p38 phosphorylation and Noxa upregulation. In addition, future work could examine the effect of ABT-199 on autophagy in BT16 cells and regulation of β-TrCP to elucidate its involvement in mediating the increase of Noxa and Mcl-1 degradation. Interestingly, Alhoshani *et al*, have described increased ROS and autophagy-associated cell death in response to ABT-199 treatment in human breast cancer cells[478].

The integrated stress response (ISR) factors, ATF3 and ATF4 have also been reported to mediate transactivation of Noxa and subsequently Mcl-1 degradation[500]. As mentioned above Roca-Portoles *et al.*, proposed metabolic reprogramming of the mitochondria by ABT-199 where the activity of complex I/II in the ETC is impaired resulting in enhanced carboxylation. Metabolic reprogramming was confirmed by Weller *et al*, who observed an increased ratio of α-ketoglutarate:citrate in response to ABT-199 causing the activation of ATF4[500]. ER stress has been associated with chemoresistance in a number of studies[557]. Moreover, ER stress has also been implicated in resistance to ABT-263 in uveal melanoma cells[558]. Therefore, it would be of interest to determine if ATF3 and ATF4 are activated in response to ABT-199 treatment in MRT cells.

Interestingly, it was observed that the phenol red indicator in the medium of BT16 cells consistently became yellow at a much more rapid rate when compared to BT12 cells,

suggesting BT16 cells may have a more glycolytic phenotype than BT12 cells, which instead may be characterised by a more oxidative phenotype. A higher oxidative phenotype may account for the higher basal levels of ROS, which this study has observed in BT12 cells. Future work could aim to further study the differences in metabolism between the two MRT cell lines and establish whether this may also play a role in their different sensitivities to cisplatin. Moreover, it would be of interest to evaluate whether the differential expression of Bcl-2 in BT12 and BT16 cell lines may be linked to their different metabolic profiles.

Poly(ADP-ribose) polymerase 1 (PARP-1) is a DNA -damage response protein that is stimulated by both single strand and double strand DNA breaks. Further study is warranted to evaluate PARP-1 activation by cisplatin-induced DNA damage in MRT cell lines. PARP-1 activation leads to NAD+ depletion followed by ATP depletion resulting in cell death. As NAD+ is an essential metabolite in both OXPHOS and glycoltsis, an examination into the role of PARP-1 activation on cellular metabolic activity may be of interest, considering the varying metabolic profiles of the panel of MRT cell lines. Furthermore, PARP-1 has been linked to DNA-damage induced autophagy; it would be of interest to examine the link between cisplatin-induced autophagy and PARP1 activation/NAD+ inhibition with metabolic profiles.

Lastly, further studies could be carried out to evaluate the role of characteristic underlying SMARCB1 mutation on the observed effects of cisplatin on autophagy, the antioxidant system, and the Bcl-2 antiapoptotic family members. To this effect, re-expressing SMARCB1 in these SMARCB1-deficient cell lines and examining cellular responses cisplatin-induced autophagy with or without inhibitors may provide further insight into the significant of this mutation of cisplatin-induced autophagy. In addition, a comparison of the role of the antioxidant system in response to cisplatin cells with re-expressed SMARCB1 may help evaluate the importance of this mutation in the context of targeting the antioxidant system for the sensitisation of MRT cells to cisplatin.

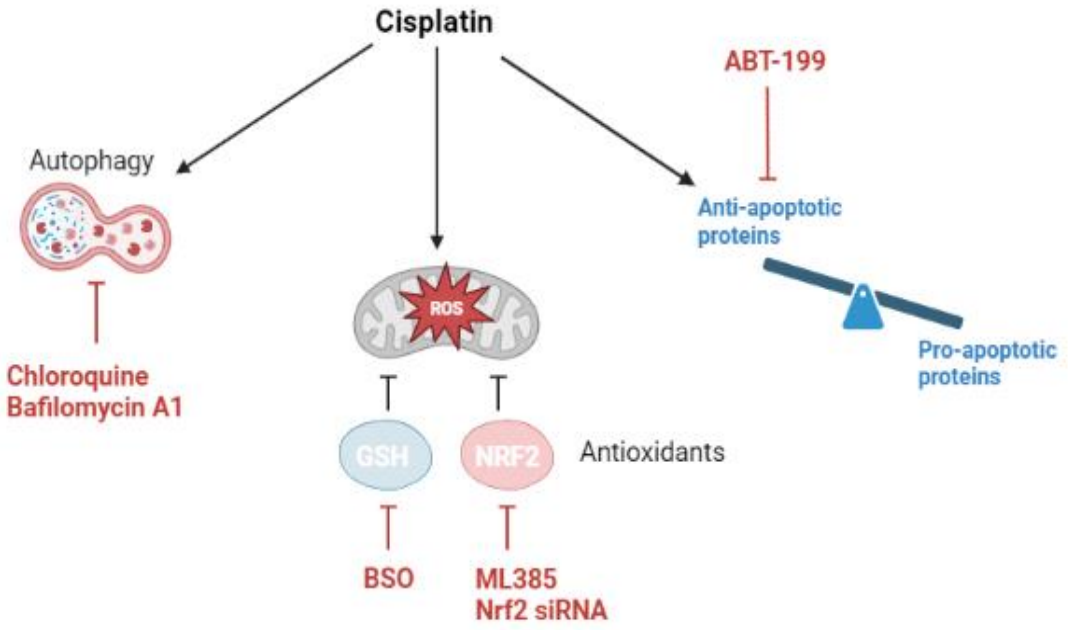

Figure 6.4 Targeting molecular mechanisms underlying cisplatin resistance in MRT cells.

In summary, this project has examined three aspects of cisplatin resistance in MRT, and results described herein suggest three potential strategies to circumvent this resistance. This study firstly evaluated the role of autophagy in mediating cisplatin resistance. Results demonstrated that cisplatin induced apoptosis and autophagy concomitantly in a panel of MRT cell lines. In addition, blocking autophagy at the early stages of the autophagic process using the pharmacological inhibitor SAR405 or through the genetic knockdown of critical autophagic protein ATG5 by siRNA did not sensitise cells to cisplatin-induced apoptosis. Collectively, these results suggest that induction of autophagy does not appear to elicit a pro-survival effect in the chemotherapeutic response of MRT cells. Nonetheless, this study found that combining cisplatin with the lysosomal inhibitors, chloroquine or bafilomycin-A1, may represent a novel treatment strategy to improve clinical outcome in MRT patients. Next, the role of the Nrf2/GSH antioxidant system was assessed. This study found a correlation between the expression profile of the antioxidant defence system and sensitivity to cisplatin. MRT cells with higher resistance to cisplatin exhibited higher levels of GSH and Nrf2 expression as well as lower levels of intracellular ROS. Most importantly, targeting either GSH with the inhibitor BSO or Nrf2 through an siRNA approach or with the small molecule inhibitor ML385 sensitised resistant MRT cells to

cisplatin-induced cell death suggesting that targeting the Nrf2/GSH antioxidant defence pathway may present a novel therapeutic avenue in the design of new treatment strategies for MRT and a means of overcoming chemoresistance.

Lastly, the role of the Bcl-2 family of proteins in mediating chemoresistance was examined. Differential expression of Bcl-2 was observed between cisplatin-sensitive BT12 cells and cisplatin-resistance BT16 cells. Importantly, the BH3 mimetic ABT-199 synergised with cisplatin to induce cell death in the cisplatin-resistant BT16 cells and a potential mechanism of action for this synergy between cisplatin and ABT-199 was proposed. BH3 mimetics are worth further evaluation for their applicability in improving the treatment of chemotherapy-resistant MRT with aberrant expression of Bcl-2 family proteins.

7. References

1. Woehrer, A. *et al.* Incidence of atypical teratoid/rhabdoid tumors in children. *Cancer* **116**, 5725-5732 (2010).
2. Brennan, B., Stiller, C. & Bourdeaut, F. Extracranial rhabdoid tumours: what we have learned so far and future directions. *The Lancet Oncology* **14**, e329-e336 (2013).
3. van den Heuvel-Eibrink, M.M. *et al.* Malignant rhabdoid tumours of the kidney (MRTKs), registered on recent SIOP protocols from 1993 to 2005: a report of the SIOP renal tumour study group. *Pediatr Blood Cancer* **56**, 733-737 (2011).
4. Tomlinson, G.E. *et al.* Rhabdoid Tumor of the Kidney in The National Wilms' Tumor Study: Age at Diagnosis As a Prognostic Factor. *Journal of Clinical Oncology* **23**, 7641-7645 (2005).
5. Beckwith, J.B. & Palmer, N.F. Histopathology and prognosis of Wilms tumor Results from the first national wilms' tumor study. *Cancer* **41**, 1937-1948 (1978).
6. Davidoff, A.M. Wilms tumor. *Advances in pediatrics* **59**, 247-267 (2012).
7. Haas, J.E., Palmer, N.F., Weinberg, A.G. & Beckwith, J.B. Ultrastructure of malignant rhabdoid tumor of the kidney. A distinctive renal tumor of children. *Hum Pathol* **12**, 646-657 (1981).
8. Weeks, D.A., Beckwith, J.B., Mierau, G.W. & Luckey, D.W. Rhabdoid tumor of kidney. A report of 111 cases from the National Wilms' Tumor Study Pathology Center. *Am J Surg Pathol* **13**, 439-458 (1989).
9. Rorke, L.B., Packer, R.J. & Biegel, J.A. Central nervous system atypical teratoid/rhabdoid tumors of infancy and childhood: definition of an entity. *J Neurosurg* **85**, 56-65 (1996).
10. Fritz, A., Edn. Third Edition. (ed. C. Percy) (World Health Organization, Geneva, Switzerland; 2000).
11. Bonnin, J.M., Rubinstein, L.J., Palmer, N.F. & Beckwith, J.B. The association of embryonal tumors originating in the kidney and in the brain. A report of seven cases. *Cancer* **54**, 2137-2146 (1984).
12. Geller, J.I., Roth, J.J. & Biegel, J.A. Biology and Treatment of Rhabdoid Tumor. *Critical reviews in oncogenesis* **20**, 199-216 (2015).
13. Bourdeaut, F. *et al.* Frequent hSNF5/INI1 Germline Mutations in Patients with Rhabdoid Tumor. *Clinical Cancer Research* **17**, 31 (2011).
14. Heck, J.E. *et al.* Epidemiology of rhabdoid tumors of early childhood. *Pediatric blood & cancer* **60**, 77-81 (2013).
15. Ostrom, Q.T. *et al.* The descriptive epidemiology of atypical teratoid/rhabdoid tumors in the United States, 2001–2010. *Neuro-Oncology* **16**, 1392-1399 (2014).
16. Brennan, B. *et al.* Outcome of extracranial malignant rhabdoid tumours in children registered in the European Paediatric Soft Tissue Sarcoma Study Group Non-Rhabdomyosarcoma Soft Tissue Sarcoma 2005 Study-EpSSG NRSTS 2005. *Eur J Cancer* **60**, 69-82 (2016).
17. Hilden, J.M. *et al.* Central nervous system atypical teratoid/rhabdoid tumor: results of therapy in children enrolled in a registry. *J Clin Oncol* **22**, 2877-2884 (2004).
18. Uwineza, A. *et al.* Rhabdoid tumor: the Irish experience 1986-2013. *Cancer Genet* **207**, 398-402 (2014).
19. Benesch, M. *et al.* High-dose chemotherapy (HDCT) with auto-SCT in children with atypical teratoid/rhabdoid tumors (AT/RT): a report from the European Rhabdoid Registry (EU-RHAB). *Bone Marrow Transplantation* **49**, 370-375 (2014).
20. Bartelheim, K. *et al.* Improved 6-year overall survival in AT/RT - results of the registry study Rhabdoid 2007. *Cancer Med* **5**, 1765-1775 (2016).

21. Nemes, K. *et al.* Clinical and genetic risk factors define two risk groups of extracranial malignant rhabdoid tumours (eMRT/RTK). *European Journal of Cancer* **142**, 112-122 (2021).
22. Biegel, J.A., Rorke, L.B. & Emanuel, B.S. Monosomy 22 in rhabdoid or atypical teratoid tumors of the brain. *N Engl J Med* **321**, 906 (1989).
23. Versteege, I. *et al.* Truncating mutations of hSNF5/INI1 in aggressive paediatric cancer. *Nature* **394**, 203-206 (1998).
24. Johann, P.D. Invited Review: Dysregulation of chromatin remodellers in paediatric brain tumours – SMARCB1 and beyond. *Neuropathology and Applied Neurobiology* **46**, 57-72 (2020).
25. Tang, L., Nogales, E. & Ciferri, C. Structure and function of SWI/SNF chromatin remodeling complexes and mechanistic implications for transcription. *Progress in biophysics and molecular biology* **102**, 122-128 (2010).
26. Phelan, M.L., Sif, S., Narlikar, G.J. & Kingston, R.E. Reconstitution of a core chromatin remodeling complex from SWI/SNF subunits. *Mol Cell* **3**, 247-253 (1999).
27. Muchardt, C. & Yaniv, M. When the SWI/SNF complex remodels … the cell cycle. *Oncogene* **20**, 3067-3075 (2001).
28. Kadoch, C. *et al.* Proteomic and bioinformatic analysis of mammalian SWI/SNF complexes identifies extensive roles in human malignancy. *Nat Genet* **45**, 592-601 (2013).
29. Wang, X. *et al.* SMARCB1-mediated SWI/SNF complex function is essential for enhancer regulation. *Nat Genet* **49**, 289-295 (2017).
30. Lu, C. & Allis, C.D. SWI/SNF complex in cancer. *Nature genetics* **49**, 178-179 (2017).
31. Nakayama, R.T. *et al.* SMARCB1 is required for widespread BAF complex-mediated activation of enhancers and bivalent promoters. *Nature genetics* **49**, 1613-1623 (2017).
32. Klochendler-Yeivin, A. *et al.* The murine SNF5/INI1 chromatin remodeling factor is essential for embryonic development and tumor suppression. *EMBO reports* **1**, 500-506 (2000).
33. Kohashi, K. & Oda, Y. Oncogenic roles of SMARCB1/INI1 and its deficient tumors. *Cancer Science* **108**, 547-552 (2017).
34. Mora-Blanco, E.L. *et al.* Activation of β-catenin/TCF targets following loss of the tumor suppressor SNF5. *Oncogene* **33**, 933-938 (2014).
35. Jagani, Z. *et al.* Loss of the tumor suppressor Snf5 leads to aberrant activation of the Hedgehog-Gli pathway. *Nature medicine* **16**, 1429-1433 (2010).
36. Duan, R., Du, W. & Guo, W. EZH2: a novel target for cancer treatment. *Journal of Hematology & Oncology* **13**, 104 (2020).
37. Knutson, S.K. *et al.* Durable tumor regression in genetically altered malignant rhabdoid tumors by inhibition of methyltransferase EZH2. *Proceedings of the National Academy of Sciences of the United States of America* **110**, 7922-7927 (2013).
38. Tang, A. *et al.* Aurora kinases: novel therapy targets in cancers. *Oncotarget* **8**, 23937-23954 (2017).
39. Kim, K.H. & Roberts, C.W.M. Mechanisms by which SMARCB1 loss drives rhabdoid tumor growth. *Cancer Genetics* **207**, 365-372 (2014).
40. Peng, L. *et al.* A Pan-Cancer Analysis of SMARCA4 Alterations in Human Cancers. *Frontiers in Immunology* **12** (2021).
41. Gröbner, S.N. *et al.* The landscape of genomic alterations across childhood cancers. *Nature* **555**, 321-327 (2018).
42. Ma, X. *et al.* Pan-cancer genome and transcriptome analyses of 1,699 paediatric leukaemias and solid tumours. *Nature* **555**, 371-376 (2018).
43. Eaton, K.W., Tooke, L.S., Wainwright, L.M., Judkins, A.R. & Biegel, J.A. Spectrum of SMARCB1/INI1 mutations in familial and sporadic rhabdoid tumors. *Pediatric blood & cancer* **56**, 7-15 (2011).

44. Sredni, S.T. & Tomita, T. Rhabdoid Tumor Predisposition Syndrome. *Pediatric and Developmental Pathology* **18**, 49-58 (2015).
45. Phi, J.H. *et al.* NPM1 as a potential therapeutic target for atypical teratoid/rhabdoid tumors. *BMC Cancer* **19**, 848 (2019).
46. Negrini, S., Gorgoulis, V.G. & Halazonetis, T.D. Genomic instability — an evolving hallmark of cancer. *Nature Reviews Molecular Cell Biology* **11**, 220-228 (2010).
47. Lee, R.S. *et al.* A remarkably simple genome underlies highly malignant pediatric rhabdoid cancers. *The Journal of clinical investigation* **122**, 2983-2988 (2012).
48. McKenna, E.S. *et al.* Loss of the epigenetic tumor suppressor SNF5 leads to cancer without genomic instability. *Mol Cell Biol* **28**, 6223-6233 (2008).
49. Kieran, M.W. *et al.* Absence of oncogenic canonical pathway mutations in aggressive pediatric rhabdoid tumors. *Pediatric Blood & Cancer* **59**, 1155-1157 (2012).
50. Hasselblatt, M. *et al.* High-resolution genomic analysis suggests the absence of recurrent genomic alterations other than SMARCB1 aberrations in atypical teratoid/rhabdoid tumors. *Genes, Chromosomes and Cancer* **52**, 185-190 (2013).
51. Clapier, C.R. & Cairns, B.R. The Biology of Chromatin Remodeling Complexes. *Annual Review of Biochemistry* **78**, 273-304 (2009).
52. Kalimuthu, S.N. & Chetty, R. Gene of the month: SMARCB1. *Journal of clinical pathology* **69**, 484-489 (2016).
53. Vitte, J., Gao, F., Coppola, G., Judkins, A.R. & Giovannini, M. Timing of Smarcb1 and Nf2 inactivation determines schwannoma versus rhabdoid tumor development. *Nature Communications* **8**, 300 (2017).
54. Torchia, J. *et al.* Integrated (epi)-Genomic Analyses Identify Subgroup-Specific Therapeutic Targets in CNS Rhabdoid Tumors. *Cancer cell* **30**, 891-908 (2016).
55. Abdullah, A., Patel, Y., Lewis, T.J., Elsamaloty, H. & Strobel, S. Extrarenal malignant rhabdoid tumors: radiologic findings with histopathologic correlation. *Cancer imaging : the official publication of the International Cancer Imaging Society* **10**, 97-101 (2010).
56. Nguyen, H., Stelling, A., Kuramoto, A., Patel, C. & Keller, J. Malignant rhabdoid tumor of the liver: Findings at US, CT, and MRI, with histopathologic correlation. *Radiology case reports* **9**, e00031-e00031 (2015).
57. Tergestina, M., Ross, B.J., Manipadam, M.T. & Kumar, M. Malignant rhabdoid tumour of the neck in a neonate. *BMJ Case Reports* **2018**, bcr-2017-223145 (2018).
58. Madan, K., Bal, A., Agarwal, R. & Das, A. Malignant extra renal rhabdoid tumour presenting as central airway obstruction. *Case reports in pulmonology* **2014**, 950869-950869 (2014).
59. Kapral, N., Melmer, P., Druzgal, C.H. & Lancaster, L. Pediatric hepatic rhabdoid tumor: A rare cause of abdominal mass in children. *Radiology Case Reports* **13**, 724-727 (2018).
60. Wykoff, C.C. *et al.* Atypical teratoid/rhabdoid tumor arising from the third cranial nerve. *Journal of neuro-ophthalmology : the official journal of the North American Neuro-Ophthalmology Society* **28**, 207-211 (2008).
61. Biggs, P.J., Garen, P.D., Powers, J.M. & Garvin, A.J. Malignant rhabdoid tumor of the central nervous system. *Hum Pathol* **18**, 332-337 (1987).
62. Tahir, F., Vol. Cureus. (ed. Z. Majid) 8 (2019).
63. Amar, A.M., Tomlinson, G., Green, D.M., Breslow, N.E. & de Alarcon, P.A. Clinical presentation of rhabdoid tumors of the kidney. *J Pediatr Hematol Oncol* **23**, 105-108 (2001).
64. Gündüz, K. *et al.* Malignant Rhabdoid Tumor of the Orbit. *Archives of Ophthalmology* **116**, 243-246 (1998).
65. Ng, W.K., Toe, B.P. & Lau, H.Y. Malignant Rhabdoid Tumor of the Mediastinum: A Case Report and Literature Review. *Journal of clinical imaging science* **9**, 7-7 (2019).

66. Sigauke, E. *et al.* Absence of expression of SMARCB1/INI1 in malignant rhabdoid tumors of the central nervous system, kidneys and soft tissue: an immunohistochemical study with implications for diagnosis. *Modern Pathology* **19**, 717-725 (2006).
67. Horazdovsky, R., Manivel, J.C. & Cheng, E.Y. Surgery and actinomycin improve survival in malignant rhabdoid tumor. *Sarcoma* **2013**, 315170 (2013).
68. Richards, A. *et al.* Outcomes with respect to extent of surgical resection for pediatric atypical teratoid rhabdoid tumors. *Child's Nervous System* **36**, 713-719 (2020).
69. Reddy, A.T. *et al.* Efficacy of High-Dose Chemotherapy and Three-Dimensional Conformal Radiation for Atypical Teratoid/Rhabdoid Tumor: A Report From the Children's Oncology Group Trial ACNS0333. *Journal of Clinical Oncology* **38**, 1175-1185 (2020).
70. Crist, W. *et al.* The Third Intergroup Rhabdomyosarcoma Study. *Journal of Clinical Oncology* **13**, 610-630 (1995).
71. Kerl, K., Holsten, T. & Frühwald, M.C. Rhabdoid Tumors: Clinical Approaches and Molecular Targets for Innovative Therapy. *Pediatric Hematology and Oncology* **30**, 587-604 (2013).
72. Nemes, K. *et al.* The extraordinary challenge of treating patients with congenital rhabdoid tumors—a collaborative European effort. *Pediatric Blood & Cancer* **65**, e26999 (2018).
73. Tekautz, T.M. *et al.* Atypical Teratoid/Rhabdoid Tumors (ATRT): Improved Survival in Children 3 Years of Age and Older With Radiation Therapy and High-Dose Alkylator-Based Chemotherapy. *Journal of Clinical Oncology* **23**, 1491-1499 (2005).
74. Jaenisch, R. & Bird, A. Epigenetic regulation of gene expression: how the genome integrates intrinsic and environmental signals. *Nature Genetics* **33**, 245-254 (2003).
75. Johann, P.D. *et al.* Atypical Teratoid/Rhabdoid Tumors Are Comprised of Three Epigenetic Subgroups with Distinct Enhancer Landscapes. *Cancer Cell* **29**, 379-393 (2016).
76. Torchia, J. *et al.* Molecular subgroups of atypical teratoid rhabdoid tumours in children: an integrated genomic and clinicopathological analysis. *Lancet Oncol* **16**, 569-582 (2015).
77. Chun, H.E. *et al.* Genome-Wide Profiles of Extra-cranial Malignant Rhabdoid Tumors Reveal Heterogeneity and Dysregulated Developmental Pathways. *Cancer Cell* **29**, 394-406 (2016).
78. Tsankova, N., Renthal, W., Kumar, A. & Nestler, E.J. Epigenetic regulation in psychiatric disorders. *Nature Reviews Neuroscience* **8**, 355-367 (2007).
79. Schuettengruber, B., Bourbon, H.-M., Di Croce, L. & Cavalli, G. Genome Regulation by Polycomb and Trithorax: 70 Years and Counting. *Cell* **171**, 34-57 (2017).
80. Kuwahara, Y., Wei, D., Durand, J. & Weissman, B.E. SNF5 reexpression in malignant rhabdoid tumors regulates transcription of target genes by recruitment of SWI/SNF complexes and RNAPII to the transcription start site of their promoters. *Molecular cancer research : MCR* **11**, 251-260 (2013).
81. Bild, A.H. *et al.* Oncogenic pathway signatures in human cancers as a guide to targeted therapies. *Nature* **439**, 353-357 (2006).
82. Nemes, K. & Frühwald, M.C. Emerging therapeutic targets for the treatment of malignant rhabdoid tumors. *Expert Opinion on Therapeutic Targets* **22**, 365-379 (2018).
83. George, R.E. *et al.* Phase I study of decitabine with doxorubicin and cyclophosphamide in children with neuroblastoma and other solid tumors: a Children's Oncology Group study. *Pediatric blood & cancer* **55**, 629-638 (2010).
84. Nemes, K. *et al.* Current and Emerging Therapeutic Approaches for Extracranial Malignant Rhabdoid Tumors. *Cancer management and research* **14**, 479-498 (2022).
85. Matthews, H.K., Bertoli, C. & de Bruin, R.A.M. Cell cycle control in cancer. *Nature Reviews Molecular Cell Biology* **23**, 74-88 (2022).
86. Tsikitis, M., Zhang, Z., Edelman, W., Zagzag, D. & Kalpana, G.V. Genetic ablation of Cyclin D1 abrogates genesis of rhabdoid tumors resulting from Ini1 loss. *Proceedings of the National Academy of Sciences of the United States of America* **102**, 12129-12134 (2005).

87. Kuwahara, Y., Charboneau, A., Knudsen, E.S. & Weissman, B.E. Reexpression of hSNF5 in malignant rhabdoid tumor cell lines causes cell cycle arrest through a p21(CIP1/WAF1)-dependent mechanism. *Cancer Res* **70**, 1854-1865 (2010).
88. Alarcon-Vargas, D. *et al.* Targeting cyclin D1, a downstream effector of INI1/hSNF5, in rhabdoid tumors. *Oncogene* **25**, 722-734 (2006).
89. Zhang, Z.K. *et al.* Cell cycle arrest and repression of cyclin D1 transcription by INI1/hSNF5. *Mol Cell Biol* **22**, 5975-5988 (2002).
90. Wetmore, C. *et al.* Alisertib is active as single agent in recurrent atypical teratoid rhabdoid tumors in 4 children. *Neuro-oncology* **17**, 882-888 (2015).
91. Venkataraman, S. *et al.* Targeting Aurora Kinase A enhances radiation sensitivity of atypical teratoid rhabdoid tumor cells. *Journal of neuro-oncology* **107**, 517-526 (2012).
92. Maris, J.M. *et al.* Initial testing of the aurora kinase A inhibitor MLN8237 by the Pediatric Preclinical Testing Program (PPTP). *Pediatric blood & cancer* **55**, 26-34 (2010).
93. Coyle, R., Slattery, K., Ennis, L., O'Sullivan M, J. & Zisterer, D.M. The XIAP inhibitor embelin sensitises malignant rhabdoid tumour cells to TRAIL treatment via enhanced activation of the extrinsic apoptotic pathway. *Int J Oncol* **55**, 191-202 (2019).
94. Ouchi, K. *et al.* A NOXA/MCL-1 Imbalance Underlies Chemoresistance of Malignant Rhabdoid Tumor Cells. *Journal of Cellular Physiology* **231**, 1932-1940 (2016).
95. Bukowski, K., Kciuk, M. & Kontek, R. Mechanisms of Multidrug Resistance in Cancer Chemotherapy. *International journal of molecular sciences* **21**, 3233 (2020).
96. Vasan, N., Baselga, J. & Hyman, D.M. A view on drug resistance in cancer. *Nature* **575**, 299-309 (2019).
97. Mansoori, B., Mohammadi, A., Davudian, S., Shirjang, S. & Baradaran, B. The Different Mechanisms of Cancer Drug Resistance: A Brief Review. *Advanced pharmaceutical bulletin* **7**, 339-348 (2017).
98. Lippert, T.H., Ruoff, H.-J. & Volm, M. Intrinsic and Acquired Drug Resistance in Malignant Tumors. *The main reason for therapeutic failure* **58**, 261-264 (2008).
99. Greaves, M. & Maley, C.C. Clonal evolution in cancer. *Nature* **481**, 306-313 (2012).
100. Santos, P. & Almeida, F. Role of Exosomal miRNAs and the Tumor Microenvironment in Drug Resistance. *Cells* **9**, 1450 (2020).
101. Ramos, A., Sadeghi, S. & Tabatabaeian, H. Battling Chemoresistance in Cancer: Root Causes and Strategies to Uproot Them. *International Journal of Molecular Sciences* **22** (2021).
102. Ralhan, R. & Kaur, J. Alkylating agents and cancer therapy. *Expert Opinion on Therapeutic Patents* **17**, 1061-1075 (2007).
103. Rocha, C.R.R., Silva, M.M., Quinet, A., Cabral-Neto, J.B. & Menck, C.F.M. DNA repair pathways and cisplatin resistance: an intimate relationship. *Clinics (Sao Paulo)* **73**, e478s (2018).
104. Li, L.-y., Guan, Y.-d., Chen, X.-s., Yang, J.-m. & Cheng, Y. DNA Repair Pathways in Cancer Therapy and Resistance. *Frontiers in Pharmacology* **11** (2021).
105. Hashizume, R. *et al.* Inhibition of DNA damage repair by the CDK4/6 inhibitor palbociclib delays irradiated intracranial atypical teratoid rhabdoid tumor and glioblastoma xenograft regrowth. *Neuro Oncol* **18**, 1519-1528 (2016).
106. Uribe, M.L., Marrocco, I. & Yarden, Y. EGFR in Cancer: Signaling Mechanisms, Drugs, and Acquired Resistance. *Cancers* **13**, 2748 (2021).
107. Hientz, K., Mohr, A., Bhakta-Guha, D. & Efferth, T. The role of p53 in cancer drug resistance and targeted chemotherapy. *Oncotarget* **8**, 8921-8946 (2017).
108. Lee, H.-J. *et al.* Drug Resistance via Feedback Activation of Stat3 in Oncogene-Addicted Cancer Cells. *Cancer Cell* **26**, 207-221 (2014).

109. Kamaruzman, N.I., Aziz, N.A., Poh, C.L. & Chowdhury, E.H. Oncogenic Signaling in Tumorigenesis and Applications of siRNA Nanotherapeutics in Breast Cancer. *Cancers* **11**, 632 (2019).
110. McCubrey, J.A. *et al.* Roles of signaling pathways in drug resistance, cancer initiating cells and cancer progression and metastasis. *Advances in Biological Regulation* **57**, 75-101 (2015).
111. Zahreddine, H. & Borden, K. Mechanisms and insights into drug resistance in cancer. *Frontiers in Pharmacology* **4** (2013).
112. Borchert, S. *et al.* Impact of metallothionein-knockdown on cisplatin resistance in malignant pleural mesothelioma. *Scientific Reports* **10**, 18677 (2020).
113. Housman, G. *et al.* Drug resistance in cancer: an overview. *Cancers* **6**, 1769-1792 (2014).
114. Zhang, N., Yin, Y., Xu, S.-J. & Chen, W.-S. 5-Fluorouracil: mechanisms of resistance and reversal strategies. *Molecules (Basel, Switzerland)* **13**, 1551-1569 (2008).
115. Bossennec, M., Di Roio, A., Caux, C. & Ménétrier-Caux, C. MDR1 in immunity: friend or foe? *Oncoimmunology* **7**, e1499388-e1499388 (2018).
116. Fojo, A.T. *et al.* Expression of a multidrug-resistance gene in human tumors and tissues. *Proceedings of the National Academy of Sciences of the United States of America* **84**, 265-269 (1987).
117. Kurimchak, A.M. *et al.* MDR1 Drug Efflux Pump Promotes Intrinsic and Acquired Resistance to PROTACs in Cancer Cells. *bioRxiv*, 2021.2012.2002.470920 (2021).
118. Mao, Q. & Unadkat, J.D. Role of the breast cancer resistance protein (BCRP/ABCG2) in drug transport--an update. *The AAPS journal* **17**, 65-82 (2015).
119. Natarajan, K., Xie, Y., Baer, M.R. & Ross, D.D. Role of breast cancer resistance protein (BCRP/ABCG2) in cancer drug resistance. *Biochemical pharmacology* **83**, 1084-1103 (2012).
120. Si, W., Shen, J., Zheng, H. & Fan, W. The role and mechanisms of action of microRNAs in cancer drug resistance. *Clinical Epigenetics* **11**, 25 (2019).
121. Ma, J., Dong, C. & Ji, C. MicroRNA and drug resistance. *Cancer Gene Therapy* **17**, 523-531 (2010).
122. van der Spek, Y.M., Kroep, J.R., Tollenaar, R.A.E.M. & Mesker, W.E. Chemotherapy resistance and stromal targets in breast cancer treatment: a review. *Molecular Biology Reports* **47**, 8169-8177 (2020).
123. Boedtkjer, E. & Pedersen, S.F. The Acidic Tumor Microenvironment as a Driver of Cancer. *Annual Review of Physiology* **82**, 103-126 (2020).
124. Wojtkowiak, J.W., Verduzco, D., Schramm, K.J. & Gillies, R.J. Drug resistance and cellular adaptation to tumor acidic pH microenvironment. *Mol Pharm* **8**, 2032-2038 (2011).
125. Sharma, M. *et al.* pH Gradient Reversal: An Emerging Hallmark of Cancers. *Recent Pat Anticancer Drug Discov* **10**, 244-258 (2015).
126. Senthebane, D.A. *et al.* The Role of Tumor Microenvironment in Chemoresistance: To Survive, Keep Your Enemies Closer. *International journal of molecular sciences* **18**, 1586 (2017).
127. Song, K.-A. & Faber, A.C. Epithelial-to-mesenchymal transition and drug resistance: transitioning away from death. *Journal of thoracic disease* **11**, E82-E85 (2019).
128. Dudas, J., Ladanyi, A., Ingruber, J., Steinbichler, T.B. & Riechelmann, H. Epithelial to Mesenchymal Transition: A Mechanism that Fuels Cancer Radio/Chemoresistance. *Cells* **9**, 428 (2020).
129. Zheng, X. *et al.* Epithelial-to-mesenchymal transition is dispensable for metastasis but induces chemoresistance in pancreatic cancer. *Nature* **527**, 525-530 (2015).
130. Singh, A. & Settleman, J. EMT, cancer stem cells and drug resistance: an emerging axis of evil in the war on cancer. *Oncogene* **29**, 4741-4751 (2010).

131. Tanabe, S., Quader, S., Cabral, H. & Ono, R. Interplay of EMT and CSC in Cancer and the Potential Therapeutic Strategies. *Frontiers in Pharmacology* **11** (2020).
132. Phi, L.T.H. *et al.* Cancer Stem Cells (CSCs) in Drug Resistance and their Therapeutic Implications in Cancer Treatment. *Stem cells international* **2018**, 5416923-5416923 (2018).
133. Auffinger, B. *et al.* Conversion of differentiated cancer cells into cancer stem-like cells in a glioblastoma model after primary chemotherapy. *Cell Death Differ* **21**, 1119-1131 (2014).
134. Shlush, L.I. *et al.* Identification of pre-leukaemic haematopoietic stem cells in acute leukaemia. *Nature* **506**, 328-333 (2014).
135. Heenatigala Palliyage, G., Ghosh, R. & Rojanasakul, Y. Cancer chemoresistance and therapeutic strategies targeting tumor microenvironment. *ScienceAsia* **46**, 639 (2020).
136. Ayestaran, I. *et al.* Identification of Intrinsic Drug Resistance and Its Biomarkers in High-Throughput Pharmacogenomic and CRISPR Screens. *Patterns* **1**, 100065 (2020).
137. Rajendran, G., Taylor, J.A. & Woolbright, B.L. Natural products as a means of overcoming cisplatin chemoresistance in bladder cancer. *Cancer Drug Resistance* **4**, 69-84 (2021).
138. Rosa, R., D'Amato, V., De Placido, S. & Bianco, R. Approaches for targeting cancer stem cells drug resistance. *Expert Opinion on Drug Discovery* **11**, 1201-1212 (2016).
139. Samuel, S.M. *et al.* Counteracting Chemoresistance with Metformin in Breast Cancers: Targeting Cancer Stem Cells. LID - 10.3390/cancers12092482 [doi] LID – 2482 (2020).
140. Riganti, C. & Contino, M. New Strategies to Overcome Resistance to Chemotherapy and Immune System in Cancer. *International journal of molecular sciences* **20**, 4783 (2019).
141. Chang, H. & Zou, Z. Targeting autophagy to overcome drug resistance: further developments. *Journal of Hematology & Oncology* **13**, 159 (2020).
142. Kwee, J.K. A paradoxical chemoresistance and tumor suppressive role of antioxidant in solid cancer cells: a strange case of Dr. Jekyll and Mr. Hyde. *BioMed research international*, 209845-209845 (2014).
143. Huo, H., Magro, P.G., Pietsch, E.C., Patel, B.B. & Scotto, K.W. Histone methyltransferase MLL1 regulates MDR1 transcription and chemoresistance. *Cancer Res* **70**, 8726-8735 (2010).
144. Hu, S. *et al.* Overexpression of EZH2 contributes to acquired cisplatin resistance in ovarian cancer cells in vitro and in vivo. *Cancer Biology & Therapy* **10**, 788-795 (2010).
145. Alimova, I. *et al.* Inhibition of EZH2 suppresses self-renewal and induces radiation sensitivity in atypical rhabdoid teratoid tumor cells. *Neuro Oncol* **15**, 149-160 (2013).
146. Jones, R.L. *et al.* A phase II, multicenter study of the EZH2 inhibitor tazemetostat in adults (rhabdoid tumor cohort) (NCT02601950). *Annals of Oncology* **29**, viii580-viii581 (2018).
147. Ishi, Y. *et al.* Therapeutic Targeting of EZH2 and BET BRD4 in Pediatric Rhabdoid Tumors. *Molecular Cancer Therapeutics* **21**, 715-726 (2022).
148. Liu, W.H. *et al.* Cisplatin-selected resistance is associated with increased motility and stem-like properties via activation of STAT3/Snail axis in atypical teratoid/rhabdoid tumor cells. *Oncotarget* **6**, 1750-1768 (2015).
149. Rosson, G.B., Vincent, T.S., Oswald, B.W. & Wright, C.F. Drug resistance in malignant rhabdoid tumor cell lines. *Cancer Chemotherapy and Pharmacology* **49**, 142-148 (2002).
150. Melcher, V. *et al.* Macrophage-tumor cell interaction promotes ATRT progression and chemoresistance. *Acta Neuropathologica* **139**, 913-936 (2020).
151. Chiou, S.H. *et al.* Identification of CD133-positive radioresistant cells in atypical teratoid/rhabdoid tumor. *PLoS One* **3**, e2090 (2008).
152. Yanagisawa, S. *et al.* Identification and Metastatic Potential of Tumor-Initiating Cells in Malignant Rhabdoid Tumor of the Kidney. *Clinical Cancer Research* **15**, 3014-3022 (2009).
153. Nodomi, S. *et al.* CD146 is a novel marker for highly tumorigenic cells and a potential therapeutic target in malignant rhabdoid tumor. *Oncogene* **35**, 5317-5327 (2016).

154. Okuno, K. *et al.* Expression of neural stem cell markers in malignant rhabdoid tumor cell lines. *Oncol Rep* **23**, 485-492 (2010).
155. Carugo, A. *et al.* p53 Is a Master Regulator of Proteostasis in SMARCB1-Deficient Malignant Rhabdoid Tumors. *Cancer Cell* **35**, 204-220.e209 (2019).
156. Hanahan, D. Hallmarks of Cancer: New Dimensions. *Cancer Discov* **12**, 31-46 (2022).
157. Shalini, S., Dorstyn, L., Dawar, S. & Kumar, S. Old, new and emerging functions of caspases. *Cell Death & Differentiation* **22**, 526-539 (2015).
158. García-Berrocal, J.R. *et al.* The anticancer drug cisplatin induces an intrinsic apoptotic pathway inside the inner ear. *British journal of pharmacology* **152**, 1012-1020 (2007).
159. Shamas-Din, A., Brahmbhatt, H., Leber, B. & Andrews, D.W. BH3-only proteins: Orchestrators of apoptosis. *Biochimica et Biophysica Acta (BBA) - Molecular Cell Research* **1813**, 508-520 (2011).
160. Li, J. & Yuan, J. Caspases in apoptosis and beyond. *Oncogene* **27**, 6194-6206 (2008).
161. Guicciardi, M.E. & Gores, G.J. Life and death by death receptors. *FASEB journal : official publication of the Federation of American Societies for Experimental Biology* **23**, 1625-1637 (2009).
162. Kumar, R., Herbert, P.E. & Warrens, A.N. An introduction to death receptors in apoptosis. *International Journal of Surgery* **3**, 268-277 (2005).
163. Ichim, G. & Tait, S.W.G. A fate worse than death: apoptosis as an oncogenic process. *Nature Reviews Cancer* **16**, 539-548 (2016).
164. Hrdinka, M. & Yabal, M. Inhibitor of apoptosis proteins in human health anddisease. *Genes & Immunity* **20**, 641-650 (2019).
165. Silke, J. & Meier, P. Inhibitor of apoptosis (IAP) proteins-modulators of cell death and inflammation. *Cold Spring Harbor perspectives in biology* **5**, a008730 (2013).
166. Martinez-Ruiz, G., Maldonado, V., Ceballos-Cancino, G., Grajeda, J.P.R. & Melendez-Zajgla, J. Role of Smac/DIABLO in cancer progression. *Journal of experimental & clinical cancer research : CR* **27**, 48-48 (2008).
167. Eckelman, B.P., Salvesen, G.S. & Scott, F.L. Human inhibitor of apoptosis proteins: why XIAP is the black sheep of the family. *EMBO reports* **7**, 988-994 (2006).
168. Lalaoui, N. & Vaux, D.L. Recent advances in understanding inhibitor of apoptosis proteins. *F1000Research* **7**, F1000 Faculty Rev-1889 (2018).
169. Vucic, D. *et al.* Engineering ML-IAP to produce an extraordinarily potent caspase 9 inhibitor: implications for Smac-dependent anti-apoptotic activity of ML-IAP. *The Biochemical journal* **385**, 11-20 (2005).
170. Mobahat, M., Narendran, A. & Riabowol, K. Survivin as a preferential target for cancer therapy. *International journal of molecular sciences* **15**, 2494-2516 (2014).
171. Kataoka, T. & Tschopp, J. N-terminal fragment of c-FLIP(L) processed by caspase 8 specifically interacts with TRAF2 and induces activation of the NF-kappaB signaling pathway. *Molecular and cellular biology* **24**, 2627-2636 (2004).
172. Safa, A.R. Roles of c-FLIP in Apoptosis, Necroptosis, and Autophagy. *Journal of carcinogenesis & mutagenesis* **Suppl 6**, 003 (2013).
173. Geserick, P. *et al.* Suppression of cFLIP is sufficient to sensitize human melanoma cells to TRAIL- and CD95L-mediated apoptosis. *Oncogene* **27**, 3211-3220 (2008).
174. Singh, R., Letai, A. & Sarosiek, K. Regulation of apoptosis in health and disease: the balancing act of BCL-2 family proteins. *Nature Reviews Molecular Cell Biology* **20**, 175-193 (2019).
175. Kale, J., Osterlund, E.J. & Andrews, D.W. BCL-2 family proteins: changing partners in the dance towards death. *Cell Death & Differentiation* **25**, 65-80 (2018).
176. Michels, J. *et al.* Functions of BCL-X L at the Interface between Cell Death and Metabolism. *Int J Cell Biol* **2013**, 705294 (2013).

177. Kvansakul, M. & Hinds, M.G. Structural biology of the Bcl-2 family and its mimicry by viral proteins. *Cell death & disease* **4**, e909-e909 (2013).
178. Adams, C.M., Clark-Garvey, S., Porcu, P. & Eischen, C.M. Targeting the Bcl-2 Family in B Cell Lymphoma. *Frontiers in oncology* **8**, 636-636 (2019).
179. Tzifi, F. *et al.* The Role of BCL2 Family of Apoptosis Regulator Proteins in Acute and Chronic Leukemias. *Advances in Hematology* **2012**, 524308 (2012).
180. Donovan, M. & Cotter, T.G. Control of mitochondrial integrity by Bcl-2 family members and caspase-independent cell death. *Biochimica et Biophysica Acta (BBA) - Molecular Cell Research* **1644**, 133-147 (2004).
181. Gabellini, C., Trisciuoglio, D. & Del Bufalo, D. Non-canonical roles of Bcl-2 and Bcl-xL proteins: relevance of BH4 domain. *Carcinogenesis* **38**, 579-587 (2017).
182. Tsujimoto, Y. & Shimizu, S. VDAC regulation by the Bcl-2 family of proteins. *Cell Death & Differentiation* **7**, 1174-1181 (2000).
183. Mojsa, B., Lassot, I. & Desagher, S. Mcl-1 ubiquitination: unique regulation of an essential survival protein. *Cells* **3**, 418-437 (2014).
184. Westphal, D., Kluck, R.M. & Dewson, G. Building blocks of the apoptotic pore: how Bax and Bak are activated and oligomerize during apoptosis. *Cell Death & Differentiation* **21**, 196-205 (2014).
185. Campbell, K.J. & Tait, S.W.G. Targeting BCL-2 regulated apoptosis in cancer. *Open biology* **8**, 180002 (2018).
186. Aguiló, N., Uranga, S., Marinova, D., Martín, C. & Pardo, J. Bim is a crucial regulator of apoptosis induced byMycobacterium tuberculosis. *Cell Death & Disease* **5**, e1343-e1343 (2014).
187. Shukla, S., Saxena, S., Singh, B.K. & Kakkar, P. BH3-only protein BIM: An emerging target in chemotherapy. *European Journal of Cell Biology* **96**, 728-738 (2017).
188. Billen, L.P., Shamas-Din, A. & Andrews, D.W. Bid: a Bax-like BH3 protein. *Oncogene* **27**, S93-S104 (2008).
189. Sinicrope, F.A. *et al.* Proapoptotic Bad and Bid protein expression predict survival in stages II and III colon cancers. *Clinical cancer research : an official journal of the American Association for Cancer Research* **14**, 4128-4133 (2008).
190. Krajewska, M. *et al.* Expression of Bcl-2 family member Bid in normal and malignant tissues. *Neoplasia (New York, N.Y.)* **4**, 129-140 (2002).
191. Ploner, C., Kofler, R. & Villunger, A. Noxa: at the tip of the balance between life and death. *Oncogene* **27 Suppl 1**, S84-S92 (2008).
192. Albert, M.-C., Brinkmann, K. & Kashkar, H. Noxa and cancer therapy: Tuning up the mitochondrial death machinery in response to chemotherapy. *Molecular & cellular oncology* **1**, e29906-e29906 (2014).
193. Kosmidou, V. *et al.* Noxa upregulation and 5-gene apoptotic biomarker panel in colorectal cancer. *European Journal of Clinical Investigation* **51**, e13353 (2021).
194. Yu, J. & Zhang, L. PUMA, a potent killer with or without p53. *Oncogene* **27 Suppl 1**, S71-S83 (2008).
195. Polcic, P., Jaka, P. & Mentel, M. Yeast as a tool for studying proteins of the Bcl-2 family. *Microbial Cell* **2**, 74-87 (2015).
196. Kerr, J.F., Wyllie, A.H. & Currie, A.R. Apoptosis: a basic biological phenomenon with wide-ranging implications in tissue kinetics. *British journal of cancer* **26**, 239-257 (1972).
197. Wong, R.S.Y. Apoptosis in cancer: from pathogenesis to treatment. *Journal of experimental & clinical cancer research : CR* **30**, 87-87 (2011).
198. Lopes, R.B., Gangeswaran, R., McNeish, I.A., Wang, Y. & Lemoine, N.R. Expression of the IAP protein family is dysregulated in pancreatic cancer cells and is important for resistance to chemotherapy. *International Journal of Cancer* **120**, 2344-2352 (2007).

199. Abd-Elrahman, I. *et al.* The Inhibitor of Apoptosis Protein Livin (ML-IAP) Plays a Dual Role in Tumorigenicity. *Cancer Research* **69**, 5475-5480 (2009).
200. Small, S., Keerthivasan, G., Huang, Z., Gurbuxani, S. & Crispino, J.D. Overexpression of survivin initiates hematologic malignancies in vivo. *Leukemia* **24**, 1920-1926 (2010).
201. Bai, L., Smith, D.C. & Wang, S. Small-molecule SMAC mimetics as new cancer therapeutics. *Pharmacology & therapeutics* **144**, 82-95 (2014).
202. Dean, E.J. *et al.* A small molecule inhibitor of XIAP induces apoptosis and synergises with vinorelbine and cisplatin in NSCLC. *British journal of cancer* **102**, 97-103 (2010).
203. Lee, E.K. *et al.* A Smac mimetic augments the response of urothelial cancer cells to gemcitabine and cisplatin. *Cancer biology & therapy* **14**, 812-822 (2013).
204. Binder, P.S. *et al.* The targeted SMAC mimetic SW IV-134 augments platinum-based chemotherapy in pre-clinical models of ovarian cancer. *BMC Cancer* **22**, 263 (2022).
205. Coyle, R., O'Sullivan, M.J. & Zisterer, D.M. Targeting inhibitor of apoptosis proteins (IAPs) with IAP inhibitors sensitises malignant rhabdoid tumour cells to cisplatin. *Cancer Treatment and Research Communications* **32**, 100579 (2022).
206. Jonges, L.E. *et al.* Caspase-3 Activity as a Prognostic Factor in Colorectal Carcinoma. *Laboratory Investigation* **81**, 681-688 (2001).
207. Wang, J. *et al.* Livin, Survivin and Caspase 3 as early recurrence markers in non-muscle-invasive bladder cancer. *World J Urol* **32**, 1477-1484 (2014).
208. Devarajan, E. *et al.* Down-regulation of caspase 3 in breast cancer: a possible mechanism for chemoresistance. *Oncogene* **21**, 8843-8851 (2002).
209. Liu, P.F. *et al.* Expression levels of cleaved caspase-3 and caspase-3 in tumorigenesis and prognosis of oral tongue squamous cell carcinoma. *PLoS One* **12**, e0180620 (2017).
210. Shen, X.G. *et al.* Downregulation of caspase-9 is a frequent event in patients with stage II colorectal cancer and correlates with poor clinical outcome. *Colorectal Disease* **12**, 1213-1218 (2010).
211. Fong, P.Y. *et al.* Caspase activity is downregulated in choriocarcinoma: a cDNA array differential expression study. *Journal of clinical pathology* **59**, 179-183 (2006).
212. Teitz, T., Lahti, J.M. & Kidd, V.J. Aggressive childhood neuroblastomas do not express caspase-8: an important component of programmed cell death. *Journal of Molecular Medicine* **79**, 428-436 (2001).
213. Harada, K. *et al.* Deregulation of caspase 8 and 10 expression in pediatric tumors and cell lines. *Cancer Res* **62**, 5897-5901 (2002).
214. Glick, R.D. *et al.* Hybrid Polar Histone Deacetylase Inhibitor Induces Apoptosis and CD95/CD95 Ligand Expression in Human Neuroblastoma1. *Cancer Research* **59**, 4392-4399 (1999).
215. Peter, M.E. *et al.* The role of CD95 and CD95 ligand in cancer. *Cell Death & Differentiation* **22**, 549-559 (2015).
216. Rozenfeld-Granot, G., Toren, A., Amariglio, N., Brok-Simoni, F. & Rechavi, G. Mutation analysis of the FAS and TNFR apoptotic cascade genes in hematological malignancies. *Experimental Hematology* **29**, 228-233 (2001).
217. Jin, Z., McDonald, E.R., III, Dicker, D.T. & El-Deiry, W.S. Deficient Tumor Necrosis Factor-related Apoptosis-inducing Ligand (TRAIL) Death Receptor Transport to the Cell Surface in Human Colon Cancer Cells Selected for Resistance to TRAIL-induced Apoptosis *. *Journal of Biological Chemistry* **279**, 35829-35839 (2004).
218. Huang, S., Chen, G., Dang, Y. & Chen, L.-H. Overexpression of DcR3 and Its Significance on Tumor Cell Differentiation and Proliferation in Glioma. *The Scientific World Journal* **2014**, 605236 (2014).
219. Baugh, E.H., Ke, H., Levine, A.J., Bonneau, R.A. & Chan, C.S. Why are there hotspot mutations in the TP53 gene in human cancers? *Cell Death & Differentiation* **25**, 154-160 (2018).

220. Muller, P.A.J. & Vousden, K.H. p53 mutations in cancer. *Nature Cell Biology* **15**, 2-8 (2013).
221. Olivier, M., Hollstein, M. & Hainaut, P. TP53 mutations in human cancers: origins, consequences, and clinical use. *Cold Spring Harbor perspectives in biology* **2**, a001008-a001008 (2010).
222. Kinoshita, Y. *et al.* Mutations of the p53 gene in malignant rhabdoid tumors of soft tissue and the kidney: immunohistochemical and DNA direct sequencing analysis. *Journal of Cancer Research and Clinical Oncology* **127**, 351-358 (2001).
223. Rosson, G.B. *et al.* Establishment and molecular characterization of five cell lines derived from renal and extrarenal malignant rhabdoid tumors. *Modern pathology : an official journal of the United States and Canadian Academy of Pathology, Inc* **11**, 1228-1237 (1998).
224. Hsueh, C. *et al.* Infrequent p53 Gene Mutations and Lack of p53 Protein Expression in Clear Cell Sarcoma of the Kidney: Immunohistochemical Study and Mutation Analysis of p53 in Renal Tumors of Unfavorable Prognosis. *Modern Pathology* **15**, 606-610 (2002).
225. Hirose, M. *et al.* Establishment and characterization of two cultured cell lines derived from malignant rhabdoid tumors of the kidney. *International Journal of Cancer* **67**, 218-223 (1996).
226. Howard, T.P. *et al.* MDM2 and MDM4 Are Therapeutic Vulnerabilities in Malignant Rhabdoid Tumors. *Cancer Research* **79**, 2404-2414 (2019).
227. Chang, Y.-C. & Cheung, C.H. An Updated Review of Smac Mimetics, LCL161, Birinapant, and GDC-0152 in Cancer Treatment. *Applied Sciences* **11** (2021).
228. Yip, K.W. & Reed, J.C. Bcl-2 family proteins and cancer. *Oncogene* **27**, 6398-6406 (2008).
229. Reed, J.C. Bcl-2 on the brink of breakthroughs in cancer treatment. *Cell Death & Differentiation* **25**, 3-6 (2018).
230. Um, H.-D. Bcl-2 family proteins as regulators of cancer cell invasion and metastasis: a review focusing on mitochondrial respiration and reactive oxygen species. *Oncotarget* **7**, 5193-5203 (2016).
231. García-Aranda, M., Pérez-Ruiz, E. & Redondo, M. Bcl-2 Inhibition to Overcome Resistance to Chemo- and Immunotherapy. *International journal of molecular sciences* **19**, 3950 (2018).
232. Davids, Matthew S. & Letai, A. ABT-199: Taking Dead Aim at BCL-2. *Cancer Cell* **23**, 139-141 (2013).
233. Seymour, J.F. *et al.* Venetoclax–Rituximab in Relapsed or Refractory Chronic Lymphocytic Leukemia. *New England Journal of Medicine* **378**, 1107-1120 (2018).
234. Xu, Y. *et al.* Combined treatment of ABT199 and irinotecan suppresses KRAS-mutant lung cancer cells. *Gene* **688**, 1-6 (2019).
235. Deng, J. & Letai, A. Priming BCL-2 to kill: the combination therapy of tamoxifen and ABT-199 in ER+ breast cancer. *Breast cancer research : BCR* **15**, 317-317 (2013).
236. Wang, Y. *et al.* ABT-199-mediated inhibition of Bcl-2 as a potential therapeutic strategy for nasopharyngeal carcinoma. *Biochemical and Biophysical Research Communications* **503**, 1214-1220 (2018).
237. Luedtke, D.A. *et al.* Inhibition of Mcl-1 enhances cell death induced by the Bcl-2-selective inhibitor ABT-199 in acute myeloid leukemia cells. *Signal Transduction and Targeted Therapy* **2**, 17012 (2017).
238. Lever, J.R. & Fergason-Cantrell, E.A. Allosteric modulation of sigma receptors by BH3 mimetics ABT-737, ABT-263 (Navitoclax) and ABT-199 (Venetoclax). *Pharmacological Research* **142**, 87-100 (2019).
239. Glick, D., Barth, S. & Macleod, K.F. Autophagy: cellular and molecular mechanisms. *The Journal of pathology* **221**, 3-12 (2010).
240. Feng, Y., He, D., Yao, Z. & Klionsky, D.J. The machinery of macroautophagy. *Cell Research* **24**, 24-41 (2014).

241. Mizushima, N. & Komatsu, M. Autophagy: Renovation of Cells and Tissues. *Cell* **147**, 728-741 (2011).
242. Kaushik, S. & Cuervo, A.M. The coming of age of chaperone-mediated autophagy. *Nature Reviews Molecular Cell Biology* **19**, 365-381 (2018).
243. Pierzynowska, K. *et al.* Autophagy stimulation as a promising approach in treatment of neurodegenerative diseases. *Metabolic brain disease* **33**, 989-1008 (2018).
244. Bernard, A. & Klionsky, D.J. Autophagosome formation: tracing the source. *Developmental cell* **25**, 116-117 (2013).
245. Carlsson, S.R. & Simonsen, A. Membrane dynamics in autophagosome biogenesis. *Journal of Cell Science* **128**, 193 (2015).
246. Nakamura, S. & Yoshimori, T. New insights into autophagosome–lysosome fusion. *Journal of Cell Science* **130**, 1209 (2017).
247. Lőrincz, P. & Juhász, G. Autophagosome-Lysosome Fusion. *Journal of Molecular Biology* (2019).
248. Lawrence, R.E. & Zoncu, R. The lysosome as a cellular centre for signalling, metabolism and quality control. *Nature Cell Biology* **21**, 133-142 (2019).
249. Melendez A, L.B. (The online review of C.elegans Biology [Internet].
250. Tsukada, M. & Ohsumi, Y. Isolation and characterization of autophagy-defective mutants of Saccharomyces cerevisiae. *FEBS Lett* **333**, 169-174 (1993).
251. Wen, X. & Klionsky, D.J. An overview of macroautophagy in yeast. *Journal of molecular biology* **428**, 1681-1699 (2016).
252. Wesselborg, S. & Stork, B. Autophagy signal transduction by ATG proteins: from hierarchies to networks. *Cellular and molecular life sciences : CMLS* **72**, 4721-4757 (2015).
253. Zachari, M. & Ganley, I.G. The mammalian ULK1 complex and autophagy initiation. *Essays in biochemistry* **61**, 585-596 (2017).
254. Wang, C. *et al.* Phosphorylation of ULK1 affects autophagosome fusion and links chaperone-mediated autophagy to macroautophagy. *Nature Communications* **9**, 3492 (2018).
255. Ohashi, Y., Tremel, S. & Williams, R.L. VPS34 complexes from a structural perspective. *Journal of Lipid Research* (2018).
256. Obara, K. & Ohsumi, Y. Atg14: a key player in orchestrating autophagy. *International journal of cell biology* **2011**, 713435-713435 (2011).
257. Di Bartolomeo, S. *et al.* The dynamic interaction of AMBRA1 with the dynein motor complex regulates mammalian autophagy. *J Cell Biol* **191**, 155-168 (2010).
258. Boutouja, F., Brinkmeier, R., Mastalski, T., El Magraoui, F. & Platta, H.W. Regulation of the Tumor-Suppressor BECLIN 1 by Distinct Ubiquitination Cascades. *International journal of molecular sciences* **18**, 2541 (2017).
259. Cebollero, E., van der Vaart, A. & Reggiori, F. Understanding phosphatidylinositol-3-phosphate dynamics during autophagosome biogenesis. *Autophagy* **8**, 1868-1870 (2012).
260. Nascimbeni, A.C., Codogno, P. & Morel, E. Local detection of PtdIns3P at autophagosome biogenesis membrane platforms. *Autophagy* **13**, 1602-1612 (2017).
261. Cebollero, E. *et al.* Phosphatidylinositol-3-phosphate clearance plays a key role in autophagosome completion. *Curr Biol* **22**, 1545-1553 (2012).
262. Zhuang, X. *et al.* ATG9 regulates autophagosome progression from the endoplasmic reticulum in Arabidopsis. *Proceedings of the National Academy of Sciences* **114**, E426 (2017).
263. Ungermann, C. & Reggiori, F. Atg9 proteins, not so different after all. *Autophagy* **14**, 1456-1459 (2018).
264. Zhou, C. *et al.* Regulation of mATG9 trafficking by Src- and ULK1-mediated phosphorylation in basal and starvation-induced autophagy. *Cell Research* **27**, 184-201 (2017).

265. Nakatogawa, H. Two ubiquitin-like conjugation systems that mediate membrane formation during autophagy. *Essays in Biochemistry* **55**, 39-50 (2013).
266. Walczak, M. & Martens, S. Dissecting the role of the Atg12-Atg5-Atg16 complex during autophagosome formation. *Autophagy* **9**, 424-425 (2013).
267. Tanida, I., Ueno, T. & Kominami, E. LC3 and Autophagy. *Methods Mol Biol* **445**, 77-88 (2008).
268. Lee, Y.-K. & Lee, J.-A. Role of the mammalian ATG8/LC3 family in autophagy: differential and compensatory roles in the spatiotemporal regulation of autophagy. *BMB reports* **49**, 424-430 (2016).
269. Pankiv, S. *et al.* p62/SQSTM1 binds directly to Atg8/LC3 to facilitate degradation of ubiquitinated protein aggregates by autophagy. *J Biol Chem* **282**, 24131-24145 (2007).
270. Liu, W.J. *et al.* p62 links the autophagy pathway and the ubiqutin-proteasome system upon ubiquitinated protein degradation. *Cellular & molecular biology letters* **21**, 29-29 (2016).
271. Dikic, I. & Elazar, Z. Mechanism and medical implications of mammalian autophagy. *Nature Reviews Molecular Cell Biology* **19**, 349-364 (2018).
272. Chen, H.-Y. & White, E. Role of autophagy in cancer prevention. *Cancer prevention research (Philadelphia, Pa.)* **4**, 973-983 (2011).
273. Debnath, J., Baehrecke, E.H. & Kroemer, G. Does autophagy contribute to cell death? *Autophagy* **1**, 66-74 (2005).
274. Kroemer, G. & Levine, B. Autophagic cell death: the story of a misnomer. *Nature reviews. Molecular cell biology* **9**, 1004-1010 (2008).
275. Liu, E.Y. & Ryan, K.M. Autophagy and cancer – issues we need to digest. *Journal of Cell Science* **125**, 2349 (2012).
276. Santana-Codina, N., Mancias, J.D. & Kimmelman, A.C. The Role of Autophagy in Cancer. *Annual review of cancer biology* **1**, 19-39 (2017).
277. Boya, P. & Codogno, P. 1-12 (Tocris Biosci Sci Rev Ser, 2015).
278. Folkerts, H., Hilgendorf, S., Vellenga, E., Bremer, E. & Wiersma, V.R. The multifaceted role of autophagy in cancer and the microenvironment. *Medicinal Research Reviews* **39**, 517-560 (2019).
279. Yun, C.W. & Lee, S.H. The Roles of Autophagy in Cancer. *International journal of molecular sciences* **19**, 3466 (2018).
280. Lin, J.-F. *et al.* Cisplatin induces protective autophagy through activation of BECN1 in human bladder cancer cells. *Drug design, development and therapy* **11**, 1517-1533 (2017).
281. Sasaki, K. *et al.* Resistance of colon cancer to 5-fluorouracil may be overcome by combination with chloroquine, an in vivo study. *Anticancer Drugs* **23**, 675-682 (2012).
282. Sasaki, K. *et al.* Chloroquine potentiates the anti-cancer effect of 5-fluorouracil on colon cancer cells. *BMC Cancer* **10**, 370 (2010).
283. Sui, X. *et al.* Autophagy and chemotherapy resistance: a promising therapeutic target for cancer treatment. *Cell Death & Disease* **4**, e838-e838 (2013).
284. Han, H.Y., Kim, H., Jeong, S.H., Lim, D.S. & Ryu, M.H. Sulfasalazine induces autophagic cell death in oral cancer cells via Akt and ERK pathways. *Asian Pac J Cancer Prev* **15**, 6939-6944 (2014).
285. Xiong, H.Y. *et al.* Autophagic cell death induced by 5-FU in Bax or PUMA deficient human colon cancer cell. *Cancer Lett* **288**, 68-74 (2010).
286. Lee, Y.J. *et al.* Molecular mechanism of SAHA on regulation of autophagic cell death in tamoxifen-resistant MCF-7 breast cancer cells. *Int J Med Sci* **9**, 881-893 (2012).
287. Watanabe, M. *et al.* Induction of autophagy in malignant rhabdoid tumor cells by the histone deacetylase inhibitor FK228 through AIF translocation. *Int J Cancer* **124**, 55-67 (2009).

288. Yoshii, S.R. & Mizushima, N. Monitoring and Measuring Autophagy. *International journal of molecular sciences* **18**, 1865 (2017).
289. Pasquier, B. Autophagy inhibitors. *Cell Mol Life Sci* **73**, 985-1001 (2016).
290. Wu, Y.-T. *et al.* Dual role of 3-methyladenine in modulation of autophagy via different temporal patterns of inhibition on class I and III phosphoinositide 3-kinase. *The Journal of biological chemistry* **285**, 10850-10861 (2010).
291. Pasquier, B. SAR405, a PIK3C3/Vps34 inhibitor that prevents autophagy and synergizes with MTOR inhibition in tumor cells. *Autophagy* **11**, 725-726 (2015).
292. Martin, K.R. *et al.* A Potent and Selective ULK1 Inhibitor Suppresses Autophagy and Sensitizes Cancer Cells to Nutrient Stress. *iScience* **8**, 74-84 (2018).
293. Qin, L. *et al.* Chloroquine enhances the efficacy of cisplatin by suppressing autophagy in human adrenocortical carcinoma treatment. *Drug design, development and therapy* **10**, 1035-1045 (2016).
294. Su, M., Mei, Y. & Sinha, S. Role of the Crosstalk between Autophagy and Apoptosis in Cancer. *J Oncol* **2013**, 102735 (2013).
295. El-Khattouti, A., Selimovic, D., Haikel, Y. & Hassan, M. Crosstalk between apoptosis and autophagy: molecular mechanisms and therapeutic strategies in cancer. *Journal of cell death* **6**, 37-55 (2013).
296. Rubinstein, A.D. & Kimchi, A. Life in the balance – a mechanistic view of the crosstalk between autophagy and apoptosis. *Journal of Cell Science* **125**, 5259-5268 (2012).
297. Eisenberg-Lerner, A., Bialik, S., Simon, H.U. & Kimchi, A. Life and death partners: apoptosis, autophagy and the cross-talk between them. *Cell Death & Differentiation* **16**, 966-975 (2009).
298. Ray, P.D., Huang, B.W. & Tsuji, Y. Reactive oxygen species (ROS) homeostasis and redox regulation in cellular signaling. *Cell Signal* **24**, 981-990 (2012).
299. Redza-Dutordoir, M. & Averill-Bates, D.A. Activation of apoptosis signalling pathways by reactive oxygen species. *Biochimica et Biophysica Acta (BBA) - Molecular Cell Research* **1863**, 2977-2992 (2016).
300. Cao, S.S. & Kaufman, R.J. Endoplasmic reticulum stress and oxidative stress in cell fate decision and human disease. *Antioxidants & redox signaling* **21**, 396-413 (2014).
301. Filomeni, G., De Zio, D. & Cecconi, F. Oxidative stress and autophagy: the clash between damage and metabolic needs. *Cell Death & Differentiation* **22**, 377-388 (2015).
302. Reczek, C.R. & Chandel, N.S. The Two Faces of Reactive Oxygen Species in Cancer. *Annual Review of Cancer Biology* **1**, 79-98 (2017).
303. Vučetić, M., Cormerais, Y., Parks, S.K. & Pouysségur, J. The Central Role of Amino Acids in Cancer Redox Homeostasis: Vulnerability Points of the Cancer Redox Code. *Front Oncol* **7**, 319 (2017).
304. Zhang, H. & Forman, H.J. Signaling pathways involved in phase II gene induction by alpha, beta-unsaturated aldehydes. *Toxicology and industrial health* **25**, 269-278 (2009).
305. Suzuki, M., Otsuki, A., Keleku-Lukwete, N. & Yamamoto, M. Overview of redox regulation by Keap1–Nrf2 system in toxicology and cancer. *Current Opinion in Toxicology* **1**, 29-36 (2016).
306. No, J.H., Kim, Y.B. & Song, Y.S. Targeting nrf2 signaling to combat chemoresistance. *J Cancer Prev* **19**, 111-117 (2014).
307. Furfaro, A.L. *et al.* The Nrf2/HO-1 Axis in Cancer Cell Growth and Chemoresistance. *Oxidative medicine and cellular longevity* **2016**, 1958174-1958174 (2016).
308. Hirai, K., Sasahira, T., Ohmori, H., Fujii, K. & Kuniyasu, H. Inhibition of heme oxygenase-1 by zinc protoporphyrin IX reduces tumor growth of LL/2 lung cancer in C57BL mice. *Int J Cancer* **120**, 500-505 (2007).
309. Nitti, M. *et al.* HO-1 Induction in Cancer Progression: A Matter of Cell Adaptation. *Antioxidants (Basel, Switzerland)* **6**, 29 (2017).

310. Sova, M. & Saso, L. Design and development of Nrf2 modulators for cancer chemoprevention and therapy: a review. *Drug design, development and therapy* **12**, 3181-3197 (2018).
311. Traverso, N. *et al.* Role of glutathione in cancer progression and chemoresistance. *Oxid Med Cell Longev* **2013**, 972913 (2013).
312. Bansal, A. & Simon, M.C. Glutathione metabolism in cancer progression and treatment resistance. *Journal of Cell Biology* **217**, 2291-2298 (2018).
313. Tonelli, C., Chio, I.I.C. & Tuveson, D.A. Transcriptional Regulation by Nrf2. *Antioxidants & redox signaling* **29**, 1727-1745 (2018).
314. Lv, H. *et al.* Unraveling the Potential Role of Glutathione in Multiple Forms of Cell Death in Cancer Therapy. *Oxid Med Cell Longev* **2019**, 3150145 (2019).
315. Lee, K.S. *et al.* Effects of buthionine sulfoximine treatment on cellular glutathione levels and cytotoxicities of cisplatin, carboplatin and radiation in human stomach and ovarian cancer cell lines. *Korean J Intern Med* **7**, 111-117 (1992).
316. Neuwelt, A.J. *et al.* Preclinical high-dose acetaminophen with N-acetylcysteine rescue enhances the efficacy of cisplatin chemotherapy in atypical teratoid rhabdoid tumors. *Pediatric blood & cancer* **61**, 120-127 (2014).
317. Sporn, M.B. & Liby, K.T. NRF2 and cancer: the good, the bad and the importance of context. *Nature reviews. Cancer* **12**, 564-571 (2012).
318. Panieri, E. *et al.* Potential Applications of NRF2 Modulators in Cancer Therapy. *Antioxidants (Basel, Switzerland)* **9**, 193 (2020).
319. Magnano, S., Hannon Barroeta, P., Duffy, R., O'Sullivan, J. & Zisterer, D.M. Cisplatin induces autophagy-associated apoptosis in human oral squamous cell carcinoma (OSCC) mediated in part through reactive oxygen species. *Toxicology and Applied Pharmacology* **427**, 115646 (2021).
320. Garvin, A.J., Re, G.G., Tarnowski, B.I., Hazen-Martin, D.J. & Sens, D.A. The G401 cell line, utilized for studies of chromosomal changes in Wilms' tumor, is derived from a rhabdoid tumor of the kidney. *The American journal of pathology* **142**, 375-380 (1993).
321. Qi, M. *et al.* Midkine rescues Wilms' tumor cells from cisplatin-induced apoptosis: regulation of Bcl-2 expression by Midkine. *J Biochem* **127**, 269-277 (2000).
322. Rampersad, S.N. Multiple applications of Alamar Blue as an indicator of metabolic function and cellular health in cell viability bioassays. *Sensors (Basel, Switzerland)* **12**, 12347-12360 (2012).
323. Crowley, L.C., Marfell, B.J., Scott, A.P. & Waterhouse, N.J. Quantitation of Apoptosis and Necrosis by Annexin V Binding, Propidium Iodide Uptake, and Flow Cytometry. *Cold Spring Harb Protoc* **2016** (2016).
324. Wlodkowic, D., Telford, W., Skommer, J. & Darzynkiewicz, Z. Apoptosis and beyond: cytometry in studies of programmed cell death. *Methods in cell biology* **103**, 55-98 (2011).
325. Chan, L.L.-Y. *et al.* A novel image-based cytometry method for autophagy detection in living cells. *Autophagy* **8**, 1371-1382 (2012).
326. Eruslanov, E. & Kusmartsev, S. Identification of ROS using oxidized DCFDA and flow-cytometry. *Methods Mol Biol* **594**, 57-72 (2010).
327. Yoon, D.S., Lee, M.H. & Cha, D.S. Measurement of Intracellular ROS in Caenorhabditis elegans Using 2',7'-Dichlorodihydrofluorescein Diacetate. *Bio Protoc* **8** (2018).
328. Kauffman, M.E. *et al.* MitoSOX-Based Flow Cytometry for Detecting Mitochondrial ROS. *React Oxyg Species (Apex)* **2**, 361-370 (2016).
329. Čapek, J. & Roušar, T. Detection of Oxidative Stress Induced by Nanomaterials in Cells-The Roles of Reactive Oxygen Species and Glutathione. *Molecules* **26** (2021).
330. Cortés-Ríos, J. *et al.* Protein quantification by bicinchoninic acid (BCA) assay follows complex kinetics and can be performed at short incubation times. *Analytical Biochemistry* **608**, 113904 (2020).

331. Khan, P. *et al.* Luminol-based chemiluminescent signals: clinical and non-clinical application and future uses. *Applied biochemistry and biotechnology* **173**, 333-355 (2014).
332. Ginn, K.F. & Gajjar, A. Atypical teratoid rhabdoid tumor: current therapy and future directions. *Frontiers in oncology* **2**, 114-114 (2012).
333. Dasari, S. & Tchounwou, P.B. Cisplatin in cancer therapy: molecular mechanisms of action. *European journal of pharmacology* **740**, 364-378 (2014).
334. Biswas, A., Kashyap, L., Kakkar, A., Sarkar, C. & Julka, P.K. Atypical teratoid/rhabdoid tumors: challenges and search for solutions. *Cancer management and research* **8**, 115-125 (2016).
335. Astolfi, L. *et al.* Correlation of adverse effects of cisplatin administration in patients affected by solid tumours: a retrospective evaluation. *Oncology reports* **29**, 1285-1292 (2013).
336. Yeldag, G., Rice, A. & Del Río Hernández, A. Chemoresistance and the Self-Maintaining Tumor Microenvironment. *Cancers* **10**, 471 (2018).
337. Zheng, H.-C. The molecular mechanisms of chemoresistance in cancers. *Oncotarget* **8**, 59950-59964 (2017).
338. Chen, S.-H. & Chang, J.-Y. New Insights into Mechanisms of Cisplatin Resistance: From Tumor Cell to Microenvironment. *International journal of molecular sciences* **20**, 4136 (2019).
339. Chun, Y. & Kim, J. Autophagy: An Essential Degradation Program for Cellular Homeostasis and Life. *Cells* **7**, 278 (2018).
340. Levine, B. & Kroemer, G. Autophagy in the pathogenesis of disease. *Cell* **132**, 27-42 (2008).
341. White, E. & DiPaola, R.S. The double-edged sword of autophagy modulation in cancer. *Clinical cancer research : an official journal of the American Association for Cancer Research* **15**, 5308-5316 (2009).
342. Mathew, R. *et al.* Autophagy suppresses tumor progression by limiting chromosomal instability. *Genes & development* **21**, 1367-1381 (2007).
343. Denton, D. & Kumar, S. Autophagy-dependent cell death. *Cell Death & Differentiation* **26**, 605-616 (2019).
344. Dalby, K.N., Tekedereli, I., Lopez-Berestein, G. & Ozpolat, B. Targeting the prodeath and prosurvival functions of autophagy as novel therapeutic strategies in cancer. *Autophagy* **6**, 322-329 (2010).
345. Levy, J.M.M., Towers, C.G. & Thorburn, A. Targeting autophagy in cancer. *Nature reviews. Cancer* **17**, 528-542 (2017).
346. Liu, T., Zhang, J., Li, K., Deng, L. & Wang, H. Combination of an Autophagy Inducer and an Autophagy Inhibitor: A Smarter Strategy Emerging in Cancer Therapy. *Frontiers in Pharmacology* **11** (2020).
347. Chude, C.I. & Amaravadi, R.K. Targeting Autophagy in Cancer: Update on Clinical Trials and Novel Inhibitors. *International journal of molecular sciences* **18**, 1279 (2017).
348. Lee, Y.E. *et al.* Repositioning disulfiram as a radiosensitizer against atypical teratoid/rhabdoid tumor. *Neuro-oncology* **19**, 1079-1087 (2017).
349. Erkek, S. *et al.* Comprehensive Analysis of Chromatin States in Atypical Teratoid/Rhabdoid Tumor Identifies Diverging Roles for SWI/SNF and Polycomb in Gene Regulation. *Cancer cell* **35**, 95-110.e118 (2019).
350. Fasler-Kan, E. *et al.* Chromosomal Heterogeneity of the G-401 Rhabdoid Tumor Cell Line: Unusual Partial 7p Trisomy. *Frontiers in Medicine* **6**, 187 (2019).
351. Elmore, S. Apoptosis: a review of programmed cell death. *Toxicologic pathology* **35**, 495-516 (2007).
352. Su, M., Mei, Y. & Sinha, S. Role of the Crosstalk between Autophagy and Apoptosis in Cancer. *Journal of Oncology* **2013**, 102735 (2013).

353. Shibutani, S.T., Saitoh, T., Nowag, H., Münz, C. & Yoshimori, T. Autophagy and autophagy-related proteins in the immune system. *Nat Immunol* **16**, 1014-1024 (2015).
354. Gomez-Puerto, M.C. *et al.* Autophagy Proteins ATG5 and ATG7 Are Essential for the Maintenance of Human CD34+ Hematopoietic Stem-Progenitor Cells. *STEM CELLS* **34**, 1651-1663 (2016).
355. Qiao, Z. *et al.* Dysfunction of ATG7-dependent autophagy dysregulates the antioxidant response and contributes to oxidative stress-induced biological impairments in human epidermal melanocytes. *Cell Death Discovery* **6**, 31 (2020).
356. Staskiewicz, L., Thorburn, J., Morgan, M.J. & Thorburn, A. Inhibiting autophagy by shRNA knockdown: cautions and recommendations. *Autophagy* **9**, 1449-1450 (2013).
357. Fernández, Á.F. *et al.* Disruption of the beclin 1–BCL2 autophagy regulatory complex promotes longevity in mice. *Nature* **558**, 136-140 (2018).
358. Gottlieb, R.A., Andres, A.M., Sin, J. & Taylor, D.P.J. Untangling autophagy measurements: all fluxed up. *Circulation research* **116**, 504-514 (2015).
359. Loos, B., du Toit, A. & Hofmeyr, J.-H.S. Defining and measuring autophagosome flux—concept and reality. *Autophagy* **10**, 2087-2096 (2014).
360. Séité, S. *et al.* The Autophagic Flux Inhibitor Bafilomycine A1 Affects the Expression of Intermediary Metabolism-Related Genes in Trout Hepatocytes. *Frontiers in Physiology* **10** (2019).
361. Fang, F., Li, Y. & Chang, L. Mechanism of autophagy regulating chemoresistance in esophageal cancer cells. *Exp Mol Pathol* **117**, 104564 (2020).
362. Liu, D., Yang, Y., Liu, Q. & Wang, J. Inhibition of autophagy by 3-MA potentiates cisplatin-induced apoptosis in esophageal squamous cell carcinoma cells. *Med Oncol* **28**, 105-111 (2011).
363. Zhan, L. *et al.* Autophagy as an emerging therapy target for ovarian carcinoma. *Oncotarget* **7**, 83476-83487 (2016).
364. Guo, S. *et al.* A rapid and high content assay that measures cyto-ID-stained autophagic compartments and estimates autophagy flux with potential clinical applications. *Autophagy* **11**, 560-572 (2015).
365. Mauthe, M. *et al.* Chloroquine inhibits autophagic flux by decreasing autophagosome-lysosome fusion. *Autophagy* **14**, 1435-1455 (2018).
366. Lin, X., Han, L., Weng, J., Wang, K. & Chen, T. Rapamycin inhibits proliferation and induces autophagy in human neuroblastoma cells. *Bioscience reports* **38**, BSR20181822 (2018).
367. Mizushima, N., Yoshimori, T. & Levine, B. Methods in mammalian autophagy research. *Cell* **140**, 313-326 (2010).
368. Zhang, X.-j., Chen, S., Huang, K.-x. & Le, W.-d. Why should autophagic flux be assessed? *Acta pharmacologica Sinica* **34**, 595-599 (2013).
369. Xia, Q. *et al.* Therapeutic Potential of Autophagy in Glioblastoma Treatment With Phosphoinositide 3-Kinase/Protein Kinase B/Mammalian Target of Rapamycin Signaling Pathway Inhibitors. *Frontiers in oncology* **10**, 572904-572904 (2020).
370. Mauvezin, C., Nagy, P., Juhász, G. & Neufeld, T.P. Autophagosome–lysosome fusion is independent of V-ATPase-mediated acidification. *Nature Communications* **6**, 7007 (2015).
371. Ye, X., Zhou, X.-J. & Zhang, H. Exploring the Role of Autophagy-Related Gene 5 (ATG5) Yields Important Insights Into Autophagy in Autoimmune/Autoinflammatory Diseases. *Frontiers in immunology* **9**, 2334-2334 (2018).
372. Tait, S.W.G. & Green, D.R. Caspase-independent cell death: leaving the set without the final cut. *Oncogene* **27**, 6452-6461 (2008).
373. Yun, C.W., Jeon, J., Go, G., Lee, J.H. & Lee, S.H. The Dual Role of Autophagy in Cancer Development and a Therapeutic Strategy for Cancer by Targeting Autophagy. *International journal of molecular sciences* **22**, 179 (2020).

374. Pabla, N. & Dong, Z. Cisplatin nephrotoxicity: Mechanisms and renoprotective strategies. *Kidney International* **73**, 994-1007 (2008).
375. Jangra, A. *et al.* Disulfiram potentiates the anticancer effect of cisplatin in atypical teratoid/rhabdoid tumors (AT/RT). *Cancer Letters* **486**, 38-45 (2020).
376. Birks, D.K. *et al.* Pediatric rhabdoid tumors of kidney and brain show many differences in gene expression but share dysregulation of cell cycle and epigenetic effector genes. *Pediatric blood & cancer* **60**, 1095-1102 (2013).
377. Wu, Y.J., Muldoon, L.L. & Neuwelt, E.A. The Chemoprotective Agent N-Acetylcysteine Blocks Cisplatin-Induced Apoptosis through Caspase Signaling Pathway. *Journal of Pharmacology and Experimental Therapeutics* **312**, 424 (2005).
378. Marquez, R.T. & Xu, L. Bcl-2:Beclin 1 complex: multiple, mechanisms regulating autophagy/apoptosis toggle switch. *American journal of cancer research* **2**, 214-221 (2012).
379. Levy, J.M.M. & Thorburn, A. Modulation of pediatric brain tumor autophagy and chemosensitivity. *Journal of neuro-oncology* **106**, 281-290 (2012).
380. Sun, C.-Y. *et al.* Scutellarin Increases Cisplatin-Induced Apoptosis and Autophagy to Overcome Cisplatin Resistance in Non-small Cell Lung Cancer via ERK/p53 and c-met/AKT Signaling Pathways. *Frontiers in Pharmacology* **9** (2018).
381. Jiang, Y. *et al.* Cisplatin-induced autophagy protects breast cancer cells from apoptosis by regulating yes-associated protein. *Oncol Rep* **38**, 3668-3676 (2017).
382. Bao, L. *et al.* Induction of autophagy contributes to cisplatin resistance in human ovarian cancer cells. *Mol Med Rep* **11**, 91-98 (2015).
383. Qu, X. *et al.* Autophagy inhibitor chloroquine increases sensitivity to cisplatin in QBC939 cholangiocarcinoma cells by mitochondrial ROS. *PloS one* **12**, e0173712-e0173712 (2017).
384. Hu, X., Ma, Z., Wen, L., Li, S. & Dong, Z. Autophagy in Cisplatin Nephrotoxicity during Cancer Therapy. *Cancers* **13**, 5618 (2021).
385. Gąsiorkiewicz, B.M., Koczurkiewicz-Adamczyk, P., Piska, K. & Pękala, E. Autophagy modulating agents as chemosensitizers for cisplatin therapy in cancer. *Investigational new drugs* **39**, 538-563 (2021).
386. Byun, J.-Y. *et al.* The Rac1/MKK7/JNK pathway signals upregulation of Atg5 and subsequent autophagic cell death in response to oncogenic Ras. *Carcinogenesis* **30**, 1880-1888 (2009).
387. Dasari, S.K. *et al.* Signalome-wide RNAi screen identifies GBA1 as a positive mediator of autophagic cell death. *Cell death and differentiation* **24**, 1288-1302 (2017).
388. Kanzawa, T. *et al.* Role of autophagy in temozolomide-induced cytotoxicity for malignant glioma cells. *Cell Death Differ* **11**, 448-457 (2004).
389. Kaina, B. Temozolomide in Glioblastoma Therapy: Role of Apoptosis, Senescence and Autophagy. Comment on Strobel et al., Temozolomide and Other Alkylating Agents in Glioblastoma Therapy. Biomedicines 2019, 7, 69. *Biomedicines* **7**, 90 (2019).
390. Dragowska, W.H. *et al.* Induction of autophagy is an early response to gefitinib and a potential therapeutic target in breast cancer. *PloS one* **8**, e76503-e76503 (2013).
391. Maycotte, P. *et al.* Chloroquine sensitizes breast cancer cells to chemotherapy independent of autophagy. *Autophagy* **8**, 200-212 (2012).
392. Chu, H.-Y. *et al.* Bafilomycin A1 increases the sensitivity of tongue squamous cell carcinoma cells to cisplatin by inhibiting the lysosomal uptake of platinum ions but not autophagy. *Cancer Letters* **423**, 105-112 (2018).
393. Ferreira, P.M.P., Sousa, R.W.R.d., Ferreira, J.R.d.O., Militão, G.C.G. & Bezerra, D.P. Chloroquine and hydroxychloroquine in antitumor therapies based on autophagy-related mechanisms. *Pharmacological Research* **168**, 105582 (2021).
394. Manic, G., Obrist, F., Kroemer, G., Vitale, I. & Galluzzi, L. Chloroquine and hydroxychloroquine for cancer therapy. *Molecular & Cellular Oncology* **1**, e29911 (2014).

395. Choi, D.S. *et al.* Chloroquine eliminates cancer stem cells through deregulation of Jak2 and DNMT1. *Stem cells (Dayton, Ohio)* **32**, 2309-2323 (2014).
396. Eng Christina, H. *et al.* Macroautophagy is dispensable for growth of KRAS mutant tumors and chloroquine efficacy. *Proceedings of the National Academy of Sciences* **113**, 182-187 (2016).
397. Redmann, M. *et al.* Inhibition of autophagy with bafilomycin and chloroquine decreases mitochondrial quality and bioenergetic function in primary neurons. *Redox biology* **11**, 73-81 (2017).
398. Yan, Y. *et al.* Bafilomycin A1 induces caspase-independent cell death in hepatocellular carcinoma cells via targeting of autophagy and MAPK pathways. *Scientific Reports* **6**, 37052 (2016).
399. Blair, H.C., Simonet, S., Lacey, D.L. & Zaidi, M. CHAPTER 7 - Osteoclast Biology, in *Osteoporosis (Third Edition)*. (eds. R. Marcus, D. Feldman, D.A. Nelson & C.J. Rosen) 151-167 (Academic Press, San Diego; 2008).
400. Xu, R., Ji, Z., Xu, C. & Zhu, J. The clinical value of using chloroquine or hydroxychloroquine as autophagy inhibitors in the treatment of cancers: A systematic review and meta-analysis. *Medicine* **97**, e12912-e12912 (2018).
401. Halcrow, P.W., Geiger, J.D. & Chen, X. Overcoming Chemoresistance: Altering pH of Cellular Compartments by Chloroquine and Hydroxychloroquine. *Frontiers in Cell and Developmental Biology* **9** (2021).
402. Boone, B.A. *et al.* Safety and Biologic Response of Pre-operative Autophagy Inhibition in Combination with Gemcitabine in Patients with Pancreatic Adenocarcinoma. *Ann Surg Oncol* **22**, 4402-4410 (2015).
403. Briceño, E., Reyes, S. & Sotelo, J. Therapy of glioblastoma multiforme improved by the antimutagenic chloroquine. *Neurosurgical Focus FOC* **14**, 1-6 (2003).
404. Kim, J.Y. *et al.* Curcumin-induced autophagy contributes to the decreased survival of oral cancer cells. *Arch Oral Biol* **57**, 1018-1025 (2012).
405. Salazar, M. *et al.* Cannabinoid action induces autophagy-mediated cell death through stimulation of ER stress in human glioma cells. *J Clin Invest* **119**, 1359-1372 (2009).
406. Schlütermann, D. *et al.* Targeting urothelial carcinoma cells by combining cisplatin with a specific inhibitor of the autophagy-inducing class III PtdIns3K complex. *Urologic Oncology: Seminars and Original Investigations* **36**, 160.e161-160.e113 (2018).
407. Li, C. *et al.* Impact of autophagy inhibition at different stages on cytotoxic effect of autophagy inducer in glioblastoma cells. *Cell Physiol Biochem* **35**, 1303-1316 (2015).
408. Chen, J. *et al.* Inhibition of autophagy promotes cisplatin-induced apoptotic cell death through Atg5 and Beclin 1 in A549 human lung cancer cells. *Mol Med Rep* **17**, 6859-6865 (2018).
409. Zhao, H. *et al.* Blocking autophagy enhances the pro-apoptotic effect of bufalin on human gastric cancer cells through endoplasmic reticulum stress. *Biology open* **6**, 1416-1422 (2017).
410. Hollomon, M.G., Gordon, N., Santiago-O'Farrill, J.M. & Kleinerman, E.S. Knockdown of autophagy-related protein 5, ATG5, decreases oxidative stress and has an opposing effect on camptothecin-induced cytotoxicity in osteosarcoma cells. *BMC cancer* **13**, 500-500 (2013).
411. Yang, S. *et al.* Pancreatic cancers require autophagy for tumor growth. *Genes Dev* **25**, 717-729 (2011).
412. Huang, S., Okamoto, K., Yu, C. & Sinicrope, F.A. p62/sequestosome-1 up-regulation promotes ABT-263-induced caspase-8 aggregation/activation on the autophagosome. *The Journal of biological chemistry* **288**, 33654-33666 (2013).
413. Mukhopadhyay, S., Panda, P.K., Sinha, N., Das, D.N. & Bhutia, S.K. Autophagy and apoptosis: where do they meet? *Apoptosis* **19**, 555-566 (2014).

414. Herzog, C., Yang, C., Holmes, A. & Kaushal, G.P. zVAD-fmk prevents cisplatin-induced cleavage of autophagy proteins but impairs autophagic flux and worsens renal function. *American journal of physiology. Renal physiology* **303**, F1239-F1250 (2012).
415. Zhao, Q. *et al.* Pristimerin induces apoptosis and autophagy via activation of ROS/ASK1/JNK pathway in human breast cancer in vitro and in vivo. *Cell Death Discovery* **5**, 125 (2019).
416. Zorov, D.B., Juhaszova, M. & Sollott, S.J. Mitochondrial reactive oxygen species (ROS) and ROS-induced ROS release. *Physiol Rev* **94**, 909-950 (2014).
417. He, L. *et al.* Antioxidants Maintain Cellular Redox Homeostasis by Elimination of Reactive Oxygen Species. *Cellular Physiology and Biochemistry* **44**, 532-553 (2017).
418. Liu, Z. *et al.* Role of ROS and Nutritional Antioxidants in Human Diseases. *Front Physiol* **9**, 477 (2018).
419. Le Gal, K., Schmidt, E.E. & Sayin, V.I. Cellular Redox Homeostasis. *Antioxidants (Basel)* **10** (2021).
420. Baird, L. & Yamamoto, M. The Molecular Mechanisms Regulating the KEAP1-NRF2 Pathway. *Mol Cell Biol* **40** (2020).
421. Loboda, A., Damulewicz, M., Pyza, E., Jozkowicz, A. & Dulak, J. Role of Nrf2/HO-1 system in development, oxidative stress response and diseases: an evolutionarily conserved mechanism. *Cell Mol Life Sci* **73**, 3221-3247 (2016).
422. Zitka, O. *et al.* Redox status expressed as GSH:GSSG ratio as a marker for oxidative stress in paediatric tumour patients. *Oncology letters* **4**, 1247-1253 (2012).
423. Kumari, S., Badana, A.K., G, M.M., G, S. & Malla, R. Reactive Oxygen Species: A Key Constituent in Cancer Survival. *Biomark Insights* **13**, 1177271918755391 (2018).
424. Van Loenhout, J., Peeters, M., Bogaerts, A., Smits, E. & Deben, C. Oxidative Stress-Inducing Anticancer Therapies: Taking a Closer Look at Their Immunomodulating Effects. *Antioxidants (Basel)* **9** (2020).
425. Xue, D., Zhou, X. & Qiu, J. Emerging role of NRF2 in ROS-mediated tumor chemoresistance. *Biomedicine & Pharmacotherapy* **131**, 110676 (2020).
426. Aboelella, N.S., Brandle, C., Kim, T., Ding, Z.C. & Zhou, G. Oxidative Stress in the Tumor Microenvironment and Its Relevance to Cancer Immunotherapy. *Cancers (Basel)* **13** (2021).
427. Zhu, H. *et al.* Molecular mechanisms of cisplatin resistance in cervical cancer. *Drug Des Devel Ther* **10**, 1885-1895 (2016).
428. Pasello, M. *et al.* Overcoming Glutathione S-Transferase P1–Related Cisplatin Resistance in Osteosarcoma. *Cancer Research* **68**, 6661-6668 (2008).
429. Rocha, C.R., Kajitani, G.S., Quinet, A., Fortunato, R.S. & Menck, C.F. NRF2 and glutathione are key resistance mediators to temozolomide in glioma and melanoma cells. *Oncotarget* **7**, 48081-48092 (2016).
430. Silva, M.M., Rocha, C.R.R., Kinker, G.S., Pelegrini, A.L. & Menck, C.F.M. The balance between NRF2/GSH antioxidant mediated pathway and DNA repair modulates cisplatin resistance in lung cancer cells. *Scientific Reports* **9**, 17639 (2019).
431. Liu, P. *et al.* Nrf2 overexpression increases risk of high tumor mutation burden in acute myeloid leukemia by inhibiting MSH2. *Cell Death & Disease* **12**, 20 (2021).
432. Singh, A. *et al.* Small Molecule Inhibitor of NRF2 Selectively Intervenes Therapeutic Resistance in KEAP1-Deficient NSCLC Tumors. *ACS Chem Biol* **11**, 3214-3225 (2016).
433. Parkhurst, A. *et al.* Dual mTORC1/2 inhibition compromises cell defenses against exogenous stress potentiating Obatoclax-induced cytotoxicity in atypical teratoid/rhabdoid tumors. *Cell Death & Disease* **13**, 410 (2022).
434. Tetz, L.M., Kamau, P.W., Cheng, A.A., Meeker, J.D. & Loch-Caruso, R. Troubleshooting the dichlorofluorescein assay to avoid artifacts in measurement of toxicant-stimulated

cellular production of reactive oxidant species. *J Pharmacol Toxicol Methods* **67**, 56-60 (2013).
435. Halasi, M. *et al.* ROS inhibitor N-acetyl-L-cysteine antagonizes the activity of proteasome inhibitors. *The Biochemical journal* **454**, 201-208 (2013).
436. Hayes, J.D., Dinkova-Kostova, A.T. & Tew, K.D. Oxidative Stress in Cancer. *Cancer Cell* **38**, 167-197 (2020).
437. Tsang, R.Y., Al-Fayea, T. & Au, H.J. Cisplatin overdose: toxicities and management, in *Drug Saf*, Vol. 32 1109-1122 (New Zealand; 2009).
438. Park, B.H. *et al.* Curcumin potentiates antitumor activity of cisplatin in bladder cancer cell lines via ROS-mediated activation of ERK1/2. *Oncotarget* **7**, 63870-63886 (2016).
439. Kleih, M. *et al.* Direct impact of cisplatin on mitochondria induces ROS production that dictates cell fate of ovarian cancer cells. *Cell Death & Disease* **10**, 851 (2019).
440. Lee, Y.J. & Lee, S.H. Pro-oxidant activity of sulforaphane and cisplatin potentiates apoptosis and simultaneously promotes autophagy in malignant mesothelioma cells. *Mol Med Rep* **16**, 2133-2141 (2017).
441. Barrera, G. *et al.* Control of Oxidative Stress in Cancer Chemoresistance: Spotlight on Nrf2 Role. *Antioxidants (Basel)* **10** (2021).
442. Salatino, A. *et al.* H-Ferritin Affects Cisplatin-Induced Cytotoxicity in Ovarian Cancer Cells through the Modulation of ROS. *Oxidative Medicine and Cellular Longevity* **2019**, 3461251 (2019).
443. Diehn, M. *et al.* Association of reactive oxygen species levels and radioresistance in cancer stem cells. *Nature* **458**, 780-783 (2009).
444. Wang, Y. *et al.* ROS-Induced DCTPP1 Upregulation Contributes to Cisplatin Resistance in Ovarian Cancer. *Front Mol Biosci* **9**, 838006 (2022).
445. Zhao, R.Z., Jiang, S., Zhang, L. & Yu, Z.B. Mitochondrial electron transport chain, ROS generation and uncoupling (Review). *Int J Mol Med* **44**, 3-15 (2019).
446. Marullo, R. *et al.* Cisplatin induces a mitochondrial-ROS response that contributes to cytotoxicity depending on mitochondrial redox status and bioenergetic functions. *PloS one* **8**, e81162-e81162 (2013).
447. Huang, S. *et al.* N-Acetylcysteine Attenuates Cisplatin-Induced Acute Kidney Injury by Inhibiting the C5a Receptor. *Biomed Res Int* **2019**, 4805853 (2019).
448. Abdel-Wahab, W.M. & Moussa, F.I. Neuroprotective effect of N-acetylcysteine against cisplatin-induced toxicity in rat brain by modulation of oxidative stress and inflammation. *Drug Des Devel Ther* **13**, 1155-1162 (2019).
449. Chen, H.H. & Kuo, M.T. Role of glutathione in the regulation of Cisplatin resistance in cancer chemotherapy. *Met Based Drugs* **2010** (2010).
450. Zhu, Z. *et al.* Glutathione reductase mediates drug resistance in glioblastoma cells by regulating redox homeostasis. *Journal of Neurochemistry* **144**, 93-104 (2018).
451. Townsend, D.M. & Tew, K.D. The role of glutathione-S-transferase in anti-cancer drug resistance. *Oncogene* **22**, 7369-7375 (2003).
452. Anderson, C.P. & Reynolds, C.P. Synergistic cytotoxicity of buthionine sulfoximine (BSO) and intensive melphalan (L-PAM) for neuroblastoma cell lines established at relapse after myeloablative therapy. *Bone Marrow Transplantation* **30**, 135-140 (2002).
453. Li, Q. *et al.* The effects of buthionine sulfoximine on the proliferation and apoptosis of biliary tract cancer cells induced by cisplatin and gemcitabine. *Oncol Lett* **11**, 474-480 (2016).
454. Villablanca, J.G. *et al.* A Phase I New Approaches to Neuroblastoma Therapy Study of Buthionine Sulfoximine and Melphalan With Autologous Stem Cells for Recurrent/Refractory High-Risk Neuroblastoma. *Pediatr Blood Cancer* **63**, 1349-1356 (2016).

455. Bao, L.J. *et al.* Nrf2 induces cisplatin resistance through activation of autophagy in ovarian carcinoma. *Int J Clin Exp Pathol* **7**, 1502-1513 (2014).
456. Song, S. *et al.* Loss of SWI/SNF Chromatin Remodeling Alters NRF2 Signaling in Non-Small Cell Lung Carcinoma. *Mol Cancer Res* **18**, 1777-1788 (2020).
457. Sun, X. *et al.* SIRT5 Promotes Cisplatin Resistance in Ovarian Cancer by Suppressing DNA Damage in a ROS-Dependent Manner via Regulation of the Nrf2/HO-1 Pathway. *Front Oncol* **9**, 754 (2019).
458. Ren, D. *et al.* Brusatol enhances the efficacy of chemotherapy by inhibiting the Nrf2-mediated defense mechanism. *Proc Natl Acad Sci U S A* **108**, 1433-1438 (2011).
459. Ji, L. *et al.* Nrf2 pathway regulates multidrug-resistance-associated protein 1 in small cell lung cancer. *PLoS One* **8**, e63404 (2013).
460. Dillon, M. *et al.* Progress on Ras/MAPK Signaling Research and Targeting in Blood and Solid Cancers. *Cancers (Basel)* **13** (2021).
461. Lopez, J. & Tait, S.W.G. Mitochondrial apoptosis: killing cancer using the enemy within. *British Journal of Cancer* **112**, 957-962 (2015).
462. Villalobos-Ortiz, M., Ryan, J., Mashaka, T.N., Opferman, J.T. & Letai, A. BH3 profiling discriminates on-target small molecule BH3 mimetics from putative mimetics. *Cell Death & Differentiation* **27**, 999-1007 (2020).
463. Vogler, M. Targeting BCL2-Proteins for the Treatment of Solid Tumours. *Adv Med* **2014**, 943648 (2014).
464. Wang, H., Guo, M., Wei, H. & Chen, Y. Targeting MCL-1 in cancer: current status and perspectives. *Journal of Hematology & Oncology* **14**, 67 (2021).
465. Morales-Martínez, M. & Vega, M.I. Roles and Regulation of BCL-xL in Hematological Malignancies. *Int J Mol Sci* **23** (2022).
466. Adams, C.M. *et al.* BCL-W has a fundamental role in B cell survival and lymphomagenesis. *J Clin Invest* **127**, 635-650 (2017).
467. Pan, R. *et al.* Selective BCL-2 inhibition by ABT-199 causes on-target cell death in acute myeloid leukemia. *Cancer Discov* **4**, 362-375 (2014).
468. Cho, H.J. *et al.* Upregulation of Bcl-2 is associated with cisplatin-resistance via inhibition of Bax translocation in human bladder cancer cells. *Cancer Letters* **237**, 56-66 (2006).
469. Townsend, P.A., Kozhevnikova, M.V., Cexus, O.N.F., Zamyatnin, A.A. & Soond, S.M. BH3-mimetics: recent developments in cancer therapy. *Journal of Experimental & Clinical Cancer Research* **40**, 355 (2021).
470. Oltersdorf, T. *et al.* An inhibitor of Bcl-2 family proteins induces regression of solid tumours. *Nature* **435**, 677-681 (2005).
471. Stamelos, V.A., Redman, C.W. & Richardson, A. Understanding sensitivity to BH3 mimetics: ABT-737 as a case study to foresee the complexities of personalized medicine. *J Mol Signal* **7**, 12 (2012).
472. Mohamad Anuar, N.N., Nor Hisam, N.S., Liew, S.L. & Ugusman, A. Clinical Review: Navitoclax as a Pro-Apoptotic and Anti-Fibrotic Agent. *Front Pharmacol* **11**, 564108 (2020).
473. Diepstraten, S.T. *et al.* The manipulation of apoptosis for cancer therapy using BH3-mimetic drugs. *Nature Reviews Cancer* **22**, 45-64 (2022).
474. Tariq, S., Khan, M., Azhar, A. & Baig, M. Venetoclax in the Treatment of Chronic Lymphocytic Leukemia: Evidence, Expectations, and Future Prospects. *Cureus* **12**, e8908 (2020).
475. Knight, T., Edwards, H., Taub, J.W. & Ge, Y. Evaluating venetoclax and its potential in treatment-naïve acute myeloid leukemia. *Cancer Manag Res* **11**, 3197-3213 (2019).
476. Juárez-Salcedo, L.M., Desai, V. & Dalia, S. Venetoclax: evidence to date and clinical potential. *Drugs Context* **8**, 212574 (2019).

477. Lochmann, T.L. *et al.* Venetoclax Is Effective in Small-Cell Lung Cancers with High BCL-2 Expression. *Clinical Cancer Research* **24**, 360-369 (2018).
478. Alhoshani, A. *et al.* BCL-2 Inhibitor Venetoclax Induces Autophagy-Associated Cell Death, Cell Cycle Arrest, and Apoptosis in Human Breast Cancer Cells. *Onco Targets Ther* **13**, 13357-13370 (2020).
479. Xu, Y. *et al.* Combined treatment of ABT199 and irinotecan suppresses KRAS-mutant lung cancer cells.
480. Bose, P., Gandhi, V. & Konopleva, M. Pathways and mechanisms of venetoclax resistance. *Leuk Lymphoma* **58**, 1-17 (2017).
481. Steele, T.M. *et al.* Obatoclax, a BH3 Mimetic, Enhances Cisplatin-Induced Apoptosis and Decreases the Clonogenicity of Muscle Invasive Bladder Cancer Cells via Mechanisms That Involve the Inhibition of Pro-Survival Molecules as Well as Cell Cycle Regulators. *Int J Mol Sci* **20** (2019).
482. Bauer, J.A. *et al.* Reversal of cisplatin resistance with a BH3 mimetic, (−)-gossypol, in head and neck cancer cells: role of wild-type p53 and Bcl-xL. *Molecular Cancer Therapeutics* **4**, 1096-1104 (2005).
483. D'Aguanno, S. & Del Bufalo, D. Inhibition of Anti-Apoptotic Bcl-2 Proteins in Preclinical and Clinical Studies: Current Overview in Cancer. *Cells* **9** (2020).
484. Xu, L. *et al.* Bcl-2 overexpression reduces cisplatin cytotoxicity by decreasing ER-mitochondrial Ca2+ signaling in SKOV3 cells. *Oncol Rep* **39**, 985-992 (2018).
485. Low, S.Y. *et al.* Suppression of BCL-2 synergizes cisplatin sensitivity in nasopharyngeal carcinoma cells. *Cancer Letters* **314**, 166-175 (2012).
486. Aharoni-Simon, M. *et al.* Bcl-2 Regulates Reactive Oxygen Species Signaling and a Redox-Sensitive Mitochondrial Proton Leak in Mouse Pancreatic β-Cells. *Endocrinology* **157**, 2270-2281 (2016).
487. Roca-Portoles, A. *et al.* Venetoclax causes metabolic reprogramming independent of BCL-2 inhibition. *Cell Death & Disease* **11**, 616 (2020).
488. Wang, Q. & Zou, M.H. Measurement of Reactive Oxygen Species (ROS) and Mitochondrial ROS in AMPK Knockout Mice Blood Vessels. *Methods Mol Biol* **1732**, 507-517 (2018).
489. Wang, L. *et al.* Mitochondrial Respiratory Chain Inhibitors Involved in ROS Production Induced by Acute High Concentrations of Iodide and the Effects of SOD as a Protective Factor. *Oxid Med Cell Longev* **2015**, 217670 (2015).
490. Chen, Z.X. & Pervaiz, S. Bcl-2 induces pro-oxidant state by engaging mitochondrial respiration in tumor cells. *Cell Death & Differentiation* **14**, 1617-1627 (2007).
491. Lagadinou, E.D. *et al.* BCL-2 inhibition targets oxidative phosphorylation and selectively eradicates quiescent human leukemia stem cells. *Cell Stem Cell* **12**, 329-341 (2013).
492. Pollyea, D.A. *et al.* Venetoclax with azacitidine disrupts energy metabolism and targets leukemia stem cells in patients with acute myeloid leukemia. *Nat Med* **24**, 1859-1866 (2018).
493. Chong, S.J.F., Low, I.C.C. & Pervaiz, S. Mitochondrial ROS and involvement of Bcl-2 as a mitochondrial ROS regulator. *Mitochondrion* **19**, 39-48 (2014).
494. Lan, D. *et al.* Exogenous glutathione contributes to cisplatin resistance in lung cancer A549 cells. *American journal of translational research* **10**, 1295-1309 (2018).
495. Rudin, C.M. *et al.* Inhibition of glutathione synthesis reverses Bcl-2-mediated cisplatin resistance. *Cancer Res* **63**, 312-318 (2003).
496. Abdul Rahman, S.F. *et al.* Co-inhibition of BCL-XL and MCL-1 with selective BCL-2 family inhibitors enhances cytotoxicity of cervical cancer cell lines. *Biochem Biophys Rep* **22**, 100756 (2020).
497. Choudhary, G.S. *et al.* MCL-1 and BCL-xL-dependent resistance to the BCL-2 inhibitor ABT-199 can be overcome by preventing PI3K/AKT/mTOR activation in lymphoid malignancies. *Cell Death Dis* **6**, e1593 (2015).

498. Smith, V.M. *et al.* Specific interactions of BCL-2 family proteins mediate sensitivity to BH3-mimetics in diffuse large B-cell lymphoma. *Haematologica* **105**, 2150-2163 (2020).
499. Zhou, F.-j. *et al.* Metformin exerts a synergistic effect with venetoclax by downregulating Mcl-1 protein in acute myeloid leukemia. *Journal of Cancer* **12**, 6727-6739 (2021).
500. Weller, S. *et al.* The BCL-2 inhibitor ABT-199/venetoclax synergizes with proteasome inhibition via transactivation of the MCL-1 antagonist NOXA. *Cell Death Discovery* **8**, 215 (2022).
501. Bate-Eya, L.T. *et al.* High efficacy of the BCL-2 inhibitor ABT199 (venetoclax) in BCL-2 high-expressing neuroblastoma cell lines and xenografts and rational for combination with MCL-1 inhibition. *Oncotarget* **7**, 27946-27958 (2016).
502. Peirs, S. *et al.* ABT-199 mediated inhibition of BCL-2 as a novel therapeutic strategy in T-cell acute lymphoblastic leukemia. *Blood* **124**, 3738-3747 (2014).
503. Stewart, D.P. *et al.* Ubiquitin-independent degradation of antiapoptotic MCL-1. *Mol Cell Biol* **30**, 3099-3110 (2010).
504. Mojsa, B., Lassot, I. & Desagher, S. Mcl-1 ubiquitination: unique regulation of an essential survival protein. *Cells* **3**, 418-437 (2014).
505. Rapino, F., Naumann, I. & Fulda, S. Bortezomib antagonizes microtubule-interfering drug-induced apoptosis by inhibiting G2/M transition and MCL-1 degradation. *Cell Death & Disease* **4**, e925-e925 (2013).
506. Willis, S.N. *et al.* Proapoptotic Bak is sequestered by Mcl-1 and Bcl-xL, but not Bcl-2, until displaced by BH3-only proteins. *Genes Dev* **19**, 1294-1305 (2005).
507. Lee, S.-J. *et al.* Berberine sensitizes TRAIL-induced apoptosis through proteasome-mediated downregulation of c-FLIP and Mcl-1 proteins. *Int J Oncol* **38**, 485-492 (2011).
508. Arai, S. *et al.* MARCH5 mediates NOXA-dependent MCL1 degradation driven by kinase inhibitors and integrated stress response activation. *Elife* **9** (2020).
509. Gomez-Bougie, P. *et al.* Noxa controls Mule-dependent Mcl-1 ubiquitination through the regulation of the Mcl-1/USP9X interaction. *Biochemical and Biophysical Research Communications* **413**, 460-464 (2011).
510. Haschka, M.D. *et al.* MARCH5-dependent degradation of MCL1/NOXA complexes defines susceptibility to antimitotic drug treatment. *Cell Death & Differentiation* **27**, 2297-2312 (2020).
511. Tonino, S.H. *et al.* ROS-mediated upregulation of Noxa overcomes chemoresistance in chronic lymphocytic leukemia. *Oncogene* **30**, 701-713 (2011).
512. Pérez-Galán, P. *et al.* The proteasome inhibitor bortezomib induces apoptosis in mantle-cell lymphoma through generation of ROS and Noxa activation independent of p53 status. *Blood* **107**, 257-264 (2006).
513. de Vos, S. *et al.* Safety and efficacy of navitoclax, a BCL-2 and BCL-X(L) inhibitor, in patients with relapsed or refractory lymphoid malignancies: results from a phase 2a study. *Leuk Lymphoma* **62**, 810-818 (2021).
514. Cang, S., Iragavarapu, C., Savooji, J., Song, Y. & Liu, D. ABT-199 (venetoclax) and BCL-2 inhibitors in clinical development. *J Hematol Oncol* **8**, 129 (2015).
515. Oakes, S.R. *et al.* Sensitization of BCL-2–expressing breast tumors to chemotherapy by the BH3 mimetic ABT-737. *Proceedings of the National Academy of Sciences* **109**, 2766-2771 (2012).
516. Alcon, C. *et al.* Sequential combinations of chemotherapeutic agents with BH3 mimetics to treat rhabdomyosarcoma and avoid resistance. *Cell Death & Disease* **11**, 634 (2020).
517. Michaud, W.A. *et al.* Bcl-2 blocks cisplatin-induced apoptosis and predicts poor outcome following chemoradiation treatment in advanced oropharyngeal squamous cell carcinoma. *Clin Cancer Res* **15**, 1645-1654 (2009).
518. Bahar, E., Kim, J.-Y., Kim, H.-S. & Yoon, H. in International Journal of Molecular Sciences, Vol. 21 (2020).

519. Bodo, J. *et al.* Acquired resistance to venetoclax (ABT-199) in t(14;18) positive lymphoma cells. *Oncotarget* **7**, 70000-70010 (2016).
520. Pham, L.V. *et al.* Strategic Therapeutic Targeting to Overcome Venetoclax Resistance in Aggressive B-cell Lymphomas. *Clinical Cancer Research* **24**, 3967-3980 (2018).
521. Wong, K.Y. & Chim, C.S. Venetoclax, bortezomib and S63845, an MCL1 inhibitor, in multiple myeloma. *Journal of Pharmacy and Pharmacology* **72**, 728-737 (2020).
522. Nakajima, W. *et al.* Combination with vorinostat overcomes ABT-263 (navitoclax) resistance of small cell lung cancer. *Cancer Biology & Therapy* **17**, 27-35 (2016).
523. Cerella, C. *et al.* Bcl-2 protein family expression pattern determines synergistic pro-apoptotic effects of BH3 mimetics with hemisynthetic cardiac glycoside UNBS1450 in acute myeloid leukemia. *Leukemia* **31**, 755-759 (2017).
524. Leisching, G., Loos, B., Botha, M. & Engelbrecht, A.-M. Bcl-2 confers survival in cisplatin treated cervical cancer cells: circumventing cisplatin dose-dependent toxicity and resistance. *Journal of Translational Medicine* **13**, 328 (2015).
525. Lucantoni, F., Lindner, A.U., O'Donovan, N., Düssmann, H. & Prehn, J.H.M. Systems modeling accurately predicts responses to genotoxic agents and their synergism with BCL-2 inhibitors in triple negative breast cancer cells. *Cell Death & Disease* **9**, 42 (2018).
526. Amstad, P.A. *et al.* BCL-2 is involved in preventing oxidant-induced cell death and in decreasing oxygen radical production. *Redox Report* **6**, 351-362 (2001).
527. Yu, S. *et al.* Glycine ameliorates mitochondrial dysfunction caused by ABT-199 in porcine oocytes. *J Anim Sci* **99** (2021).
528. Zhang, Q. *et al.* BCL-2 Antagonist ABT-199 Combined with Complex I Inhibitor IACS-010759 Blocks Mitochondrial Respiration and Facilitates Anti-Leukemia Efficacy in Pre-Clinical AML Models. *Blood* **130**, 1362 (2017).
529. Nguyen, L.X.T. *et al.* The Bcl-2 inhibitor venetoclax inhibits Nrf2 antioxidant pathway activation induced by hypomethylating agents in AML. *J Cell Physiol* **234**, 14040-14049 (2019).
530. Hoang, D.H. *et al.* Arsenic Trioxide and Venetoclax Synergize against AML Progenitors by ROS Induction and Inhibition of Nrf2 Activation. *Int J Mol Sci* **23** (2022).
531. Brozovic, A., Ambriović-Ristov, A. & Osmak, M. The relationship between cisplatin-induced reactive oxygen species, glutathione, and BCL-2 and resistance to cisplatin. *Critical Reviews in Toxicology* **40**, 347-359 (2010).
532. Celli, A., Que, F.G., Gores, G.J. & LaRusso, N.F. Glutathione depletion is associated with decreased Bcl-2 expression and increased apoptosis in cholangiocytes. *American Journal of Physiology-Gastrointestinal and Liver Physiology* **275**, G749-G757 (1998).
533. Ong, F., Kim, K. & Konopleva, M.Y. Venetoclax resistance: mechanistic insights and future strategies. *Cancer Drug Resist* **5**, 380-400 (2022).
534. Lin, K.H. *et al.* Targeting MCL-1/BCL-XL Forestalls the Acquisition of Resistance to ABT-199 in Acute Myeloid Leukemia. *Scientific Reports* **6**, 27696 (2016).
535. Chiou, J.-T., Lee, Y.-C., Wang, L.-J. & Chang, L.-S. BCL2 inhibitor ABT-199 and BCL2L1 inhibitor WEHI-539 coordinately promote NOXA-mediated degradation of MCL1 in human leukemia cells. *Chemico-Biological Interactions* **361**, 109978 (2022).
536. Janssen, M. *et al.* Venetoclax synergizes with Gilteritinib in FLT3 wildtype high-risk Acute Myeloid Leukemia by suppressing MCL-1. *Blood* (2022).
537. Chanvorachote, P. & Pongrakhananon, V. Ouabain downregulates Mcl-1 and sensitizes lung cancer cells to TRAIL-induced apoptosis. *Am J Physiol Cell Physiol* **304**, C263-272 (2013).
538. Lynch, J.T. *et al.* The role of glucocorticoid receptor phosphorylation in Mcl-1 and NOXA gene expression. *Molecular Cancer* **9**, 38 (2010).

539. Sun, L. *et al.* Dichloroacetate enhances the anti-tumor effect of sorafenib via modulating the ROS-JNK-Mcl-1 pathway in liver cancer cells. *Experimental Cell Research* **406**, 112755 (2021).
540. Chi, S.N. *et al.* Intensive multimodality treatment for children with newly diagnosed CNS atypical teratoid rhabdoid tumor. *J Clin Oncol* **27**, 385-389 (2009).
541. Fulda, S. Autophagy in Cancer Therapy. *Frontiers in Oncology* **7**, 128 (2017).
542. Li, X. *et al.* Autophagy: A novel mechanism of chemoresistance in cancers. *Biomedicine & Pharmacotherapy* **119**, 109415 (2019).
543. Bhutia, S.K. *et al.* Autophagy: cancer's friend or foe? *Advances in cancer research* **118**, 61-95 (2013).
544. Button, R.W., Roberts, S.L., Willis, T.L., Hanemann, C.O. & Luo, S. Accumulation of autophagosomes confers cytotoxicity. *J Biol Chem* **292**, 13599-13614 (2017).
545. Zhao, X.G. *et al.* Chloroquine-enhanced efficacy of cisplatin in the treatment of hypopharyngeal carcinoma in xenograft mice. *PLoS One* **10**, e0126147 (2015).
546. Zhang, S. *et al.* Toosendanin, a late-stage autophagy inhibitor, sensitizes triple-negative breast cancer to irinotecan chemotherapy. *Chinese Medicine* **17**, 55 (2022).
547. Molero-Valenzuela, A. *et al.* A Novel Late-Stage Autophagy Inhibitor That Efficiently Targets Lysosomes Inducing Potent Cytotoxic and Sensitizing Effects in Lung Cancer. *Cancers (Basel)* **14** (2022).
548. Yang, Y. *et al.* Lysosomal dysfunction and autophagy blockade contribute to autophagy-related cancer suppressing peptide-induced cytotoxic death of cervical cancer cells through the AMPK/mTOR pathway. *Journal of Experimental & Clinical Cancer Research* **39**, 197 (2020).
549. Chen, Y., Jungsuwadee, P., Vore, M., Butterfield, D.A. & St Clair, D.K. Collateral damage in cancer chemotherapy: oxidative stress in nontargeted tissues, in *Mol Interv*, Vol. 7 147-156 (United States; 2007).
550. Saha, S., Buttari, B., Panieri, E., Profumo, E. & Saso, L. An Overview of Nrf2 Signaling Pathway and Its Role in Inflammation. *Molecules* **25** (2020).
551. Wu, S., Lu, H. & Bai, Y. Nrf2 in cancers: A double-edged sword. *Cancer Med* **8**, 2252-2267 (2019).
552. Zhang, J. *et al.* ROS and ROS-Mediated Cellular Signaling. *Oxid Med Cell Longev* **2016**, 4350965 (2016).
553. Bao, L. *et al.* ABCF2, an Nrf2 target gene, contributes to cisplatin resistance in ovarian cancer cells. *Mol Carcinog* **56**, 1543-1553 (2017).
554. Fraser, C., Ryan, J. & Sarosiek, K. BH3 Profiling: A Functional Assay to Measure Apoptotic Priming and Dependencies. *Methods Mol Biol* **1877**, 61-76 (2019).
555. Ramsey, H.E. *et al.* A Novel MCL1 Inhibitor Combined with Venetoclax Rescues Venetoclax-Resistant Acute Myelogenous Leukemia. *Cancer Discovery* **8**, 1566-1581 (2018).
556. Seo, S.U., Kim, T.H., Kim, D.E., Min, K.J. & Kwon, T.K. NOX4-mediated ROS production induces apoptotic cell death via down-regulation of c-FLIP and Mcl-1 expression in combined treatment with thioridazine and curcumin. *Redox Biol* **13**, 608-622 (2017).
557. Yadav, R.K., Chae, S.-W., Kim, H.-R. & Chae, H.J. Endoplasmic reticulum stress and cancer. *Journal of cancer prevention* **19**, 75-88 (2014).
558. Bellini, L. *et al.* Endoplasmic reticulum stress mediates resistance to BCL-2 inhibitor in uveal melanoma cells. *Cell Death Discovery* **6**, 22 (2020).
559. ROCHA, Clarissa Ribeiro Reily; SILVA, Matheus Molina; QUINET, Annabel; CABRAL-NETO, Januario Bispo; MENCK, Carlos Frederico Martins. DNA repair pathways and cisplatin resistance: an intimate relationship. Clinics, v. 73, n. suppl 1, e478s, Aug. 2018.

560. Brand, M.D. Mitochondrial generation of superoxide and hydrogen peroxide as the source of mitochondrial redox signaling. Free Radical Biology and Medicine 100, 14-31 (2016).

Publication

Cancer Treatment and Research Communications 32 (2022) 100584

Contents lists available at ScienceDirect

Cancer Treatment and Research Communications

journal homepage: www.sciencedirect.com/journal/cancer-treatment-and-research-communications

Evaluation of targeting autophagy for the treatment of malignant rhabdoid tumours

Patricia Hannon Barroeta [a,*], Stefania Magnano [a], Maureen J O'Sullivan [b], Daniela M Zisterer [a]

[a] School of Biochemistry and Immunology, Trinity Biomedical Sciences Institute, Trinity College Dublin, Dublin 2, Ireland
[b] The National Children's Research Centre, Children's Health Ireland at Crumlin, Dublin 12, Ireland

ARTICLE INFO

Keywords:
Malignant rhabdoid tumour
Apoptosis
Autophagy
Chemoresistance

ABSTRACT

Malignant rhabdoid tumour (MRT) is a rare and aggressive paediatric tumour that typically arises in the kidneys or central nervous system (CNS). The malignancy often affects patients under the age of three and is associated with an extremely poor survival rate, with most deaths occurring within the first year of presentation. Thus, there is an unmet and urgent medical need for novel therapeutic strategies for this malignancy. One of the major issues when treating MRT patients is the emergence of chemoresistance. Autophagy has become an area of focus in the study of chemoresistance due to its reported dual role as both a pro-survival and pro-death mechanism. The role of autophagy in the chemotherapeutic response of MRT remains largely unknown. A greater understanding of the role of autophagy may lead to the development of therapeutic strategies to enhance chemotherapeutic effect and improve the clinical outcome of MRT patients. This study evaluated the cellular response to cisplatin, a representative chemotherapeutic agent used in the treatment of MRT, and the role of autophagy in mediating cisplatin resistance. Our results demonstrated that cisplatin induced apoptosis and autophagy concomitantly in a panel of MRT cell lines. Furthermore, inhibition of caspase-induced apoptosis with Z-VAD-FMK also inhibited autophagy levels demonstrating a complex interplay between these two pathways. In addition, blocking autophagy at the early stages of the autophagic process using the pharmacological inhibitor SAR405 or through the genetic knockdown of critical autophagic protein ATG5 by siRNA did not sensitise cells to cisplatin-induced apoptosis. Collectively, these results suggest that induction of autophagy does not appear to elicit a pro-survival effect in the chemotherapeutic response of MRT cells.

Introduction

Malignant rhabdoid tumour (MRT) is a very rare and highly aggressive form of neoplasm that occurs primarily in infants and young children. This tumour is primarily found in the kidneys, the central nervous system (CNS) and less commonly, in the liver and any soft tissue sites. Tumours located in the kidney are typically referred to as malignant rhabdoid tumour of the kidney (MRTK) and tumours located in the CNS are referred to as atypical teratoid malignant tumour (AT/RT) [1]. A common characterising feature of MRTs is a mutation in the SWI/SNF related, matrix associated, actin dependant regulator of chromatin, subfamily b, member 1 (*SMARCB1*) gene. *SMARCB1* is a tumour suppressor gene coding for the SMARCB1 protein, a component of the SWI/SNF chromatin remodelling complex. SMARCB1 is inactivated in the majority of rhabdoid tumours. Interestingly, MRTs have a remarkably stable genome, with biallelic SMARCB1 inactivation being the only recurring genetic event [2]. Diagnosis of MRT relies primarily on the histological analysis of a tumour biopsy, clinical features and detection of the SMARCB1 mutation. Tumours are identified as MRTs due to certain histological characteristics such as large nucleoli, filamentous cytoplasmic inclusions, and a significant amount of eosinophilic cytoplasm [1]. Immunohistochemical staining of SMARCB1 was developed in 2004 and has since become a useful diagnostic tool in identifying MRT [1–4]. Clinical similarities can be observed across different cases of MRTs. Therefore, a combination of tests with clinical assessment should be used to correctly diagnose MRTs. Diagnosis frequently occurs at advanced stages of disease due to the aggressive and rare nature of these tumours [5,6].

Although it is also diagnosed in older children and adults, MRT typically occurs in infants under the age of three. The patients' age poses significant restrictions when planning intensive therapy due to their low tolerance to radiotherapy and chemotherapy. This, combined with the

* Corresponding author.
E-mail address: hannonbp@tcd.ie (P. Hannon Barroeta).

https://doi.org/10.1016/j.ctarc.2022.100584

Available online 3 June 2022

higher stage at presentation means that the prognosis for MRT is very poor with an estimated 2-year survival rate of 30% [7–9]. Collectively, this indicates that there is an urgent need to better understand the molecular mechanisms underlying chemoresistance in rhabdoid tumours to reduce the toxicities associated with aggressive chemotherapeutic regimens in young children.

Autophagy is an evolutionarily conserved catabolic process by which the cell degrades and recycles its own components. There are three types of autophagy described in literature: chaperone-mediated autophagy (CMA), microautophagy and macroautophagy [10]. CMA is the chaperone-mediated recruitment of proteins to the lysosome via KFERQ-like pentapeptide sequence where they are internalised and degraded. In microautophagy, smaller components are engulfed through the invagination of the lysosomal membrane and subsequently recycled. The term "macroautophagy" is often used interchangeably with "autophagy" in literature and is the best characterised form of autophagy. The process of macroautophagy consists of the formation of a double membrane sequestering compartment called the phagophore. This isolates the cytoplasmic components to form an autophagosome which then fuses with the lysosome to form an autolysosome, where the cargo is degraded [11]. From here on, the term "autophagy" will be used to refer to "macroautophagy".

Autophagy is essential in the maintenance of cellular homoeostasis, however, dysregulation of the autophagic process has been implicated in numerous diseases such as diabetes, neurodegenerative disorders and cancer [12]. Autophagy is described as a "double-edged sword" in cancer due to its dual role in tumorigenesis [13]. Depending on the context, autophagy has been shown to exhibit both pro-survival and pro-death activity. For this reason, both the inhibition and induction of autophagy have been considered as potential anti-cancer treatments. On the one hand, autophagy is believed to suppress tumorigenesis at early stages by removing damaged cellular components and reactive oxygen species [14]. On the other hand, it is believed to promote tumorigenesis at advanced stages by facilitating cell survival in stressful conditions such as nutrient starvation and hypoxia [15]. Moreover, autophagy can modulate the tumour environment (TME) through several factors such as tumour-associated macrophages (TAM) amongst other immune cells, cytokines and antibodies, thereby influencing treatment effectiveness in a context-dependant manner [16–18]. Autophagy is also believed to be upregulated in cancer cells to promote survival in response to genotoxic stress induced by chemotherapeutic treatment, implicating it as a key process in chemoresistance [18,19]. In contrast, there have also been studies to suggest a pro-death role for autophagy in response to chemotherapy in several cancers [20,21]. However, the role of autophagy in mediating chemoresistance in MRT remains poorly understood.

The results presented in this study demonstrate a concomitant induction of apoptosis and autophagy in MRT cells in response to cisplatin, a standard MRT chemotherapeutic agent which induces genotoxic stress by producing interstrand and intrastrand DNA cross-links. Moreover, treatment with Z-VAD-FMK, a caspase inhibitor, appeared to inhibit both apoptosis and autophagy indicating crosstalk between the two pathways. This study also investigated the effect of targeting autophagy using early and late-stage pharmacological inhibitors (SAR405, chloroquine and baflomycin-A1) as well as through the genetic knockdown of the key autophagic protein, ATG5. The findings in this report provide new insights into the role for autophagy in response to chemotherapy in MRT.

Materials and methods

Reagents

Cisplatin (Sigma-Aldrich; cat no. A9165) was dissolved in sterile 0.9% NaCl. Baflomycin-A1 (Sigma-Aldrich; cat no. B1793), SAR405 (APExBIO; cat no. A8883) and Z-VAD-FMK (Calbiochem; cat no.627610) were dissolved in DMSO (Sigma-Aldrich; cat no. 102,952). Rapamycin and chloroquine were supplied in the CytoID® Autophagy Detection kit (Enzo Life Sciences (UK) LTD; cat no. ENZ-51,031-K200) and prepared according to the manufacturers' instructions. Stock solutions were stored at −20 °C and working solutions were prepared fresh in sterile PBS (Sigma-Aldrich; cat no. 14,190–094) the day of the treatment.

Cell culture

BT12 and BT16 cell lines are epithelial AT/RT cells isolated from a 2-month-old female and a 2-year-old male, respectively. These cell lines were kindly donated by Peter Houghton, St. Jude Children's Research Hospital (Memphis, TN, USA). G401 cells (American Type Culture Collection, Manassas, VA, USA) were derived from a 3-month-old male who was originally misdiagnosed with Wilms Tumour, but it was later identified to be a kidney rhabdoid tumour cell line. BT12 and BT16 cell lines were cultured in Gibco RPMI-1640 GlutaMAX (Biosciences, Dublin, Ireland). G401 cells were cultured in Gibco Dulbecco's modified Eagle's medium (DMEM) GlutaMAX (Biosciences). All media used was supplemented with 10% (v/v) foetal bovine serum (FBS; Biosciences), 100 U/ml penicillin and 100 μg/ml streptomycin (Biosciences). Cultured cells were incubated at 37 °C with 5% $CO2^{22}$.

Cell viability

BT12, BT16 and G401 cell lines were seeded at densities of 10×10^3, 10×10^3 and 5×10^3 cells/well, respectively, in 96-well plates. Cells were left overnight to adhere and then treated with a range of concentrations of cisplatin for 24, 48 and 72 h. Viability was assessed via the alamar blue assay. After the relevant incubation period, 20 μl of AlamarBlue™ (Invitrogen; Thermo Fisher Scientific, Inc. Waltham, MA, USA) was added to each well and the plate was left to incubate in the dark for 5 h at 37 °C. Fluorescence was measured on a SpectraMax plate reader at an excitation wavelength of 544 nm and an emission wavelength of 590 nm. All alamar blue assays were performed in triplicate. Dose response curves were obtained and used to determine the IC50 values (GraphPad Prism 5.0) [22].

Apoptosis analysis

2 mL of cells were seeded in 6 well plates in complete media at seeding densities of 1×10^5 cells/mL for BT12 and BT16 and 5×10^4 cells/mL for G401 cells. The following day the cells were treated with the relevant drugs for the required timepoint. Apoptosis analysis was performed using annexin V- fluorescein isothiocyanate (FITC, Accuscience; cat no. IQP–120F) and propidium iodide (PI, Sigma-Aldrich; cat no. P4170) staining as previously described [22] .

Autophagy analysis

Autophagy analysis was performed using the CytoID® Autophagy Detection kit. 2 mL of cells were seeded in 6 well plates at a density of 1×10^5 cells/mL in complete media and the following day were treated with the relevant drugs for the required timepoints. After incubation, cells were harvested and stained with the CytoID® Green dye solution, as per manufacturer's instructions.

Western blot analysis

Western blotting was conducted as previously described [18]. Blots were probed with antibodies from Cell signaling Technology: caspase 3 (1:1000; cat no. 9662S), cleaved caspase 3 (1:500; cat no. 9664S), LC3 (1:1000; cat no. 3868), ATG5 (1:1000; cat no. 2630), ATG7 (1:1000; cat no. 2631), beclin-1 (1:1000; cat no. 3738S) and p62 from Abcam (1:1000, cat no. ab56416). All blots were re-probed with anti-GAPDH

(1:5000, Calbiochem, cat no. 6C5), actin or anti-α-tubulin (1:5000, Calbiochem, cat no. CP06) to ensure equal loading.

ATG5 knockdown using small interfering (si)RNA

On-target plus human ATG5 siRNA SMART pool (GE Healthcare Dharmacon, Inc.; cat no. L-004,374–00–0005) was employed for ATG5 knockdown, while non-targeting pool served as negative control. Cells were seeded in 6 well plates at a density of 1×10^5 cells/mL in antibiotic free media. The following day, ATG5 siRNA or non-targeting siRNA was transfected into cells using Lipofectamine (Thermo Fisher; cat no. 11,668–027) at a final concentration of 50 nM, as per manufacturer's instructions and as previously described by Magnano et al. [23]. Western blot analysis was employed to confirm ATG5 knockdown at 48 h post-transfection.

Statistical analysis

GraphPad Prism 5 (GraphPad Software, Inc., La Jolla, CA, USA) was used for statistical analysis of experimental data. Results are displayed as the mean ± standard error of the mean. Statistical analysis was performed using a one-way ANOVA with Tukey's post hoc test. Values of $*p < 0.05$, $**p < 0.01$ and $***p < 0.001$ were deemed statistically significant.

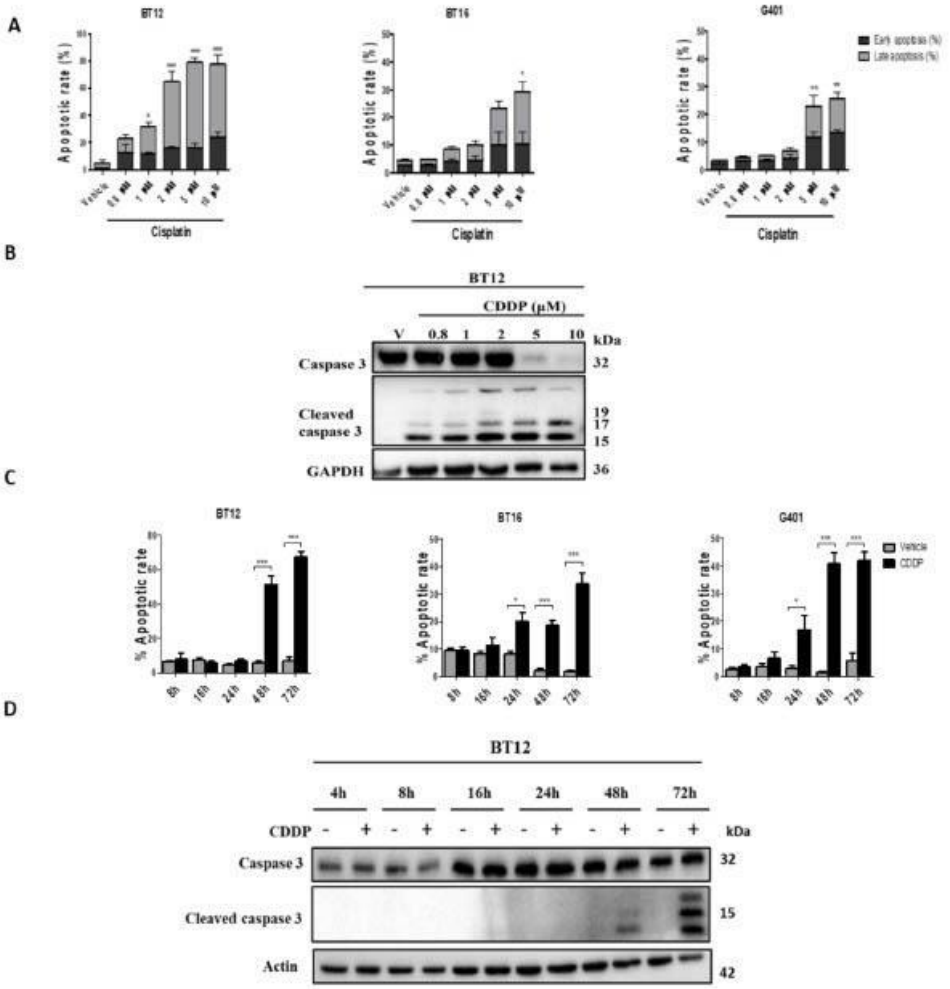

Fig. 1. Cisplatin induces apoptosis in a dose- and time-dependant manner in MRT cell lines.
A. Cells were treated with increasing concentrations of cisplatin or vehicle (0.009% NaCl) for 48 h. Apoptosis was assessed via flow cytometric analysis of Annexin V/PI-stained cells. B. Cells were treated with increasing concentrations of cisplatin or vehicle (0.009% NaCl) for 48 h. Caspase 3 and cleaved caspase 3 were examined via western blot analysis on a 15% gel. GAPDH served as a loading control. C. MRT cells were treated with cisplatin (CDDP) or vehicle (0.009% NaCl) for the indicated timepoints (BT12 cells were treated with 1 μM while BT16 and G401 were treated with 10 μM CDDP). Apoptosis was assessed via flow cytometric analysis of Annexin V/PI-stained cells. D. BT12 cells were treated with 1 μM CDDP for the indicated timepoints. Caspase 3 and cleaved caspase 3 were examined via western blot analysis. Actin served as a loading control. The results are representative of mean ± S.E.M of three independent experiments. Statistical analysis was performed using a one-way ANOVA with Tukey's post hoc test $***p < 0.001$, $**p < 0.01$, $*p < 0.05$.

Results

Cisplatin induces apoptosis in a dose- and time-responsive manner in MRT cell lines

Viability of BT12, BT16 and G401 cell lines was assessed upon treatment with cisplatin, a chemotherapeutic agent commonly utilised in the treatment of MRT. All three cell lines were responsive to treatment with cisplatin. BT12 cells were the most sensitive, followed by G401 cells with the BT16 cell line showing the greatest resistance (**Fig S1, Table S1**).

Induction of apoptosis in response to cisplatin was next assessed in the MRT panel. Apoptosis was measured through flow cytometric analysis of annexin V/PI-stained cells. Treatment of cells with a range of concentrations of cisplatin resulted in a marked induction of apoptosis in a dose-dependant manner (Fig 1**A**). BT12 cells were noted to be particularly sensitive to cisplatin in comparison to BT16 and G401 cells. For this reason, BT12 cells were treated with 1 μM cisplatin at varying timepoints whereas BT16 and G401 cells were treated with a higher concentration of 10 μM cisplatin. A significant induction of apoptosis was observed in all cell lines in a time-dependant manner (Fig 1**C**).

These results were confirmed using western blot analysis of caspase 3 cleavage in BT12 cells which demonstrated the progressive disappearance of the caspase 3 band and the appearance of cleaved caspase 3 fragments (Fig. 1**B, D, Fig S2**). Caspase 3 (a cysteine-aspartic acid protease) is an enzymatic protease which plays a critical role in the execution phase of the apoptotic cascade. Caspase 3 itself is activated through proteolytic cleavage. Cleaved fragments of caspase 3 can be detected via western blotting and are a commonly used method of detecting apoptosis [24].

Collectively, these results demonstrate that cisplatin induces apoptosis in a dose- and time-dependant manner in MRT cell lines. These results also indicate that BT12 cells have a higher sensitivity to cisplatin in comparison to BT16 and G401 cell lines.

Cisplatin induces autophagy in a dose- and time- responsive manner in MRT cell lines

To evaluate the basal levels of autophagy in the MRT cell lines, the autophagic flux (defined as the balance between autophagosome generation and clearance) was evaluated by utilising bafilomycin-A1, a late-stage autophagy inhibitor which acts by preventing degradation of autophagosomes. As shown in Fig. 2**A**, western blot analysis demonstrated an accumulation of LC3-II in cells treated with bafilomycin-A1 compared to vehicle-treated cells, suggesting that basal levels of autophagy are constitutively activated in all three MRT cell lines under normal conditions. Furthermore, conversion of LC3-I to LC3-II and degradation of p62, in cells starved of nutrients (through treatment with EBSS) demonstrated autophagy activation, confirming the ability of these cell lines to undergo autophagy in response to external stimuli. Having established this, the effect of cisplatin on autophagy levels was next assessed. Cells were treated with various concentrations of cisplatin for 48 h and stained with CYTO-ID green dye for flow cytometric analysis. An increase in fluorescence indicated an increase in autophagic vesicles in response to cisplatin treatment in all three MRT cell lines (Fig 2**B**). Of note, a decrease in vesicles was observed at higher concentrations of cisplatin in BT12 cells where extremely high levels of cell death affected the ability to detect autophagic vesicles. A representative flow cytometric histogram of vehicle and cisplatin treated BT12 cells alongside the rapamycin/chloroquine positive control is shown in supplementary **Fig S3**.

This result was confirmed by western blot analysis which demonstrated a degradation of p62 as well as a conversion LC3-I to LC3-II in response to cisplatin in BT12 cells (Fig 2**C**). The effect of cisplatin on autophagy was next assessed at various timepoints from 4 h up to 72 h (Fig 2**D, E**). Interestingly, an increase in autophagic vesicles was not observed in BT12 cells until 48 h, the same time point that apoptosis is first detected in these cells. An increase in LC3-I to LC3-II was also observed and a significant decrease in p62 levels was again detected at 48 h indicating that autophagy is induced alongside apoptosis in response to cisplatin. Next, to confirm that the increase in autophagic vesicles detected was due to an induction of autophagy, and not due to the inhibition of the last stage of autophagy (the degradation of autophagic vesicles), cells were treated with cisplatin and a late-stage autophagy inhibitor, chloroquine, alone and in combination. A significant increase in autophagic vesicles was observed in co-treated cells when compared to cells treated with cisplatin or chloroquine only (Fig 2**F**), indicating that cisplatin indeed induces autophagic flux. Taken together, these results suggest that cisplatin induces apoptosis and autophagy in MRT cell lines, concurrently.

Inhibition of apoptosis partially abrogates cisplatin-induced autophagy in MRT cell lines

Having established that cisplatin induces caspase 3-dependant apoptosis in MRT cells, the effect of the pan-caspase inhibitor, Z-VAD-FMK, on both apoptosis and autophagy was evaluated. Through flow cytometric analysis, Z-VAD-FMK was shown to significantly reduce the levels of cisplatin-induced apoptosis (Fig 3**A**). Furthermore, pre-treatment of cells with Z-VAD-FMK followed by cisplatin inhibited autophagy as shown by the significant accumulation of LC3-II and p62 when compared to treatment with cisplatin alone (Fig 3**B**). These results taken together indicate that blocking apoptosis results in the inhibition of autophagy, suggesting complex interplay between the two pathways.

Inhibiting autophagy using late-stage inhibitors sensitises MRT cells to cisplatin

Autophagy has been reported to be activated as a pro-survival or pro-death mechanism in response to chemotherapy treatment in a cell-type and/or drug-specific manner, but the role of autophagy in MRT remains unclear. The effect of targeting autophagy on cisplatin-induced apoptosis was next evaluated. Since autophagic flux can be blocked at different stages, two late-stage autophagy inhibitors, chloroquine and bafilomycin-A1 respectively, were firstly selected to block autophagic flux. Inhibition of autophagy by both inhibitors was again confirmed via western blot analysis, demonstrating enhanced accumulation of p62 and LC3-II in both BT12 and BT16 cells (Fig 4**A, D**). Densitometric analysis is shown in supplementary **Fig S4**. Interestingly, treatment of cells with chloroquine significantly enhanced cisplatin-induced apoptosis in both BT12 and BT16 cell lines as demonstrated by flow cytometric analysis and western blot analysis of cleaved caspase 3 (Fig 4**B, C**). Similar findings were also observed upon co-treatment with bafilomycin-A1 (Fig 4**E, F**). These results initially suggested that autophagy may play a pro-survival role in MRT and therefore could potentially be targeted in the treatment of MRT. However, both these pharmacological inhibitors have been reported to elicit off-target effects, therefore these results required further substantiation.

Targeting early-stage autophagy has no effect on cisplatin-induced apoptosis in MRT cells

Having determined that cisplatin upregulates autophagy and that inhibition of autophagic flux sensitises cells to cisplatin-induced apoptosis, this study next aimed to confirm these results by blocking autophagy through early-stage inhibition of autophagy. The early-stage pharmacological inhibitor, SAR405, was employed for this purpose. Inhibition of early-stage autophagy was confirmed via western blot analysis which demonstrated a reduction of LC3-I to LC3-II conversion and a marked accumulation of p62 in MRT lines (Fig 5**A**). In marked contrast to the result obtained with the late-stage autophagy inhibitors, SAR405, tested at three different concentrations, was found to elicit no

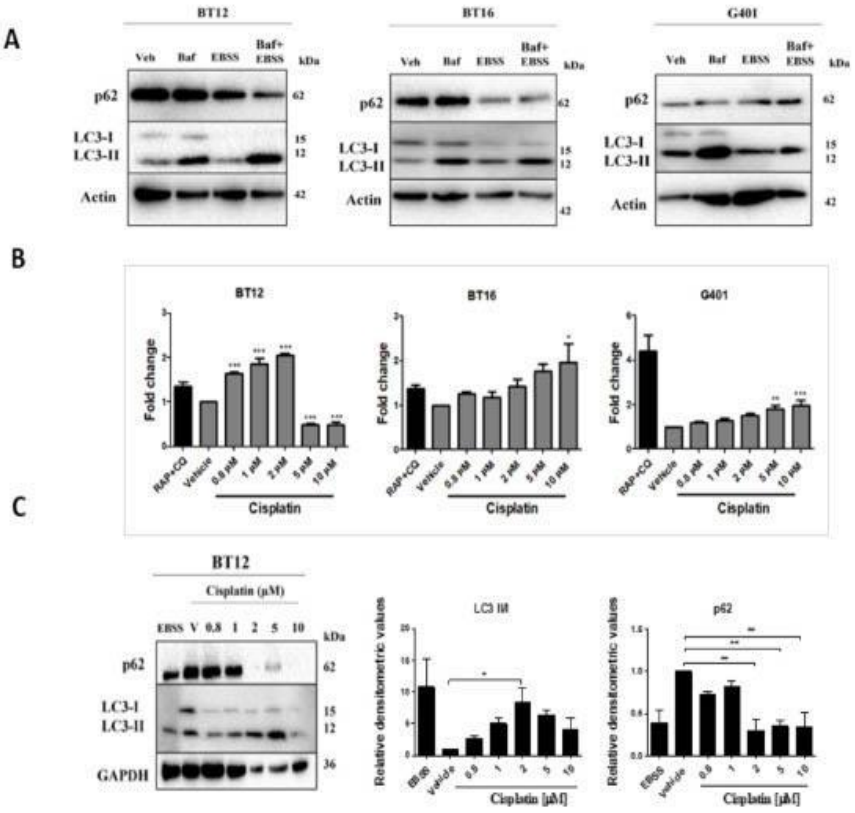

(caption on next page)

Fig. 2. Cisplatin activates autophagy in a dose- and time-dependant manner in MRT cell lines.
A. BT12, BT16 and G401 cells were left untreated, treated with EBSS for 4 h, treated with bafilomycin-A1 (100 nM) for one hour or a combination of EBSS and bafilomycin-A1. After the incubation period, the cells were harvested and lysed. 20 μg of protein lysate was loaded onto a 15% SDS-PAGE gel. The protein was then transferred onto a PVDF membrane, incubated in blocking milk for one hour and probed for LC3 and p62. Actin was used as a loading control. This figure is representative of three independent experiments. **B.** MRT cells were treated with cisplatin (CDDP) or vehicle (0.009% NaCl) at varying concentrations and stained with Cyto-ID green dye for flow cytometric analysis. Co-treatment of rapamycin and chloroquine (RAP + CQ) was used as a positive control. **C.** BT12 cells treated with increasing concentrations of CDDP for 48 h were probed for p62 and LC3 via western blot analysis. GAPDH served as a loading control. Cells were starved with EBSS for 4 h as a positive control. **D.** BT12 cells treated for up to 72 h with CDDP (1 μM) and probed for p62 and LC3 via western blot analysis. Actin served as a loading control. Densitometry analysis was performed on p62, LC3-I and LC3-II bands, using the ImageLab software. Data was normalised by the loading control and to the vehicle control. **E.** BT12 cells were treated with 1 μM cisplatin (CDDP) or vehicle (0.009% NaCl) at varying timepoints and stained with Cyto-ID green dye for flow cytometric analysis. Co-treatment of rapamycin and chloroquine (RAP + CQ) was used as a positive control. **F.** BT12 and BT16 cell lines were treated with CDDP (1 μM or 10 μM respectively), chloroquine (CQ) (20 μM) or combination of both for 48 h and stained with Cyto-ID green dye for flow cytometric analysis. The results are representative of mean ± S.E.M of three independent experiments. Statistical analysis was performed using a one-way ANOVA with Tukey's post hoc test. $***p < 0.001$, $**p < 0.01$, $*p < 0.05$.

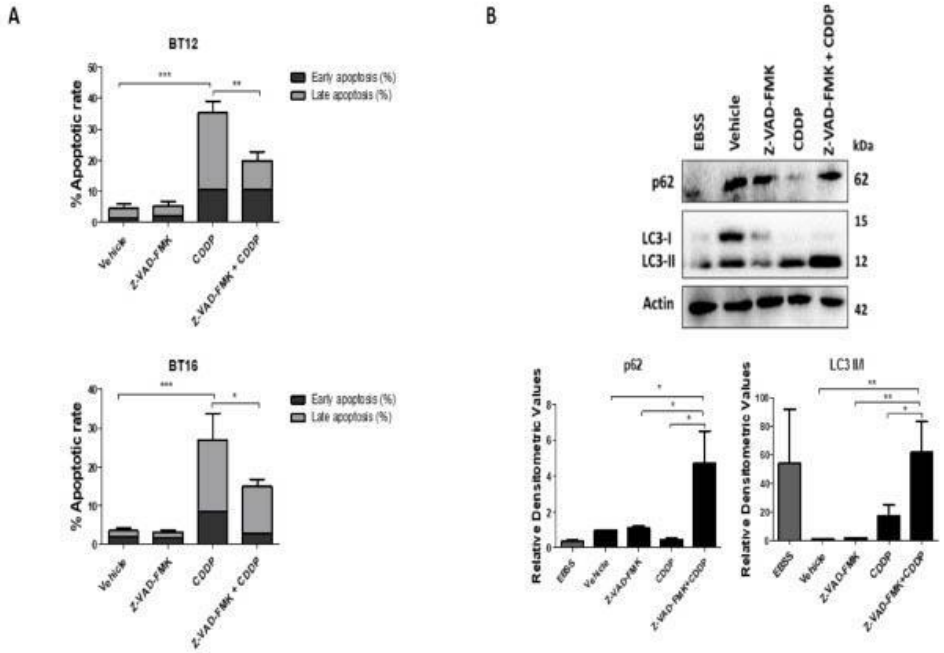

Fig. 3. The pan-caspase inhibitor Z-VAD-FMK elicits a protective effect against cisplatin-induced apoptosis and autophagy in MRT cell lines.
BT12 and BT16 cells were pre-treated with Z-VAD-FMK (20 μM) for 1 h before being treated with CDDP (1 μM and 10 μM, respectively) for 48 h. The cells were stained with Annexin V/PI for flow cytometric analysis (A) and BT12 cells were probed for p62 and LC3 via western blot analysis (B). Actin served as a loading control. Densitometry analysis was performed on p62, LC3-I and LC3-II bands using the ImageLab software. The values represent mean ± S.E.M for three independent experiments. Statistical analysis was performed using a one-way ANOVA with Tukey's post hoc test. $***p < 0.001$, $**p < 0.01$, $*p < 0.05$.

effect on cisplatin-induced apoptosis levels when compared to cells treated with cisplatin only (Fig 5B). In order to substantiate this result, RNA interference was employed to block autophagy through the silencing of a key autophagic player, ATG5. This autophagic protein is involved in autophagosome formation through induction of the autophagy elongation complex (ATG5–12/16). This method has a higher degree of specificity when compared to the use of pharmacological inhibitors which are often associated with off-target effects. BT12 cells transfected with ATG5 siRNA exhibited a marked reduction in ATG5-ATG12 protein expression and a corresponding significant reduction in the LC3-II levels compared to NT siRNA transfected cells and lipofectamine treated control cells (Fig. 5C). Next, the effect of genetic inhibition of autophagy on cisplatin-induced apoptosis was examined. Results obtained using flow cytometric analysis showed no difference in cells that were transfected with non-targeting siRNA and cells transfected with ATG5 siRNA (Fig 5D). This supports the results obtained using the early-stage pharmacological inhibitor SAR405 and indicates that early-stage inhibition of autophagy does not sensitise MRT cells to cisplatin. Collectively, these findings indicate that autophagy is not activated as a pro-survival mechanism and is not likely to be implicated in cisplatin resistance in MRT cells.

Discussion

MRT is a very aggressive tumour occurring in infants and is associated with an extremely poor prognosis. Due to its aggressive nature, it is

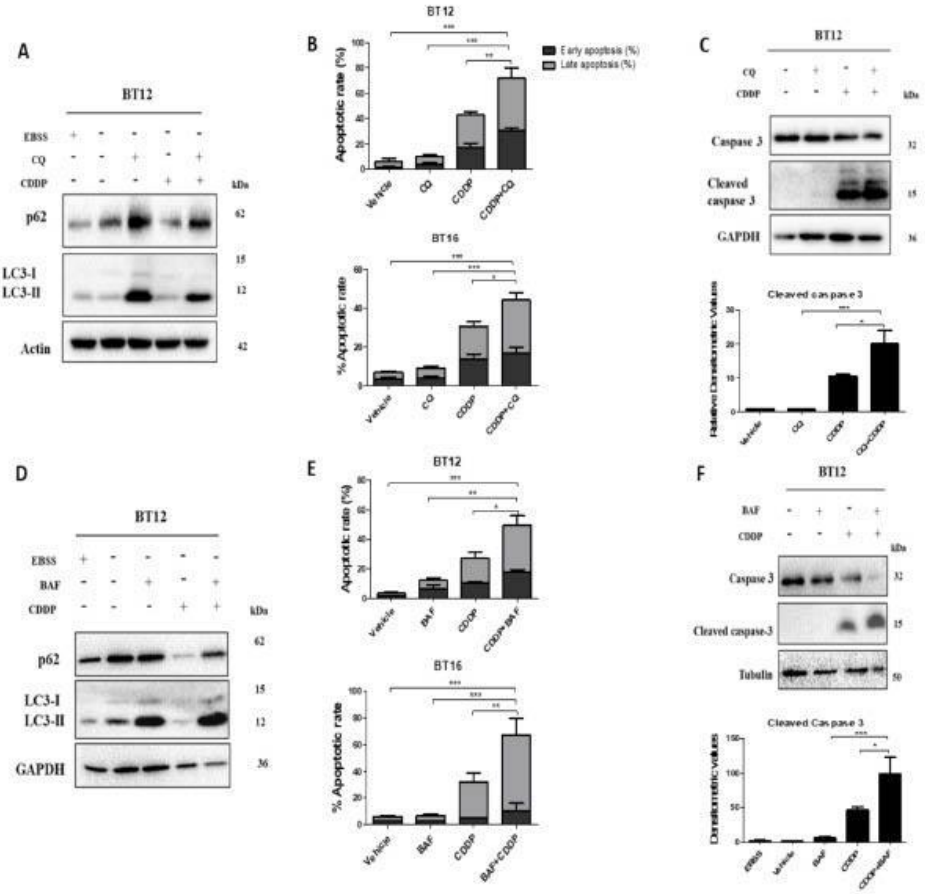

Fig. 4. Inhibition of autophagy with the late-stage pharmacological inhibitors, chloroquine, and bafilomycin-A1, enhanced cisplatin-induced apoptosis in MRT cells. **A** BT12 cells were treated with CQ (20 μM) and CDDP (1 μM) alone and in combination for 48 h and probed for p62 and LC3 via western blotting. **B** BT12 and BT16 cells were treated with CDDP (1 and 10 μM, respectively) alone and in combination with CQ (20 μM) for 48 h. After the incubation period, the cells were stained with Annexin V/PI for flow cytometry. **C.** BT12 cells were treated with CQ and CDDP alone and in combination for 48 h and probed for caspase 3 and cleaved caspase 3 via western blotting. **D** BT12 cells were treated with bafilomycin-A1 (BAF, 2.5 nM) and CDDP (1 μM) alone and in combination for 48 h and probed for p62 and LC3via western blotting. **E** BT12 and BT16 cells were treated with CDDP (1 and 10 μM, respectively) alone and in combination with bafilomycin-A1 (2.5 nM) for 48 h. After the incubation period, the cells were stained with Annexin V/PI for flow cytometry. **F** BT12 cells were treated with bafilomycin-A1 and CDDP alone and in combination for 48 h and were probed for caspase 3 and cleaved caspase 3 via western blotting. The values represent mean ± S.E.M for at least three independent experiments. Statistical analysis was performed using a one-way ANOVA with Tukey's post hoc test. $^{***}p < 0.001$, $^{**}p < 0.01$, $^{*}p < 0.05$.

often diagnosed at advanced stages. This, in combination with the young age of MRT patients, results in limited treatment options which are often associated with grave toxicities. For this reason, there is an urgent need to develop novel therapeutic options to sensitise rhabdoid tumour cells to chemotherapeutics. To date, there is no established treatment protocols for these tumours and our understanding of their molecular biology remains elusive [1,25]. Therefore, a better understanding of the cellular mechanisms underlying chemoresistance in these tumours is critical.

Autophagy is necessary to maintain cellular homoeostasis. However, dysregulation of this process has been implicated in several diseases, including cancer. The role of autophagy in cancer progression and chemoresistance has been a subject of debate in cancer studies due to its paradoxical role [26]. Autophagy can have a preventative role against tumorigenesis through the removal of damaged organelles. In contrast, autophagy facilitates tumour survival by recycling cellular components to meet the metabolic requirements of the tumours and promotes cellular proliferation. Its role in chemoresistance is also considered to be "context-dependant" [27]. On one hand, autophagy is thought to be upregulated in response to chemotherapeutic-induced stress on the cells [28]. On the other hand, there have been reports of "autophagic cell death" whereby autophagy responds to chemotherapeutic stress by inducing cell death [21,29].

The role of autophagy in MRT chemoresistance remains unclear. In one study in MRT, the histone deacetylase inhibitor FK228 was shown to induce both apoptosis and autophagy [30]. Inhibition of autophagy by

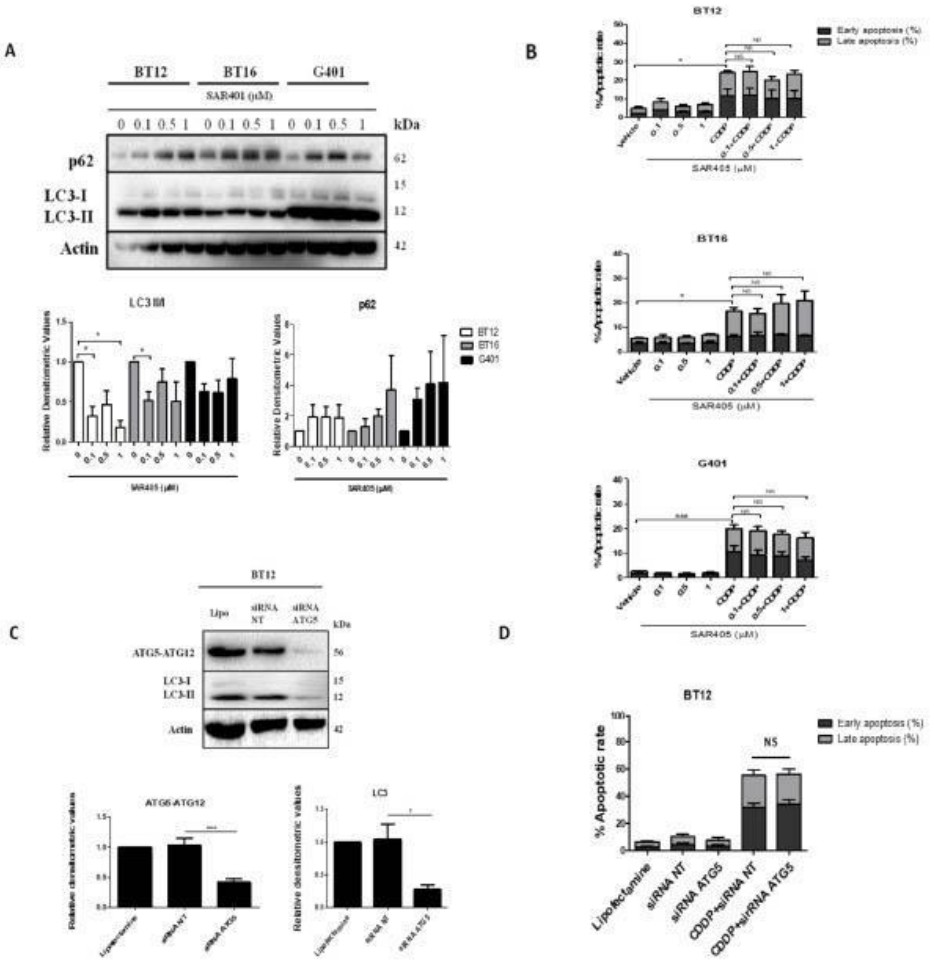

Fig. 5. Targeting early-stage autophagy via genetic knockdown of ATG5 and the pharmacological inhibitor SAR405 does not affect cisplatin-induced apoptotic death in MRT cells.

A BT12, BT16 and G401 cell lines were treated with increasing concentrations of SAR405 (0.1, 0.5 and 1 μM) and probed for p62 and LC3 via western blotting. Actin served as a loading control. **B** MRT cells were treated with concentrations of SAR405 alone and in combination with cisplatin for 48 h. Cells were stained with Annexin V/PI and analysed via flow cytometric analysis. **C** BT12 cells were transfected with Non-Targeting (NT) control siRNA or with ATG5 siRNA with Lipofectamine 2000™ (Lipo) for 48 h. Cells treated with Lipo alone served as negative control. ATG5-ATG12 and LC3-I/II levels were assessed by western blotting. Actin served as loading control. Densitometric analysis was performed using ImageLab. **D** BT12 cells were transfected with NT and ATG5 siRNA for 24 h. After 24 h, cells were treated with CDDP (10 μM) alone and in combination with NT and ATG5 siRNA for a further 24 h. The values represent mean ± S.E.M for at least three independent experiments. Statistical analysis was performed using a one-way ANOVA with Tukey's post hoc test. $^{***}p < 0.001$, $^{**}p < 0.01$, $^{*}p < 0.05$, NS = non-significant.

the pharmacological autophagy inhibitors chloroquine and 3-methlyadenine enhanced FK228-induced cell death suggesting that, under these circumstances, autophagy is activated as a pro-survival protective mechanism [30]. In a further study, Levy and Thorburn examined the effects of lomustine and cisplatin on paediatric medulloblastoma and MRT cell lines with varying results and found that genetic inhibition of autophagy through targeting ATG7 and ATG12 had no effect on tumour cell survival [31]. In contrast, Carugo et al. developed MRT embryonic mosaic mouse models and found that these tumours were highly sensitive to the inhibition of autophagy and induction of proteotoxic stress due to their active unfolded protein response (UPR) which was regulated by the MYC-p53 axis, suggesting a rationale for combination of autophagy and proteosome inhibitors for patients with MRT [32,33]. These contradictory results provide a rationale for further study into the role of autophagy in MRT and exploration of its potential as a therapeutic target.

In this present study, cisplatin was found to induce apoptosis and autophagy simultaneously, in a panel of MRT cell lines suggesting a

complex interplay between the two pathways (Figs. 1, 2). This agrees with several reports in the literature that demonstrate that cisplatin induces both apoptosis and autophagy concomitantly in human bladder cells [34], in lung cancer cells [35]and in breast cancer cells [36]. It is also in agreement with a recent report in OSCC cells whereby autophagy and apoptosis were concurrently upregulated in response to cisplatin treatment and appeared to have an intricately linked relationship [23].

To further study the interplay between apoptosis and autophagy, a pan-caspase inhibitor, Z-VAD-FMK was employed. Z-VAD-FMK was found to significantly protect MRT cells from cisplatin-induced apoptosis confirming cisplatin cytotoxicity is in part, caspase-mediated (Fig. 3). Interestingly, Z-VAD-FMK was also shown to significantly inhibit autophagic flux, as demonstrated by an accumulation of p62 and LC3-II, further supporting the observation that there is crosstalk between apoptotic and autophagic signalling pathways in MRT cell lines. This result is in agreement with that observed in the study in OSCC cells by Magnano et al., who demonstrated that Z-VAD-FMK abrogated cisplatin-induced apoptosis and significantly inhibited cisplatin-induced autophagy [23]. Moreover, Herzog et al. observed that Z-VAD-FMK inhibits cisplatin-induced autophagic flux in porcine kidney proximal tubule epithelial cells [37]. In contrast, Martinet et al. have shown that Z-VAD-FMK induced autophagy and non-apoptotic cell death in macrophages [38]. These reports suggest that the relationship between autophagy and apoptosis is highly context-dependant and may differ depending on cell type and stressor.

Having observed that autophagy is upregulated in response to cisplatin treatment, this study next aimed to target autophagy to establish whether its role is pro-death or pro-survival in the context of chemotherapeutic treatment. Treatment of cells with two late-stage lysosomal inhibitors, chloroquine and bafilomycin-A1, in combination with cisplatin resulted in a significant enhancement in apoptosis levels indicating that targeting autophagy at later stages may be a potential therapeutic strategy in MRT treatment (Fig. 4).

In contrast, treatment with the early-stage autophagy inhibitor SAR405 had no notable effect on cisplatin-induced apoptosis (Fig. 5B). These conflicting results suggest that targeting autophagy may have different effects depending on which stage of the autophagic process is being modulated. Furthermore, it is worth noting that pharmacological inhibitors are often associated with limited specificity for autophagy. For example, some studies in breast and tongue carcinoma cells have reported that both chloroquine and bafilomycin-A1 may sensitise cells to therapy due to off-target effects which are unrelated to autophagy suppression [39,40].

To address this, a genetic approach was employed to modulate autophagy. An siRNA approach was used to silence the key autophagic protein, ATG5. Inhibition of ATG5 and LC3-I/LC3-II conversion was confirmed using western blot analysis (Fig 5C). Results demonstrated no discernible difference in cisplatin-induced apoptosis in cells transfected with non-targeting siRNA compared with cells transfected with ATG5 siRNA suggesting that cisplatin-induced autophagy does not represent a protective mechanism in MRT cell lines (Fig 5D). These results are in agreement with Magnano et al., which showed a significant increase in cisplatin-induced cytotoxicity when OSCC cells were treated in combination with chloroquine, but no enhancement of cytotoxicity when autophagy was targeted with early-stage inhibitors or with ATG5 siRNA [23]. However, due to the multiple and complex interactions between autophagy and apoptosis pathways, it cannot be excluded that opposing effects on chemosensitivity may be obtained depending on the stage of autophagy and/or the autophagic protein targeted.

In conclusion, this study has shown that cisplatin induces simultaneous activation of both apoptosis and autophagy in MRT cells and inhibition of apoptotic signalling through the use of a pan-caspase inhibitor also inhibited autophagy, suggesting an interplay of the two pathways in response to chemotherapeutics. Interestingly, autophagy inhibition using the late-stage autophagy inhibitors chloroquine and bafilomycin-A1 sensitised MRT cells to cisplatin-induced apoptosis and it would be of interest in future studies to confirm these findings in an *in vivo* model of MRT. However, both these pharmacological inhibitors have been reported to exert off-target effects therefore no firm conclusions can be made on whether their modulation of cisplatin sensitivity is solely due to autophagy inhibition. Nonetheless, these results demonstrate that combining chemotherapy with chloroquine or bafilomycin-A1 may represent a novel treatment strategy to improve clinical outcome in MRT patients. In contrast, autophagy inhibition using a specific early-stage autophagy inhibitor SAR405 had no effect on cisplatin sensitivity, suggesting that cisplatin-induced autophagy may not represent a protective mechanism in MRT. This conclusion was supported by data demonstrating that the genetic knockdown of ATG5 had no effect on sensitivity of MRT cells to cisplatin. Thus, the role of autophagy in MRT is complex and further study into understanding the intricate relationship between apoptosis and autophagy in MRT is warranted. There are many proteins controlling autophagy at various steps in the process and a more comprehensive genetic targeting of these may be worthwhile.

Ethical statement

None.

Funding statement

This work is supported by a Trinity College Dublin PhD Provost Award.

CRediT authorship contribution statement

Patricia Hannon Barroeta: Methodology, Validation, Formal analysis, Investigation, Writing – original draft, Visualization. **Stefania Magnano:** Methodology, Conceptualization, Writing – review & editing. **Maureen J O'Sullivan:** Resources, Writing – review & editing. **Daniela M Zisterer:** Resources, Writing – original draft, Supervision, Project administration, Funding acquisition.

Declaration of Competing Interests

The authors declare that they have no known competing financial interests or personal relationships that could have appeared to influence the work reported in this paper.

Supplementary materials

Supplementary material associated with this article can be found, in the online version, at doi:10.1016/j.ctarc.2022.100584.

References

[1] J.I. Geller, J.J. Roth, J.A. Biegel, Biology and treatment of rhabdoid tumor, Crit. Rev. Oncog. 20 (2015) 199–216.
[2] K.H. Kim, C.W.M. Roberts, Mechanisms by which SMARCB1 loss drives rhabdoid tumor growth, Cancer Genet. 207 (2014) 365–372.
[3] A. Tang, et al., Aurora kinases: novel therapy targets in cancers, Oncotarget 8 (2017) 23937–23954.
[4] E. Sigauke, et al., Absence of expression of SMARCB1/INI1 in malignant rhabdoid tumors of the central nervous system, kidneys and soft tissue: an immunohistochemical study with implications for diagnosis, Mod. Pathol. 19 (2006) 717–725.
[5] A. Abdullah, Y. Patel, T.J. Lewis, H. Ehamaloty, S. Strobel, Extrarenal malignant rhabdoid tumors: radiologic findings with histopathologic correlation, Cancer Imaging 10 (2010) 97–101.
[6] H. Nguyen, A. Stelling, A. Kuramoto, C. Patel, J. Keller, Malignant rhabdoid tumor of the liver: findings at US, CT, and MRI, with histopathologic correlation, Radiol. Case Rep. 9 (2015) e00031-e00031.
[7] J.S. Lee, T.R. Sanchez, S. Wootton-Gorges, Malignant renal tumors in children, J. Kidney Cancer VHL 2 (2015) 84–89.
[8] L. Lafay-Cousin, et al., Central nervous system atypical teratoid rhabdoid tumours: the Canadian paediatric brain tumour consortium experience, Eur. J. Cancer 48 (2012) 353–359.

[9] T.M. Tekautz, et al., Atypical teratoid/rhabdoid tumors (ATRT): improved survival in children 3 years of age and older with radiation therapy and high-dose alkylator-based chemotherapy, J. Clin. Oncol. 23 (2005) 1491–1499.
[10] K.R. Parzych, D.J. Klionsky, An overview of autophagy: morphology, mechanism, and regulation, Antioxid. Redox Signal. 20 (2014) 460–473.
[11] N. Mizushima, M. Komatsu, Autophagy: renovation of cells and tissues, Cell 147 (2011) 728–741.
[12] K. Jing, K. Lim, Why is autophagy important in human diseases? Exp. Mol. Med. 44 (2012) 69–72.
[13] R. Chavez-Dominguez, M. Perez-Medina, J.S. Lopez-Gonzalez, M. Galicia-Velasco, D. Aguilar-Cazares, The double-edge sword of autophagy in cancer: from tumor suppression to pro-tumor activity, Front. Oncol. 10 (2020).
[14] H.-Y. Chen, E. White, Role of autophagy in cancer prevention, Cancer Prevent. Res. (Philadelphia, Pa.) 4 (2011) 973–983.
[15] C.W. Yun, S.H. Lee, The roles of autophagy in cancer, Int. J. Mol. Sci. 19 (2018) 3466.
[16] S.O. Bustos, F. Antunes, M.C. Rangel, R. Chammas, Emerging autophagy functions shape the tumor microenvironment and play a role in cancer progression - implications for cancer therapy, Front. Oncol. 10 (2020).
[17] B. Janji, G. Berchem, S. Chouaib, Targeting autophagy in the tumor microenvironment: new challenges and opportunities for regulating tumor immunity, Front. Immunol. 9 (2018), 887-887.
[18] H. Folkerts, S. Hilgendorf, E. Vellenga, E. Bremer, V.R. Wiersma, The multifaceted role of autophagy in cancer and the microenvironment, Med. Res. Rev. 39 (2019) 517–560.
[19] C.W. Yun, J. Jeon, G. Go, J.H. Lee, S.H. Lee, The dual role of autophagy in cancer development and a therapeutic strategy for cancer by targeting autophagy, Int. J. Mol. Sci. 22 (2020) 179.
[20] G. Kroemer, B. Levine, Autophagic cell death: the story of a misnomer, Nat. Rev. Mol. Cell Biol. 9 (2008) 1004–1010.
[21] J. Debnath, E.H. Baehrecke, G. Kroemer, Does autophagy contribute to cell death? Autophagy 1 (2005) 66–74.
[22] R. Coyle, K. Slattery, L. Ennis, M.J. O'Sullivan, D.M Zisterer, The XIAP inhibitor embelin sensitises malignant rhabdoid tumour cells to TRAIL treatment via enhanced activation of the extrinsic apoptotic pathway, Int. J. Oncol. 55 (2019) 191–202.
[23] S. Magnano, P. Hannon Barroeta, R. Duffy, J. O'Sullivan, D.M. Zisterer, Cisplatin induces autophagy-associated apoptosis in human oral squamous cell carcinoma (OSCC) mediated in part through reactive oxygen species, Toxicol. Appl. Pharmacol. 427 (2021), 115646.
[24] P.-P. Liu, et al., Expression levels of cleaved caspase-3 and caspase-3 in tumorigenesis and prognosis of oral tongue squamous cell carcinoma, PLOS ONE 12 (2017), e0180620.
[25] K.F. Ginn, A. Gajjar, Atypical teratoid rhabdoid tumor: current therapy and future directions, Front. Oncol. 2 (2012), 114-114.
[26] S.K. Bhutia, et al., Autophagy: cancer's friend or foe? Adv. Cancer Res. 118 (2013) 61–95.
[27] X. Li, et al., Autophagy: a novel mechanism of chemoresistance in cancers, Biomed. Pharmacother. 119 (2019), 109415.
[28] H.-C. Zheng, The molecular mechanisms of chemoresistance in cancers, Oncotarget 8 (2017) 59950–59964.
[29] D. Denton, S. Kumar, Autophagy-dependent cell death, Cell Death Differ. 26 (2019) 605–616.
[30] M. Watanabe, et al., Induction of autophagy in malignant rhabdoid tumor cells by the histone deacetylase inhibitor FK228 through AIF translocation, Int. J. Cancer 124 (2009) 55–67.
[31] J.M.M. Levy, A. Thorburn, Modulation of pediatric brain tumor autophagy and chemosensitivity, J. Neuro-Oncol. 106 (2012) 281–290.
[32] A. Carugo, et al., p53 is a master regulator of proteostasis in SMARCB1-deficient malignant rhabdoid tumors, Cancer Cell 35 (2019) 204–220, e209.
[33] P. Mraouel, A. Carugo, G. Genovese, Targeting proteostasis and autophagy in SMARCB1-deficient malignancies: where next? Oncotarget 10 (2019) 3979–3981.
[34] J.-P. Lin, et al., Cisplatin induces protective autophagy through activation of BECN1 in human bladder cancer cells, Drug Des., Devel. Ther. 11 (2017) 1517–1533.
[35] C.-Y. Sun, et al., Scutellarin increases cisplatin-induced apoptosis and autophagy to overcome cisplatin resistance in non-small cell lung cancer via ERK/p53 and c-met/AKT signaling pathways, Front. Pharmacol. 9 (2018).
[36] Y. Jiang, et al., Cisplatin-induced autophagy protects breast cancer cells from apoptosis by regulating yes-associated protein, Oncol. Rep. 38 (2017) 3668–3676.
[37] C. Herzog, C. Yang, A. Holmes, G.P. Kaushal, zVAD-fmk prevents cisplatin-induced cleavage of autophagy proteins but impairs autophagic flux and worsens renal function, Am. J. Physiol. Renal Physiol. 303 (2012) F1239–F1250.
[38] W. Martinet, D.M. Schrijvers, A.G. Herman, G.R. De Meyer, z-VAD-fmk-induced non-apoptotic cell death of macrophages: possibilities and limitations for atherosclerotic plaque stabilization, Autophagy (2) (2006) 312–314 (United States; .
[39] P. Maycotte, et al., Chloroquine sensitizes breast cancer cells to chemotherapy independent of autophagy, Autophagy 8 (2012) 200–212.
[40] H.-Y. Chu, et al., Bafilomycin A1 increases the sensitivity of tongue squamous cell carcinoma cells to cisplatin by inhibiting the lysosomal uptake of platinum ions but not autophagy, Cancer Lett. 423 (2018) 105–112.